Johns Hopkins APL

TECHNICAL DIGEST

April-June 1982, Vol. 3, No. 2

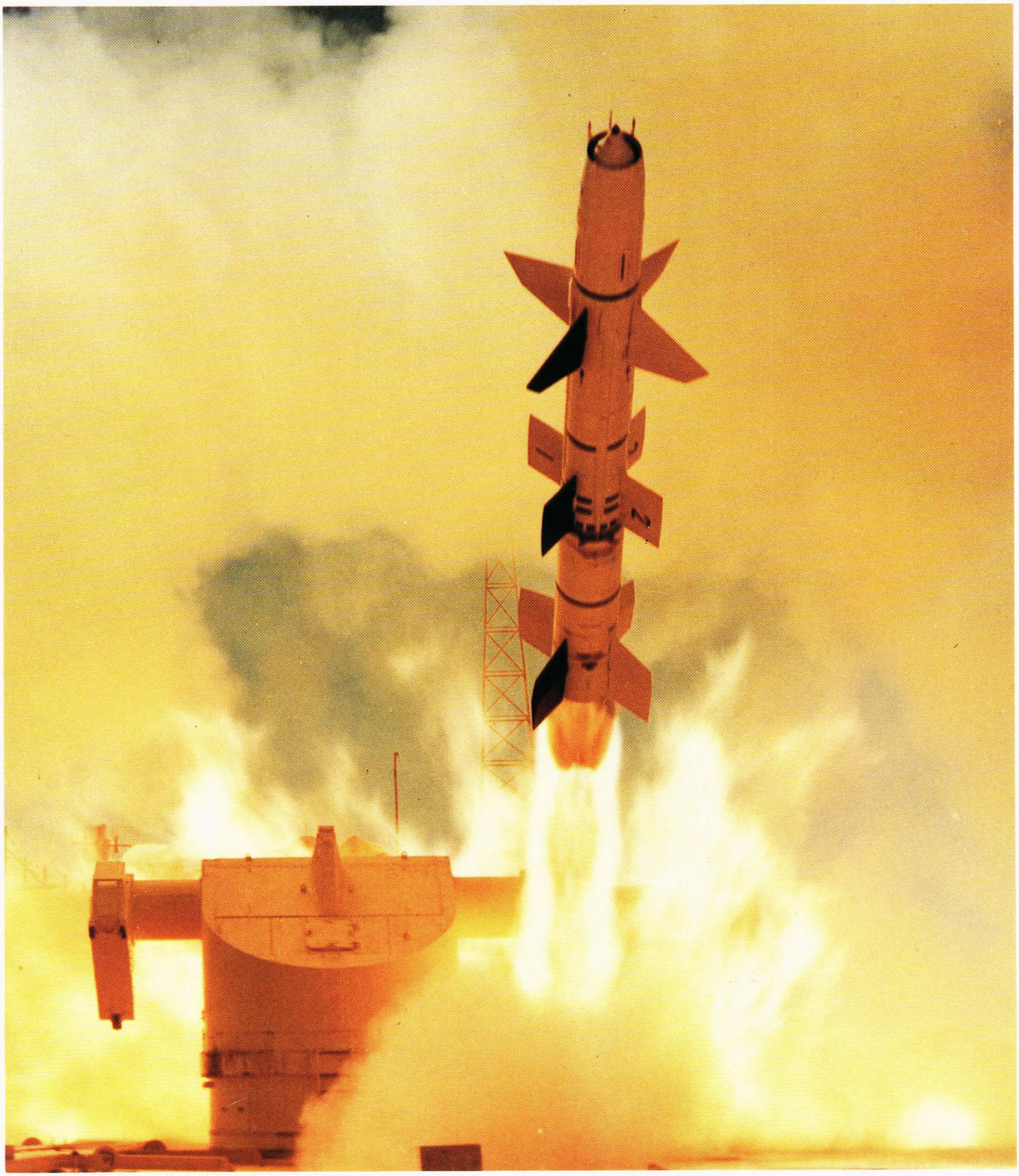

The Talos Missile

114	Editorial	W. G. Berl
115	Guest Editor's Introduction	F. A. Dean
116	Talos in Retrospect	W. H. Goss
117	Evolution of the Talos Missile	W. Garten, Jr., F. A. Dean
123	The Unified Talos	F. A. Dean
126	The Talos Propulsion System	W. B. Shippen, W. G. Berl, W. Garten, Jr., E. J. Hardgrave, Jr.
135	The Talos Booster Rockets	W. H. Avery
138	Talos Aerodynamics	L. L. Cronvich
142	The Talos Guidance System	J. Gulick, W. C. Hyatt, O. M. Martin, Jr.
154	The Talos Control System	F. C. Paddison
157	The Talos Continuous-Rod Warhead	C. R. Brown, C. F. Meyer
160	Talos Flight Test Facilities	
161	The Talos Land System	
162	The Talos Ship System	E. D. Robinson
167	The Talos Shipboard Test Program	D. D. A. Gray
170	Operational Lessons Learned	RADM W. E. Meyer, CAPT R. W. Anderson
171	Annotated Bumblebee Initial Report	W. G. Berl
180	A Post-Voyager View of Saturn's Environment	S. M. Krimigis
189	Combat Casualty Care: Can Technology Help?	S. Koslov
207	In Memoriam: Merle Antony Tuve	
218	Publications, Presentations, and The Authors	

▲ TOP

EDITORIAL

APL is recalling this year events that occurred during the four decades after a contract was made between the Office of Scientific Research and Development (OSRD) and The Johns Hopkins University to support and administer a large applied physics laboratory. The contract was signed in March 1942. It was the low ebb in the fortunes of war of the Allied powers. The Laboratory was then almost exclusively engaged in the crash development of a radio-activated proximity fuze for use in the defense of ships against hostile aircraft attacks. In less than a year a working fuze was in production and use. The first assignment to the Laboratory had been accomplished with record speed.

This issue of the *Technical Digest* contains several reflections on that 40-year period. Included is a set of recollections, a "bouquet of reminiscences," by colleagues and friends of Merle A. Tuve (p. 207). Tuve, the founder and first director of the Applied Physics Laboratory, joined the Department of Terrestrial Magnetism of the Carnegie Institution of Washington in the 1920's. He carved out a brilliant career in experimental physics, searching for explanations for the anomalous propagation of radiowaves in the ionosphere and for the forces (then only dimly perceived) within the nuclei of atoms.

Fourteen years later, when the conflict between the United States and the Axis powers became well-nigh inevitable, and the inadequate state of U.S. military preparedness became clear, if only to a few, Tuve gave up his career in basic research and became a key participant in the program of the National Defense Research Council (NDRC). It was set up by Franklin D. Roosevelt in June 1940, and placed under the direction of Vannevar Bush, then the president of the Carnegie Institution of Washington. The aim of NDRC was to bring to bear the insights of physicists and chemists on building up the U.S. war effort. Tuve selected the fuze project, which had been discussed earlier in military circles as a desirable ordnance device but never seriously pursued. He soon showed its feasibility by a convincing field demonstration. Important tasks to provide acceptable reliability and to supervise large-scale production remained to be solved. His Applied Physics Laboratory was the vehicle to bring the project to fruition.

A substantial part of the *Technical Digest* is given over to a description of a subsequent APL undertaking, the development of a Fleet defense missile system that became known as Talos. Much more complex and chancy than the fuze program, it was first seriously thought about early in 1944. It became a formal technical assignment in January 1945, when the outcome of World War II was no longer in doubt. It laid the groundwork for guided missile technologies yet to come. More than ten years went by before the system became operational and part of the Fleet armament.

Talos demonstrated the powers of a dedicated technical team to design and develop a complex mechanical system. Tuve, on the other hand, will be remembered as an individual with consummate skills in his profession, who, in time of need, had the ability to inspire his colleagues to push on into unexplored fields.

President Steven Muller recently summarized his thoughts on the relationship of the Applied Physics Laboratory and The Johns Hopkins University in words that Merle Tuve would have been pleased to hear:*

> If there is a dominant ethos in modern science and modern learning, it is that we are rational. Therefore, as a rational institution that fosters reason, it makes sense to conclude that the use of force to resolve disputes is not rational and that the use of nuclear weapons as part of the employment of force is, in fact, insanity.
>
> But we do not live in a purely rational world. We live in a world that is imperfect spiritually and rationally. In that world, rational analysis must conclude that security and defense are a precondition of peace and the avoidance of force. Because of that, a deep commitment to reason and to peace and an equally deep commitment to national security and national defense are not inconsistent or opposed to each other.
>
> I regard them as twin missions of this institution. I regard them as complementary, and I see in this Laboratory and in this University the mirror image of the problems that face the world and our nation where there is an overwhelming commitment on the part of the most rational and civilized people to peace, and an equally firm commitment, until that day when peace can be assured by other means, to defense and security as the best investment we can make to avoid the use of force.

WALTER G. BERL

*Speech given at the APL 40th Anniversary Dinner for the Principal Professional Staff, March 8, 1982.

GUEST EDITOR'S INTRODUCTION

Secretary of Defense Caspar Weinberger said at the launching ceremony of the Aegis ship USS *Ticonderoga* (CG-47), "We are christening the most capable antiair warfare system ever put to sea." Similar words were spoken twenty years earlier at the christening of the Talos cruiser USS *Galveston* (CLG-3). In both instances the statements were true. Though Aegis reflects the technological advancements and refinements of the past decade, it was the broadly based research and development efforts of the Talos program that supplied the underlying technology that gave birth to the present generation of surface-to-air missiles.

The assignment of Task F to APL by the Chief of the Bureau of Ordnance on January 11, 1945, provided the official start of the Bumblebee program, which led to the development and production of the ship-launched Talos, a ramjet-propelled antiaircraft guided missile.

Guided missile technology was virtually nonexistent when the Bumblebee program was begun: supersonic ramjets were not known to have been successfully flown; rockets large enough for boosting a ramjet to flight speed had not been developed; knowledge of supersonic aerodynamics was limited to a few ballistic studies on shells; missile control was limited to airplane autopilot developments; guidance technology, at best, was confined to remote control schemes for low-speed vehicles; and an effective warhead had yet to be invented and developed.

Engineers and scientists were assembled into teams of specific expertise so that an energetic effort could be made on the many problems that such a task presented. Progress in all areas was rapid: test facilities were built and design data were collected; solid-fuel boosters and test vehicles for the 28-inch-diameter ramjet engine were designed, built, and flight tested; supersonic aerodynamics and control technologies were fully developed; beamriding control at supersonic speeds was demonstrated; and the interferometer homing system was invented. By 1951, sufficient information was in hand to formulate general specifications for the Talos prototype missile. In January 1955, the Talos missile was ready for production, and later that year the first missiles were delivered to the Navy.

The following articles describe the development of this first ramjet-powered guided missile, spanning the time from the early concepts to the deployment of a mature guided missile system. Since the Talos missile went through numerous design changes, the first two articles are devoted to the evolution of its development. Six subsequent articles discuss specific technical areas, followed by two sections that are concerned with shipboard placement. The last article summarizes operational lessons learned during the program. It is hoped that these contributions will instill in the reader the excitement felt by the participants in seeking solutions to problems that had not been faced previously.

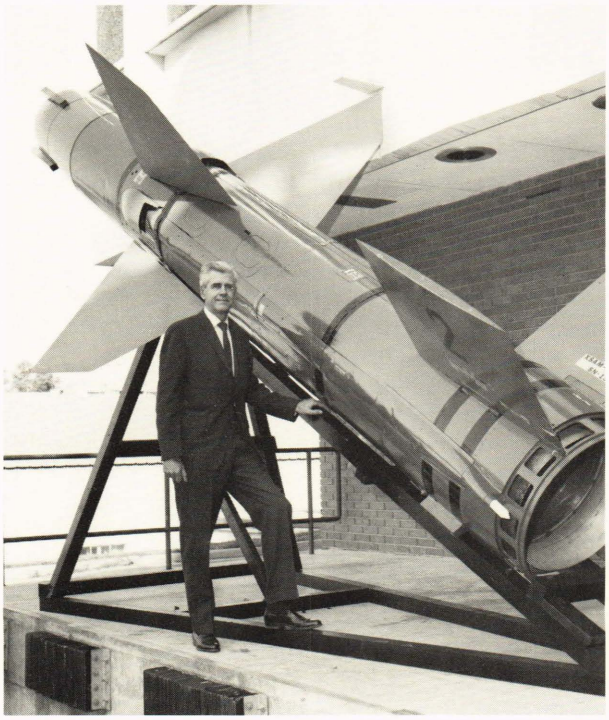

Roy W. Larson

Guidance and motivation for the preparation of these articles were provided by Mr. Roy Larson. His knowledge of all phases of the program was extensive, and his interest in it was enduring. Outlines and some first drafts had been submitted for his approval when we learned of his sudden death.

The authors were closely associated with Mr. Larson during the development of the Talos missile. It was their desire to proceed with the publication project, not only because they thought the story would be of interest, but to complete the plan initiated by their long-time colleague. It is our hope that this collection of articles is a fulfillment of what Roy had in mind.

FRANK A. DEAN

WILBUR H. GOSS

TALOS IN RETROSPECT

The Talos system, a product of the oldest of the U.S. Navy's antiaircraft guided missile programs, has recently been retired from the Fleet after 22 years of active service. The heavy cruisers for which it was designed as the primary armament have been mothballed or retrofitted with newer systems. USS *Oklahoma City*, with the last Talos missile system on board, was decommissioned in 1980.

Talos was the largest and most powerful weapon in the Navy's arsenal of antiaircraft missiles. During its years of development, and by successive retrofits during deployment, its range grew from 10 nautical miles to well in excess of 100 nautical miles, with midcourse guidance and a terminal homing system of deadly accuracy. Its capabilities were expanded to intercept ships as well as aircraft; to employ features that made it virtually unjammable; to include a nuclear warhead capable of destroying aircraft flying in formation; and to offer a shore bombardment mode.

At its inception, when controlled supersonic flight was in its infancy and when the concept of guided missile warfare was only just being formulated, the Talos program set out to pioneer, to chart new territory — to do things that had not been done before. Such a pioneering program generates "firsts." It developed the first rocket-launched supersonic ramjet engine, the first interferometric homing guidance, and the first beamriding missile system. It was the first to incorporate a tactical nuclear warhead and the first to develop an explosive warhead capable of ejecting a continuous, expanding steel ring.

The ramjet engine deserves a special comment. Following its extensive development and testing phase, it was manufactured for years without a single production engine ever being test-fired prior to use; conformity to production specifications was the sole acceptance criterion. The engines had to ignite reliably at the instant of separation of the missile from the booster rocket at speeds greater than twice the speed of sound and had to maintain controlled speed throughout flight, while delivering up to 70,000 horsepower. No ramjet engine failed to meet these requirements in more than 750 successive flights.

In the Vietnam conflict, Talos distinguished itself in early engagements by its deadly accuracy at long range. The presence of a Talos cruiser in the Gulf of Tonkin was sufficient to suppress all enemy fighter aircraft flights over the Vietnam coastal strip.

In retrospect, perhaps the most important aspect of the Talos effort was not the missile system itself, in spite of its achievements, but rather what developed from it: the current and future generations of antiaircraft missile systems — both hardware and concepts — and a technology that is now making contributions in fields ranging from satellite systems to biomedical engineering.

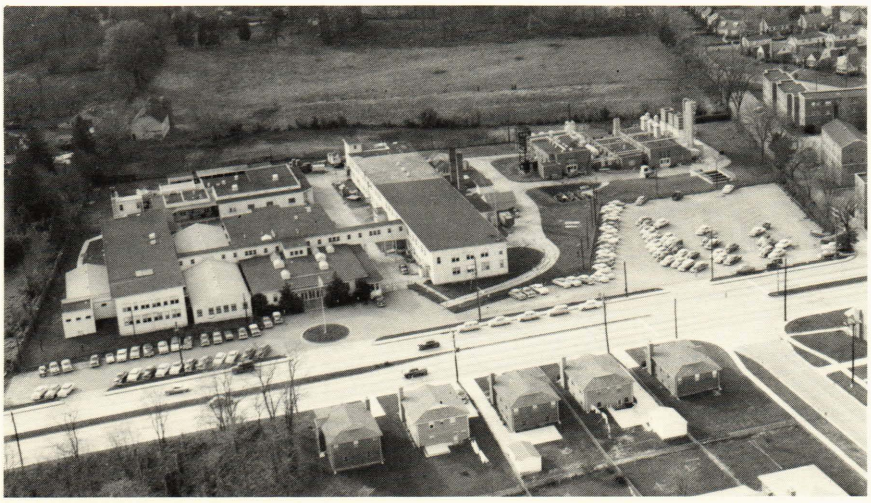

Aerial view, in the early 1950's, of APL's Forest Grove Station on Georgia Ave., Silver Spring, Md. The Burner Lab, behind the large parking lot at right, was the site of early ramjet research, development, and testing, which culminated in the Fleet's operational Talos missiles. Midnight explosions and other earshattering sounds emanating from this facility led ultimately to the choice of the rural setting of the present facilities in Howard County, Md.

WILLIAM GARTEN, JR. and FRANK A. DEAN

EVOLUTION OF THE TALOS MISSILE

In 1945, the Bumblebee Program began work directed toward determining the feasibility of building a supersonic guided missile. It was to be ramjet propelled and guided by radar. Because the state of the required technology was then very limited, many problems needed solutions. This article is an overview of the work done to bring the Talos missile into the Navy's arsenal.

At the beginning of World War II, the principal threat to Allied surface ships was from dive-bombing or torpedo-carrying aircraft, with speeds on the order of 250 knots. The airplanes had to make a long, slow, straight-in approach rather close to the target in order to deliver their weapons. This put them in positions where antiaircraft gunfire was quite effective and attrition rates were high.

With the advent of proximity-fuzed antiaircraft shells in 1943, enemy planes were even less able to mount conventional attacks without incurring unacceptable losses. However, it was foreseeable that this advantage of defense over attack would not long continue. As high-performance turbojet and rocket engines became available, and with the advent of radio-guided bombs, it was evident that small, high-speed, air-launched missiles might become a threat to ships whose antiaircraft shells had insufficient range to prevent enemy airplanes from launching such missiles.

A solution to this dilemma was to provide ships with defensive weapons of such range, accuracy, and speed that attacking airplanes would be unable to approach near enough to launch antiship missiles. In the fall of 1944, responding to an inquiry by the Bureau of Ordnance (BuOrd) regarding the feasibility and time scale of such a development, APL proposed a program for a supersonic, radar-guided, ramjet-propelled missile, launched by a solid propellant booster rocket and carrying a payload of about 600 pounds of explosives. It was suggested that, in a period of two to three years and with an expenditure of 10 to 20 million dollars, an initial version of such a "chaser missile" could be produced or, conversely, that proof could be provided that such devices could not be built. It was also proposed that such a development should be sharply focused on the specific objective of developing a supersonic guided missile and be carried out by a closely integrated team responsible for the solution of the overall problem. The anticipated time scale foresaw limited military use in the latter stages of World War II.

In December 1944, the Chief of Naval Operations, Admiral E. J. King, directed BuOrd to proceed with the development of such a missile on an urgent basis. The other Navy bureaus were to give all possible support and assistance.

On January 11, 1945, Admiral G. F. Hussey, Jr., the Chief of BuOrd, assigned the following task to the Applied Physics Laboratory:

> Task "F" — A comprehensive research and development program shall be undertaken, embracing all technical activities necessary to the development of one or more types of rocket-launched, jet-propelled, guided, antiaircraft missiles. The desired performance characteristics are to be defined in consultation with the Bureau of Ordnance as the work progresses, in accordance with the objective of obtaining a weapon of useful military characteristics in the shortest feasible time.
>
> This program shall include pertinent basic research, investigations and experiments, and the design, fabrication and testing of such missiles, their component parts, and supplementary equipment. Alternative modes of promising technical approach are to be pressed either singly or simultaneously, as deemed most effective for the rapid development of a useful weapon. The work shall include cooperation and joint activity, as may be feasible, with those groups in the Armed Services and other agencies which are actively concerned with the development, testing, production and use of similar or related missiles for the United States Government. The work also may include, on request of the Bureau of Ordnance, supervision and guidance of the technical work under other Navy contracts which may be assigned work related to this Task.
>
> The Bureau of Ordnance does not expect by this request and in the immediate future to obtain an ideal or

ultimate antiaircraft weapon, and is aware that the actual results of these efforts cannot be guaranteed or accurately predicted. The Bureau believes, nevertheless, that an immediate attack must be made on this problem, and expects that this will result at the best in the production of an advanced antiaircraft weapon which may be available in the latter stages of this war, and at the least in considerable valuable progress in research and development on jet propulsion techniques, self-guided techniques, and other technical matters of great importance to the future of ordnance.

This was the beginning of the "Bumblebee" program, the development of the technology necessary to build a supersonic surface-to-air guided missile. The key problems were the development of a ramjet engine, supersonic maneuvering, a guidance system that directed the missile to the vicinity of the target, and a warhead that would explode at the appropriate instant.

The program consisted of a family of direct Navy contracts with universities and industry under the integrating technical direction of APL. Initially, industry and APL collaborated in the R&D effort. With the passage of time, industry's role changed from co-developer to that of missile contractor. Bendix Aviation Corp., Mishawaka, Ind., assumed this role for the Talos missile. To maintain the continuity between R&D and production, the engineering program at Bendix was under the technical direction of APL.

INITIAL GOALS

Initial goals were to intercept an airplane target at a horizontal range of 10 nautical miles and 30,000 feet altitude and with a shooting accuracy of 2 mils (2 feet per 1000 feet of target range). Large warhead weights (300 to 600 pounds) were required to achieve kill probabilities of 0.3 to 0.6. This, in turn, meant that a large and fast guided missile was needed to deliver such warheads effectively. Subsonic turbojets were too slow to achieve such intercepts with high-speed targets. Rockets had not been developed at that time to reach such distances. The choice of ramjet propulsion was dictated primarily by the required range and the possibility of extending it by minor alterations in missile geometry, as was done later. Powered flight right up to target intercept was the goal.

EARLY BUMBLEBEE MISSILE DEVELOPMENTS

The development of the Bumblebee missile required ground and flight tests with a variety of test vehicles, each designed to investigate or verify the operation of a specific missile subsystem. These were the following: (a) launching test vehicles that evaluated the performance of the large solid-fuel booster rockets; (b) burner test vehicles to study ramjet engine performance; (c) subsonic control test vehicles that tested radar beamriding; (d) supersonic test vehicles (STV) for the study of guidance and control during supersonic flight; and (e) the XPM, a prototype ramjet-propelled guided missile that incorporated all previous developments. The relationships between these developments are shown in Fig. 1.

STV-3 test vehicles, the most complex of the rocket-propelled test vehicles, were launched by a booster rocket and sustained in supersonic speed by a small solid-fuel rocket. As the first successful supersonic beamriding missiles ever to be flown, they were recognized by both the Navy and APL to have potential as a short-range antiaircraft missile if the telemetry section were replaced with a fuze and warhead. APL accepted responsibility for developing a prototype missile from this test vehicle. The missile was named Terrier.

RATIONALE OF THE TALOS DESIGN

Since the small Terrier missile was to cover short-range antiair targets and was expected to be deployed much sooner than the ramjet-propelled version of the Bumblebee missile (to be known as Talos), goals for the large missile were extended. Maximum range was increased to 50 nautical miles or more, and a terminal homing guidance requirement was generated.

As early work on Task F began to develop confidence that a ramjet missile would be successfully developed, an appropriate name for this missile was sought. From Bulfinch's *Age of Fable*, the name Talos was selected. Talos was a demigod who watched over and guarded the island of Crete. He was made of brass and was reputed to fly through the air at such terrific speed that he became red hot. His method of dealing with his enemies was to clasp them tightly to his breast, turning them to cinders at once. Talos was approved as the name for the new ramjet missile by BuOrd and by the Guided Missiles Subcommittee of the Aeronautical Board on January 5, 1948.

Beamriding for midcourse guidance was an obvious choice, based on successful experience in development of the STV-3. Even though the maximum range requirement of Talos precluded the missile from traveling on a direct line-of-sight trajectory from launch to target (because of excessive fuel consumption on such a flight path at low altitude), it was realized that a guidance beam could be programmed in elevation so that a missile riding along its axis could be made to follow a fuel-conserving trajectory. Beamriding also offered the possibility of simultaneously guiding several missiles with a single guidance beam.

Since beamriding guidance could not provide sufficient accuracy for precise intercepts at ranges of 50 to 100 nautical miles, a terminal guidance phase with a semiactive target seeker was envisaged. The interferometer seeker proved to be the most accurate among the surface-to-air missile seekers of the Navy.

Development of the missile along the above lines led to the pilot line production of the First Tactical Talos missile (SAM-N-6b) shown in Fig. 2. This configuration was flown in 1952, and the First Tactical

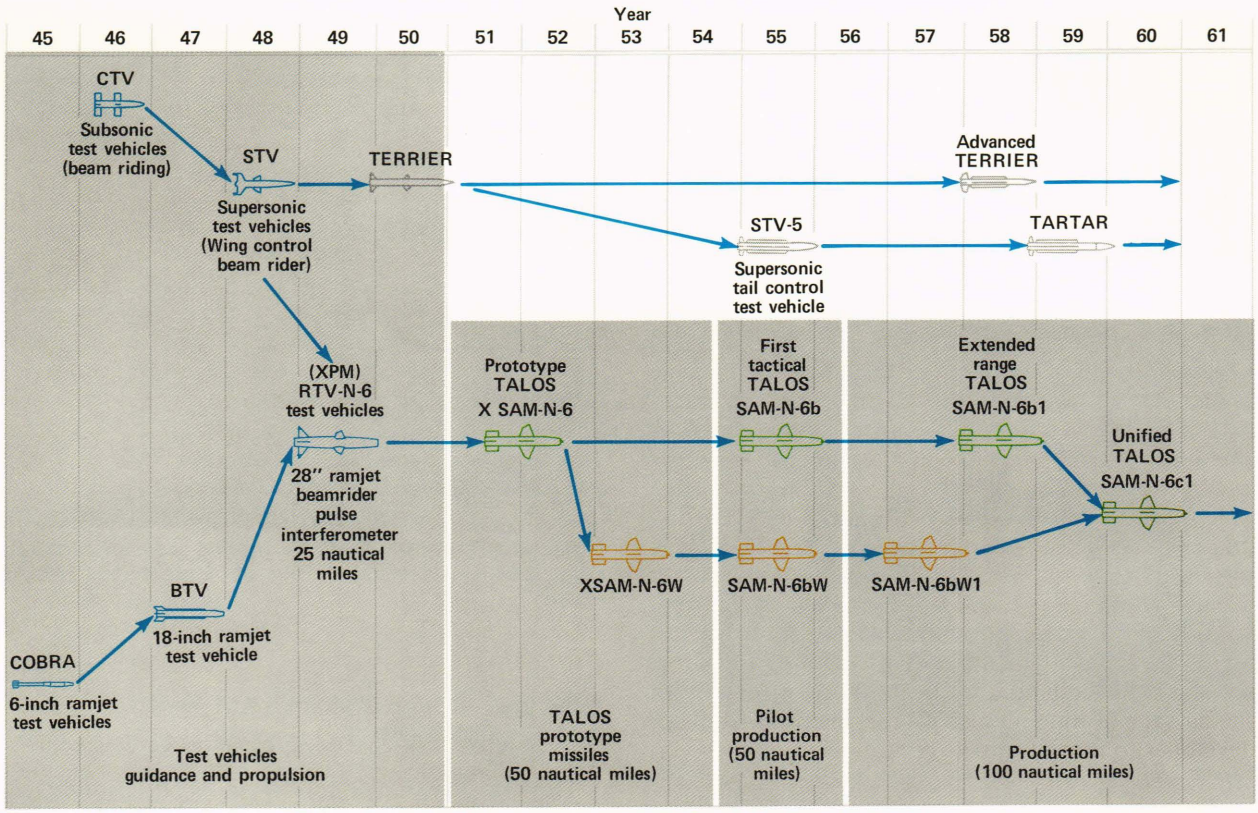

Figure 1 — The evolution of Talos started with the development of Bumblebee test vehicles to investigate operation of missile subsystems and ended with the production of the Unified Talos missile. Bumblebee test vehicles also led to the Terrier and Tartar missile programs.

Talos missile was introduced into the Fleet in May 1958, with the recommissioning of USS *Galveston* (CLG-3). The principal time-determining factor in introducing Talos to the Fleet was ship conversion, a four-year task, following a decision to proceed on a satisfactory missile design.

RATIONALE OF THE TALOS W DESIGN

Analysis of the basic capabilities of the Talos semiactive interferometer homing system included a study of guidance accuracy under conditions where the missile could simultaneously receive microwave energy reflected from two or more aircraft flying in formation. It showed that, for target separations of a few hundred feet, the missile would have a large miss distance. The Talos weapon system was therefore vulnerable to simple tactics that could be used by a well-informed attacker.

A solution to this vulnerability was seen when it became known that a small nuclear bomb was being developed (in 1951) for use by fighter-bomber aircraft. Since this bomb had a smaller diameter than the Talos missile, it was feasible to adapt it as a warhead for Talos.

Talos W, capable of carrying a nuclear warhead, would be guided all the way to the target by the beamrider system used for Talos midcourse guidance. The accuracy of this system at maximum range and the basic need to force large separation distances for attacking aircraft required the kill radius for the warhead to be 1000 to 2000 feet. Estimates of warhead effectiveness showed that gust loading would generally be the kill mechanism at longest range, but that both overpressure and thermal radiation could produce significant effects.

The large value for tolerable miss distance for Talos W translated into a relatively low missile maneuver requirement. As a result of the more forward location of the center of gravity, which increased the missile's dynamic stability, the Talos W maneuver capability was diminished relative to Talos but remained adequate to meet the system requirement.

All aerodynamic surfaces, the combustion chamber, exit nozzle, fuel tank, fuel controls, and the actuators for wing control of Talos W were identical with those of prototype Talos. A modified front end, with an enlarged inner body, was necessary to accommodate the nuclear warhead.

When the Talos W missile development was initiated, it was decided to develop a new beamrider receiver, beacon transponder, and control system electronics. The microwave frequency for the Talos W beamrider and beacon was in the 5 to 6 gigahertz band intended for the tactical Talos weapon system rather than the 9 to 10 gigahertz band then being used in the prototype Talos flight testing. Electronic packaging compatibility between Talos and Talos W was attained in later production missiles.

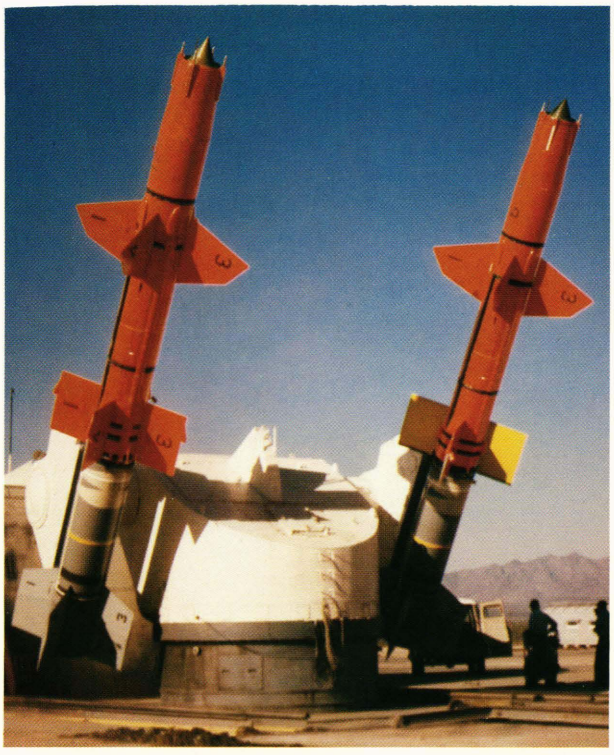

Figure 2 — The First Tactical Talos missiles (SAM-N-6b) are shown on the launcher at White Sands Missile Range. Introduced into the Fleet in May 1958, Talos had a 50-nautical-mile range that employed midcourse beamriding and semiactive pulse homing.

Development along the above lines led to the first successful flight test of a prototype in 1953 (Fig. 3). This was accomplished in 18 months from initiation of hardware design to this first flight. Tactical missile (SAM-N-6bW) production followed the initial 12 prototype missiles. Early in its development, Talos W was seen as a possible new weapon for land defenses and a little later as a possible first anti-ICBM weapon. These possibilities motivated programs to use Talos for the defense of the continental United States.

TALOS CONFIGURATIONS

Capabilities of the missile were enhanced by a succession of configuration variations of Talos (see Fig. 4 and Table 1) beyond First Tactical Talos (identified as SAM-N-6b and SAM-N-6bW). The development program, known as Extended Range Talos (identified as SAM-N-6b1 and SAM-N-6bW1), encompassed a reoptimization of missile flight capabilities for the separate conventional and nuclear versions of Talos. A further development, known as Unified Talos (SAM-N-6c1), took advantage of electronic miniaturization, which made it feasible to package all the electronics of the homing system within the space available for electronics in the nuclear missile. This made it possible to design a single Talos missile configuration for either conventional or nuclear warheads.

Figure 3 — The first Talos W missile was successfully flight tested in December 1953 at White Sands Missile Range.

Extended Range Talos (SAM-N-6b1 and SAM-N-6bW1)

Exploitation of the full-range capability inherent in the ramjet engine was expedited by the interest of the Air Force in the use of Talos for defense of Strategic Air Command bases against rocket-launched missiles. The development of a 100-nautical-mile Talos took place in the 1950's, with the first Fleet firing taking place in 1961.

This development began in 1953 with studies carried out by the missile airframe contractor and APL looking at a possible redesign of the Talos missiles (prototype and W versions) to achieve higher performance. As the analysis proceeded, the improved performance was defined as an increase of the altitude ceiling from 60,000 to 70,000 feet and of the range under optimum conditions from 50 to 100 nautical miles.

The more efficient design of these missiles (greater maneuverability, lower maneuver-induced drag, and greater engine thrust and efficiency) resulted in a higher operating ceiling, the capability to engage faster and more maneuverable targets, and tolerance of greater levels of residual low-frequency angular motion of the guidance beam due to imperfect beam stabilization. Greater missile speed was a factor in obtaining this increase in efficiency and also a decrease in the weapon system tie-up time for any one engagement, with an increase in weapon system firepower.

Modifications to achieve the improved performance were:

1. Increased flight speed at high altitude from 2000 to 2400 feet per second;
2. Increased missile tail fin span and increased speed, providing greater maneuverability, high-

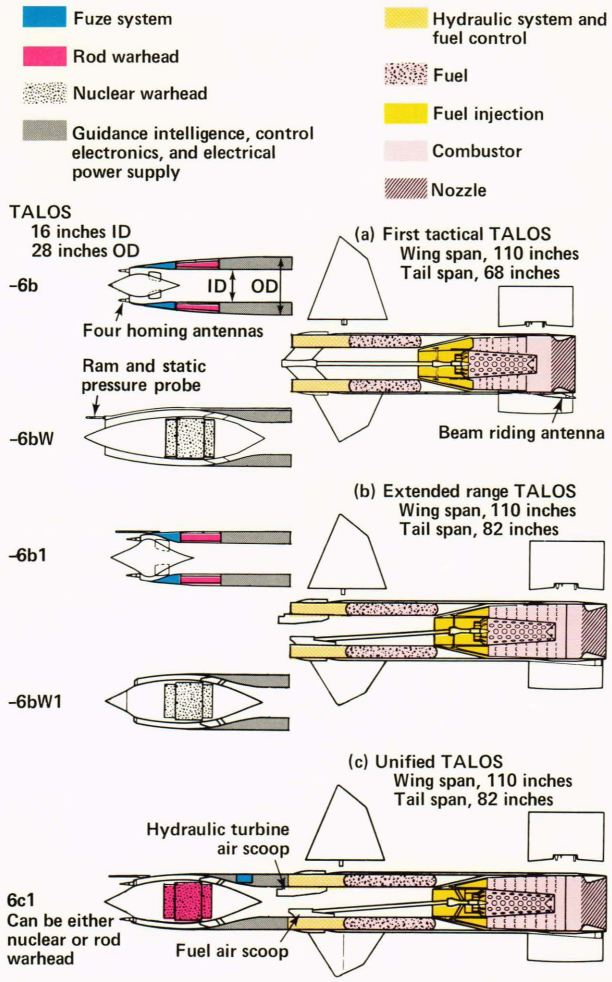

Figure 4 — The Talos configurations can be divided into three classifications: First Tactical Talos, Extended Range Talos, and Unified Talos. (a) The First Tactical Talos employed beamrider midcourse guidance and semiactive pulse homing for terminal guidance. The warhead was annular and surrounded the diffuser. The nuclear version required a special front end. (b) The Extended Range Talos was achieved by enlarging the fuel tank, redesigning the combustor, and improving the aerodynamic efficiency. Air turbine scoops for the fuel and hydraulic systems were placed on the wall of the diffuser. Separate warhead sections were required. (c) The Unified Talos configuration was basically the nuclear version of the Extended Range Talos with a solid-state continuous wave seeker added. The inner body normally contained a rod warhead, but it could also accommodate a nuclear warhead. All subsequent versions of Talos were obtained by exchanging subsystem modules on the basic configuration.

er lift-to-drag ratio, and more linear aerodynamic characteristics;

3. Lengthened fuel tank, providing about 20% more fuel capacity;
4. Six-inch lengthening of the combustion chamber, giving greater combustion efficiency at high altitudes;
5. Double-cone engine inlet, resulting in greater thrust margins at high altitudes;
6. A more powerful booster, providing adequate launch speed for these heavier missiles.

Unified Talos (SAM-N-6c1)

Still unsolved at this stage of development were two problems that forced the next development step. Low-altitude target intercepts were precluded because of excessive sea clutter. Also, the use of two missile types (carrying either nuclear or high-explosive warheads) posed logistic problems and required a determination of the number of each type to be allocated to a ship. In a nonnuclear war situation, vital stowage would be taken up by missiles that would never be launched.

The solution to this dilemma lay in providing interchangeable warheads so that any missile aboard ship could be equipped at will with either a high-explosive or a nuclear warhead. To accomplish this, it was necessary to develop a high-explosive rod warhead to be packaged in the inner-body space occupied by the nuclear warhead and to find space in the SAM-N-6bW1 design for a target seeker and fuze in addition to the beamrider. Fortunately, since a shift from pulse seeker to continuous wave seeker was required to permit low-altitude intercepts, it was possible to meet the space demands simultaneously by developing this new seeker with space-conserving solid-state devices.

Studies carried out in 1956 established the feasibility of adding interferometer homing to the SAM-N-6bW1 missile. This configuration provided the Talos weapon system with missiles that could be used with either a conventional or a nuclear warhead.

The Unified Talos (SAM-N-6c1) was essentially a SAM-N-6bW1 with an alternative, interchangeable, high-explosive warhead and a solid-state continuous wave seeker. The modular construction of this missile provided invaluable versatility. All subsequent versions of the Talos missile were obtained by simply exchanging subsystem modules in this basic SAM-N-6c1 airframe.

Flight testing of the XSAM-N-6c1 configuration began in June 1959. Production of missiles for ship deployment began in the early 1960's.

Talos Antiradiation Missile (RGM-8H)

The need for an antiradiation missile became evident early in the Vietnam conflict, and work was started in 1965 to develop a missile that would passively home on a radar installation. The system and missile requirements were quickly defined and implemented. Successful demonstrations of the system occurred at White Sands Missile Range during 1967, and this was followed by deployment of antiradiation missiles on USS *Long Beach* in 1968.

While specific details of combat applications cannot be released, the radiation-seeking capability was demonstrated by the fact that shore batteries were silenced by missiles fired from ships located in the Gulf of Tonkin. The target discrimination capabilities of Talos also permitted long-range kills of MiG aircraft over land. The long-range intercept capacity limited the enemy air tactics whenever a Talos ship was present. An opportunity to use the surface-to-surface capability did not occur.

Table 1 — Missile designations.

Description	*Designations*	
	Former	*Current* *
Talos prototype, 50-nautical-mile range	XSAM-N-6	None
Talos prototype, 50-nautical-mile range	XSAM-N-6a	None
Nuclear warhead Talos prototype	XSAM-N-6aW	None
First Tactical Talos	SAM-N-6b	RIM-8A
First Tactical Talos W (nuclear)	SAM-N-6bW	RIM-8B
Extended Range Talos, 100-nautical-mile range, modular packaging	SAM-N-6b1	RIM-8C
Extended Range Talos W (nuclear)	SAM-N-6bW1	RIM-8D
Modified RIM-8D, first CW seeker	SAM-N-6b1-CW	RIM-8F
Unified Talos, CW seeker, solid-state electronics and an interchangeable high-explosive or nuclear warhead	SAM-N-6c1	RIM-8E
Antiship capability and guidance improvements		RIM-8G
Antiradiation missile, 120-nautical-mile range		RGM-8H
Unified Talos (final version). Improved seeker, electronic counter-countermeasures, chaff rejection, multiple target discrimination, 130-nautical-mile range (dimer fuel), low-altitude fuzing		RIM-8J

*Missile designations as revised by the Department of Defense in 1963.

THE END OF AN ERA

From the commissioning of USS *Galveston* in May 1958 to the decommissioning of USS *Oklahoma City* in September 1980, Talos missiles protected the Fleet for 22 years. Eventually, the time came to consider their retirement, for several reasons. First, although their one-to-one capability to engage planes at long range was clearly demonstrated and has never been matched, it required the exclusive dedication of a midcourse guidance beam for essentially the full flight time of the missile. This degraded defensive capabilities against multiple azimuth attacks. Second, long-range target identification problems had to be solved before the long-range missile capability was really usable in a congested battle environment. Third, Talos missiles required relatively large launchers and occupied considerable storage space. Fourth, maintenance of the aging Talos ships was expensive. Fifth, new weapon systems using smaller missiles and capable of handling many targets simultaneously had been developed and were available for the threats of the 1980's.

Thus, with the decommissioning of USS *Oklahoma City* the Talos missile deployment came to an end. Yet the technology that was developed and the concepts it engendered continue to exercise an influence over much of modern missilery. Many of the operational missiles in the Fleet today reflect the proud parentage of Talos. We hope they will serve as long and as well.

FRANK A. DEAN

THE UNIFIED TALOS

This article describes the final version of Talos, known as Unified Talos.

The final version of Talos is shown in Fig. 1. Four interchangeable warhead assemblies were available: nuclear, nuclear training, continuous-rod, and exercise warhead with telemetry. The innerbody provided packaging space for the warhead and also acted as part of the annular diffuser for the ramjet engine. Interferometer antennas were placed on the lip of the diffuser inlet. The outer annular region of the forward compartment contained the electronic hardware for the guidance system, behind which were compartments containing the hydraulic power supply and wing control actuators for missile control, batteries for electronic power, and fuel pump and flow regulators for the propulsion system. An 85 gallon fuel tank holding JP-5 or dimer fuel completely encircled the missile and was part of the airframe. Missile speed was regulated by control of the fuel flow.

The electronic equipment was packaged in modules and designed to facilitate checkout and repair. Modules were physically and functionally interchangeable to permit replacement in the event of equipment failure. Interchangeable wings and fins were provided that could quickly be attached to or removed from the missile and booster assembly.

A summary of overall weights and dimensions is given in Table 1.

The missile had four independently movable wings that provided for roll control and steering maneuvers. They were angularly positioned by hydraulically powered actuators through differential-current servo valves. Attitude and roll stabilization were maintained during boost by wing control, assisted by the booster fins. In the midcourse and homing phases, the control system combined outputs from motion-sensing elements with outputs from the missile guidance receiver to provide error signals to steer the missile.

The missile was launched at elevation angles from 25 to 55° (Fig. 2). It was boosted to nominal flight speeds of over 2000 feet per second by a solid-fuel

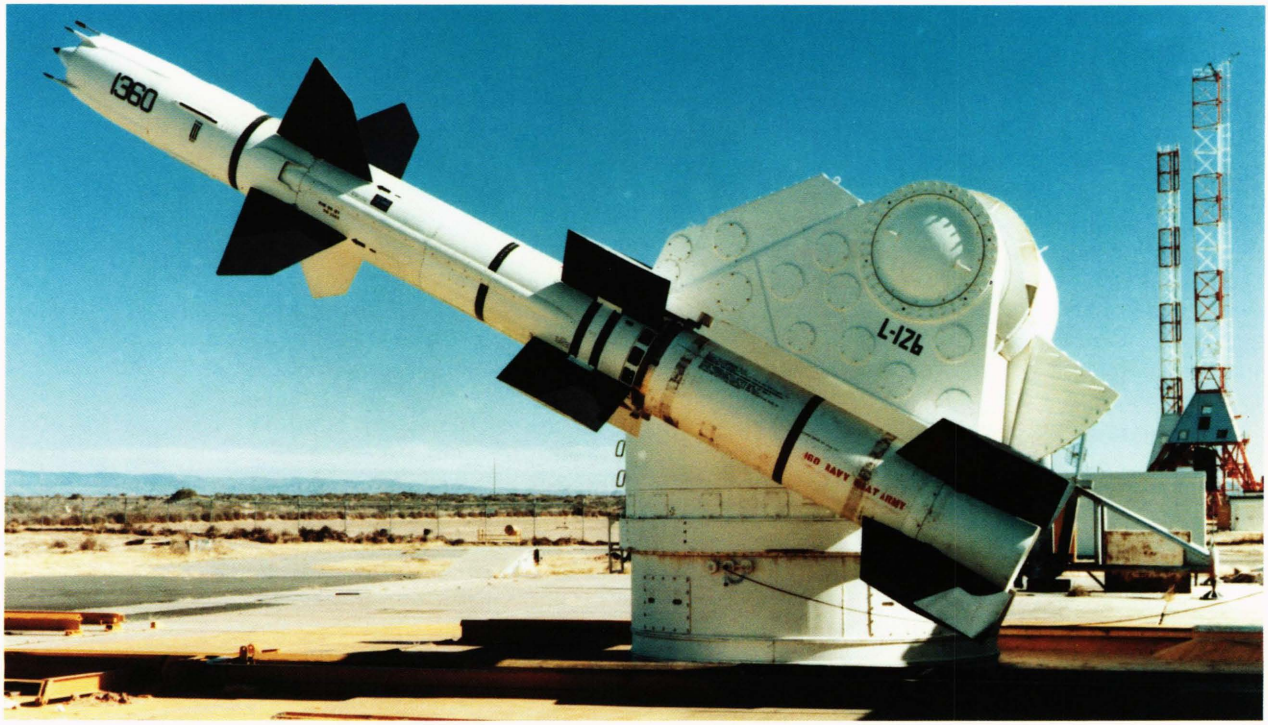

Figure 1 — The Unified Talos is shown in the missile-booster configuration, mounted on the *Desert Ship* launcher at White Sands Missile Range in 1972. This missile could employ either a conventional or a nuclear warhead. Guidance and control modules were physically and functionally interchangeable. The missile was designated RIM-8E. Improved versions of the missile, RIM-8G, RGM-8H, and RIM-8J, were made by substitution of modules.

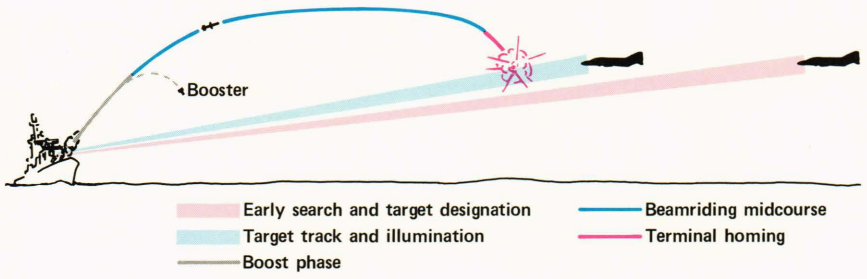

Figure 2 — The operational concept was to launch at elevation angles from 25 to 55°. After the boost phase, the booster rocket was automatically separated from the missile and the ramjet engine was ignited. The missile was then controlled by midcourse beamriding. Near the end of the midcourse phase, the missile was sent a signal that activated the semiactive homing system and armed the warhead.

Table 1 — Unified Talos weights and dimensions.

	Missile	*Booster*
Weight (pounds)	3360	4360
Dimensions (inches)		
Length	254	132
Body diameter	28	30
Wingspan	110	—
Tailspan	82	72

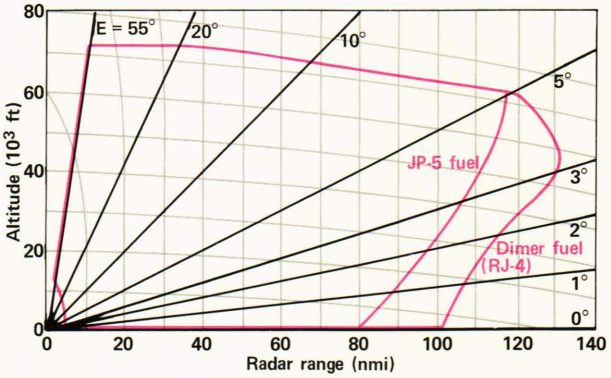

Figure 3 — Kinematic performance envelope for the Unified Talos. The long-range boundaries are determined by fuel exhaustion. The short-range boundary is determined by the time required for boost and 6 seconds of homing. The close-in high-altitude boundary is limited by the maximum climbout angle of 55°.

booster rocket that provided approximately 590,000 pound-seconds impulse for 5 to 6 seconds. After boost, the rocket booster was automatically separated from the missile, the ramjet engine was ignited, and the midcourse flight phase was initiated.

A beamriding system was used during the midcourse phase to steer the missile to a predicted intercept. Near the end of the midcourse flight phase, the missile received a signal that activated the homing system and armed the warhead.

A semiactive continuous-wave interferometer homing system was employed during the terminal phase. Rapid acquisition of the desired target Doppler signal was achieved by a ground-aided acquisition signal derived from the fire control and guidance radars and transmitted via the illuminator beam. The semiactive homing system provided reliable guidance in the presence of sea or land clutter and homed on a jammer at target illumination frequencies in lieu of a target Doppler signal.

An active target-detecting device (proximity fuze) initiated a firing pulse when the missile was within lethal range. Optimum timing of the warhead detonation was calculated using data supplied by the missile homing system.

The intercept envelope was primarily a function of target size, speed, crossing angle, and altitude. The maximum missile-intercept envelope occurred for directly incoming targets (Fig. 3). For small targets at long range, the Talos missile intercept ranges extended beyond the detection capabilities of the ship's radar system.

A fire control channel could engage only one target at a time but could fire a single missile or a two-missile salvo every 46 seconds. That firing rate was considered adequate for long-range targets if short-range targets were covered by other missiles with a higher engagement-rate capability.

Talos had an impressive antiship capability. Its kinetic energy alone extensively damaged any ship it struck, even though there was no warhead. The missile was launched in an antiair mode at a high angle and was programmed to approach the target at a high dive angle. Maximum range capability for that antiship mode depended on the ability of the fire control radar to track and illuminate the surface target.

A surface mode was available for engaging large surface or shore targets. It was designed for firing beamriding missiles on a trajectory that was optimized for a nuclear warhead with command fuzing. The maximum engagement range for a surface target was limited by the guidance radar horizon and the desired altitude of the air burst. Shore targets at distances up to 40 nautical miles were engageable. Flight accuracy when operating against shore targets depended on target position data, set and drift of the ship, ship heading and speed, and ship location. Data on both ship and target position had to be entered into the fire control system by special data transmitters. Several methods were developed for entering those data into the weapon system.

Table 2 — Talos missiles built and flown.

Missile Configuration	*Missile Firings*		*Missiles Built*
	WSMR	*Fleet*	
First Tactical Talos	137	40	229
First Tactical Talos W	60	12	111
Extended Range Talos	57	164	234
Extended Range Talos W	32	56	101
Unified Talos	176	615	1729
Total	462	887	2404

The Talos antiradiation mode made it possible to destroy shore target by homing on radar radiation. Target radiation characteristics, such as frequency and pulse rate, had to be known within certain tolerances to permit target discrimination. Two separate configurations of the homing receiver were required to cover the desired frequency bands. The missile flew a high-altitude trajectory with a maximum range of 120 nautical miles.

A summary of the number of Talos missiles built and flown (not including missiles flown as supersonic targets) is shown in Table 2. The period covers 1955 through 1978, the last record of a Talos flight. The success rate for the missile was greater than 80%. The success rate of the entire system was about 40%.

WILLIAM B. SHIPPEN, WALTER G. BERL, WILLIAM GARTEN, JR., and
EVERETT J. HARDGRAVE, JR.

THE TALOS PROPULSION SYSTEM

Development of the ramjet engine for Talos required the solution of many new engineering problems, including maintenance of stable engine operation at high as well as low altitudes; assurance of engine durability during long periods of high-temperature operation; maintenance of stable and efficient intake performance; and provision of a fuel system that would store, pump, distribute, and control the fuel rate.

In January 1945, APL was authorized by the Navy Bureau of Ordnance to commence basic and applied research in support of the development of a guided missile. Until that time, no ramjet-powered flights were known to have taken place, even though the basic idea for the ramjet had been enunciated by René Lorin of France as early as 1913. Intelligence reports of German activities during World War II, and captured documents as well, showed that ramjet engines had been developed for subsonic and supersonic flights, but no applications were made.

The ramjet engine is similar in principle to the turbojet but relies completely on its forward velocity to supply high-pressure air for the combustion chamber. It is not self-starting and requires a rocket booster for acceleration to the minimum operable flight velocity at which it develops sufficient thrust to maintain flight speed or accelerate further. The major components of the ramjet (Fig. 1) are: (a) an air inlet, designed to capture the desired amount of air at supersonic speeds and convert its dynamic pressure to a high static pressure at low velocity for subsonic combustion; (b) a fuel system that provides and controls the fuel flow; (c) a combustion chamber, where heat is added by burning the fuel; and (d) an exit nozzle, where the heated products of combustion are increased in velocity and expanded to ambient pressure.

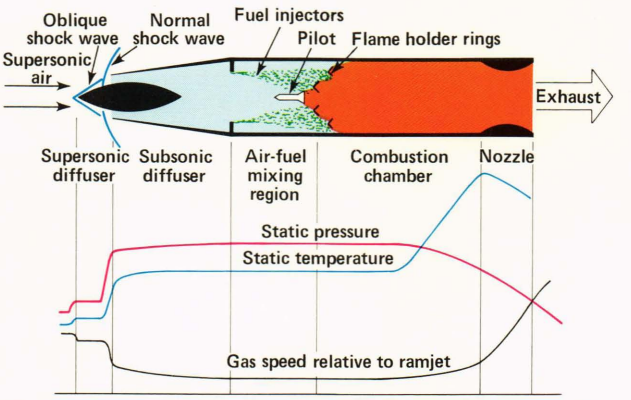

Figure 1 — The ramjet principle is based on increasing the momentum of air passing through the engine. Air enters through a multiple-shock inlet and is converted from supersonic flow at ambient static pressure to subsonic flow at high static pressure. Fuel is mixed with the air, ignited by a pilot flame, and burned in a combustion zone stabilized by flameholders. Energy added to the gases by combustion produces an increase in the momentum of the exhaust. The exhaust momentum and pressure are in equilibrium with internal pressures in the ramjet. Thrust is produced by the vector sum of the forces resulting from pressures on the internal parts of the ramjet.

EARLY HISTORY OF RAMJET DEVELOPMENT

At the start of the program, it was essential to provide laboratory facilities in which ramjets of various sizes could be tested under conditions simulating those expected in flight. Construction of a facility for testing 6-inch-diameter ramjets at the APL Forest Grove Station in Silver Spring, Md., began in February 1945. Plans were made for construction of a full-scale ramjet test facility and supersonic wind tunnel to be located adjacent to the Lone Star Steel Company at Daingerfield, Tex., where large-capacity, high-pressure air blowers were available. The Consolidated Vultee Aircraft Company (CVAC) accepted an associate contract to build and operate this facility, which was later named the Ordnance Aerophysics Laboratory (OAL). Construction of OAL began in June 1945 and was completed in November 1946; testing was initiated in August 1945.

To provide an early indication of the feasibility of ramjet propulsion, a flight test program was started at Island Beach, N.J., utilizing a cluster of high-velocity aircraft rockets (HVAR Model 38) to accelerate 6-inch-diameter ramjet test vehicles to supersonic speed. The first flight tests were conducted on February 16, 1945, to provide data on supersonic drag and to test telemetering performance. The first unambiguous demonstration of ramjet thrust at supersonic speed occurred on June 13, 1945, using carbon disulfide as fuel, less than six months after initiation of the Bumblebee project. The first test demonstrating thrust in excess of drag at supersonic speed occurred in October 1945, using heptane as fuel (Fig. 2). This test vehicle design was modified in early 1946 by in-

THE SUNDAY SUN

BALTIMORE, SUNDAY, JUNE 9, 1946

THE BUMBLEBEE—Here is a model of the Navy's new ram jet engine called "The Bumblebee," taking off from a launching platform (bottom photo). The model in flight (upper photo) is capable of supersonic speeds up to 1,500 miles per hour at high altitudes.

Navy Reveals Supersonic Engine Exceeding 1,400 Miles An Hour

Ram Jet Weighs Only 70 Pounds Has No Moving Parts And Develops 2,000 Horsepower

By WILLIAM J. PERKINSON
[*Sun Staff Correspondent*]

Washington, June 8—The Navy's newest supersonic engine—The Bumblebee—which has hurtled through the air at speeds greater than 1,400 miles per hour was disclosed to the public tonight.

Developing more than 2,000 horsepower, the engine contains no moving parts, and weighs but 70 pounds. Conventional engines capable of producing that much power now weigh more than 2,000 pounds.

The ram jet engine, also known as the "Flying Stovepipe," which has been successfully flown a number of times, is described by the Navy Department as "neither a rocket, missile nor airplane, but simply a vehicle to get through the air at the speed of sound."

Launching Device Secret

Since the ram jet operates inefficiently at low speeds, there must be some way used to bring it up to high speeds. This is done by the use of catapults or rockets. After launching, the engine moves under its own power. Details of the Navy's launching device are still covered by the secrecy of the classified list.

The 600 scientists who are connected with the Bumblebee project faced the same problems as other scientists and engineers trying to perfect an engine capable of driving a plane or missle at supersonic speeds.

The problem is this:

Up to speeds approaching that of sound (743 miles per hour at sea level) scientists do not have to worry about the compressibility of air.

Air behaves like a liquid, thus as in a canoe if you wish to go faster you have to paddle faster and use more energy. But in airplanes and guided missiles, this energy comes from a power plant. The more energy a power plant developed the heavier it had to be.

Builds Up To Barrier

At the speed of sound this compressibility of the air builds up rapidly until it becomes a barrier that is extremely hard to penetrate. More power is needed, and before the advent of the jet engines with their high output for low weight, the problem seemed insurmountable.

Once on the other side of the barrier, in the realm of supersonic speeds, the resistance of the air to passage through it again decreases.

Yet within six months after the problem of producing a supersonic engine was turned over to the Hopkins scientists, the laboratory had successfully flown its first ram jet engine.

Looks Like Stovepipe

"The ram jet looks very much like a stovepipe," Dr. Richard B. Roberts, director of Project Bumblebee disclosed, with openings at both ends.

"It will not operate at speeds below 300 to 500 miles per hour, so we developed a special launching device to get the engine to that speed," he added.

As the engine hurtles through the air, air is scooped into a cone-shaped narrow front opening and compressed by the speed of the jet. This forward portion of the pipe is known as the diffuser. Approximately one third of the length of the pipe is used for diffusing the air, which is mixed with fuel from two injectors.

Wall Of Flame

To the rear of the diffuser is a combustion chamber where a wall of flame increases the momentum of the air as it expands in the diffuser.

This flame front also produces a back pressure which is exerted on the walls of the conical shaped diffuser. The forward thrust of the air on the diffuser's inner walls is what makes the jet engine go. The reaction to this forward thrust is flaming exhaust gases, whose temperatures are above 1,000 degrees Fahrenheit.

Even after it was determined in just what proportion the flame front, fuel inlets and diffusers were to be spaced, other problems arose.

There was the need to record data obtained by actual experiments, and the need to obtain a testing ground.

Must Be Tested In Motion

The ram jets cannot be tested statically, that is on the ground. They must be moved through the air, either in free flight or in a wind tunnel.

But there wasn't time to construct the supersonic wind tunnels necessary. It was decided to test the missiles in flight off Island Beach, N.

At the time the tests were started there was only one supersonic wind tunnel in the country; that was located at Aberdeen Proving Ground. (The Germans are reported to have had 30 such supersonic tunnels.)

The ram jet was first launched "cold"; that is, without the use of its fuel. This was necessary so that scientists could determine the flight characteristics of the engine's carrier. Later the engine was fired, using its own power.

Small Instruments Needed

Since the ram-jet engines being tested were extremely small, it was necessary to develop new means of telemetering information back to the ground. Telemetering is a method by which such data as pressure, temperatures, fuel flows and altitude can be broadcast back to field equipment at the test site.

It was necessary to develop equipment so small and compact that a four-channel radio system, complete with power supplies, measuring instruments and broadcasting equipment, could be contained in a space only slightly larger than a man's two hands.

Here the laboratories' prior work on the proximity fuse, and its close connections with other universities and industrialists paid off.

"Without the components developed for the proximity fuse, the job of relaying the data back to the ground for analysis could not be done," Dr. Roberts said.

Figure 2 — *The Sunday Sun* of Baltimore, reported on June 9, 1946, the development of a supersonic ramjet engine. © 1946, *The Baltimore Sun*. Photo courtesy of World Wide Photos.

creasing the diameter of the forward section to 8.5 inches in order to provide additional packaging space for fuel, fuel metering equipment, instrumentation, and telemetering, as well as to increase the drag to make the unit less likely to accelerate to destruction when operated with fuel-rich fuel-air mixtures. This unit, Model 3B, was named Cobra because of the enlarged front end (Fig. 3).

In late 1945, representatives of Curtiss-Wright, CVAC, and APL met to plan an 18-inch-diameter prototype missile called the Ramjet Test Vehicle (RTV). This RTV was built by the Cornell Aeronautical Laboratory and was first tested at OAL in December 1945. It was designed to carry guidance equipment and a warhead but was unable to withstand the structural stresses of a ground test in a free jet. The only flight test of an RTV used kerosene fuel and produced a maximum acceleration of 2.5 g and a maximum velocity of 2200 feet per second. Further tests of 18-inch-diameter engines were conducted using a similar unit, called the Burner Test Vehicle (BTV), in which the guidance and warhead weight allowance was relocated in a stronger structure.

With the demise of the RTV as a prototype, a larger unit, called the Experimental Prototype Missile (XPM), was designed in late 1946, with a body diameter of 28 inches and a combustion chamber diameter of 24 inches (Fig. 4). The first XPM propulsion test vehicle was flown in March 1949 at the Naval Ordnance Test Station, China Lake, Calif. The predicted thrust was produced, but the engine was extinguished after 7 seconds of operation because improper fuel control caused an excessively fuel-rich mixture. Later flight tests were successful.

The ramjet engine designs, from the 6-inch Model 3B up to the 24-inch XPM, were all basically similar. They had "normal-shock" air inlets that were simple in design and not prone to producing pressure oscillations when the heat release of the combustion chamber or the presence of a tandem booster prevented maximum capture of the inlet air stream. The fuel injectors were simple tubes. The flameholders were combinations of blunt baffles to provide sheltered burning zones and interconnecting "gutters" to spread flame from the more sheltered piloting zones to the main fuel-air stream (Fig. 5). Fuel control progressed from constant fuel flow devices to more sophisticated ones, culminating in the XPM fuel control that throttled the fuel flow within the allowable combustion limits to provide constant-Mach-number flight.

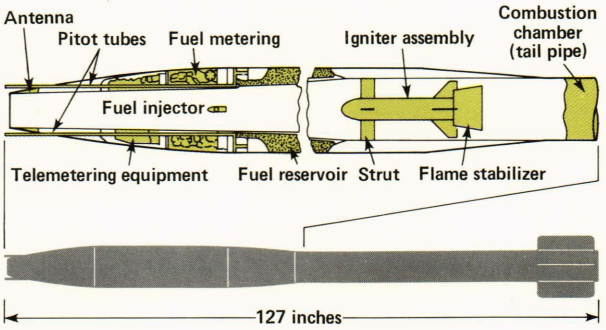

Figure 3 — Cobra ramjet (Model 3B) was the first of a series of test vehicles. Ram pressure was employed to force the fuel out of a flexible neoprene bag into the air duct near the diffuser intake where static pressure was low. The fuel rate was determined by the pressure differential that occurred across a fixed orifice. Ignition of the fuel mixture was by a pyrotechnic flare that burned throughout flight. The tailpipe was made from a stainless steel exhaust pipe from a fighter aircraft. Although the Cobra weighed only 70 pounds, it developed between 2000 and 3000 horsepower — as much as a big bomber engine.

THE TALOS COMBUSTION CHAMBER

High-Altitude Performance

The major problem with early Bumblebee ramjet engines was their inability to provide stable, efficient combustion for long periods at an altitude of 60,000 feet and an airspeed of 2000 feet per second. At these conditions, the combustion chamber had to operate at a pressure of one third atmosphere and at an inlet air temperature of 200°F. To meet this goal, CVAC had initiated tests of a "can"-type flameholder, based on turbojet technology. This development led to a completely different type of flameholding system (Fig. 6) that offered a solution for satisfactory operation at high altitude. Low- and high-altitude tests were conducted on this design in the summer of 1950. The development was successful, and all Talos combustion chambers used this general configuration. The design was unique in its ability to burn efficiently at low air temperatures and pressures. Combustion efficiencies (the ratio of theoretical to actual fuel flow for a given heat release) met or exceeded the ini-

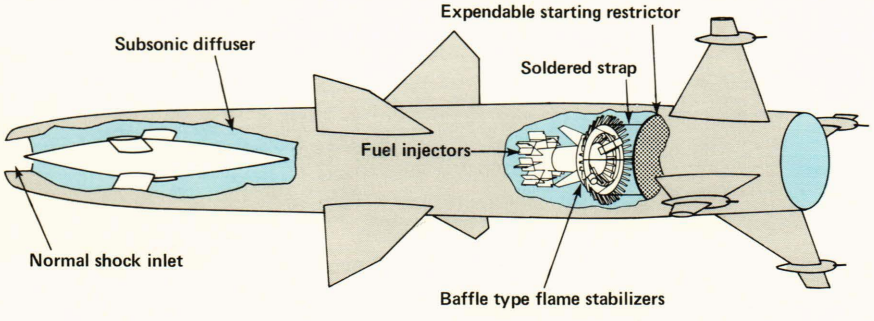

Figure 4 — The XPM ramjet engine required a starting restrictor to permit ignition. This starting restrictor was attached within the combustion chamber with soldered straps to block the duct partially and reduce the flow velocity. On ignition, the solder melted gradually and the restrictor was blown out of the exit.

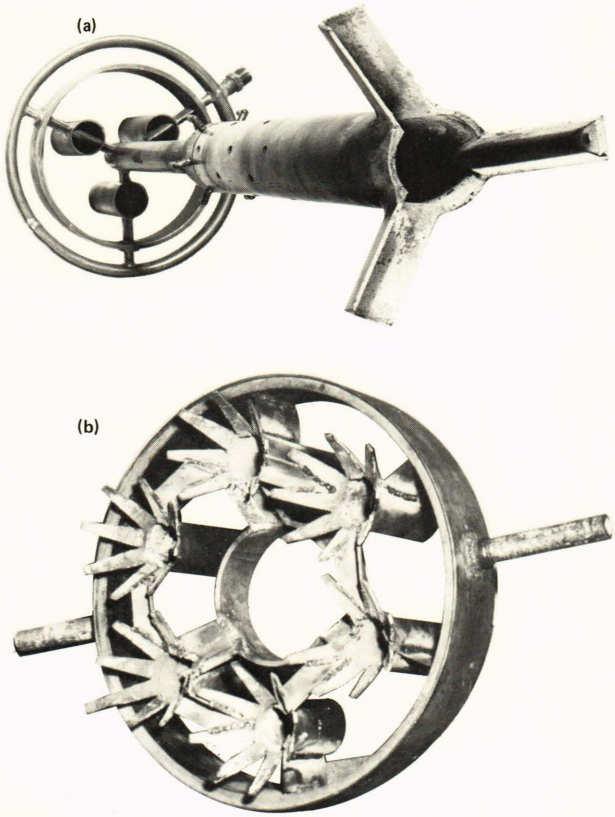

Figure 5 — Flameholder hardware for ramjets in 1946 were combinations of blunt baffles to provide sheltered burning zones and interconnecting gutters to spread flame from sheltered piloting zones to the main fuel-air stream. View (a) shows the fuel injector and radial gutter developed for a 6-inch ramjet. View (b) shows a piloted rake for an 18-inch combustor. The central ring fits into a pilot cone and connects the pilot to the rakes by radial gutters.

tially desired values. This combustion chamber design was frozen on June 1, 1951.

Combustion Chamber and Tailpipe Durability

An ensuing development problem of this combustion chamber design was to improve durability — the ability to maintain the integrity of the sheet metal "can" structure needed for flame stabilization. This problem is placed in perspective when one considers that stoichiometric burning will produce gases at about 3500°F and the melting point of stainless steel is no higher than 2800°F. The solution consisted of providing carefully controlled coatings of zirconia on all surfaces exposed to hot gases to prevent oxidation and to interpose cooling air between the hot combustion products and the metal structures. Persistent burnthrough was located at the intersection of the pilot can and the cooling shroud, where fuel tended to collect in the dead zone. The solution was to operate the pilot as fuel-rich as possible to provide enough fuel in the dead zone for fuel cooling in a local atmosphere too rich to burn. Another durability problem was caused by flow wakes behind fuel system components, which resulted in local reduction of airflow into the cooling shroud and hence degradation of wall cooling. This problem was solved by the installation of small airfoil sections, termed turbulators, to reenergize the boundary layer and the wake. The last of the durability problems was revealed by the first two low-angle shipboard firings of the higher speed Unified Talos (SAM-N-6c1). Both missiles failed because of burnthrough of the combustion chamber wall. The solution was found in increasing metal and zirconia thicknesses, but with a penalty of added weight.

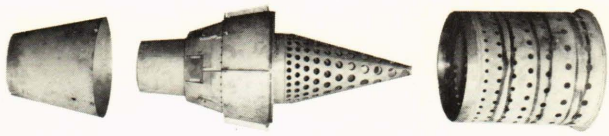

Figure 6 — The can-type flameholder operated with good efficiency at both high and low altitudes. A fuel-air mixture flows through holes in the can wall, and recirculation zones are established behind the holes to act as flame-stabilizing elements.

Combustion Efficiency

A major improvement in combustion efficiency was made for the higher speed and longer range missiles. The higher speed made it possible to reduce the exit nozzle throat diameter and thereby reduce the air velocity within the engine. Six inches were added to the combustion chamber length to improve combustion efficiency for high-altitude cruise. Combustor pressure losses were reduced somewhat by minor redistribution of airflow within the combustion chamber and careful attention to the angle and concentricity of the flow dividers at the combustion chamber entrance.

THE INLET

The function of a ramjet air inlet is to capture the desired airflow and reduce the air velocity from supersonic speeds to values acceptable to the combustion system with the highest practical pressure recovery. Fundamental studies by Oswatitsch in Germany and Kantrowitz and Donaldson in the United States demonstrated both analytically and experimentally what variations of pressure recovery could be expected in supersonic flow, as a function of Mach number, for single shock and multiple external conical shock air inlets. This established the fundamental design requirements for subsequent supersonic diffuser development.

For external multiple shock inlets, the compression is a three-stage process. In the first stage, the airspeed is decelerated to a reduced Mach number in passing through one or more conical shock waves. The second stage is the compression through a normal shock wave near the intake lip to produce subsonic flow. The third stage is the subsonic diffusion of air to produce high pressure at the combustion chamber.

All Talos engines were designed to operate subcritically, that is, at less than maximum air capture (Fig. 7) when the pressure within the combustion chamber

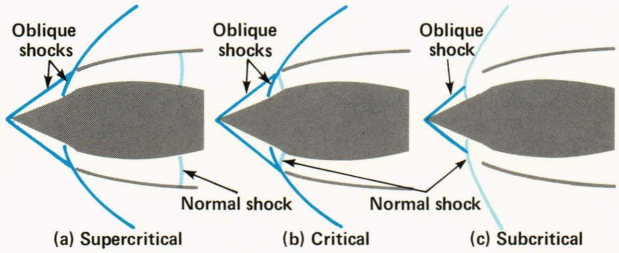

Figure 7 — Modes of diffuser operation are supercritical, critical, and subcritical. (a) Supercritical operation results when the normal shock is downstream from the cowl lip. It occurs at lean fuel/air mixtures. (b) Critical operation occurs when the normal shock is near the cowl lip. This takes place at an intermediate fuel/air mixture and is the most efficient operating point. (c) Subcritical operation results when the normal shock is ahead of the cowl lip. This occurs at rich fuel/air mixtures.

was high, providing maximum engine thrust. Operation in the subcritical regime tends toward instability of the overall diffuser-combustor system, permitting pressure oscillations that cause reduced thrust, missile structure vibration, and extinction of the combustion when operating near the combustion stability limit. Much of the inlet development effort was devoted to establishing the limits of acceptable subcritical operation by wind tunnel tests and overall engine free-jet tests.

Three air inlet designs were implemented before the Unified Talos configuration was established. The initial air inlet for the prototype Talos was a single-cone design, based on National Advisory Committee for Aeronautics (NACA) data that produced significantly better pressure recovery than did a normal shock inlet. During 1953, the entire ramjet system was redesigned for the first tactical missile. The cone angle of the inlet was increased to provide higher supersonic compression. These changes permitted an increase in inlet capture area from 205 to 235 square inches and a decrease in exit nozzle throat size from 70 to 65% of the body area, resulting in an increase in thrust capability. The "W" versions (nuclear warhead capability) of Talos had identical inlet cone shapes forward of the cowl lip but a slightly reduced capture area to compensate for the additional internal pressure loss in the annulus surrounding the larger inner body. In the latter part of 1953, another inlet redesign was needed to accommodate higher operating Mach numbers. A double-cone external compression surface was selected, with a forward cone half-angle of 25° and a second half-angle of 35°. This higher compression angle, combined with higher flight Mach numbers, resulted in a maximum inlet capture area of 360 square inches. The exit nozzle throat size was kept at 65% of the body area.

FUEL SELECTION CRITERIA

Selection of a suitable fuel for a prescribed flight envelope of missile speed and altitude for the ramjet engine depends on optimizing three criteria: (a) the fuel should have favorable thermochemical performance characteristics, expressible in terms of fuel specific impulse; (b) its rates of reaction with air should be such that an uncomplicated combustion chamber can be designed that will provide high combustion efficiency; and (c) fuel handling characteristics and costs should be within reasonable bounds. What weight is to be placed on each criterion depends on the specific engine performance to be achieved. For example, flight range is a very sensitive function of combustion efficiency and favorable thermochemical characteristics of the fuel. If long flight range is desired, criteria (a) and (b) need to be maximized.

The Talos system was designed to begin self-sustained operation at the termination of the solid rocket boost phase and to accelerate to Mach 2.5 during climb to cruise altitude. Long range was to be achieved by flying at altitudes of approximately 60,000 feet. These flight conditions of speed and altitude fixed the temperature/pressure regime for the combustion chamber in which fuel was to be injected, ignited, and burned. The thrust-producing temperature changes in the working fluid were achieved by varying the concentration of fuel in the air streams. At the start of the Talos development program, fuels were selected in which the reaction rate criterion (b) was emphasized at the expense of high thermochemical performance. Proof of principle was achieved with carbon disulfide and propylene oxide, both substantially more reactive than fuels based on carbon and hydrogen (hydrocarbons) alone.

As experience with the design of effective fuel injectors and flame stabilization devices grew, it became possible to turn to hydrocarbon-based fuels that would satisfy criteria (a) and (b) and also meet the operational requirements of reasonable cost and safe handling. By and large, hydrocarbon fuels rank high in all three of the fuel-selection criteria and have, therefore, been used as the preferred fuels. Only boron hydrides (in which boron acts as the hydrogen "carrier") offer substantial improvements in both criteria (a) and (b), with some reduction in criterion (c).

Table 1 summarizes the suitability of fuels that were investigated in the course of the Talos development. Some sulfur- and oxygen-containing fuels offer benefits of ease of ignition and rapid flame propagation but at the expense of thrust per unit weight of fuel. Boron hydrides provide superior kinetic performance and high fuel specific impulses but at the expense of cost and ease of handling. Saturated aliphatic or aromatic hydrocarbons, while somewhat deficient in reactivity, nevertheless perform well when extreme flight ranges are not of vital importance.

As military specifications were developed for jet engine fuels, JP-5 was selected for use in the early production Talos. The value of higher density fuels in providing additional range capability was recognized early in the engine development program, and tests with tetralin were conducted at OAL. A less expensive high-density fuel was methylcyclopentadiene

Table 1 — Suitability of fuels in Talos ramjet engines.

	S_a	S_f	$S_{f,d}$	*Kinetics*	*Toxicity*	*Storage*	*Thermal Stability*	*Viscosity*	*Cost*
Carbon disulfide	P	P	P	E	F	G	G	G	G
Kerosene	G	G	F	F	E	E	E	G	E
Propylene oxide	F	F	F	G	G	F	F	G	F
Methylcyclopentadiene dimer	G	G	G	F	G	F	F	G	F
Kerosene-boron slurries	G	E	G	F	E	F	E	P	F
Methylacetylene	E	G	F	E	G	F	F	G	F
Boron hydrides	E	E	E	E	P	F	P	G	P

P = Poor
F = Fair
G = Good
E = Excellent

S_a = air specific impulse (stream thrust at sonic velocity divided by air mass flow)
S_f = fuel specific impulse (S_a/(fuel/air ratio))
$S_{f,d}$ = density specific impulse ($S_f \times$ density)

dimer, which has 12% higher volumetric heat release than JP-5. The dimer fuel was successfully tested in the first tactical combustor at OAL in 1955. In 1964, when additional range was desired for the Unified Talos, the use of that fuel was reconsidered. However, its storage stability characteristics were unsatisfactory because, as an unsaturated hydrocarbon, it tended to polymerize with time. A program was completed to hydrogenate the dimer to form a stable saturated compound. This fuel was used after 1966.

THE FUEL SYSTEM

The Talos fuel system provided fuel to the combustion chamber to maintain stable combustion and to control engine thrust. For maximum stability of operation, the pilot required fuel at a rate that provided an approximately constant and optimum fuel-to-air ratio. For the main combustor, the fuel rate was varied from zero to a maximum near the overall stoichiometric fuel-to-air ratio to provide the required thrust. Fuel systems for the prototype and First Tactical Talos controlled the fuel flow to maintain constant speed. Since the temperature-sensing units used to control velocity were prone to malfunction, the fuel systems for Extended Range Talos and Unified Talos were designed to control Mach number as a function of altitude.

The fuel controls operated from sea level to 70,000 feet altitude, representing a 17:1 variation in airflow through the engine. They also had to provide fuel for engine ignition within a few tenths of seconds after missile separation from the rocket booster. Fuel had to be injected into the air stream to provide local air-to-fuel ratios that were within the burning limits of the fuel. Other considerations for fuel system design included: (a) high flight accelerations (about 15 g longitudinally during boost and up to about 15 g laterally in flight); (b) accelerations when missile roll-control was established; (c) low combustion chamber pressure at high altitude; (d) vibration and heating during flight; and (e) sudden variations in pressure and airflow at the time of rocket booster separation. Small volume and weight, compatibility with the annular packaging space of the missile, long storage life, reliability, and low cost were additional design considerations.

Figure 8 shows the main elements of the Talos fuel system. The outlet of the annular fuel tank was sealed by a valve controlled by nitrogen pressure. Stored under pressure, nitrogen was released by a valve that was opened by acceleration during boost, pressurizing the fuel bladders inside the fuel tank and opening the fuel tank valve. Fuel flow from the tank was maintained during periods of high missile acceleration by channels within the tank formed of perforated sheet-metal segments. The bladder material had to withstand the stresses generated by fuel motion and the heating by the hot walls of the central air duct.

A centrifugal pump driven by an air turbine was the chief means of moving the fuel to the fuel nozzles. High-pressure air bled from the central air duct provided a suitable energy source for the air turbine. Fuel pump inlet pressure was provided by the nitrogen pressurization.

Separate regulators were used for the pilot and main fuel. A probe ahead of the engine inlet provided freestream pitot and static pressure measurements for the fuel system. These pressures were used to measure flight Mach number, altitude, and engine airflow. The fuel regulators were required to control fuel flow rates over a range of about 20:1 for the pilot burner and more than 100:1 for the main burner.

Main and pilot fuel entered the combustion chamber in concentric pipes. In either case, the fuel was

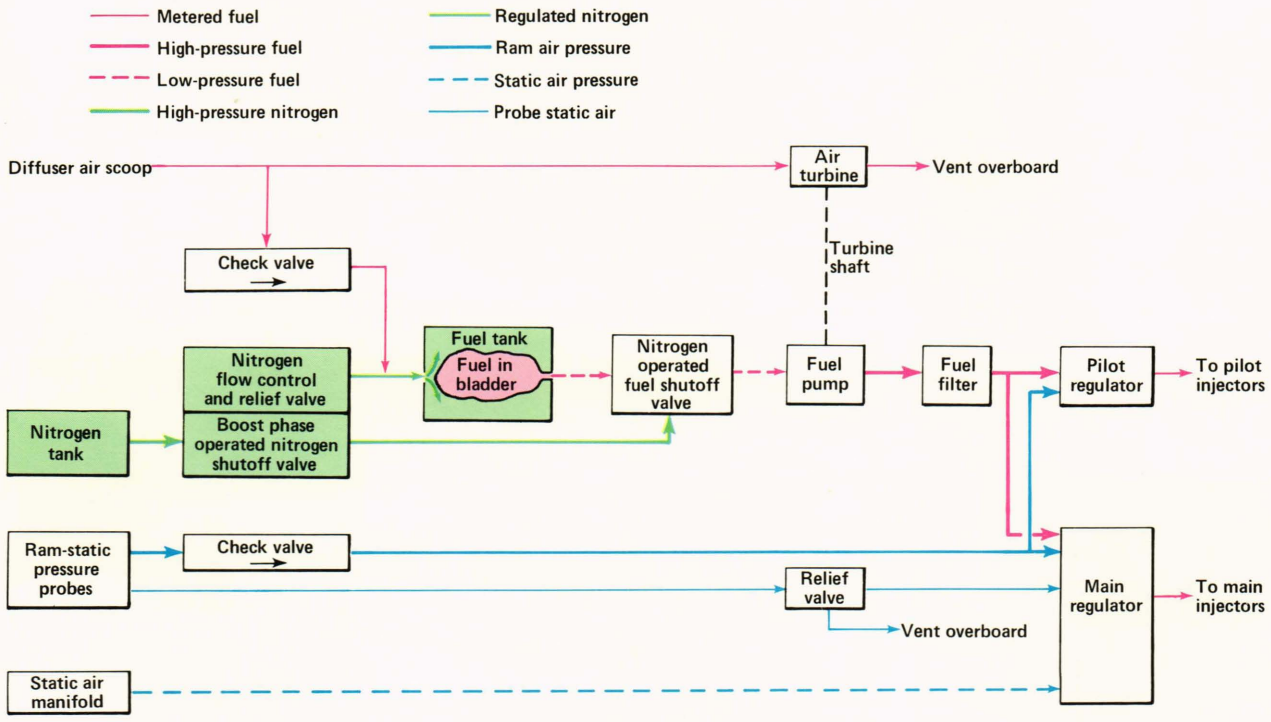

Figure 8 — The Talos ramjet fuel system maintained stable combustion and controlled engine thrust. The fuel tank was normally pressurized with nitrogen, but diffuser pressure was also available as backup. A centrifugal pump driven by an air turbine provided high-pressure fuel to the pilot and main fuel regulators. Ram and static air pressures were used to regulate the fuel flow. The regulator compartment was vented to the atmosphere through louvers and was employed as an atmospheric sump for the regulator.

discharged into the air stream through an annular array of nozzles. The injector system maintained proper fuel distribution during high-g lateral maneuvers and sustained proper fuel flow in the presence of variations in air pressure. Nozzles used in the pilot injector had linear pressure-versus-fuel flow characteristics that assured uniform flow distribution to the pilot. The main fuel injectors used spring-loaded, fixed-pressure nozzles and a fuel distribution valve to maintain uniform fuel distribution to the individual nozzles.

THE UNIFIED TALOS RAMJET PROPULSION SYSTEM

No major changes were made to the ramjet design after the Unified Talos configuration was established. This final design provided reliable and adequate propulsion for all flight conditions that fell within the Talos operating envelope.

The supersonic inlet employed double-cone external compression and was designed for best operation for flight Mach numbers ranging from 2.0 to 2.5. The engine operated subcritically at low Mach number but inlet stability was maintained at maximum engine thrust.

The fuel rate was controlled so that the flight Mach number was regulated between 2.0 and 2.5 depending on the ambient static pressure (which is related to altitude). Dimer or JP-5 fuel could be used with minor adjustments to the fuel regulator. The capacity of the fuel system provided a maximum range of 130 nautical miles with dimer and 115 nautical miles with JP-5.

The final Talos combustor is shown in Fig. 9. The combustor was constructed of conical sections and assembled to provide concentric regions where pilot flame and main air-fuel mixtures are combined to provide stable combustion. Holes in the central cone produced vortex wakes of relatively low speeds (less than the spreading speed of the flame), which provided the flameholding action (Fig. 10). Burnout of the combustor was prevented by proper distribution of the air and fuel and by appropriate zirconia coatings. Ramjet ignition was by a spark plug located in the pilot region. The length of the combustion chamber provided adequate time for efficient combustion. A contracting/expanding exit nozzle was employed to reduce air speed in the combustor and to match the combustor with the inlet.

A summary of Talos ramjet propulsion capabilities is given in Fig. 11. Two independent relations are shown: the maximum acceleration due to thrust, and deceleration due to drag. Horizontal flight and properties of the atmosphere for an NACA Standard Atmosphere are assumed. For a given altitude, the difference between the maximum acceleration from

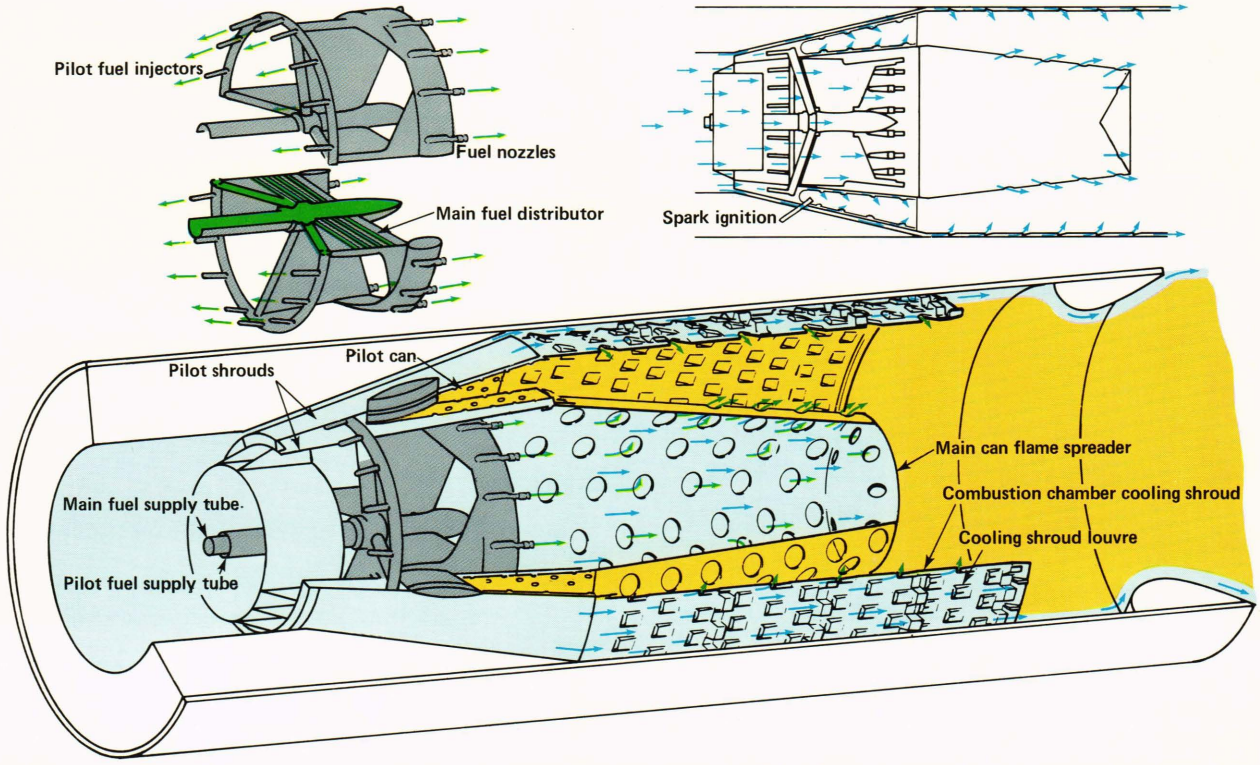

Figure 9 — The Talos combustion chamber design used approximately 20% of the captured inlet air along the outer wall for combustion chamber wall and nozzle cooling. Another 15% of the air passed into a pilot section, where pilot fuel was injected through high-pressure spray nozzles to maintain stable combustion under all conditions of flight. The remainder of the air flowed through the center of the engine to the main flamespreading section, where fuel was injected through low-pressure nozzles and burned to produce the engine thrust. Combustion chamber parts were ceramic-coated to prevent oxidation at high temperatures.

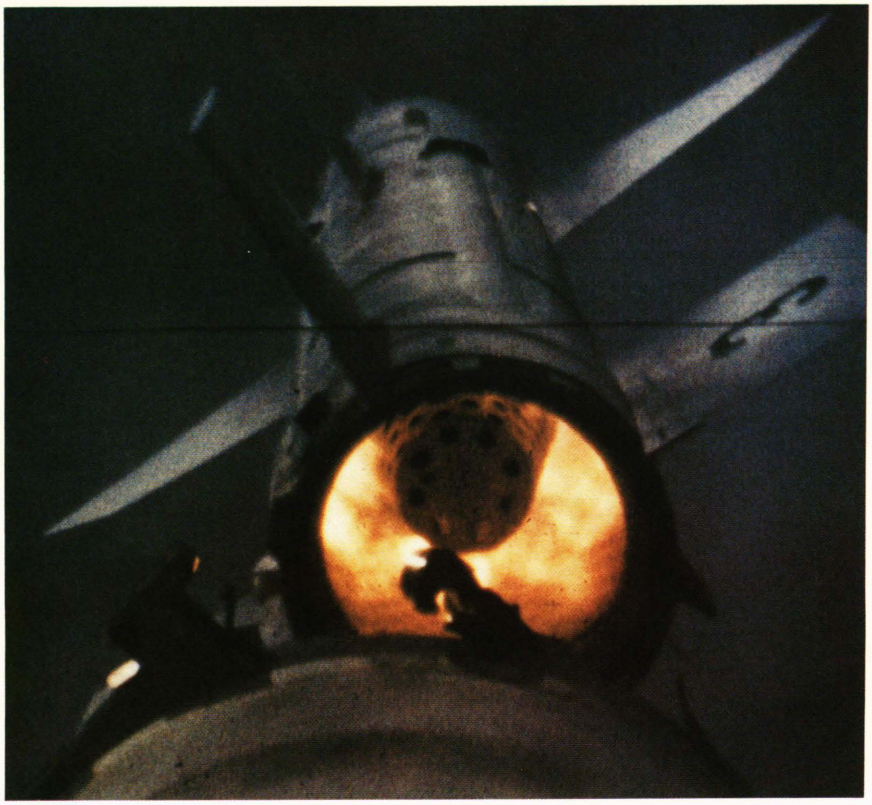

Figure 10 — Flameholding action in the Talos combustion chamber was accomplished by vortex wakes produced by jets from holes in the central cone. Flameholding action during a Talos flight test is shown as viewed from a booster rocket.

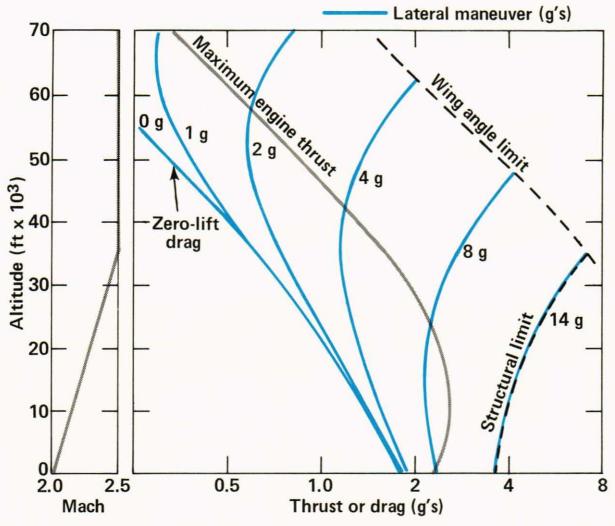

Figure 11 — Unified Talos ramjet engine performance is shown for the Mach number and altitude relation displayed at the left of the figure. Two independent relations are presented in the main figure: (a) maximum acceleration due to thrust, and (b) deceleration due to lateral maneuver. For a given altitude, the difference between relation (a) and relation (b) gives net available acceleration along the flight path. Operating points that occur to the right of the maximum engine thrust line will result in missile slowdown.

engine thrust and deceleration resulting from lateral maneuver gives the net available acceleration along the flight path. Operating points that occur to the right of the maximum engine thrust line will result in missile slowdown.

The characteristics shown in Fig. 11 have been demonstrated by comparison with over a hundred flight tests. The mean error in the thrust-minus-drag coefficient was less than 0.01, and the 1σ scatter about the mean was about 0.01. These errors are equivalent to errors in pressure of about 1% and represent better accuracy than can be found for individual points in ground testing.

RELIABILITY

Almost 1200 missiles using the Talos ramjet engine have been launched. During 25 years of testing, an overall system success rate of 96% was demonstrated. In the ongoing Vandal program that employs the Talos airframe and propulsion system as a supersonic target, an even better reliability of about 98% is being achieved, using propulsion systems that were built about 20 years ago.

WILLIAM C. CAYWOOD, ROBERT M. RIVELLO, and LOUIS B. WECKESSER

TACTICAL MISSILE STRUCTURES AND MATERIALS TECHNOLOGY

Significant advances have occurred in missile structures and materials technology since the late 1940's. Some of the advances were the result of improvements in design concepts and material properties; others were from the development of new materials and fabrication techniques. Rapid strides in computer technology and methods of structural analysis have also played an important role. This article discusses the structural design requirements for the next generation of missiles and reviews the technological advances that will make it possible to meet those requirements.

INTRODUCTION

The Applied Physics Laboratory's experience in tactical missile structural design began with the development of the rocket-powered Terrier and the ramjet-powered Talos in the late 1940's. The airframes for those missiles were designed with conventional aircraft materials, using slide rules, mechanical desk calculators, handbooks, and rule-of-thumb procedures. To ensure adequate safety margins, conservative analytical procedures were pursued, followed by extensive environmental testing. Simple aluminum and steel structures operating at temperatures below 300°F for Terrier and 600°F for Talos made up the major portion of the missiles. Terrier was constructed primarily from machined castings. Talos, shown in Fig. 1 with its central air duct configuration, used sheet metal construction. The early Talos production missiles contained no magnesium, but after alloys capable of withstanding aerodynamic heating temperatures to 600°F and suitable fire- and corrosion-preventive coatings were developed, magnesium was introduced into the primary and secondary structural components of Talos. The remaining structure, except for the aluminum tail fins and forward nonstructural covers, was made from sheet steel.

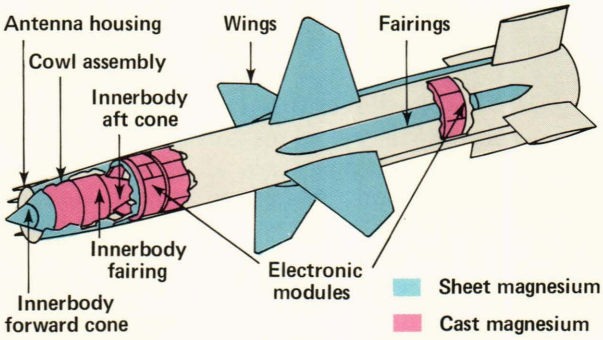

Figure 1 — Magnesium components in Talos represented 13% of the weight of the primary load-carrying structure and 10% of the gross launch weight.

The next major missile airframe development at APL was the Mach 4 Long Range Typhon (Typhon LR) in 1958-1960 (Fig. 2). The airframe was fabricated from superalloys of nickel and cobalt, using lightweight honeycomb and corrugation-stiffened panel construction. As with Talos, the Typhon's external airframe in the region of the combustor was protected from the hot combustion-chamber gases by means of an air-cooled shroud liner system that bypassed a portion of the relatively cool internal duct

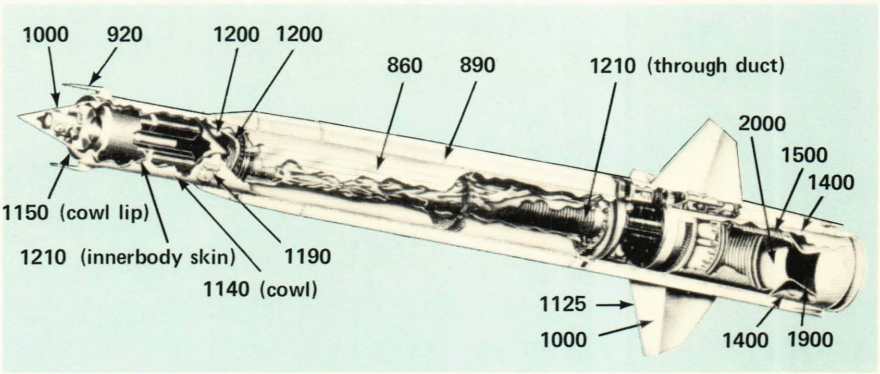

Figure 2 — The maximum temperatures (°F) of the structural components of the Long Range Typhon missile. Temperatures reached 1210°F as a result of aerodynamic heating and 2000°F from ramjet combustion.

air. Also, flame-sprayed zirconium dioxide coatings maintained the combustion-chamber components within acceptable temperature limits. The structural capability of the missile at speeds up to Mach 4.2 and at altitudes of 55,000 to 100,000 feet was demonstrated in successful flight tests at White Sands Proving Ground in 1960-1962. Studies conducted for NASA in 1963[1] indicated that the structure would be capable of operating at Mach 4.5 at high altitudes.

Subsequent advances in ramjet structural design technology have been in exploratory and advanced development programs that have not yet progressed to flight demonstration. However, structural improvements with flight demonstration have been incorporated into the successive upgrades of the rocket-powered Standard Missile. The improvements in the structure of Standard Missile, which provide higher speed, longer range, and higher temperature operating capability, have been achieved primarily by the use of external thermal protection. The Standard Missile-2 ER structural arrangement is illustrated in Fig. 3.

Proposed missile concepts for two classes of airbreathing engines are being examined in exploratory development programs. The first class uses subsonic combustion ramjets with more advanced technology than those of Talos and Typhon LR. The Advanced Surface-to-Air Ramjet (ASAR) shown in Fig. 4 is an example of this class. ASAR has an integral-rocket-ramjet engine in which a single combustion chamber is used for both the solid-rocket boost phase and the liquid-fuel ramjet sustain phase. The second class of engine uses supersonic combustion that extends the operating speed of ramjet missiles to above Mach 5. All of these missile concepts have guidance systems that require forward-viewing radar, infrared sensor windows, or electro-optical sensor windows instead of the interferometer antennas used on Talos and Typhon LR.

DESIGN REQUIREMENTS

Thermal Environment

The maximum speeds of future tactical missiles are expected to move from the supersonic (between Mach 1 and 5) to the hypersonic (Mach > 5) regime. Figure 5 shows the maximum temperatures that will occur in major components of missiles cruising at Mach 5 to 8 at 80,000 feet. Similar data for Mach 4 at

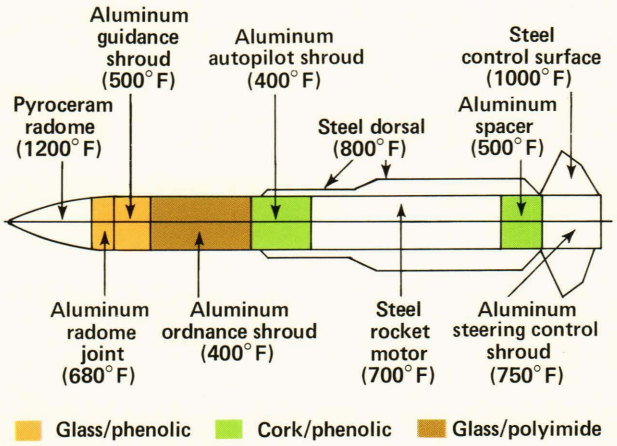

Figure 3 — The structural and thermal protection materials for Standard Missile-2 ER (without booster) and the maximum temperatures to which the structural materials are exposed.

sea level are given in Table 1. The radome, body, and swept leading edge temperatures apply to both rocket and airbreathing missiles, whereas the remaining temperatures are for airbreathing propulsion components.

In the hypersonic regime, a dual combustion ramjet propulsion system (DCR) is more efficient than a subsonic combustion ramjet. The DCR uses a supersonic combustion chamber in tandem with a much smaller subsonic dump combustion chamber that acts as a fuel-rich gas generator and flame holder (see the "Tactical Missile Design Concepts" article in this issue). As shown in Fig. 5 and Table 1, one of the structural advantages of the DCR over the pure subsonic ramjet is that the very high temperatures that

Table 1 — Typical maximum component temperatures (°F) for Mach 4 at sea level.

Radome	1500
Nose tip and unswept leading edges	1550
Swept leading edges	1475-1520
Forebody skin and control surfaces	1460-1480
Aft body skin	1275-1300
Subsonic inlet ducts	1600
Supersonic inlet ducts	1470
Gas generator	4600
Combustor	3660
Nozzle	3500

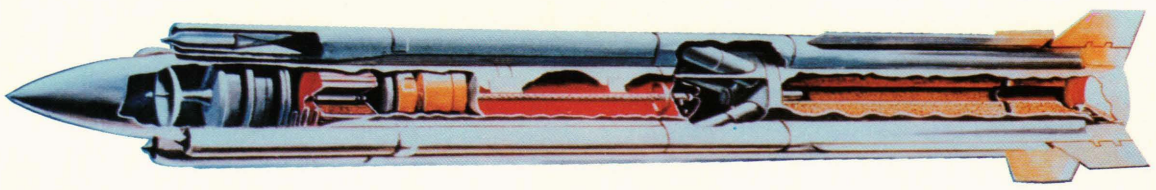

Figure 4 — Typical integral-rocket-ramjet concept. The aft section of the missile serves as both the solid-rocket booster case and the ramjet combustion chamber.

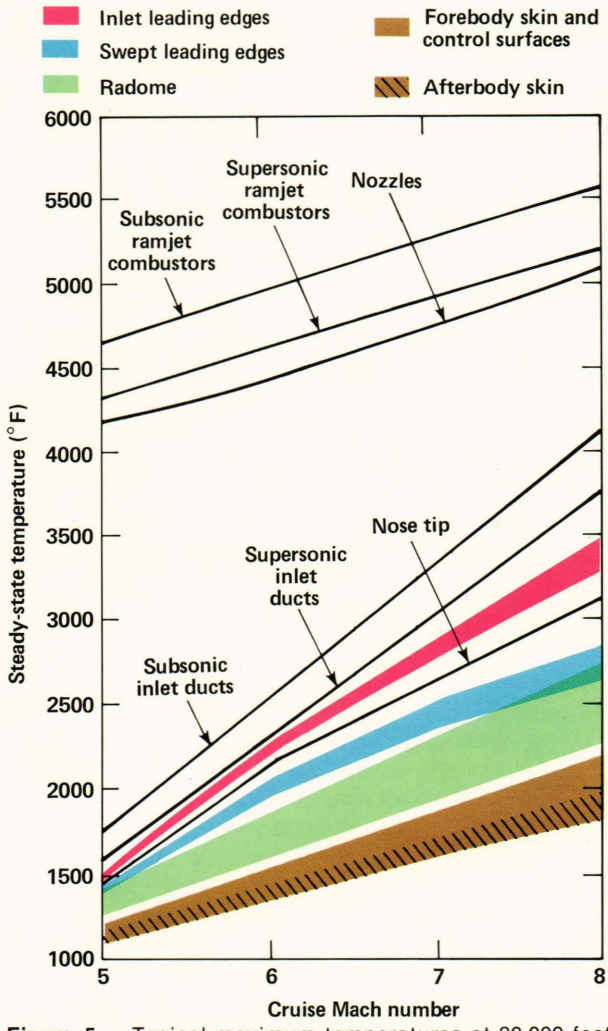

Figure 5 — Typical maximum temperatures at 80,000 feet altitude as a function of cruise Mach number for critical components.

occur in the subsonic inlet ducts and combustor of the DCR are restricted to small sections of the engine. Of even greater importance, at a given free-stream Mach number and altitude, the pressures and heat fluxes to walls in the supersonic inlet ducts and combustor are much lower than in the subsonic inlet ducts and combustor, so that both mechanical and thermal stresses are lower.

Loads Environment

Missile structures must be designed to withstand the loads imposed by shipboard shocks, launch, boost, and sustain flight conditions as well as the thermal stresses and distortions generated by aerodynamic and propulsion system heating. Little change is expected in the shipboard shock environment; however, newly developed vertical launching systems may include shock mitigation systems to alleviate the transmitted shock loads. Boost- and sustain-maneuver loads are likely to increase for advanced self-defense and area-defense missiles, but little change is expected for missiles in other mission categories.

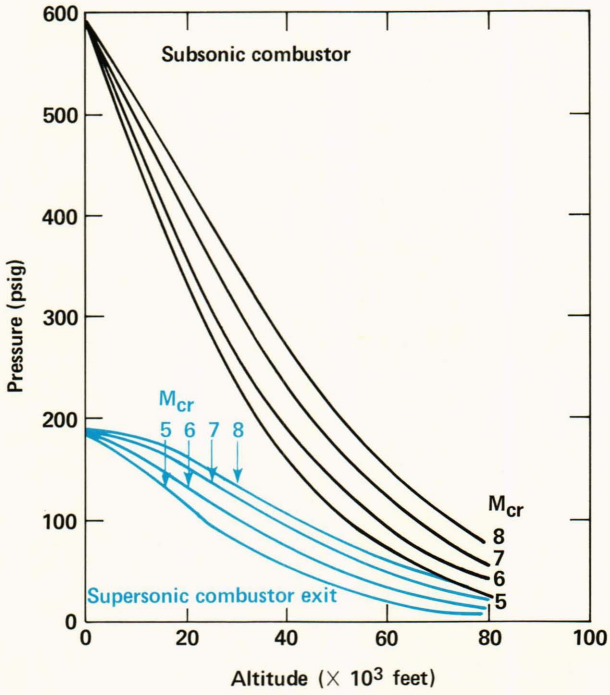

Figure 6 — Bursting pressures in subsonic and supersonic combustion chambers for a fuel equivalence ratio of 1.0 and Mach-altitude boundaries that vary linearly from Mach 4 at sea level to indicated cruise Mach number (M_{cr}) at 80,000 feet.

At a constant Mach number, the internal pressures in airbreathing engines decrease rapidly with increasing altitude. It is therefore common practice to establish Mach-altitude (*M-Z*) design boundaries that permit the Mach number to increase with altitude. Figure 6 shows typical maximum pressures in subsonic and supersonic combustion chambers for nominal *M-Z* boundaries in which *M* varies linearly with altitude from Mach 4 at sea level to a prescribed cruise Mach number (M_{cr}) at Z = 80,000 feet. Pressures in subsonic and supersonic inlet ducts show similar reductions with altitude.

For the assumed *M-Z* boundaries, the highest engine temperatures occur during high-altitude cruise; those temperatures dictate the choices of materials and insulation thicknesses for engine components. However, the highest internal pressures occur at sea level, and, depending upon the selected *M-Z* boundary, they may determine the structural thicknesses of the engine components.

Range Requirements

Flight times for wide-area-defense missiles can exceed 10 minutes even though the average speed is hypersonic. When these flight times are combined with the temperatures shown in Fig. 5, the oxidation of structural materials, the cooling of avionics, and the thermal protection of fuel and missile subsystems become problems. Materials with high-temperature capability frequently have lower strength and higher density than those with lower-temperature capability.

Trade-off studies are required to determine whether structures using low-density, high-strength structural materials that require insulating or ablative materials to protect them are lighter or more volumetrically efficient than those using high-density, low-strength materials that do not require thermal protection.

Launching Requirements

Launching systems impose dimensional constraints on missile designs. For future surface-to-surface, area-defense, and wide-area-defense missiles, the principal launcher is the vertical launching system that is being developed for new ship construction. Unlike existing launching systems, the system is not trainable and is located below decks. The weapon, housed in the shipping container, is stowed in a cell and is launched vertically from its container. The internal dimensions of the container restrict the weapon size to approximately 21 inches in diameter and 256 inches in length. The current weight limit on the weapon is 4100 pounds. Relatively slow or short-range missiles will benefit from the vertical launching system because the designer will be allowed greater dimensional freedom and the installation of a shock mitigation system will be permitted. On the other hand, the system will constrain the size and weight of long-range high-speed missiles. This constraint will place increased importance on the development of minimum-weight structures and minimum-volume thermal protection systems for these weapons.

STRUCTURAL MATERIALS

Structural weight, which is a primary consideration in the selection of materials, is inversely proportional to a material weight efficiency parameter that depends upon the geometry of the structure, the type of loading, and the failure criteria. For pressure vessels such as rocket motor cases, combustion chambers, and inlet ducts with circular cross sections, this parameter is F_{tu}/ω, where F_{tu} is the ultimate tensile strength and ω is the density. The parameter for body skins that fail by buckling due to compressive or bending loads is $E^{1/2}/\omega$, where E is the modulus of elasticity. If the body skin design is dictated by vibration frequency requirements rather than buckling, E/ω is the appropriate parameter.

Homogeneous Metallic Materials

The parameters F_{tu}/ω and $E^{1/2}/\omega$ for several commercially available metal alloys are shown as functions of temperature in Figs. 7 and 8. Further advances in material technology will have the effect of moving the curves up and to the right. However, it is expected that the changes will be modest and will not affect the general trends that are displayed. The magnitudes of the material weight-efficiency parameters drop rapidly as temperature increases. As a result, the unprotected hypersonic missile structures made of commercially available metal alloys will be much heavier than the structures of current supersonic missiles.

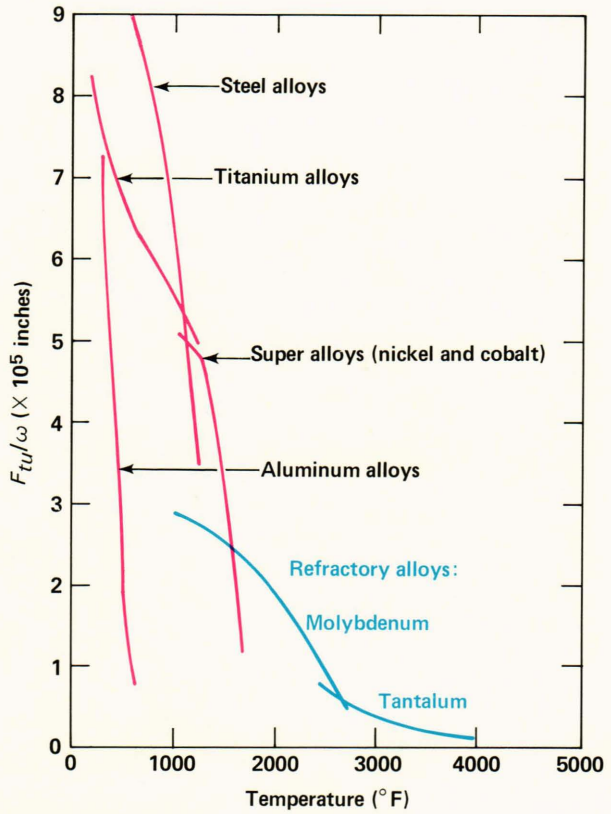

Figure 7 — Ultimate specific strength of commercially available metal alloy classes at elevated temperatures.

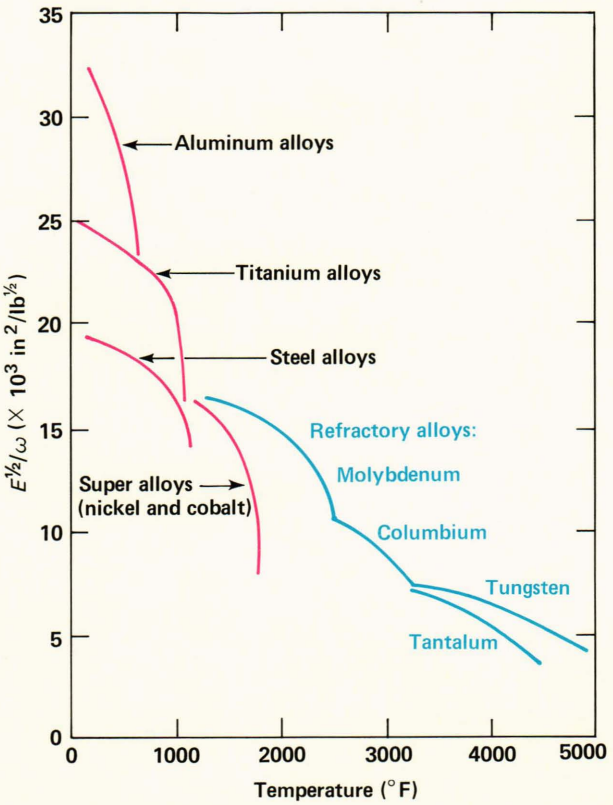

Figure 8 — Buckling efficiency parameter, $E^{1/2}/\omega$, of commercially available metal alloy classes at elevated temperatures.

It is seen from Figs. 5, 7, and 8 that superalloys (alloys of nickel and cobalt) may be used for external skins away from leading edges for speeds up to Mach 7 at 80,000 feet and for inlet ducts for speeds up to approximately Mach 5.5. At higher Mach numbers, refractory alloys (alloys of molybdenum, columbium, tantalum, and tungsten) will be required for those components. Refractory metals will also be required for unswept and swept leading edges at speeds above Mach 5.5 and 6, respectively, at 80,000 feet. The combustion chamber and nozzle temperatures are beyond the limits of metals and require thermal protection or construction from carbon materials.

Composite Materials

The concept of composite materials dates back several thousand years to the use of straw to reinforce dried-mud building blocks. The use of steel to reinforce concrete, or of carbon black and fabrics to reinforce rubber, has been commonplace for nearly a century. Fiberglass-reinforced plastics have had limited use in aircraft since the 1940's, but only now are advanced high-strength composites being used in aircraft structures. In missiles, composites were first used in fiberglass-epoxy radomes of subsonic missiles and filament-wound rocket motor cases of strategic missiles.

The high-strength reinforcing material in a composite can take the form of long filaments, short fibers or whiskers, or a finely divided particulate. Filament materials include glass, boron, graphite, organic fibers such as Kevlar, and silicon carbide (SiC), which is also used as a particulate material. Epoxy resin is the most commonly used matrix material for applications to 400°F. Polyimide and polybenzimidazole matrix resins are being developed for applications to 700 and 850°F, respectively, and it is predicted that future resin systems will have short-time capabilities to 1000°F.

Aluminum, magnesium, and titanium metal matrix materials are also undergoing development. The aluminum and titanium matrix composites will be useful to temperatures of approximately 600 and 1000°F, respectively. At the high end of the temperature scale, carbon-carbon composites consisting of graphite filaments in a pyrolyzed and graphitized pitch or resin matrix have been used in rocket nozzle applications where the temperatures approach 6500°F.

Two-dimensional filamentary composites are made by stacking and bonding together lamina composed of unidirectionally oriented filaments embedded in a matrix material. By selecting the filament and matrix materials, the volume fraction of the filaments, the stacking order of the lamina, and the directions of the filaments in each lamina, the designer can tailor the laminate to provide the necessary strengths and stiffnesses in all directions. The design procedures are complex, and computer programs are required to predict laminate properties. Three-dimensional filamentary composites are made by weaving the filaments and infiltrating the resulting preform with the matrix material.

The ultimate tensile strength and stiffness of unidirectional filamentary lamina are lower than those of the filament; in turn, the ultimate stress and stiffness of the multidirectional laminate are less than those of the lamina. Multidirectional laminates usually are required in practical applications and one cannot directly compare the strengths of monolithic materials with those of filaments or unidirectional composites. A more rational approach, but one that does not take full advantage of the ability to tailor the composite to the loading, is to compare the properties of monolithic materials with those of "pseudo-isotropic" composites. In these composite materials, the unidirectional lamina are oriented to provide the same properties in all directions lying in the plane of the laminate.

Figure 9 compares the room temperature values of F_{tu}/ω and E/ω of several unidirectional and pseudo-isotropic composite materials with conventional metals. The results show the reason for the current interest in developing the composites to reduce weight in flight-vehicle structures.

The temperature limits on the composite materials exceed those of the matrix materials for short exposure times; e.g., the temperature limit of a graphite-aluminum composite is roughly 100°F greater than that of monolithic aluminum. Unprotected titanium matrix composites will be useful for skins away from leading edges at speeds to Mach 5.5 at 80,000 feet, and carbon-carbon has the ability to

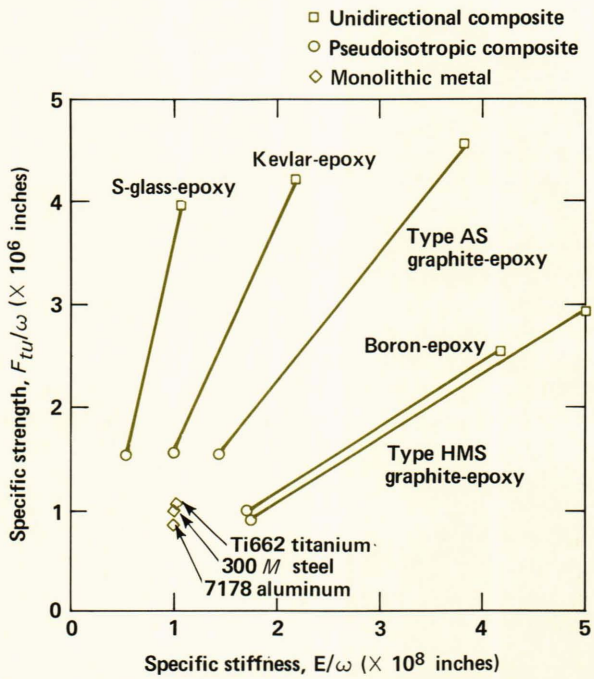

Figure 9 — Comparision of room temperature values of ultimate specific strength, F_{tu}/ω, and specific modulus, E/ω, of unidirectional and pseudoisotropic composite materials with commercially available metal alloys.

operate under the most severe temperatures shown in Fig. 5. However, most composites will require thermal protection for hypersonic missile applications. It remains to be determined whether the composites with thermal protection material will be more weight and volume efficient than the unprotected metal structures.

Filament-wound rocket motor cases of glass-epoxy and Kevlar-epoxy are operational, and graphite-epoxy cases are under development. For higher temperature applications, polyimide is expected to replace epoxy as the matrix material. While rocket nozzles of carbon-carbon are operational, there are extensive developmental efforts to improve the properties and reliability of those materials while reducing costs. Carbon-carbon appears to be a satisfactory material for combustion chambers and nozzles operating in a fuel-rich (reducing) environment, as is usually the case for solid-fuel rockets. For ramjet-powered hypersonic missiles, however, it will be necessary to develop ways to protect the material from oxidation by the hot combustion gases.

THERMAL PROTECTION SYSTEMS

The use of external insulation is generally restricted to the load-carrying structure; it can be either an ablating material or a low-conductivity material with sufficient structural integrity to withstand handling conditions and aerodynamic loads. Most ablators are resin compositions of Teflon (fluorinated ethylene propylene copolymer), silicone, or phenolic. Teflon is generally used in applications where a "clean" ablation is desired, such as over a radar transmission window. It converts from a solid directly to a gas (sublimation) when heated above about 700°F and, in so doing, does not attenuate the radar transmission. A good example of a Teflon ablator is Duroid 5650M. Reinforced silicone and phenolic ablators develop a char layer during the ablation process that provides additional thermal protection. Two charring ablators that have been considered for long-range hypersonic missiles are S-10 (a reinforced silicone resin) and HSHS, a heat-shrinkable heat shield that is a modified silicone rubber. External insulation is primarily used to keep the structure temperature below its allowable limit for strength and stiffness, but it also is used to reduce temperature gradients that could produce undesirable thermal stresses and to maintain a rocket case temperature below the pyrolyzation temperature of internal insulation.

Internal insulation materials must have low thermal conductivity and low density to minimize both weight and volume. Two attractive materials are Min-K and the high-purity quartz insulation Refrasil. These insulations are made in different forms for different temperature ranges. Min-K is a bonded structure reinforced with fibrous media; it contains appreciable quantities of very small particulate matter. Its maximum operating temperature is specified by the manufacturer as 2000°F, but it can be used up to 2600°F for times of less than 10 minutes. In the case of the insulation in a supersonic combustion chamber of a hypersonic ramjet, that temperature is exceeded, and an intermediate layer of zirconium dioxide felt insulation is proposed for short-time operation to 4600°F.

These materials are flexible and must be held in place by a secondary structure, usually made of 3-mil metal or rigidized refractory cloth. Assembly and accessibility requirements govern the design of the support material.

Internal rocket-case insulation must be able to protect the structure from gas temperatures as high as 6000 to 7000°F. For booster or short-range missile applications, the time of exposure may be only 5 to 10 seconds, and the liner material can be quite thin (about 0.1 inch). Ramjet combustors usually operate at lower temperatures, but the combustion gases are more oxidizing than the rocket gases and burn times may last for 5 to 10 minutes. Ramjet combustor insulation varies, depending on the missile speed and whether the missile uses a subsonic or a supersonic combustion chamber. For the Talos missile, whose speed does not exceed Mach 3 and which contains a subsonic combustion chamber, a coating of flame-sprayed zirconium dioxide on the air-cooled liner provided sufficient protection. For the supersonic combustion chamber of the proposed hypersonic dual combustion ramjet engine, flame temperatures up to 5000°F are predicted. Experimental investigations showed that a pyrolytic graphite coating over a carbon-carbon substrate is a good candidate system.

Considerable attention has been given in the past to the development of integral-rocket ramjets whose combustion chamber is used both for the rocket and ramjet (see Fig. 4). A special insulation material has been developed to provide thermal protection of the combustion chamber case during both phases of propulsion. The material (Dow Corning DC 93-104) is a silicone ablator containing a high percentage of silica that forms a low-conductivity char after the material has pyrolyzed. Considerable effort has been expended in developing a thermal model to predict the ablation and temperature response of this material.[2] An experimental demonstration of this material's thermal protection capability has been performed in both the Air Force's Advanced Strategic Air-Launched Missile ramjet flight test program and the Navy's Advanced Surface-to-Air Ramjet prototyping program. Future missile designs using a rocket-ramjet should be able to use DC 93-104 in the combustion chamber with reasonable confidence.

SENSOR WINDOWS

For radar-guided missiles, the window through which the radar must "look" is a radome; for vehicles guided by infrared radiation, the window is called an infrared (IR) dome. The windows are generally located in the missile's nose to provide a wide forward view, and they are shaped, as much as possible, to minimize drag. The frequency ranges for mi-

crowave (radar), infrared (including laser systems), and electro-optical systems are: 3×10^8 to 3×10^{11}, 3×10^{12} to 3×10^{14}, and 4.3×10^{14} to 7.5×10^{14} hertz, respectively, for which the protecting windows must have transmittances. Thus, materials with low dielectric constants (generally below 10) are used primarily. There are two important differences between radomes and infrared or optical windows: (1) the thickness-to-wavelength ratio for the radome is nearly always less than 1 (usually ½), whereas for an infrared or optical window it can be in the hundreds; and (2) the electromagnetic signal passed by the radome is usually polarized and coherent, whereas the infrared or optical signal is not polarized and is noncoherent unless the energy emanates from a laser. Stated differently, if the radome design problem were scaled to infrared or optical frequencies, the radome wall thickness would be a thin film less than 10^{-6} inch thick, and it would be suitable for transmitting laser-type energy with minimum aberration and maximum efficiency.

Radomes

For the missile technologist, the word "radome" denotes a window of any shape and size that protects a radiating and/or receiving electromagnetic antenna with minimum aberration and maximum efficiency. The first airborne radomes were used in aircraft and were made of ¼-inch plywood, but the problem of moisture absorption in the plywood resulted in a search for better materials. Glass-fiber-reinforced plastic (FRP) is now used for aircraft radomes and low-speed missiles. Some of the more widely used resins in RF radome materials are polyester, epoxy, phenolic, and silicone. Epoxies generally are superior for speeds less than Mach 2 at sea level. Their maximum use temperature is about 400°F. Phenolic resins have somewhat higher temperature resistance, low cost, high mechanical strength properties, and resistance to a large range of environmental conditions, but relatively poor electrical properties. Silicone resins yield good performance when electrical properties are of prime importance and temperatures to about 550°F are encountered.

Some investigations are in progress to determine the feasibility of using an ablative coating over an FRP radome for Mach 3 to 5 applications. Two candidate ablators are Duroid 5650M and Avcoat 8029, both of which provide good rain-erosion resistance and operation over a broad frequency band because of their relatively low dielectric constant.

An FRP radome can be attached to the main body structure by conventional shell structure methods. Joints may be made by using bolts, screws, rivets, latches, clamp rings, adhesive bonding, or straight threading of the radome attachment edge. The greatest departure from convention is found in the special techniques used to reinforce the attachment edge of the radome for the proper transfer of design loads. The reinforcement must be designed to overcome the "weak links" inherent in glass-reinforced plastics: interlaminar shear, interlaminar tension, and bearing strength.

Ceramic radomes generally are used for missiles that fly faster than Mach 3. Ceramic materials have a higher temperature capability than FRP and high resistance to rain erosion at supersonic velocities. However, most of them are susceptible to thermal shock. Also, because of their brittleness and relatively low coefficient of expansion compared to those of metals, special care must be taken in the design of the radome attachment.

Ceramic radome design must take into account electrical, thermal, and mechanical conditions. Generally, the electrical design is addressed first and establishes the thickness of the wall – usually one-half the wavelength of the radar for which the radome is designed. For 10 gigahertz, this is about 0.20, 0.25, and 0.33 inch for alumina, Pyroceram 9606, and slip-cast fused silica, respectively. Good electrical performance can also be obtained with a thin-wall design whose thickness is about one-twentieth of the wavelength. Thin walls reduce the thermal stresses but are more susceptible to damage from handling and flight through rain.

For a number of years, APL worked on the development of a method to predict the environmental flight performance boundaries for ceramic radomes. That work was combined into a unified radome limitations (URLIM) computer program[3] that can predict the flight limits of radome materials on the basis of electrical degradation, surface melting, thermal stress, and mechanical load. By means of this code, limitations were defined for alumina, fused silica, and Pyroceram 9606. The alumina and Pyroceram 9606 were found to be limited by thermal stress, and the fused silica was limited by radar performance degradation. Even though alumina has high strength and a high melting point, its high expansion coefficient causes thermal-stress limitations for nominal accelerations to velocities between 3000 and 4000 feet per second. The thermal-stress performance of several X-band radome materials was computed for a thermally severe trajectory (Fig. 10). The results indicate that Pyroceram 9606 experiences thermal stresses very near its design allowable stress, while the other materials demonstrate a comfortable margin.

To explore further the capabilities of the slip-cast fused silica, two experimental programs were carried out in which Standard Missile-size radomes were subjected to flow conditions simulating a hypersonic environment.[4,5] Figure 11 is a photograph of a free jet test at the nominal flow conditions of Mach 2.8, total pressure of 200 pounds per square inch, absolute and total temperature of 4000°F. On the basis of an equivalent heat flux, these conditions simulate a Mach 8 flight at 86,000 feet altitude. An X-band radome and its attachment survived a 35 second test that included 10 seconds at 15° angle of attack. The fused silica withstood the hypersonic environment, but more development work is needed on the attachment. The low strength and thermal expansion of

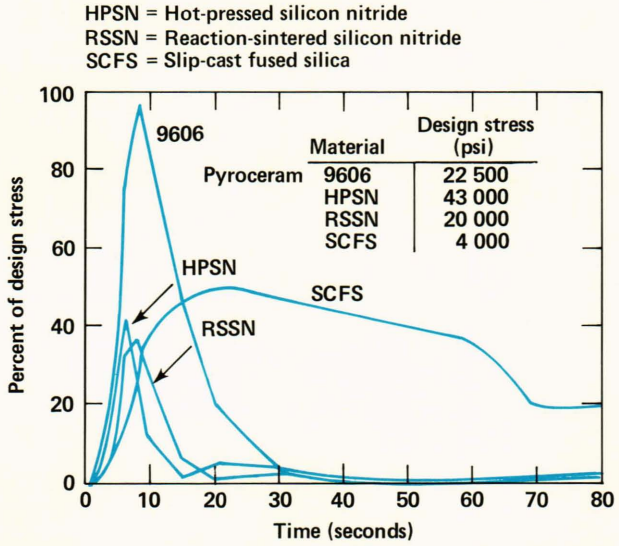

Figure 10 — Thermal stress performance of several radome materials.

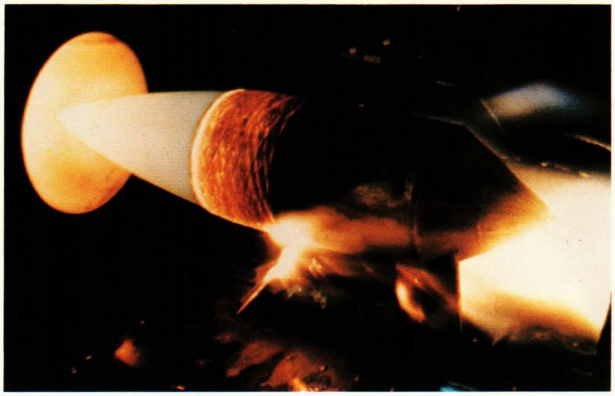

Figure 11 — Fused silica radome in free jet test. Conditions simulate flight at Mach 8 at 65,000 feet altitude.

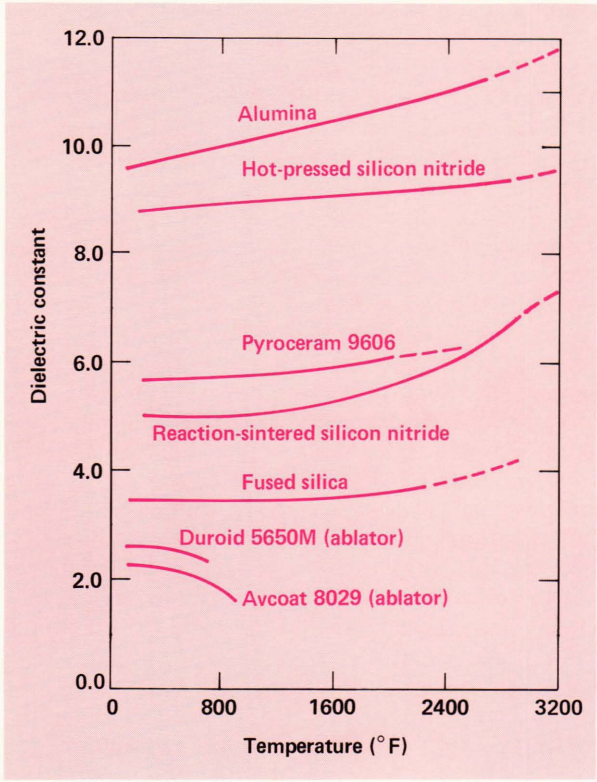

Figure 12 — Dielectric constant of several radome materials as a function of temperature.

fused silica combined with the high temperatures experienced in hypersonic flight make the attachment design difficult.

Figure 12 presents dielectric constants of several radome materials as functions of temperature. Of particular interest is the negative slope on ablator materials. Because these materials lose thickness during flight, it would be desirable to have positive slopes. Fused silica's small variation in dielectric constant with temperature is a very attractive characteristic.

Infrared and Electro-Optical Windows

In recent years, infrared and electro-optical guidance systems have become strong competitors of microwave guidance systems for tactical missiles; they offer greater tracking precision, smaller dimensions, and lower weight and cost in addition to passive homing, which is of primary importance in short-range encounters.

The wavelength range for electro-optical systems is the optical bandwidth (0.4 to 0.68 micrometer), while infrared (heat-seeking) systems are restricted to regions in which there is good transmission through the atmosphere. The near-infrared windows are 0.75 to 1.3, 1.5 to 1.8, and 2.0 to 2.5 micrometers. The intermediate- and far-infrared windows are 3 to 5 and 8 to 13 micrometers, respectively. If the missile is to be used against targets having particularly hot areas (i.e., a tailpipe, nose, or leading edge), the guidance system can operate in the near-infrared window. If the missile is to have a broader capability in which detection of target plume radiation and hot surface radiation is required, the guidance system would have to operate in the intermediate-infrared window. A more advanced infrared system may use "cold body tracking," which would make use of the far-infrared atmospheric window and require infrared dome materials that transmit in the 8 to 13 micrometer range.

The previous discussion shows that the selection of an infrared dome for a particular missile application is intimately connected with the intended capability of the missile and the type of target for which it is designed. Current systems generally work in the near or intermediate windows. However, there is a trend toward the longer wavelengths (i.e., low-temperature targets), and future missiles may operate in the far-infrared window.

In considering the flight environment, there are three problem areas in infrared or electro-optical dome design: the hot window, rain erosion, and ther-

mal shock. Of the three, the last imposes the most critical requirements on the dome material.[6]

Sapphire, spinel ($MgAl_2O_4$), and IRG-11 ($Ca\text{-}Al_2O_3$) are the infrared dome materials that have the best thermal shock capabilities. Of the electro-optical materials, the silicas and VYCOR 7913 are very attractive. For most applications, the sapphire material cannot be considered because of cost, leaving spinel and IRG-11 as the best candidates for infrared applications where thermal shock is a design problem. Spinel is a magnesium aluminate glass having good thermal shock resistance and good infrared transmittance for wavelengths beyond 5 micrometers. IRG-11 is a calcium aluminate glass that has good thermal shock resistance because of its high tensile strength. A disadvantage is its slight solubility in water, which necessitates a protective coating, but it deserves special attention for infrared dome applications. For the near-infrared window, the VYCOR 7913 material may be most attractive since a 2-millimeter thick layer has a transmittance above 90% out to a wavelength of 2.5 micrometers. Thermal shock is not a major problem with most of the electro-optical materials; however, the low thermal expansion combined with the thin wall increases the difficulty of designing a suitable mount for the domes. Special compliant joints must be used to ensure that the dome is not overstressed by differential expansion at the mount.

For supersonic missile applications, the infrared dome temperatures will increase approximately in proportion to the flight velocity. These elevated temperatures generally reduce transmittance of the dome material as well as cause energy to radiate to the seeker, both of which affect the signal-to-noise ratio. Some data on transmissivity and emissivity as a function of temperature have been reported, but additional measurements must be made before a high-speed dome can be designed.

Because of reduced visibility, infrared and electro-optical systems generally are not expected to perform in bad weather conditions, but this does not fully remove the requirement that the domes must be able to withstand flights through rain. Missiles carried aboard aircraft are subject to rain, and a multimode guidance, long-range missile may have to fly through rain before reaching its terminal phase near the target. In the past, nearly all infrared and electro-optical domes were hemispherical (future domes may take on a lower-drag aerodynamic shape), which presented a vulnerable region where frontal and near-frontal raindrop impacts were possible. Numerous reports (among them Ref. 7) have shown that rain erosion is proportional to the normal velocity component, and considerable damage to hemispherical domes exposed to rain at supersonic speeds might be expected. Efforts are in progress to develop suitable rain-erosion-resistant coatings for infrared and electro-optical domes and to use aerodynamic shapes that reduce the angle of incidence of the rain.

CONCLUDING REMARKS

Future missiles designed to meet the wide-area defense needs of the Navy's surface Fleet may fly at hypersonic speeds for up to 10 minutes. External aerodynamic and internal combustor heating will place stringent demands on structural materials, in many cases necessitating the use of external insulation to protect airframes and internal insulation to protect internal components. Flight environments also impose demanding requirements on guidance systems, necessitating the development of new and improved sensor window materials. New, high-firepower launching systems will impose weight and volume restrictions on missile designs. The incorporation of advanced resin, metal matrix, and carbon composites into missile airframes has the potential of increasing structural efficiency through improved weight and volume control.

REFERENCES

1. W. B. Shippen and W. C. Caywood, *Feasibility Study of the Use of the Long Range Typhon Ramjet Engine for Tests on the X-15 Airplane,* JHU/APL TG 542 (Dec 1963).
2. L. B. Weckesser and L. L. Perini, "Evaluation of Thermal Models for DC-93-104," *Proc. 14th JANNAF Combustion Meeting* (Aug 1977).
3. R. K. Frazer, "A Unified Radome Limitations Computer Program," *Proc. 12th Symp. on Electromagnetic Windows* (12-14 Jun 1974).
4. C. A. Murphy, L. B. Weckesser, and N. E. Poulos, "Thermal Testing of Slip-Cast Fused Silica Radomes," *Proc. U. S. Air Force-Georgia Tech. Symp. on Electromagnetic Windows* (Jun 1966).
5. L. B. Weckesser and R. K. Frazer, "Evaluation of Radomes for Hypersonic Flight," AIAA paper presented at the Fourth Thermophysics Conference (23-25 Jul 1969).
6. F. Megerlin and L. Rayburn, "Thermal Shock of Infrared Missile Domes during High Speed Missile Flight," *Proc. Tenth Symp. on Electromagnetic Windows* (Jul 1970).
7. G. F. Schmitt, Jr., and A. H. Krabill, *Velocity-Erosion Rate Relationships of Materials in Rain at Supersonic Speeds,* AFML-TR-70-44 (Oct 1970).

ROLAND E. LEE, ROBERT TURNER, and RICHARD C. BENSON

OPTICAL MEASUREMENTS FOR RAMJET ENGINE DEVELOPMENT

Two optical instruments, the laser anemometer and the coherent anti-Stokes Raman scattering (CARS) spectrometer, were recently studied at APL's Propulsion Research Laboratory for use as combustion diagnostic tools. Recent test results of the laser anemometer used in a typical exhaust flow environment of a combustion chamber and of CARS in graphite surface oxidation studies are discussed.

INTRODUCTION

Advanced propulsion systems involve highly complex combustion flow processes. Extensive and accurate flowfield measurements can help to guide and support engine development. For example, in the hypersonic dual-combustor ramjet, the subsonic combustion chamber operating at fuel-rich conditions generates a complex multiphase combustion flow comprising liquid fuel droplets, soot particles, and reacting gases. The complexity of this flow is intensified by its subsequent downstream interaction with air at supersonic speeds. In such reacting flows, conventional mechanical probes can disturb the local flow environment as well as be subjected to impact and thermal damage. Optical instruments that have been developed and used in laboratory experiments of less complex combustion flows avoid these difficulties. However, their application in the harsh flow environment of ramjet engine combustion is more difficult and needs to be approached cautiously. In contrast to mechanical probes, optical instruments generally are nonintrusive; produce minimum flow disturbance; have a faster response, higher data rate capability, and better spatial resolution; and, in some cases, can measure more than one flow parameter per instrument.

Flow modeling requires accurate flowfield measurements of stream velocity, temperature and pressure distributions, and, when chemical reactions are present, the chemical species concentration distributions. For a reacting flow containing a considerable amount of particulates, the characteristics and distributions of these particles need to be measured. The particulate flow is important because it can strongly affect both the performance of optical diagnostic devices and the combustion efficiency. In relatively clean combustion flows, such as most laboratory flames, the particulates are generally of submicrometer size. In the fuel-rich ramjet flows, however, soot particles and unburned fuel droplets can extend the particle size range from submicrometer size to as large as 50 micrometers.

In principle, all of the above flow parameters may be determined by optical instruments. APL's Aeronautics Division, in collaboration with the Research Center, is currently reviewing and test-evaluating selected optical instruments for use in supersonic ramjet combustion flowfield measurements. Figure 1 lists the techniques considered and the flow parameters they are expected to measure. In some cases, an intermediate parameter is used to obtain the desired flow parameter; e.g., the laser anemometer measures particle velocity, and the gas flow velocity is deduced from modeling of particle drag.

At the onset of this program, there was very little information on the size, number density, or index of refraction of particles generated by a fuel-rich hydrocarbon combustor. The first two instruments for measuring particle size were selected on the basis of laser light transmission at two wavelengths and laser light scattering at two viewing angles. They were abandoned early in the program because analysis showed that the upper range of particle sizes of interest could not be measured. Follow-on evaluation and testing showed the laser anemometer and Raman spectrometer to be viable instruments that could withstand the hostile engine-testing environment and provide data on a number of the pertinent flow parameters. The laser anemometer observes laser light scattered by particulates embedded in the flow to deduce the particle and flow velocities, the particle size, and the particle number density. The Raman spectrometer relates the laser light scattered by molecules in the combustion medium to flow temperature and gaseous species concentrations.

The evaluation of the laser anemometer instrument included: (a) analysis with laser light scattering (Mie theory) and light diffraction computer programs; (b) calibration with a cold-air supersonic flow (Mach 3.5) with controlled particle seeding; and (c) actual measurements in a small-scale combustor that can be operated at pressures up to 4.5 atmospheres, inlet air temperatures from 650 to 870 K, and fuel-air equivalence ratios between 0.8 and 4.0, using JP-5 fuel.

PARTICLE SIZING

Various optical techniques have been developed that use scattered light to measure the micrometer-

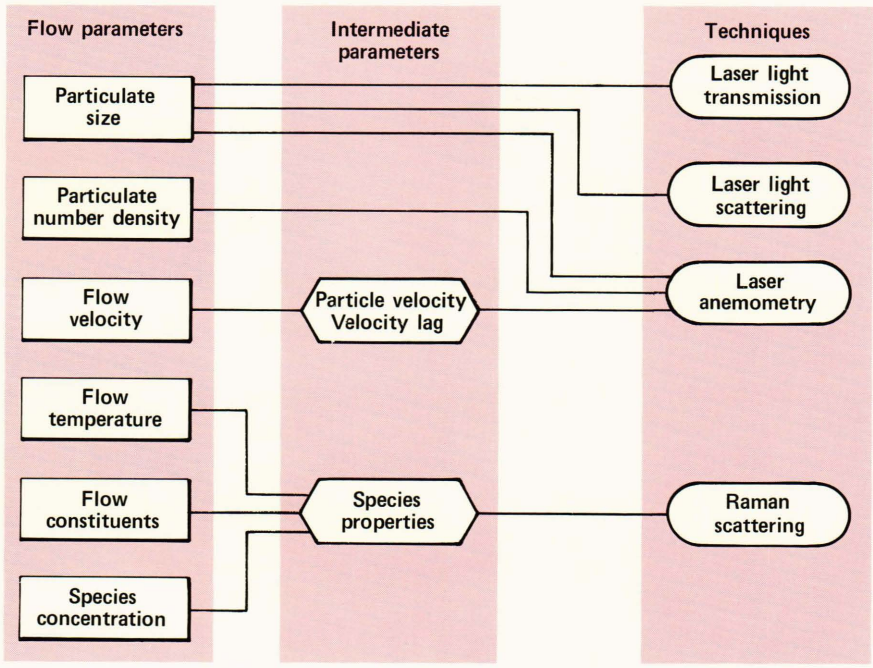

Figure 1 — Optical flow diagnostic parameters and techniques.

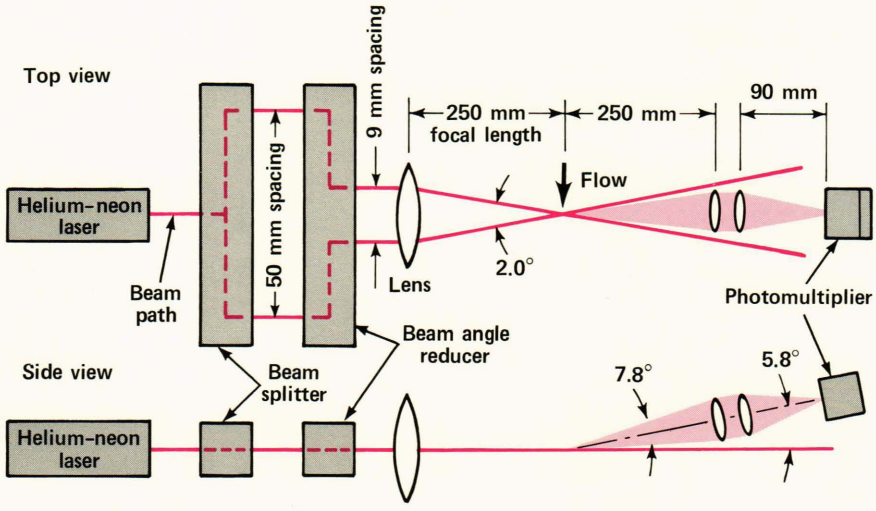

Figure 2 — Laser Doppler velocimeter optical configuration.

size particles found in combustion experiments. In general, all such techniques make assumptions about the particle size distribution, particle shape, index of refraction, and size relative to the wavelength of the light source. Some methods use relative amplitude measurements; others use absolute measurements. Some observe the signal from a single particle; others observe the signal produced by a number of particles. The actual method chosen depends to a large extent on the parameters to be determined and the adaptability of the instrument to the particular application. A standard dual-beam laser anemometer, normally used to measure particle velocity, was adapted to provide a simultaneous measurement of particle size (in the range of 3 to about 100 micrometers) and speed (550 to 1400 meters per second), the density of particles greater than about 1 micrometer, and the attenuation of a laser anemometer beam produced by particles smaller than 100 micrometers.

Figure 2 is a schematic diagram of the Thermo-Systems, Inc., laser anemometer, which uses a 5-milliwatt helium-neon laser, configured for forward scattering at an elevation angle of 5.8°. The two laser anemometer beams cross at an angle of 2° to produce an ellipsoidal scattering volume. The measured signal is a function of a particle's position in each beam; as a result, constructive and destructive interference can occur as the particle moves through the beams. It is often convenient to think of the particle as being illuminated by light and dark fringes, with a spacing of 17.6 micrometers in this case. The minor axis of the scattering volume, in the direction of flow, is 250 micrometers; the major axis, perpendicular to the flow, is 2 millimeters. A 250-micrometer aperture in the

collection optics limits the field of view at the center of the region to 16 fringes. Particles moving at speeds of 550 to 1400 meters per second will produce scattered light pulses from 0.5 to 0.2 microseconds wide that are modulated at frequencies from 30 to 80 megahertz. Figure 3 is a photograph of the laser anemometer instrument configured for use in the full-scale ramjet engine combustor.

The size of the particle producing the scattered light can be derived from the signal visibility (V), which is the ratio of the depth of the modulation of the scattered signal to the mean amplitude [$V = (I_{max} - I_{min})/(I_{max} + I_{min})$, where I_{max} and I_{min} are the maximum and minimum of the light intensities], and from the mean amplitude of the signal directly. The two methods for determining particle size are complementary. With the present laser anemometer, the intensity of the light scattered by small particles (< 3 micrometers) is low, but the visibility is high (about 1); the intensity of light scattered by large particles (> 20 micrometers) is large, but the visibility is low (less than 0.3). The intensity measurement is absolute; it generally increases monotonically with particle size and can have a large dynamic range. Visibility is a relative measurement, and because the particle size can be multivalued for a given visibility, the dynamic range is generally less than 10. This can present a problem in its application if the size range of interest is not defined beforehand. References 1 through 5 describe aspects of the visibility and scattered light measurements that are relevant to the work described here.

Particle sizing by means of the signal visibility is of recent origin, and there has been considerable discussion about its interpretation and application. The visibility and intensity techniques are both extremely sensitive to the f number of the collection optics and to their location relative to the incident laser beams. In fact, the visibility and intensity dependence on particle diameter can be tailored by the proper choice of scattering angle and collection aperture. Because of this, it is important that the instrument be calibrated and also that its response function be calculated for the conditions actually used.

Visibility curves computed for spherical particles are shown in Fig. 4 for three conditions. Curve A is calculated for the collection optics centered between the laser anemometer beams and in the plane of the beams. The visibility is approximated by:

$$V = 2[J_1(\pi D_p/\delta_f)]/(\pi D_p/\delta_f), \qquad (1)$$

where $J_1(\pi D_p/\delta_f)$ is the first-order Bessel function of $(\pi D_p/\delta_f)$, D_p is the particle diameter, and δ_f is the fringe spacing.[1] Curve B is calculated using the standard diffraction approximation for the detector mounted 5.8° above the plane of the two beams. Cal-

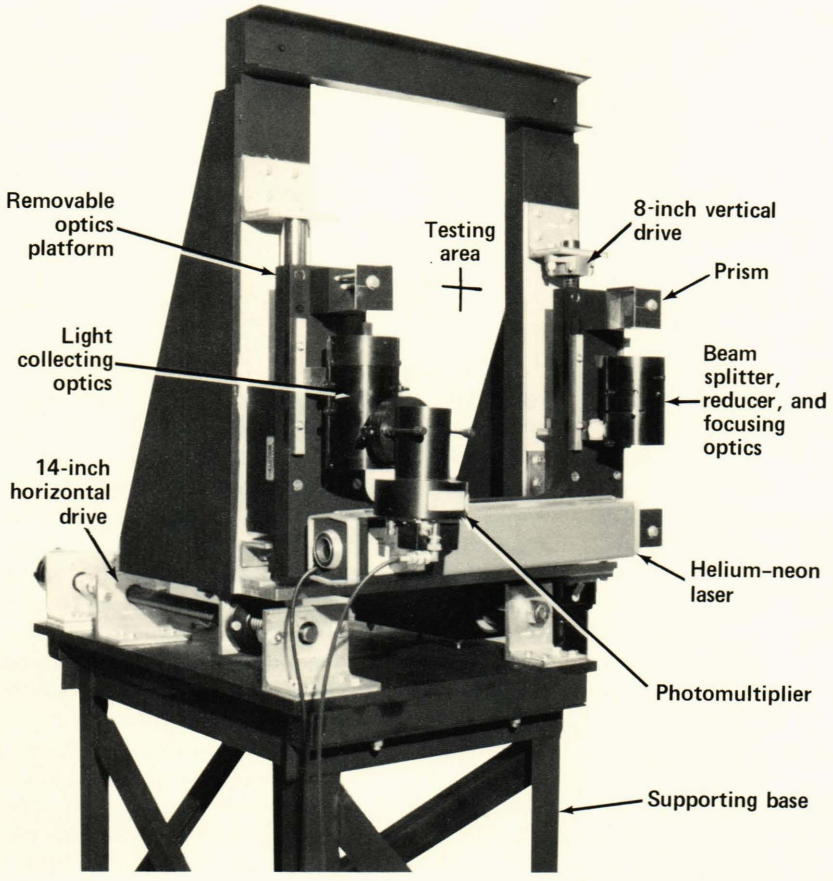

Figure 3 — Photograph of the laser Doppler velocimeter mounted on motorized two-component traverse.

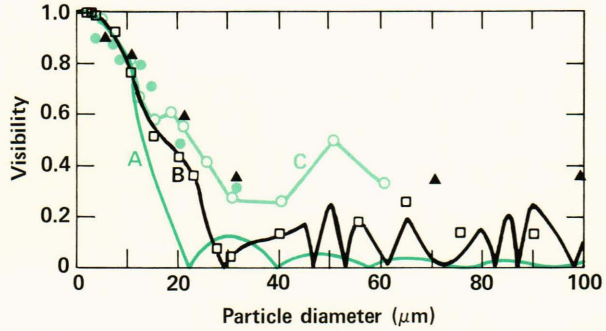

Figure 4 — Calculated and measured visibility as a function of particle diameter. The plotted data, except for A, are for a detector with a 250-millimeter focal length lens, an aperture of 34 millimeters, and a scattering angle of 5.8°. A is the visibility using the approximation of Ref. 1. B is calculated using the diffraction approximation. C, shown by the symbol ○, is the calculation using the Mie theory for dioctyl phthalate. □ indicates points calculated using Mie theory for soot-hydrocarbon particles (n = 1.67—i0.33); ▲ indicates measured values for polystyrene (n = 1.59—i0.00); and • indicates measured values for dioctyl phthalate (n = 1.49—i0.00).

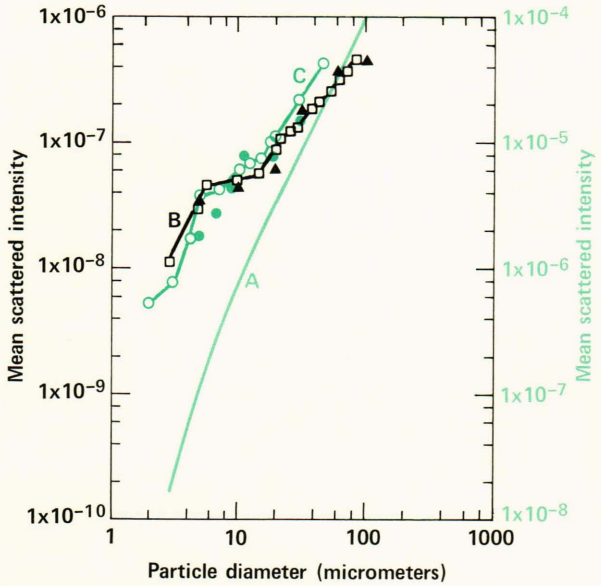

Figure 5 — Calculated and measured values of the mean scattered intensity as a function of particle size. A is the intensity calculated using the diffraction approximation with the detector centered between the beams in the plane of the laser Doppler velocimeter beams. B is the intensity calculated with the diffraction approximation at an angle of 5.8°. C, shown by the symbol ○, is the intensity calculated with the Mie theory for dioctyl phthalate. □ indicates points calculated for soot-hydrocarbon particles (n = 1.67—i0.33); ▲ indicates measured values (relative) for polystyrene (n = 1.59—i0.00); and • indicates measured values (relative) for dioctyl phthalate (n = 1.49—i0.00).

culations using the diffraction approximation are suspect when the measurements are made off-axis and the index of refraction (n) of the particle becomes a factor. In this case, the more exact Mie theory must be used.[6] The visibility calculated for selected points using the Mie theory for dioctyl phthalate (n = 1.59—i0.00) and for a soot-hydrocarbon mixture (n = 1.67—i0.33), representative of partially burned fuel, are indicated in Fig. 4. The diffraction approximation is reasonable for the expected combustion products, but the effect of the index of refraction must be considered in the calibration and for unburned fuel drops. Figure 5 shows the calculated intensities for the same two positions of the collection optics using the diffraction approximation and the Mie theory for dioctyl phthalate and the soot-hydrocarbon mixture.

The laser anemometer was calibrated with solid polystyrene spheres and liquid aerosols. Single 5- to 100-micrometer polystyrene spheres were mounted on a rotating disc that provided a particle speed of 20 meters per second. In this case, the laser anemometer output could be identified with a particle whose size, shape, index of refraction, and position in the scattering volume were known. The results of individual measurements, plotted in Figs. 4 and 5, are in reasonable agreement with the Mie theory calculations. A Bergulund-Liu aerosol generator was used to provide dioctyl phthalate aerosols up to 50 micrometers in diameter, moving at 3 meters per second (the normal velocity of the aerosols from the generator) or up to 400 meters per second when they were injected into a small supersonic wind tunnel. The results at 3 meters per second are plotted in Figs. 4 and 5. Measurements in the small wind tunnel agreed with the low-speed results for particles of up to 12 micrometers in diameter. The measurements with the larger aerosols were erratic but generally similar to those produced by smaller particles. The erratic results are attributed to the breakup of the large dioctyl phthalate drops in the high-speed flowfield.

Two selection processes are applied to each laser anemometer pulse to ensure, as far as practical, that data from only one particle are being collected and that the particle is illuminated by the maximum intensity of each incident beam. Only scattered light pulses that are less than 0.5 microseconds wide and have exactly 16 cycles of modulation are processed. Figure 6 is a simplified block diagram of the signal processing used. The laser anemometer signal is filtered with a low-pass filter to provide the mean scattered intensity $(I_{max} + I_{min})/2$; it is also filtered with a bandpass filter and rectified to give $(I_{max} - I_{min})/2$. The two outputs are stretched, sampled at their peaks, and held for 20 microseconds. The output of the bandpass filter is also used by two fast discriminators. One provides a pulse for each laser anemometer output, above a threshold equivalent to a particle larger than 1 micrometer, to start a time-to-pulse height converter and to provide a 0.5-microsecond gate and a 20-microsecond hold/reset pulse for the peak sense-and-hold circuits. The output of the second discriminator is a train of pulses equal to the number of cycles of modulation produced by the particle. If there are exactly 16 pulses, the maximum number at the center of the scattering volume, the single channel analyzer stops the time-to-pulse height

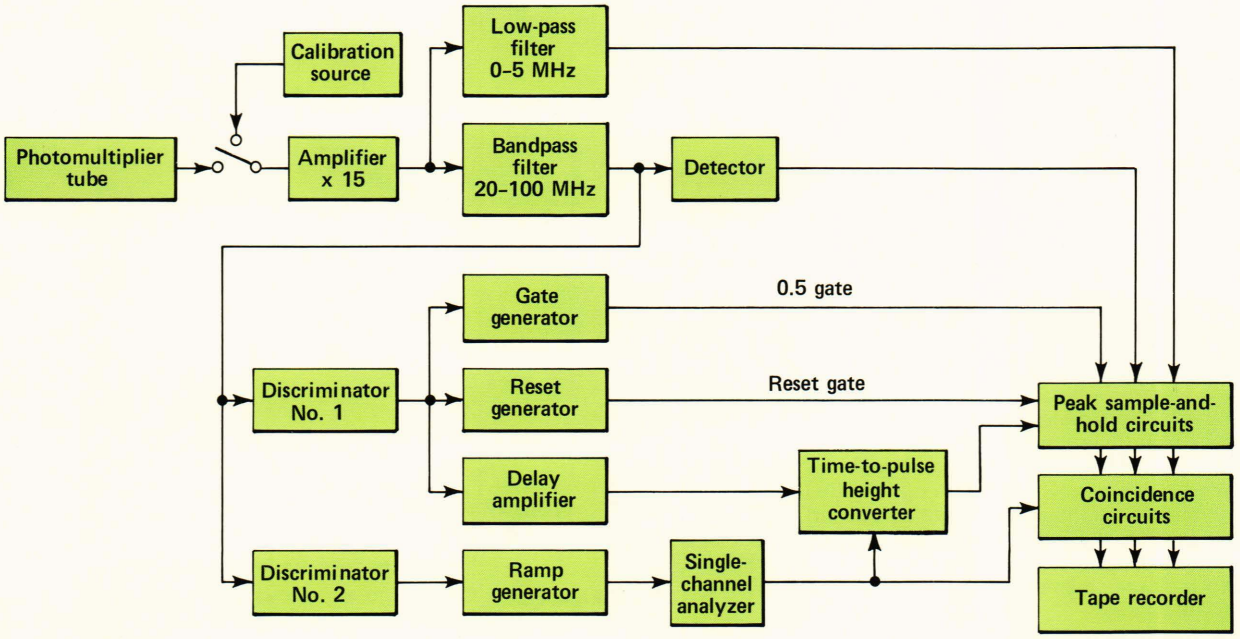

Figure 6 — Schematic of particle sizing instrument.

converter. The time-to-pulse height converter output, which is a measure of particle speed, is also sampled and held. The $(I_{max} + I_{min})/2$, $(I_{max} - I_{min})/2$, and time-to-pulse height converter voltages are recorded if a single channel analyzer pulse is present. From these data, the particle's speed and two measures of its size are derived. The output of discriminator No. 1 is also counted to indicate the flux of particles passing through the scattering volume.

The transmission ratio (I/I_0), where I is the measured intensity with the particles present and I_0 is the intensity when no particles are present, of the laser beam through the flowfield was measured to indicate the amount of material with diameters of less than about 100 micrometers in the flow, evidence of multiple scattering or refractive effects, and to reinforce the sizing results obtained from the visibility and intensity measurements. The transmission ratio is determined by the integrated effect of particle density (N), extinction efficiency (Q_{ext}), particle area (S), and path length (l) through the particulate flow:

$$I/I_0 = \exp(-\alpha l) \qquad (2)$$

where α, the attenuation coefficient per centimeter, equals $NQ_{ext}S$. The extinction efficiency is close to 2 for the large particles of interest; it is near 1 for the great number of smaller particles that contribute to the beam attenuation. Because this measurement is an average along the path of the beam through the flame, average values have been used, and an extinction efficiency of 2 has been assumed for all calculations. The path length was derived from photographs of the scattered light.

Tests were made on the fuel-rich ramjet combustor to evaluate the suitability of the instrument for the intended application and to uncover problems, resulting from refractive effects or loss of coherence, associated with the environment. Measurements were made with the laser anemometer scattering volume located on the centerline of the exhaust jet at selected distances ranging from 6.4 to 229 millimeters from the combustor nozzle exit. The combustor was operated at a nominal pressure of 240 kilopascals (35 pounds per square inch, absolute), an air inlet temperature of 650 to 870 K, and fuel-air equivalence ratios of 1.6 and 2.6 for the results described here. A typical run lasted 30 to 60 seconds, during which time particle size and velocity information was obtained on more than 1000 particles.

The spread in the measured particle diameters and speeds was large; in particular, there were large particles moving at much higher speeds than expected. Figure 7 contains plots of the average diameter, the average particle speed, and the attenuation coefficient at selected distances from the nozzle for an equivalence ratio of 1.6. In the first 50 millimeters, the speed of the particles increased from 260 to 820 meters per second; this is the region of accelerating flow. The particle speed then decreased with increasing distance to 528 meters per second, the lower limit of the instrument. The particle diameter increased in the first 50 millimeters from the nozzle, decreased for about 100 millimeters, and then increased again farther downstream.

Since small particles accelerate faster and slow down faster than large particles, and so enter or leave the velocity selection window at different times, the size distribution will be skewed to the smaller-sized particles near the nozzle and to the larger-sized particles at greater distances. This is clearly the case at distances greater than 125 centimeters from the noz-

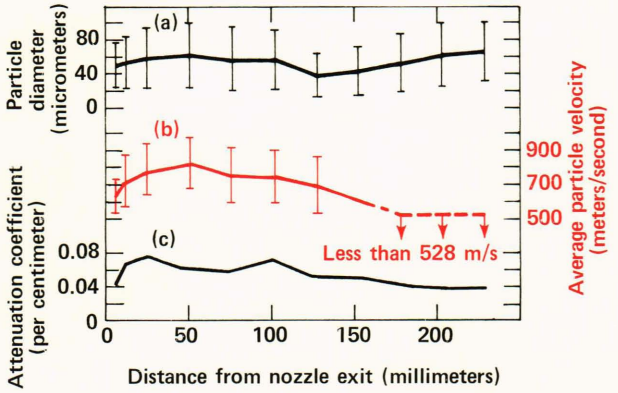

Figure 7 — The average values of the measured (a) diameter, (b) speed, and (c) attenuation coefficient, plotted as a function of distance from the exhaust nozzle for an equivalence ratio of 1.6.

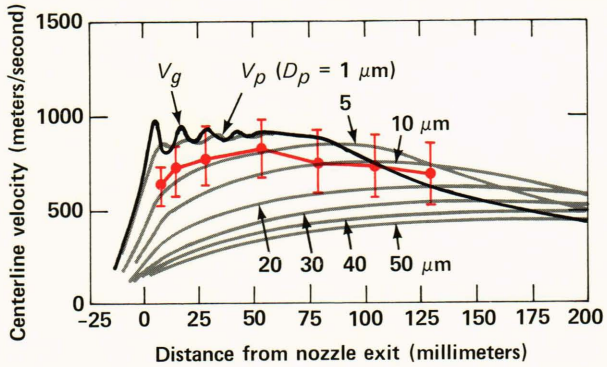

Figure 8 — Computed particle velocities for selected particle size (D_p) as a function of distance from the nozzle. The combustor pressure is 254 kilopascals, (37 pounds per square inch, absolute) and T_C = 2800°R. Velocity data for an ER of 1.6 are plotted in color.

zle. The slower particles drop below the minimum speed for which their diameter can be measured before the faster large particles do, resulting in more large particles being measured than small particles and so giving a larger average particle diameter. In general, the fluctuations of the transmitted signal increased with distance from the nozzle.

Wide variations in the particle count were observed, particularly at the greater distances; the average was about 40,000 counts per second at all positions. The number density of particles greater than about 1 micrometer was 70 particles per cubic centimeter at 12.7 millimeters from the nozzle; the value increased to 140 particles per cubic centimeter at 229 millimeters. The attenuation coefficient varied from 0.04 to 0.08 per centimeter as the distance increased from 6.4 to 229 millimeters. The large attenuation coefficient indicates that most of the particulate mass is carried by particles of less than 1 micrometer.

The results at an equivalence ratio of 2.6 were similar and consistent with those obtained at an equivalence ratio of 1.6. The maximum velocity was slightly lower (780 meters per second at 50 millimeters) and dropped off more rapidly. The attenuation coefficient was about twice that measured at the lower equivalence ratio (0.14 relative to 0.08) at the larger values, multiple scattering is becoming important. The particle count rate was approximately constant at 100,000 counts per second.

The difference between the particle velocity and the velocity of the flowfield can also be used to estimate the size of the particles in the flow. The velocity of a given size spherical particle (V_p) in a flowfield of velocity V_g was calculated using the model of Ref. 7. The model describes single particle flow in a supersonic nozzle where the particle drag coefficient is determined empirically. The gas velocity distribution was obtained as follows. For the region upstream of the nozzle exit, the one-dimensional isentropic flow equations based on the local flow cross-sectional area were used; for the near flow region downstream of the nozzle exit, V_g was obtained from a pitot probe survey of the unheated airflow. At distances of more than 90 millimeters from the nozzle, the free-circular jet approximation ($V_g \approx 1/x$) was used. The peaks in the V_g curve are related to the location of the oblique shock waves.

Figure 8 shows the computed particle speeds as a function of distance from the nozzle for spherical fuel drops 1 to 50 micrometers in diameter and for a combustor pressure of 254 kilopascals (37 pounds per square inch, absolute). In the shock region, particles larger than a few micrometers lag the gas velocity by a considerable amount. The measured velocity data for an equivalence ratio of 1.6 are also plotted on Fig. 8; they fit particles 5 micrometers or less near the nozzle and even larger particles at greater distances.

The discrepancy between the average particle size derived from the velocity lag and the laser anemometer measurements is too large to be explained by experimental error or approximations in the calculations. Since the combustor is being operated in a fuel-rich condition, most of the large particles observed are in all likelihood unburned fuel drops. The drops would be deformed into flattened, high-drag objects as they are accelerated through the nozzle and would probably break up into a large number of smaller drops, as has been observed under similar conditions, but at much lower speeds, by others. Breakup of the fuel drops can be expected when the Weber number exceeds 10 to 20. The Weber number is defined as:

$$W_e = U^2 D_p \rho_g / \sigma \qquad (3)$$

where U is the velocity of the particle relative to the flow velocity, σ is the particle surface tension, D_p is the particle diameter, and ρ_g is the gas density. At 6.4 millimeters from the nozzle, the calculated Weber number for a 50-micrometer drop of jet fuel (JP-5) is 288, far in excess of the breakup value. The large number of smaller particles after breakup scatter more energy. The actual scattered signal depends on

the number of particles in the field of view of the laser anemometer. One 50-micrometer particle is equivalent in volume to one thousand 5-micrometer particles, while only ten 5-micrometer particles are needed to give the observed signal. It is not unlikely, then, that a cluster of 10 particles, all moving at the same high speed, is in the scattering volume at one time and appears to the instrument as a single large particle.

The results of these tests indicate that the instrumented laser anemometer can be used to measure the size and speed of large solid particles in high-speed flows. However, the simultaneous measurement of size and speed indicated that particles with large measured diameters were moving faster than expected. These "large" particles are probably a number of small particles moving together in a cluster that remains after the breakup of the initial large fuel drops or the coalescence of the small drops. While the breakup of fuel drops is advantageous for their later combustion, the presence of clusters of small particles appearing to be large particles makes the interpretation of the results more difficult. The simultaneous measurement of particle size and speed is essential where particle breakup appears likely. Additional measurements with optical techniques specifically designed to measure clusters of small-size particles are required to confirm these conclusions.

COHERENT ANTI-STOKES RAMAN SCATTERING

Turning our attention from light scattered by particles to light scattered by molecules, the most common processes are illustrated in Fig. 9. Incident photons at frequency ω_0 interact with molecules and are scattered over 4π steradians with elastic and inelastic components. The elastic scattering, referred to in the past as Rayleigh scattering, is the phenomenon that results in the blue appearance of the sky and the red sun at sunrise and sunset (because shorter wavelength blue light is scattered more than red). Because the process is elastic, the scattered light is of the same frequency as the incident light; it is not specific to the molecule causing the scattering. Thus, the technique can be used for total density measurements but not for individual species concentrations.

The inelastic scattering of light by molecules is known as spontaneous Raman scattering and is termed rotational, vibrational, or electronic, depending on the nature of the energy change that occurs in the molecule. As illustrated in Fig. 9, Raman scattering consists of weak components at fixed frequency separations on both sides of ω_0. The frequency separations are related to the characteristic frequencies of the molecule, as for example, the vibrational frequency, ω_v, in Fig. 9. The Raman component that is displaced toward a longer wavelength is known as the Stokes band (ω_s) and that toward a shorter wavelength as the anti-Stokes band (ω_{as}). These bands are the result of a true scattering process; i.e., the incident photons are not absorbed and re-emitted as in

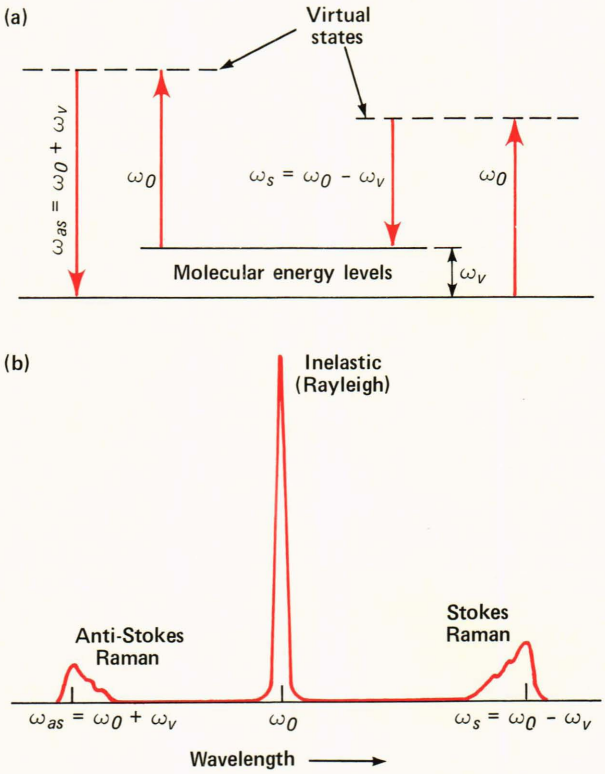

Figure 9 — Spontaneous Raman scattering. (a) Energy level diagram and (b) spectrum. The intensities are not to scale; the Raman bands are actually much weaker.

fluorescence. Hence, any incident wavelength can be used, although visible radiation is preferred because of the high sensitivity of detectors in the visible region and the fact that the intensity of the Raman scattering scales as ω_0^4. In vibrational Raman scattering, the interaction between the radiation and the sample depends on the vibrational modes of the molecule and is, therefore, species specific. Because the energy distribution in the vibrational modes depends on the molecular temperature, the spectral distribution of the Raman scattering can be used to measure the gas temperature, which is assumed to be equal to the molecular temperature. In addition to the ω_0^4 dependence, the Raman scattering intensity is linearly proportional to the species number density and the power of the incident laser.

Unfortunately, spontaneous Raman scattering is a very weak effect and usually is not amenable to practical combustion diagnostics. However, the advent of high-power lasers made it possible to devise new Raman processes that result in larger signals. One such process is coherent anti-Stokes Raman scattering (CARS). Although CARS was discovered in the early '60s,[8] it was not until the mid-seventies when high-peak-power tunable lasers became generally available that investigations of the technique became widespread. Numerous experiments in CARS have been conducted on laboratory flames,[9-11] and intensive work is in progress at various development labo-

ratories to use it as a nonintrusive probe of jet engines.

In CARS two laser beams at the frequencies ω_1 and ω_2 interact with the sample molecules in a nonlinear manner to generate a new coherent beam at frequency $\omega_3 = 2\omega_1 - \omega_2$, as illustrated in Fig. 10. When the frequency difference $\omega_1 - \omega_2$ is close to the vibrational frequency, ω_v, of a Raman active mode, the magnitude of the CARS signal at ω_3 becomes very large. The incident beams, however, must be aligned so that the nonlinear interaction is properly phased. In gases, phase matching can occur when the beams are collinear. Although this is easy to produce optically, the interaction length is rather long, leading to poor spatial resolution. The problem is overcome by separating the incident beams and crossing them at the correct phase-matching angles.

A narrowband laser at a fixed frequency is used to generate ω_1, and, since $\omega_1 - \omega_2$ must be varied to coincide with a molecular resonance, ω_2 must be obtained from a tunable source such as a dye laser. There are two methods of tuning ω_2 to generate the CARS spectrum. In one, ω_2 is generated from a narrowband dye laser, and the CARS spectrum is obtained by scanning the dye laser frequency and using a single channel detector. In the other method, ω_2 is generated from a broadband dye laser and the entire CARS spectrum can be obtained simultaneously for several species using a multichannel detector. Although the latter approach is not as sensitive, it allows fast time-resolved measurements to be made on fluctuating phenomena.

The CARS instrument being tested at APL is modeled after that developed by Eckbreth at the United Technologies Research Center.[10,12] A schematic of the optical configuration is shown in Fig. 11. A frequency-doubled Nd:YAG laser is used to generate the primary beam (ω_1) at a wavelength of 532 nanometers. Because frequency doublers are not 100% efficient, there is residual 1064-nanometer radiation from the laser that can be utilized by passing it through a second frequency doubler (KD*P crystal). This additional 532-nanometer beam pumps a dye laser that produces a broadband output centered at ω_2. The dye laser beam and the pump beam are adjusted to the same diameter using Galilean telescopes, ensuring optimum focusing of the beams. (The prisms and half-wave plates are used in polarization-dependent experiments.) The pump beam is split into two components that can be directed independently to the focusing lens; a rotatable optical flat allows for minor steering of the dye laser beam. This

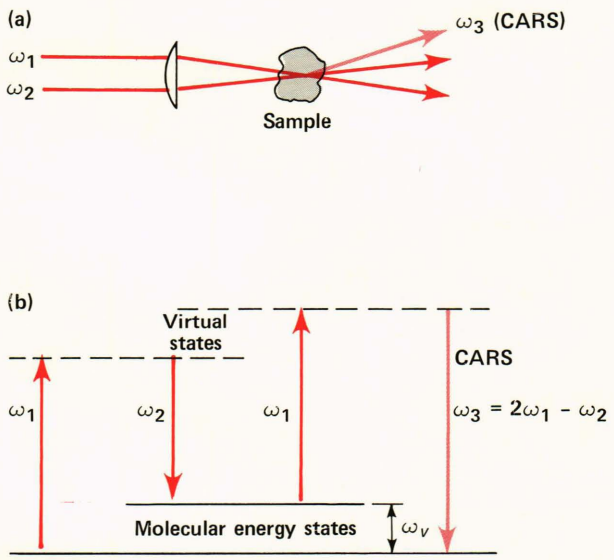

Figure 10 — Coherent anti-Stokes Raman scattering. (a) General approach and (b) energy level diagram.

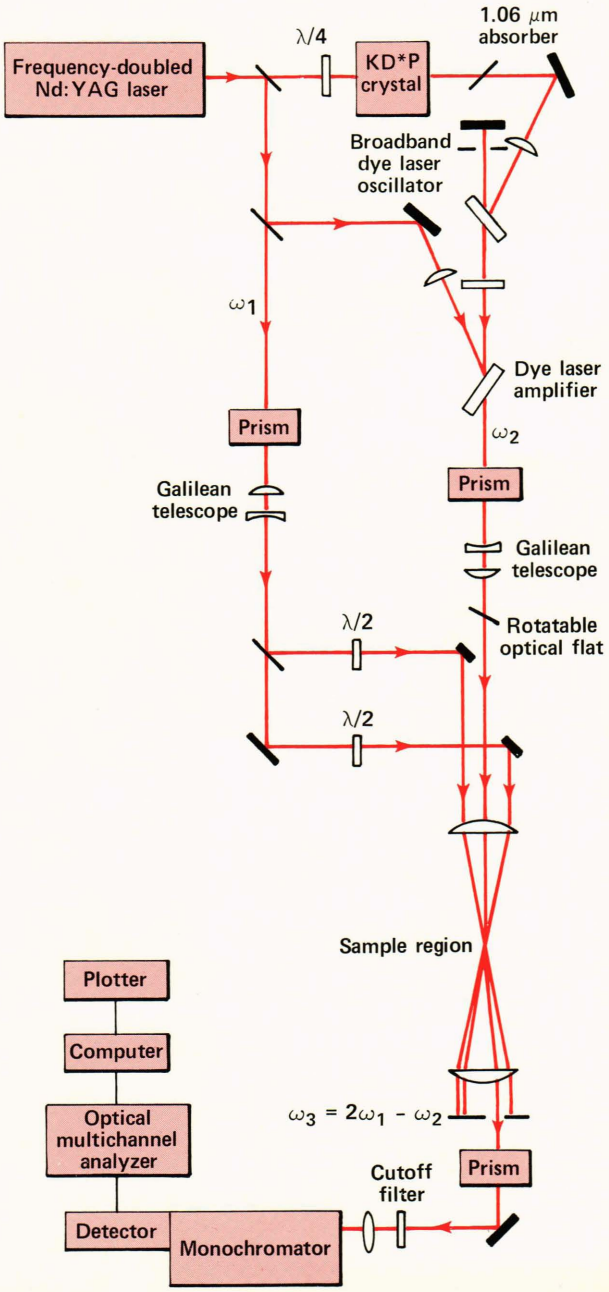

Figure 11 — Schematic of CARS system.

enables the beams to be aligned at the proper angles for phase matching, while achieving good spatial resolution in the focal region. After being focused into the medium, the incident beams and the newly generated CARS beam are recollimated by a collection lens. The CARS beam, which is spatially separated from the other beams, passes through an aperture and a cutoff filter and is then detected by an optical multichannel analyzer.

From a systems standpoint, spontaneous Raman scattering has several advantages over the CARS technique, the most important being that it is much simpler in both optical layout and interpretation of data. The relationship between the Raman signal and the species concentration and temperature is straightforward. The spatial resolution, approximately 20 micrometers for lenses of moderate focal length, is excellent. Unfortunately, those advantages are often outweighed by low sensitivity and, especially in combustion applications, by background luminosity and laser-induced interferences such as fluorescence and particulate incandescence. The CARS technique, although much more complex than the spontaneous Raman method, overcomes most of the disadvantages of the latter when probing combustion processes. CARS is a rather strong process that results in signal levels many orders of magnitude larger than those from spontaneous Raman scattering. Because the CARS radiation is itself essentially a laser beam, all of it can be collected. On the other hand, in spontaneous Raman scattering the photons are scattered over 4π steradians and are collected only over a limited solid angle. A more important consequence of the coherent nature of the CARS radiation is that it can be spatially separated (normally with just an aperture) from the incident pump beams, and elaborate double monochromators are not required. Because only a very small solid angle is required to collect all of the CARS radiation, interferences from background luminosity and laser-induced particulate incandescence are small. Furthermore, the CARS beam is in a spectral region (the anti-Stokes region) that is free of laser-induced fluorescence.

Despite all of the significant advantages of CARS, there are a few disadvantages. Although the signal is rather intense, the sensitivity is limited by interferences from the nonresonant background. Polarization-dependent experiments have recently been used to suppress this background but at a cost of losing some of the desired CARS signal. The spatial resolution is not as good as in spontaneous Raman scattering, with typical interaction regions 1 millimeter long and 0.2 millimeter in diameter. Another disadvantage is the complex dependence of the CARS signal on species concentration and temperature; that dependence requires extensive analysis and calibration.

The initial work on CARS at APL has used the technique to measure the concentration of gaseous species near a hot graphite surface in various oxidizing environments. The experimental results will be used to improve the theoretical procedure for predicting the amount of material loss resulting from ablation in supersonic ramjet combustors. Preliminary measurements using the existing ablation apparatus were encouraging in that carbon monoxide produced during the oxidation of graphite was detected with moderate spatial resolution. It should be noted that spontaneous Raman scattering could not be used in this application because of the extremely bright incandescence from the hot graphite surface. However, the entire CARS signal can be collected using small solid-angle optics, which eliminated most of the incandescent background. Improvements to the ablation apparatus and the CARS system are in progress so that accurate measurements of species concentration can be made as a function of distance above the ablating surface.

CONCLUSIONS

Because of their nonintrusive nature, fast time response, and high spatial resolution, optical measuring devices are attractive for measuring complex and unstable combustion flowfields. Because of their limitations, however, their application must be scrutinized carefully, and they must be well calibrated and adapted to the environment. The importance of these points was clearly demonstrated in the application of a laser anemometer for particle sizing.

REFERENCES

1. W. M. Farmer, "Measurement of Particle Size, Number Density and Velocity Using a Laser Interferometer," *Appl. Opt.* **11**, 2603 (1972).
2. W. M. Farmer, "Observations of Large Particles with a Laser Interferometer," *Appl. Opt.* **13**, 610 (1974).
3. W. M. Farmer, "Visibility of Large Spheres Observed with a Laser Velocimeter: A Simple Model," *Appl. Opt.* **19**, 3660 (1980).
4. D. Holve and S. A. Self, "Optical Particle Sizing for in Situ Measurements," Parts 1 and 2, *Appl. Opt.* **18**, 1632 (1979).
5. F. Durst, "Review-Combined Measurements of Particle Velocities, Size Distributions, and Concentrations," *J. Fluids Eng.* **104**, 284 (1982).
6. G. Grehan and G. Gouesbet, "Mie Theory Calculations – New Progress, with Emphasis on Particle Sizing," *Appl. Opt.* **18**, 3489 (1979).
7. W. J. Yanta, "Measurements of Aerosol Size Distribution with a Laser Doppler Velocimeter (LDV)," in *Aerosol Measurements,* NBS special publication 412, pp. 73-88 (7 May 1974).
8. P. D. Maker and R. W. Terhune, "Study of Optical Effects due to an Induced Polarization Third Order in Electric Field Strength," *Phys. Rev.* **137A**, 801 (1965).
9. W. M. Tolles, J. W. Nibler, J. R. McDonald, and A. B. Harvey, "A Review of the Theory and Application of Coherent Anti-Stokes Raman Spectroscopy (CARS)," *Appl. Spectrosc.* **31**, 253 (1977).
10. A. C. Eckbreth, P. A. Bonczyk, and J. F. Verdieck, "Combustion Diagnostics by Laser Raman and Fluorescence Techniques," *Prog. Energy Combust. Sci.* **5**, 253 (1979).
11. G. L. Eesley, *Coherent Raman Spectroscopy,* Pergamon Press, New York (1981).
12. A. C. Eckbreth, "BOXCARS: Cross-Beam Phase-Matched CARS Generation in Gases," *Appl. Phys. Lett.* **32**, 421 (1978).

ACKNOWLEDGMENTS – We would like to acknowledge the assistance of the following people in the various aspects of this work: R. A. Murphy and S. Favin of the Research Center in the particle sizing experiment; J. Funk and C. E. Stevens of the Propulsion Research Laboratory in the actual combustor measurements in the test cell; and H. Y. Chiu in the CARS experiments on graphite ablation. We would also like to thank A. C. Eckbreth of the United Technology Research Center for help in the design of the CARS system and R. Antcliff and O. Jarrett of NASA Langley for help in the initial checkout of CARS.

H. J. Unger

Knowledge of the performance of rockets requires carefully documented research of their exhaust gases. This is being done, in a high-velocity wind tunnel developed at APL, by infrared spectroscopic analysis of the composition and temperature of gases flowing from a burning solid-propellant rocket. This method of testing under severe environmental conditions uses a specially modified spectrometer and associated recording equipment so ruggedly constructed and mounted as to maintain the requisite optical alignment.

Development of INFRARED SPECTROMETER for Rocket Gas Analysis

A high-velocity wind tunnel using a solid-propellant rocket as a source of gas was developed several years ago in the Fluid Mechanics Group of the Research Center by F. K. Hill and H. A. Wallskog. This type of rocket was used because it was a convenient source of high-temperature gas for studying the dynamics of high-speed gas flow through the supersonic portions of a nozzle. Associated with this effort has been a program to develop apparatus and a technique for determining rocket exhaust gas composition without disturbing the gas flow. The usual probe method is not satisfactory since, when a sampling probe is introduced into the stream, the temperature and pressure increase and new conditions exist, so that the sample actually taken does not have the same composition it had in the free stream. Of particular interest is to establish at what position in the nozzle the chemical reactions begin to lag behind the expansion process. Experimental departure from equilibrium theory can be expected at about 1500°K and 100 psia, i.e., very close to the throat of the nozzle for the present rockets.

Since three of the exhaust gas components (CO, CO_2, and H_2O) are active in the infrared region without serious overlapping of their bands, it was believed practical to use infrared spectroscopy to determine the gas composition; it was also hoped that temperature determinations could be made in this way. Rugged equipment that will withstand the vibration of the rocket has now been developed for this application, and some quantitative results have been obtained.

The Rocket

The rocket grain used is a double-base solid-propellant (cellulose nitrate dissolved in nitroglycerin) developed and proof-tested by the Allegany Ballistics Laboratory. The gases produced

during burning are typically those common to most high-impulse rockets, namely, CO, CO_2, H_2, N_2, and H_2O. (The absorption bands of a number of the oxides of nitrogen have been observed during and after the tests.) The combustion chamber pressure and temperature have been found to be approximately 1100 psi and 2500°K, respectively. With end-burning, a 25-lb charge lasts 10 sec and gives relatively constant flow conditions for 9 sec. The composition of the product gases is assumed to be governed at high temperatures and pressures by the water-gas reaction $CO + H_2O \rightleftarrows CO_2 + H_2 + 9.6$ kcal.

Equipment Development

A diagram of the rocket gas generator (enclosing the solid propellant), the expansion nozzle, tunnel, and associated test equipment is shown in Fig. 1. The combustion chamber orifice, which is the throat of the nozzle, is 0.63 in. in diameter. The nozzle has a conical expansion up to 4 in. where the cylindrical test section is attached, followed by a converging-diverging diffuser. The nozzle is made of molybdenum and is water-cooled to minimize erosion and wall-temperature effects.

One of the chief obstacles to applying infrared spectrometer techniques to a study of rocket exhaust gases is the vibration set up when the rocket is in operation. The sound level in the test building reaches the order of 150 db, and the resulting vibrations are sufficient to shake the building and its foundations; any instrumentation must, therefore, be well shock-mounted. The test cell is constructed of reinforced concrete and is both fire- and fragment-proof. The side of the cell opposite the tunnel exhaust is open and the surrounding area is protected by an earthen parapet. The recording equipment is housed in a separate building for the safety of personnel and also for isolation from the vibration.

There is no commercial infrared spectrometer that is sufficiently rugged to operate in this environment. It was necessary, therefore, to modify considerably a conventional instrument, in this case a Perkin-Elmer Mod. 83 Monochromator, so that it could withstand the test conditions. A signal-to-noise ratio of 100 was deemed to be necessary. On each side of the tunnel is a massive table on tracks. On these tables are the light source, the collimating system, the light chopper, wavelength sweeping mechanism, and detector. The arrangement of the scanning spectrometer system and recording equipment is shown in Fig. 2. The instruments are now so ruggedly mounted that they can be transported and assembled in test position in a few minutes.

To make adequate optical and spectroscopic measurements in a nozzle, it is necessary to have observation ports of relatively constant transmission characteristics. The problem of "dirty" gas which blackens everything it reaches has been solved by recessing the window and flushing its inner surface with an inert gas such as nitrogen. If a sufficient gas flow is used to bal

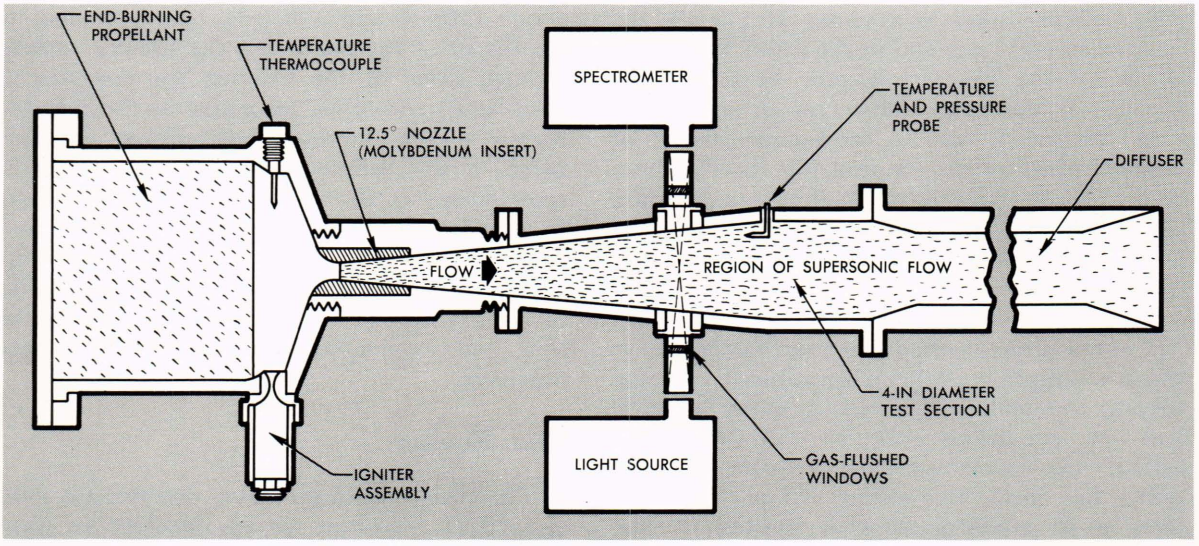

Fig. 1—Diagram of the high-temperature rocket tunnel showing arrangement of equipment for conducting spectroscopic analysis as well as for pressure and temperature measurements in the gas stream.

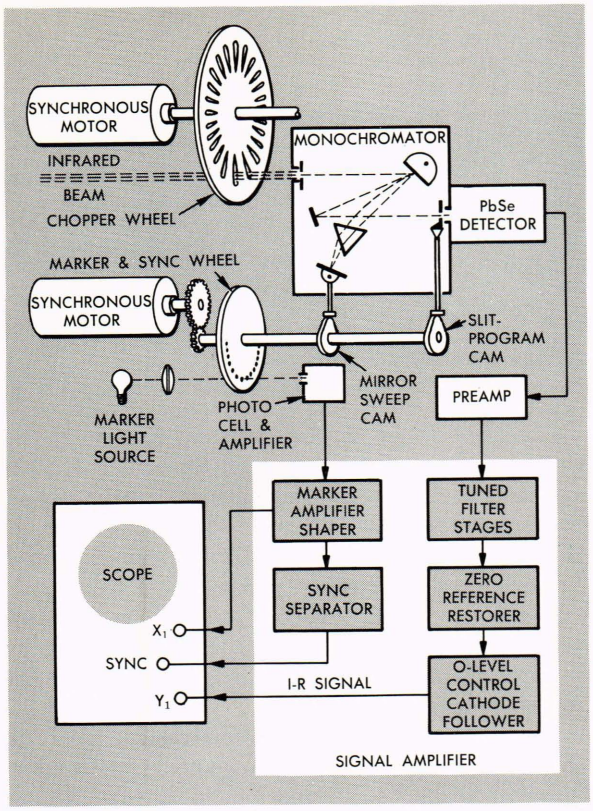

Fig. 2—Schematic diagram of the fast-scanning infrared spectrometer.

ance the nozzle pressure at the wall, no soot enters the side tube supporting the window. This flushing method has been so successful that optical windows of even such fragile, crystalline materials as rock salt and calcium fluoride have been used without damage, and twenty-five successive tests have been run in which the change in transmission factor of the cell windows was less than 1%.

The spectral region in the infrared in which CO, CO_2, and H_2O have fundamental vibration bands (at 4.25, 4.73, and 6.09μ, respectively) is suited to rapid scanning (0.7 sec per spectrum). Two high-speed detectors have been used successfully: lead selenide (PbSe) and gold-doped germanium (Au-Ge). At the liquid-nitrogen temperature (76°K) to which they are cooled, the time constant of the detectors is of the order of 10^{-6} sec. Therefore, high-speed light choppers may be used, and the advantages of AC amplifiers may be explored. Visual observations of the spectra are made on a 21-in. oscilloscope screen while recording is accomplished with a 5-in. oscilloscope and a 35-mm continuous-drive camera.

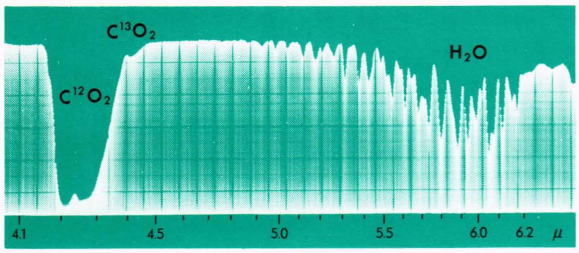

Fig. 3—Spectrogram of the atmospheric absorption in the 120-in. path of the spectrometer. Carbon 13 occurs in about 1.1% of atmospheric CO_2. Time sweep increases from right to left; total sweep time is 0.83 sec.

In order to obtain satisfactory analysis of the gases in the absorption cell, all of the light path in the spectrometer must be free from absorbing material. The spectrometer system is therefore enclosed in metal boxes and flushed with air that has been purified by passing it through activated alumina. This method removes all of the CO_2 and most of the H_2O. As a test of the potential sensitivity of this method of analyzing gases, atmospheric absorption over the entire light path of 120 in. was measured first; the results are indicated in Fig. 3. The nominal composition of the air by volume is 0.03% CO_2 and 1.8% H_2O at 50% relative humidity. In addition to showing the fundamental absorption bands of CO_2 and H_2O, this figure also shows the absorption due to the isotopic species CO_2. It is known that C^{13} occurs in 1.1% concentration in ordinary carbon, and the $C^{13}O_2$ bands should be very similar to those of $C^{12}O_2$ but shifted slightly to the long-wavelength side because of the mass difference; this shift may be observed on the spectrogram.

Results

In applying this spectrometric equipment to gases from rocket exhausts, satisfactory results have been obtained. In a typical run, Fig. 4, immediately upon ignition of the rocket it is

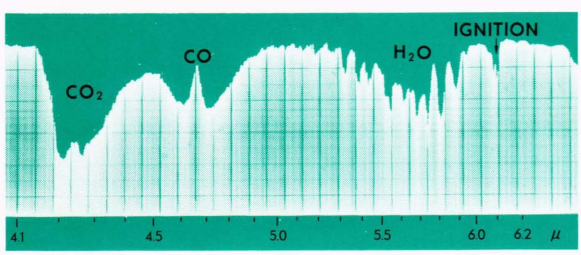

Fig. 4—Spectrogram of the first sweep of the spectrometer at ignition of the propellant.

TABLE I
INFRARED SPECTROMETER RUNS: CONDITIONS AND RESULTS
(Nozzle Angle—12.5°)

TEST NUMBER	STATION DIAMETER (in.)	MEASURED CHAMBER TEMPERATURE (°K)	MEASURED CHAMBER PRESSURE (psia)	STATIC NOZZLE PRESSURE (psia)	CALCULATED MACH NUMBER	TEMPERATURE (°K)		
						THEORETICAL	EXPERIMENTAL	
							T_{CO_2}	T_{CO}
148	2.37	2270	1050	8.22	3.64	918	917	950
150	1.86	2230	1110	14.82	3.29	1050	—	1050
154	2.37	2300	1065	7.95	3.64	918	910	—
156	1.35	2320	1100	37.50	2.68	1328	1345	1300

noticed that there is a transient phenomenon which lasts for approximately 0.01 sec and consists of a momentary decrease in transmission over the entire spectral region, sometimes followed by a short period of emission. This is caused by the luminosity of solid particles burning in the residual oxygen in the tunnel. After this transient, equilibrium is established quickly and the absorption bands for CO_2, CO, and H_2O appear as in Fig. 5, which was taken between 5 and 6 sec after ignition.

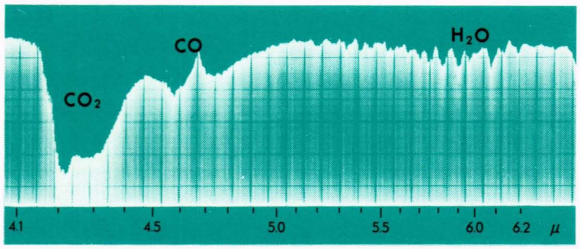

Fig. 5—Spectrogram of the seventh sweep after ignition. The 4.25 μsec CO_2 band is noticeably broadened from that in Fig. 3 owing to the high temperature (1350°K).

In making average gas temperature determinations by this method, use could be made of the separation between the maxima of the P and R branches of the CO_2 and CO absorption bands. In most of the spectrograms obtained thus far, the maxima of the branches appear to be "washed out" (as can be observed in Fig. 4) because of the presence of small amounts of N_2O and NO and some overlapping of bands caused by temperature broadening. However, in some of the spectrograms obtained most recently these branches are quite sharp and have led to the calculation of temperatures that agree reasonably well with the theoretical values. Table I summarizes the temperature calculations from the infrared data.

Several successive tests were made at most of the six stations used to date, and reproducible absorption data were obtained. The absorption path across the nozzle has been varied from 4.0 to 1.35 in. and the corresponding pressure varied from 1.8 to 38 psia. Since the percentage absorption at a particular wavelength is a function of the product of the path length and the density, it turns out that the absorption due to each gas or vapor increases as the stations advance toward the nozzle throat. The observed absorption data are consistent with this.

This exploratory work has shown that the "ruggedized" equipment developed and the techniques employed can be used satisfactorily in the severe environmental conditions present during operation of a rocket motor. The results obtained suggest that this equipment may be useful, when fully developed, in obtaining quantitative analysis and temperature determinations of exhaust gases from rocket propellants.

JAMES L. KEIRSEY and RICHARD T. CUSICK

AUTOMATED AIRBREATHING PROPULSION TEST FACILITIES

The development of airbreathing propulsion systems requires ground test facilities that provide true simulation of flight Mach number, altitude, and angle of attack for testing full-scale engines and components. These facilities must therefore have large systems for the storage and supply of air to the test article, and the air heaters and exhaust systems are powered by the discharge of large heat-energy sources during brief test runs. APL's Propulsion Research Laboratory and other such facilities require automated systems for accurate control and repeatibility of test conditions, and high-speed data aquisition systems.

THE PROBLEM

Early in the development of a new engine concept, great emphasis is placed on analytical evaluation of the engine cycle and its components to narrow the choice of design options to those most attractive for further development. Repeated ground testing, although expensive and difficult, is the necessary next step because it is not generally possible to model analytically all the engine's physical phenomena from first principles. This is especially true for new, high-speed (hypersonic) engines where the state of the art in most technical disciplines (fluid dynamics, combustion, materials, etc.) is pushed beyond conventional bounds. Thus, the importance of ground testing is underscored.

Flight simulation on the ground can be a complex undertaking. With the test engine mounted rigidly to the ground, flight is simulated by placing the engine in a high-speed air jet that produces the proper conditions of velocity, pressure, and temperature both external and internal to the engine. To produce this jet, air from a high-pressure and high-temperature supply is expanded through a supersonic (or hypersonic) nozzle. Consistent with the conservation of energy, when air at conditions of high supply pressure and temperature is expanded to the desired supersonic velocity, the proper conditions of local static pressure and temperature are produced to simulate the desired altitude. Ground test facilities therefore must have capacities for compressing, storing, and heating large quantities of air and must be provided with control systems to supply the proper flow for these large jets. In addition, there must be systems to supply fuel, water, exhaust suction, etc.

SIMULATION REQUIREMENTS

True simulation of flight conditions in a ground test facility involves reproducing Mach number, altitude, angle of attack, and flight duration with a full-scale engine. The engine must be tested full scale because combustion phenomena that involve turbulent mixing and chemical reaction kinetics are not amenable to scaling. Individual engine components, such as air inlets and diffusers, may be tested part scale if the Mach numbers and Reynolds numbers are properly simulated.

The facility requirements for engine testing are related to flight conditions as follows:

1. Mach number and altitude. The facility must produce the correct air velocity, total pressure, and total temperature. The velocity requirements determine the needed overall pressure ratio for the facility.
2. Angle of attack. (a) For free jet tests, the proper angular orientation of engine-air inlet to air-jet axis is required. (b) For direct-connect tests, the airflow profile into the test engine duct must be simulated.
3. Flight duration. (a) Prove-in tests of flight-weight components require full duration testing and possibly simulation of flight trajectory (altitude and Mach number as a function of time). (b) The development of optimum engine/combustor configurations is usually done with heavyweight test hardware and involves short run times, rapid data acquisition rates, and highly reproducible conditions for repeated testing.

The principal simulation requirements therefore relate to the mass flow rate and temperature of the air supply and to the evacuation pressures of the facility versus time. If the engine is not axisymmetric, angle-of-attack simulations may include both pitch and yaw.

PRIMARY FACILITY SYSTEMS

Any propulsion ground test facility (such as the APL Propulsion Research Laboratory described later) will have similar systems to meet testing re-

quirements, although designs may differ according to the state of the art and the availability of materials at hand. Air is stored in steel tanks at high pressure (typically 2000 to 10,000 pounds per square inch) and the airflow rate is regulated by control valves to the pressure and mass flow rate required for simulation.

The air temperature is raised to the required value by means of in-line heaters using either thermal storage or chemical or electrical energy, depending on the air temperature required. These types of air heaters are illustrated (along with various engine test arrangements) in Figs. 1 to 3. A thermal storage type heater such as that indicated in Fig. 1 is used where process air temperature up to 1000°C is required to simulate moderate supersonic flight speeds (Mach 2 to 3.5). This heater uses a storage medium such as a metal or ceramic matrix that is heated over a period of several hours by means of a gas- or oil-fired burner, and the process air is then passed through the medium during test operation. A second type, illustrated in Fig. 2, is the chemical heater, which uses in-stream combustion of a fuel such as propane or hydrogen either to boost the temperature from a partially heated condition or to heat completely the process air to temperatures between 1000 and 2000°C. This heating technique permits the simulation of higher supersonic flight speeds (Mach 3 to 5). Since this mode of heating adds combustion products to the air, additional oxygen is added to the stream to reestablish the same mole fraction of oxygen as in atmospheric air. An electric arc heater such as that indicated in Fig. 3 is generally used for hypersonic flow simulation (Mach 5 and above), where the arc is in direct contact with the flow stream and air temperatures of up to 3000 and 4000°C are produced.

Altitude simulation may be provided by an exhaust system that evacuates the test chamber to low pressure by means of a steam ejector system that uses the momentum exchange principle. Energy for this system may be stored in the form of hot water that is flashed to steam, as required, during test operation.

The operation of a facility such as that described above is based upon the "blowdown principle," wherein the various forms of energy (i.e., high pressure air, heat, electrical energy, steam, etc.) are accumulated over a relatively long period of time (typically several hours) and discharged rapidly during a test run, typically seconds or minutes in duration.

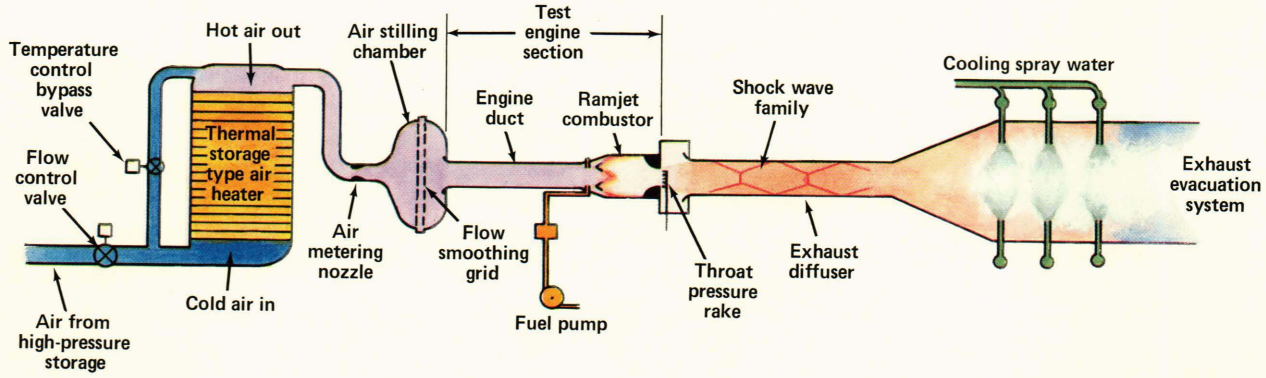

Figure 1 – A subsonic combustor being tested in direct-connect mode to determine performance. To simulate flight engine internal flow conditions, high-pressure air from the facility air storage is heated as it flows to the engine with a thermal-storage type air heater. Supersonic flight speeds in the Mach 2 to 3.5 range can be simulated using this technique.

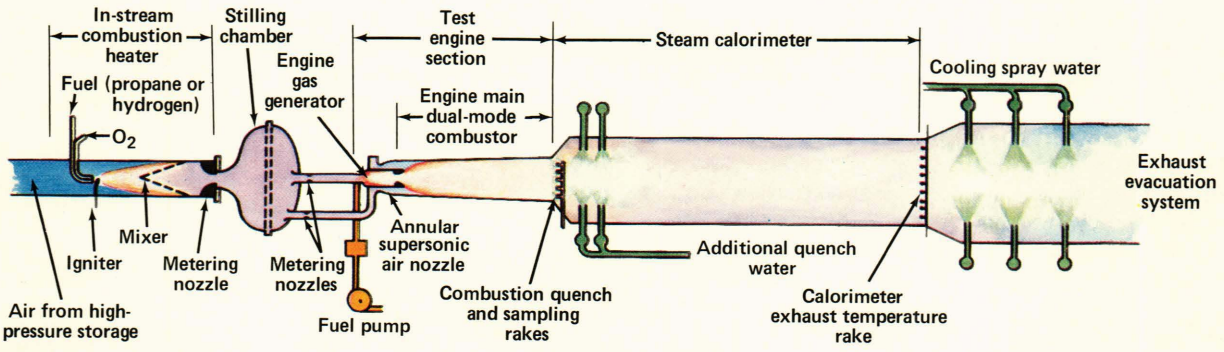

Figure 2 – A higher speed ramjet, known as a dual-mode (subsonic/supersonic combustion) ramjet, being tested in direct-connect mode to determine performance. The engine cycle shown was invented at APL and is a dual-combustor type of dual-mode ramjet. It uses a small gas generator (which uses a small portion of the engine airflow) embedded in the forward end of the main dual-mode (subsonic/supersonic) combustor to pilot the process. The in-stream combustion heater permits simulation of flight speeds up to Mach 5.

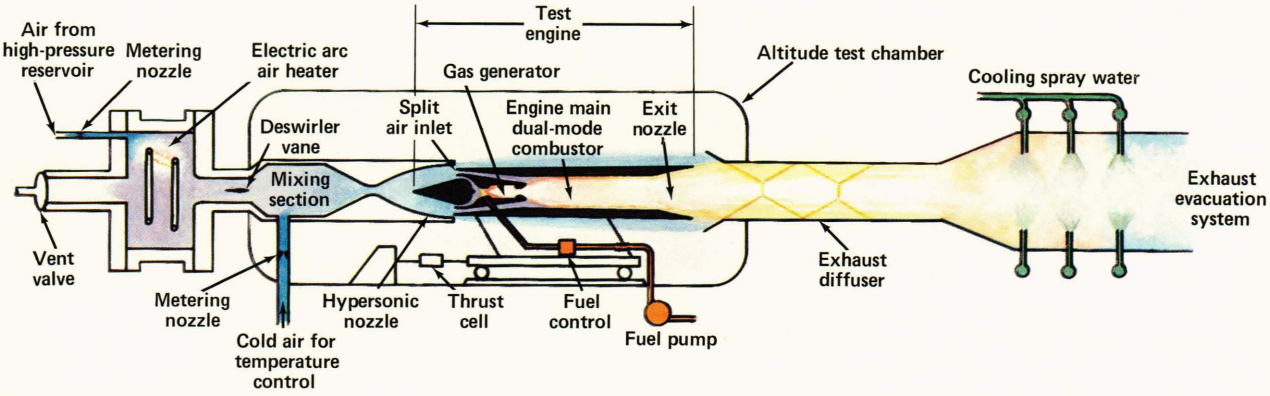

Figure 3 – A complete hypersonic dual-combustion ramjet engine, mounted on a thrust stand in a sealed test cabin to simulate high altitude, being tested in a free jet to determine performance. Note that an appreciable quantity of airflow is spilled around the engine to ensure proper simulation of air inlet flow conditions. An electric-arc heater can produce air temperatures as high as 4000°C, simulating flight up to Mach 10 in the atmosphere.

Blowdown testing operations are sometimes more practical than continuous supply test modes because of the lower demand for peak power, but they place severe constraints on testing operations because of the short test duration. Such constraints are partially mitigated by the use of automatic controls, which provide rapid, precise changes in test conditions so that more conditions are tested per run.

Figures 1 to 3 also indicate several types of airbreathing engine ground tests. Figure 1 depicts the facility to test the combustor for a subsonic combustion ramjet in a "direct-connect" mode. Each individual engine component (air inlet, combustor, exit nozzle, and fuel system) is developed first in separate tests, followed by validation of the overall engine operation in a free jet test. The direct-connect mode of operation is less demanding of the facility capabilities (flow and pumping pressure ratio) than an engine free jet test and is used in the extensive tests that are needed to optimize the combustor design (flameholders, fuel injectors, igniters, etc.). Combustor performance in this configuration is determined from measurements of total pressure using a rake at the exit-nozzle throat, or by measuring engine static pressures or thrust with the use of a thrust stand. Engine mass flow is determined from the upstream metering nozzle. The engine exit nozzle is simulated only to the sonic throat for two reasons: (a) it facilitates the measurement of the engine exit stream thrust by having a known (Mach 1.0) condition at the exit plane, and (b) it eliminates the need to know the thrust efficiency of the supersonic portion of the exit nozzle in evaluating combustor performance. The thrust efficiency of the supersonic portion of the exit nozzle is determined from separate tests.

The exhaust products from the engine are evacuated through the facility exhaust system. They are first passed through an exit diffuser, which acts as an exhaust pump by converting the kinetic energy associated with the high-speed exit jet to potential energy (higher pressure) through a series of shock waves. The exhaust combustion products are then quenched and cooled by a water spray system. Following this, the exit stream passes through other stages of facility exhauster pumps, usually steam-driven ejectors, before being discharged to the atmosphere.

Figure 2, in contrast to the setup in Fig. 1, depicts a direct-connect arrangement for testing the combustor for a higher speed ramjet, known as a dual-mode (subsonic/supersonic combustion) ramjet. The particular engine cycle shown was invented at APL and is known as a dual-combustor type of dual-mode ramjet. It involves the use of a gas generator (a small subsonic dump combustor using a small part of the engine airflow), embedded in the forward end of the main dual-mode (subsonic or supersonic) combustor, to pilot the process. The engine may operate either in a subsonic combustion mode, which is optimum for moderate supersonic speeds (Mach 3 to 5), or in a supersonic combustion mode, which is more effective for higher speeds (above Mach 5).

Although the use of this dual-mode propulsion cycle permits a single airbreathing engine to operate efficiently over a broad Mach number range, it presents a more difficult problem in ground testing for performance evaluation than the subsonic combustion ramjet, because the exit of the combustor will not necessarily have a known sonic (or choked) flow plane. For a supersonic combustion engine, the combustion efficiency as well as a representative average stream Mach number must be determined at the combustor exit plane to obtain stream thrust. These properties, together with known engine mass flow rates, are sufficient to define combustor performance but involve special measuring techniques. To make such measurements, the supersonic combustion process is quenched at the combustor exit plane by an appropriately designed water injection rake, as indicated in Fig. 2. The combustion gases are cooled by flashing this water to steam, and a careful heat balance is performed on the "steam calorimeter" to determine the gas enthalpy at the supersonic combustor exit plane. The process requires an accurate evaluation of total enthalpy of the entire stream (exhaust gas plus water

vapor) at the calorimeter exit plane. The water injection must be carefully controlled to produce a temperature high enough to ensure that all the water within the calorimeter is vaporized.

This calorimetric information, together with measurements of all other system enthalpies (inlet air, cooling water, fuel, etc.), permits the determination of combustion efficiency. The adiabatic flame temperature at the exit plane of the supersonic combustor can then be approximated, assuming average gas properties (specific heats). Gas sampling is helpful in defining the constituent products. To obtain the combustor exit Mach number, "representative" pressures are measured at that plane using rakes that sample across the stream. This is a difficult undertaking, and much development testing is required to evolve appropriate probe designs and suitable probe locations within the stream that do not interfere with the supersonic combustion process being measured.

Figure 3 depicts a complete dual-combustion ramjet engine being tested. Here the engine is placed in a sealed test cabin, with the engine inlet immersed in a supersonic free jet that simulates high-speed flight in the atmosphere. The quantity of airflow required for testing a complete engine is greater than that passing through the engine because in producing a realistic flow field at the air inlet much of the air in the jet is spilled around the engine. A shock system is formed by the flow at the inlet, such as that shown in the spark photograph (Fig. 4). All engine internal flow characteristics (aerodynamics and combustion) properly simulate free flight, and overall performance is measured with a thrust stand. Many detailed measurements of pressure, temperature, fuel flow rate, heat flux, etc. are also made within the engine and are used to analyze the operation of engine components. The exhaust system must have the capacity to pump the total exhaust mass flow (including water vapor) from a low pressure in the sealed test cabin (corresponding to the required test altitude) to an atmospheric final-discharge condition.

Other engine components such as air inlets and fuel systems and portions of the vehicle structure (radomes, inlet leading edges, engine tailpipe and exit nozzles, etc.) are tested and developed individually. Figure 5, which shows a radome being tested under conditions that simulate a Mach 8 flight, indicates the severe aerodynamic heating at hypersonic speeds.

The requirement for repeated ground testing for the development of advanced propulsion systems also places emphasis on proper facility control system design so that test conditions can be reproduced accurately. Great emphasis also is placed on high-speed data acquisition and real-time display of engineering data for test control and monitoring, especially for tests at hypersonic speeds, where run times are of short duration.

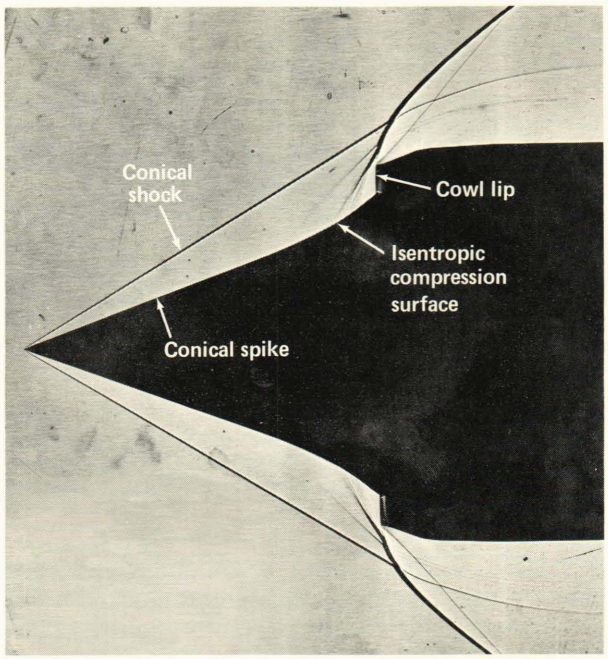

Figure 4 – An "isentropic-spike" type of air inlet operating at supersonic conditions. A conical shock is generated from the conical spike tip, followed by a series of weaker compression waves ahead of the cowl lip. High inlet efficiency is achieved in this manner. The family of weak compression waves coalesce to form a strong shock outboard of the cowl lip.

Figure 5 – A missile radome test under conditions that simulate a Mach 8 flight indicates the severe aerodynamic heating at hypersonic speeds. Other missile components such as leading edges are also developed in ground test facilities.

TESTING OPERATIONS

The simulation parameters described above are applied in a sequence of operations that is normally described as a "test" or "run." The test sequence is sometimes performed manually and sometimes automatically, but it generally will include the following steps:

Pretest Checkout

1. Test and calibrate (end-to-end simulation) all instrumentation signals and control channels.
2. Measure energy levels of all supplies:
   Air supply system
   Fuel and air heater temperatures

Steam accumulator
Fuel system(s)
Water system(s)
Battery power supply

3. Operate and check out engine fuel and ignitor systems.

Facility Startup

1. Start data acquisition, display, safety monitoring, and recording systems
2. Start airflow and bring to required flow rate
3. Start heater and set air temperature
4. Set cooling water flows to initial levels
5. Set steam ejector (altitude) vacuum level
6. Check that facility is "on the point."

Engine Startup

1. Set fuel flow to initial conditions, bypassing engine
2. Set fuel heater temperature
3. Start ignitor sequence:
   Start oxygen
   Start hydrogen
   Activate spark
   Check "ignitor lit" signal
4. Divert fuel flow from bypass to the engine
5. Check "engine lit" signal.

Sequencing of Engine and Facility Conditions

The primary variable in the engine test sequence is usually the fuel flow rate expressed as an equivalence ratio (ER), which is a ratio of the actual fuel flow to the stoichiometric rate. When the fuel flow rate is changed to a new equivalence ratio setting and stabilized, the engine controls are said to be "on the point," and data are taken before moving to the next condition. Probe sampling or injector combinations are often sequenced as well. Whenever feasible, the facility air mass flow or temperature is changed to a new set of simulated altitude and speed conditions, and the engine fuel flow rates are resequenced.

This exploration of "test space" whose dimensions are speed, altitude, and fuel flow rate is limited in magnitude and duration by the quantities of stored energy in the various facility systems (air, heat energy, steam, water, etc.). In some tests, significant savings can be made in the cost of the model and associated test hardware by using uncooled or "heat sink" combustors and hardware. In that case, the test duration is limited by the maximum permissible combustor wall temperature.

Engine and Facility Shutdown

Following the final engine sequence, the engine fuel flow is cut off and all fuel lines are purged, generally with gaseous nitrogen. The facility airflow and temperature are then sent through a programmed shutdown sequence to provide gradual cooling of the hardware, thus avoiding excessive thermal shock.

Shutdown of the facility and engine test operation may be performed in an "abort" mode, an emergency shutdown mode, or the standard shutdown mode. In any of these modes, the systems are sequenced according to a predetermined plan.

TEST OPERATIONAL PROCESSES

The various operations required as part of a propulsion test can be arranged into groups of tasks called processes. These processes can be classified according to function in a hierarchical arrangement such as that shown in Fig. 6. This arrangement of processes or something similar will be seen for various types of tests and is almost always used in propulsion tests. Task groupings such as these were originated in manual operations, where test hardware was grouped around a human operator. In those applications, interprocess synchronization was accomplished by verbal communication among the operators, each one having the equipment required for his process clustered about him. Of course, even in manual tests, certain tasks have been automated for years, but they too were clustered together under the control of an operator. When considering automation of a test operation, it is attractive to adopt this same organization for the design of the Instrument and Control System, to minimize interprocess communications at these proven functional interfaces.

Supervisory Control Process

This type of control is concerned with the scheduling, synchronization, and coordination of all the subordinate test processes. Such control can be as simple as strict synchronization, called a sequencer, or can be more sophisticated – proceeding through a simple, logical progression while receiving status feedback from the controlled processes. It may be even more sophisticated, as implemented in a "programmable

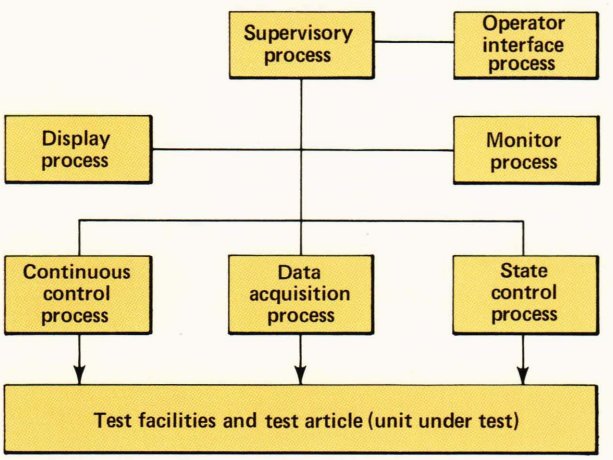

Figure 6 – Test operational processes are groups of tasks performed in real time. They are allocated to hardware in many different arrangements in actual instrument and control systems.

controller," in which case it proceeds in a preprogrammed logical progression with preprogrammed alternative sequences that can be chosen on the basis of an internal program interacting with status feedback from the controlled processes. The designs of the alternative sequences are implemented to react to any of the likely failures in the test operation or the test equipment. Such sequences would provide an automatic shutdown based on the particular fault and the test conditions at the time the fault was detected or a relight cycle might be originated if an engine "flameout" occurs early in a run.

A fully implemented supervisory control process is resident in a digital computer directs dependent processes resident in the same or in other computers. It communicates with the other processes in transactions involving the bilateral exchange of data, e.g., transmitting set point values and other process control instructions, and receiving status feedback confirming that control action has been achieved. It can respond to external events in the dependent system in a way that tends to stabilize the overall test operation and drive it to a successful conclusion, even under conditions of failure in the operation or hardware.

Continuous Control

All control processes are, by nature, temporal. However, a distinction is made between "continuous" processes and "state" control of a test. Because of hardware considerations, the continuous control process is further classified into direct digital and analog control.

Direct Digital Control. Originally, in the process control industry, supervisory control systems did not have computers in the subordinate processes; they made use of existing banks of pneumatic and electronic analog controllers for the closed loop control of individual parameters. As individual groups of electronic controllers were replaced by computers, the hierarchical relationship was often retained, but this newer type of implementation was referred to as "direct digital control," as opposed to "supervisory control," of which it was a dependent part.

As defined in this article, direct digital control uses digital techniques for the continuous control of individual parameters in a test or in the facility operation. With it, the control algorithm or transfer function for each individual parameter is resident in a central processor (computer). Its use in propulsion tests has been mainly to provide a more rapid response of gaseous flows by means of metered flow control (as with digital valves) to generate the required downstream pressure response through the use of feed-forward predictive control in connection with a simple system model. Open-loop flow control of this type gets around the limitation of closed-loop response times for major flow changes. Flow is then "trimmed" using closed-loop response. Forms of this type of control have been used for both fuel flows and process airflows at APL and elsewhere.

Analog Control. Analog control, in our context, refers to a process associated with a particular type of closed-loop control hardware used in industry. These systems (to be described below) preceded the use of computer control and are still widely used today.

In an analog control system or subsystem, there are a number of electronic amplifier controllers. Each controller is used to regulate a particular parameter to the series of "set-point" values corresponding to various test conditions.

In propulsion research, analog systems are often still used to control the temperature, pressure, and flow rate of liquids, such as water and hydrocarbon fuels, and of gases, such as hydrogen, oxygen, propane, and steam.

The electronic controllers used in these systems are designed to take manual or computer input of a set-point value, and to provide a control signal to a final control element such as a valve or positioner. The controller regulates the controlled parameter to the required value by comparing the set-point value with the measured value (feedback error). The units are called proportional integral derivative (PID) controllers because they generate a control signal that is proportional to the sum of three components: the error signal, the integral of the error signal, and the time derivative of the error signal. The proportional component of each error signal is adjusted in the initial setup of the system during the tuning process.

In supervisory control applications, set points for each loop are dictated from the supervisory control process for each test condition in the sequence, and loop status is fed back for each condition.

A typical loop status consists of three binary signals:

1. On the point. The controlled parameter is, or is not, within the allowed error band from the set point.
2. High saturation. The final control element (valve or positioner) is, or is not, nearing the open end of its control range.
3. Low saturation. The final control element is, or is not, nearing the closed end of its control range.

All three loop status signals are conditioned to ignore transient conditions such as oscillation or overshoot that could lead to an erroneous response. A typical response for an indication that a valve was almost wide open (high saturation) would be for the supervisor process to call for a new test condition at lower flows, which would permit the valve to move back to midrange operation.

State Control Process

The state control process determines the physical configuration of the facility and the test article for various test conditions. The final control elements in this process are binary in nature, so that the valves, positioners, and switches would be "on" or "off" or, in the case of steering (three-way) valves, flow would be from the normally open or normally closed

port. For fault detection and synchronization, the state of each final control element is sensed and compared with the command signal. When all of the final control elements have reached their commanded state, within the permitted operational time, the state control system is on the point.

Data Acquisition Process

In an automated facility, the data acquisition process includes the acquisition of all data and also encompasses the operation of transducers, signal conditioning, remote submultiplexers, multiplexers, and analog-to-digital converters, as well as data formatting and recording. Computer-controlled data acquisition techniques are used routinely in most modern facilities because computer control of data acquisition equipment provides the capability to specify (under program control) such items as sampling rate and sequence, channel gain, and the format for the data recording media. In addition, if the data acquisition system is coupled to the test controller, it can be commanded by the controller to provide data processing and data compression aids such as variable sampling rates, variable sampling sequences, and critical data flagging. Use of a computer can also provide a capability for post-test data processing and engineering units display of key test parameters immediately after a run. The computer can also be used as a tool for automatic pretest checkout of the data system itself.

Monitor Process

The monitor process includes the special real-time data processing required to determine actual or impending fault conditions, unsafe trends, parameters that are out of limits, and the routing of messages, data, and indicators to the supervisor process or to displays for the test facility operators.

In any test, failure of test articles in performance or in hardware can cause damage to the facility or other test hardware. In propulsion testing, the energy levels are so high that failure can result in very serious damage, causing delays to the program for weeks or even months, in addition to hardware replacement costs. For these reasons, there has long been a requirement to provide a capability for monitoring test data in real time so as to provide an output signal or action in response to off-normal test conditions. Many times in the past, the condition to be monitored could not be measured directly, and much time and effort was spent developing, building, and installing "black boxes" that could input signals from directly measurable parameters and perform calculations to determine the occurrence of a condition to be monitored. The major drawback to the provision of these protective items usually was related to the narrow applicability of the devices and the difficulty of testing and debugging them in the propulsion testing environment. Final debugging of such a device *in situ* usually involved monitoring its performance in connection with a propulsion test.

Implementation of the display and monitor process on a digital computer provides the flexibility and capability required to perform this task efficiently, using existing signals and without regard for the environmental or reliability concerns of a new hardware design. Test parameters can be measured and manipulated as a function of the test sequence and related test conditions, and results can be output as status signals or fault alarms to the supervisor process. The supervisor process then adapts the test sequence or shuts down the test under way, and key data can be displayed in graphical form at the test operator's panel.

A properly designed and implemented monitor process will have a highly significant effect on the efficient operation of a test facility and on the successful and timely conduct of experimental programs conducted in it.

THE APL PROPULSION RESEARCH LABORATORY (PRL)

The Propulsion Research Laboratory, shown in Fig. 7, is an automated test facility. Since its construction at APL's Howard County site in 1961, test programs have been carried out on a wide variety of airbreathing missile research engines and related components over a Mach number range from subsonic to Mach 7 and at simulated altitudes from sea level to 120,000 feet. In developing the facility, emphasis has been placed on the flexibility of test conditions and on maximizing data obtained in short blowdown runs.

The principal elements of the facility are the air systems (storage, supply, and heating), the steam and exhauster systems, the fuel systems, the water cooling and quench systems, and the instrumentation and control systems.

Air Systems

A total of 58,000 pounds of air is stored in tanks at a pressure of 3000 pounds per square inch (psi). A 10,000-psi storage system also exists at PRL but has not been used in a number of years. High-pressure air is supplied to any of the five test cells at flow rates up to 150 pounds per second. The flow is controlled either by the analog control system in connection with three conventional analog control valves or by computer-controlled digital control valves, depending on the test requirements.

To simulate flight conditions properly in the test cell, the high-pressure process air must be heated. Three different types of heaters are used, depending on the temperature required. The storage heater (Fig. 1) contains a stainless steel matrix core that is preheated by an oil burner to a temperature of 1800°F. This core has a total heat capacity (referred to atmospheric reference temperature) of 3.2×10^6 British thermal units, and heat energy is added to the process air as it passes through the core. The air temperature is controlled by varying the ratio of bypass air to that

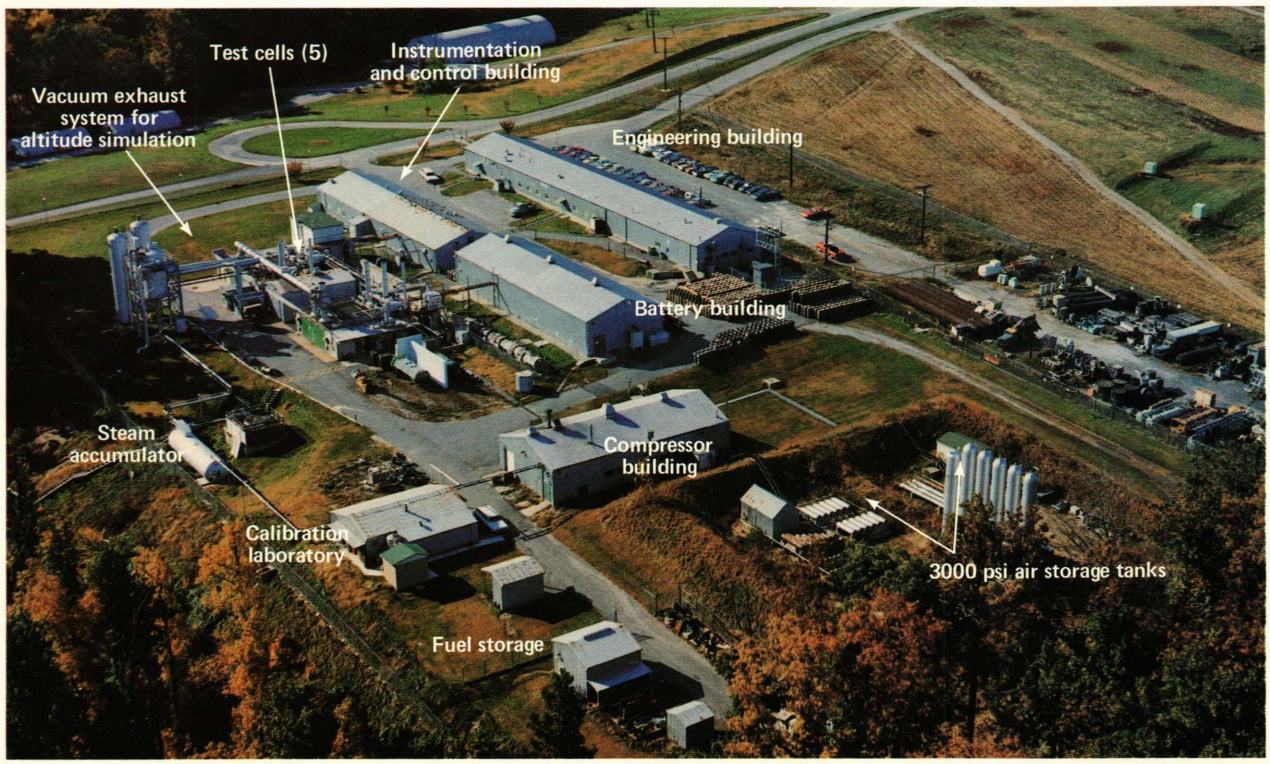

Figure 7 – The APL Propulsion Research Laboratory, a highly automated test facility. Since its construction in 1961, test programs have been carried out on a wide variety of airbreathing missile research engines and related components over a Mach number range from subsonic to Mach 7 and at simulated altitudes from sea level to 120,000 feet.

passing through the core. This heater can be used to supply air to the test cells at a maximum flow rate of 100 pounds per second at 800°F, down to 10 pounds per second at up to 1500°F.

For higher temperatures, a vitiation (in-stream combustion) heater (Fig. 2), which uses either hydrogen or propane and oxygen, can be used alone or as a topping heater in conjunction with the storage heater. The combustion heater can raise the air temperature to over 3000°F, has a 1000-psi maximum pressure, and has a maximum flow rate of 80 pounds per second (these three maxima cannot be attained simultaneously).

For still higher air temperatures, the DC electric arc heater is used (Fig. 3). Arc heaters are available to heat the air to total enthalpies greater than 3000 British thermal units per pound (approximately 7400°F) at 500 psi. In those heaters, an arc is struck between two parallel copper-tube electrodes in a chamber through which process air is flowing. Both the electrodes and the chamber are water cooled. The power supply for driving the arc is a DC battery consisting of 1216 2.1-volt submarine cells; the battery is housed in a separate building (see Fig. 7). This battery can deliver up to 14 megawatts, depending on the charge state and mode of connection, but it is usually run at about 10 megawatts or less.

Steam and Exhauster Systems

If required, an exhaust system with two steam ejectors removes the engine exhaust products and air from the test section and provides altitude simulation. The steam for driving these ejectors is generated by flashing hot water from a pressurized accumulator as it is expanded through a valve. The blow-down steam system can operate for as long as 4 to 5 minutes during a run, after which replenishment is required. The steam exhauster will pump air and combustion products at a rate of 20 pounds per second at atmospheric pressure (sea level). At a minimum pressure of 0.75 psia (67,000 feet), it pumps at a rate of 1 pound per second.

Fuel Systems

Special fuel handling and supply systems involving pyrophoric and toxic fuels have been developed for the extensive experimental supersonic combustion programs conducted at APL since 1961. Typical of these fuels were the boranes (ethyldecaborane and pentaborane) and tri-ethyl aluminum. Fuel systems were also developed for metal slurries, but current programs concentrate on more conventional hydrocarbon fuels.

Water Systems

These systems are needed in propulsion testing for quenching and cooling exhaust products as well as cooling facility and test equipment. Five separate water systems are used to support the wide variety of testing at PRL. They vary from low-pressure, high-flow-rate systems to a high-pressure (2000 psi) blow-

down system where two 300-cubic-foot steel tanks are filled with water, which is then expelled under pressurized conditions provided by the 3000-psi air storage system. The lower pressure systems are used for such purposes as cooling the air compressors, the storage air heater, the arc heater ballast resistor, and other facility components, as well as for quenching combustion products. The high-pressure system is required for cooling arc heater electrodes, nozzles, heaters, and other equipment where more severe heating is experienced.

Instrument and Control System

The requirement for remote control of a complex test sequence involving 50 to 100 on/off valves and positioners, 3 to 10 proportional control loops, and possibly 350 channels of test measurement instrumentation, coupled with the monitoring of facility and test article operation in this high-energy environment, has led to the development of a hierarchical computer control and data acquisition system. The system includes a capability for joint operation of the facility and the test article with both a facility operator and a test operator in the loop. For the more complex tests, the supervisor computer memory contains the complete test sequence and preprogrammed alternative sequences. During test operation, the actual sequence path is chosen in real time by the computer on the basis of status feedback from the test or commands from the operators or both.

The present implementation of the instrumentation and control system is shown diagrammatically in Fig. 8. In this system, the supervisory control process is resident in a Texas Instruments 960 minicomputer. This supervisor computer is connected to several other minicomputers and microcomputers that, together, implement the test operational processes described earlier, in the subsystems shown. The monitor and the analog control subsystems are not implemented in a computer in the present system. Planning calls for the monitor process to be implemented in the host processor of the data acquisition subsystem. Real-time display of test data is currently available using that same processor.

The direct digital control process is also implemented in another Texas Instruments 960 minicomputer and includes dedicated sensors for measuring temperatures and pressures for the control of facility process air mass flow and temperature when the storage heater is used. It interacts with the supervisor in the same way as the other control subsystems, in that it is continuously looking to the supervisor computer for the set-point value of each of the controlled parameters and it is continuously generating status feedback data on those same parameters.

The analog control subsystem consists of a number of PID controllers that regulate the value of the controlled parameter to that commanded by the supervisor. Set-point values for each condition are output to the analog control subsystem in voltage levels corresponding to engineering unit values (psi, degrees Celsius, etc.) through a programmable translator unit. This unit, which is part of the analog control subsystem, is designed to enable the test engineer to

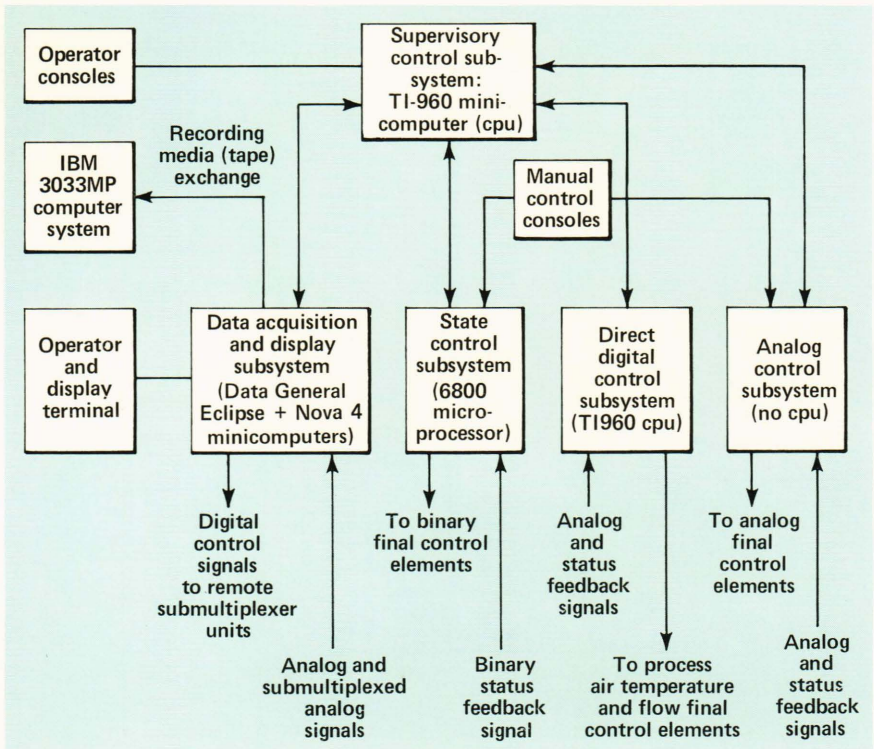

Figure 8 – The implementation of the PRL instrument and control system shown here illustrates the present allocation of operational processes to hardware having different computers, software, and communications protocols, thus making it difficult to maintain and upgrade the system. To remedy this problem, a new system is being designed that will build on the existing (new) data acquisition system hardware. The probable configuration of this system is shown in Fig. 9.

redefine the values in his set-point sequence for each analog control loop without changing the supervisor computer software.

Status feedback for each analog and digital control channel includes an "on the point" signal indicating regulation within tolerable limits and a "HIGH" or "LOW" saturation signal indicating that the control valve is almost wide open or almost closed and that the channel is about to go out of control. The appropriate response to a saturation signal is often to jump ahead in the supervisory control sequence to some less stringent set-point value that will bring the control channel back into regulation. Test condition sequences in a blow-down facility such as PRL are usually constructed to go from the more stringent conditions (higher temperatures, pressures, and flows) to the less.

At present, the state control subsystem is implemented using a Motorola 6800 microprocessor in conjunction with a diode-programmable read-only memory that serves as a programmable translator for this system. It contains 64 words addressable from the supervisor computer. Each word is 128 bits long, so that each can represent a required state of a system having up to 100 on/off valves or other such binary devices (28 bits are used internally). The state of each binary device (called a final control element) is measured using position or proximity switches, and the status is fed back and compared with the output command of the read-only memory by the 6800 microprocessor. When all of the final control elements have reached their commanded state, an "on the point" signal is transmitted to the supervisor. If any element does not change state within the time permitted for that valve, or if it fails in an illegal state (neither open nor closed), then the supervisor is notified so that an appropriate action can be taken.

Future plans call for the state control process to be implemented in a minicomputer on the bus network described below.

A new data acquisition and display subsystem has recently been installed. It has been designed to permit expansion to meet the complete testing requirements for some years to come. It was designed to provide the kernel of a refurbished instrument and control system that can be expanded to take over from existing subsystems that are obsolete or inadequate for the task.

The new system (Fig. 9) consists of two computers configured in a master/slave arrangement. During data acquisition, all the high-speed multiplexing, analog-to-digital conversion, and operation of remote submultiplexers are under control of the slave processor, whereas the operations requiring more memory and computing power such as on-line data reduction for display, the monitor process, and data formatting

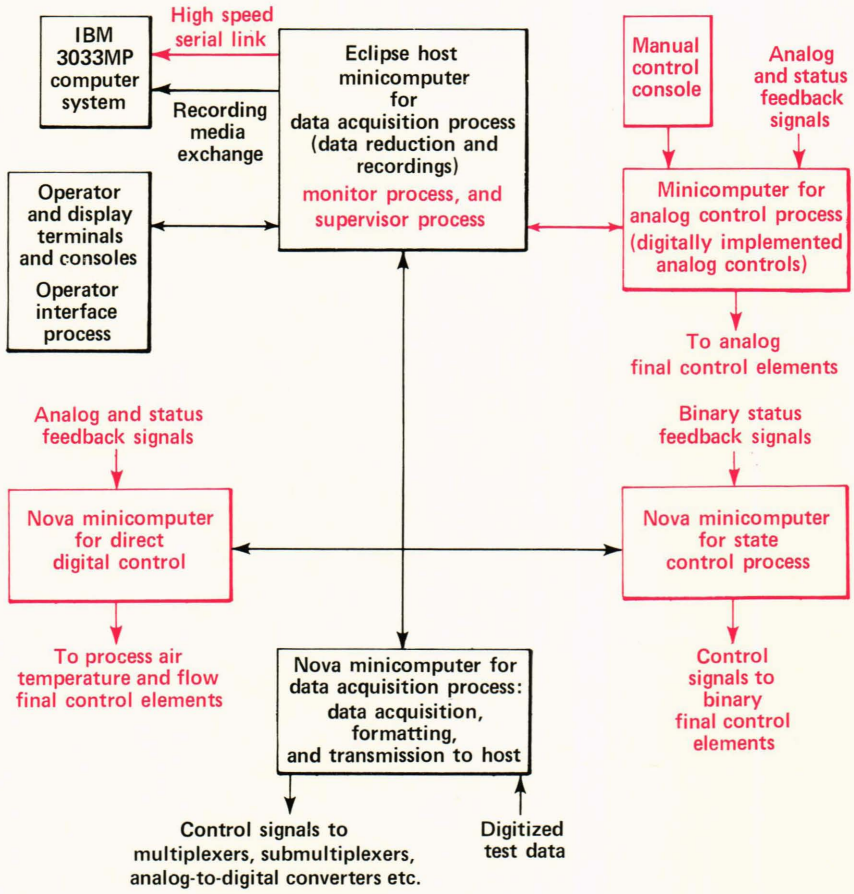

Figure 9 – This figure shows (in black) the existing data acquisition and display subsystem at PRL and also illustrates the difficulty in evolving and implementing a new design while continuing to use the old. Modern developments in computer technology involving multitasking systems usable in real-time control applications have led us to consider reallocation of operational processes to the hardware as shown in red. High-speed direct memory access interprocessor communications and larger random access memory, coupled with multitasking, suggest a shared data base design with the monitor and the supervisor processes in the host computer, in addition to the real-time display and recording currently implemented.

and recording are performed in the host. The data acquisition software resident in the NOVA 4 operates analog multiplexers to acquire high-speed data at sampling rates of up to 1000 samples per second per channel. Simultaneously, remote submultiplexers in the test cell are being driven under program control to sample up to 640 additional channels at sampling rates of up to 20 samples per second. All of these data are transmitted via direct memory access to the host computer, where they are formatted and recorded on 9-track magnetic tape. Copies of those data that are required to support the monitor or the display processes are also retained for processing in the multitasking environment of the host. After processing, the data for real-time display are output to display terminals in formats requested by operators at the terminals. Output from the monitor process is used for decision making either at the test engineer's terminal or directly in the supervisor process.

Off line, the host processor (Data General Eclipse) is used for all software development and for maintenance of the various data bases required in the operation of the facility. Software for the slave processor is down-loaded from the host for real-time operation. With this arrangement, all of the expensive programming-support peripherals (mass storage, printer, etc.) need not be replicated when additional processors are added for real-time applications. Up to 14 computers (including the host processor) may be connected to the bus.

Current plans call for moving the supervisory control process to the host processor and adding additional computers to the bus to provide input/output ports and signal processing for state input/output and direct digital control. This may change somewhat if there is insufficient room (and processor time) in the host for the supervisor, the display, and the monitor process. Since the monitor process requires immediate access to the data and faster, more powerful, arithmetic capability it will reside in the host processor to minimize communications requirements.

During the pretest checkout phase, all of the multiplexers and submultiplexers in the system can be operated from terminals via the host computer. In addition, software routines can be invoked to operate the signal conditioning, the data acquisition system, and certain diagnostic hardware (voltmeters, counters, etc.) in an automatic (diagnostic monitor) process that checks operation of the system end to end and prints out error messages listing any malfunctioning equipment. The diagnostic monitor saves many hours of manual checking of the sensors, signal conditioning, and digital recording hardware, and permits additional checks to be made right up until test time. The need for automatic testing of equipment of this type has required that a built-in test capability be designed into all subsystems and interfaced to the data acquisition system computer.

A data base management capability exists in the host in connection with the Advanced Operating Systems™ (AOS), the multiprocessing operating system. Word processing and other applications software running under AOS permits various facility support personnel to create, store, retrieve, and sort data, records, and textual documentation in the system. The data are accessible on terminals throughout the facility. To directly support the data acquisition process, the complete sensor inventory is included in one such data base along with the historical calibration records for each unit. When the data acquisition program is initialized for a particular experiment, the latest calibration data from all the sensors listed in the data acquisition sequence for that experiment are automatically retrieved from the inventory data base. Calibration constants required for data reduction in APL's IBM 3033 facility are recorded on the same 9-track tape on which the test data will be logged. Calibration constants are also retained in the host for sensors where output data are to be displayed in real time in engineering units.

The sensor inventory data base is accessed when new tests are being designed in order to locate and designate sensors for the measurement of various parameters. Drawing documentation records, technical memoranda, and manuals for various facility equipment are also stored in the host processor for instant access to determine the latest issue available. Textual documentation is updated, making use of the word processor software resident in the system.

WILLIAM H. AVERY

THE TALOS BOOSTER ROCKETS

Major problems had to be solved before solid booster rockets could be produced in the size required for Talos. Five years after booster rocket development was started, booster technology had reached a level where propellants and metal parts could be tailored confidently to meet the Bumblebee Program needs. The first Talos missile was launched in 1952.

As with other parts of the Talos program, the development of rockets to accelerate a 2000-pound ramjet missile to supersonic flight speed in a few seconds required major strides into unexplored areas of technology. In 1945, only the newest types of military rockets in production were capable of attaining supersonic speeds, with payloads generally a minor fraction of rocket weight. With the freedom then available to engineer, plan, and carry out development programs, it was possible to accomplish the ramjet booster rocket objectives in only 2½ years.

As an interim measure, existing rockets were used for launching the 6-inch-diameter Cobra ramjet, the Control Test Vehicle, and the Supersonic Test Vehicle. A group of rockets, arranged in a cluster and manifolded at the forward end to equalize thrust, was used in each application. For example, four (and later six) high velocity aircraft rockets were used to launch the Cobra, four British UP-3 rockets for the Control Test Vehicles, and four T10E1 rockets (developed by Division 8 of the National Defense Research Center) for the Supersonic Test Vehicles. On the whole, these clustered boosters proved adequate, although their low impulse-to-weight ratio and the necessity of relying on the uniformity of thrust of the individual units made extension of this design to the larger vehicles and service missiles highly undesirable.

INDIVIDUAL PROBLEMS

Three major problems required solution before solid rocket boosters could be produced in sizes required by the missiles envisaged in the Bumblebee Program. The status of rocket development in 1945 is summarized in Refs. 1 and 2. The problems were: (a) the development of techniques for producing propellant grains[3] in sizes five to ten times larger than those used in the ongoing production of rockets,[4] (b) the development of special propellant granulations and compositions to achieve maximum loading density and increased overall specific impulse,[5,6] and (c) the development of propellant compositions having a greatly reduced dependence of burning rate on rocket chamber pressure to permit the use of lighter metal parts with a corresponding increase in the propulsive efficiency of the system.[7]

In addition, it was considered essential to strengthen the existing organizations engaged in solid-fuel rocket development and to establish new facilities for the experimental production of developed units.

TECHNICAL PROGRESS

The development of solid-fuel rockets five to ten times as large as those then available was a task of major magnitude. To ensure an early solution of the problem, parallel programs were initiated at Aerojet Engineering Corporation and Allegany Ballistics Laboratory (ABL), with the objective of establishing the techniques and facilities necessary for the production of large rockets.

In the fall of 1945, the decision was made to develop for use with the ramjet test vehicle (RTV) a single booster rocket having a diameter that would permit it to be inserted and attached to the 18-inch ramjet combustion chamber. Separate tasks were assigned to Aerojet and to ABL to provide a unit capable of accelerating a missile weighing 1000 pounds to a velocity of about 1800 feet per second in approximately 2 seconds.

Jet-assisted takeoff rockets that used a castable propellant made of a mixture of potassium perchlorate and asphalt had been developed previously by Aerojet. By replacing the asphalt with a polymeric resin and the potassium perchlorate with ammonium perchlorate, a propellant with a satisfactory specific impulse and reasonable physical properties was produced. The work at ABL was to be based on smokeless powder, either in the conventional extruded granulation or, preferably, in large single grains. A process for preparing grains of double-base powder[8] by the casting technique had been developed but had not been established as reliable.

AEROJET DEVELOPMENT OF BOOSTER FOR RTV

Initial emphasis was placed on development of the Aerojet booster, which was accomplished quickly. Full-scale units suitable for boosting the RTV were produced in early 1946. These rockets used a charge of two 400-pound tubular grains that were supported in the rocket chamber by circumferential tie rods. Al-

though it was known that insufficient development had been carried out to establish reliable performance of these units, the time scale of the ramjet development necessitated launching an RTV at the earliest practicable time. Therefore, five units were ordered from Aerojet and, at the same time, a program of propellant research was instituted to improve the product and to establish reproducible controls in its fabrication.

The Aerojet booster was used successfully in firing two RTV's. The first cold round to test stability and separation was fired on May 23, 1946. The second round, which successfully demonstrated ramjet operation on an 18-inch scale for the first time, was fired on September 24, 1946, 22 months after the program was started.

A third RTV and a redesigned 18-inch burner test vehicle (BTV) of reduced weight and improved airflow were launched with Aerojet boosters in January 1947. In neither instance did the rocket perform satisfactorily. Failures of the rear propellant grain occurred before the end of burning, which, in the second round, resulted in blowup of the rocket. In view of these propellant failures, it was decided to interrupt the BTV program until either the Aerojet booster could be redesigned or the ABL booster could be proved in. The discouraging results of these tests led to a vigorous effort to analyze the source of the failure. It was concluded that the tubular grain design and mode of support, combined with the marginal strength of the propellant, were inadequate to withstand the high accelerations and vibration loads imposed on the propellant during boost.

ALLEGANY BALLISTICS LABORATORY DEVELOPMENT

Although the Aerojet booster for the BTV was considered to satisfy the immediate need of the ramjet propulsion program in the original plan, the smokeless powder booster development at ABL was pursued with the objective of producing a thoroughly reliable unit with higher performance. Three alternative designs were considered to maximize the likelihood of producing at least one fully satisfactory unit. Two used extruded smokeless powder grains, and the third used full-diameter grains of cast double-base powder. The progress made in developing the casting process made it possible to terminate the two less efficient alternatives in mid-1946.

At ABL, it became apparent that there were inherent advantages in the design of a booster rocket that used a propellant bonded to the rocket case. The uniform support at the circumference greatly reduced the maximum grain stresses and also protected the case from the high temperature of the propellant gases. Thus, a more efficient and more reliable booster could be made with this design. Accordingly, after the Aerojet booster failures, all effort was turned to the development of the cast double-base booster rocket.

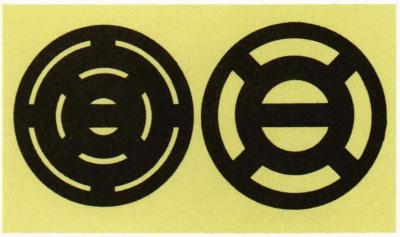

Figure 1 — Cross-section geometry of two types of powder grain used in Allegany Ballistics Laboratory (ABL) 51,000-pound thrust units. These grain geometries were designed to provide approximately constant surface area during the burning process and thus provide a constant level of thrust.

In Fig. 1, cross sections of two types of powder grain are illustrated. As a by-product of one of these, a 7-inch-diameter rocket with an aluminum case was developed that had an extraordinarily high overall specific impulse. This rocket, designated the "Deacon," was used to launch aerodynamic test vehicles for APL and for the National Advisory Committee for Aeronautics.

The development of the cast double-base booster for the BTV was completed in the spring of 1947. After five successful static tests at ABL, five launching test vehicles (LTV) with attached fins and a nose cone were flown successfully in June and July of 1947. To compensate for the absence of the BTV, a lead weight was placed in the nose cone of the LTV, which gave it a total weight that would result in about 20% higher acceleration than the BTV launch configuration to ensure a margin of safety for its use as a BTV booster.

Telemetry showed that the rocket chamber pressure during flight duplicated the static results, indicating that no propellant breakup was caused by booster acceleration and flight-induced vibrations. It was possible then to proceed confidently with adoption of the ABL booster for further ramjet testing. This confidence was fully justified by later developments. An interesting account[4] of the first 10 years of cast double-base propellant developments states that in 1956, when many thousands of boosters had been flown, not a single booster failure caused by the propellant had been recorded.

Because work leading to an improved Aerojet booster had not been completed at that time, it was decided to standardize on the ABL unit for subsequent BTV flights. The work at Aerojet was redirected along more fundamental lines. The ABL rocket performed in a highly satisfactory manner in the first BTV flight test in August 1947. A typical record of pressure and acceleration as a function of time is shown in Fig. 2. Figure 3 is a drawing of the launch configuration. This unit demonstrated a high degree of reliability and yielded telemetered pressure-time records in flight corresponding to those obtained in static firings.

On the basis of experience obtained in development of booster rockets for the BTV, work was

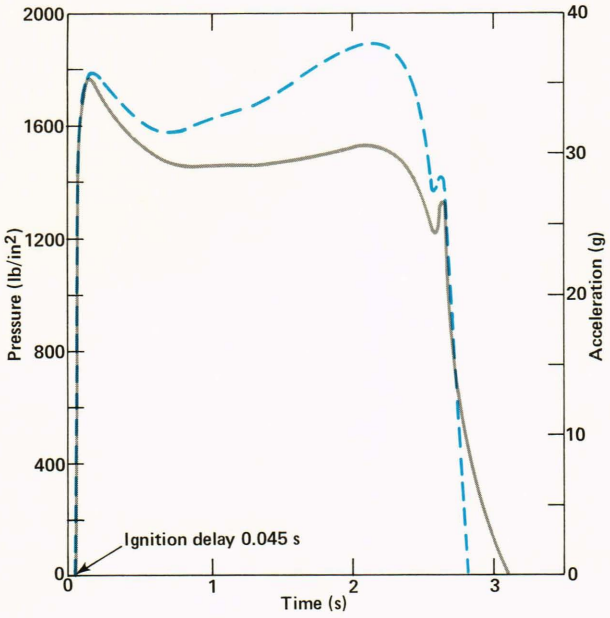

Figure 2 — Typical telemetered record of pressure (solid line) and acceleration (broken line) versus time for ABL burner test vehicle (BTV) booster shows nearly constant pressure during the rocket burn. Rocket chamber pressure is directly related to the thrust. The acceleration curve shows the effect of weight loss during the burn.

begun in January 1948 on a scaled-up version suitable for launching the XPM, the prototype Talos missile. Fabrication of the larger propellant grain, tests to tailor the thrust and burning time to the desired values, and a series of prove-in tests were completed by the end of June 1948. Increasing the size of grains produced by the casting process involved no basic difficulties and established the procedures for subsequent booster rockets for the Talos series of missiles. The first flight test of the XPM booster was made on July 1, 1948. This LTV weighed 3000 pounds and provided 90,000 pounds of thrust for 3.5 seconds. Three additional LTV's were flown between July and December while construction and tests of the XPM (dummy) airframe were in progress, and on December 2, 1948, the first flight of the booster rocket attached to the XPM airframe occurred.

That test and the following one were unsuccessful because flight instability of the launching configuration led to failure of the booster fins, although the rocket performed as predicted. This trouble was prevented on the third flight on March 30, 1949, in a flight without missile wings that demonstrated successful booster and ramjet operation. The stability problem and other program work delayed the next flight until March 6, 1950, when completely satisfactory operation was demonstrated.

With these flights, booster rocket technology had reached a state in which the propellant and metal parts could be tailored with confidence to meet new program needs, and further booster research and development turned to improvements in the specific impulse and reductions in hardware weight and cost.

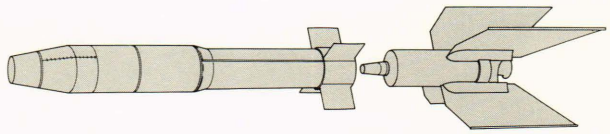

Figure 3 — BTV and launching carriage after separation. This configuration was flown successfully in 1947.

Modifications to the XPM in the spring of 1949 led to the need for a larger booster rocket, and on June 6, 1949, an LTV was launched with 105,000 pounds of thrust (average). It weighed 3720 pounds and contained 2063 pounds of propellant. Although the XPM was a prototype, the Talos missile required a still larger booster. Development of this booster, which also needed a significant reduction in the weight of the booster case and thorough prove-in of its reliability, was carried out at ABL during 1950 and 1951.

On October 28, 1952, the first Talos missile was launched. The total weight of the launching configuration was 7455 pounds. The booster alone weighed 4425 pounds. Further minor modifications were made to the booster to accommodate the requirements of the various versions of Talos over the years, but Talos booster development was essentially complete at this point. At least 1400 tactical Talos boosters were flown without a single failure during the lifetime of the Talos program.

LIQUID-FUEL BOOSTER ROCKETS

In view of possible limitations in the ultimate size of solid-fuel booster units, the development of liquid-fuel systems for short duration use was initiated at the M. W. Kellogg Company early in 1947. The objective of this work was to provide all the engineering data required to evaluate the relative merits of solid- and liquid-fuel boosters as a function of thrust and total impulse required.

Preliminary work indicated that it would be possible to design an efficient liquid-fuel rocket having thrust and duration comparable with those of the solid-fuel booster for BTV. However, the success of the solid booster development eliminated the need for liquid boosters, and further development was discontinued.

REFERENCES and NOTES

[1] *Rockets and Underwater Ordnance*, Office of Scientific Research and Development, National Defense Research Council, Washington, D.C. (1946).

[2] R. E. Gibson, "Personal Reflections on the Origins of CPIA," *CPIA Bull.* (Oct 1981).

[3] A rocket propellant grain is a single piece of propellant of a particular geometrical configuration, developed to produce a specified rate of production of propellant gases or burning.

[4] L. G. Bonner, 12th Meeting, Joint Army, Navy, Air Force Solid Propellant Group, NOL, White Oak, Md. (7 May 1956).

[5] Specific impulse is thrust divided by weight.

[6] W. H. Avery and J. Beek, *Propellant Charge Design of Solid Fuel Rockets,* OSRD Report 5890, ABL Report 13-4, George Washington Univ. (Jun 1946).

[7] W. H. Avery, R. E. Hunt, and M. N. Donin, *Burning Rate Studies of Double Base Powder,* OSRD 8527, ABL 8-1, George Washington Univ. (Jan 1946).

[8] Highly nitrated guncotton plasticized with nitroglycerin.

LESTER L. CRONVICH

TALOS AERODYNAMICS

During development of the aerodynamic configuration for the Talos missile, several technological constraints and problems existed whose solutions added significantly to the body of design principles used in subsequent missile designs.

STATE OF THE ART IN 1945

The small group of aerodynamicists associated with the Bumblebee Program who initiated aerodynamic investigations of supersonic missiles in 1945, had limited experience in supersonic aerodynamics; their experience had been primarily with subsonic aircraft before and during World War II. The status of supersonic aerodynamics at that time was assessed at a symposium held at APL on December 6 and 7, 1945 that was attended by representatives from 49 organizations. A survey of the field revealed progress in fundamental theory, which included shock-wave theory, expansion theory, cone theory, and a method of characteristics for two-dimensional flow. For the vehicle designer there existed linear theories for bodies of revolution, for thin finite-span wings, and for ducted bodies, as well as linear and second-order theories for two-dimensional wings.

Some experimental data on projectile aerodynamics were available from the spark photography ranges of the Ballistics Research Laboratory at Aberdeen Proving Ground, Md. There were also some limited test data on small models in the two operating supersonic wind tunnels in the United States, one at the Guggenheim Aeronautical Laboratory in Pasadena, Calif., and one at the National Advisory Committee for Aeronautics, Langley Field, Va. In 1945, these were the only wind tunnels in the United States in which models could be tested at supersonic speeds, but they were too small to be of significant value for designing large guided missiles. A somewhat larger facility was available at the Ballistics Research Laboratory, but it was not yet operational. Thus, a decision was made to develop a wind-tunnel facility of sufficient size to permit testing models of approximately 1/10 scale, a size that would permit testing of relatively complicated models at desirably large Reynolds numbers. This decision led to the development of the Ordnance Aerophysics Laboratory at Daingerfield, Tex., for both aerodynamic and engine testing (Fig. 1). The aerodynamic wind tunnel eventually covered a test range of Mach numbers from 1.25 to 2.75 in a 19 × 27.5 inch test section. It proved to be the principal aerodynamics ground-test facility for the Talos program and for many other missile programs until it was closed in 1958.

Only limited flight test data were available to aerodynamicists because most supersonic testing was related to the ballistics of shells rather than to the aerodynamics of missiles. Early in the Talos program, high-velocity aircraft rockets were used as missile models for acquiring information on base pressure, drag, wing pressures, and missile accelerations attainable through deflections of movable wings. Most of the aerodynamic flight testing was carried out at the Naval Ordnance Test Station, China Lake, Calif., and later at White Sands Missile Range, N.M.

A team of associate contractors from industry and the universities was formed to assist APL in carrying out research and development in several aerodynamics areas related to the design of guided missiles. Their activities were guided by a panel of experts (known as the Bumblebee Aerodynamics Panel) whose charter was to provide broad planning of the aerodynamics program and whose goals were (a) to develop prototype information for defining an early design, (b) to develop information to improve the prototype's range and maneuverability, and (c) to foster basic research.

CONSTRAINTS IMPOSED BY OTHER TECHNOLOGIES

Low Angle of Attack for Engine

Since a key element in the development of the long-range missile was the ramjet engine, it was essential to operate the engine as efficiently as possible. This led to the decision to fly the missile at a low angle of attack, which would permit optimum engine performance, and to depend on movable wings to provide the desired maneuverability. Thus, the missile would be maintained at a small angle to the oncoming airflow while the wings would be deflected by an amount sufficient to provide the necessary lift to achieve the desired maneuverability.

Skid-to-Turn Steering

The original choice of beamriding guidance with commanded maneuvers in two orthogonal planes dictated a cruciform arrangement of wings and tail stabilizers. In addition, the wings served as control surfaces to steer the missile in pitch or yaw through de-

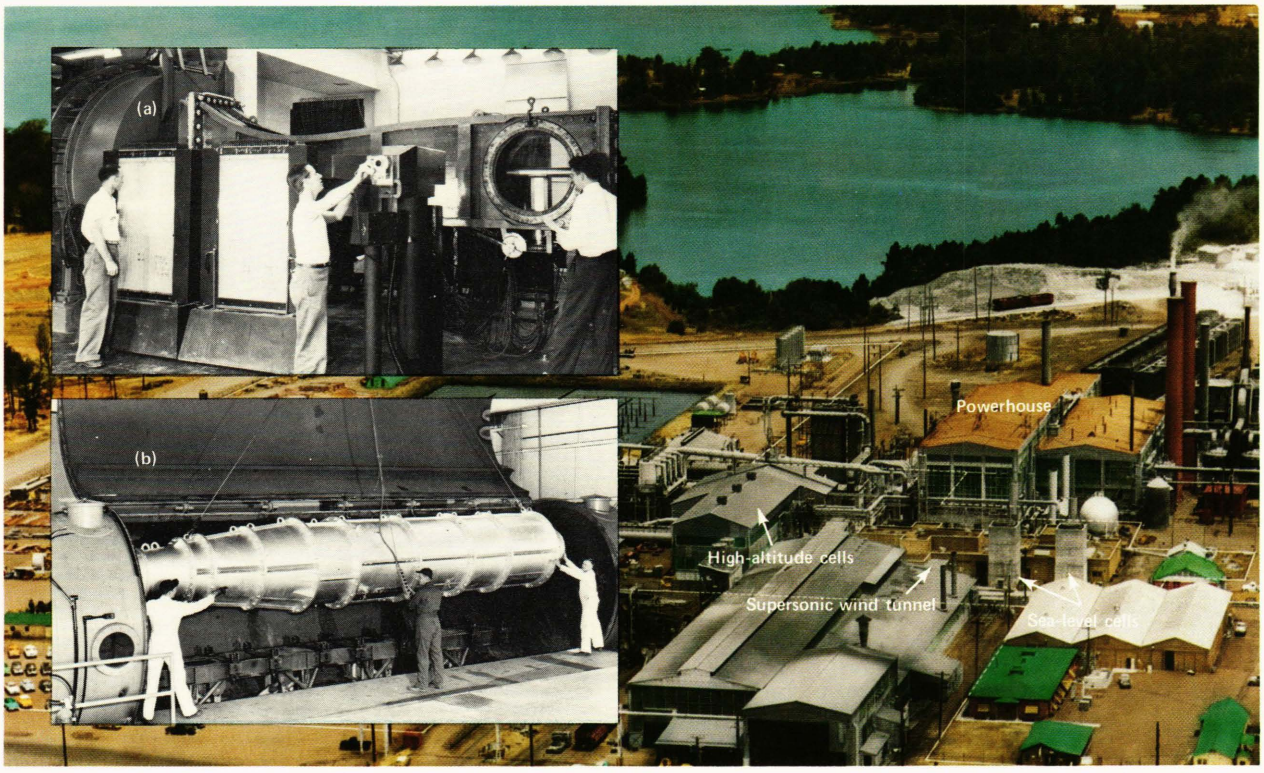

Figure 1 — The Ordnance Aerophysics Laboratory used blast-furnace blowers available at the adjacent steel plant to supply large volumes of high-pressure air for operation of a wind tunnel and burner facility. (a) Test section of the wind tunnel, where airflow from Mach 1.25 to 2.75 was available at a test section of 19 × 27.5 inches. (b) Test cell for full-scale combustor tests, where maximum air capacity was 15,000 pounds of air per minute at a pressure of 45 pounds per square inch absolute or 7500 pounds of air per minute at a pressure of 124 pounds per square inch absolute.

flections of pairs of wing panels and to stabilize it in roll through differential deflection of all four panels.

Minimum Space for Control Servos

Because the ramjet engine required a central air duct, the servos needed for operating the wing control system had to be housed in the annular region of the body around the central duct where space was limited. This restriction led to a study of wing planform shapes to find one that would result in the smallest hinge moments required to deflect the wings over the full range of operating Mach numbers and angles of attack. The planform finally selected became known as the Bumblebee planform.

Boost Phase Control

Another important factor in ramjet engine design is the need for a secondary propulsion system to boost the missile to the ramjet "take-over" speed. Thus, two aerodynamic configurations must be considered, one consisting of the missile alone and the other consisting of the missile combined with the attached rocket booster, which must fly stably until it attains the speed at which the booster can be dropped and the ramjet engine ignited for its climb to cruise altitude. The missile's relatively large wings, necessary to provide the desired maneuverability, posed a problem as a destabilizing aerodynamic surface well ahead of the center of gravity of the missile-booster combination during the boost phase. This situation required large stabilizing fins to be placed on the booster or, since space in a shipboard system is at a premium, some type of control that could permit a reduction in the size of the booster fins.

SIGNIFICANT PROBLEMS AND PHENOMENA, AND THEIR SOLUTIONS

Wing Design

A design decision was made to achieve lift primarily from the deflected wings (Fig. 2). Consideration had to be given to the problem of maximizing lift while minimizing drag, to structural requirements, and to the need for minimizing servo requirements for deflecting the wings. A combination of aerodynamic and structural considerations led to the choice of a double circular arc (biconvex) wing cross section because of its low drag per unit stress. During the subsequent production engineering phase, a modified double-wedge section was chosen, with minimum loss in aerodynamic or structural efficiency. Taper in both thickness and chord was used primarily for reasons of structural design and weight reduction. A tip rake appropriate for the Mach number regime was chosen to minimize the losses in lift associated with the tip, thus providing a more nearly two-dimensional wing lift, except for the root portion. Force testing on this so-called Bumblebee

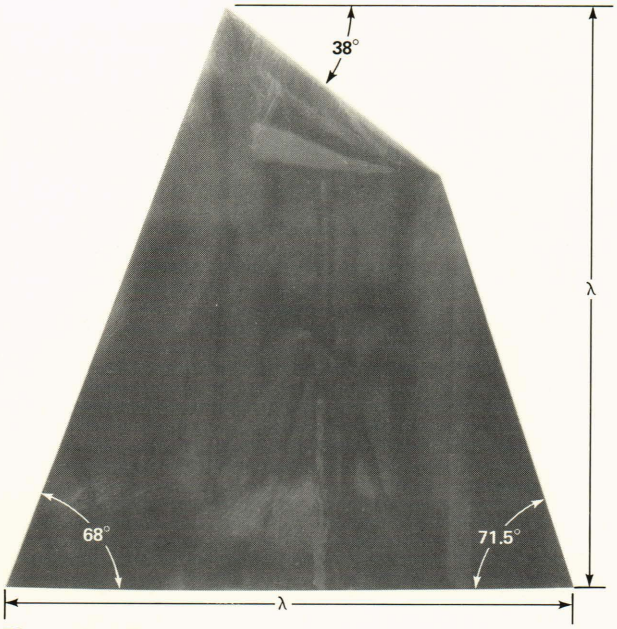

Figure 2 — The unique planform shape of the wings became known as the Bumblebee planform (from the name of the program itself). Its special shape minimized torque requirements on the servos that drove the wing controls.

planform showed rather small variations in chordwise center of pressure over the operating ranges of Mach numbers, angles of attack, and wing incidence so that it was possible to select a hinge line that minimized the design hinge moments. This particular planform shape exhibited very favorable characteristics over an extended Mach number range and has been used in nearly all other Navy surface-to-air missiles and in several non-U.S. missiles.

Roll Reversal (Tail Redesign)

Because the missile was to be roll-stabilized, it was necessary to have a roll-control system in addition to the control systems for pitch and yaw. At first, differential deflection of wings was considered for producing a roll torque and was tried in supersonic test vehicles. In flight, however, the roll obtained on the vehicle was opposite that expected from the torque produced by the wings. Because flow interaction was suspected, a research program to find the cause of the problem was established. Meanwhile, an immediate solution was to provide roll control by small flippers at the tips of the tail-stabilizing fins. Later, when the phenomena associated with this reverse roll were better understood and their effects were quantified, the tail planform was redesigned and the wings were again used to control all angular motion.

Since three angular motions (pitch, yaw, and roll) were to be controlled by four deflected panels, the choice of deflections was made definite by the use of a so-called "squeeze mode" on the wings, which required that deflections would be chosen that would minimize drag. The development of three-axis control by the wings during the missile's sustain phase led naturally to the introduction of the concept of wing control during boost.

Stabilization During Boost (Wing Control)

The early test vehicles were stabilized during boost with large booster fins that were necessitated by the presence of large wings ahead of the center of gravity of the missile-booster combination. However, the limitations of stowage and launcher space stimulated consideration of reducing the size of the booster fins by active control of the missile during the boost phase. The missile control system was designed to operate during boost as well as during sustained flight. Thus, it was possible to reduce the size (and weight) of the fins with only a small additional demand on the control system.

Duct Resonance (Exhaust Vents)

A problem that had to be faced during the flight testing program was the occurrence of resonance of the air column in the diffuser duct and combustion chamber during the boost phase when the air column was blocked by the tandem booster. Flight tests revealed a severe pressure oscillation in the duct ("organ pipe effect") that produced two problems: the pressure oscillation caused the inlet innerbody, which housed the warhead, to oscillate violently; it also prevented a clean separation of the booster from the missile, allowing the booster to recontact and damage the missile during a low point in the pressure oscillation.

The problems were solved by providing exhaust vents near the aft end of the missile to relieve the pressure buildup in the duct during boost. Because those vents were near the center of gravity of the configuration and did not alter the booster fin's effectiveness in stability, no special problems in the aerodynamic behavior of the missile were introduced.

Aeroelastic Phenomena

Because the nose-inlet ramjet engine is truly a "flying stovepipe," (i.e., a body with a large void along the center), it was expected that the design would have to account for the deflection of the missile under load and to establish the aerodynamic characteristics of the distorted configuration. Such quasi-static corrections to aerodynamics are usually needed only when the principal air load (the wing load) is applied at a point and the mass is distributed uniformly, resulting in a banana-shaped body, depending on its rigidity. For the Talos missile, it was found that at low altitudes the flexibility of the structure caused a considerable reduction in the maneuverability achievable per unit deflection of the wings (Fig. 3). The forward portion of the missile (diffuser ducting section) was less rigid than the aft portion (combustion chamber section). However, for a given maneuver, the angle of attack and control incidence increased with altitude, and these angles caused a redistribution of air loads, which must balance the fixed inertia loads. Thus, at high altitudes (such as 60,000 feet) that redistribution of loads caused the body to behave more like a rigid body.

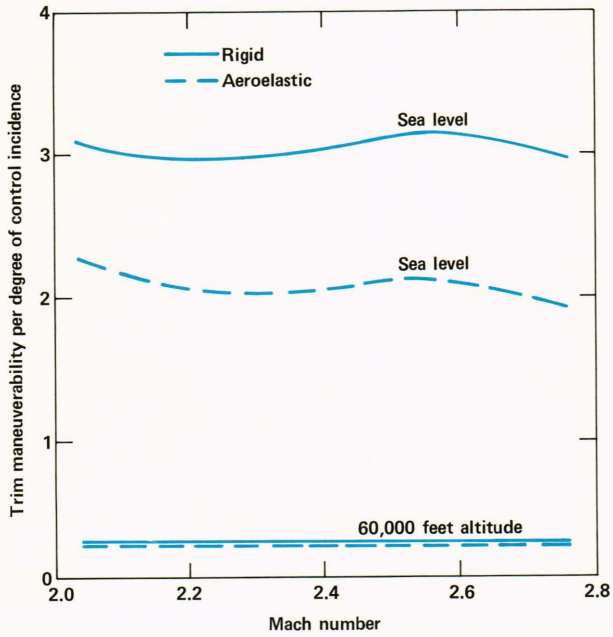

Figure 3 — The aeroelasticity of the missile under the high loading at sea level reduces the attainable maneuverability for a given wing incidence to two-thirds of that available for a rigid missile. At higher altitudes, the effect is negligible.

Effects on Later Missile Programs

As noted earlier, the modified double-wedge cross section for the wing with the tapered planform and raked tip (i.e., the Bumblebee planform) was found to have desirably low hinge-moment characteristics. The planform has been used over a wide range of Mach numbers for control surfaces of many other missiles, including the Terrier, Tartar, and Standard missiles of the United States, the French Masurca, the Italian Indigo, and the British Bloodhound. A somewhat similar planform appears on the British Sea Dart and the Russian Atoll and Gainful.

The procedure followed in the Talos program to account for the effects of elasticity of the missile on the static aerodynamics was also applied to the nose-inlet, wing-tip-controlled Long Range Typhon missile of the early 1960's. On the basis of previous Talos experience, it was decided to vent the diffuser pressure during boost of the Long Range Typhon missile through openings in the adapter section between the missile and the booster to avoid the "organ-pipe" oscillations in the duct. In addition, as further experience was gained in operating the inlets at higher angles of attack, it became evident that the restriction to low angles of attack (requiring wing incidence for lift) could be partially removed. In fact, the Long Range Typhon test vehicle used large fixed wings with wing-tip controls and achieved maneuverability through body angle of attack with satisfactory engine performance.

Thus, the Talos aerodynamic program, lacking an adequate supersonic aerodynamics data base, had to embark on a course that generated a new body of aerodynamic data and design principles. These were in the fields of aerodynamic stability, forward surface control, wing-body and wing-tail interference, aeroelastic effects on static aerodynamics, and inlet effects on aerodynamics. A control surface shape, the well-known Bumblebee planform, was developed that minimized center-of-pressure travel.

ALVIN R. EATON

BUMBLEBEE MISSILE AERODYNAMIC DESIGN: A CONSTANT IN A CHANGING WORLD

This article discusses the development of the basic Terrier, Tartar, Standard Missile tail-control aerodynamic configuration as an example of Project Bumblebee technology not yet outdated. Solution of the problem of reverse roll at supersonic speeds is highlighted as a step toward final aerodynamic design. It is emphasized that tail control provides a noncritical aerodynamic configuration that can be efficiently divided into functionally separate elements (i.e., sectionalized) to facilitate development, production, and testing. As a result, it has been possible to implement a remarkable degree of interchangeability of parts between large- and small-ship missiles and to simplify the introduction of new missile capabilities. Pertinent systems engineering approaches and techniques are outlined. Similarities among worldwide aerodynamic designs are indicated.

INTRODUCTION

The fiftieth anniversary of the Applied Physics Laboratory provides a welcome opportunity for reminiscing about the historical role of APL in the development of supersonic surface-to-air guided missiles. It is quite natural to recollect with pride that many of the most significant achievements in the field can be attributed to APL. It is also appropriate and gratifying to note that APL scientists and engineers are continuing to make unique and timely contributions to the design of guided missile systems at a time when technology is changing rapidly and many organizations are involved. But there is a pertinent and intriguing question not often considered. Are there specific APL-originated ideas or missile design approaches from the early days—the pioneering days—that are not yet outdated? Is it possible to identify achievements of the distant past that have current significance in spite of the phenomenal advances in technology that have been made over the years?

In this article, primary consideration is given to only one aspect of guided missile design: the basic aerodynamic/dynamic configuration. It is evident that most modern supersonic guided missiles employ tail control; four tail surfaces are typically used in a cruciform arrangement to provide all aspects of pitch, yaw, and roll control. Some missiles have fixed forward lifting surfaces (wings or "dorsal fins") and some are wingless, but tail control is now the prevailing choice for high-performance missiles. Yet tail control was by no means the initial direction of guided missile development; at APL, and elsewhere in the world, primary emphasis was on the use of forward control surfaces, either large wings or smaller "canards." At APL, however, early interest in high levels of performance led toward tail control; more than 40 years ago, APL originated the aerodynamic design approach that is now in worldwide use.

To put the tail-control development story in perspective, it is necessary to emphasize that supersonic aerodynamics appropriate to missile design was truly in its infancy at the inception of the Bumblebee project in 1945. Simple linear theories were available for bodies of revolution or thin wings in isolation, but basic aspects of wing–body–tail (or even wing–body) interactions were a mystery; there was no hope of calculating stability and control parameters to the required degree of accuracy. Very limited wind tunnel lift and drag data obtained from tests in small tunnels in Europe and the United States were available for projectiles and airfoils, but there was no supersonic wind tunnel capable of providing adequate data (including essential stability and control measurements) for missile design. In fact, there was no general agreement (even at APL) that any affordable wind tunnel would ever provide data relevant to flight conditions (at representative Reynolds numbers). In 1947, during a classic Wilbur Wright lecture, Theodore von Kármán would still be referring to supersonic aerodynamics as "a collection of mathematical formulas and half-digested, isolated experimental results."[1]

STV–2 FLIGHT TESTS AND REVERSE ROLL

It was necessary to make exploratory flight tests in the late 1940s to establish the most fundamental aerodynamic design characteristics and to measure (telemeter) as many flight data as possible. The first APL supersonic control test vehicle (STV-2) is shown in Figure 1. The large aft lifting surfaces (tails) were fixed; the forward movable surfaces (termed wings, though relatively small in area compared with the aft surfaces) provided pitch and yaw control; and small flippers (rollerons) located between the wings were designed to furnish roll control. Results of a

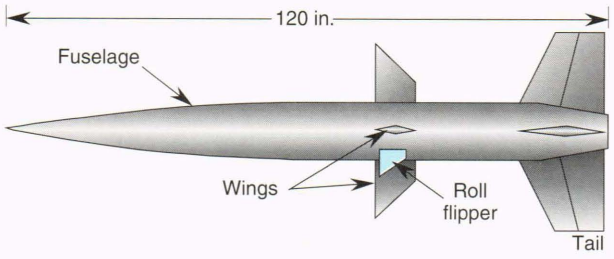

Figure 1. STV-2 aerodynamic configuration.

representative flight are shown in Figure 2; roll was indeed achieved on schedule, but—and it seemed incredible at the time—the direction of roll was opposite to the sense predicted from theory and subsonic experience.[2]

During the next few months, the STV-2 flight-test investigations of roll control were continued.[3] Two additional tests were conducted with the initial aerodynamic configuration, corroborating the previous data. Two flights were made with the roll flippers moved forward of the wings (to minimize flipper–wing interactions), and one was carried out with the rollerons removed and the small wings used to provide roll; during all three flights, the direction of roll was reversed at supersonic speeds.

Another flight test did provide roll results compatible with subsonic experience, however—one that led the way into the future. In this test, the tail surfaces were differentially deflected (with the forward rollerons removed), and roll performance was entirely consistent with expectations. It was immediately apparent that predictable roll control could be achieved by use of aft surfaces, even in the nonuniform flow field created by the wings.

SUPERSONIC WIND TUNNEL DEVELOPMENT AND TESTING

In the meantime, remarkable progress had been made toward the development of a suitable supersonic wind tunnel. Early in 1945, shortly after the beginning of Project Bumblebee, it had been decided that construction of a major test facility should be undertaken to provide for a large supersonic wind tunnel (as well as a "burner" laboratory to permit testing of large-scale ramjets under conditions of supersonic flow). For the wind tunnel, a test section area of "at least three square feet" was selected for testing of models "at least as large as tenth-scale, to facilitate making the complicated and precise models anticipated," and operation at relatively high pressures was specified as a requirement to provide acceptable Reynolds numbers. The defined power and compressor requirements were enormous (about 15,000 lb/min of air at a pressure of 30 lb/in^2 gauge), and the appropriate compressor and power-production facilities had to be identified and made available in a wartime environment.[4]

It did prove possible, however, to locate a standby blast furnace (at the Daingerfield, Texas, plant of the Lone Star Steel Company) with a blower capable of furnishing half of the required flow. The Navy arranged for the necessary access, and the Reconstruction Finance Corporation found a second blower of equal capacity that could be transferred to Daingerfield. Assistance in the overall de-

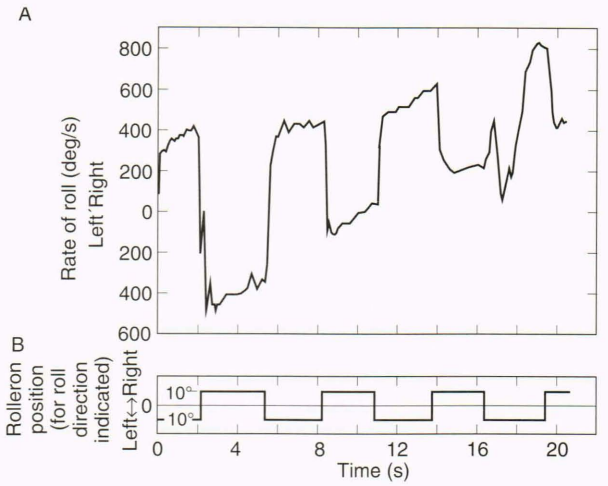

Figure 2. STV-2 Serial No. 24 telemetering data. **A.** Rate of roll versus time. **B.** Rolleron position versus time.

sign of the wind tunnel was obtained from the California Institute of Technology along with the detailed design of the nozzles intended to provide uniform flow in test sections of 19 × 27.5 in. for Mach (M) numbers ranging from 1.25 to 2.50. Construction of the Ordnance Aerophysics Laboratory (OAL) was started in June 1945, and initial exploratory tunnel tests with a full-scale nozzle were being run by June 1946. By March 1947, calibration of the $M = 1.73$ nozzle had been completed, demonstrating unusually uniform flow conditions (see Fig. 3), and a highly accurate rolling-moment balance system had been developed by the Consolidated Vultee Aircraft Corporation (CVAC), which was responsible for operation of the OAL facility under the technical direction of APL.

In March 1947, wind tunnel tests confirmed the reverse-roll results of the prior STV-2 flight tests (see Fig. 4); additional tests demonstrated the suitability of aft roll-control surfaces.[5] To minimize overall configurational changes for STV-2, it was decided to effect roll control by employing roll flippers located at the extremes of the tail surfaces (see Fig. 5), and flight success was immediate. In August 1947, roll stabilization at supersonic speeds was accomplished, and in March 1948, successful beam-riding guidance was demonstrated in a memorable flight.[6]

THE PHYSICAL EXPLANATION OF REVERSE ROLL

It is notable, however, that selection of the final STV-2 design (with aft roll-flipper control) had been made without a physical understanding of the phenomenon of reverse roll at supersonic speeds. Finally, after many false leads had been pursued, the breakthrough explanation occurred in June of 1947 between sessions of an Aerodynamics Panel meeting at OAL. The initial clues were negative in nature. It proved possible to deduce—conclusively—that no existing aerodynamic theory (wing upwash/downwash, body upwash effects, etc.) could possibly account quantitatively for the indicated results. It therefore became evident that an entirely new aerodynamic concept was required. When a particular possibility was identified by the author—late at night—it seemed so obviously correct

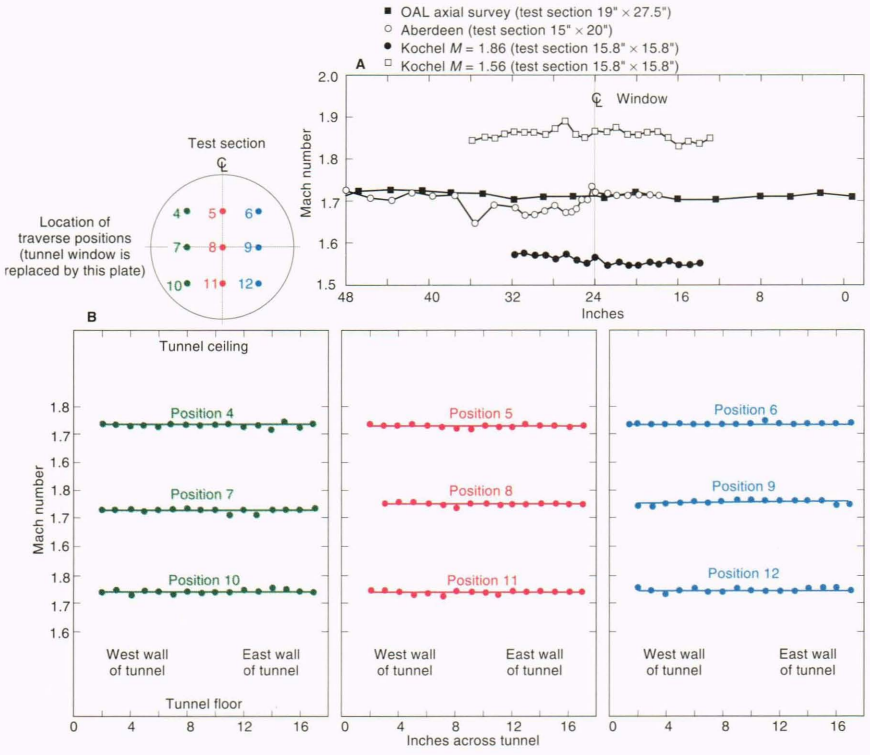

Figure 3. Mach number variations in supersonic wind tunnel test sections. **A.** Axial static pressure survey results for the Ordnance Aerophysics Laboratory (OAL), Kochel (Germany), and Aberdeen wind tunnels (Mach number versus nozzle abscissae). **B.** Uniformity of Mach number in test section (M = Mach number).

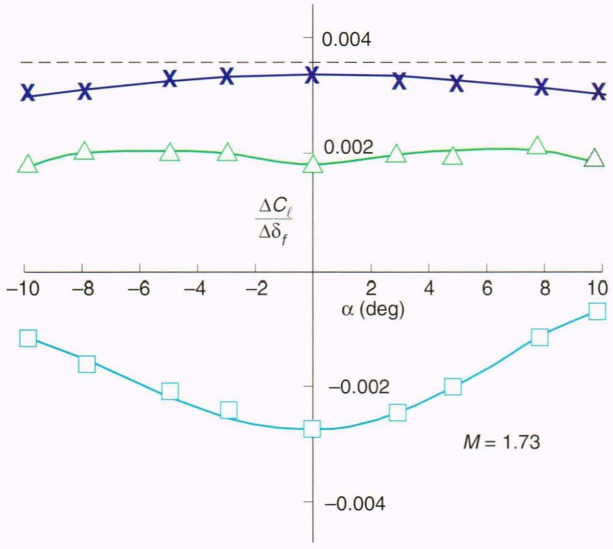

Figure 4. Wind tunnel roll-control data for the STV-2 test vehicle. ($\Delta C_\ell/\Delta\delta_f$ = rolling moment per degree of flipper differential deflection; α = body angle of attack; dashed line = theory, assuming no interference; x = roll-flipper effectiveness, wings and tails off; Δ = roll-flipper effectiveness, wings on and tails off; □ = roll-flipper effectiveness, complete configuration; M = Mach number.)

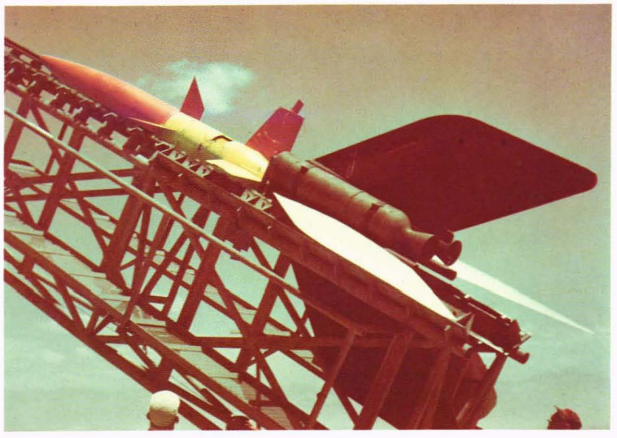

Figure 5. STV-2 test vehicle on launcher.

that immediate steps were initiated to provide experimental verification in the OAL wind tunnel. A simplified diagram of the nonconformist idea—which seems entirely obvious in retrospect—is presented in Figure 6. It seemed apparent that a strong interaction of pressure fields at the wing–body juncture must be occurring in direct contradiction to existing theory.

A postmidnight telephone call led to reopening of the wind tunnel facility and, with the essential cooperation of the CVAC tunnel operators, to an all-night effort to arrange a demonstration for the Panel on the following morning. Perhaps for the first time, two subsonic wind tunnel techniques were used to furnish a visual (and photographic) representation of supersonic flow patterns. In one approach, an oil-and-lampblack mixture was placed inside of a "Tinkertoy" model so that flow through model joints would occur when the model was exposed to the low pressures present during tunnel operation; in the other, tufts (short silk threads) were attached to the model in appropriate locations.[7] The resulting photographs (see Figs. 7 and 8) have deteriorated with time, but they still show that the essence of the physical theory was effectively proved by the initial experiments. Clear evidence can be seen of an interaction of pressure fields emanating from the root sections of the differentially deflected surfaces, leading to swirl around the body in the

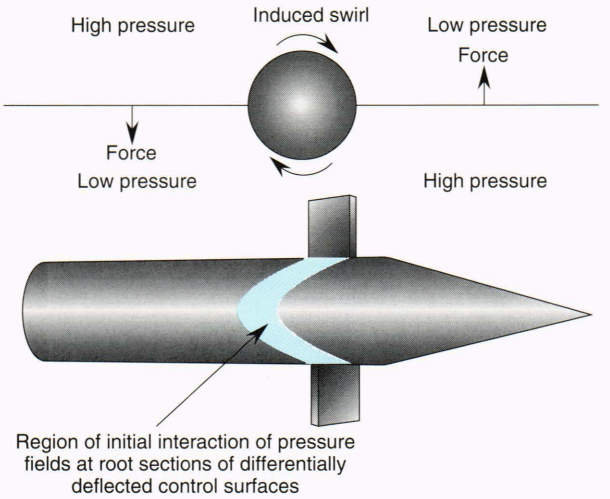

Figure 6. Origin of cross-flow and swirl from interaction of pressure fields at root sections of differentially deflected control surfaces.

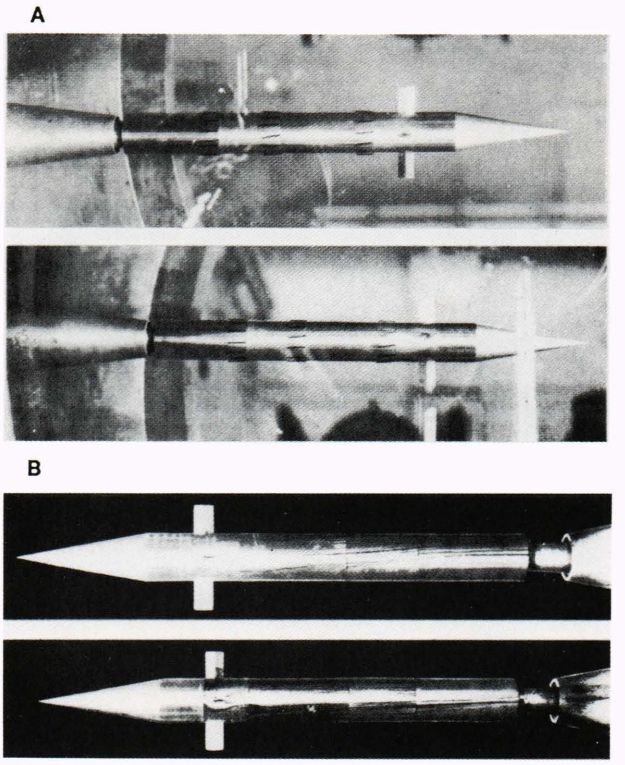

Figure 7. Photographs of tufts and oil-lampblack survey illustrating interaction of pressure fields. **A.** Tufts indicate swirl in the direction expected from the interaction of pressure fields at root sections of differentially deflected control surfaces. **B.** Oil-lampblack flow indicates swirl in direction expected from interaction of pressure fields at root sections of differentially deflected control surfaces. (Vertical flippers deflected 10° differentially, body angle of attack = 0°, Mach number = 1.73. Photographs taken from opposite sides of the tunnel.)

direction needed for reverse roll. (The swirl impinges on aft surfaces, causing the development of reverse rolling moments.) The field of swirl was evident for small flippers representative of the STV-2 design (see Fig. 7); crucially, in respect to the physical explanation, the swirl was also present for large-span differentially deflected surfaces (see Fig. 8) for which the flow at the root sections could not possibly have been affected (at supersonic speeds) by wing-tip phenomena.

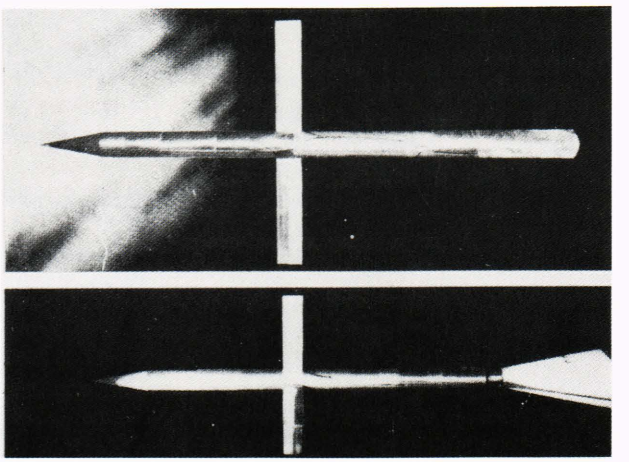

Figure 8. Photographs of oil-lampblack survey indicating swirl in direction expected from interaction of pressure fields at root section of differentially deflected wings. (Horizontal wings deflected 10° differentially, body angle of attack = 0°, M = Mach number. Photographs taken from opposite sides of the tunnel.)

Shortly after the flow patterns were identified, the results were confirmed by detailed pressure measurements, again in regimes that could not physically be affected by wing-tip flow.[7] Additional wind tunnel rolling-moment data were obtained for a wide range of configurations; typical results are shown in Figure 9. With aft surfaces substantially larger than differentially deflected forward surfaces, reverse roll is invariably encountered at supersonic speeds.

The reverse-roll story has been told in some detail to emphasize that supersonic aerodynamic theory was in a state of turmoil in the 1940s. In fact, after the Reference 7 paper had been delivered at a Bumblebee Aerodynamics Symposium in November 1948, reactions were mixed. A few well-recognized theoreticians in the United States and Europe denounced the reverse-roll (both flight and wind tunnel) results as impossible. Some time passed before it was generally agreed that the wind tunnel and flight results were correct and conclusive as presented, that the physical explanation was entirely valid, and that the relevant physical principles had previously been misinterpreted. In defense of those who reacted adversely, it should be mentioned that the OAL wind tunnel rolling-moment results could not be duplicated elsewhere at that time. The uniformity of OAL wind tunnel flow and the accuracy of OAL roll-measurement instrumentation were unique in the world. Furthermore, computational techniques available at the time could not possibly have predicted the rolling moment results, and it is interesting to note that—to the author's knowledge—modern methods have not yet been applied to this problem.

STV–3 AND TERRIER AERODYNAMIC DESIGN

For STV-3, which was intended as a forerunner of the Talos ramjet aerodynamic configuration, roll control was again achieved by use of rollerons at the tips of the fixed

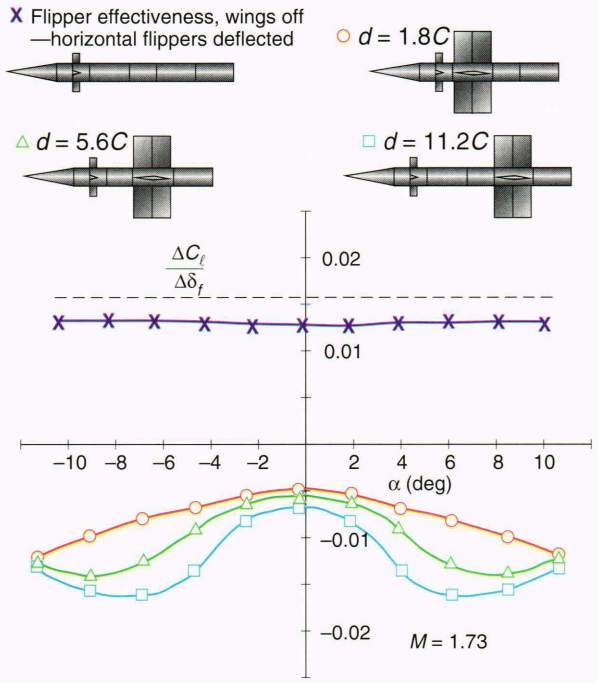

Figure 9. Effect of distance between rectangular flippers and rectangular wings (cruciform wings in line with flippers; horizontal flippers deflected). ($\Delta C_\ell/\Delta\delta_f$ = change in rolling moment per degree of flipper differential deflection; α = body angle of attack; dashed line = theoretical; d = distance from flipper trailing edge to wing leading edge; C = flipper chord length = 0.40 in.; flipper span = 0.60 in.; wing span = wing chord = 2.00 in.; body diameter = 1.00 in.)

tail surfaces, and pitch and yaw control were again (as for STV-2) accomplished by deflection of forward wings. By employing wings substantially larger than those of STV-2, it was possible to develop a viable design that would provide adequate maneuverability at low angles of attack, thereby simplifying in-process Talos ramjet propulsion development. For a ramjet, it is difficult to achieve appropriate air-inlet flow conditions at high angles of attack.

For STV-3, control-test-vehicle flights began in April 1948, and an extensive series of tests was conducted (throughout 1948) to establish correlation between wind tunnel and flight results. It was shown that predictions based on wind tunnel results had become dependable—assuming that considerations relating to nonrigid structures (structural dynamics) were appropriately taken into account (see Ref. 8). The STV-3 aerodynamic characteristics were defined in detail. As a result, when the decision was made in April 1949 to produce a tactical missile (Terrier) with solid rocket propulsion (to provide the earliest possible operational guided missile capability), it was prudent to proceed with minimal changes in the STV-3 configuration. Except for small changes in missile length and wing location and an increase in the size of the rollerons, the Terrier aerodynamic design (see Fig. 10) was virtually identical with that of STV-3.

TALOS AERODYNAMIC DESIGN

In respect to Talos design, it was initially decided that rollerons at the extremes of tail surfaces would be used

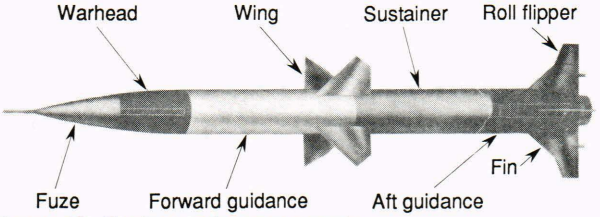

Figure 10. Terrier I major components.

for roll control (as for STV-3 and Terrier), but structural dynamics and control difficulties developed for the tail location on the ramjet tailpipe (the controls could not be directly coupled through the tailpipe). Fortunately, it was determined that, with a further increase in wing area (so that the wings were significantly larger than the tails), it would be possible to generate adequate roll control by differential deflection of the wings for the limited flight regime of Talos (nearly constant Mach number). It was also established that wing control would provide acceptable maneuverability throughout flight for the virtually fixed center-of-gravity location of the ramjet design. As a result, a well-understood aerodynamic configuration could be selected, known structural problems could be avoided, and a single control system could be used.[9]

INITIAL TAIL–CONTROL DEVELOPMENTS

Early in 1950, the need for a follow-on solid rocket missile of significantly higher performance (termed Terrier II) was identified, and an opportunity was provided to make a major change in aerodynamic design. By December of that year—on the basis of wind tunnel tests alone, since tunnel–flight data correlation had been clearly demonstrated—tail control had been selected.[10] It had been established that, for the desired high maneuverability, tail control would significantly improve controllability (much larger, more linear control moments; more linear static stability characteristics; reduced rolling moments due to pitch and yaw angles of attack). Since the center of gravity of the rocket motor could be located approximately at the overall center of gravity of the missile (not possible for wing control with solid rocket propulsion), center-of-gravity travel during flight could be minimized. Because stability variations with Mach number would also be limited for tail control, missiles could be designed for near-zero static stability and maximum speed of response while minimizing control system power requirements and drag due to maneuver.

By early 1951, a specific "final" Terrier II aerodynamic configuration had been chosen, essentially all required wind tunnel data had been obtained, a detailed Navy Ordnance Specification had been prepared, and work had started on the construction of four test vehicles with a view toward flights in early 1952 (employing Terrier I components where possible). The plans for Terrier II included both beamriding and homing guidance versions; the objective was to double the range of Terrier I while significantly improving both high- and low-altitude performance. To allow for the homing system dimensions and rocket characteristics that seemed to be needed, a

diameter of 15 in. had been selected for Terrier II in contrast to 13.5 in. for Terrier I (see Fig. 11).

During 1951 and 1952, however, it became necessary to reduce hardware efforts directed toward Terrier II in order to concentrate on major developmental and production problems that had arisen for the original Terrier. Actually, the delays were beneficial because time was provided for additional studies as well as further component development. In late 1952, a complete Terrier II program review was initiated to assure that maximum advantage would be taken of all available research data and hardware components.

In May 1953, a major report was published,[11] providing in effect a composite design textbook for the future. Included were future program outlines for homing as well as beamriding guidance along with comprehensive aerodynamic and dynamic tail-control design data , extensive tactical analyses, detailed performance calculations, and illustrative discussions of shipboard installations. Selection of the original STV-4 aerodynamic configuration (with a large fixed wing) was confirmed as a best-bet design for homing, but a second tail-control configuration (wingless) was deemed to be of special interest. For the wingless design, it was evident that there would be even more desirable stability and control (and drag) characteristics as well as shipboard handling advantages (obviation of the requirement to install missile surfaces during the launching cycle). As shown in Figure 12, both configurations permitted ideal sectionalization (i.e., division of the missile into functionally separate elements to facilitate development, production, and testing).

The sole difficulty with the wingless missile related to the design and production of a radome that would meet guidance requirements for accurate homing while also withstanding the effects of high temperatures and rain erosion at supersonic speeds (speeds at which the impact of raindrops is similar to that of steel pellets). To realize small missile-to-target miss distances for a homing missile, it is necessary to achieve highly precise measurements of the rate of change of the line-of-sight from missile to target. For the type of guidance system involved, the measurements are made by tracking the target with a gimballed antenna system and measuring the motion of the antenna in space; the antenna system is mounted within a radome. Errors are introduced into the measurement process by aberrations in the radome that cause an apparent motion of the target as the missile moves in response to maneuver commands. As a result of these radome boresight errors, the true target position differs from the apparent target position, and the measured rate of change of the line-of-sight to the target differs from the true rate of change.

For a given missile configuration, the radome boresight error slopes that can be accommodated without significant degradation of miss distance are a direct function of the rate at which a missile develops lift with

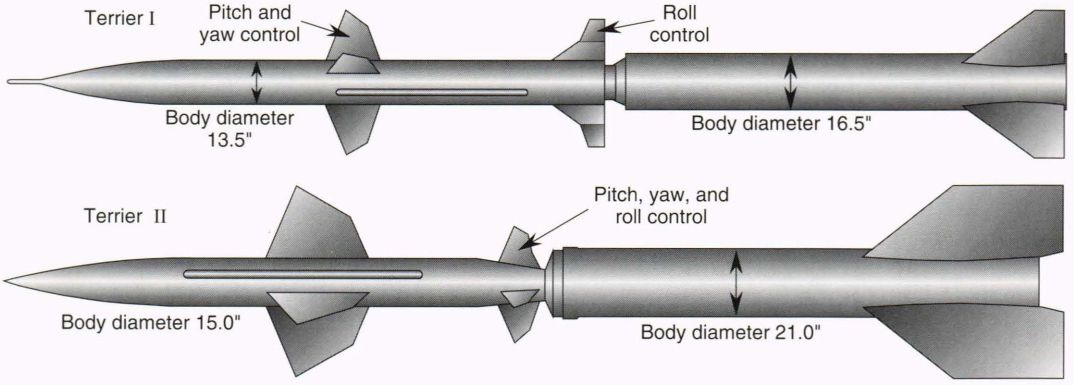

Figure 11. Comparison of Terrier I and Terrier II configurations.

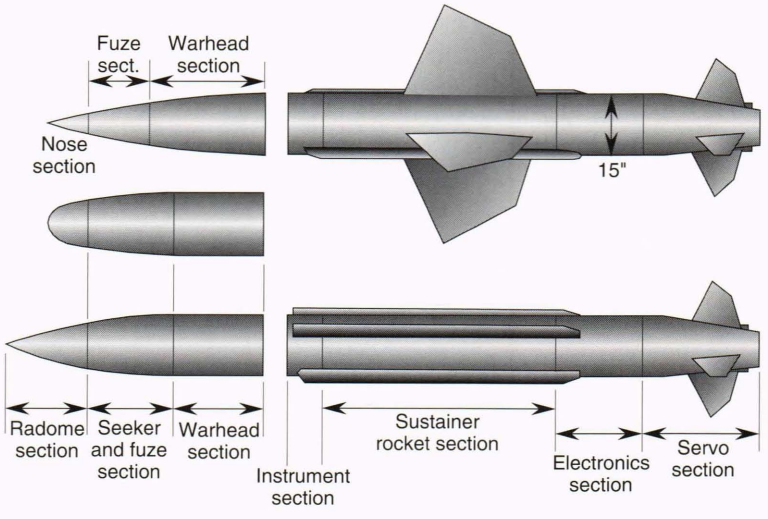

Figure 12. Winged and wingless Terrier II missiles.

increases in angle of attack. For the tail-control configuration with wings (and a high rate of lift development), the radome boresight error slope requirements (the characteristics essential to satisfactory homing) were considered to be consistent with design expectations for a radome of an acceptable (ogival) aerodynamic shape. For the wingless configuration, the requirements appeared at the time to be manageable only for an undesirable (high-drag hemispherical) nose shape.[11]

It was certain, however, that the wingless design would be preferable for beamriding guidance, and it seemed possible that ongoing radome research programs would lead to a radome design suitable for the wingless configuration. Two of the four previously designed STV-4 test vehicles were therefore converted to the wingless design. By October 1954, flights of both winged and wingless versions had been conducted with outstanding success, confirming in detail the preflight aerodynamics and control predictions from analyses and wind tunnel data.[12]

SELECTION OF THE PRODUCTION TAIL–CONTROL DESIGN

In the same time period, studies were undertaken of a compromise configuration, one that would improve the lift versus angle-of-attack characteristics of the wingless configuration—thus alleviating the radome design problem—while maintaining the shipboard handling advantages of the wingless approach. The concept involved using dorsal fins with span limited to the span of "folded" missile tails; the folded tails and the dorsal fins could then be retained on the missile body during the shipboard launching cycle, thus simplifying shipboard handling. The dorsal fins would furnish additional lift (potentially enough to make a significant difference in connection with the radome issue) and would also provide a further advantage in regard to stability and control. It appeared that the static stability of the airframe could be adjusted to required levels for different missile versions simply by altering the dorsal fin length.

Calculations for the designs with dorsal fins were very promising, indicating that the radome design issue might be successfully resolved for a highly desirable missile design. On the other hand, calculational techniques then available were not considered to be dependable for the parameters involved; consequently, the first relevant wind tunnel tests were awaited with intense interest. When the tests were conducted in November 1954, the results exceeded expectations.[13] The lift effects were greater than anticipated—to the extent that the radome boresight error slope requirements appeared to be achievable (within research expectations) even for a pointed radome. In addition, the wind tunnel stability and control data were entirely consistent with the very favorable estimates.

By late 1954, there had also been significant reductions in packaging volume requirements for homing guidance as well as notable improvements in rocket impulse. Putting all of the results together, it was realized that the advanced-missile diameter could be reduced to 13.5 in. to take maximum advantage of previous Terrier developments. A joint APL–Convair presentation (CVAC had become Convair, a Division of General Dynamics Corporation) was made to the Navy in December 1954, identifying the 13.5-in tail-control missile with dorsal fins as the ultimate program objective.[14] At that time, however, the Terrier Growth Program did include advanced wing-control missiles as potential production versions to provide interim levels of improved performance in the event that delays were encountered in meeting the tighter radome tolerances required for tail control. Navy acceptance of the program proposal was immediate.

During 1954, manufacture of another test vehicle series, STV-5, had been undertaken as a step in the winged Terrier II program (15-in. diameter). In accordance with the revised program plan, the STV-5 wings were replaced by dorsal fins, and the first control flight test of the new configuration was carried out, very successfully, in November 1955. By that date, impressive progress had also been made in radome design, and again there were program changes. In January 1956, in another joint APL–Convair presentation, it was recommended to the Navy—again with immediate Navy acceptance—that only tail-control missiles with dorsal fins be produced as elements of the Terrier Growth Program.[15]

TERRIER–TARTAR INTERACTIONS

In the meantime, yet another major program decision had been made. Over a period of years, studies had been directed toward the development of a "small-ship" missile (Tartar) that could be used on destroyers or as a secondary battery on larger ships. Initially, efforts had focused on the design of a new missile. By early 1955, however, an intensive study[16] had been conducted "to determine if the Terrier Improvement Program could also lead directly to the development of a missile suitable for use aboard small ships." As noted in the reference, "The outcome of the study was successful beyond initial expectations. A program based on the results of this study was approved by the Navy early in 1955 and all previous work reoriented accordingly . . . To a major extent, a single missile is being developed to meet both requirements for the Navy . . . It should be emphasized that this evolution is made possible by the Terrier concept of sectionalization and by the use of a missile configuration that is not sensitive to changes in missile dimensional and weight characteristics."[16]

The "Tinkertoy" approach to missile development and production (see Fig. 13) was outstandingly successful, both with respect to the several Growth Program versions of Terrier and with regard to Terrier–Tartar interactions. To streamline the development process, the Terrier program was given responsibility for primary aspects of aerodynamics, dynamics, and control system design for Tartar as well as Terrier,[17] and the Tartar program was made responsible for homing system and warhead design for Homing Terrier as well as for Tartar.[17,18] In general, problem solutions developed for one missile type could be employed for others.

SOLUTION OF THE RADOME PROBLEM

In 1957, an especially timely and noteworthy success was achieved in the radome research program. As men-

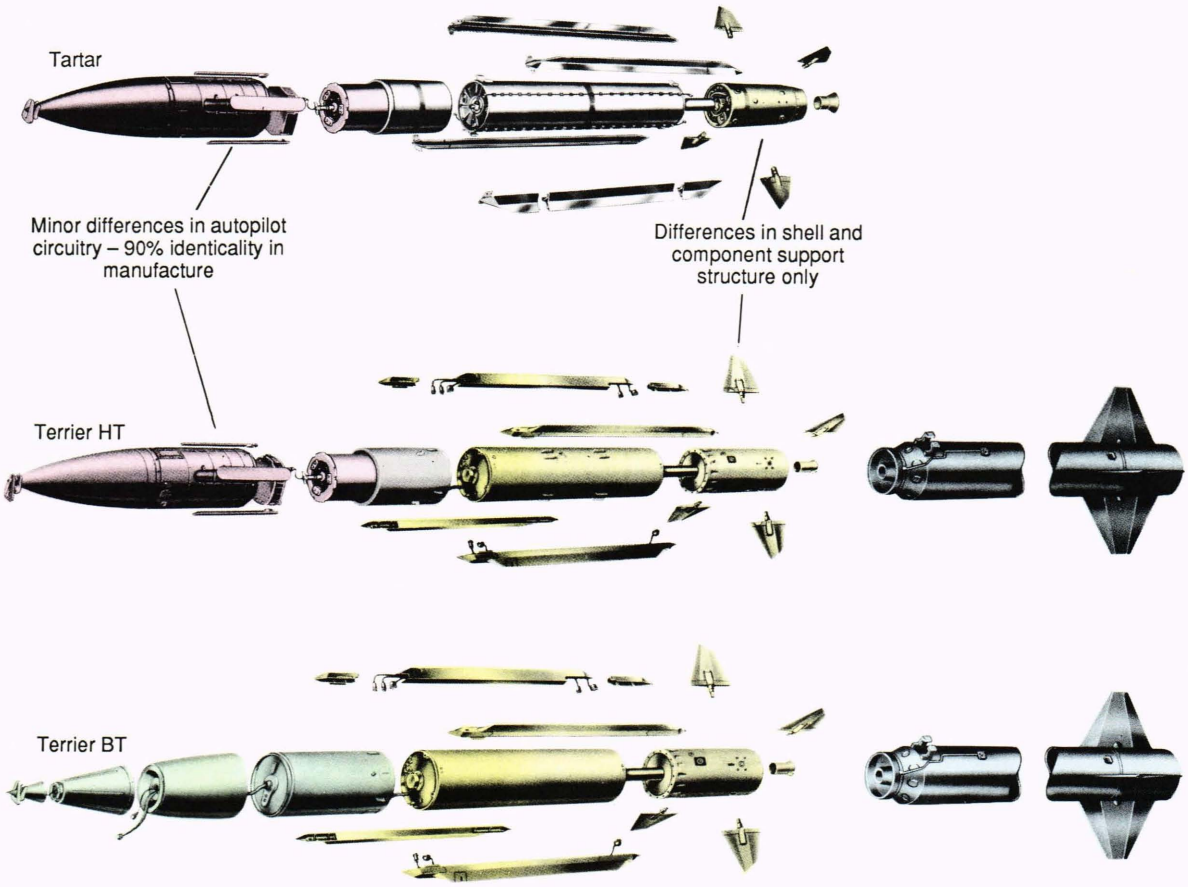

Figure 13. "Tinkertoy" approach to missile design.

tioned previously, to permit accurate homing with tail control, it was necessary to develop radomes that would meet electrical design requirements (very low values of radome aberrations) while also fulfilling mechanical design requirements (suitable structural characteristics under conditions of high flight temperatures and potential rain erosion). In the rain-erosion test program, samples of a new class of materials (termed cerams) were obtained from the Corning Glass Company—initially because of the promise of excellent mechanical properties. Prior to heat treatment, these materials behaved as high–melting-point glasses and could be fabricated into desired shapes by conventional glass-forming techniques; after forming, they could be heat-treated to change them from a glass to a fine-grained crystalline material. The material of greatest interest—a pyroceram—passed all mechanical tests, demonstrating remarkable rain-erosion resistance.

Fortuitously, it was determined that the electrical properties of the same material might also be unusually attractive if precise control of composition could be accomplished in production. Under Department of Defense sponsorship, a pilot production project was quickly established—first to develop production techniques and then to furnish flight radomes for Tartar and Terrier. Once again, the results exceeded all expectations. It proved possible to produce a material of requisite uniformity; as a result, radomes with outstanding electrical characteristics (including the required boresight error slopes) could be provided at low cost.[19] By this achievement, the major risk taken in the selection of the tail-control configuration with dorsal fins had been eliminated—and the Corning Glass Company had a new product available for commercial applications.

DESIGN FOR PRODUCTION

In all design areas, progress was made rapidly—though not smoothly. Structural dynamics problems (steady-state deflections and flutter) had led to STV-3 and Talos flight-test failures; flutter problems also developed for the Terrier/Tartar tail surfaces. Flutter theory was inadequate at the time, but ultimately the problems were solved by use of a straightforward dynamic balancing approach developed at APL.[20] Additional structural dynamics issues plagued the development of the first high-performance acceleration-feedback autopilots. Abstruse coupling modes, such as coupling between body longitudinal bending and tail torsional modes and between tail spanwise bending and roll system design parameters, were discovered in ground tests—degrees of interaction that were certainly not anticipated. For high angle-of-attack conditions, aerodynamic interactions among pitch, yaw, and roll modes of motion had to be accounted for in control system design.[19, 21, 22] Rocket shock, vibration, and flame-burst problems had to be solved; malfunction of components caused by extreme flight environments was common. Fortunately, flight failures were deemed to

be necessary elements of the learning process, not reasons for program cancellation; management efforts could therefore be concentrated on program accomplishment, not on program defense. As a result, problems were solved expeditiously, schedules were maintained, and all design objectives were fully met.

For the beamriding tail-control Terrier (Terrier BT), pilot production began in mid-1958. By December 1958, all thirty of the missiles in the pilot program had been formally accepted by the Navy—12 months after the first successful tail-control flight with beamriding guidance and 18 months after the first successful control-test-vehicle flight with the dorsal fin configuration. Terrier BT was in full-scale, high-rate production early in 1959.[17]

INTERCEPT OF BALLISTIC TARGETS

Successful formal Navy evaluations of Terrier BT performance were conducted at the Naval Ordnance Test Station (now the Naval Air Warfare Center), China Lake, California, and on tactical ships; however, an additional, unusual flight-test program was carried out to provide flight demonstrations against potential tactical ballistic missile targets. For this program, Terrier I Beamriding/Wing Control (Terrier BW) missiles were converted by APL for use as targets (with wings removed); a missile-to-target miss-distance measuring system was included. The targets were launched from San Nicolas Island (off the coast of California, in the Pacific Missile Range) by a U.S. Marine Corps Battalion; the Terrier BT interceptor missiles were flown from the USS *Norton Sound,* a ship that had been converted for experimental Terrier flight tests. The Terrier BW missiles (targets) were flown on ballistic trajectories to altitudes of about 115,000 ft; the Terrier BT missiles were fired for planned intercepts during the downward phase of the target flights.

On August 16, 1960, an intercept was achieved at an altitude of 64,500 ft, with a measured miss distance of 56 ft—presumably the first intercept of a ballistic missile target by a supersonic guided missile. On August 18, a second ballistic missile intercept occurred at approximately 80,000 ft; the miss distance indicator malfunctioned, but a close miss or direct hit seemed to be indicated. In the same program, designated TOP HAT (Terrier Operational Proof, High Altitude Target), Terrier BT successfully intercepted (on August 17) a Regulus II Missile Drone flying at Mach 2 at an altitude of 44,000 ft,[23] foreshadowing programs to intercept airborne missile targets.

TERRIER–TARTAR INTERCHANGEABILITY

Production of the Tartar missile was started late in 1959; Homing Terrier (HT) production, in 1961. Because of the sectionalized nature of the missile designs and the noncritical aerodynamic configuration, improvements on a "block-change" basis could be conveniently introduced.[24] The Terrier/Tartar concept of interchangeability—the capability for substitutions and common usage of missile elements with no modifications or adjustments—resulted in striking advantages during development, production, and fleet utilization. For development: concentration of design talent on fewer components with concomitant reductions in documentation requirements and in the number of items to "debug" in ground and flight tests. For production: reduction in documentation requirements and in tooling for parts fabrication; quantity purchase of common items; standardization of assembly techniques; multiple usage of test equipment, inspection facilities, and gauges. For fleet utilization: quantity purchasing; reduced inventory of spares, test equipment, and assembly tools; common shipping and handling methods; reduced training time.[25] For the overall program: substantially reduced costs.

When production of Homing Terrier and the corresponding improved version of Tartar was fully integrated in 1961 (see Fig. 14), approximately 85% of the dollar value of the guidance, control, and airframe elements was in terms of directly interchangeable parts. Achieving the indicated levels of interchangeability entailed minor costs, for each of the missiles necessarily carried a small number of extra components and circuits as a result of requirements for a different missile. The costs of interchangeability were, however, entirely negligible by comparison with the advantages.

STANDARD MISSILE DESIGN

At a later date, when initial ship defense requirements had been met and homing system designs had been proven, a decision was made to stop production of the beamriding version of Terrier. At that time, the follow-on versions of Homing Terrier and Tartar were designated Standard Missile to emphasize the "single missile" nature of the development process.[26] The value of the program approach was further evidenced when Standard Missile versions were quickly and efficiently developed for applications other than surface-to-air defense of the fleet, for example, as air-to-surface antiradiation missiles or antisurface missiles with active guidance.[27]

SYSTEMS ENGINEERING TECHNIQUES

As previously stated, the sectionalized missile designs and the noncritical aerodynamic configuration were essential to effective implementation of the interchangeability concept for Terrier/Tartar/Standard Missile. It is important to note, however, that the programs could not have been successful without the concurrent development of requisite systems engineering approaches and techniques. Reference 28 specifically discusses systems engineering for the initial tail-control beamriding Terrier program, but the design philosophy and methodology were applied for all of the interactive programs.

It is emphasized in Ref. 28 that the process of defining performance requirements was closed-loop, involving preliminary design trade-offs to assure that the specified performance would be consistent with the goal of designing a high-performance missile capable of large-scale production on an established schedule (see Fig. 15). The general approach is outlined as follows:

1. An over-all missile design is selected that appears to provide a substantial margin of performance over the stated requirements; a combination of aerodynamic, dynamic, and structural characteristics is chosen that seems appropriate to noncritical design.

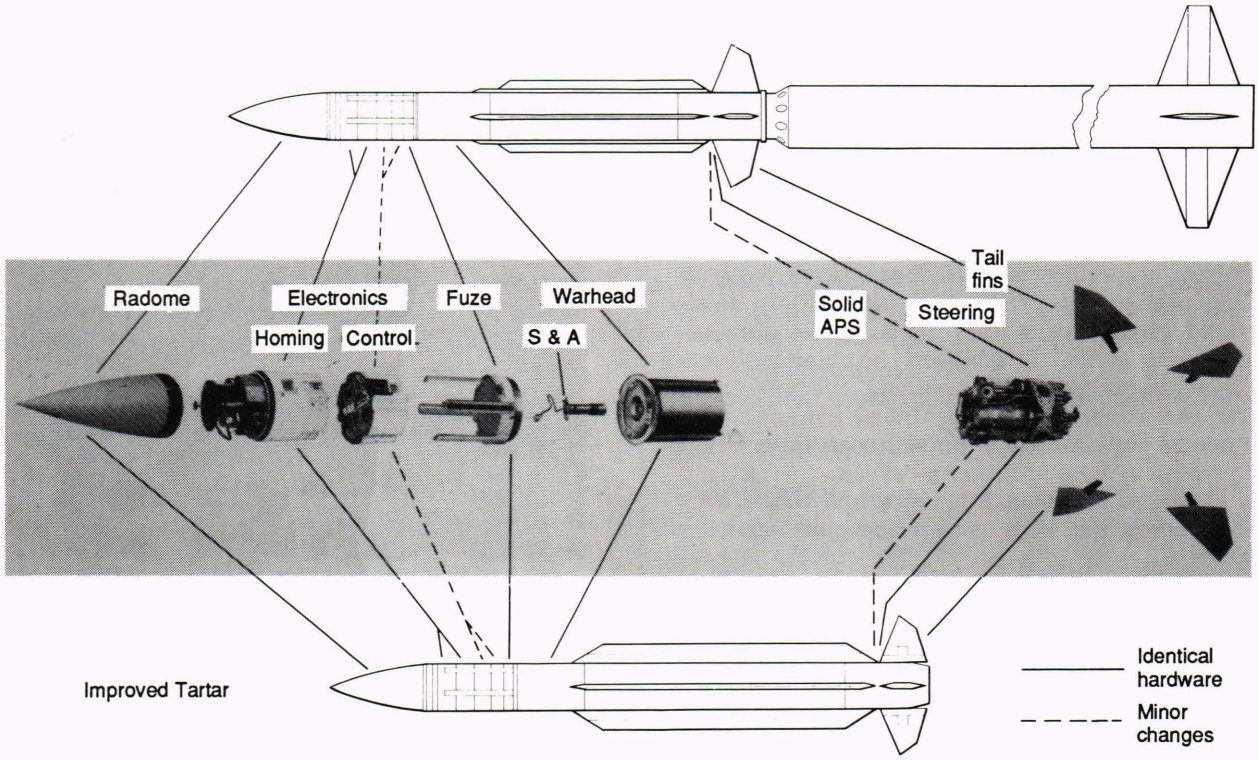

Figure 14. Terrier HT (Homing Terrier) and improved Tartar showing interchangeable hardware (APS = auxiliary power supply, S & A = safety and arming).

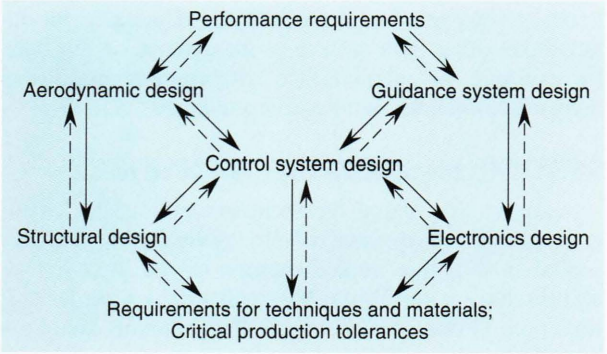

Figure 15. Terrier BT (Beamriding Tail-Control) Preliminary Design Approach.

2. The design is subdivided (sectionalized) along functional lines, to permit flexibility of design in functionally separate areas and to minimize coordination problems.
3. The design areas of greatest difficulty are determined, and all design requirements are organized to provide maximum latitude in those areas.
4. Each element of the missile is designed for required performance, rather than for maximum possible performance; simplification of design and broadening of tolerances are emphasized rather than improvement of performance beyond the given requirements.
5. Reserve design margins are provided in the preliminary design phase to "leave room" for unforeseen problems.
6. The number of engineering challenges is minimized by employing techniques well within the state-of-the-art; techniques not yet proved in production are used only where absolutely essential.[28]

In the development of production tolerances,

> Statistical (Monte Carlo) methods are employed to evaluate the effects of production tolerances on performance; the possibility of a small percentage of functional failures is allowed in order to permit general broadening of tolerances. Studies are directed toward broadening of permissible tolerances in areas of design difficulty; an attempt is made to determine the best balance of tolerances for the stated over-all performance goal.[28]

Overall, the intent was to develop and use production designs as early as possible during the flight-testing programs so that there could be a relatively smooth transition from development to production. In the latter stages of the flight demonstration/validation programs, the prototype missiles were very similar to the planned pilot production designs.

For each section of the missile, all functional design requirements were specified in APL "Performance and Compatibility Requirements" documents (see, for example, Fig. 16 for Standard Missile), and interface control among elements was maintained by using "Correlation Drawings" that defined electrical, mechanical, and spatial requirements. Formal, continuing studies were conducted under APL direction with representation by all contractors affected by a particular interface to ensure that an appropriate balance of interface requirements had been achieved.

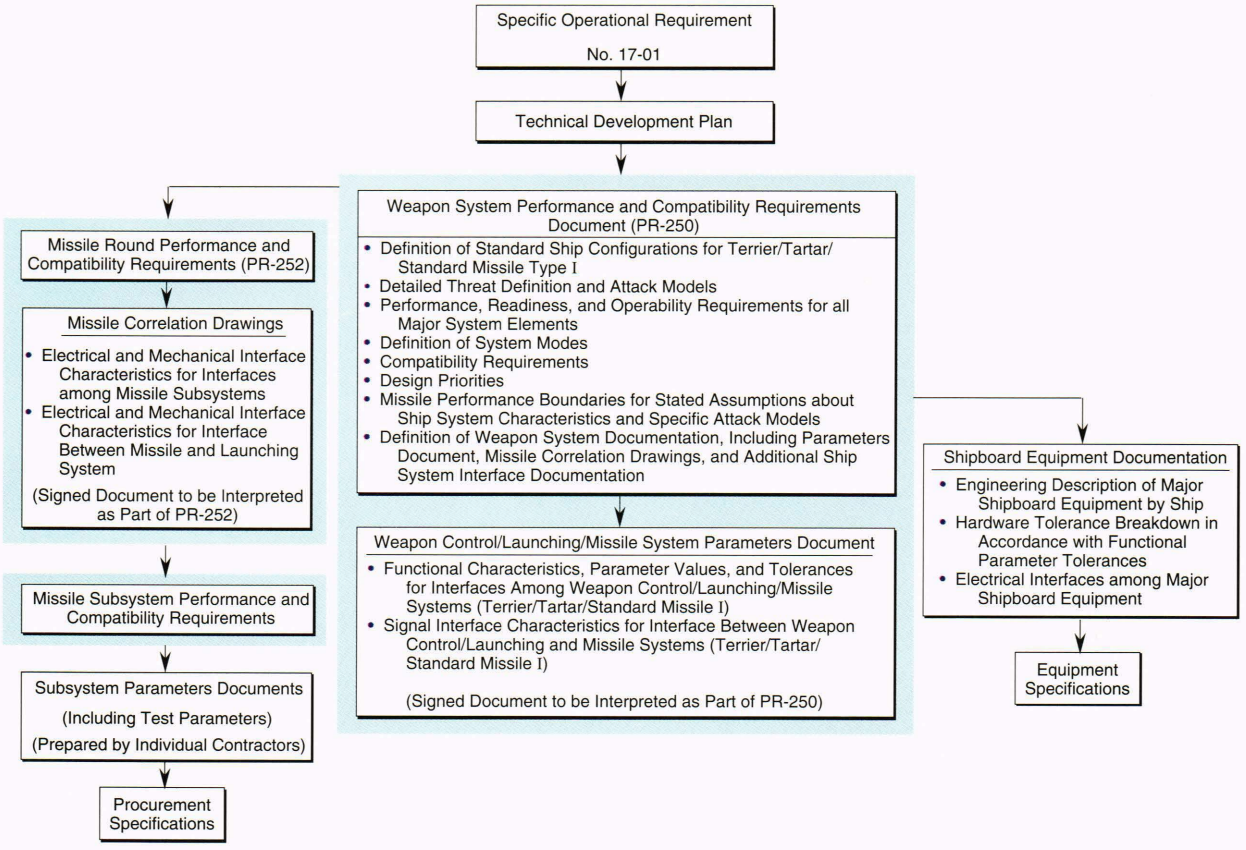

Figure 16. Hierarchy of APL Performance and Compatibility Requirements documents for the Standard Missile.

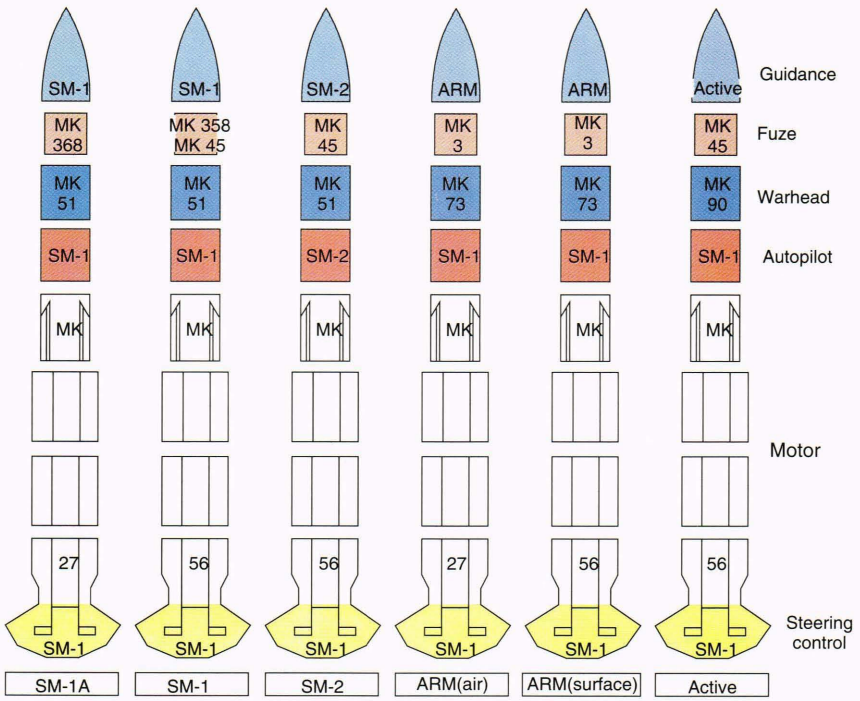

Figure 17. Medium-range Standard Missile family, including antiradiation and active-guidance missiles, derived from combination of components (ARM = antiradiation missile).

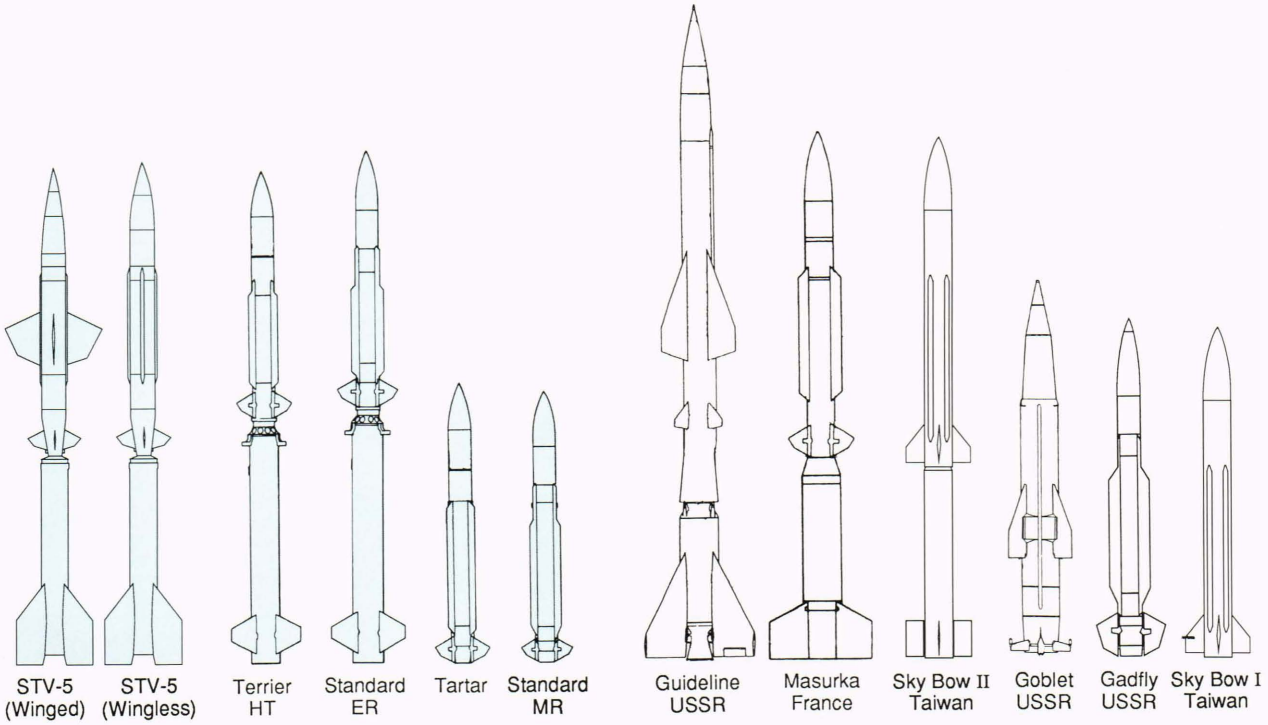

Figure 18. Missile configuration comparisons (ER = extended range, MR = medium range).

RECOGNITION OF THE STANDARD MISSILE APPROACH

It is worth noting that the value of the overall program approach was recognized and commended in a widely distributed report in 1974.[29] To quote from the reference:

> An outstanding example of the manner in which carefully-controlled interface specifications can provide a framework for evolution of variants of a mission-critical system is the Navy's Standard Missile program. The program involved the evolution of missiles to meet different threats in a field of rapidly changing technology. It invoked standard interfaces with the platform, launchers, etc., so that the new Standard Missiles could be employed on the older Terrier and Tartar ships with only minor (usually electrical) modifications required aboard ship. Intramissile interfaces were established and controlled so that new technology or new capability could be added a section at a time, and as a result new missiles representing completely new capabilities have been developed while making use of existing, available standard and proven missile sections and elements.
>
> The sketch [see Fig. 17] illustrates the several members of the Standard Missile (medium-range) family and the degree to which standardization has been achieved. Not shown is the fact that the Standard Missile-1 (SM-1) was itself developed by using many prior proved components, assemblies and sections from Terrier and Tartar.
>
> The benefits of this approach can be seen in two areas. First, the manpower in man-months and the calendar time required to achieve the first successful guided test vehicle of each successive type have been substantially smaller than what was required for the initial Standard Missile. Second, despite continuing performance improvement in successive missile types (e.g., doubling in altitude capability, quadrupling in range), missile production costs have stayed essentially constant.

WORLDWIDE AERODYNAMIC DESIGNS

With respect to the basic aerodynamic design of Terrier, Tartar, and Standard Missile, it is interesting to make comparisons with missile configurations that have evolved—some quite recently—in other countries (see Fig. 18).[30] Since fundamental aspects of aerodynamics and control technologies are involved, it is probable that many of the designs were derived independently, but the similarities are compelling. In any event, it is clear that the specific tail-control aerodynamic configurations pioneered by APL during the Bumblebee days are in widespread use and have not been outdated by subsequent developments.

REFERENCES

[1] von Kármán, T., "Supersonic Aerodynamics—Principles and Applications," The Tenth Wright Brothers Lecture, in *Collected Works of Theodore von Kármán, Vol. IV 1940–1951*, Butterworths Scientific Publications, London, pp. 271–326 (1956).

[2] *Survey of Bumblebee Activities*, JHU/APL Bumblebee Series Report No. 49, pp. 15–19 (Dec 1946).

[3] *Survey of Bumblebee Activities*, JHU/APL Bumblebee Series Report No. 54, pp. 10–11 (Feb 1947).

[4] Looney, C. T. G., *The Design and Construction of the Ordnance Aerophysics Laboratory*, JHU/APL Bumblebee Series Report No. 78 (May 1948).

[5] *Survey of Bumblebee Activities*, JHU/APL Bumblebee Series Report No. 56, pp. 13–14 (Mar 1947).

[6] *Survey of Bumblebee Activities*, JHU/APL Bumblebee Series Report No. 77, pp. 19–20 (Mar 1948).

[7] Eaton, A. R., "Experimental Investigations of Roll-Reversal Effects for Generalized Missile Configurations at Supersonic Velocities," in *Proc. Bumblebee Aerodynamics Symposium, 4–5 November 1948*, The Johns Hopkins University Applied Physics Laboratory, Silver Spring, Md., pp. 237–265 (1948).

[8] Eaton, Jr., A. R., *Telemetering in the Bumblebee Program*, JHU/APL TG 138, pp. 2–7 (1 Jul 1952).

[9] Cronvich, L. L., ' Talos Aerodynamics," *Johns Hopkins APL Tech. Dig.* **3**(2), 138–141 (1982).

[10]Eaton, A. R., "Tail Control vs. Wing Control; Plans for Type II Terrier," in *Bumblebee Aerodynamics Panel, Minutes of Fourteenth Regular Meeting, San Diego, California, 5 & 6 December 1950,* JHU/APL TG 14-11, Appendix V (Feb 1951).
[11]Amsler, B. E., Eaton, A. R., Garrison, J. B., Goldbach, F. P., Waddell, M. C., et al., *Terrier II Program Review,* TG 192 (1 Jul 1953).
[12]*Semi-Annual Summary of Bumblebee Activities,* JHU/APL Bumblebee Report No. 233, p. 24 (Jul–Dec 1954).
[13]Marley, E. T., *Aerodynamic Report of the STV-5 (Control Test Vehicle) Missile,* JHU/APL Bumblebee Series Report No. 255 (Jul 1956).
[14]*Survey of Bumblebee Activities*, JHU/APL Bumblebee Report No. 227, p. 4 (Jul 1955).
[15]Convair, *Terrier Growth Program as of January 1956,* Convair Report 300–005, Pomona, Calif. (Jan 1956).
[16]Amsler, B. E., Eaton, A. R., Floyd, J. F. R., Goldbach, F. P., Sheppard, T. W., et al., *The Tartar Missile, Adaptation of the Terrier Missile to Small Ship Use,* JHU/APL TG 258 (13 Oct 1955).
[17]Goldbach, F. P., *Terrier Section, APL History,* The Johns Hopkins University Applied Physics Laboratory, Silver Spring, Md. (Dec 1961).
[18]Fraser, L. W., and Sheppard, T. W., *Tartar History*, JHU/APL FS 508 (21 Jan 1964).
[19]*APL Accomplishments in the Bumblebee Program, FY 1957,* JHU/APL TG 277, pp. 2–3, 10 (Dec 1957).
[20]Kearns, J., *Flutter Analysis in the Bumblebee Program*, JHU/APL Bumblebee Report No. 225 (Dec 1954).
[21]Cronvich, L. L., and Amsler, B. E., "Pitch-Yaw-Roll Coupling," AGARD Specialists' Meeting on Aircraft Stability and Control, Brussels (10–14 Apr 1961).
[22]Cronvich, L. L., "Aerodynamic Considerations for Autopilot Design," in *Tactical Missile Aerodynamics, Progress in Astronautics and Aeronautics,* Vol. 104, Hemsch, M. J., and Nielsen, J. N. (eds.), American Institute of Aeronautics and Astronautics, Inc., Brooklyn, N.Y. (1986).
[23]Williamson, A. C., *Top Hat Summary Report*, JHU/APL TG 389 (Apr 1961).
[24]Eaton, A. R., and Foley, W. J., "A Comprehensive Evaluation of the Performance of Terrier and Tartar Homing Missiles in Special Environments Including Low Elevation Targets, Multiple Targets, Countermeasures and Multi-Ship Operations; Definition of a Retrofit Program to Provide Major Improvements," JHU/APL MPO-A-067 (Nov 1964).
[25]*Report on Terrier/Tartar Interchangeability Achievements,* Prepared for Bureau of Naval Weapons by General Dynamics, Pomona, Calif., and The Johns Hopkins University Applied Physics Laboratory, Silver Spring, Md.
[26]Oliver, M. E., and Sweet, W. N., "Standard Missile: The Common Denominator," *Johns Hopkins APL Tech. Dig.* **2**(4), pp. 283–288 (1981).
[27]Kemp, R. M., "Versatile Navy Weapon," *National Defense* **61** (337), pp. 44–47 (Jul–Aug 1976).
[28]Eaton, A. R., "Systems Engineering in a Missile Program," Operations Research and Systems Engineering, An Intensive Course for Management, The Johns Hopkins University, Silver Spring, Md. (6–17 Jun 1960).
[29]Gates, Jr., H. P., Gourary, B. S., Deitchman, S. J., Rowan, T. C., and Weimer, C. D., *Electronics-X: A Study of Military Electronics with Particular Reference to Cost and Reliability, Final Report for Period February 1973–October 1973,* Report R-195, Institute for Defense Analyses Science and Technology Division, Arlington, Va., pp. 281–284 (Jan 1974).
[30]*The World's Missile Systems*, Seventh Edition, General Dynamics, Pomona Division, Pomona, Calif. (Apr 1982).

THE AUTHOR

ALVIN R. EATON received his A.B. in physics from Oberlin College and his M.S. in aeronautical engineering from the California Institute of Technology. Relative to the subject of this article, he received a U.S. Navy Meritorious Public Service Citation as "personally responsible for most of the aerodynamic design of Terrier, and for the solution of many difficult problems, such as supersonic roll reversal, which threatened to halt the successful development of the missile." He was responsible for direction of the tail-control Terrier program from inception into production. After supervising other missile programs, he became Head of the Missile Systems Division in 1965, Head of the Fleet Systems Department and Assistant Director for Tactical Systems in 1973, Assistant Director in 1979, and Associate Director from 1986 to 1989. He is currently a Senior Fellow and Director of Special Programs. He has received a U.S. Navy Distinguished Public Service Medal and numerous commendations from other agencies. He is listed in *Who's Who in America* and *Who's Who in the World.*

MATERIALS for structural use

In the era from 1970 to 1980, manned orbital flights may be quite commonplace. It has been estimated, for example, that the United States alone could have requirements for orbiting up to 1000 passengers each year. Based on disposable rocket systems of the type now employed or under development, it is predicted that even at this level of operation, the cost would remain at the rather extravagant figure of 2.7 million dollars per passenger round trip.[1] It has also been predicted that the cost could be reduced to $20,000 per passenger with a reusable launch system employing an airbreathing turbo-ramjet to power the first stage.[1] A system that would use the cold hydrogen fuel to accumulate and store liquid oxygen during first-stage flight has been proposed in order to achieve such economy. The liquid oxygen would be used to power second- or third-stage rockets. Such a scheme involves substantial development risks, but the prospect of such an important economy suggests that some developmental effort should be expended in this direction.

The advantages of airbreathing propulsion have long been recognized at APL, and the Aeronautics Division is currently involved in research that will be of notable importance in the development of hypersonic propulsion systems. The supersonic combustion ramjet (SCRAM) has special advantages that have been investigated under the direction of W. H. Avery and G. L. Dugger of APL.* It has been shown, for example, that it is theoretically possible to develop an airplane based on this type of propulsion that would be capable of achieving orbital velocity with substantially better payload efficiencies than can be gotten with chemical rockets. For missile applications, the supersonic

[1] R. A. Bailey and D. L. Kelley, "The Potential of Recoverable Booster Systems for Orbital Logistics," *Astronautics and Aeronautics*, 2, Jan. 1964, 54–59.

* Dr. W. H. Avery is supervisor of the Aeronautics Division and Dr. G. L. Dugger is supervisor of the Hypersonic Propulsion Group.

ABOVE 3000°F

Hypersonic projects at APL and elsewhere are generating the need for improved materials for use in complex structures that must operate at temperatures up to 5000°F. The present paper discusses the behavior of metallic alloys under stress at temperatures above 3000°F. The usable strength at a given temperature may vary by a factor of ten because of the way in which strength depends on the rate at which the materials are deformed. Estimates of the design allowables *are given for currently available alloys, along with predictions of developments for the next decade.*

M. L. Hill

ramjet can provide substantial speed and range advantages over conventional rockets, and much of the current research at APL is being conducted with this application in mind.

One of the difficult problems with such hypersonic vehicles is the intense heat that is generated by the friction of the air moving across the structure. At speeds around Mach 10, and at an altitude of about 15 miles, an uncooled or uninsulated structure would rise to temperatures near the 5000°F of the "white hot" filament in an incandescent light bulb. Thus, hypersonic airplanes or missiles will have to employ insulating materials and special cooling techniques to counteract these severe temperatures. In the case of the orbiting airplane, before the very cold liquid hydrogen fuel is burned in the ramjet engines, it would be pumped through passages in the skin to absorb frictional heat. Missile airframes, by virtue of their short-duration missions might be protected by a passive insulation or an ablative material in much the same way that re-entry vehicles are protected; they are therefore expected to have substantially simpler structures than the regeneratively cooled airplane.

Successful development of such cooling or insulating techniques would permit the use of conventional aircraft materials such as titanium, aluminum, and steel for the major portion of the structures. It is certain, however, that there will be critical regions in which it will be difficult or impossible to hold temperatures to the 500°F to 2000°F range that these materials can tolerate. For this reason the Laboratory is engaged in a program of evaluating metallic alloys of columbium, tantalum, and molybdenum, as well as graphites and refractory oxides, carbides, silicides, and other ceramics for possible use in a hypersonic environment at temperatures in the range of 2000° to 5000°F. At temperatures where ordi-

nary steel melts, some of these have strengths exceeding that of an automobile bumper. However, as temperatures exceeding 3000°F are reached, even these lose strength rapidly, and it is necessary to be intimately familiar with their properties in order to employ them efficiently.

Problems associated with high temperatures are, of course, also encountered in rockets that fly outside the atmosphere. The overall efficiency and, often, the difference between success and failure depend to a great extent on the performance of critical components of rocket propulsion plants that operate at high temperatures. Regardless of the specific modes of propulsion that might be employed, the practical limits of future space and defense programs will be strongly influenced by materials availability and capabilities. Consequently, there is an intense curiosity about what improvements in materials are likely to be achieved in the next decade or so.

The most reasonable basis on which such predictions can be made is an assessment of what has already been accomplished and over what period of time. A brief assessment of this nature is therefore given here; and in the light of it some predictions are made about the probable materials developments during the next decade.

High-Temperature Materials Reviewed

The progress that has been made toward providing high-strength metallic alloys for engineering applications is summarized in Fig. 1 in a general way. As described below, this figure also presents a picture of the current state of affairs, and in another sense it illustrates what some of the problems are in going to higher temperatures.

Shown in this figure are the tensile strengths of a variety of metals and alloys at temperatures up to 5000°F. The upper, heavy boundary line shows the highest strength alloys that have been developed to date (1964), while the dotted extensions of the various segments show the general temperature dependence of the individual alloys. Also shown (lower left) are the strengths of the metallic elements on which the alloys are based. Arrows are drawn to show how much increase in strength has been achieved by application of metallurgical strengthening mechanisms.

Development of Steel—By far the most profound achievement has been in the area of converting iron to steel by the addition of other elements such as carbon, nickel chromium, and others. However, modern-day metallurgists cannot take much credit for this, for as everyone who watches late TV shows knows, iron-masters in the service of King Louis XIV discovered this strengthening quite by accident when they hurriedly dumped a freshly cast cannon into the castle moat to prevent the enemy from confiscating it. Hollywood researchers are open to metallurgical criticism, however, for it is certain that a cannon of the size shown in their films would have cracked to pieces when quenched in water. Besides, they probably could have made a far more interesting film about Damascus swords, which were hardened centuries earlier by thrusting the red hot blade into the thigh of a choice slave.

This facetious discussion is made only to point out that much of the development of high-strength steels from iron took place over several centuries and in the absence of scientific understanding of the process. Basic understanding of the transformation—hardening of steels—was obtained about 50 years ago, and as a result of this understanding usable strengths have been extended from about 150,000 psi to the 350,000 psi now obtainable. Newer knowledge of dislocation behavior, phase transformations, and fracture mechanisms has resulted in achievement of 450,000 psi in recent experimental steels,[2] and a half-a-million-psi tensile strength steel may be an engineering reality within the next decade.

Recent Alloy Development—In contrast to the centuries of steel development, the large increase in strength of titanium alloys has been achieved almost entirely within the last decade.[3] When recovery of this metal from ores became economically feasible, no time was lost in applying previously accumulated metallurgical knowledge of phase changes, precipitation-hardening, cold-working, and other strengthening mechanisms. Because of their relatively low density and high strength, titanium alloys are currently used in many aircraft applications. Total world production in 1950 was only a few thousand pounds, while in 1963, U.S. production alone amounted to about 7000 tons. Higher strength alloys are still under development, and some of the current research on titanium alloys is aimed at increasing their temperature capability. It is reasonable to expect the knee of

[2] C. W. Marshall, "Hot-Cold Working of Steel to Improve Strength," Battelle Memorial Institute DMIC Report 192, Oct. 1963.

[3] "The Current Status and 1970 Potential of Selected Defense Materials," Battelle Memorial Institute DMIC Memo 183, Oct. 1963.

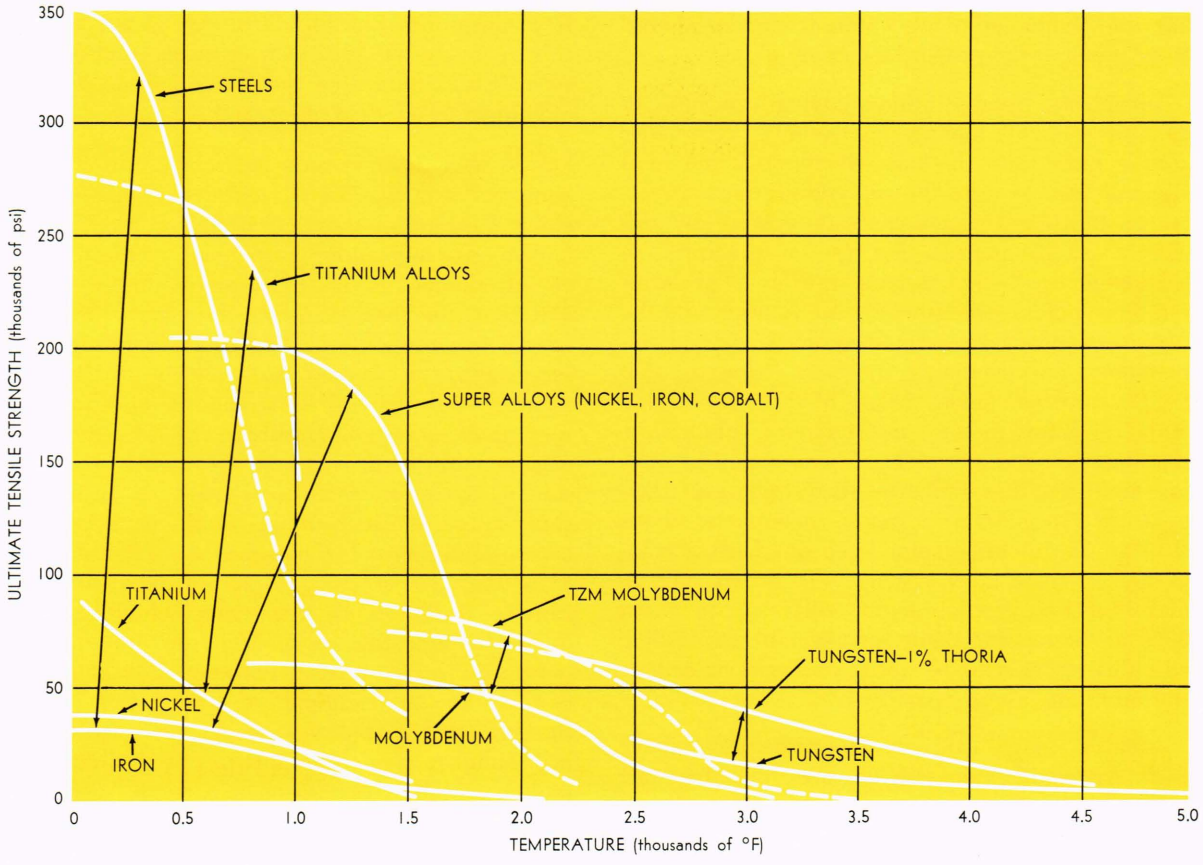

Fig. 1—Summary of tensile strengths of a variety of metals and metal alloys at temperatures to 5000°F.

this curve to be shifted out to perhaps 1300°F during the next decade.

Much of the credit for improvements in super alloys belongs to those who have been involved in the theoretical aspects of metal physics. A number of methods of increasing strength and decreasing creep rate were suggested by modern theories about imperfections and dislocations in metallic crystals. Many of these ideas have been converted into practical usage and remarkable engineering gains. For example, during the past two decades the aircraft turbine has evolved from a risky, inefficient propulsion plant of practical interest to only a few military planners into a reliable and unsurpassed system for commercial transport. The role of metallurgy in this development was not minor.

Some gains in strength of these nickel, cobalt, and iron-base "super alloys" are still forthcoming, but it is unlikely that the knee of this curve can be shifted much above 1700° to 1800°F.[3] Major improvements in fabricability are being made, particularly with respect to welding. Alloys similar to TD nickel[3] (a dispersion of thoria powder in nickel) will probably be more common. These will have substantially less strength than shown here for super alloys at 1600°F, but will retain usable strength to 2400°F.

In the area in which we are currently most interested (2000°F and up) it is seen that relatively small improvements in strength have been accomplished. Unfortunately this is not the result of mere lack of understanding or inadequate effort; it is a reflection of basic properties that frustrate most attempts to add strength. Conventional strengthening mechanisms such as phase-transformation, precipitation-hardening, and cold-working, which are widely employed in aluminum, steels, and titanium, are usually ineffective above the recrystallization temperature of the base metal. In a simplified sense this is the temperature at which thermal activation is sufficiently intense to permit easy diffusion of atoms within the crystal lattice. In pure metals it usually occurs at about one half the melting point. It is an inherent property, but

like the boiling point of water, it can be altered by a "pinch of the proper kind of salt."

In general, solid-solution alloying (addition of metallic elements having slightly larger or smaller atomic radii than the base element) is the most effective way to raise the recrystallization temperature. Shifting this temperature upward by this means usually permits the use of precipitation hardening up to higher temperatures. The latter is a more potent strengthening mechanism, and the two mechanisms are often combined to yield appreciable improvements in both strength and temperature resistance. Many of the alloy studies in the refractory metals—molybdenum, columbium, tantalum and tungsten—have been aimed at finding additions that raise the recrystallization temperature. In general, however, increases to above 60% of the melting point have not been accomplished in these alloy systems.[4] In others such as nickel, recrystallization temperatures up to about 80% of the melting point have been accomplished, and this appears to be about as far as it can be shifted in any useful system.

Metallic alloys can, of course, be used above their recrystallization temperatures, but then one finds that they behave somewhat like highly viscous fluids. Their ability to carry loads depends strongly on the velocity at which they are deformed and on the temperature. Parameters used to characterize the flow of metals[5, 6] are distantly analogous to Reynolds number of fluid flow. Insofar as is known, this behavior has not been critically reviewed by specialists in fluid flow, but it does show promise of being a fertile field of research.

DISPERSION HARDENING—At temperatures much above recrystallization, the only effective strengthening mechanism that has been employed is one known as dispersion hardening. This consists of introducing an insoluble phase into the alloy matrix in the form of a fine dispersion. To some extent the presence of this phase can raise the recrystallization temperature, but it usually contributes some measure of strength even above the recrystallization temperature. The foreign phase can be produced by heat treatments that are similar to aging treatments used to strengthen super alloys, it can be mixed with metal powders before sintering (TD nickel is an example), or, as in the case of most refractory metal alloys, it can be produced by traversing solubility limits during solidification or cooling from forging temperatures (TZC, a relatively new alloy of molybdenum, is an example of the latter, where titanium and zirconium carbides are formed during cooling). Some attempts to mix powders with molten metals have also been partially successful.

The dispersion hardening principle is somewhat analogous to the process of blending sugar with butter. Many male readers of this text are possibly familiar with this process because it is essential to baking a good cake, and many wives become fatigued by it as a result of the stiffness of the mixture. In dispersion-hardened alloys, phases of hard particles of oxide or carbides are generally used in the ductile matrix of the base metal to strengthen the composite alloy. Dislocation theory has dealt with the detailed atomic mechanisms of plastic flow in the presence of such particles, but in a simplified view the particles can be interpreted

[4] J. E. Campbell, H. B. Goodwin, H. S. Wagner, R. W. Douglas, and B. C. Allen, "Introduction to Metals for Elevated Temperature Use," Battelle Memorial Institute DMIC Report 160, Oct. 1961.

[5] F. R. Larson and J. Miller, "A Time Temperature Relationship for Rupture and Creep Stresses," *Trans. Am. Soc. Mech. Engrs.*, **74**, 1952, 765–771.

[6] S. S. Mansen and A. M. Haferd, "A Relation for Extrapolation of Creep and Stress Rupture Data," NACA Report TN 2890, 1953.

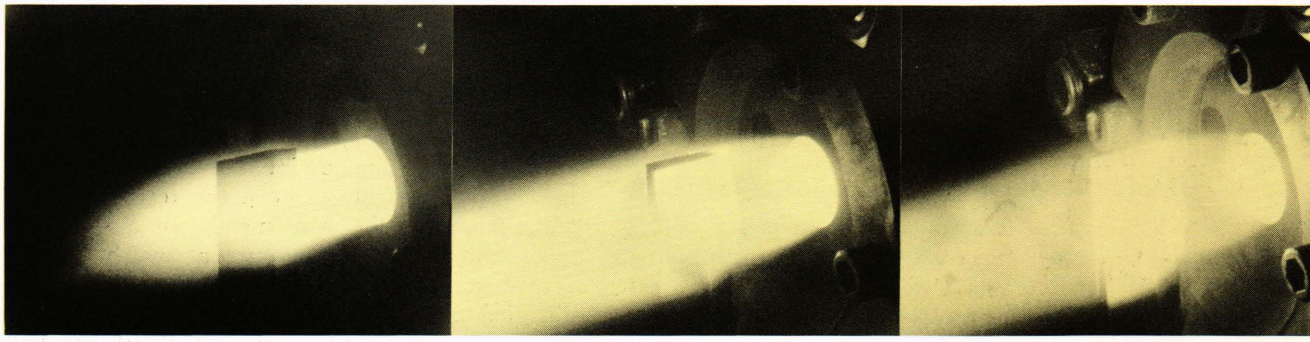

Plasma arc test, in the Propulsion Research Laboratory, of a pyrolytic graphite wing-leading

as increasing the viscosity of an already very viscous fluid.

Unfortunately, some of the other characteristics of the sugar-butter analogy are also present in dispersion-hardened alloys. In the case of the sugar-butter mixture, a homogeneous caramel-like fluid is formed as the temperature is raised. In dispersion alloys the particles usually dissolve at some temperature well below the melting point, and become ineffective. In general the analogy goes one step further. Cooling of the melted sugar-butter mixture results in the binder used for making peanut-brittle candy. Likewise, cooling of an overheated dispersion-hardened alloy often results in a brittle material; this occurs in practically all refractory metal alloys, and it severely limits the welding and general fabricating of such alloys.

Assessment of the Future

With this simplified analogy in mind, the directions of research that may lead to stronger alloys for service above 2500°F are reasonably obvious. The first is, of course, that of raising the recrystallization temperature by means of adding soluble elements to the matrix; the second is to find dispersed phases with increased resistance to dissolving in the matrix. Major research projects in the first area have been underway for the past decade. Binary and ternary systems for raising the recrystallization temperature of molybdenum, tantalum, columbium, and tungsten have been reasonably well surveyed. The TZM now available has a recrystallization temperature around 2700°F, this being 60% of the melting point. Several columbium alloys having recrystallization temperatures at 60% of their melting points are also available commercially. A few tantalum-tungsten alloys with this characteristic are also available. This 60% level may be close to the practical limit in these alloy systems since it has been found that alloy additions that are effective in pushing the recrystallization temperature above this point usually result in brittleness of the alloys at room temperature. In this sense these alloy systems are far more limited than nickel alloys in which the pure element is very ductile and tolerant to many alloy additions.

The few programs in progress that are aimed at studying the solubility of promising dispersed phases in refractory metals are generally side-line efforts in specific alloy development programs. A more fundamental approach to this problem would probably yield more useful results. This is also true of the role that diffusion of dissolved species away from the reaction region may play in obtaining maximum possible strength. Some advantages may be gained in this area, particularly in materials for the missile structures that may be designed to perform their entire function within a few seconds. The time required for solution and diffusion of dispersed phases above 3000°F is of the same order of magnitude. A challenging complication in this part of the problem is the fact that both the solubility and the subsequent diffusion rates are often significantly changed by the minor alloy additions used to raise the recrystallization temperature. Substantial confusion can result if the fundamental factors are not understood separately.

Considering all aspects of the problems of developing strength and maintaining fabricability, it appears likely that the next decade will not see a lot of improvement in strength of metallic materials beyond the values that are shown in Fig. 1 for the tungsten-thoria alloy above 3000°F. Instead, the major progress will probably deal with improvements in the fabricability and quality of alloys whose strengths fall below that of this material.

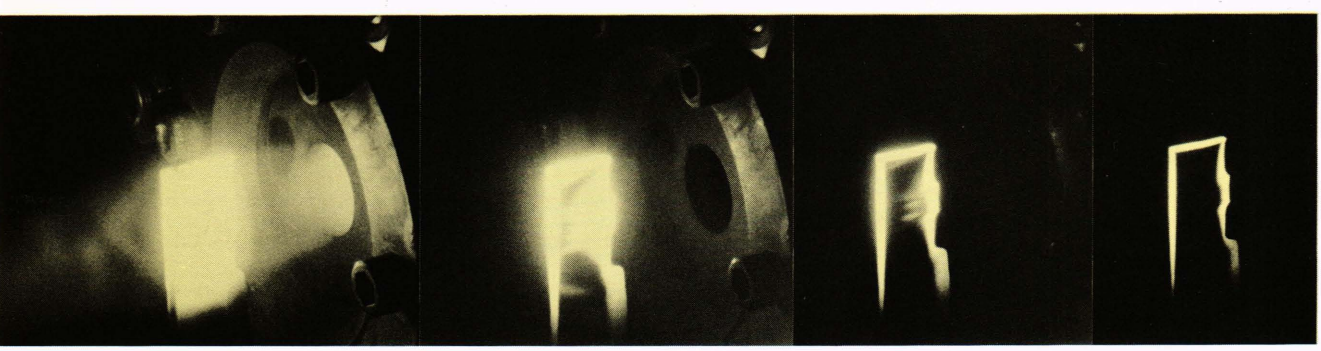

edge section, showing representative variations of the heating rate on different areas of the sample.

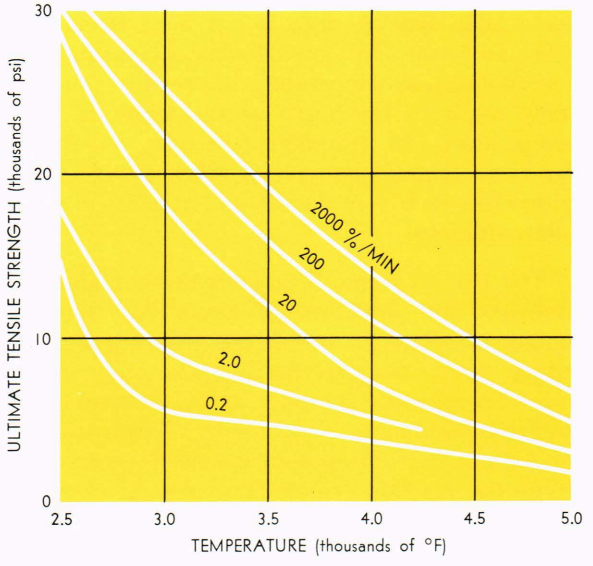

Fig. 2—Tensile strength of tungsten as a function of strain rate and temperature.

BEHAVIOR ABOVE RECRYSTALLIZATION TEMPERATURE—The basic pattern of behavior at temperatures above the recrystallization temperature is described by data in Fig. 2. Here we see the ultimate tensile strength of commercially pure tungsten at temperatures from 2500° to 5000°F.[7] The family of curves demonstrates the high dependence of strength on the rate at which the material is elongated. For example, the bottom curve was obtained in tests in which the strain rate was held constant at 0.2%/min, while in the top curve the strain rate was 2000%/min. At temperatures around 3000°F, we see that the material is about five times as strong at the fast strain rate as it is at the slow rate. The higher strength at fast strain rates persists at all temperatures up to 5000°F, but the magnitude of the effect changes with temperature. The lower two curves show a steepening at lower temperatures, caused primarily by a variable degree of recrystallization that occurs during such tests.

Recrystallization is both time- and temperature-dependent, and in very rapid tests, or in slow tests at low temperatures, the rate of recrystallization can lag behind the rate at which the structure is deformed. Whenever recrystallization lags behind the deformation rate, extra strength is obtained. In a simplified sense this is the reason for the higher strength at fast strain rates. Atomically scaled processes known as "recovery" or "relaxation" are also involved, but it is generally easier to think in terms of recrystallization since this is something that can be readily observed in optical microscopes. Large variations in the yield strength of materials also result from changes in the rate of strain. The effect can be even larger than the five-fold increase in the ultimate tensile strength shown in Fig. 2. A ten-fold variation in yield strength occurred in similar tests.

DESIGN FACTORS—In the midst of these variations in strength it is not a straightforward matter to specify *stress allowables* in terms of a certain percentage of yield or ultimate tensile strength as is often done in engineering design. In order to build a reliable and efficient structure, it will be necessary to take this behavior into account and develop strength data with the specific requirements in mind. One way would be to decide first what degree of deformation can be tolerated by a given component and then evaluate the material in terms of the stress it can withstand without exceeding this deformation during a temperature-time simulation of the missile flight. *Design allowables* determined in this way will permit the use of *minimum* safety factors, so essential because of the inordinately heavy structures that can result from overdesign with these relatively dense materials.

There is currently very little creep information on refractory metals above 3000°F that is amenable to this kind of an approach. Even standard tensile tests are quite expensive and tedious to perform, and as a result only a sketchy description of ordinary tensile properties is available for many of the alloys that are now being publicized.

In Fig. 3 a comparison is made between steady-state creep properties[8,9,10] and the short-time, tensile, ultimate strength of tantalum,[10] molybdenum,[11] and tungsten.[12] The data shown as broken lines indicate the tensile stress that results in 1% creep elongation during a 1-min exposure at steady temperature (this does not include thermal or elastic expansion). The tensile data are all from tests conducted at a strain rate of

[7] P. F. Sikora and R. W. Hall, "Effect of Strain Rate on the Tensile Properties of Tungsten," NASA Report TN-d 1094, 1962.

[8] W. V. Green, M. C. Smith, and D. M. Olson, "Short Time Creep Behavior of Molybdenum at High Temperatures," *Trans. Am. Inst. Mining Met. Engrs.*, **215**, Dec. 1959, 1061–1066.

[9] W. V. Green, "Short Time Creep Rupture Behavior of Tungsten at 2250 to 2800°C," *Trans. Am. Inst. Mining Met. Engrs.*, **215**, Dec. 1959, 1067–1072.

[10] J. B. Preston, W. P. Roe, and J. R. Kattus, "Determination of Mechanical Properties of Aircraft Structural Materials at High Temperature After Rapid Heating," Southern Research Institute Report WA DE TR 57–649, Jan. 1958.

[11] R. W. Hall and P. F. Sikora, "Tensile Properties of Molybdenum and Tungsten from 2500 to 3700°F," NASA Memo 3–9–59E, Feb. 1959.

[12] P. F. Sikora and R. W. Hall, "Tensile Properties of Wrought and Sintered Tungsten," NASA Technical Note D-79, Sept. 1959.

0.05 in./in./min. The tantalum and molybdenum creep data are seen to correspond quite closely to these particular ultimate strength curves, each of which must be recognized as one of a family similar to that in Fig. 2. For tungsten the correlation is not as good, but this could well be caused by variations in purity and/or by experimental errors in different laboratories. However, it is apparent that for all three materials, design allowables derived from these particular ultimate strength data would be of the correct magnitude for a structure limited to 1% deformation during one minute. This is a case of practical interest in missile application. Other correlations for smaller deformations, shorter or longer times, or varying temperature and load can also be derived. Eventually design with such materials will be done best by using computers to estimate design allowables for transient loads and temperatures. These, however, will require specific creep data that are as yet unavailable for most alloys.

The behavior of alloy systems (above recrystallization temperatures) follows that of the base metals reasonably well. Therefore, until such time as creep data become available, it is reasonable to use the ultimate strength (determined in tensile tests at strain rates of about 0.05 in./in./min) for preliminary estimates of the weight and size of components that are permitted 1% deformation. Because strain rates in the vicinity of 0.05 in./in./min are usually employed in preliminary evaluation of alloys, much of the tensile data are applicable. However, we should point out that unusually high strengths are sometimes reported without an accompanying reference to the fact that abnormally high strain rates were used.

Tensile Strengths of Refractory Alloys—The ultimate tensile strength of the highest-strength refractory alloys that have thus far been made available commercially are shown in Fig. 4. All of these were obtained in tests at strain rate of 0.05 in./in./min. They therefore represent the best estimates that can be made currently of design allowables that might be used for preliminary planning and evaluation of structure weights for hypersonic missiles. Data for pure tungsten are shown for comparison.

The columbium alloy B-66 is not very useful above 3000°F. Most columbium alloys are highly fabricable, have good impact resistance and have ductile weld characteristics. Such advantages compensate somewhat for relatively high cost, and these alloys are usually the preferred choice for service from 2000° to 2700°F. The density of B-66 is 0.32 lb/in.^{3}, and current cost is about $120.00/lb.

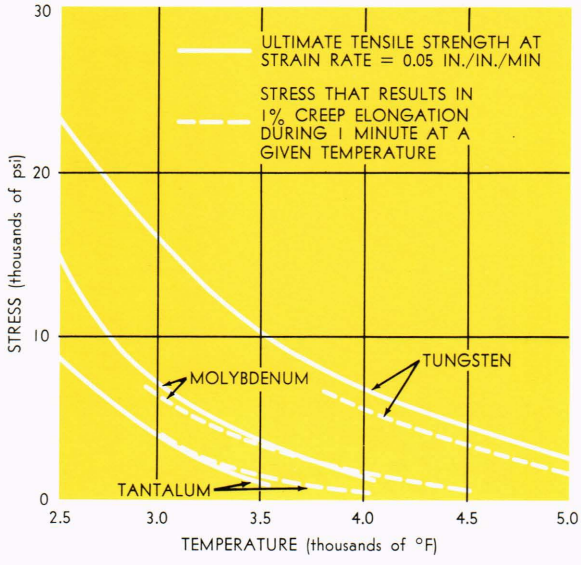

Fig. 3—Comparison of ultimate tensile strength with steady-state creep strength for tungsten, molybdenum, and tantalum.

A molybdenum-base alloy, TZM, was also developed, primarily for service below 3000°F. This alloy is reasonably fabricable and it can be formed in dies or spun into shapes. It is ductile at room temperature except when subjected to impact loads. While it can be joined by fusion welding, the welds are very brittle at temperatures below about 500°F. This imposes severe restrictions on the structural use of TZM. The material has a density of 0.36 lb/in.^{3}, and the current price is about $25.00/lb.

A tantalum-base (Ta–10W–2.5Hf) alloy, which is ductile at room temperature and can be joined by welding, is T-222. Because it is relatively easy to fabricate into complex shapes, T-222 is probably the best candidate for complex structures under high-temperature conditions. No strength data are available above 3500°F; strength will probably be found to drop below that of tungsten at temperatures above ≈ 4000°F, but should remain at about 80% of the strength shown here for tungsten up to 4500°F. The alloy has a density of about 0.61 lb/in.^{3}; the current cost is about $150.00/lb.

The tungsten-1% thoria alloy is used primarily in wire form as filaments in incandescent lights and electronic tubes[13] but is available in limited sizes of strip and rod. A drawing operation is a necessary part of the process for developing strength.

[13] R. W. Hall, P. F. Sikora, and G. M. Ault, "Mechanical Properties of Refractory Metals and Alloys Above 2000°F," *Proc., Am. Inst. Mining Met. Engrs., Technical Conference on Refractory Metals and Alloys*, Detroit, 1960 (Interscience Publishers, London, 1961), 483–503.

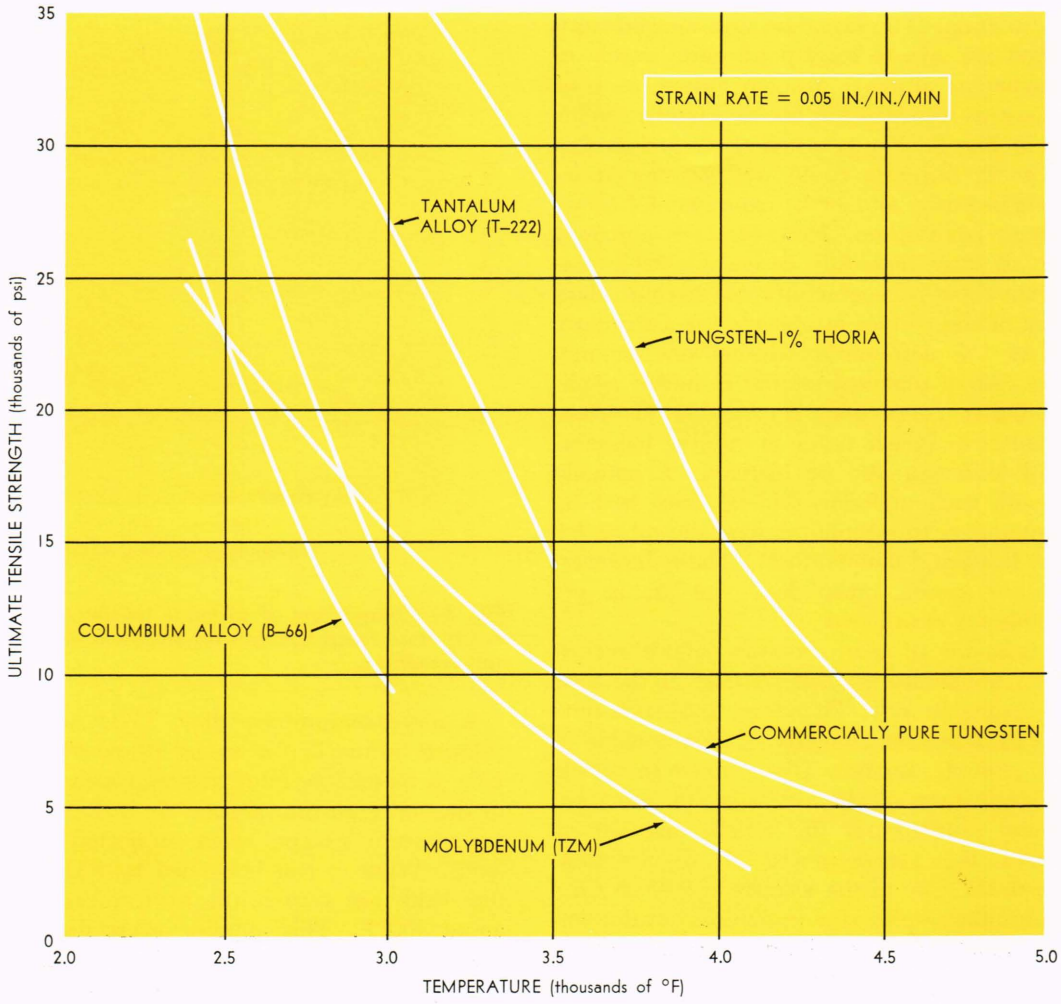

Fig. 4—Ultimate strengths of the five best refractory metal alloys available in 1964.

Both tungsten and tungsten-1% thoria are very brittle at temperatures below about 300°F, therefore have limited fabricability, and are usable in welded forms. The density of tungsten is 0.70 lb/in.^{3}, and current cost is about $30.00/lb.

The tungsten-1% thoria alloy is essentially a dispersion-hardened alloy. As we have mentioned, this is the only effective strengthening mechanism at temperatures above about 3000°F. Some improvement in strength may be possible by altering the size and distribution of the dispersion in such alloys, but the curve shown here is probably close to the upper limit of strength that can be achieved in any metallic alloy system. Major emphasis of alloy-development effort during the remainder of this decade will probably be on raising the strength of fabricable alloys up to this limit rather than attempting to push tungsten alloys beyond it. For purposes of planning for 1970, therefore, it seems unreasonable to assume a design allowable in excess of the tensile strength of this material.

Comparison of Ceramic and Metallic Materials

The term *ceramics* is derived from the Greek word for earthenware, and its common meaning still applies only to pottery, tiles, or other articles made by baking clay, oxides, silicates, titanates, etc., found in the earth's crust. In the technical sense today, the term includes a host of other compounds such as carbides, borides, silicides, nitrides, beryllides, and other intermetallic compounds having high melting points.

Use of ceramics in engineering applications has been limited because they are inherently brittle and their strength varies widely as a result of minor

changes in processing or composition.[14] In spite of this the severe requirements of missiles and rockets have stimulated interest in them, and some promising research programs aimed at understanding the behavior and use of brittle materials are underway. The result of these efforts will very likely be that they will permit the development of oxidation-resistant materials with modest but reproducible strength properties, rather than an unusually high strength at extreme temperatures.

Ceramic materials exhibit the same general tendency as metals to lose strength rather drastically at temperatures above about half the melting point. This is due primarily to a change in the fracture mechanism, in which fracture usually occurs along grain boundaries at high temperature but passes through grains at low temperature.[14] Some plasticity sets in at temperatures of about two-thirds of the melting point, and the brittle fracture problems then become less severe. However, ductility seldom reaches the amount characteristic of metals (often 100% elongation) and fracture typically occurs at less than 5% elongation. Creep under stress is also observed in such materials, and, characteristically, the creep strengths fall below those of refractory metals.

The tensile strengths of several oxides at elevated temperatures are shown in Fig. 5. The steep decrease in strength at temperatures from 2000° to 3000°F is quite evident, and at temperatures above 3000°F the strengths fall in a range not exceeding ≈ 500 psi.

These tensile tests were made on material of the highest density that could be produced in the laboratory (probably < 1% porosity).[14] Generally, most commercial ceramics—and particularly pure oxides—contain fine pores equal to about 10% of the total volume. This porosity results in substantially less strength than that of the fully dense materials. Figure 6 shows how the room-temperature strength of alumina decreases with porosity.[15] This porosity effect persists at all temperatures of practical interest and causes comparable losses in the creep strength when tested above one-half the melting point. Porosity is the factor that is probably most responsible for the variability of properties of commercially available materials. To some extent the strength values normally published in current handbooks do not represent the true strength that might be available with better quality control during manufacture.

[14] W. D. Kingery, "Oxides for High Temperature Applications," *Proc., International Symposium on High Temperature Technology,* Stanford Research Institute, Oct. 1959 (McGraw-Hill Book Co., New York, 1960), 108–133.

[15] R. L. Coble and W. D. Kingery, "Effect of Porosity on Strength of Aluminum Oxide," *J. Am. Ceram. Soc.,* **39,** 1956, p. 377.

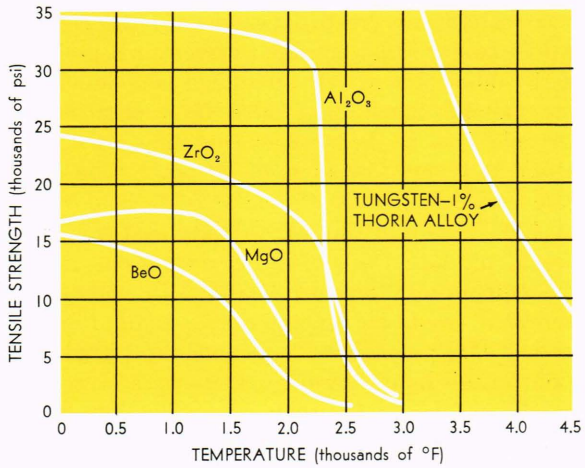

Fig. 5—Tensile strengths of a variety of ceramic oxides at elevated temperatures.

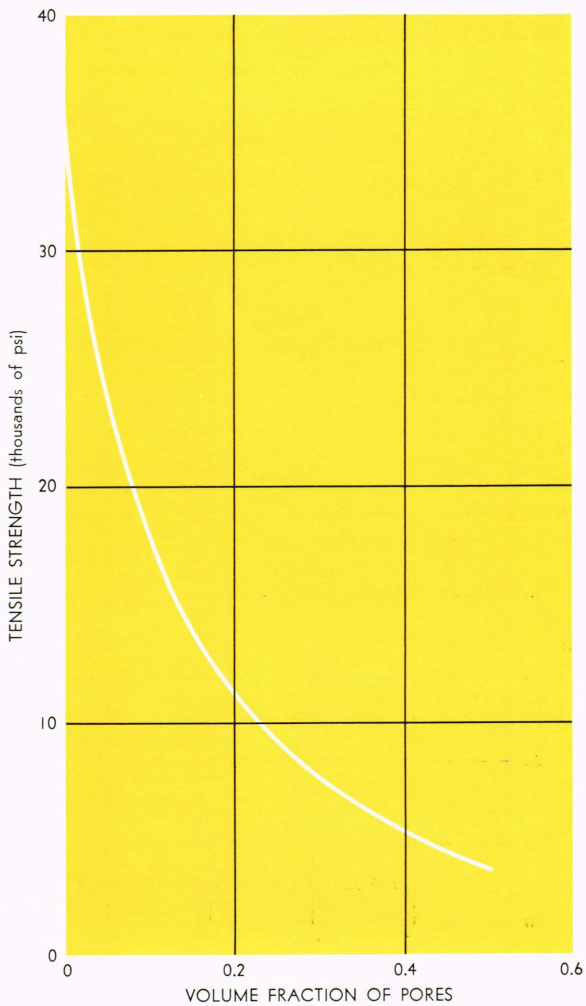

Fig. 6—Effect of porosity on the relative strength of alumina at ambient temperature.

Essentially no creep data exist for the ceramic oxides, and it is not possible to ascertain a probable design allowable as was attempted here previously for metals. Some data have been obtained on zirconia (one of the stronger ceramic oxides available) at a very low stress of 50 psi.[14] The creep rate varied from 0.003%/sec at 3450°F to 0.36% at 4200°F. From this we estimate that this stress would produce 1% elongation during one minute at temperatures around 3700°F. In comparison tungsten would be expected to sustain loads of about 7000 psi without exceeding the 1% elongation; in this light, ceramic oxides appear very poor candidates for true structural applications above 3500°F.

In Fig. 7 the tensile strengths of a variety of materials are shown in order to compare nonoxide ceramics, oxide ceramics, graphite, and metals.[16] These show the strongest of each breed. Zirconium carbide has a strength about equal to the oxide. It is not known at what temperature the strength of this material will drop off sharply, but it is likely to occur below 3500°F. Molybdenum disilicide shows a gradual increase in strength up to about 2200°F and then a sudden drop. The rise in strength probably is associated with the onset of ductile behavior (or less susceptibility to the nucleation of brittle fracture mechanisms). The same is probably true of titanium boride,[17] and of pyrolytic graphite,[18] which appears in this figure as the highest-strength material at temperatures above 3200°F.

Pyrolytic graphite is a special form of carbon that is obtained by a high-temperature process in

[16] R. I. Jaffee and D. M. Maykuth, "Refractory Materials," Battelle Memorial Institute DMIC Memo 44, Feb. 1960.

[17] V. Mandorf, J. Hartung, and E. J. Seldin, "High Temperature Properties of Titanium Diboride," *Proc., Am. Inst. Mining Met. Engrs., Technical Conference on Refractory Metals and Alloys,* Detroit, 1960 (Interscience Publishers, London, 1961), 455–467.

[18] "Pyrolytic Graphite Engineering Handbook," General Electric Company Form PG-63-1, Detroit, Michigan, 1963.

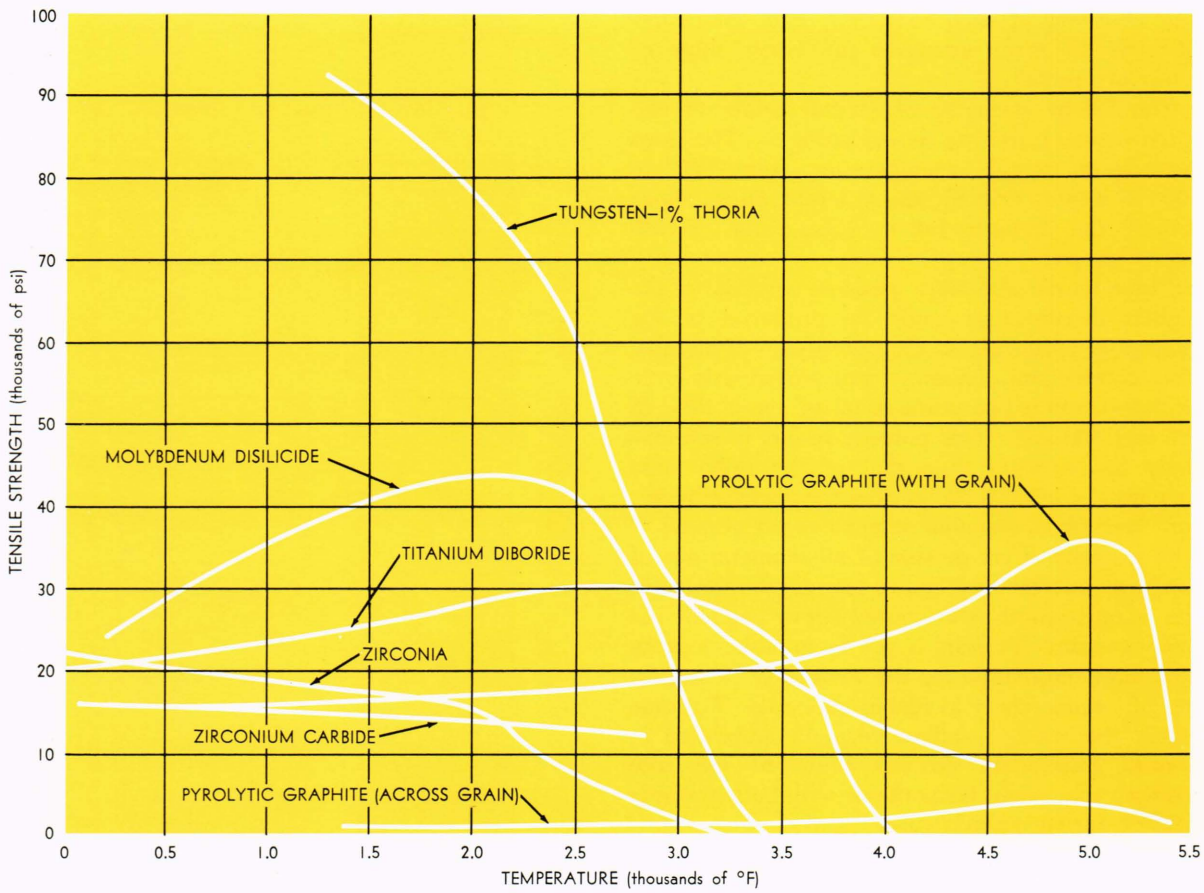

Fig. 7—Summary comparison of the strengths of various metals, metal alloys, and ceramics at elevated temperatures.

TABLE I

CRITICAL PROPERTIES OF SOME HIGH-TEMPERATURE MATERIALS

Material	*Melting Point, °F*	*Density, lb/in.³*	*Heat Capacity, BTU/lb °F*		*Thermal Conductivity, $\frac{BTU\ ft}{ft^2\ °F\ hr}$*		*Thermal Expansion Coefficient 78°F (10^{-6} in./in. °F)*	*Modulus of Elasticity, 10^6 psi*		*Maximum Temperature For Use In Oxidizing Atmosphere, °F*
			78°F	*3000°F*	*78°F*	*3000°F*		*78°F*	*3000°F*	
Tungsten	6170	0.70	0.033	0.040	97	74	2.5	60	17	3500†
Tantalum	5425	0.60	0.033	0.041	32	42	3.7	27	8	3000†
Molybdenum	4730	0.37	0.061	0.098	85	69	3.0	48	9	3150†
Columbium	4379	0.31	0.065	0.083	30	≈40	3.9	18	4	2900†
Zirconia*	4620	0.20	0.10	0.15	1.0	1.4	3.7	22	≈0	4620
Alumina	3690	0.14	0.16	0.33	7.0	0.5	4.5	53	≈0	3690
Magnesia	5072	0.13	0.23	0.40	24	3.0	7.5	31	≈8	≈4800
Beryllia	4660	0.11	0.24	0.50	121	9.0	4.3	45	≈0	4660
Zirconium carbide	6390	0.24	—	—	12	—	3.7	—	—	3000
Titanium diboride	5000	0.16	—	—	—	24	5.5	63	54	≈3000
Molybdenum disilicide	3400	0.23	—	—	19	—	—	—	—	3150

* Stabilized with 4% CaO and 4% HfO_2.
† Coated.

which methane is decomposed and the resultant graphite deposited with a highly oriented hexagonal crystal structure. The process was discovered late in the last century, and the material was of interest to Edison, among others, for filaments in incandescent bulbs. New interest has been stimulated by the severe requirements of rocket propulsion systems, and much progress in understanding the material has been made in the past five years. Owing to its highly anisotropic structure, it exhibits wide variations in strength, thermal and electrical conductivity, and other properties when tested in different directions with respect to the crystal orientation. The material is brittle at room temperature, but like some ceramics it becomes ductile at elevated temperatures. Owing to the grain of its structure, it is relatively weak in one direction and has a tendency to split like wood. As a result, fabrication techniques similar to the "hole and peg" methods used in early American furniture have been used in some quite modern structures. Pyrolytic graphite is not very resistant to oxidation at extreme temperatures, and it has an unfavorable tendency to shrink in some directions and expand in others when heated above about 4000°F. In spite of all these problems, the material has been used successfully in operational rockets.

Pyrolytic materials with two or three times the strength shown here will probably be available within the next decade, and many of the problems that have been encountered due to directionality will be better understood and used to good advantage. Apart from purely structural applications, the material is of great interest because of its unique ability to conduct heat along its grain as rapidly as does copper, and yet insulate as well as asbestos across the grain. This attractive characteristic will stimulate continued progress in this class of materials.

Apart from pyrolytic graphite, it appears that the strengths of nonmetallic materials at temperatures much greater than half their melting points may also be limited, by some inherent characteristics, to values ranging in the hundreds of pounds per square inch at temperatures above 3000°F. However, ceramic materials have not been explored as much as metals, and it is possible that the predominant trend for low strength at these temperatures could be altered by better scientific understanding. Unfortunately the current level of effort on this problem in this country is meager compared with what it should be, and improvements during the next decade are not likely to be very numerous.

A comment should be made here on the use of ordinary tensile strength as a basis for comparison of materials, rather than the ratio of ultimate tensile strength to density that is generally more significant in airframe uses. In many applications of these materials in hypersonic vehicles, the geometry of a component is limited by aerodynamic factors such as drag and shock deflection. It is often not possible to use thicker sections of lower density material; thus maximum strength within the fixed volume must be achieved. The ultimate strength/density ratio is, of course, more appropriate in cases where such limitations do not exist. Likewise, there are areas where such thermal properties as conductivity, heat capacity, oxidation rate, etc., are more important than strength, and where final selection of material will be based on combinations of all such properties. For a general comparison, Table I has been assembled to show the properties of some of the materials discussed in this paper.

JOSEPH GULICK, W. COLEMAN HYATT, and OSCAR M. MARTIN, JR.

THE TALOS GUIDANCE SYSTEM

The Talos guidance system evolved from a series of development efforts within the Bumblebee and Talos programs — specifically, the first beamriding system and the first semiactive interferometer homing system. The guidance system that evolved was virtually unjammable, and it provided the missile with capabilities against manned aircraft, antiship missiles, surface ships and boats, and radar targets.

INTRODUCTION

When the Bumblebee Program was conceived, missile guidance technology was in its infancy. The early guidance development work was based on pulse radar technology since pulse radars were well developed by 1945. The first guidance concept was that a radar beam, following the target, could be used to guide the missile to the target. It was determined early, however, that the maximum allowable miss distance could not be achieved by such a "beamriding" system at ranges beyond approximately 10 nautical miles. When the target intercept range for the missile was increased, the guidance concept was revised to use beamriding for the midcourse phase with semiactive homing for the terminal phase. This resulted in a guidance system that produced very small miss distances, essentially independent of intercept range. During the later Talos years, the major guidance effort was focused on the homing system. This effort resulted in a monopulse homing system that was virtually unjammable and an antiradiation missile seeker that enabled the missile to home on radar targets.

MIDCOURSE GUIDANCE

In a beamriding system, departure of the missile from the axis of a conically scanned radar beam causes deflection of the aerodynamic surfaces to return the missile to the beam axis. Basically, the missile must determine the vector that indicates the angular direction and distance to the scan axis. The distance is determined by observing the amplitude of the modulation produced by the conically scanned beam, and the angular direction is determined by the phase of the amplitude modulation with respect to the scan frequency reference signal.

The beamriding system for Talos was the result of a joint effort by APL and Farnsworth Television and Radio Corp. It employed a conically scanned radar beam (Fig. 1) and, together with a sinusoidal variation of the pulse repetition frequency, provided the missile-borne receiver with the signals needed to measure missile angular distance and direction perpendicular to the nutation axis of the guidance beam (Fig. 2). The missile was roll stabilized in flight by a free gyro so that the error signals would be directed to the proper aerodynamic steering surface.

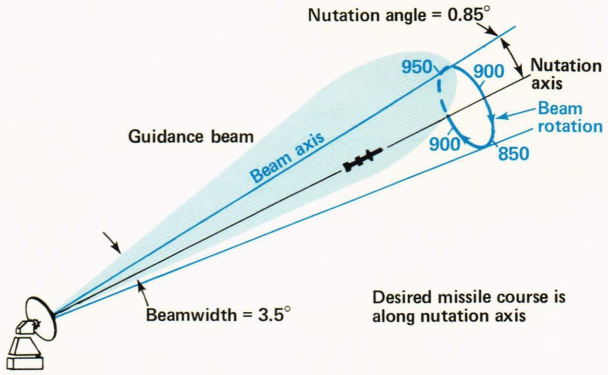

Figure 1 — The guidance beam for the beamrider missile was conically scanned at 30 hertz with a clockwise rotation, as viewed from behind the radar antenna. The radar pulse rate, nominally 900 pulses per second, was varied by ±50 pulses per second in synchronism with the conical scan.

The guidance transmitter radiated pulse groups at a nominal rate of 900 pulses per second. Each group consisted of three pulses that were coded by interpulse timing to identify the guidance beam to the missile. Nutation position information was transmitted by frequency modulating the pulse group rate at the nutation frequency (30 hertz) with a deviation of ±50 groups per second. The maximum pulse group rate occurred for a nutation position that was up and left. On board a ship, an inertial system was required to compensate the pulse group modulation for roll and pitch.

A simplified block diagram of the beamrider receiver is shown in Fig. 3. Microwave pulses were detected and passed through a decoder to produce one pulse for each valid code group. The decoded pulses were then applied to a 30-hertz amplitude detector, a 30-hertz frequency modulation detector, and a beacon transmitter. Outputs from the frequency modulation detector were used as references for the

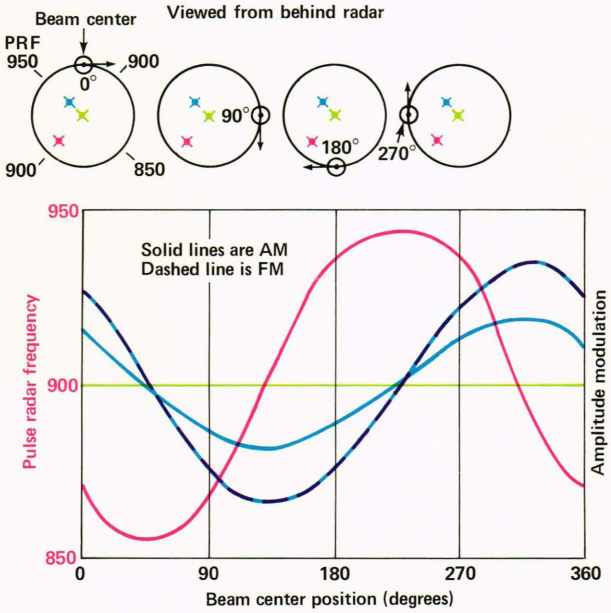

Figure 2 — Signal modulations detected by the beamriding receiver were processed to determine missile position with respect to the guidance beam. Angular direction and distance from the scan axis were determined by comparing the phase and amplitude of the 30-hertz amplitude-modulated signal with the frequency-modulated reference signals.

steering channel phase comparators. The phase comparators were used to resolve the in-phase component of the amplitude modulation detector output to obtain steering-error signals for each wing plane.

As a flight progressed, the direction of the guidance beam was programmed by the fire-control computer to cause the missile to fly the desired midcourse trajectory. Missile range was determined by automatically range tracking the missile-borne beacon pulses. That range was used by the fire-control computers to control the beam program and compute the time at which a homing enable pulse code was transmitted to the missile, permitting target acquisition by the homing system.

Subsonic beamriding along a fixed beam was accomplished by a guidance test vehicle in January 1947. The first supersonic beamriding Talos was demonstrated in 1950.

TERMINAL GUIDANCE

A terminal-guidance phase following the midcourse beamriding phase had been envisioned from almost the beginning of the development program. The task was to devise a homing system that would be compatible with the constraints imposed by the ramjet diffuser and that would rapidly acquire the target without requiring accurate missile-to-target line-of-sight positioning information. The goal of intercepting small targets at long range (about 100 nautical miles) placed a premium on high receiver sensitivity as well as on good target resolution.

The interferometer homing system was chosen for terminal guidance for the following reasons:

1. Widely spaced body-fixed antennas were compatible with ramjet inlet constraints.
2. The body-fixed antennas were simple compared with a gimballed dish antenna.
3. Rapid target acquisition was possible without the need for missile-to-target angle data.
4. It was desired to have the largest possible aperture and, hence, the most accurate measurement of the line-of-sight angular rate.

The basic principle of the interferometer system is illustrated in Fig. 4. Two widely spaced antenna elements of an interferometer have a composite antenna pattern consisting of a series of peaks and nulls. The peaks and nulls are moved by a phase shifter, resulting in amplitude modulation of the target signal. A discriminator tuned to this modulation frequency provides an output that is proportional to the angular rate of the target line of sight. If the target line-of-sight rate with respect to an inertial reference is maintained at zero, a proportional navigation homing trajectory to the target is executed. It is therefore only necessary to control the missile turning rate so that the line-of-sight rate is maintained at zero to effect an intercept.

THE FIRST TALOS HOMING SYSTEM

Guidance concepts consisting of body-fixed, widely spaced antennas to be used as a radar interferometer were proposed almost simultaneously by the Defense Research Laboratory (DRL) of the University of Texas and the Massachusetts Institute of Technology. Both concepts used widely spaced antennas but different methods of signal processing. Because the basic system proposed by DRL (which employed an independent interferometer channel for each wing-control plane) was judged to be more consistent with the state of the art, the first Talos homing system was based on that concept.

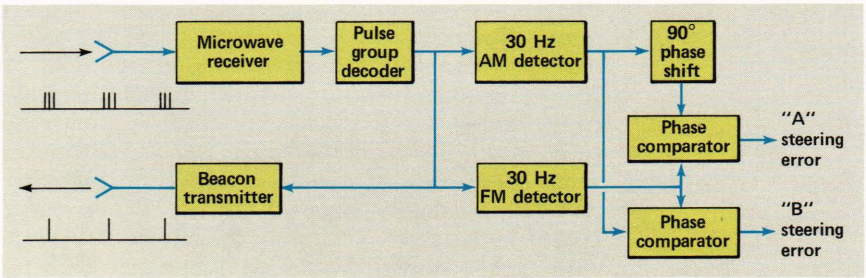

Figure 3 — The beamrider receiver detected and processed guidance beam signals to generate commands for the missile control planes and the radar beacon responses.

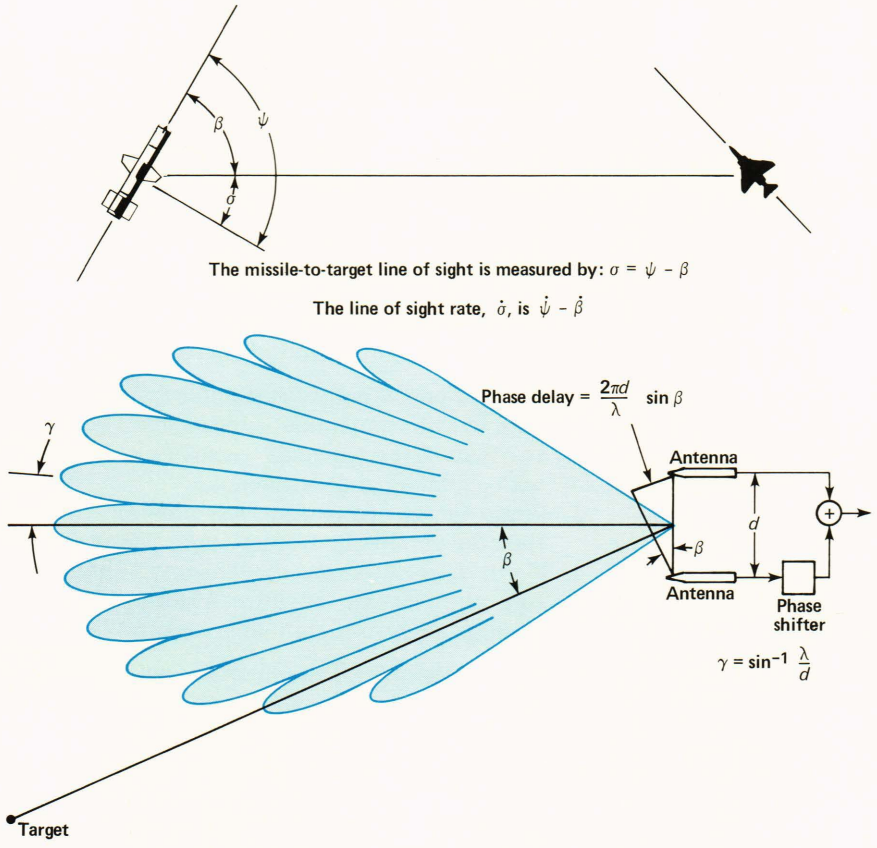

Figure 4 — Interferometer parameters and symbols used in the article are defined in this figure.

The receiver (Fig. 5) used a scanning interferometer system. Target signals at the antenna were:

$$\begin{aligned} X_1 &= A_1 \sin \omega t \\ X_2 &= A_2 \sin (\omega t + \theta) \\ &= A_2 \sin \left(\omega t + 2\frac{\pi d}{\lambda} \sin \beta\right), \end{aligned} \tag{1}$$

where ω is the microwave frequency and θ is the electrical phase difference at the antennas. A_1 and A_2 are the amplitudes, which may be different, but the scanning process was essentially insensitive to that difference. The scanning phase shifter advanced the phase of X_2 by $\Phi(t)$ as follows:

$$\Phi(t) = \omega_S t + \Phi, \tag{2}$$

where ω_S is the scan frequency and Φ is the initial phase shift. The X_3 can be written as

$$X_3 = A_2 \sin \left[\left(\omega + \omega_S + 2\frac{\pi d}{\lambda} \dot{\beta} \cos \beta\right) t + \Phi \right]. \tag{3}$$

The addition of X_3 and X_1 gives X_4:

$$\begin{aligned} X_4 &= A_1 \sin \omega t \\ &+ A_2 \sin \left[\left(\omega + \omega_S + 2\frac{\pi d}{\lambda} \dot{\beta} \cos \beta\right) t + \Phi \right]. \end{aligned} \tag{4}$$

X_4 can be seen to be a carrier signal at ω and is amplitude modulated at

$$\omega_S + 2\frac{\pi d}{\lambda} \dot{\beta} \cos \beta. \tag{5}$$

The heterodyne process in the receiver changed the carrier from microwave to a lower frequency but did not affect the modulation and, therefore, did not change the basic $\dot{\beta}$ information. It is also apparent that because the desired information was the frequency of the modulation, changes in amplitude of the signal had no direct effect upon the measurement of $\dot{\beta}$. Decoupling of body motion to provide the line-of-sight rate measurement ($\dot{\sigma}$) was accomplished by use of a body-mounted rate gyroscope where the gyro output frequency modulated an oscillator to produce a carrier frequency (ω_0) with a deviation proportional to the missile body turning rate ($\dot{\psi}$). The term N in the gyro channel was an estimate of cos β. A fixed value of N for all flight conditions proved to be unsatisfactory. Therefore, Talos had a selection of two values based upon the crossing component of the target speed. That value was set into the missile at the time of launch. Double modulation eliminated the scan-

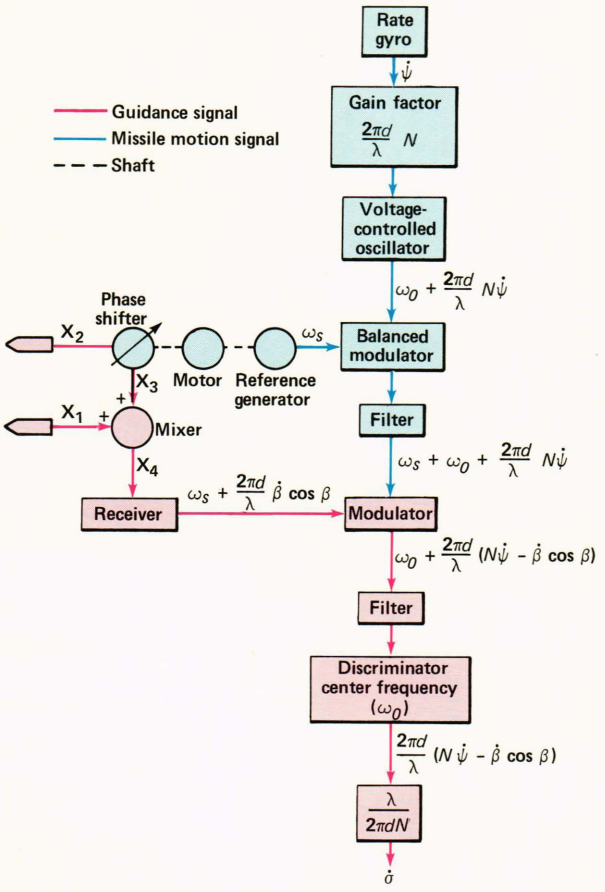

Figure 5 — The first Talos homing receiver (1950) used a scanning interferometer. The system shown here was for a single control plane. An identical system was used for the orthogonal control plane. Output from a body-mounted rate gyro was used to decouple the effect of body motion on the interferometer signals. The term N was an estimate of cos β. The output from the discriminator was a signal proportional to $\dot{\sigma}$.

phase shifter frequency (ω_S) from the final term and allowed a frequency discriminator tuned to ω_0 to provide an output that was proportional to $(2\pi d/\lambda)$ $(N\dot{\psi} - \dot{\beta} \cos \beta)$. The discriminator output, neglecting biases, was approximately proportional to the desired $\dot{\sigma}$. This form of signal processing was used in a number of test flights and for the first Talos production receiver.

STABLE PLATFORM PHASE FOLLOW-UP SYSTEM

Two major problems associated with the first Talos homing system were the following:

1. A bias resulted from any offset between the voltage-controlled oscillator and the discriminator center frequency,
2. A stable gyro gain factor equal to $(2\pi d/\lambda)N$ was difficult to maintain.

Both problems were solved by the Stable Platform Phase Follow-Up System (STAPFUS).

The scanning interferometer using STAPFUS is shown in Fig. 6. As before, a motor drove the phase shifter and a reference generator. A single-degree-of-freedom free gyro was coupled to a synchro-resolver to make phase corrections for missile body motion. The gear ratio between the gyro and resolver provided a constant gain factor for the gyro coupling. The difference in phase between the reference signal and the interferometer signal was obtained by the rotor shaft position in a phase-following servo. A potentiometer driven by the phase servo provided an output that, when differentiated, was a measure of the desired line-of-sight rate. Differentiation after the phase-subtraction process eliminated bias. A simple initializing circuit was provided to ensure that the potentiometer started at the zero position. There was no inherent bias in the system because the source of the bias had been eliminated.

Shortly after the incorporation of STAPFUS into the missile system, it was realized that a phase detection of the two signals driving the phase servo could provide an excellent indication of the presence of a signal suitable for steering, especially in a home-on-jammer mode. For this reason, a phase detector was eventually included in a major receiver design program to support home-on-jammer operations.

STAPFUS proved to be an extremely precise measurement system; after it was incorporated into the Talos missile, the majority of the intercepts resulted in direct hits (Fig. 7).

DEVELOPMENT OF THE CONTINUOUS WAVE INTERFEROMETER HOMING SYSTEM

During the 1950's, the microwave pulse-interferometer homing system was developed, and capability against medium-to-high-altitude targets was successfully demonstrated. During that period, the application of Talos to low-altitude targets, particularly over land, was being explored. In that situation, the target-tracking radar, operating at low elevation angles, illuminated the earth's surface and resulted in a large clutter signal that obscured the target (Fig. 8).

The technique developed in the Talos Program to permit low-altitude operation made use of the familiar Doppler effect. Because of the incoming target's velocity, its reflected radar signal is slightly higher in frequency than is the return from the clutter, which is stationary. This frequency separation is the unique signal characteristic that permits rejection of the undesired clutter signals. Tracking the target Doppler signal with a narrow bandpass filter effectively eliminates the massive clutter signals. A typical spectrum of the Doppler signals received by the missile in flight is shown in Fig. 9.

Attention was first given to the excellent work by Raytheon on the Lark (DPN-15) and the Sparrow (DPN-24) homing systems. The initial work on the continuous wave (CW) interferometer for Talos used much of the circuit design of those systems. Six flight

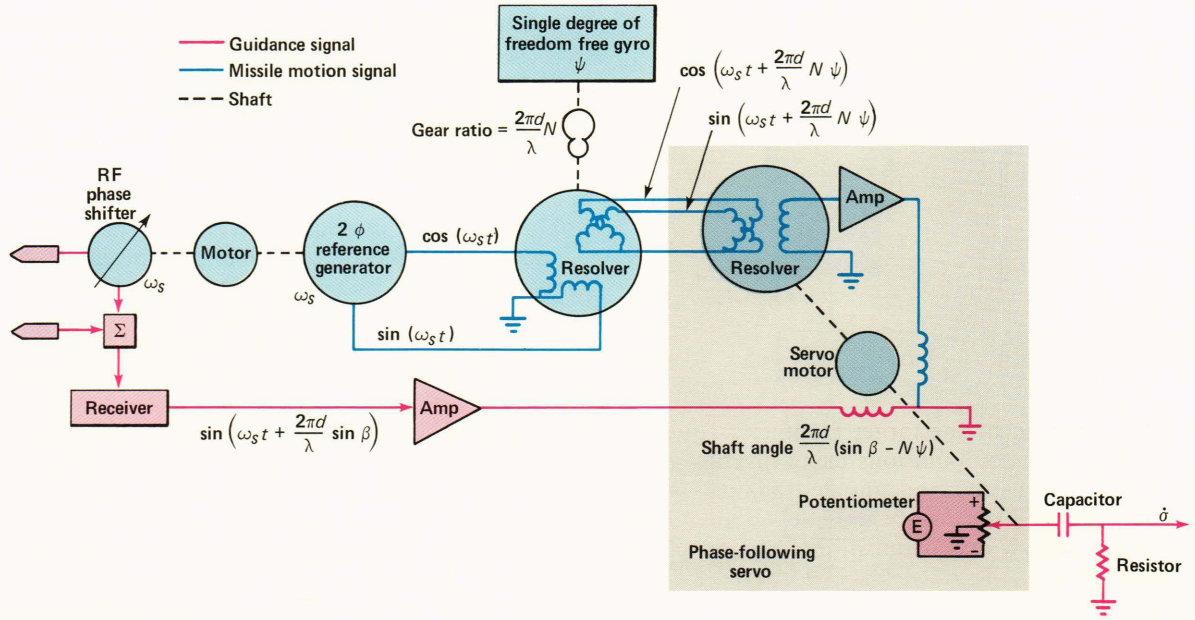

Figure 6 — STAPFUS was a more precise method for decoupling body motion from the scanning-interferometer output. The figure shows a single control channel. A synchro-resolver mechanically coupled to a free gyro (stable platform) was used to shift the phase of the reference generator. A phase-following servo positioned the resolver shaft at an angle that corresponded to $(2\pi d/\lambda)$ (sin β – $N\psi$). That shaft was also coupled to the arm of a potentiometer. The output from the potentiometer was differentiated by a resistor-capacitor network and resulted in a signal proportional to $\dot{\sigma}$.

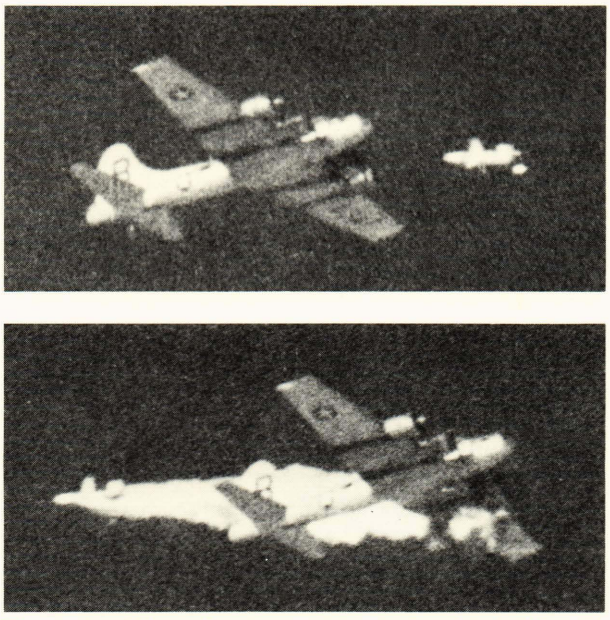

Figure 7 — Miss distances were reduced significantly following the introduction of STAPFUS. The B-17 target shown in this figure was destroyed by a direct hit. The warhead was not used in this test.

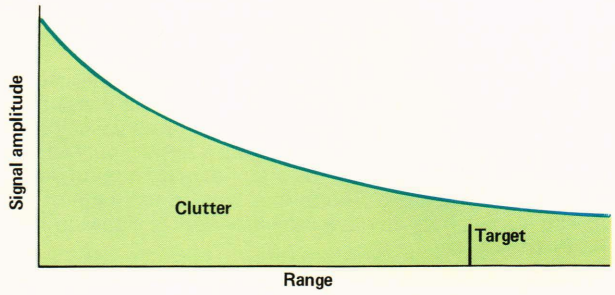

Figure 8 — Pulse radar signals from a moving target can be obscured by large, stationary reflecting surfaces such as the sea or land masses.

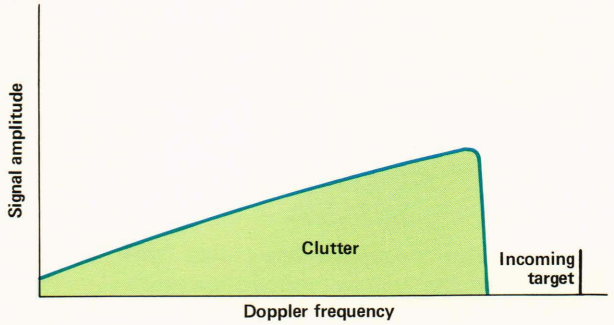

Figure 9 — Continuous wave (CW) radar signals from a moving target can be detected by filtering at the Doppler frequency.

tests were made during 1955-56 using the Sparrow homing-system design but modified for an interferometer antenna system. These tests revealed or confirmed the existence of characteristics that would need to be significantly improved to meet the goals set for the Talos homing system.

The Talos CW homing receiver was designed around the following features:

1. The superheterodyne receiver used quartz-crystal filters to establish a stable and narrow

bandpass that would remove the clutter signals from the target signal.

2. The klystron local oscillator, used in the conversion of the microwave input signals to an intermediate frequency, was controlled by phase-locking the klystron to the illuminator signal from the fire-control radar. That was essential if the target signal was to be kept within the narrow passband (100-hertz bandwidth) of the receiver. The phase-lock loop also provided a convenient way to offset the klystron frequency for automatic tracking of the target Doppler signal.
3. A prediction of the target Doppler frequency, based upon computations using measurements from the target- and missile-tracking radars, was transmitted to the missile to aid in the target search and acquisition function of the receiver. This feature reduced the initial Doppler search bandwidth from 50 kilohertz to 3.5 kilohertz and provided target acquisition in less than 2 seconds in most cases.
4. The solid-state circuit design provided low package volume, stability of adjustment, and immunity to vibration and shock.
5. The missile-to-target angle-measuring system of the interferometer was retained because of its precision and other advantages for the Talos ramjet configuration.

With the timely availability of cavity-stabilized, high-power (1 to 5 kilowatts) klystron amplifiers for the CW radar illuminator, the missile could operate against small aircraft at a range of 100 nautical miles, which coincided with the improved range of the ramjet at that time.

Figure 10 is a block diagram of the phase-locked klystron loop and the ground-aided acquisition loop. The klystron was electrically pretuned prior to launch to the approximate frequency of the illuminator. Automatic frequency control pull-in occurred at the time the ship-based CW illuminator began radiating, about 15 seconds before intercept. The target Doppler frequency, f_D, was computed using radar data and transmitted to the missile by a 400-kilohertz plus f_D frequency modulation on the illuminator frequency. That estimate of the Doppler was used in the ground-aided acquisition loop to establish the initial frequency for the voltage-controlled oscillator. In that way, the klystron frequency was very close to the correct value, and only a minimal search was required to acquire the target.

Figure 11 includes the front receiver with its narrowband quartz crystal filters and discriminators, and the Doppler tracking loop. The loop served to control the voltage-controlled oscillator and, therefore, the klystron in order to keep the target signal in the center of the receiver's narrow bandpass. As long as tracking of the target Doppler signal was maintained, the interferometer angle data could be processed by the STAPFUS system to steer the missile.

The SAM-N-6c1 Missile with its CW homing receiver had some fundamental characteristics that contributed to the missile's capabilities in a countermeasures environment. First, there was limited exposure to the hostile environment as a result of the narrowband characteristics of the seeker and the short (6 to 10 second) homing time. Second, the high-speed phase-tracking loop in STAPFUS provided a nominal angle-tracking sensitivity (volts per degree per second) when it was tracking, independent of the signal-to-noise ratio. Finally, inherent in the Talos phase-interferometer angle processing was the capability to resolve signals from two or more separate sources (for example, from multiple noise jammers) if there was a small power difference ($\geq$2 dB) between them.

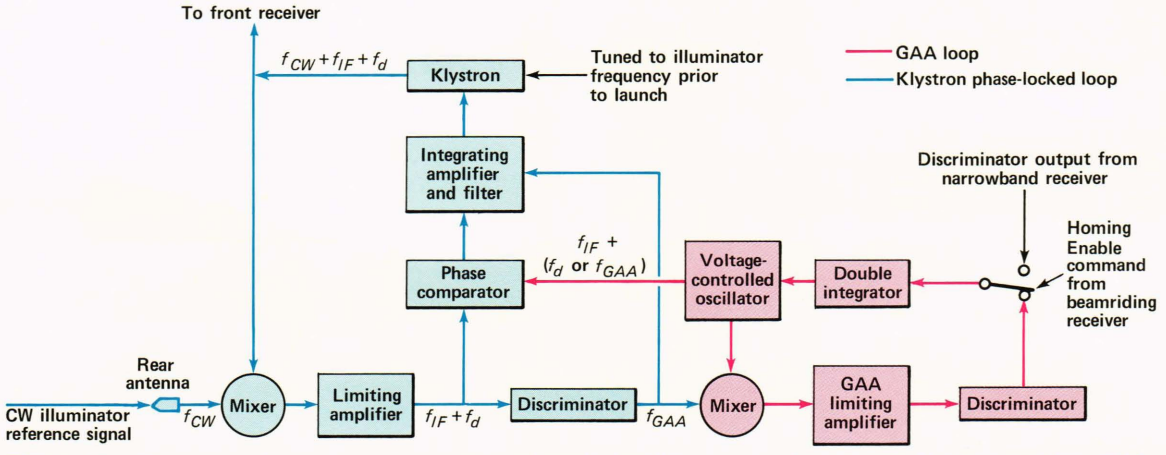

Figure 10 — The rear reference receiver used a phase-locked klystron and a ground-aided acquisition (GAA) loop. The klystron frequency was coarsely corrected by the discriminator to the frequency of the illuminator signal, followed by exact frequency control by the phase-locked loop. The voltage-controlled oscillator frequency was offset from the intermediate frequency by the f_{GAA} loop and caused the klystron frequency to be offset precisely for the target signal entering the front receiver (see Fig. 11).

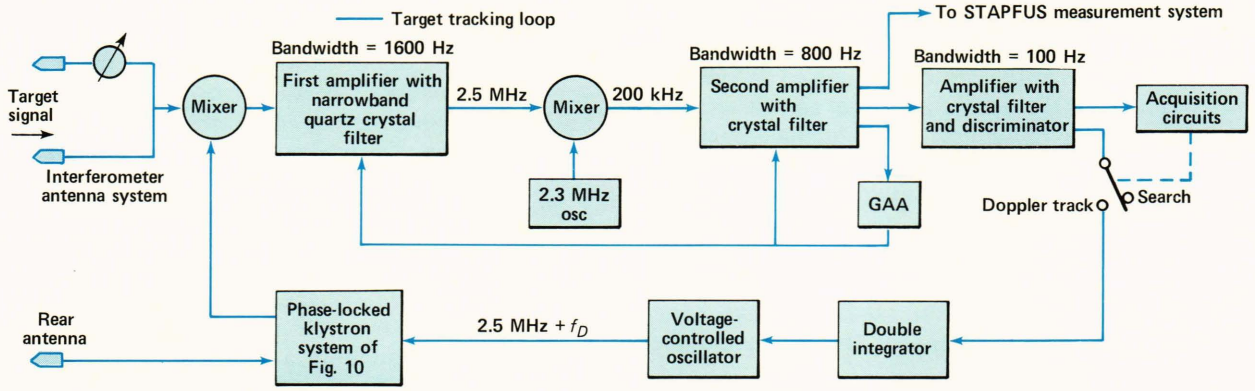

Figure 11 — A target signal having a Doppler frequency equal to f_{GAA} would pass through the amplifiers and narrow-bandpass quartz crystal filters and be detected by the acquisition circuit. Upon detection, the discriminator output readjusted the frequency of the voltage-controlled oscillator to keep the target signal in the center of the receiver bandpass. The narrow-bandpass filters removed the land and sea clutter signals entering the antennas.

As the flight test program proceeded, it became of interest to determine if the CW guidance system would perform well against surface targets. In this application, the target signal and the sea clutter signals do not have a useful Doppler frequency separation. But the combination of the 800-hertz and 100-hertz filter bandwidths maintained a signal-to-clutter ratio suitable for guidance. Figure 12 shows the massive destruction of a destroyer escort vessel as the result of a direct hit by a Talos missile.

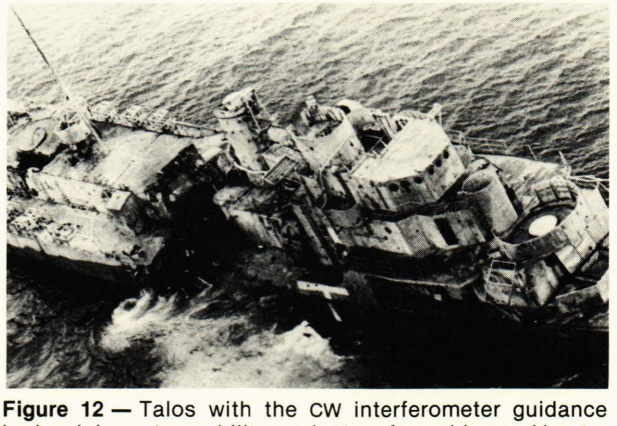

Figure 12 — Talos with the CW interferometer guidance had an inherent capability against surface ships and boats. The capability to engage these targets at ranges well beyond the radar horizon and in the presence of extensive land clutter required only minor changes to the missile and to the shipboard fire control system. The missile for this intercept did not have an active warhead.

MONOPULSE* HOMING SYSTEM

The original SAM-N-6c1 Missile performed extremely well against many types of jamming — its capabilities far exceeded those of any other missile of its day. However, its RF sequential lobing (scanning) angle processing, its slow automatic gain control, and its time-consuming Doppler search routines limited its capabilities against some types of deception countermeasures.

One of the principal objectives of the monopulse seeker design was to enable the missile to win any one-on-one encounter with an aircraft employing any conceivable AM and/or FM noise or deception jamming, even if the designer of the jammer had full knowledge of the Talos guidance system. By the mid-1960's, a seeker emerged that was virtually unjammable by an attacking aircraft. However, the system was not introduced to the Fleet until 1971 because of the high-priority antiradiation missile effort.

Two different monopulse receiver concepts were initially examined. APL examined the concept that took the intermediate frequency (IF) signals associated with antenna pairs and, after the narrowband filtering, multiplexed them into a common IF. Meanwhile, Bendix pursued the idea of the parallel channel, that is, two IF's in parallel for each guidance plane. With the solid-state technology that existed in the early 1960's, the parallel-channel concept became the most attractive: it lent itself to the use of hard-limiting IF's (no automatic gain control; phase tracking appeared satisfactory; the four IF's could be packaged within the same volume occupied by the two IF's in the original CW homer; and it would provide a simpler design than would be possible with a multiplex receiver.

One requirement for the Talos monopulse seeker was that it be compatible with the existing STAPFUS. STAPFUS, as discussed earlier, required a scan reference (ω_S) and a scan ($\omega_S + (2\pi d/\lambda) \sin \beta$) signal. As illustrated in Fig. 13, the Talos monopulse receiver was designed to provide those two signals. The receiver can be likened to the scanning receiver, with the exception that a pseudo scan was introduced at IF following narrowband filtering. That was accomplished by offsetting the frequencies of the second IF amplifiers by an amount equal to the pseudo scan. To ensure that the pseudo scan would not be vulnerable to electronic countermeasures (ECM), the scan

*The word "monopulse" is often used to describe a missile guidance system that employs simultaneous lobe comparison and may or may not employ pulses. For Talos monopulse, the signals were CW.

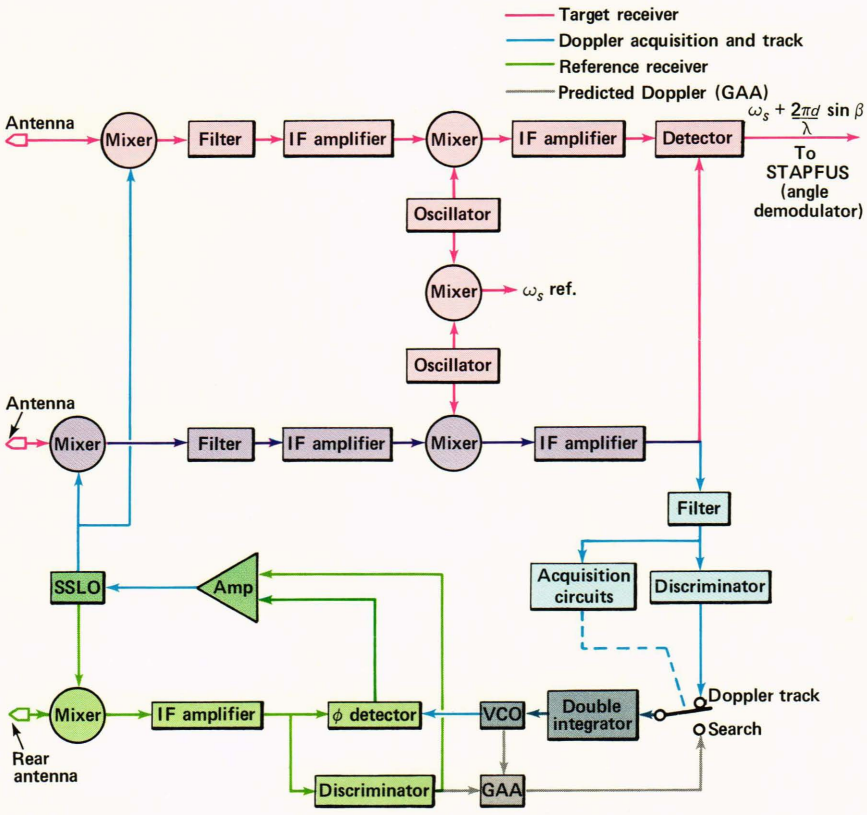

Figure 13 — The monopulse seeker was a refinement of the original CW seeker. The target and/or jammer signals were processed through a two-channel receiver (per guidance plane). Narrowbanding occurred almost immediately following the microwave mixers. The intermediate frequency (IF) amplifiers were hard limited on receiver noise. The Doppler tracking loop was closed through the microwave local oscillator and the first mixer. Predicted Doppler information provided by the ship was used to aid target search. The home-on-jamming mode employed the same narrow bandwidth and angle processing circuits used for tracking the target echo.

reference was chosen to be greater than the bandwidth of the narrow input filters. There was also a conversion of the scan signals and the scan reference signals to the lower frequency signals required by STAPFUS.

The Doppler search routines in the original CW seeker were deficient in that target reacquisition was slow or in some cases could be prevented entirely. Two contributing characteristics were the relatively slow sweep-repetition rate and the total reliance on memory for positioning the sweep. The original search patterns had been designed to provide a high first-look acquisition probability under minimum-signal-level conditions. That limited the maximum search speed that, in turn, was in conflict with the electronic counter-countermeasures requirement for fast reacquisition. Reacquisition must be fast since a jammer can cause the seeker to lose acquisition repeatedly throughout the homing phase. A compromise was sought for the monopulse seeker wherein the sweep speed was increased to a point where the single-look probability for the small signal case was lower than before but, after a second or two, was comparable because of the increased number of looks. Late in the homing phase, when the target signal-to-noise ratio was relatively high, the probability of single-look acquisition was essentially unity and, thus, the desired fast reacquisition was achieved. The problem of positioning the Doppler search center was alleviated by using the predicted Doppler information provided by the ship during the homing phase. The new search routines ensured continuous STAPFUS angle tracking under virtually all conceivable electronic countermeasures conditions and made the system far more tolerant of Doppler prediction errors.

The control of critical guidance functions was based on the coherency of the angle data. That provided a way to resolve a signal emanating from essentially a point source forward of the missile (target skin echo or a jammer) from other signals such as sea clutter, scattered chaff, receiver noise, and so on. There was no need for a detector dedicated to the home-on-jammer (HOJ) mode. The only circuit dedicated to HOJ was the HOJ timer, which delayed guidance switchover from midcourse to homing in cases where acquisition of the target echo was not achieved immediately. That was to prevent immediate HOJ on a standoff jammer. The guidance control logic is shown in Fig. 14.

TESTS OF THE CW AND MONOPULSE HOMING SYSTEM

Extensive laboratory testing of the CW and monopulse homing systems was conducted by the countermeasures group at the Naval Ordnance Laboratory, Corona, Calif. The results of that evaluation provided convincing evidence that the Talos missile with the monopulse seeker would be virtually undefeatable by any self-protection noise or deception jammer. Twenty-five of the 26 valid flight tests of the

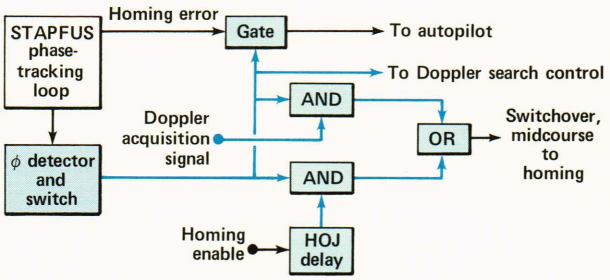

Figure 14 — Guidance-control logic used to implement guidance switchover from midcourse to homing, to gate the steering information once homing began, and to control Doppler-search routines was based on the coherency of the angle data. The signal used for that was obtained from a phase detector that monitored the STAPFUS phase-tracking loop.

Unified missile were successful. Of the 25, nine were with the monopulse seekers against a broad selection of electronic countermeasures types and parameters. Two of the successful tests were against multiple jammers, one of which is shown in Fig. 15.

An interesting observation can be made about how self-protection jamming affected the guidance accuracy (miss distance) of the Talos monopulse missile (see Fig. 16). Note that the Talos performance against the jamming targets was superior to that against the nonjamming targets. This is understandable when one recognizes that a jammer generally provides point-source enhancement of the target; that is, it literally provides a beacon that the missile can home on.

DEVELOPMENT OF MULTIMODE/ MULTIBAND HOJ SYSTEM

The long-range capabilities of Talos made it a desirable weapon to engage standoff jammers or to force them to remain at great distances. However, there was a guidance problem. If the Fleet's surveillance and fire control radars were jammed so as to deny good information about the location of the jammers and the jammers were indeed at long ranges, the midcourse guidance could not be programmed to put the missile close enough to the jamming aircraft for reliable semiactive homing.

The principal objective for the multimode multiband HOJ homing system was to enable the missile to home on jammers in S, C, and X bands. If the missile could home on one of the jammers, the midcourse guidance requirements could be relaxed. All of the semiactive and on-frequency HOJ capabilities of the monopulse homing system were to be retained. A secondary objective was to enable the missile to home on radars operating in those bands. Finally, the homing system had to be compatible with existing Talos missiles, with easy retrofitting possible. Changes to the midcourse guidance were also defined that would have extended the missile's range. Two complete guidance kits were fabricated, but the system was not introduced into the Fleet because of the planned deactivation of Talos.

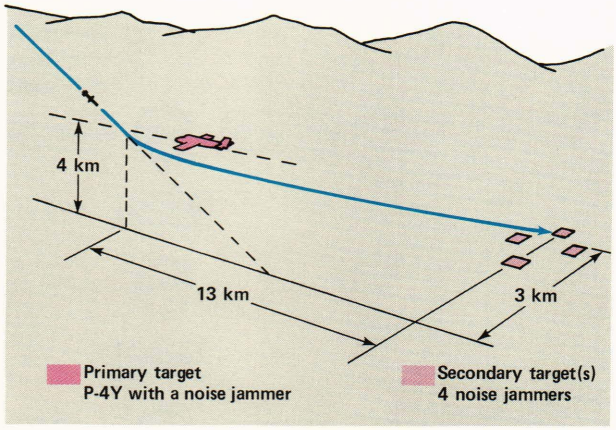

Figure 15 — Multiple jammer flight tests were conducted to demonstrate dichotomous angle-tracking capabilities inherent in the Talos interferometer guidance system. Briefly, if signals from multiple sources were present simultaneously, the missile would track one of them if a power differential of 2 decibels or greater existed within the narrow bandwidth of the receiver. In practice, the missile would nearly always intercept one of the targets. For the multiple jammer test illustrated here, the primary target was a P-4Y aircraft with a noise jammer. After achieving a near miss on the aircraft, the missile successfully intercepted the westernmost jammer on the ground.

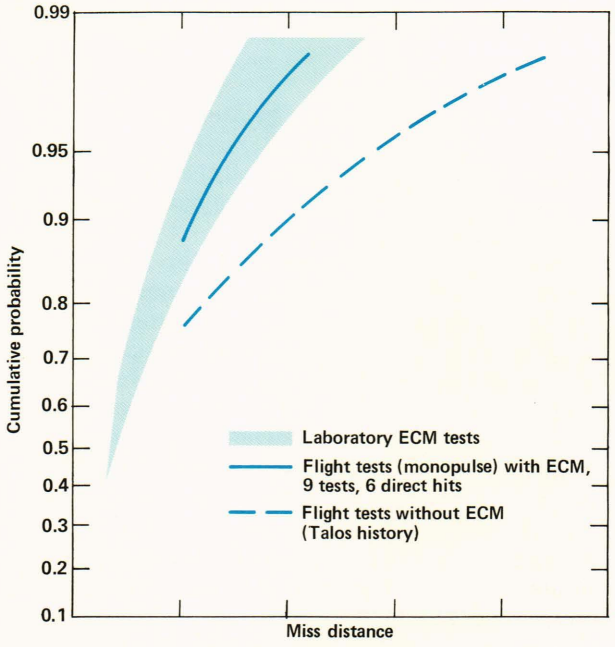

Figure 16 — The effect of self-protection electronic countermeasures (ECM) on miss distance is illustrated. The curves were derived from miss distance data obtained from laboratory ECM tests conducted at the Naval Ordnance Laboratory, Corona, Calif., from the monopulse flight tests against jamming targets, and from historic test data of Talos flight tests against nonjamming targets. Note that the performance against the jamming targets was superior to that against the nonjamming targets.

A simplified block diagram of the homing system is shown in Fig. 17. The basic system was the semiactive monopulse seeker. The principal modifications

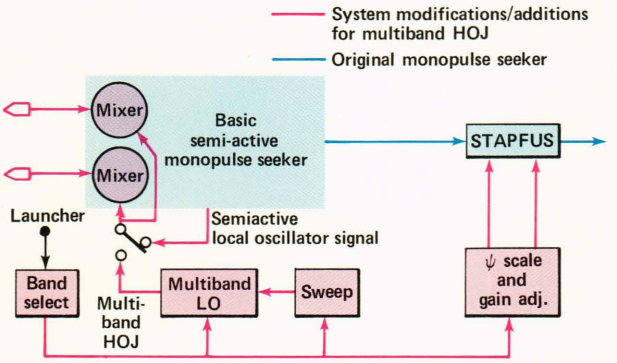

Figure 17 — The multiband HOJ system was basically an expansion of the semiactive monopulse homing system. The microwave portions of the original system were changed to provide the desired wideband operation. Frequency selection (typically 30 or 200 megahertz bandwidth) was by digital message prior to launch. Conventional semiactive homing could be activated in flight.

involved new, wideband antennas and microwave mixers and the addition of a wideband local oscillator. (The original local oscillator was used for semiactive homing.) A missile body motion ($\dot{\psi}$) and guidance gain scaler was added to adjust for the sensitivity of the interferometer to wavelength (frequency).

The multiband HOJ design was based on the simple concept that if the narrow Doppler filters of the semiactive system were excited by an intermittent signal (blinking ECM or pulse radar) at a sufficiently high rate, the output of the filters would be uninterrupted CW signals from which excellent angle information could be obtained. To ensure that the target signal could excite the Doppler filters without having to resort to the complexities of additional target recognition, acquisition, and automatic frequency control tracking circuits, the microwave local oscillator was swept at an appropriate rate over the RF band of interest. The result was a wideband seeker, the bandwidth of which was determined by the extent of the local oscillator sweep. Typically, the width of the band was either 30 or 200 megahertz. If multiple signals were present in the selected band, guidance favored the strongest signal.

The selection of the RF frequency for the multiband HOJ operation was accomplished via a digital message to the missile. Semiactive homing could be initiated in flight (if desired) in the same way as for a conventional antiair engagement.

Since it was assumed that the multiband HOJ feature would be used when target range was unknown, it was planned for the missile to fly at the fuel-conserving cruise altitude until seeker logic initiated homing. Homing always started at that altitude. For the engagement of a radar target (on land or a ship) at long range (over the horizon) but whose general location was known, a midcourse trajectory employing a terminal dive was used.

Flight hardware was fabricated, but there were no flight tests of the multimode/multiband HOJ system. In 1965, however, there were successful flight tests against radar targets at the White Sands Missile Range with Talos missiles using the same guidance concept as in the multiband HOJ system.

DEVELOPMENT OF ANTIRADIATION MISSILE GUIDANCE

Early in the Vietnam conflict, the need for an effective long-range antiradiation missile (ARM) to suppress enemy radars was evident. The Talos ARM program was authorized as a fast-reaction effort to respond to that need. The long-range capabilities and the ease with which the missile could be adapted for new missions made Talos a desirable choice for radar suppression. A feasibility demonstration flight test against an S-band radar target was successfully conducted at the White Sands Missile Range on October 26, 1965, only 35 days after initiation of the effort. Two additional guidance system designs subsequently were developed and flight tested, each progressively more sophisticated. The final design, first deployed on USS *Long Beach*, was completed in 24 months.

A unique operational concept had to be developed for ARM because it was not possible for the ship to track the target and implement missile guidance as it did for the engagement of air targets. For ARM, the target information consisting of geographic location and RF emission characteristics (frequency, pulse-repetition frequency etc.) was provided by appropriate techniques. Ship coordinates were established by means of several navigational techniques, including the Navy Navigation Satellite System. The ship then directed the missile to the vicinity of the target using the beamrider midcourse guidance. As the missile approached the target, the missile was put into a dive and the homing system was activated. Two different terminal geometries were used; one caused the missile to approach the target in an approximate 45° dive, while the other caused the missile to approach from a near-vertical dive.

The principal requirement for the ARM homing system was that it be monopulse, since the low pulse repetition frequency of some target radars was not compatible with the scan frequency used by the earlier semiactive seekers. Also, a system with a high sensitivity was desired that would provide continuous guidance on the low sidelobe levels from the target. Finally, the ARM guidance system had to be compatible with the existing Talos airframe. Modification of existing antiair warfare missiles to antiradiation missiles had to be accomplished by the relatively simple replacement of subsystem modules.

A simplified block diagram of the ARM seeker is presented in Fig. 18. The receiver used two parallel IF amplifiers (per guidance plane) with subsequent in-phase and quadrature processing. A very large instantaneous dynamic range (greater than 120 dB) was achieved by using limiting amplifiers. The differential phase shift between these amplifiers was maintained at a low level by careful attention to circuit design. Good phase tracking was attained with input peak power levels greater than 10 watts.

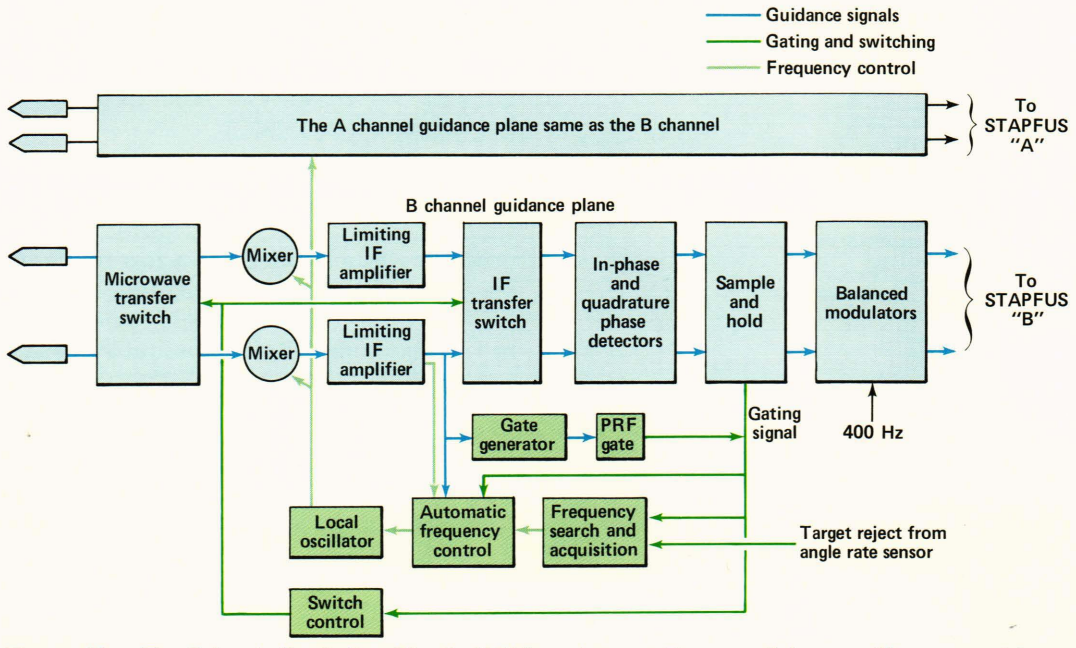

Figure 18 — The Talos Antiradiation Missile (ARM) seeker used two parallel IF amplifiers per guidance plane with subsequent in-phase and quadrature processing. A signal that satisfied the prelaunch frequency and pulse repetition frequency requirements provided the gating signal to the angle channel.

Against very-low-frequency targets (L band), the guidance error associated with as much as 10 electrical degrees differential phase shift between the receiver channels was undesirable. The error was virtually eliminated with the addition of microwave and IF transfer switches that, on a pulse-to-pulse basis, would allow radar pulses to be processed alternately through one channel and then the other. The internally generated errors would then average zero. The measured angle error arising from differential phase shift as a function of signal power level is shown in Fig. 19. The errors with and without the transfer switches operating may be seen.

In parallel with the angle channels was the acquisition and discrimination channel. The receiver was self-gating. A signal that satisfied the radiation and pulse repetition frequency requirements designated at launch would provide a gate to the angle channel. The seeker was able to discriminate between two signals if their operating frequencies differed by 3 megahertz or more. Leading-edge gating was used to minimize the effects of multipath reflections near the target. The angle phase-comparator outputs were multiplied by a 400-hertz signal to provide an amplitude-modulated signal to drive the STAPFUS resolvers.

Geometric discrimination was obtained by the seeker measuring the line-of-sight rate to the target at the time of target acquisition. The ship, via the midcourse beamriding guidance, caused the missile to

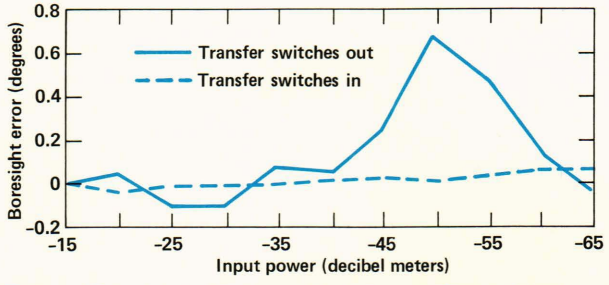

Figure 19 — Angle bias resulting from differential phase shift between the receiver channels was virtually eliminated with the use of radio frequency and of IF transfer switches that operated on a pulse-to-pulse basis.

dive toward a point that was approximately 4 miles beyond the intended target. This resulted in a missile-to-target line-of-sight rate that was in the down direction. If that downward angular rate was not detected during the target acquisition process, the signal was rejected and the seeker continued to search for another target. If the target was accepted, the missile executed a down maneuver to the target. That also enabled the missile to intercept the target at an elevation angle of approximately 90°.

Missile flight tests verified the unique design by exercising the various discriminants. Guidance accuracy was demonstrated with many direct hits (Fig. 20).

Figure 20 — A Talos ARM flight test conducted in October 1965 at White Sands Missile Range is illustrated by the sequence of pictures: (a) just before intercept of radar target, (b) impact and warhead detonation, (c) radar target after intercept. The damage mechanism is the warhead explosion plus the kinetic energy of the missile at impact.

Criteria for radiation patterns, cross-over gain, and modulation sensitivity are analyzed for conical-scan-type tracking antennas using amplitude- or phase-comparison methods. It is shown that the radiation patterns of interest are not, as generally believed, the individual static patterns, but their RF vector sum and difference. A method of measuring these sum and difference patterns is suggested.

T. C. Cheston

Criteria for CONICALLY-SCANNED TRACKING ANTENNAS

Tracking antennas often obtain high angular resolution by a time-sequential lobe-comparison method. The radiation pattern is scanned (nutated) about the boresight direction in such a way that it traces out a cone, a method called conical scanning. Figure 1 shows two radially opposite positions of the radiation pattern. When the target is in the boresight direction, a continuous-wave (CW) signal is obtained. When the target is off boresight, the signal is amplitude-modulated at the nutation frequency; the magnitude and phase of that modulation define the direction of the target. In this discussion, the tracking antenna will be considered as a receiving antenna, with the target separately illuminated.

Introduction

RADIATION PATTERNS—The antenna tracks after having acquired the target. In this way, the target is always, at least approximately, in the boresight direction. If the only signal at the tracking antenna is an undistorted plane wave front arriving from a single target, then the only antenna pattern characteristics of interest are gain and modulation sensitivity in the boresight, or cross-over, region. Such other characteristics as sidelobe structure are irrelevant under these conditions.

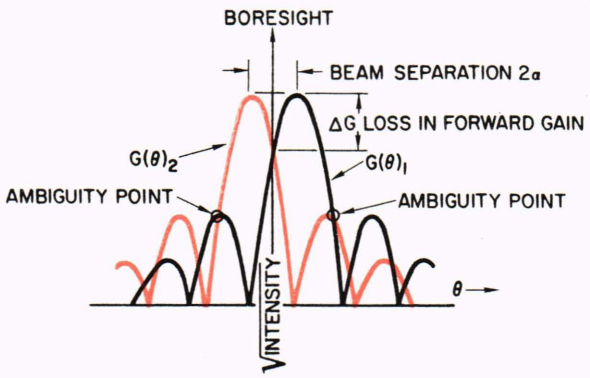

Fig. 1—Lobe comparison—static patterns.

The complete radiation pattern characteristics are of interest only if one or more additional signals from secondary sources in other directions arrive simultaneously at the antenna. These secondary sources may be real or virtual and may or may not be phase-coherent with the signal

from the target. Only coherent secondary sources will be considered here, though it can be shown[1] that similar arguments apply if the secondary sources are not phase-coherent.

The signals from the target and secondary source considered here are thus of the same frequency. Virtual secondary sources may arise if the target signal is received from two or more directions because of reflections from the ground or from obstacles or because of distortions of the plane phase front. Radomes give rise to both reflections and phase-front distortions, and the aberrations of a radome may be regarded as errors due to virtual secondary sources. Real secondary sources can result from the presence of additional targets moving with the same radial velocity. Small, incoherent variations in relative radial velocity may, in such cases, be regarded as noise.

Since the antenna tracks the primary target, a constant RF signal from that target is always present; its amplitude is determined by the cross-over gain. The return from the secondary source, modulated at the nutation frequency, is added *vectorially* to that signal. Phase is meaningful since both the primary and secondary signals co-exist at the same output terminal. Therefore, the modulation that results from the secondary source, that gives erroneous directional information, arises from the *vector* difference of the static patterns in the direction of that secondary source as a function of time. Similarly, a component is obtained from the vector sum of the static patterns, which gives erroneous amplitude information. The radiation patterns of interest are, therefore, the sum and the difference patterns obtained by the *vectorial addition and subtraction* of the static patterns; these are exactly equivalent to the familiar sum and difference patterns of monopulse-type antennas. In fact, the conically-scanned tracking-type antenna may be regarded, in this respect, as a monopulse antenna operating on a time-sharing basis.

The vector sum and difference patterns, as opposed to static patterns, correspond to a secondary source that has the worst possible phase relationship with the primary target signal. Under real conditions, this phase relationship can have any value and there can be no control over it. The worst case must therefore be taken for assessing antenna performance.

A simple example shows how misleading it can be to assess antenna performance only from static patterns. Figure 2A shows ideal sidelobe-free sum (Σ) and difference (Δ) patterns. Figure 2B shows the equivalent static patterns that each contains one large, but desirable, sidelobe. Figure 8 shows how, in the case of a phase-comparison system, a large sidelobe in the static pattern is inherently present but is in no way detrimental.

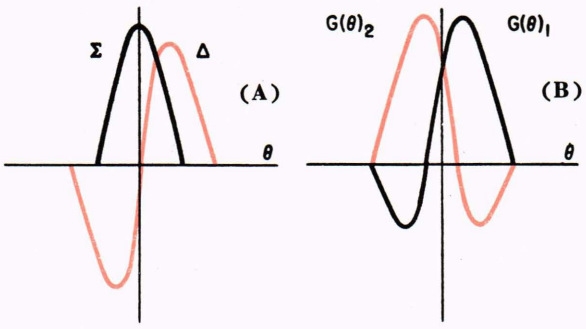

Fig. 2—(A) Ideal sum and difference patterns, and (B) static patterns for ideal Σ and Δ.

CROSS-OVER GAIN AND MODULATION SENSITIVITY—Forward, or cross-over gain, is the gain of the radiation pattern in the boresight direction and is defined by the loss in gain (ΔG) relative to the peak gain (Fig. 1). Modulation sensitivity is a measure of the amount of modulation obtained for a small, given, off-set of the target from the boresight direction and may be defined as

$$S = 100 \frac{d}{d\theta} \left(\frac{G(\theta)_1 - G(\theta)_2}{G(\theta)_1 + G(\theta)_2} \right)_{\theta=0} \% \text{ per unit angle.} \quad (1)$$

Alternatively, it may be defined as

$$S' = \frac{d}{d\theta} \left(20 \log \frac{G(\theta)_1}{G(\theta)_2} \right)_{\theta=0} \text{db per unit angle.} \quad (2)$$

Referring to Fig. 1, an increase in beam separation 2α is accompanied by a decrease in forward gain and an increase in modulation sensitivity. The minimum permissible cross-over gain is determined from the overall system requirements and characteristics and must be adequate to give an acceptable signal/noise ratio for the weakest expected target returns. Increasing the gain beyond that minimum value will not normally lead to system improvements. Increasing the modulation sensitivity, on the other hand, continuously improves the direction-finding and tracking capabilities, up to limitations imposed by other parts of the system. Excess cross-over gain may, therefore, be usefully traded for increased modulation sensitivity.

[1] T. C. Cheston, "Criteria for Conically-Scanned Tracking Antennas," The Johns Hopkins University, Applied Physics Laboratory, CM-992, Feb. 1961.

Similar to monopulse systems, an antenna radiation pattern may be conically scanned by the equivalent of an amplitude- or phase-comparison method. The general criteria for both these methods will be analyzed.

Amplitude Comparison

In the amplitude-comparison system of conical scanning, the beam is displaced by a tilted phase front that rotates to scan the beam conically. A typical example of such a system would be a nutating feed in the focal plane of a reflector or lens-type antenna.

Optimum Beam Displacement for Small Sidelobes—In the following analyses, the problem is treated one-dimensionally. Referring to Fig. 3,

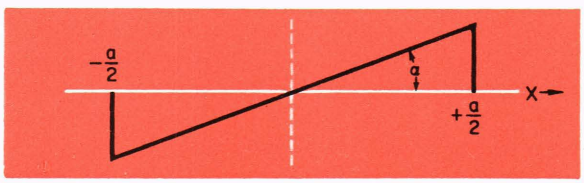

Fig. 3—Aperture phase distribution.

the antenna aperture extends from $x=-a/2$ to $x=+a/2$ and has an amplitude distribution $F(x)$. The phase distribution across the aperture is linear and is given by $k\alpha x$, where $k=2\pi/\lambda$ and α is the beam tilt angle.

The radiation pattern is then given by the Fourier transform of the amplitude and phase distribution

$$G(\theta)=\int_{-a/2}^{+a/2} F(x)\ e^{-jk\alpha x}\ e^{-jk\theta x}\ dx.$$

The sum radiation pattern is obtained from two amplitude distributions with opposite phase slopes:

$$\begin{aligned} G(\theta)_\Sigma &= \frac{1}{2}\int_{-a/2}^{+a/2} F(x)\ e^{-jk\alpha x}\ e^{-jk\theta x}\ dx \\ &+ \frac{1}{2}\int_{-a/2}^{+a/2} F(x)\ e^{+jk\alpha x}\ e^{-jk\theta x}\ dx \qquad (3) \\ &= \int_{-a/2}^{+a/2} F(x)_\Sigma\ e^{-jk\theta x}\ dx, \end{aligned}$$

where

$$F(x)_\Sigma = F(x)\ \cos(k\alpha x).$$

Similarly, the difference pattern is

$$G(\theta)_\Delta=\int_{-a/2}^{+a/2} F(x)_\Delta\ e^{-jk\theta x}\ dx, \qquad (4)$$

where

$$F(x)_\Delta = jF(x)\ \sin(k\alpha x).$$

If the aperture had been excited with constant phase, its radiation pattern would have been

$$G(\theta)_{cp}=\int_{-a/2}^{+a/2} F(x)\ e^{-jk\theta x}\ dx. \qquad (5)$$

Thus, the sum radiation pattern is derived from an amplitude distribution that equals the original (constant-phase) amplitude distribution multiplied by cos $(k\alpha x)$. Similarly, the difference radiation pattern is derived from an amplitude distribution that equals the original (constant-phase) amplitude distribution multiplied by j sin $(k\alpha x)$.

With constant amplitude distribution, the smallest sidelobes would be obtained in the sum pattern when $\cos(k\alpha x)=0$, with $x=\pm a/2$. In the difference pattern, the smallest sidelobes would be obtained when $\sin(k\alpha x)=0$, with $x=\pm a/2$, but this amount of beam tilt would cause the sum pattern to split, having zero forward gain.

The maximum value of the beam tilt angle is thus limited by considerations of the sum pattern. Low sidelobes in both sum and difference patterns, however, may still be obtained by suitably tapered amplitude distributions.

Other considerations may be used to define optimum beam tilt angles. Rhodes[2] suggests that the product of the sum signal and the slope of the difference signal should be a maximum. This maximum is broad and corresponds approximately to a 3-db loss in forward gain. It agrees reasonably with the optimum requirement for low sidelobes.

Modulation Sensitivity—All usual radiation patterns of an antenna may conveniently be described, with sufficient accuracy for present purposes, in terms of 3-db beamwidth, BW, of the static pattern, by substituting $\frac{\frac{8}{9}}{BW}$ for a/λ, giving

$$G(\theta)=\frac{\sin\left(\frac{P}{BW}\ \theta\right)}{\frac{P}{BW}\ \theta},$$

where

$$P=8\pi/9.$$

[2] D. R. Rhodes, "Introduction to Monopulse," McGraw-Hill Book Co., New York, 1959.

The static patterns of Fig. 1 are then

$$G(\theta)_1 = \frac{\sin\left\{\frac{P}{BW}(\theta-\alpha)\right\}}{\frac{P}{BW}(\theta-\alpha)},$$

and

$$G(\theta)_2 = \frac{\sin\left\{\frac{P}{BW}(\theta+\alpha)\right\}}{\frac{P}{BW}(\theta+\alpha)}, \qquad (6)$$

where α is the beam tilt angle.

Equations (1), (2) and (6) give the modulation sensitivity for the cross-over region as

$$S = 279\left\{\frac{1}{P\frac{\alpha}{BW}} - \cot\left(P\frac{\alpha}{BW}\right)\right\}\% \text{ per } BW, \qquad (7)$$

$$S' = 48.5\left\{\frac{1}{P\frac{\alpha}{BW}} - \cot\left(P\frac{\alpha}{BW}\right)\right\} db \text{ per } BW. \qquad (8)$$

Figure 4 shows the modulation sensitivity as a function of beam separation, and Fig. 5 shows it

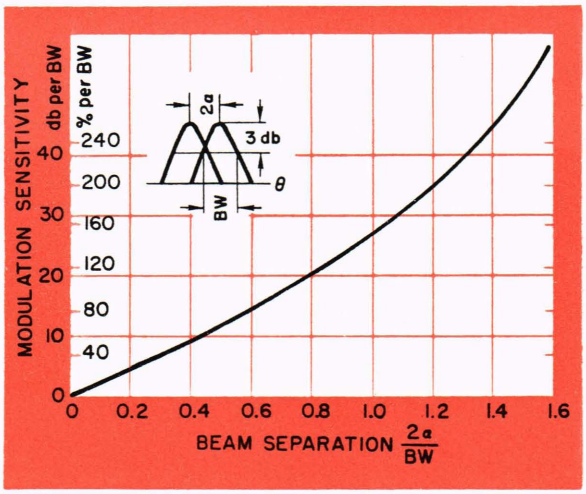

Fig. 4—Amplitude comparison—modulation sensitivity versus beam separation.

as a function of ΔG, the loss in forward gain at cross-over, where

$$\Delta G = -20 \log\left(\frac{\sin\left(P\frac{\alpha}{BW}\right)}{P\frac{\alpha}{BW}}\right) \text{db}. \qquad (9)$$

When ΔG is smaller than about 2 db, then Eq. (9), combined with Eq. (7) or (8), gives approximately

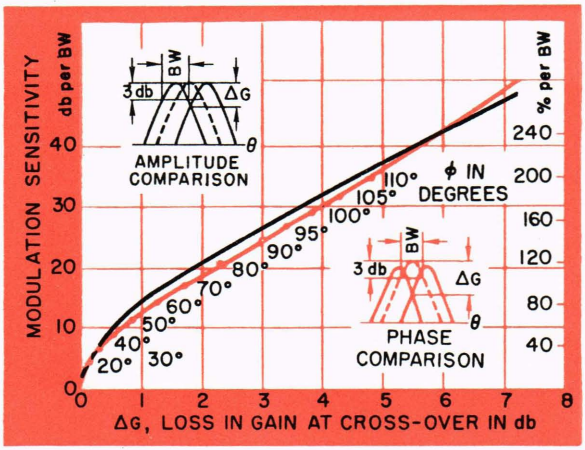

Fig. 5—Modulation sensitivity versus cross-over gain.

$$S \simeq 77\sqrt{\Delta G}/BW \qquad \% \text{ per degree},$$

$$S' \simeq 13.5\sqrt{\Delta G}/BW \qquad \text{db per degree},$$

where ΔG is expressed in db and BW in degrees. These results agree with published data.[3]

Phase Comparison

In a phase-comparison system, the aperture is divided into separate parts. For example, for a line-source system, the aperture may be divided into parts A and B (Fig. 6). The phase distribution across A and B is constant, and the two radiation patterns have maxima pointing in the same direction. The two apertures are displaced in space; hence, off-boresight radiation received by A will differ in phase from that received by B. For a monopulse system, the signal received by

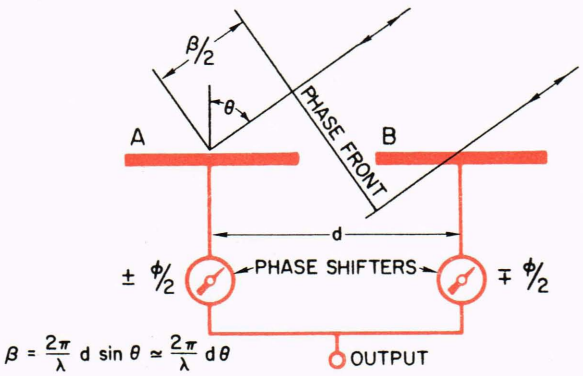

Fig. 6—Phase comparison.

[3] J. B. Damonte and D. J. Stoddar, "An Analysis of Conical Scan Antennas for Tracking," *I.R.E. National Convention Record*, **4**, 1, 1956.

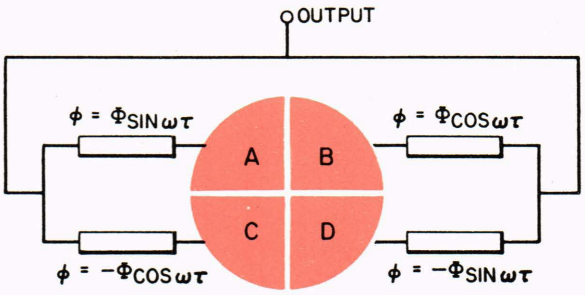

Fig. 7—Conical scan with phase comparison.

A and B may be combined in a hybrid, such as a magic-T, whose outputs are the sum and difference channels. The two apertures are thus excited in phase for the sum pattern and in antiphase for the difference pattern. For scanning, apertures A and B may be coupled to a common output through variable phase shifters, as shown in Fig. 6. In a two-dimensional system, a conically-scanned beam can be obtained from apertures A, B, C, and D, with four phase shifters as shown in Fig. 7. The insertion phase for each aperture varies sinusoidally with time, adjacent apertures being in phase quadrature and diagonally opposite apertures being in phase opposition. The beam tilt angle and modulation sensitivity are defined by the amount of phase shift.

RADIATION PATTERNS—Let A and B denote the radiation patterns of apertures A and B, respectively, as shown in Fig. 6. Let $G\theta_1$ be the combined radiation pattern (static) when the phase shifts to apertures A and B are $+\phi/2$ and $-\phi/2$, respectively, and let $G(\theta)_2$ be the equivalent pattern (static) with phase shifts of $-\phi/2$ and $+\phi/2$.

The radiation patterns $G(\theta)_1$ and $G(\theta)_2$ are given by

$$G(\theta)_1 = \frac{1}{\sqrt{2}} A\ e^{j\beta/2}\ e^{j\phi/2} + \frac{1}{\sqrt{2}} B\ e^{-j\beta/2}\ e^{-j\phi/2}, \tag{10}$$

$$G(\theta)_2 = \frac{1}{\sqrt{2}} A\ e^{j\beta/2}\ e^{-j\phi/2} + \frac{1}{\sqrt{2}} B\ e^{-j\beta/2}\ e^{+j\phi/2}, \tag{11}$$

where β is the difference in phase of the incoming signal as received by apertures A and B.

The sum $G(\theta)_\Sigma$ and difference $G(\theta)_\Delta$ radiation patterns are then obtained by adding and subtracting $G(\theta)_1/2$ and $G(\theta)_2/2$ vectorially. Where the apertures A and B are adjacent and have identical amplitude distributions, i.e., when $A \equiv B$ and $d = a/2$, this gives

$$G(\theta)_\Sigma = \sqrt{2}\ A\ \cos\left(\frac{\pi}{2}\frac{a}{\lambda}\theta\right)\ \cos(\phi/2), \tag{12}$$

$$G(\theta)_\Delta = \sqrt{2}\ A\ \sin\left(\frac{\pi}{2}\frac{a}{\lambda}\theta\right)\ \sin(\phi/2), \tag{13}$$

and the ratio

$$\frac{G(\theta)_\Sigma}{G(\theta)_\Delta} = -\tan\left(\frac{\pi}{2}\frac{a}{\lambda}\theta\right)\tan(\phi/2). \tag{14}$$

The shape of both sum and difference radiation patterns are seen to be entirely independent of the value of ϕ. This is also true when the apertures are neither adjacent nor identical. The pattern shapes are determined only by the amplitude and phase distribution across the apertures and the spacing d. The distribution of power between sum and difference patterns, and hence the modulation sensitivity, is determined by ϕ. Figure 8 shows how static patterns and sum and difference gain patterns vary with ϕ. Static patterns $G(\theta)_1$ and $G(\theta)_2$ change with ϕ from the sum pattern, when $\phi = 0$, to the difference pattern, when $\phi = \pi$. For intermediate values of ϕ, such as $\phi = \pi/2$, large "sidelobes" will, therefore, appear in the static patterns. As previously discussed, these are not undesirable.

Equations (12) and (13) show that $\phi = \pi/2$ gives a cross-over gain ($\theta = 0$) which is 3 db down from the gain of the apertures excited in phase ($\phi = 0$).

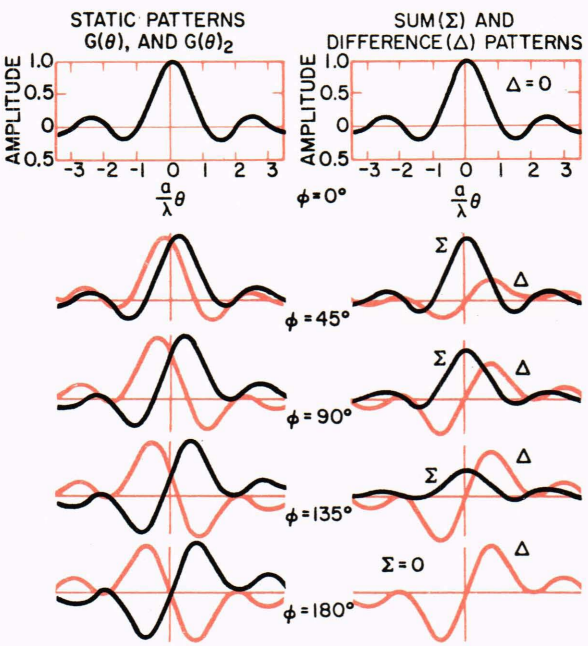

Fig. 8—Phase comparison—effects of varying ϕ. Apertures are adjacent and have a constant distribution.

If the amplitude distribution is constant and the two apertures are adjacent and of equal size a/λ, then

$$G(\theta)_{\Sigma} = \sqrt{a}\,\frac{\sin\left(\pi\,\frac{a}{\lambda}\,\theta\right)}{\pi\,\frac{a}{\lambda}\,\theta}\cos\left(\phi/2\right), \qquad (15)$$

and

$$G(\theta)_{\Delta} = \sqrt{a}\,\frac{1-\cos\left(\pi\,\frac{a}{\lambda}\,\theta\right)}{\pi\,\frac{a}{\lambda}\,\theta}\sin\left(\phi/2\right). \qquad (16)$$

These patterns, $G(\theta)_{\Sigma}$ and $G(\theta)_{\Delta}$, will be recognized as the radiation patterns from a constant-amplitude distribution aperture excited, respectively, in phase and in anti-phase.[4]

The normalized sum and difference radiation patterns obtained with amplitude- and phase-comparison methods are compared in Fig. 9. In both cases, the amplitude distribution is constant and the loss in forward gain is 3 db. The amplitude-comparison method gives a wider sum pattern and a narrower difference pattern beamwidth than the phase-comparison method.

Modulation Sensitivity—From Eqs. (1), (2), and (14), the modulation sensitivity for the cross-over region is with adjacent and equal apertures:

$$S = 50\,\pi\,\frac{a}{\lambda}\,BW\,\tan\left(\phi/2\right) \quad \%\text{ per } BW, \qquad (17)$$

$$= 2.74\,\frac{a}{\lambda}\,\tan\left(\phi/2\right) \quad \%\text{ per degree}, \qquad (18)$$

and

$$S' = 8.7\,\pi\,\frac{a}{\lambda}\,BW\,\tan\left(\phi/2\right) \text{ db per } BW, \qquad (19)$$

$$= 0.47\,\frac{a}{\lambda}\,\tan\left(\phi/2\right) \text{ db per degree}. \qquad (20)$$

Equations (18) and (20) show that with two identical apertures, the modulation sensitivity per degree is entirely independent of radiation patterns, beamwidth, or amplitude distribution. This is also true if the two apertures are not adjacent. This result agrees with Rhodes' data.[2]

The above results may be expressed in terms of beamwidth to yield good approximations, for adjacent apertures which are not identical, by

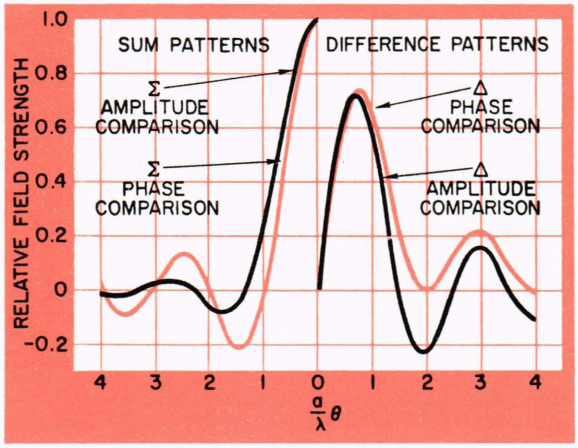

Fig. 9—Amplitude and phase comparison patterns.

the substitution $a/\lambda = \frac{\frac{8}{9}}{BW}$. This gives

$$S = 140\,\tan\left(\phi/2\right) \quad \%\text{ per } BW, \qquad (21)$$

$$S' = 24\,\tan\left(\phi/2\right) \quad \text{db per } BW, \qquad (22)$$

The loss in forward gain is obtained from Eq. (12),

$$G = -20\,\log\cos\left(\phi/2\right) \text{ db}. \qquad (23)$$

Figure 5 shows the modulation sensitivity as a function of loss in forward gain and compares the results with those obtained with amplitude comparison. For a two-dimensional conical-scan system, the required peak-to-peak value of sinusoidally-varying phase shift is $\sqrt{2}$ times the value of ϕ shown. Experimental verification within 5% has been obtained.

Radiation Pattern Improvements—Overall pattern improvements may be achieved by providing coupling between the adjacent regions of the four separate apertures of Fig. 7, particularly near the center. This coupling has no effect on the sum pattern where all apertures are excited in phase. For the difference pattern, the apertures are excited in anti-phase. The aperture distribution for the difference pattern is therefore reduced in amplitude for those regions where the coupling is effective. Coupling can thus give a suitable difference pattern distribution, with the amplitude smoothly reduced to zero at the center and, at the same time, permit a suitable sum pattern distribution with maximum amplitude at the center.

In one antenna, mutual coupling was used to reduce the measured sidelobes in the difference pattern from about −9 db without coupling to

[4] J. F. Ramsay, "Fourier Transforms in Aerial Theory," *Marconi Review*, Nos. 83-89, 1946.

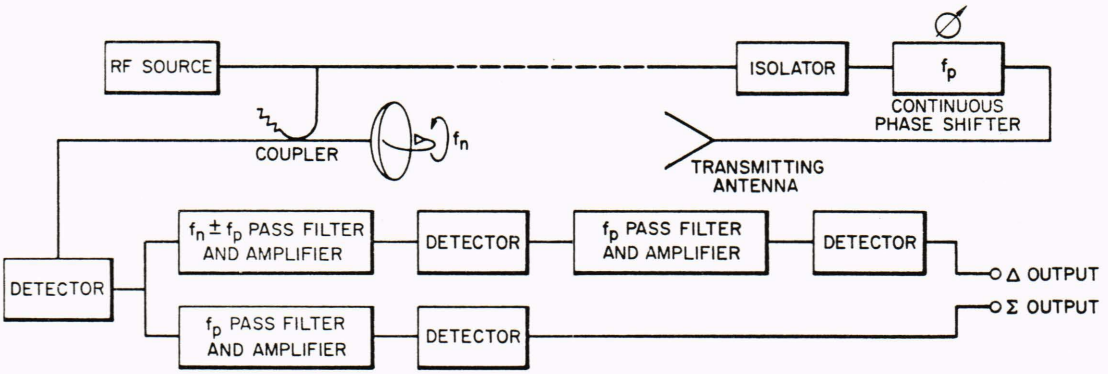

Fig. 10—Measurement of sum and difference patterns.

about −18 db with coupling, without affecting the sum pattern.

Antenna Pattern Measurements

Special techniques are required to measure the sum and difference patterns of conically-scanned beams where the amplitude-comparison method is used. These patterns are the vector sum and difference of the static patterns. Even with the beam nutating, they cannot be measured directly since the RF phase would have to be "remembered" from the time the beam points in one direction to the time when it points in the opposite direction. Figure 10 shows a simple method of measuring the sum and difference patterns.

The antenna under test is used as receiver. The beam is nutated in the normal operating mode at frequency f_n. Some of the transmitter power is tapped off and added to the received signal so that the received signal power is always small in comparison to the power added. The crystal detector then acts as a linear mixer where the IF frequency is zero. With the correct phasing of the two signals, the DC variations in the output would be a measure of the sum pattern, and the output at the nutation frequency, a measure of the difference pattern.

To avoid point-by-point phase adjustments and DC measurements, the transmitted power is single-side-band-modulated at a low frequency, f_p, ($f_p \ll f_n$) by a continuously-variable phase shifter such as, for example, described by Fox.[5] The mixer output may then be continuously analyzed in two channels: first, in a channel which passes only the frequency f_p and whose output measures the sum pattern; second, in a channel which passes $f_n \pm f_p$. Detection then yields f_p, which measures the difference pattern.

[5] A. G. Fox, "An Adjustable Waveguide Phase Changer," *Proc. I.R.E.* 35, Dec. 1947.

With conically-scanned antennas where the phase-comparison system is used, sum and difference patterns may be measured directly by adjusting the phase shifters to +90° and −90°, respectively, for the difference pattern and to 0° for the sum pattern. Alternatively, a conventional monopulse-type feed system may be connected to the apertures with sum and difference channel outputs.

Conclusions

It has been shown that, in contrast to generally accepted theory, the radiation pattern characteristics which are of interest for a conically-scanned tracking antenna are identical with the equivalent monopulse sum and difference patterns.

For an amplitude-comparison system, it has been shown that the sum and difference patterns are those derived from the given amplitude distribution multiplied by a cosine or sine function, respectively. The modulation sensitivity has been calculated and plotted as a function of beamwidth and beam separation, or loss in forward gain.

For a phase-comparison system, it was found that the sum and difference patterns were invariant functions of the antenna, entirely independent of the amount of modulation. The static patterns, however, vary with modulation from the sum pattern to the difference pattern. The sum pattern may be optimized by a suitable amplitude distribution and, concurrently and independently, the difference pattern may be optimized by the use of coupling between the separate apertures. The modulation sensitivity of a phase-comparison antenna made up of identical apertures has been shown to be a function only of the spacing of the antennas and the amount of modulation, but independent of the amplitude distribution.

The problem of radar ocean surface reflection is reviewed, emphasizing its effect on beam-riding missile guidance. A vector model of the radar signal, which assumes the total signal to be the vector sum of a noise-free direct signal and a reflected signal, is developed. The over-all effect is readily studied by means of a real-time analog simulation. This permits evaluation of missile performance for any prescribed sea state and target position.

LOW-ANGLE BEAM RIDING

Over the Ocean

W. S. Thompson

In the long-range transmission of electromagnetic radiation, energy reflected from the earth's surface, when combined with that propagated over a direct line-of-sight path, produces an interference pattern in space. If the radiation is composed of microwave signals transmitted by a radar that is used to track a target or guide a missile in flight, the resulting interference pattern induces noise on the tracking or guidance information; its severity depends on the relative amount of reflected energy available. When the microwave transmission takes place over the ocean, the interference pattern becomes dependent upon the physical state of the reflecting surface, where a continuing loss of coherent structure is observed with increasing height of ocean waves.

This discussion is confined to the effects of ocean surface reflections on beam-riding missile guidance at low elevation angles where the effects are most pronounced. These effects have been thoroughly studied by analog simulation techniques. The results are by no means strictly limited to beam-riding guidance but are easily extended to low-angle target tracking, which may be viewed as the reverse of beam riding.

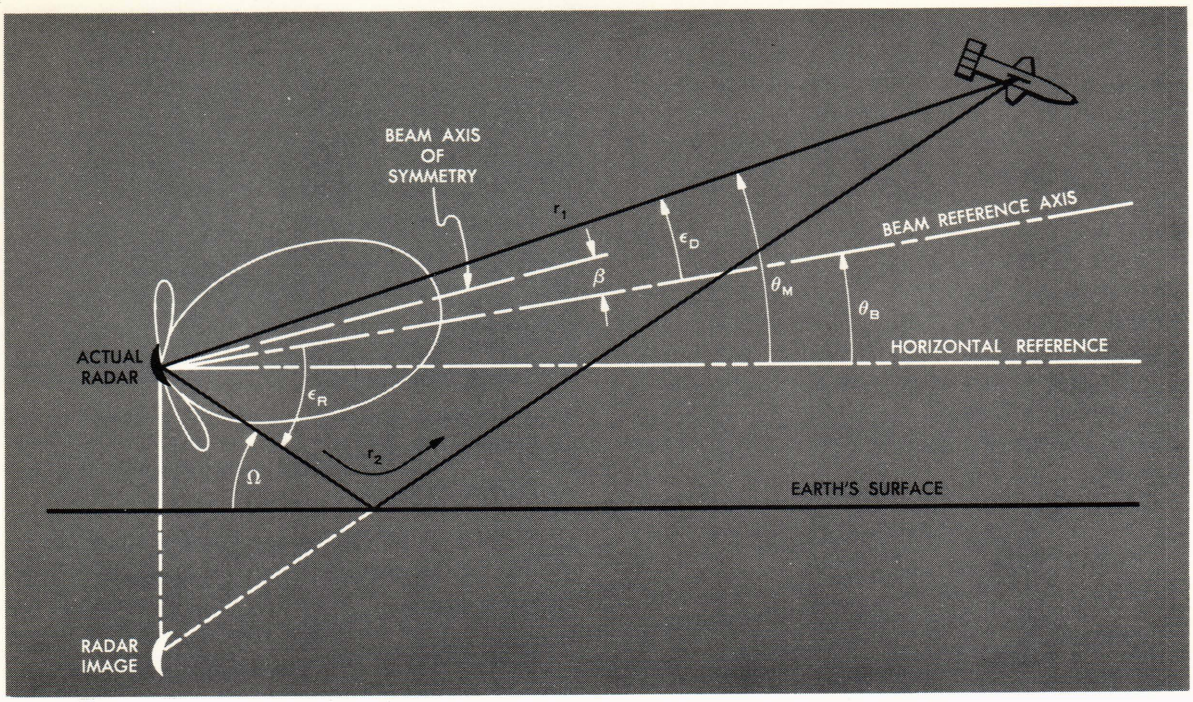

The low-angle beam-riding geometry is presented in two dimensions. The reflected signal appears to originate from an image radar below the ocean surface.

Low-Angle Interference Theory

Consider a missile located at a range r_1 from its guidance radar and at elevation θ_M above a horizontal reference. Considering the microwave signals as electric vectors, the total signal **T** appearing at the missile receiving antenna is the vector sum of a direct signal **D** propagated along the path r_1 and of a reflected signal **R** propagated along the path r_2 but appearing to originate at a radar image directly beneath the actual radar and below the reflecting surface. This vector addition is represented by

$$\mathbf{T} = \mathbf{D} + \mathbf{R} . \qquad (1)$$

Assuming no atmospheric attenuation of the signals, the amplitude of **D** is dependent only upon the radar antenna gain distribution. The antenna gain in a given direction is a function of the angle measured from the axis of symmetry of the beam, and on the basis of physical optics can be considered as a Fraunhofer diffraction pattern of a circular aperture. For simplicity, a polar plot of an antenna gain distribution is superimposed on the geometry in the first illustration.

The amplitude of **R** is also dependent on the antenna gain and, in addition, on the amount of attenuation upon reflection from the ocean surface. For convenience **R** is assumed further decomposed into electric vector components **C** and **I** where **C** represents that portion that is coherent with respect to **D**, and **I** is the incoherent portion assumed random in both amplitude and phase.

The vector **I** is actually the vector sum of the reflected signals from a very large number of infinitesimal random scatterers on the fluctuating ocean surface, each adding with its respective amplitude and phase. From statistical theory **I** is considered composed of two independent orthogonal noise vectors, $\mathbf{I}_x$ and $\mathbf{I}_y$, each possessing a Gaussian amplitude distribution with zero mean and standard deviation σ.[1]

The vector summation of all the components yields, for the total signal,

$$\mathbf{T} = \mathbf{D} + \mathbf{C} + \mathbf{I}_x + \mathbf{I}_y, \qquad (2)$$

which can be represented by the vector diagram. The angle ϕ between **C** and **D** represents the instantaneous phase difference between the two signals. In addition, it is the sum of the phase differences arising from the phase distribution

[1] C. I. Beard, I. Katz, and L. M. Spetner, "Phenomenological Vector Model of Microwave Reflection from the Sea," *I. R. E. Transactions* Vol. AP-4, No. 2, April 1956, 162-167.

of the radar antenna pattern, the phase shift of **C** upon reflection, and the path length difference between the direct signal and the reflected signal. If **R** consists only of **C**, i.e., no incoherent reflection, the interference pattern can be considered to result from the superposition of two Fraunhofer diffraction patterns where the phase angle ϕ alone determines the positions of the maxima and minima.

As the missile moves through the interference pattern, the angle ϕ changes continuously. Customarily for this dynamic situation, the change in ϕ is assumed to result from the change in the path-length difference $(r_2 - r_1)$. This proportionality results in an angular rate of change in ϕ of

$$\omega_i = \frac{d\phi}{dt} = \frac{2\pi}{\lambda} \frac{d}{dt} (r_2 - r_1), \qquad (3)$$

where λ, in the constant of proportionality, is simply the wavelength of the microwave radiation. The angular rate ω_i is expressed in terms of radians per second which, when converted to the lobe cutting or interference frequency f_i in cycles per second, can be expressed to a first approximation, in terms of the geometric quantities, as

$$f_i = \frac{2d}{\lambda} \cos \theta_M \frac{d\theta_M}{dt}, \qquad (4)$$

where d is the height of the radar antenna above the reflecting surface and θ_M is the missile elevation angle.

For a perfectly smooth reflecting surface, the

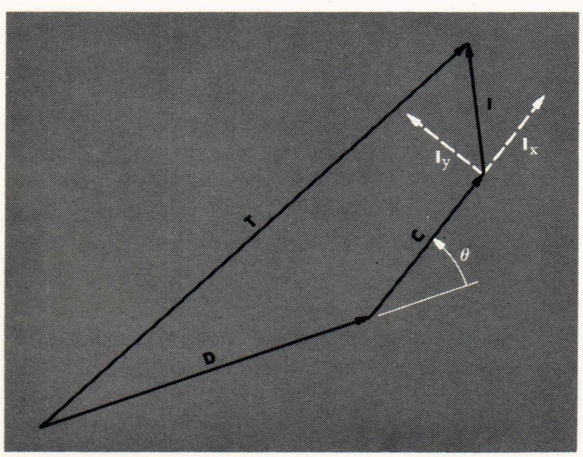

The total microwave signal is represented vectorially as the vector sum of its direct and reflected components.

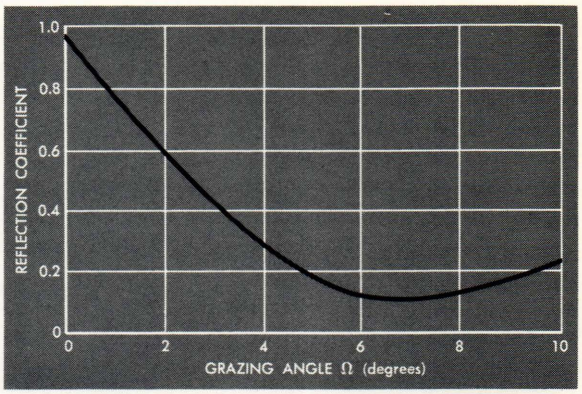

A typical variation in the reflection coefficient as a function of the grazing angle is shown for the particular case of a vertically polarized signal with a wavelength of 2 in.

amount of attenuation upon reflection is determined by the surface reflection coefficient. The latter is defined as the amplitude ratio of the reflected signal to the incident signal and, for a given signal wavelength and polarization, is dependent upon the grazing angle Ω defined in the first illustration. A typical plot of the variation of the reflection coefficient with the grazing angle is also shown for a vertically polarized signal with a wavelength of 2 in.

When ocean waves form on the surface, additional signal attenuation results, this being determined by applying correction factors to the coherent and incoherent components. A plot of the correction factor for each component is illustrated as a function of a surface roughness parameter $\frac{h\,\Omega}{\lambda}$ where Ω and λ are the same as previously defined and h is the root-mean-square amplitude of the ocean waves. This plot exhibits a decrease in the amplitude of **C** with increasing ocean surface roughness, while σ, the standard deviation of **I**, builds up rapidly to a constant value. The constancy of σ implies that the total noise power in the incoherent component remains unchanged; however, consideration must also be given to the noise bandwidth. Experimental evidence[2] has shown that the noise bandwidth increases approximately linearly to about 1.5 cycles per second at a value of 500 mils for $\frac{h\,\Omega}{\lambda}$, which indicates that even though the total noise power remains constant with increasing surface rough-

[2] C. I. Beard and I. Katz, "The Dependence of Microwave Radio Signal Spectra on Ocean Roughness and Wave Spectra," *I. R. E. Transactions*, Vol. AP-5, No. 2, April 1957, 183-191.

ness, the power per unit frequency decreases.

The above considerations of amplitude and phase yield a beat effect on the total signal **T** as the missile moves through the interference pattern. This beat effect can be visualized in connection with the vector diagram as a continuous rotation of **C** about the terminus of **D**, while **I** can assume at any instant an arbitrary direction and an amplitude characteristic of its given value of σ.

Low-Angle Beam-Riding Simulation

Beam-riding missile guidance is accomplished by a closed-loop control system employing the principle of negative feedback where the primary aim is to null the difference between the output and an input reference. In this case, the input reference is simply the elevation angle θ_B of the radar reference axis of the first plot. Ideally, the output is the missile elevation angle θ_M which, when fed back and compared with the input, yields the error angle $\theta_B - \theta_M$ denoted by ϵ_D. This forms a single loop feedback system; however, when reflection is present the system assumes a multiple loop character as will be shown.

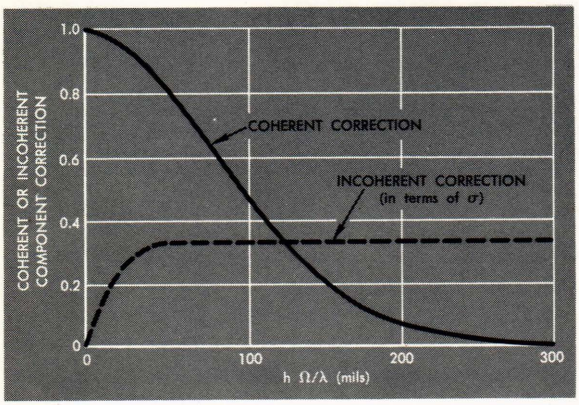

The relative rough sea corrections for both the coherent and incoherent components of the reflected signals are shown as they vary with a roughness parameter.

For the missile to maneuver in the proper direction to null the error angle, knowledge of the magnitude and sense of the error angle must be provided to the missile. This is accomplished by employing the microwave radiation from the radar as a carrier signal upon which the error information is impressed as amplitude modulation. The modulation is provided through the process of conical scan action of the radar beam.

Conical scan may be visualized through the following brief explanation. A right circular cone in space, with the vertex at the radar, is defined by revolving the generatrix (the beam axis of symmetry) around the cone axis (the beam reference axis) with a fixed vertex angle. The vertex angle β is defined in the two-dimensional geometry of the first illustration, in which the beam axis of symmetry is assumed to lie instantaneously at the extreme upper point of its path of revolution. As the antenna gain pattern revolves with the beam axis of symmetry, a solid figure is generated. The revolution, maintained at a constant frequency which is low compared with the carrier signal frequency, results in a sinusoidal variation or modulation impressed upon the microwave carrier signal. The missile receiver detects the amount of amplitude modulation which, for an ideal beam shape, is directly proportional to the off-axis angle ϵ_D. The sense of the error angle is established by comparing the phase of the detected modulation with a synchronized reference scan signal transmitted from the radar to the missile by means of a frequency modulation of the carrier signal. The error signal thus obtained provides the necessary steering intelligence information to the missile.

Due to the conical scan action, the reflected carrier signal also contains an amplitude modulation of the same nature but with a different amplitude, depending on the angular position of the reflected signal path in the nutating beam pattern. The addition of the reflected signal to the direct signal results in an amplitude modulation on the total signal that is not indicative of the true off-axis error angle. In general, the resulting error signal contains biases plus random noise where each is dependent upon the physical state of the sea surface, the height of the guidance radar, and the range, elevation, and trajectory of the missile.

Low-angle beam riding is most conveniently studied by a real-time analog simulation. Starting at the left of the diagram shown, a 25-kilocycle sine wave is employed as the analog of the microwave carrier signal. The signal is fed to both an upper channel for development of the direct signal and to a lower channel for development of the reflected signal.

The conical scan action is simulated first in each channel; DC voltages representing the respective off-axis error angles are inputs, along with the scan frequency signal, to beam angle computers. The output is the analog of the

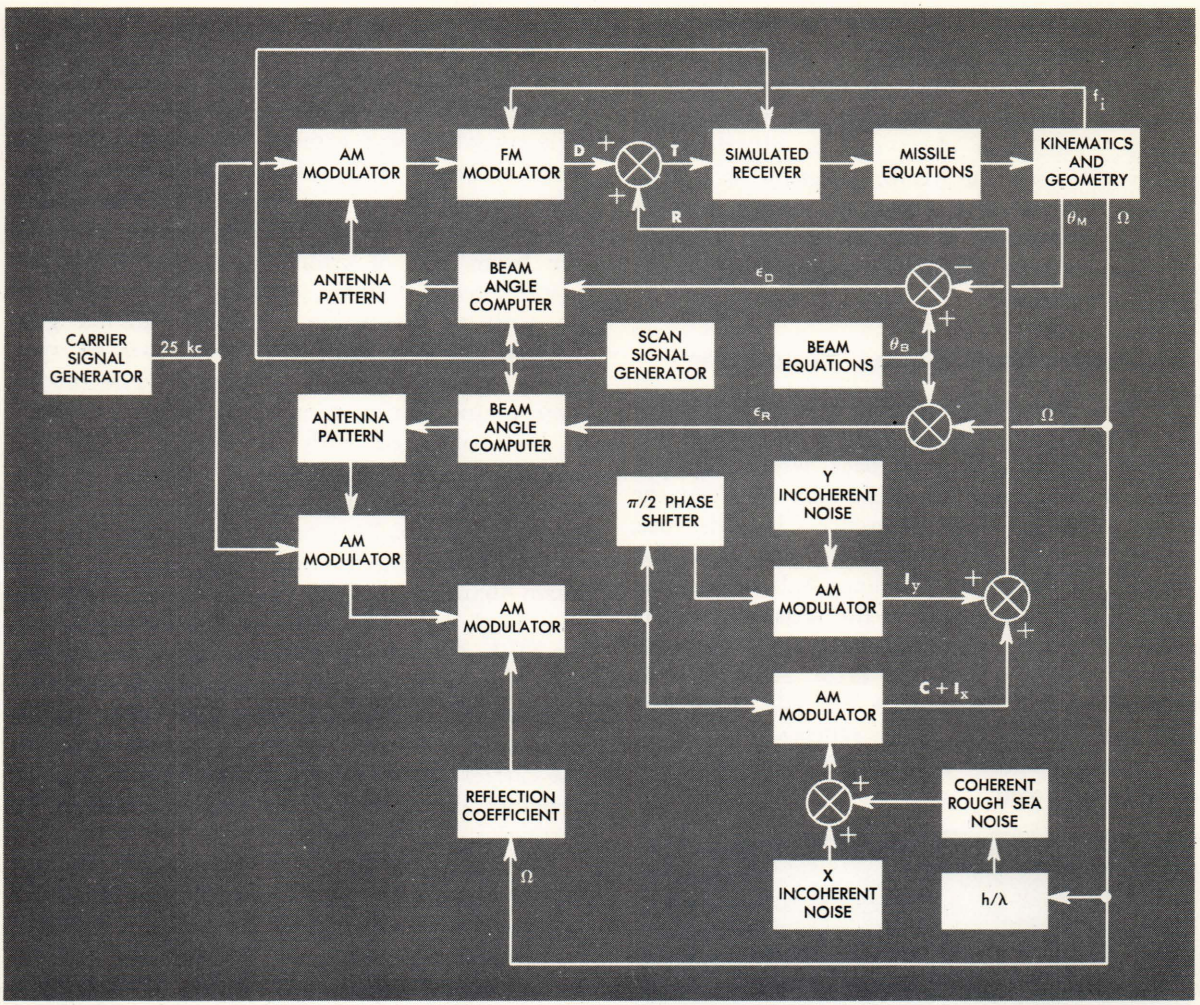

The complete low-angle beam-riding simulation is represented by a simplified closed-loop block diagram.

angle between the beam axis of symmetry and the respective signal path which is varying in a sinusoidal manner about the error angle due to the conical scanning action. A static representation of the radar antenna pattern is contained in a function generator which receives the computed beam angle and generates the proper amplitude level of the simulated carrier along with its modulation component. These signals are then fed to the respective AM (amplitude modulation) modulators which yield the analogs of the direct and reflected signals as they depart from the radar on their respective paths of propagation.

The direct signal is shifted in frequency in the FM (frequency modulation) modulator by an amount equal to the interference frequency which is computed from the kinematic expression given in Eq. 4 above. This shift in frequency will yield the proper interference beat frequency when the direct signal is later summed with the reflected signal.

Meanwhile, the reflected signal is further developed in the sea model simulation. The signal is first modulated by the reflection coefficient of the third illustration. The rough sea correction is then applied by two separate subchannels, one for the inphase signal $\mathbf{C} + \mathbf{I}_x$ and the other for the orthogonal signal $\mathbf{I}_y$.

The coherent rough sea correction as a function of the surface roughness parameter $\frac{h\,\Omega}{\lambda}$ is obtained from the coherent correction curve. This is summed with the inphase incoherent correction noise possessing the standard deviation σ and the bandwidth characteristic of the sea state under investigation. Amplitude modulation of the carrier with the summed signal completes the rough sea correction for the inphase component.

The orthogonal component is developed by first shifting the carrier phase by $\pi/2$ radians, then amplitude-modulating it with the incoherent noise correction from a separate noise source possessing the same statistical characteristics as the inphase noise source.

Summation of the two subchannel outputs then results in the analog of the reflected signal **R** which, when summed with the direct signal **D**, yields the total signal **T**.

The simulated missile receiver accepts the total signal and performs the essential operations of automatic gain control (AGC), carrier envelope detection, and phase comparison of the detected signal with the scan reference signal to yield the steering intelligence signal ϵ. If sea reflection were not present, the error angle ϵ_D would be truly represented by the error signal ϵ which, when plotted as a function of time, would appear as a DC voltage with the amplitude varying linearly with ϵ_D. If smooth sea reflection only were present, ϵ would assume a cycloidal shape, as shown in the last illustration, where the frequency of the oscillations is simply the interference or lobe cutting frequency. Increasing roughness of the ocean surface would result in the loss of the coherent structure of the curve which, for an extremely rough ocean surface, would appear only as random noise.

The error signal is the input to the missile equations which simulate the missile computer, the autopilot, the wing servomechanism, and the aerodynamic response. Ideally the missile computer accepts the error signal and computes the magnitude of the missile acceleration required to null the error. The autopilot accepts the computed acceleration command and determines the necessary wing deflection which is effected by the wing servomechanism. For the given wing deflection, the aerodynamic response yields a missile acceleration characteristic of the missile speed, weight, and altitude.

The kinematic and geometric simulator computes the output variables which are used in the feedback loops. The output θ_M—the missile elevation angle—is compared with the beam elevation angle θ_B to generate the error angle ϵ_D for the direct signal. The grazing angle Ω is summed up with θ_B to form the corresponding error angle ϵ_R for the reflected signal. The interference frequency feedback into the FM modulator and the grazing angle feedback into the sea model complete the closed-loop diagram.

The beam equations, which provide the beam elevation angle θ_B continuously, determine the trajectory that the missile takes to the target. The type of trajectory, such as ballistic, line-of-sight, long-range cruise, etc., determines to a great extent the behavior of the missile in the interference region.

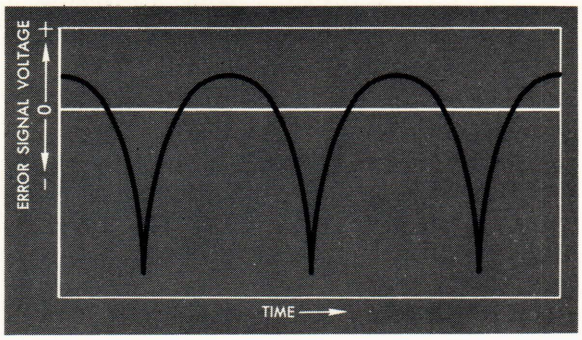

A typical beam-riding error signal resulting from smooth sea reflection appears as a cycloidal signal at the characteristic interference or lobe cutting frequency.

An error signal such as the typical one shown permits to some extent a prediction of the behavior of a missile when the specific characteristics of the missile equations are known. Theoretically, the error signal from an ideal receiver would possess a zero mean value over a complete cycle; however, the actual result is that the sharp negative spikes never reach the full theoretical value, yielding an integrated bias that appears as a net "fly-up" error. Additional filtering and nonlinearities in the missile equations yield weird combinations of "fly-up" and "fly-down" net biases that can only be resolved through a series of simulated missile flights.

The missile behavior over a rough sea is not as easily predicted. Analysis of many rough sea simulation runs has shown that the missile closed-loop behavior may be worse than for smooth sea reflection; this, however, is not necessarily so since, in certain situations, actual improvement is obtained.

A prime interest in a study of this nature is to determine the distance by which a missile misses an assigned target. The real-time simulation presented readily permits a determination of the miss distances obtained in the presence of any prescribed low-angle environment. If the established miss distances are found to be greater than the specific tolerances, proposed changes in the system can easily be incorporated into the simulation and evaluated by additional flight simulations.

RADOME THERMAL DESIGN

for a Mach 4 Missile

Theoretical and experimental work was done to obtain an efficient thermal design of a radome for a Mach 4 missile. Theoretical studies showed that for both pointed and blunted Von Karman-shaped radomes, maximum tensile thermal stresses were nearly identical. Therefore, because of its lower aerodynamic drag the pointed radome was favored. Experimental verification that the pointed radome could withstand the flight stresses was obtained in full-scale free-jet tests.

R. P. Suess and L. B. Weckesser

The evolution of a radome design for a given missile may follow a devious path. Choice of material and thickness of wall are controlled primarily by electrical requirements, while definition of shape is influenced by aerodynamic and packaging-space demands. After a preliminary radome design has then been determined from these factors, a thermal and stress analysis must be performed to determine its ability to withstand the most severe flight environments expected. If these results suggest potential structural failures (an example of a radome structural failure occurring during a wind-tunnel test is shown in Fig. 1), the design must be reviewed and modified until a high degree of confidence in its structural adequacy is achieved.

Pyroceram as a proven missile-radome material merited attention in the design study for a new Mach 4 missile. *Pyroceram,* a product the housewife has become familiar with in recent years under the trade name of Corningware,* is essentially a material that has been converted from its original glassy state into a crystalline ceramic by the use of heat treatment. Although this material has good thermal and electrical properties, a Mach 4 environment is more severe than any it had previously encountered. A thorough temperature and stress analysis had, therefore, to be made to insure that the radome could withstand the flight thermal stresses.

Definition of Critical Thermal Environment

Before temperature and stress analyses were performed it was necessary to choose the one missile trajectory that would be thermally most severe.

* Registered trademark of Corning Glass Works, Inc.

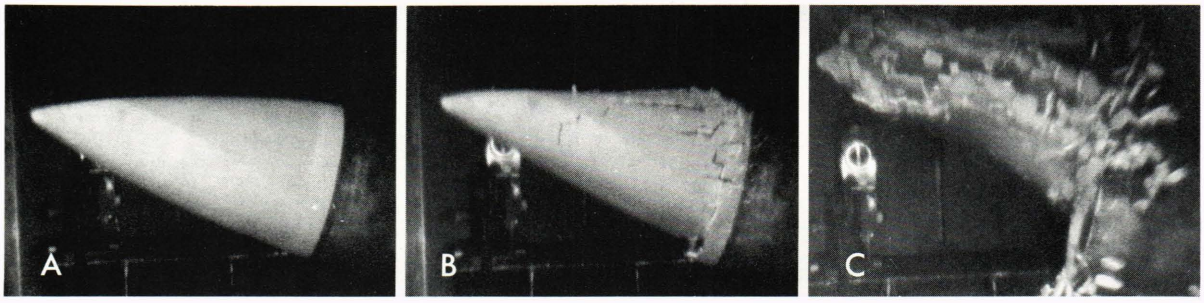

Fig. 1—Photographic sequence of a test-radome structural failure, showing the Pyroceram radome (A) before the start of the failure, (B) 0.003 sec after the start of the failure, and (C) 0.006 sec after the start of the failure. (Printed by permission of the Daingerfield Division, General Dynamics/Pomona.)

Since this could not be done by inspection, a trajectory analysis was made in which 21 representative trajectories, both ballistic and line-of-sight, were considered. Each of these trajectories was used to generate aerodynamic heating on several dummy geometries, each of various thicknesses.

The trajectory chosen as the one that would generate maximum radome thermal stress was the one giving the highest rate of heat input, that is, generating the steepest temperature-time slope. Two interesting results arose from the trajectory analysis:

1. The line-of-sight trajectories gave higher heating rates than the ballistic trajectories, and it was noted that the launch angle did not influence the heating rate significantly.
2. When different radome wall thicknesses were investigated, the same trajectory was found to be thermally most severe for all.

Figure 2 presents the Mach number and altitude history of the trajectory found thermally most severe. Note that the maximum Mach number of this trajectory is considerably below the design number (4.0) of the study. The trajectory analysis revealed that those trajectories that achieved Mach 4.0 were not critical from a radome thermal-stress viewpoint.

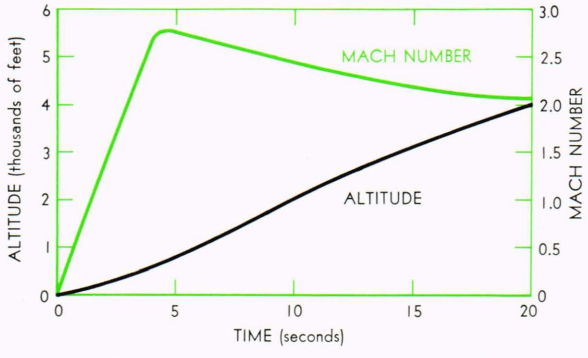

Fig. 2—Trajectory used to obtain the maximum radome thermal stress.

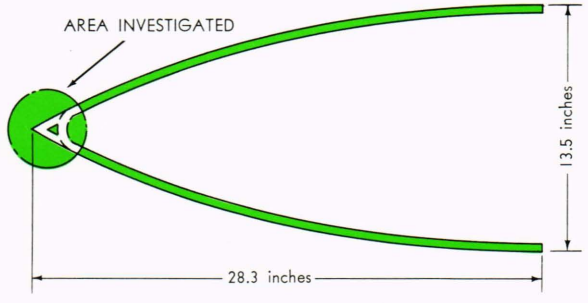

Fig. 3—Sketch of the radome cross-section, showing both the pointed and blunted nose areas.

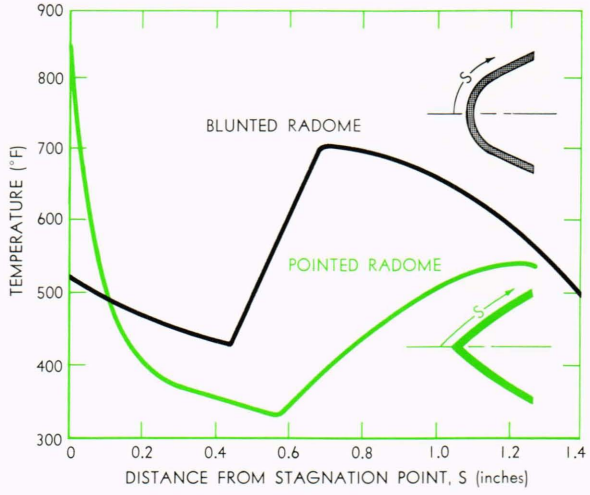

Fig. 4—Outside surface temperatures of the pointed and blunted radomes at a flight time of 5 sec.

Radome Temperature and Stress Analysis

The Von-Karman radome shape (discussed in Ref. 1) and the radome thickness were dictated by other than thermal considerations. The latter did, however, initiate an effort to determine if slightly blunting the radome would result in a reduction of thermal stresses. Since the maximum stress capability of Pyroceram had never been firmly established, and the new environment was more severe than any previously encountered, it was feared that the material would be pushed to near the limit of its thermal stress capability. Any means of reducing the thermal stresses was, therefore, felt worthy of examination. Figure 3 is a sketch of the two radomes analyzed, one a standard Von-Karman shape and the other a Von-Karman blunted with a 1.35-in. radius. Only the extreme forward portion of each radome was analyzed since experience had shown that this was the region of maximum thermal stress.

Two-dimensional temperature analyses of both radomes were performed by means of an IBM 7094 computer program. The program is quite general in nature and can handle complicated three-dimensional geometric configurations involving heat transfer by radiation, conduction, and convection. The theoretical method used for computing aerodynamic heating makes use of the Colburn equation,[2] as modified by Seban and

[1] T. Von Karman, "The Problem of Resistance in Compressible Fluids," Guggenheim Aeronautical Library, California Institute of Technology, Publication No. 75, 1936.

[2] A. P. Colburn, "A Method of Correlating Forced Convection Heat Transfer Data and a Comparison with Fluid Friction," *Trans. Am. Inst. Chem. Engr.*, **29**, 1933, 174–210.

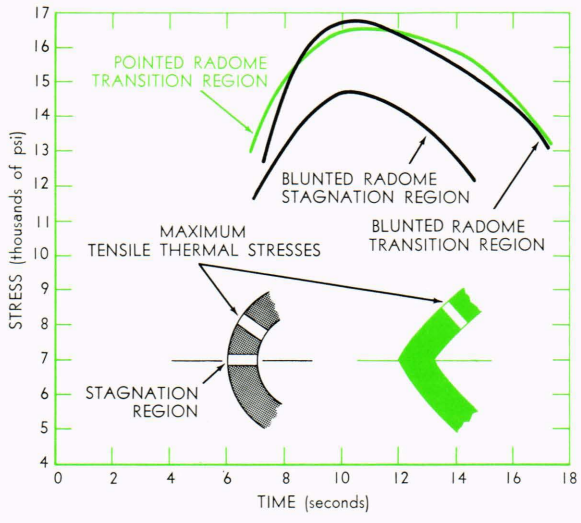

Fig. 5—Tensile thermal stress histories of the pointed and blunted radomes.

Doughty,[3] combined with the reference enthalpy method presented by Eckert.[4] In addition to convective heat transfer, a forward finite difference method is used to handle the differential equation of heat conduction, and the radiation is computed by means of the Stefan-Boltzmann law.

Because radome-shaped bodies do not lend themselves to exact theoretical stress solutions, they must be analyzed assuming the stresses can be approximated by cylindrical or spherical shell theory. In these radome stress analyses, spherical theory was chosen since it yields more conservative (higher) numbers than does cylindrical theory. The stresses were hand-computed using the temperature distributions generated from the heat transfer program described above.

Analyses on both the pointed and blunted radomes produced temperature variations over the surface such as those shown in Fig. 4. It is obvious from this figure that a sharp rise in temperature occurs at the transition point from laminar to turbulent flow on the shell portion of each radome. On both radomes the transition Reynolds number was assumed to be 1.5×10^6. On the pointed radome the maximum temperature (855°F) occurs at the stagnation point, as would be expected. However, on the blunted radome the maximum temperature (705°F) occurs not at the stagnation point but at the transition point. Figure 4 was used as an aid to locate the points of maximum stress since these points can be expected to occur at locations where the highest heat input has generated the highest temperatures early in flight.

Because the maximum temperature on the blunted radome occurred at the transition point, we expected that the maximum stress would also occur at that point. Figure 5 shows this to be true. The maximum stresses at the transition and stagnation points are 16,850 psi and 14,800 psi, respectively. These values are tensile stresses on the inside surface, which are the most critical because of the relatively low tensile strength of ceramics.

Figure 4 shows that the maximum temperature on the shell portion (i.e., away from the stagnation point) of the pointed radome occurred at the transition point. Consequently, the maximum stress on the shell portion also occurred at that point. This stress was computed and is compared with the maximum stress on the blunted radome in Fig. 5. As can be seen, the stresses are nearly identical. The conclusion to be drawn from this figure is that on the shell portion of the pointed radome the *tensile* stresses are no more severe than those on the blunted radome. In this area little value is gained by blunting the radome, and the drag penalty caused by blunting cannot be justified.

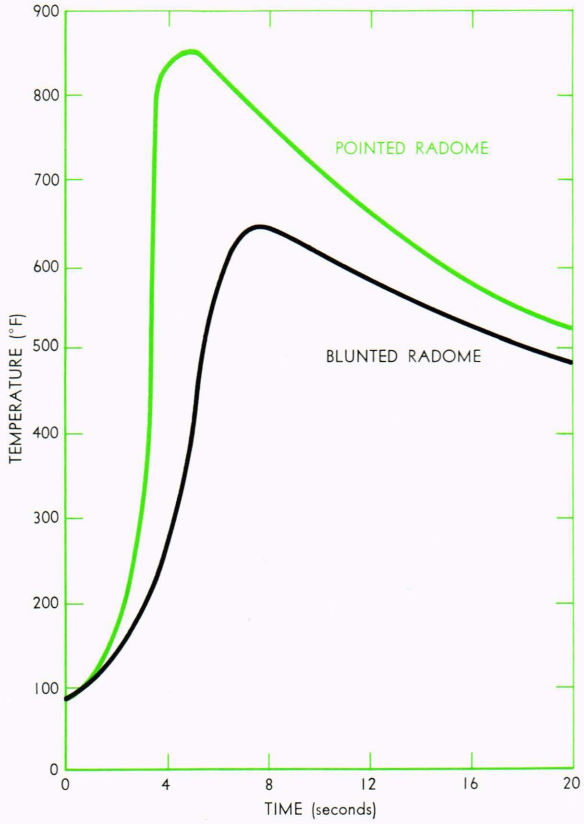

Fig. 6—Stagnation point temperature histories of the pointed and blunted radomes.

[3] R. A. Seban and D. L. Doughty, "Heat Transfer to Turbulent Boundary Layers with Variable Free Stream Velocity," *Trans. ASME*, **78**, Jan. 1956, 217–223.

[4] E. R. G. Eckert, "Survey on Heat Transfer at High Speeds," WADC Technical Report 54–70, April 1954.

However, by reference to Fig. 6, it would seem that a substantial *thermal* stress advantage could be gained at the stagnation point by blunting the radome. This impression is given by the fact that the blunted radome reaches a maximum stagnation-point temperature of only 635°F in 7.5 sec, while the pointed radome reaches 855°F in just 5 sec. At this time there is an extreme temperature gradient along the centerline of the pointed radome. Though large, this gradient generates on the outside surface compressive thermal stresses that are far less critical than are tensile thermal stresses. However, the passing of time would see a progressive decrease of compressive thermal stresses on the outside surface and a build-up of tensile stresses on the inside surface. It should be evident that the discussion of the pointed-radome stagnation-point region has thus far been confined to temperature results. The reason for this is that, because of the geometry of the area, no theoretical method, exact or approximate, is known by which to calculate the thermal stresses in the immediate region of the stagnation point.

Preliminary Experimental Compressive Stress Evaluation

In order to obtain an indication of whether the pointed radome could withstand the high compressive stresses at the stagnation point, a test was set up to determine what thermal environment would be necessary to cause a compressive stress failure at the point. Figure 7 is a schematic of the test apparatus used for this purpose. Small samples of Pyroceram measuring 0.25 × 0.125 × 3.0 in. were plunged into a molten aluminum bath and placed in contact with the bottom of the container which had been heated to the desired temperature. The sole purpose of the molten aluminum was to wet the surface of the samples and increase the thermal conductivity between the bottom of the container and the sample. After each test the specimens were examined under a 120-power microscope. No failure was noted at 1100°F or in subsequent tests at 2000°F.

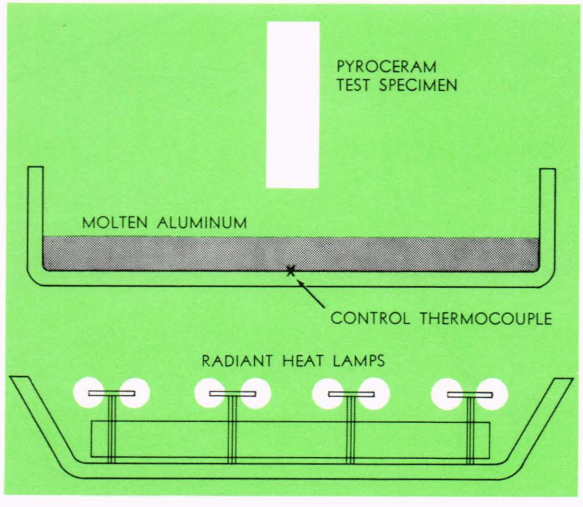

Fig. 7—Sketch showing the test arrangement used in the compressive thermal-stress evaluation of Pyroceram.

In an effort to find what was needed to generate a compressive thermal stress failure, an oxy-acetylene torch was applied to the surface of a sample. The torch generated temperatures high enough locally to soften the material—that is, approximately 2500°F. Cracking was noted after the test, indicating that a compressive thermal stress failure had occurred. There was some concern that the observed crack had occurred during the rapid cool-down of the sample after the test. This was disproved when the test was repeated on another sample that was slowly cooled after the test and on which a similar failure was noted. The conditions causing this failure were obviously far more severe than those expected in Mach 4 flight. For this reason a preliminary conclusion was drawn that no compressive thermal stress problem would exist with a pointed radome at Mach 4.

As a result of the theoretical and preliminary experimental work just described, the conclusion was reached that a pointed Pyroceram radome would be satisfactory for a Mach 4 missile. Because of the complexity and the resulting uncertainty of the theoretical analyses, it was decided to verify the conclusion by testing several radomes at the Ordnance Aerophysics Laboratory (OAL), Daingerfield, Texas.

Full-Scale Wind-Tunnel Tests

The first experiments at OAL showed that the radomes could withstand comfortably the maximum flight tensile thermal stresses that they might face (17,000 psi). Next it was decided to test three radomes to the limit of the facility in order to attempt to cause tensile thermal stress failures.

The testing procedure employed for the Pyroceram radomes was as follows. The radomes were held below the airstream until the tunnel conditions had stabilized as much as possible (this required 4 to 6 sec). The radomes were then injected into the airstream (injection time 0.5 sec) and remained there for 14 sec, which was 1 sec after the computed time of peak thermal stress. The radomes were then withdrawn from the airstream. Just prior to a run the radomes were cooled to an

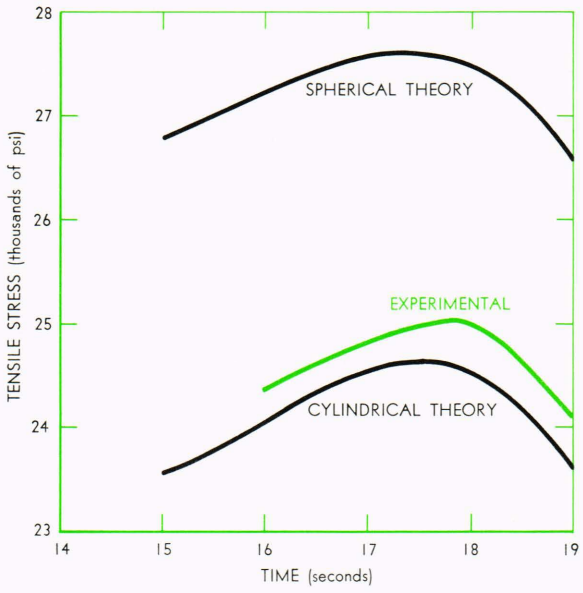

Fig. 8—Tensile thermal stresses measured during wind-tunnel test No. 1 compared with those computed using spherical and cylindrical theory.

initial temperature of +50°F or −10°F, depending on the stress level sought. This was accomplished with a CO_2 spray inside the radomes. In order to hold the radomes at these reduced temperatures, each was wrapped in an asbestos cloth that would blow off upon injection into the airstream. The radomes were tested at Mach 2.44, a total pressure of 215 psi, and an average total temperature of approximately 1350°F.

On two of the three tests, good strain-gauge data were obtained; the results are shown in Figs. 8 and 9. The tunnel flow conditions were essentially the same for both runs. The difference noted in maximum stress between the two runs is due to the difference in initial temperatures.

Comparison of Wind-Tunnel Data with Theory

Because the radomes were instrumented with strain gauges, there was an opportunity to compare measured stresses with those theoretically computed. In order to make this comparison, theoretical predictions were made, using the heat transfer computer program previously described. By this time the program had been amended so that it would compute stresses (based on cylindrical or spherical shell theory[5]) in addition to temperatures. The theoretical results shown in Figs. 8 and 9 were generated by this combined program and are for a location approximately two inches behind the stagnation point.

The experimental data from the first test are shown in Fig. 8, compared with theoretical predictions based on cylindrical and spherical shell theory. Maximum stresses agree within 2% if cylindrical theory is used for the comparison, and within 10% if spherical theory is used. In addition, the shape of the experimental and theoretical curves is quite similar. The agreement is excellent, particularly since the analysis began with only the wind-tunnel pressure and temperature-time histories and Mach number as inputs. The comparison from the second test is shown in Fig. 9. Theoretical and experimental maximum stresses once again compare favorably (2% or 11%, depending upon whether cylindrical or spherical theory is used). However, the shapes of the theoretical curves differ from the experimental, for reasons not known. As mentioned previously, the test conditions were essentially the same as those of the first test, with the exception of the initial radome temperature. The difference noted in maximum stress is attributed to the change in initial temperature.

Considering the large number of variables involved in the theoretical predictions, and the uncertainties in the instrumentation, the comparison of theoretical and experimental stresses is good. Thus, the adequacy of the theoretical method has been demonstrated for use in radome thermal design.

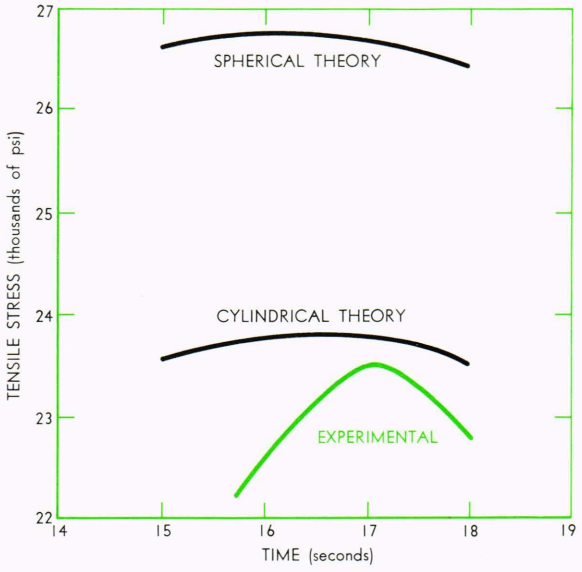

Fig. 9—Tensile thermal stresses measured during wind-tunnel test No. 2 compared with those computed using spherical and cylindrical theory.

[5] S. Timoshenko and J. N. Goodier, *Theory of Elasticity* (2nd ed.), McGraw-Hill Book Co., Inc., New York, 1951.

Conclusions

The thermal design study for a Pyroceram radome for a Mach 4 missile was successfully conducted. Investigation of the effect on thermal stress of blunting the radome disclosed that little or no reduction in maximum tensile thermal stress may be expected with a 1.35-in.-radius nose. Thus, one cannot automatically assume that the increased drag caused by blunting is justified by the reduction in thermal stress.

Preliminary laboratory tests and later wind-tunnel tests showed that the large compressive stress at the point of the radome would not cause any structural problem. Finally, correlation of strain-gauge measurements made during wind tunnel tests demonstrated that both the theoretical method used to predict temperature gradients and the cylindrical theory used to determine thermal stresses give acceptable results for use in radome thermal design.

---

a scientist and his hobby

the TECHNOLOGY of WINE-MAKING

G. H. Mowbray

Wine has been called many things since the first known reference to it in Middle Eastern writings dating from 2100 B. C. To Aeschylus it was "the mirror of the heart"; to Shakespeare, "a good familiar creature"; and to William Gilbert, "a panacea for ev'ry conceivable ill."

The author in his vineyard keeps a close watch on the growth and health of highly prized imported vines.

Others have expressed their feelings less kindly, if no less poetically. Milton spoke of "the sweet poison of misuséd wine"; Pope, of "inflaming wine, pernicious to mankind"; while in Proverbs we are warned that "it biteth like an adder and stingeth like a serpent." No matter which of these positions one espouses—and all of them have merit on occasion—officially, wine is the fermented juice of the grape used as a beverage, or so says the Oxford Dictionary.[1] Federal description, however, is a little more verbose, defining grape wine as "wine produced by the normal alcoholic fermentation of the juice of sound, ripe grapes (in-

---

G. H. Mowbray, an experimental psychologist, is a member of the staff of the Theoretical Problems Group of the Research Center. Dr. Mowbray is the author of "Some Human Perceptual Limits" in the *Digest* of Jan.-Feb. 1962.

[1] *Oxford Universal Dictionary on Historical Principles,* 3rd ed. (rev.), Clarendon Press, London, 1955.

W. MALCOLM GRAY AND ROBERT W. WITTE

GUIDANCE SYSTEM EVALUATION LABORATORY

The APL Guidance System Evaluation Laboratory (GSEL) is a test facility that interfaces missile guidance hardware and real-time computer simulation in a way that closely resembles actual missile flight.

INTRODUCTION

The original APL Guidance System Evaluation Laboratory (GSEL), constructed during 1963-64, was used to evaluate continuously the guidance performance of successive versions of the Navy's Terrier, Tartar, and Standard missiles. During the intervening 15 years, many improvements were made in Naval weaponry to keep pace with corresponding advances in countermeasures and tactics. With the development of Standard Missile-2, resident test capabilities began to fall short of test requirements. Consequently, the Navy approved a major upgrading of the GSEL. This article describes the primary features of the new laboratory, which became operational in February 1980.

BACKGROUND

"Standard Missile" designates a family of surface-to-air missiles deployed on many Navy ships. A common feature is an ability to "home," i.e., guide some or all of the flight by means of target-reflected energy. The source of the energy is a high-power, continuous-wave shipboard radar illuminator. (This type of guidance is called "semiactive" because the transmitter and receiver are not colocated.) To cope with electronic countermeasures, the missile receiver is also designed to home passively on radio frequency (RF) energy emanating from the target.

Figure 1 is an illustration of the many RF signals that can be present at the missile's receiving antenna. Various processing techniques are used to discriminate between those signals, including amplitude, frequency, coherency, and angle-of-arrival measurements. In simplest terms, a guidance evaluation is a determination of how well a missile receiver performs the task of selecting the best available signal to derive steering information. The preferred measure of performance is usually miss distance, although receiver angle error signal quality is used frequently.

FUNCTIONAL OPERATION

Figure 2 illustrates how actual guidance hardware is interfaced with a real-time simulation to model the dynamics of closed-loop homing guidance. The guidance section under test is mounted at one end of the shielded, reflection-free chamber. Its front seeker receives the RF signal(s) emanating from an array of antennas located on the other side of the room. Typically, the RF environment consists of the target skin return combined with on-board jamming, standoff jamming, or both. Considerable care is taken to represent the characteristics of the incident waveforms in terms of their range-

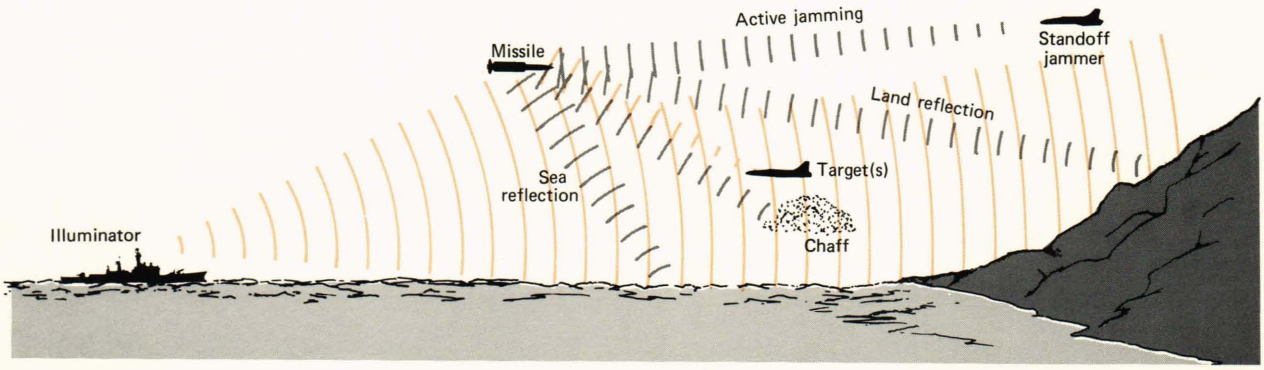

Fig. 1—Typical signals received by the missile in flight. Various discriminants are used to distinguish between the many signals arriving at the missile front antenna. Good steering information can usually be derived from either target-reflected energy or on-board target jamming. Interfering signals, which can exceed the target skin return by many orders of magnitude, must be rejected. Interference derives from natural and man-made environments, both friendly and unfriendly.

dependent power variations, amplitude and frequency modulations, and angles of arrival.

After isolating and processing a preferred RF signal, the guidance section generates pointing commands to update the look angle of the gimballed front antenna. Steering commands are also generated that serve as inputs to a computer simulation of the missile's flight control system. Depending on the trajectory being flown, the modeling of the control system can vary from a simplified to a highly complex representation of the autopilot, propulsion, and aerodynamics. In general, a simplified model is usually sufficient for a low altitude, short range intercept while more sophisticated modeling is required for a high altitude, long range engagement.

In either case, computation of the missile – target geometry and updating of the relative angular position through the RF array permit the homing loop to be closed through space across the chamber. Just prior to intercept, the process is stopped and the characteristics of the end game, including the miss distance, are determined by extrapolation.

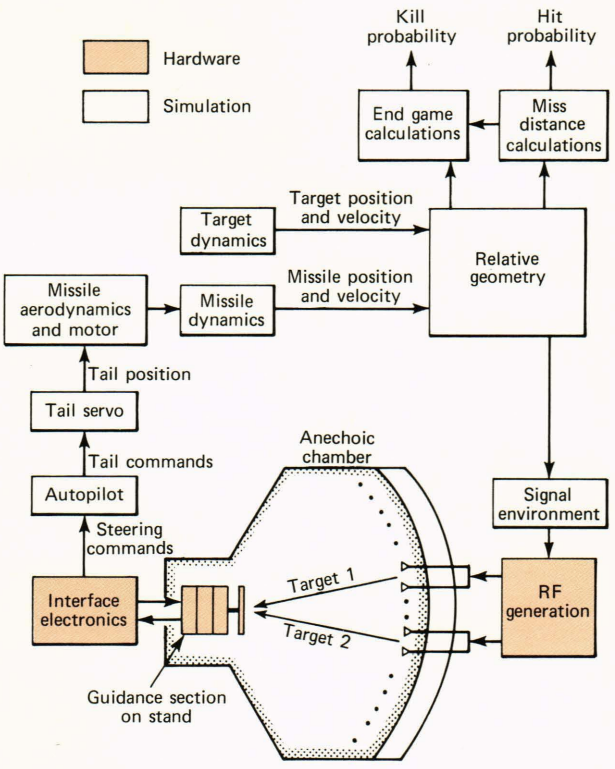

Fig. 2—GSEL hardware simulation interface. A combination of actual missile hardware and real-time computer simulation is used to determine closed-loop guidance performance under carefully controlled conditions. RF signals representing a particular flight environment are transmitted across an anechoic chamber. Missile-computed steering commands, typically based on angle and Doppler frequency measurements, serve as inputs to a simulation of the missile flight control system. The target angle relative to the missile is continuously updated through the array until just prior to closest approach. The geometry of the intercept, including the miss distance, is determined by extrapolation.

UPGRADE REQUIREMENTS

Facility requirements were defined to meet the needs of future test programs. The primary objective was to test an improved version of Standard Missile-2 (SM-2), which is being developed as part of the new Aegis Combat System, with applicable versions for upgraded Terrier and Tartar Combat Systems. SM-2 differs from its predecessors in that it has a midcourse guidance system, including communication links, that extends its effectiveness to longer ranges. In addition, it is designed to operate in more complex threat environments.

The results of the requirements definition studies and the corresponding capabilities of the former GSEL are summarized in Table 1. One of the most striking differences involves angular coverage. Simulations and analyses showed that the new chamber should span ±45° to ensure that miss distance would not be corrupted by room restrictions. Certain formation target tactics, as well as widely spaced standoff jammers, led primarily to this requirement. It is believed that the upgraded facility has the widest angular coverage of any test chamber in the country.

Table 1

GSEL UPGRADE REQUIREMENTS

Parameter	*Upgrade Requirement*	*Previous Capability*
Angular coverage	±45°	±18°
Room length	20 ft	12 ft
Frequency coverage	3-50 GHz	3-18 GHz
Dimensionality	2D + airframe motion*	2D
Target capability	3	2
Polarization	Vertical and/or horizontal	Vertical, horizontal, or circular
Angular rate	≥200°/s	60°/s
Angular acceleration	≥2000°/s^2	265°/s^2

*With future addition of a two-axis table.

Although the former chamber was long enough to test X-band seekers with antenna apertures slightly greater than 1 ft in diameter, an increase in room length to 20 ft was deemed advisable in reconstructing the chamber in order to provide a capability for testing higher frequency seekers. Requirements on both frequency coverage and maximum power output of the RF array are a compromise between the desired capability and what is achievable at reasonable cost. Similarly, the representation of missile/target flight dynamics in a single, arbitrary plane has been retained because of the much higher cost associated with RF generation in two angular coordinates. Three independent kinematic RF sources permit missile performance to be examined in threat situations involving several combinations of penetrating targets and standoff jammers. The simultaneous availability of the two orthogonal polarizations provides the desired degree of flexibility for that parameter.

DESCRIPTION

Figure 3 is a cutaway view of the new facility. The major elements are an anechoic chamber, a fixed-element RF array, RF generators, a hybrid computing system, and monitoring and control equipment. The main anechoic chamber is a screen room in which all interior surfaces are lined with RF absorbing material. A cylindrical wall across the wide end of the chamber supports the target arrays. The guidance section front antenna is located across the room at the focal point of the cylindrical wall (Fig. 4). Both the seeker antenna and the target horns are positioned midway between the floor and ceiling of the chamber. The RF generators occupy a second screen room that effectively shares a common wall with the test chamber. The dual screen rooms protect the guidance equipment under test from possible external interference while confining internally generated radiations.

The array system is one of the more unusual features of the facility. There are two separate interleaved arrays, each consisting of 64 microwave horns. One is equipped with a single set of feeds and the other with a dual set to allow a total of three independently controlled targets to be represented simultaneously. The line-of-sight angle of each target is obtained by varying the relative amplitude of the RF signals supplied to an appropriate pair of horns. Designing the digitally controlled variable power divider that performs this function was one of the more challenging engineering tasks. Under computer control, the target angle can be varied linearly across the array in 0.045° steps.

The RF generators provide: the wide variety of

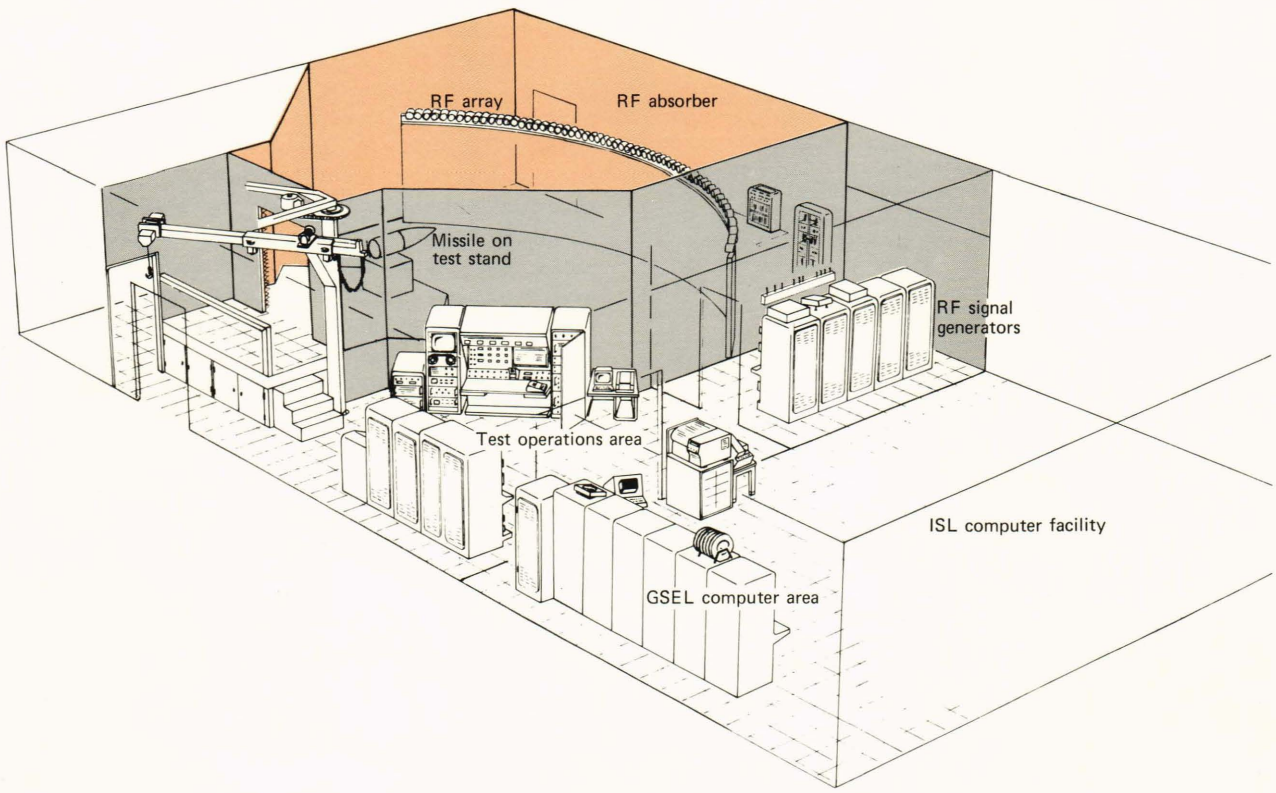

Fig. 3—Cutaway view of the upgraded GSEL. Major features of the upgraded GSEL include a large anechoic (nonreflective) chamber containing a fixed-element RF array, a screen room housing RF signal generation equipment, a test operations area, and a hybrid computer system located in an adjacent room. The new laboratory became operational in mid-February 1980.

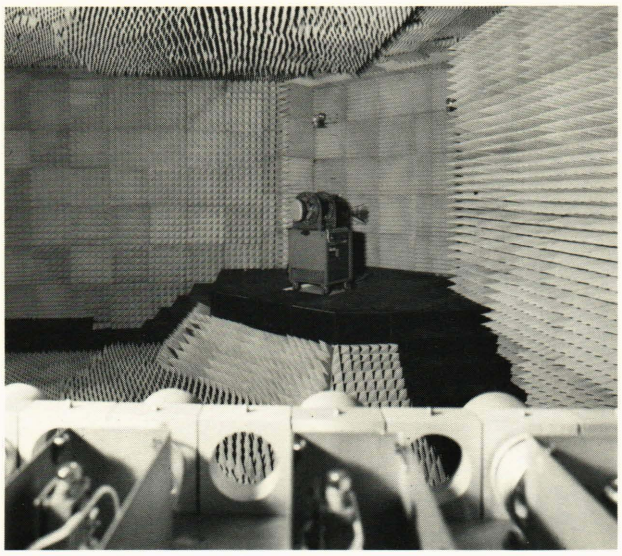

Fig. 4—Guidance section on test stand looking from behind the array. The guidance hardware, an SM-1 unit used for validation purposes, is located 20 ft away at the focal point of the RF antenna array. Absorber-lined interior surfaces suppress reflections, simulating a free-space environment. Mounting holes are for a second, interleaved array capable of representing two additional targets. Circuitry for making final amplitude and phase adjustments is in the foreground.

signals required to test Standard Missile seekers, including a rear reference signal; simulated returns for three targets, each with appropriate Doppler offset from the rear reference signal; and other signals shown in Fig 1. The power level of all signals is controlled to account for range changes. Amplitude modulation is applied to represent target fading. Many of the amplitude and frequency modulations associated with jamming types of interest are preprogrammed; others are easily synthesized.

A Pacer 600 Hybrid Computer System is situated in the adjacent Interactive Simulation Laboratory (ISL). The analog portion of the Pacer system is used to model the missile-target homing loop, including a detailed representation of the missile autopilot and kinematics. The digital portion controls detailed test operations, simulates aerodynamics, and recovers and processes data. Its capability is extended by a suite of microcomputers dedicated to performing specific tasks. The Pacer system has typical peripherals, including a tape recorder, disk storage, a card reader, a printer, and ancillary strip chart recorders. When fully implemented, it will support launch-to-intercept trajectories for all intercepts within the Aegis/SM-2, SM-2, or Tartar/ SM-2 performance envelopes.

The focus of test activities is the test operations area, where the operator's console is located. Other equipment includes a built-in test system to check the operability of the arrays, target generators, and digital communications exclusive of the Pacer computer, and a monitor and control console for interconnecting and monitoring most elements of the system.

CURRENT STATUS

Test operations in the upgraded facility began in mid-February 1980 with the receipt of a guidance section of the next-generation SM-2. Before the former facility was dismantled, closed-loop homing runs were made using an available SM-1 guidance section. When the tests were repeated in the new laboratory, essentially the same results were obtained except that certain second-order guidance effects could be observed that had not been apparent previously.

Much remains to be done before the capabilities of the new facility are fully utilized. However, the objective has been achieved of converting GSEL from a largely manually operated facility that could evaluate missile guidance performance against one or two targets at close range to a largely automated facility that simulates launch-to-intercept trajectories in threat situations involving multiple, widely spaced emitters. It is anticipated that future GSEL operations will continue to contribute significantly to Navy surface missile system programs.

FLETCHER C. PADDISON

THE TALOS CONTROL SYSTEM

The Talos autopilot was specifically designed to steer the ramjet missile with minimum angles of attack and to stabilize the missile in roll during the boost, midcourse, and terminal phases. The autopilot system evolved from late World War II designs by using such new components and system concepts as the hydraulic amplifying servo valve and the Sensitivity Feedback Autopilot developed by the Bumblebee Program.

The Talos wing control system was a powerful electromechanical-hydraulic system. It rotated the missile's wing surfaces to control the airframe in response to commands from the guidance system and automatically compensated for changes in aerodynamic sensitivity and stability associated with the considerable changes in missile speed (low subsonic to more than twice the speed of sound), altitude (sea level to more than 70,000 feet), and center of gravity (resulting from fuel consumption).

Talos was controlled by four independently movable wings mounted close to the center of gravity of the missile. Opposite pairs of wings moved together to control the missile in two orthogonal control planes (see Fig. 1). The missile was accelerated laterally and/or up and down when wings were deflected since the wings provided most of the missile lift. The control surfaces were sized to produce lateral accelerations that exceeded 14 g for altitudes up to 40,000 feet, above which the maximum attainable acceleration decreased. The wings were moved differentially to produce torque about the missile longitudinal axis to control missile roll. Wing control, with the attendant small angles of attack, was most desirable for Talos because airflow into the ramjet engine inlet was affected adversely by large angles of attack.

The Talos control surfaces had many design virtues, one of which was the limited motion of the center of pressure with Mach number and angle of incidence allowing the selection of the axis of rotation to minimize wing hinge moment. The effectiveness of the control system was sensitive to how quickly the control surface could move to produce lift. Accordingly, the control system was designed to move the wings at a maximum rate of 170 degrees per second.

As with all missiles, Talos had body vibrational modes during flight that necessitated care in the placement of sensing instruments, in particular those used for the control system. Even then, compensation and filtering of their signals were required. Furthermore, since the control surfaces were near the center of gravity and also near a point of maximum body vibration, the control surface had to be properly mass balanced to prevent coupling or flutter.

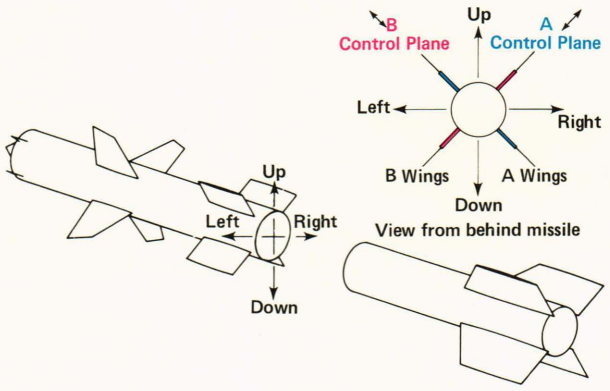

Figure 1 — The orientation of the Talos missile during all flight phases is shown. This orientation, termed "X configuration," provides maximum vertical and lateral acceleration.

The control system was functionally different for each of the three flight phases: boost, midcourse, and terminal homing. During the boost and midcourse phases, it operated as a conventional wing position system, and during the terminal phase, as an adaptive autopilot.

The servos that drove the wings were hydraulic, drawing prime power from a duct air-driven turbine. During the short early boost phase, when the air turbine was unable to supply the required hydraulic power, energy was provided by stored high-pressure nitrogen that pressurized the hydraulic system. The servos required approximately 25 horsepower.

THE BOOST-PHASE AUTOPILOT

Talos was actively stabilized during the boost phase to compensate for an aerodynamically unstable booster-missile configuration. Stabilization in the steering planes maintained the missile's orientation in space parallel to that at the time of launch. This was accomplished by command signals from a free gyroscope that had been uncaged just prior to launch. Rate gyroscopes were used in each of the two wing planes to provide damping. Figure 2 is a block diagram of the control system during the boost phase. The aerodynamic gain increased significantly during

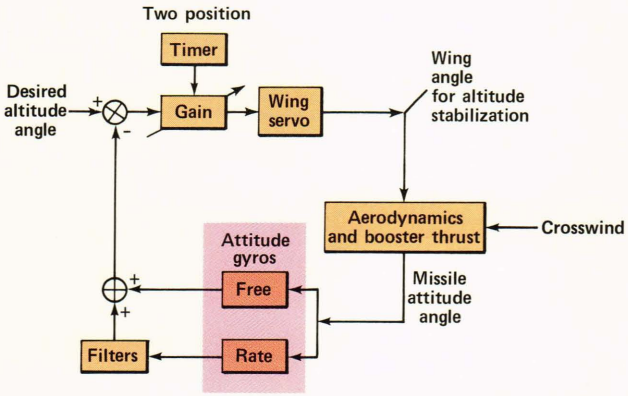

Figure 2 — The attitude control system maintained stability of the missile booster configuration during the boost phase. Two identical control channels were employed, one of which is shown. The free gyro, which was uncaged just prior to launch, provided an inertial attitude reference during the boost phase. The rate gyro was used to provide weathercock damping.

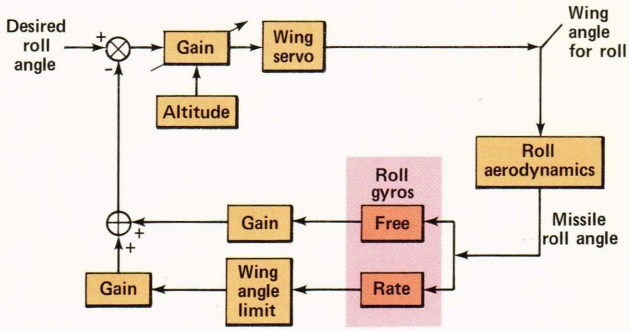

Figure 3 — Roll control was maintained during the boost and midcourse phases. The roll free gyro was uncaged at launch and provided an inertial vertical reference, while the roll rate gyro provided damping. Gain of the control loop was varied with altitude. To minimize roll-yaw-pitch coupling during the terminal phase, the roll free gyro was disconnected and a lag-lead shaping network added.

boost and, accordingly, the controller gain was reduced. This was done by a timer that reduced the gain by a factor of 2.6 at 1.75 seconds after launch. Since the effects of aerodynamic misalignments and mass unbalance, booster jet misalignment, launcher tipoff, and crosswinds during the boost phase were minimized, this boost-phase control reduced the launch dispersion and allowed the use of a relatively narrow guidance beam.

Roll control was the same for the boost phase and for the midcourse beamriding phase. Figure 3 is a block diagram of the roll system. The missile's roll position on the launcher was maintained both during the boost phase and after separation from the booster. The roll moment-of-inertia and aerodynamic characteristics during the boost phase were, of course, quite different from those during the post-separation phase. The response of the missile to roll disturbances was considerably faster after separation.

THE MIDCOURSE AUTOPILOT

Following separation from the booster, the ramjet engine was ignited. The velocity of the missile was controlled by a Mach-sensing fuel-control system, while steering was controlled by a beamrider link. During this phase, the guidance radar was programmed by target position, missile range, and previously determined parameters, all of which caused the missile to fly a trajectory that properly positioned it to begin the terminal phase.

After separation from the booster, the missile was aerodynamically stable, and control was switched from the attitude stabilization mode to a midcourse beamriding mode. An error signal, proportional to the angular off-beam error, was generated by the beamrider receiver (Fig. 4) and resolved into orthogonal components that were fed to the appropriate steering channels.

The autopilot was designed to respond to commands directing the missile to maintain its position in the guidance beam. Response was as rapid as possible without overshooting the desired position or exciting the missile's natural tendency to oscillate about its center of gravity (called weathercock oscillation). The autopilot response time varied with altitude. However, the character of the response was maintained essentially the same by programming autopilot sensitivity with altitude. Altitude was measured by a series of reliable and accurate switches that sensed the ambient static pressure. Compensation for velocity was not required since the flight Mach number was controlled. A gravity bias was used to compensate for gravity so that the missile would not fly below the center of the guidance beam as a result of gravitational force.

THE TERMINAL PHASE (HOMING)

After the midcourse phase had placed the missile into a favorable position relative to the target, a signal from the guidance transmitter activated the terminal phase of guidance. Target acquisition was normally completed soon enough after activation to permit at least 10 seconds of homing before intercept. Although 10 seconds seems a short time, it was adequate to remove missile heading errors and compensate for target maneuvers. To achieve this, the autopilot compared the requested lateral acceleration and the actual achieved acceleration produced by the control surfaces, and adjusted the internal gain of the autopilot to maintain optimum response. This "sensitivity feedback system" replaced the pressure-activated gain control used in midcourse. The block diagram for the terminal phase (homing) is shown in Fig. 5.

During the homing phase, it was desirable to rate-stabilize the missile in roll to eliminate roll-yaw-pitch coupling. Accordingly, the free gyro was not used, but control was referenced to a roll rate gyroscope to minimize the rate of roll.

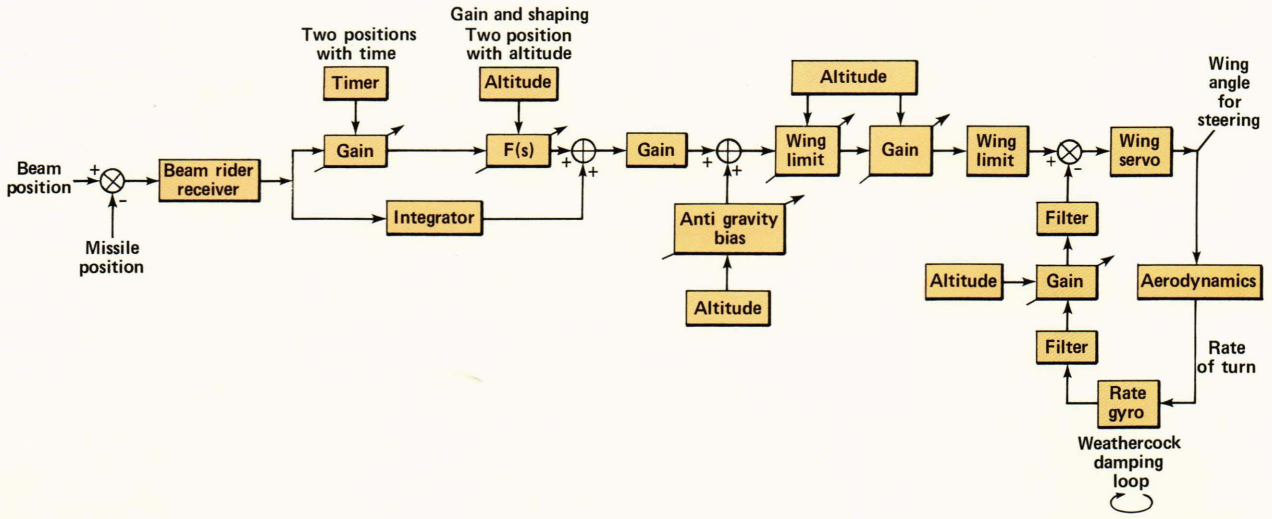

Figure 4 — Midcourse steering was controlled by a beamrider link. The beamrider receiver outputs were converted to wing commands for each control plane. These outputs were corrected for beam divergence and gravity bias by the control system. Loop gain was varied with altitude. Only one steering plane is shown.

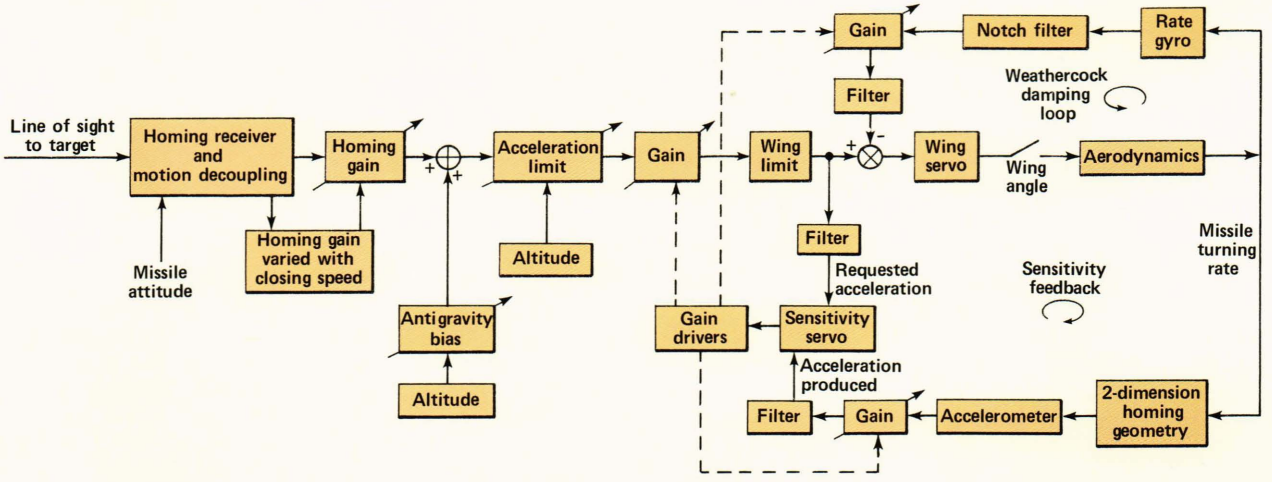

Figure 5 — Terminal steering placed the missile on a collision course by minimizing the rotation rate of the line of sight to the target. This figure shows the steering channel for one control plane. Line-of-sight rates, provided by the seeker, were converted to acceleration commands by the control system, which used the comparison of requested and achieved accelerations to adjust the gain of the autopilot and maintain optimum response. This "sensitivity feedback system" automatically compensated for changes in altitude and speed.

SUMMARY

In retrospect, the initial Talos autopilot system was an extension of World War II designs. These early systems required that the gain of the autopilot be adjusted as a function of altitude and Mach number, and programmed with time to compensate for changes in missile center of gravity as a result of fuel expenditure. The sensitivity feedback system improved the performance of the autopilot and eliminated the necessity for air density and Mach number changes to autopilot sensitivity. Talos was the first to use this sensitivity feedback design.

The outstanding performance of the Talos autopilot, despite its relative simplicity, was the result of developments in both system and component design. Many electronic, hydraulic, and electromechanical components, including end-instruments, were developed as part of the Bumblebee Program. These subsystems, components, and overall system concepts have since been used in many high-performance missiles and aircraft.

Feedback Technique Efficiency

W. Seamone

A hydraulic servomechanism is often chosen for flight control applications because of its known capability of high dynamic response from a small package. This performance advantage is usually gained at the expense of low system efficiency that is characteristic of hydraulic systems. The reason for this characteristically low efficiency may be understood by examining the basic operation of a hydraulic servomechanism. A typical block diagram of a hydraulic servo is as follows:

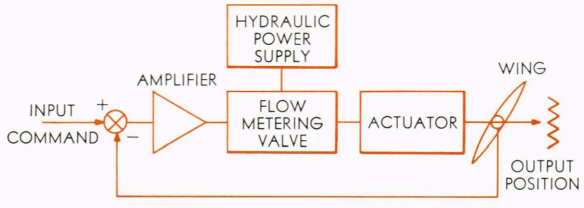

The basic controller in this loop is the flow-metering valve whose function is to meter or control the flow rate to the actuator in accordance with the amplifier drive signals. This is accomplished by varying an orifice restriction between the hydraulic supply and actuator. Assuming a constant pressure-supply source, the metering process has a maximum efficiency of 66% when the actuator pressure drop due to load is 2/3 of the supply pressure, and is progressively less efficient as the actuator load is decreased to zero.[1] Since many flight-control servos commonly undergo simultaneous high actuator velocities and low loads, system efficiency may suffer as a result.

The need for improved system efficiency while maintaining performance is particularly acute in small missiles and in space applications, where size and weight of the primary power source are at a premium. Assuming that a hydraulic servomechanism is chosen for these applications in order to meet performance requirements, the hydraulic power source should be designed for minimum power consumption. This source must be capable, however, of furnishing peak power upon servo demand without affecting dynamics of the servo.

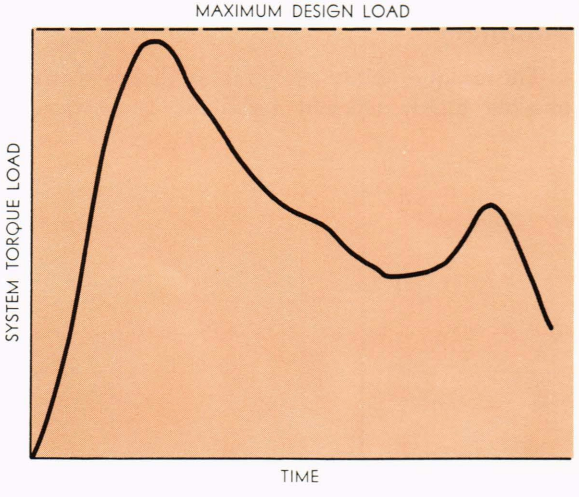

Fig. 1—Typical flight load-time history for an anti-aircraft-missile control servo.

[1] W. A. Good and F. C. Paddison, *"A Method for the Selection of Valves and Power Pistons in Hydraulic Servos,"* CM-717, The Johns Hopkins University, Applied Physics Laboratory, Jan. 26, 1952.

Improves of Hydraulic Servos

Hydraulic servos have been widely used in applications where good dynamic performance at high power levels is required. Power sources for such systems are often overdesigned to provide good transient load capability, at the expense of system efficiency for the average load duty cycle. A system concept is reported in this paper, which attempts to match the required input power to the servo as a function of actual load demand. Such a system has potential improved power efficiency. Tests performed on an experimental model have shown encouraging results.

This latter requirement and other system considerations often lead the designer to choose one of the simplest hydraulic power configurations, that is, the constant-pressure system.

Implementing this system in its simplest form is generally accomplished by employing a constant-rpm motor driving a fixed-displacement pump to deliver a constant flow rate. To maintain a fixed pressure level for the system, a relief valve is used to bleed off flow not commanded by the servo. Such a pressure source is sometimes referred to as a fixed-displacement-pump/constant-pressure system. This hydraulic power source operates at 100% pressure and flow at all times and thus can be quite inefficient for many applications. This system, however, enjoys widespread usage because of its simplicity and inherent reliability.

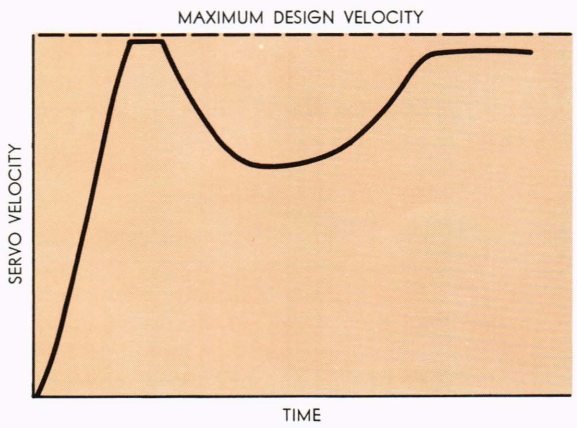

Fig. 2—Typical flight velocity-time history for an antiaircraft-missile control servo.

Recent work at APL has shown that system improvements in efficiency without sacrificing performance may be possible in a fixed-displacement-pump/constant-pressure system by using a hydraulic-load feedback loop around the servo actuator and hydraulic pump. This technique is predicated on the use of a unitized hydraulic servo in which the hydraulic power and servo elements for each servo application are packaged into self-contained servo power packs. Such a system allows a load sensor to be used to sense and control the system pump pressure as a function of the instantaneous external load on the servo. The servo-valve pressure drop remains constant for all load conditions under this arrangement; hence, the servo closed-loop bandwidth and performance is made independent of the variable system pressure operation.

Feasibility studies of this concept have been conducted on an experimental model of the unitized hydraulic package developed under subcontract to APL by the Kearfott Company. This model employs a simplified two-pressure-level system that was designed to check basic feasibility of the concept under dynamic operating conditions. All experimental data discussed in this paper are for this simplified system.

The Servo Load Environment

A quantitative definition of the servo load environment is one of the more difficult parameters to pin down in many servo applications. Maximum design loads may be readily calculated, but the

frequency of peak loading or load-duty-cycle profile is often difficult, if not impossible, to predict. A servo application in a missile control system, for example, has a load duty cycle that is a function of the exact flight conditions for each particular flight. The torque load requirements generally reach a maximum during an early portion of the flight and may drop to a moderate or even negligible value for the remainder of the flight. Such a variable load environment requires that this type of a system be designed to handle peak loads at any time during flight.

The minimum power requirements for a given servo are dictated by the servo-torque-load duty cycle and the actuator velocity requirements for its particular mission. Typical plots of instantaneous load and velocity requirements versus time for the antiaircraft missile control servo are given in Figs. 1 and 2. The maximum required power for such a system would be the product of these two curves. The average required power, however, is considerably less than the maximum value since it is dependent on the time duration of peak load demands. Most actual systems have load duty cycles such as shown in Fig. 3, which result in average power requirements typically 20 to 30% of peak system requirements. The problem then becomes one of a design trade-off to provide the instantaneous peak power as required, and yet consume average power proportional to the actual duty cycle in an effort to keep the system efficiency high.

A common approach taken in some hydraulic system designs is to provide a motor pump, sized to provide the average load duty cycle and to include

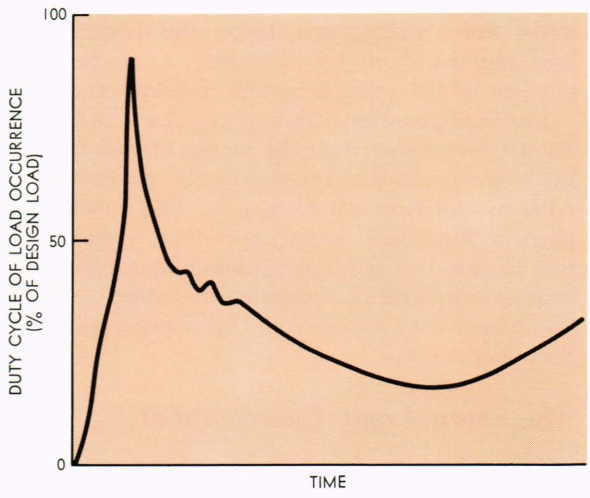

Fig. 3—Typical load duty cycle as a function of time for an antiaircraft-missile control servo.

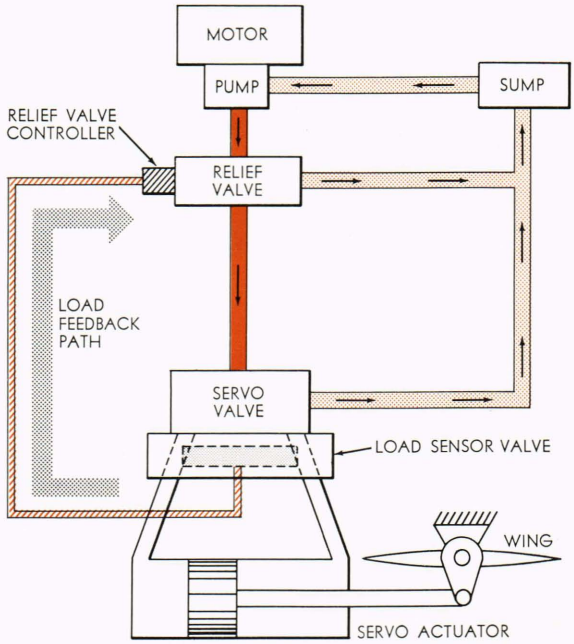

Fig. 4—Schematic diagram of a servo power system with load-sensing variable-pressure control. (Different color values indicate variations in pressure.)

a hydraulic air-oil accumulator for short-term peak-power demands. Although accumulators have been in widespread use for a number of years, missile applications have pointed up many problems, particularly in regard to the long-term storage of high-pressure air. The incorporation of an accumulator in a missile control system may require that the user perform field service maintenance on the equipment. The objections to the accumulator may be overcome by use of a variable displacement pump in lieu of the accumulator; however, this will result in additional system complexity and cost. This paper addresses the problem of how the system efficiency can be improved for a low-duty-cycle system *without* the complexity of *stored energy elements* or a variable-displacement pump.

Load Sensor Feedback

An efficiently designed power system for an application such as a missile control servo would be one whose input power is directly a function of the actual load duty cycle. Theoretically this implies that both flow and pressure should be varied as a direct function of output load. The problem is somewhat simplified for the typical system described in Figs. 1, 2, and 3 by noting that the servo velocity demand is relatively high throughout the flight period, and that a system that simply modu-

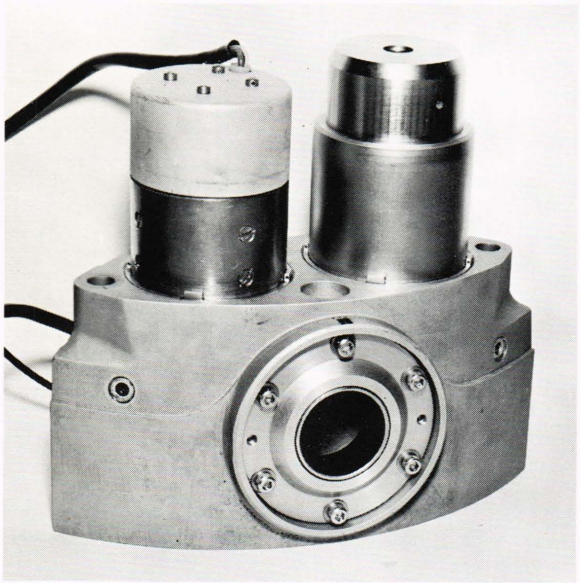

Fig. 5—Unitized hydraulic actuator modified with a load-feedback sensor.

lates input power as a function of torque demands can offer appreciable power savings for the system. Such a system is, of course, a load-controlled variable-pressure system.

Instrumentation of a load-controlled variable-pressure system in a flight-control servo appears feasible by providing each hydraulic servo with its own individual hydraulic power source. This packaging concept is sometimes referred to as a unitized hydraulic servo package; it allows the flexibility of individual pressure control for each servo by sensing its load and controlling the pressure accordingly. A conventional, single, hydraulic power source arrangement, where one pressure source is used for several servos, does not appear feasible for this type of load sensing because of possible conflict of load requirements from each servo.

Instrumentation of a load-controlled variable-pressure system may be accomplished as shown in the system diagram, Fig. 4. In this hydraulic system the relief valve is set at a minimum pressure level for the system when no external load is applied to the servo actuator. Upon encountering a load, the servo actuator will develop a differential pressure to sustain the load. A feedback path is employed to send back a signal to the relief valve to cause it to go to a higher value proportional to the encountered load. This will result in a hydraulic pressure source whose output is controlled by the actual load seen by the servo actuator. An important secondary benefit of the system is that the pressure drop across the servo control valve remains constant, independent of load. This is due to the fact that the incremental rise in supply pressure is equal to the load demand. This constant pressure drop across the servo valve tends to keep the servo valve gain constant and independent of load. This provides for a constant bandwidth servo system over the load operating range.

Experimental Model Design

In order to study experimentally the basic feasibility and dynamic characteristics of the load-feedback/variable-pressure system, a unitized hydraulic actuator package, shown in Fig. 5, has been modified with a load-feedback sensor. The instrumentation scheme chosen for this first model included a differential pressure load sensor and a two-level pressure-relief valve controlled by the load sensor. This simplified system was designed to determine possible dynamic interaction of the load feedback loop and servo dynamics. The load sensor and relief-valve mechanization employed in the experimental model are shown in Fig. 6. The load sensor valve is a spool-type valve whose displacement from null is a function of the magnitude of the external load on the servo. The metering ports across the spool have a controlled dead zone before pressure is allowed to be connected to the actuation piston of the relief valve. The relief valve is held at its lower pressure setting of 1500 psi by a mechanical stop. When the external load exceeds 400 in.-lb for either direction of load, system pressure of 1500 psi is connected by the load sensor valve to the relief valve actuation piston to force it to the mechanical stop corresponding to the

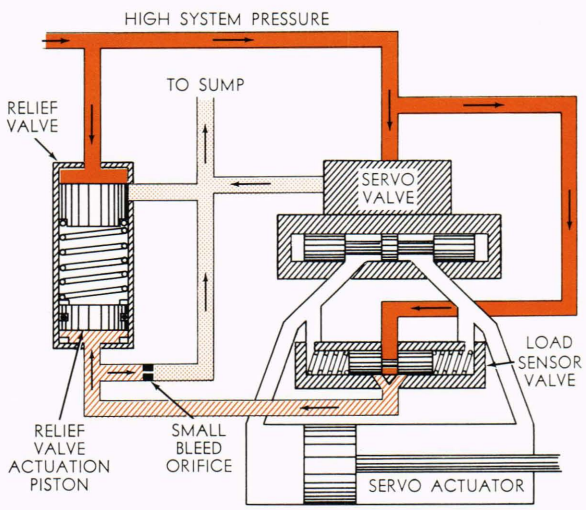

Fig. 6—Schematic diagram of a two-pressure-level system used in an experimental model.

high-pressure, 3000-psi setting. The system pressure will remain at this setting until the high load demand is removed from the servo.

The two-level pressure system in the experimental model operates at a 60% input-power level for loads up to 400 in.-lb and at 100% rated power at loads up to the design maximum of 1500 in.-lb. This power saving of 40% can be appreciable when we consider the basic size and weight of the primary power source.

Experimental Model Results

In order to exercise the load feedback characteristics of the system, the servo power package was operated against a torsion bar load. The servo bandwidth was set up to give 45° phase lag across the servo at approximately 45 cps to determine if there were any serious dynamic effects in a typical high-bandwidth system. The experimental model had its load feedback system set up with the following parameters:

(a)	No-load pressure	1500 psi
(b)	No-load motor current	12 amps at 56 volts
(c)	Torque-load switching point	± 400 in.-lb
(d)	High-load pressure	3000 psi
(e)	High-load motor current	20 amps at 56 volts

The servo was operated in this mode for approximately 10 hr of test time. The transition from a small-load to a high-load condition appeared smooth for a variety of input signal conditions.

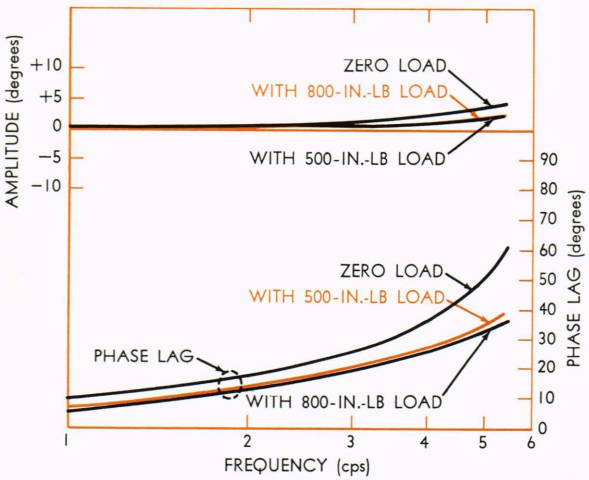

Fig. 7—Unitized actuator frequency-response characteristics with power-matching pressure-control system.

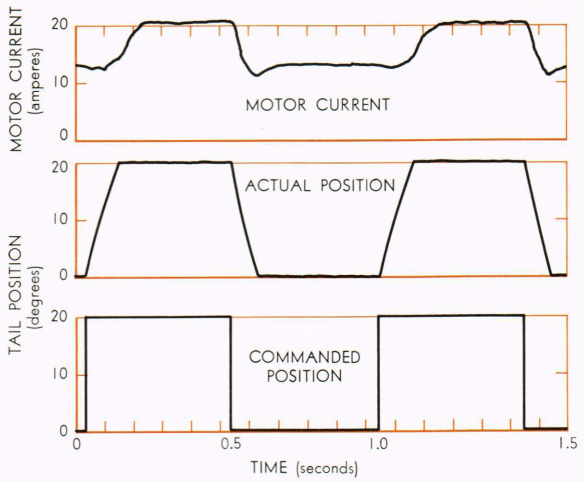

Fig. 8—Unitized actuator step-response characteristics with power-matching pressure-control system. Torsion-bar load is 37 in.-lb per degree.

Servo transfer characteristics were measured at no load, 500-in.-lb, and 800-in.-lb loadings, and are given in Fig. 7. These data show that the bandwidth actually increased as the load was increased above the load sensor switching point. Increasing the torque load switching point to a higher value will reduce this over-compensation of servo gain with increasing load.

In order to insure that the load feedback mechanism would work properly during transient inputs, a step command was applied to the servo. This test yielded typical system performance of Fig. 8. This and other tests with various command signals have not shown any evidence of dynamic instability associated with the load feedback scheme.

Conclusions

The satisfactory demonstration of the experimental model of a hydraulic power servo with load sensor feedback has indicated that this technique is sufficiently promising to warrant additional studies. The model operated at 60 and 100% power levels as a direct function of the load, showed no evidence of dynamic instabilities, and introduced no undesirable transients into the servo. The additional hardware complexity was small and is not expected to affect long-term reliability for missile applications.

A linear load feedback sensor has not been designed as of this date, but it is of interest since it offers the promising possibility of complete power matching to the actual load requirements. Such a system would allow the designer to use the high performance of hydraulic servos and retain high efficiency as well.

SELF-ERECTING MISSILE FIN

During wartime fleet operations there is a problem of defense against high-performance enemy aircraft attacking in large numbers from several directions and at varying altitudes. In order to meet attacks of this kind successfully, missile ships must be able to launch large numbers of missiles at high firing rates. To do so it has been suggested that in addition to existing launchers missile ships be equipped, at strategic locations on board, with one or more multiple-unit "tube" or "box" missile launchers having rapid-fire capability. An important factor in designing this type of launcher is the size of the box or tube needed to accommodate the span of the missile fins; this in turn determines the number of missiles that can be carried for immediate launching. It is clear that it would be desirable for the missiles to be equipped with self-erecting folding fins so that they could be stowed in the launcher with fins in the folded position.

There have been studies, made by APL and by missile contractors, aimed at devising a box- or tube-type launching system for Tartar or Tartar-type missiles.* As can be surmised, however, each proposal has run up against the problem of the volume required for storing missiles with fins erected. In the case of the Tartar missile with fins extended, for example, a box with an end opening approximately 36 in. square is required. On the other hand, with fins folded, the same missile can be contained in a box of the same length that has only a 24-in.-square opening, representing a volume saving of 55%. It is therefore obvious that if the missiles can be stored in launcher cells with fins folded, the number of cells in a given launcher can be significantly increased.

To achieve this, automatic fin erection immediately after the missile leaves the launcher cell is essential. Several methods of erection have been studied in the past, which require the use of external hardware that is ejected from the missile when fins are erected. Such concepts have not proven to be desirable solutions because of both their inherent unreliability in operation and the presence of loose parts that are exposed to rocket blast and may be thrown back on the launching ship at high velocity, with possible damage to equipment and injury to personnel.

At APL five engineering models of a self-erecting folding fin have been developed by S. Kongelbeck, W. F. Williams, and J. M. Snapp, which provide the self-erecting capability necessary for box- or tube-launch installations.† A number of tests of these fins have been conducted successfully to establish operational characteristics as well as functional reliability. As a result, the feasibility of the concept has been thoroughly demonstrated.

The APL-designed, spring-loaded, self-erecting

* The Tartar missile is among those developed for the U.S. Navy at the Applied Physics Laboratory.

† S. Kongelbeck is supervisor and W. F. Williams is assistant supervisor of the Central Laboratory Facilities Group. J. M. Snapp is a design engineer in the same organization.

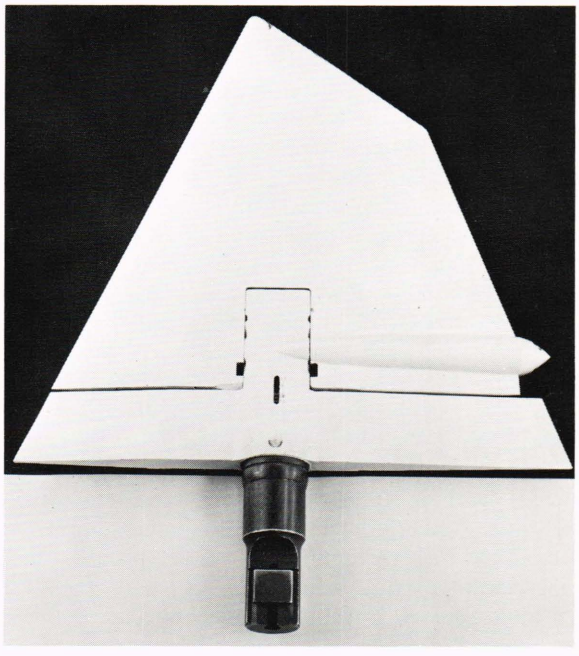

Fig. 1—Self-erecting missile fin engineering prototype.

fin (Fig. 1) fulfills the requirements for a compact, fully automatic, self-contained erection unit that does not depend on external springs or other erection mechanisms. This fin is an adaptation of the folding fin now in use on Tartar missiles.

In principle the folding and latching mechanism of the self-erecting fin is the same as that employed on the Tartar folding fin, except that such recent design changes as the improved latch and hinge-pin design, stronger latch pin, and positive stops have been incorporated. The detent mechanism has been eliminated since it is not required for a self-erecting fin. In its place an external means for holding the self-erecting fin in the folded position must be provided, and with a suitable release mechanism that depends on missile motion at launch or triggering at a predetermined time during the launch cycle. Several acceptable release mechanism designs have been studied.

Figure 2 shows the details of the erection spring and latch mechanism. The upper fin panel has been modified to include a torsion-spring housing along the hinge-pin centerline. The housing is an integral part of the upper fin panel and is aerodynamically faired to the fin at the forward and aft ends, as can be seen in Fig. 1. The torsion-coil-spring subassembly consists of the spring, with a keying ring attached to its forward end, and a housing-enclosure plug attached to the aft end. In the fin assembly the aft-hinge pivot is attached to the fin lower spar by a roll pin, and the aft end of the pivot is slotted to receive the key in the keying ring on the forward end of the torsion spring. Assembly of the torsion spring to the fin is very easily done by sliding the spring into the housing from the aft end until the spring key engages the slot in the end of the aft-hinge pivot and the housing closure is in position. The housing closure is pinned in place and, with the fin erected, the torsion spring is pre-loaded to 20-in.-lb torque by rotating the aft plug and pinning it in position. With a 20-in.-lb pre-load, the spring will develop approximately 70 in.-lb of torque when the fin is in the folded position.

A number of tests have been run to establish functional operability and reliability of the mechanism. The engineering prototypes have been subjected to repetitive folding and spring-erection cycles, with no indication of mechanical weakness or failure. Laboratory bench tests have determined the unfolding cycle times for four different fins; the results of 10 measurements on each fin showed a variation of unfolding time ranging between 0.17 and 0.20 sec.

In the box-launch concept the fins automatically erect just after the missile has left the launcher

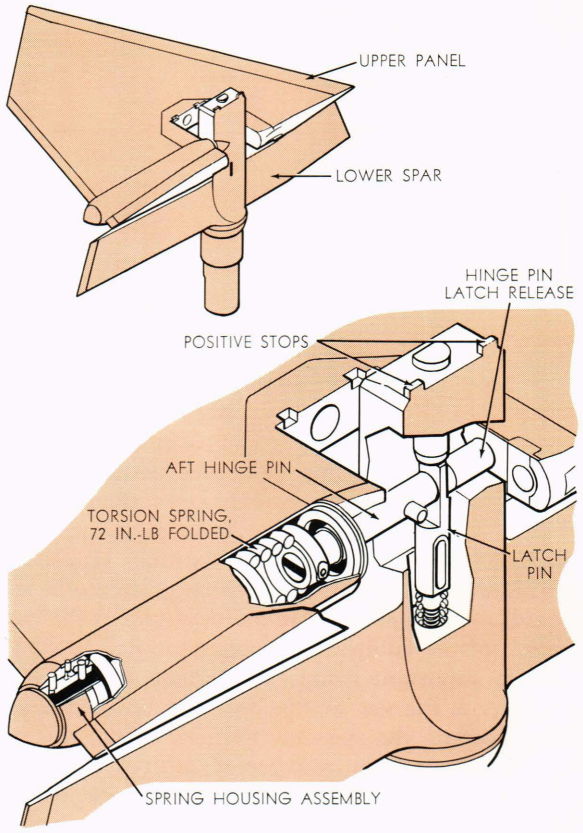

Fig. 2—Cutaway drawing of the self-erecting missile fin shown partially folded.

cell. At this time the missile is traveling at a relatively low speed and may be subjected to high-velocity winds, either broadside or at some intermediate angle to the flight path. To determine the effect of this type of wind loading on the erection-cycle time of the self-erecting fins, tests were run in which such a wind-load condition was simulated. Four self-erecting fins were installed in a missile boattail section, and means were provided for triggering the release of the fins from the folded position. The boattail was mounted on a pedestal at one end of a framework, with a high-speed camera mounted at the opposite end. This assembly was then mounted on an elevated wooden structure on a flat-bed truck in order to be exposed to the undisturbed wind stream when the truck was in motion. With the truck moving at 60 mph, the fins were triggered and erected, and the erection cycle was recorded by the camera. Several runs were made, with the boattail axis perpendicular to the air stream or facing into it at angles of 30° and 60°. No difficulty was experienced in erecting the fins during any of the runs, and analysis of the films showed only a negligible increase in erection time ($\approx$ 0.03 sec) caused by crosswind loading.

FLUIDIC ANGULAR RATE SENSOR -

a replacement for rate gyroscopes ?

T.M. Rankin, A.G. Moore, and
W.C. Schuemann

A very simple fluidic angular rate sensor is described wherein angular rate information is obtained by sensing the deflection of a laminar jet flowing from a nozzle. Both the electrofluidic jet position sensor and no-rotating-parts fluidic pump, which are instrumental in yielding a low cost, long life, self-contained fluidic angular rate sensor, are discussed. The prime advantages of this rate sensor when compared with the conventional mechanical rate gyroscopes are its over-range capabilities, inherent long life, freedom from rotating parts, and extreme ruggedness.

As a result of APL's participation and encouragement, the Allegany Ballistics Laboratory (ABL), a Division of Hercules Incorporated, is developing a fluidic rate sensor. APL has participated in this development by defining requirements, testing early devices, and by direct financial support. The Fleet Systems Division at APL, having a continuing interest in gyro development, particularly in the areas of low cost and long life, has partially funded the development of the fluidic rate sensor for possible future application to shipboard systems. The inherent low frequency response fluidics had directed early attention toward shipboard applications since missile system applications generally required higher frequency response. Recently however, self-contained fluidic sensors have been developed in the standard miniature rate-gyro-size (1 in. diameter x 2 in. long) with a linear range to 1000 degrees per second having a dynamic capability to 50 Hz.

Description and Mechanization

The basic description of the sensor is contained in its name, "Fluidic Angular Rate Sensor." "Fluidic" is a term that has evolved in recent years to describe fluid systems where signals as well as power are transmitted by the fluid medium. Angular rate sensor means a device which, through its mechanization, yields an indicated output proportional to an input angular rate about a particular axis. In the fluidic angular rate sensors discussed here, the fluid medium is air, nominally at atmospheric pressure.

Before the technical details of operation and performance of the fluidic angular rate sensor are discussed, a simplified description of the device and its mechanization will be presented. Referring to the simplified sketch (Fig. 1), an air pump connected to a long, small-diameter tube creates a laminar air jet which, when undisturbed, flows along the centerline of the drift tube which houses

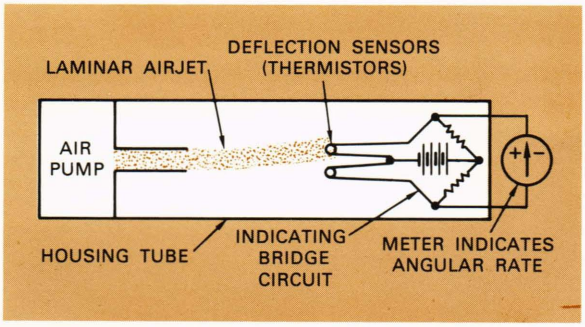

Fig. 1—Sketch of fluidic angular rate sensor.

the device. When the device is subjected to an angular rotation about an axis perpendicular to the centerline of the jet, the inertial properties of the air jet cause it to be deflected laterally. The magnitude and sense of the deflection are proportional to the magnitude and sense of the input angular rate. The two tiny thermistor deflection sensors are positioned symmetrically about the undisturbed air jet and separated a distance approximately equal to the jet nozzle diameter. The thermistors are electrically connected into a simple bridge circuit (as shown in the sketch) which provides enough current to cause self-heating of the two thermistors. In the undisturbed state the bridge is balanced and the meter indicates zero. When the air jet is deflected away from its normal centerline position, the velocity of the air flowing by one thermistor (toward which the jet is deflected) is greater than the velocity of air flowing by the opposite thermistor. This causes an unbalance in the cooling of the two thermistors. Since the thermistor resistance increases with decreasing temperature, the electronic bridge becomes unbalanced; this unbalance is indicated by a positive deflection of the meter. When the air jet is deflected in the opposite direction by a negative input angular rate, the other thermistor is cooled, thus unbalancing the bridge in the opposite sense. This causes the meter to indicate a negative value. Thus the device yields an indicated output, the magnitude and sense of which are proportional to the input angular rate about a particular axis.

Jet Deflection Mechanism—Referring to Fig. 2, which shows a schematic diagram of the fluidic angular rate sensor, a free jet having a mean velocity V_j emerges from a nozzle and is deflected from the nozzle centerline by an amount d due to rotation of the system.

If the rotation is at a constant angular rate ω in the plane of the jet position sensors, the tangential velocity of the nozzle will have a value of $Vn = X\omega$, the resulting tangential velocity of the jet position sensors will be $Vs = (X + L)\omega$, and their difference will be $Vs - Vn = (X + L)\omega - X\omega = L\omega$. Let t be the time for an increment of fluid to travel from the nozzle to the receiver ports. Then the deflection of the fluid beam is:

$$d = (Vs - Vn)\, t = (L\omega)\, t = Lt \cdot \omega = \frac{L^2}{V_j}\omega .$$

By letting L and V_j be constant, the deflection of the jet from the jet position sensor will be proportional to ω.

Naturally the above calculation holds only for small deflections. As will be shown later, the deflections in a practical device are very small compared to the length of the fluid beam and, therefore, the errors involved in the linear approximation are negligible.

It should be clear by inspection that the device is not sensitive to a constant velocity in any direction. Jet deflection is also not affected by a constant acceleration in any direction. The jet is completely submerged within the housing (drift tube) so that acceleration identically affects each element of the jet and the air in this space. Acceleration can, however, produce a constant density gradient in the housing. The change in the density may cause some second or higher order effects, but these effects should be very small.

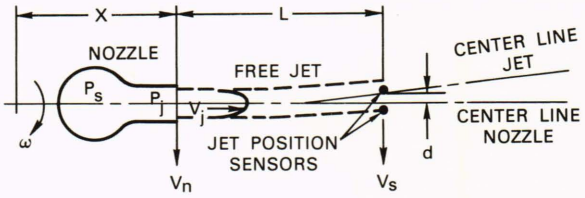

Fig. 2—Schematic diagram of fluidic angular rate sensor.

Jet Position Detection—Detection of the magnitude and direction of deflection of the fluid beam is necessary if a usable output signal is to be generated which indicates the input angular rate. Because of the fluid entrainment property of a laminar submerged jet, the velocity distribution takes on approximately the parabolic shape shown in Fig. 3. Since the velocity varies across the jet beam, the dynamic pressure resulting from the velocity distribution also varies across the jet beam, as do many other properties of the jet. Any one of these properties could be used to determine the deflection of the jet. However, in the present designs, the fluid beam position is detected by the use of two thermistor beads located in the flow as shown in Fig. 3. Two 0.01-in.-diameter thermistor beads are mounted in a drift tube downstream from the nozzle and electrically connected into a

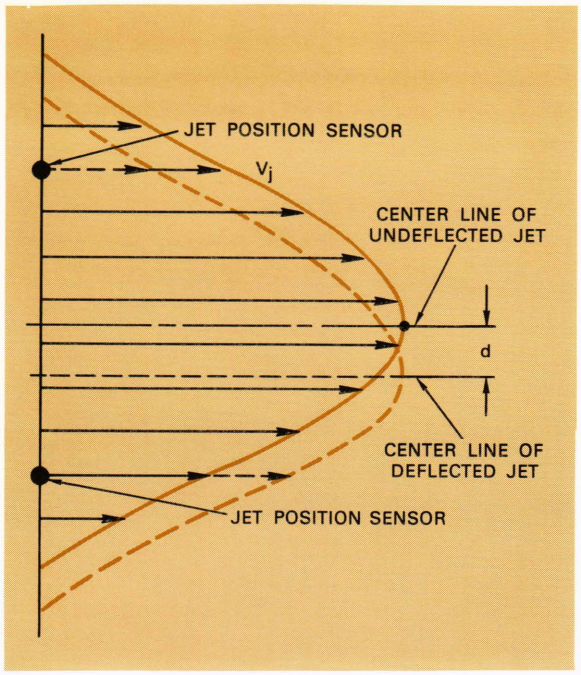

Fig. 3—Velocity profile at jet position sensor location.

balanced bridge configuration. The bridge is excited with a DC voltage and adjusted to allow enough current to flow to cause the thermistor beads to be self-heated to a temperature just above the ambient fluid temperature. As a result, heat is transferred to the ambient fluid as it flows past the tiny beads. Since the velocity distribution varies across the jet, the rate of cooling of the self-heated beads will vary with their positions in the jet. If the matched beads are both located at positions in the jet so that the velocity across each is equal, the cooling of each bead will be the same, their resistances will be equal, and the bridge will be balanced. With the beads properly spaced and symmetrically placed in a jet having the correct velocity profile, the electrical output, which results from differential cooling that occurs as the jet is deflected, can be made proportional to jet deflection over a wide range of values. The ± sense of the input angular rate is contained in the ± output voltage.

Some of the physical characteristics of the jet, nozzle, and deflection are as follows:

Nozzle diameter, $D = 0.125$ in.

Jet mean velocity, $V_j = 100$ in./sec

Distance to jet position sensors, $L = 1$ in.

Reynolds Number (Re) at nozzle $= \frac{DV_j\rho}{\mu} \cong 350$, where ρ and μ are density and viscosity of air at standard conditions. The flow is laminar if Re < 1000.

The time for a sample fluid to travel from the nozzle to the jet position sensor is: $t = L/V_j = 0.01$ sec.

Resulting deflection values for input angular rates as computed from the equation

$$d = \frac{L^2}{V_j} \cdot \omega = \frac{(1)^2}{57.3\ (100)} \cdot \omega$$

are $d = 3.5 \times 10^{-3}$ in. at $\omega = 20°$/sec and $d = 1.75 \times 10^{-6}$ in. at $\omega = 0.01°$/sec.

These deflections are certainly small compared to the length of the fluid beam L, and hence the linear approximation equation for deflection holds and second-order effects are very small.

This fluidic angular rate sensor could be designed as a flueric angular rate sensor (that is an all-fluid sensor) by locating the two input control ports of a very sensitive fluidic amplifier at the respective locations designated as jet deflection detectors (in Fig. 3) in such a manner so as to be most sensitive to the dynamic pressure of the jet. The output of such a device would be a fluid

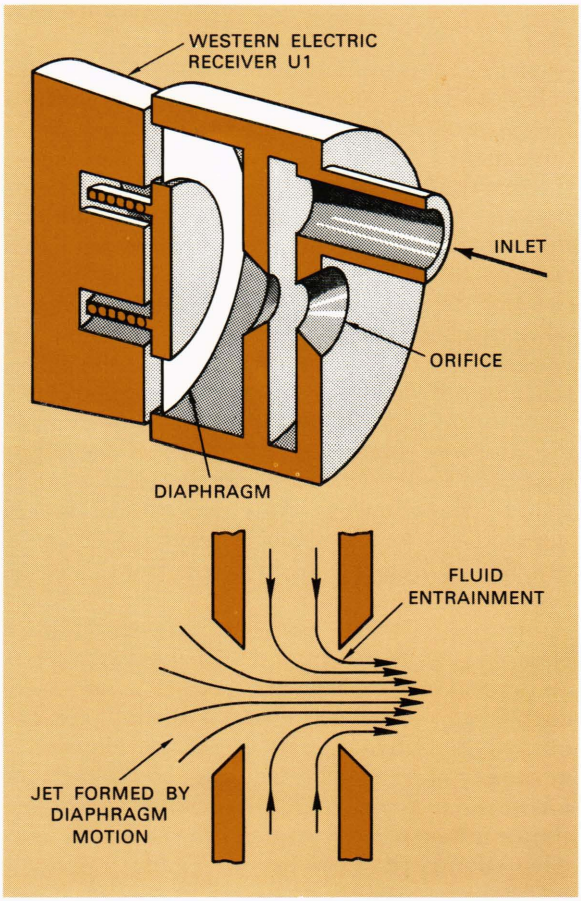

Fig. 4—Fluid pump cross section and pumping mechanism.

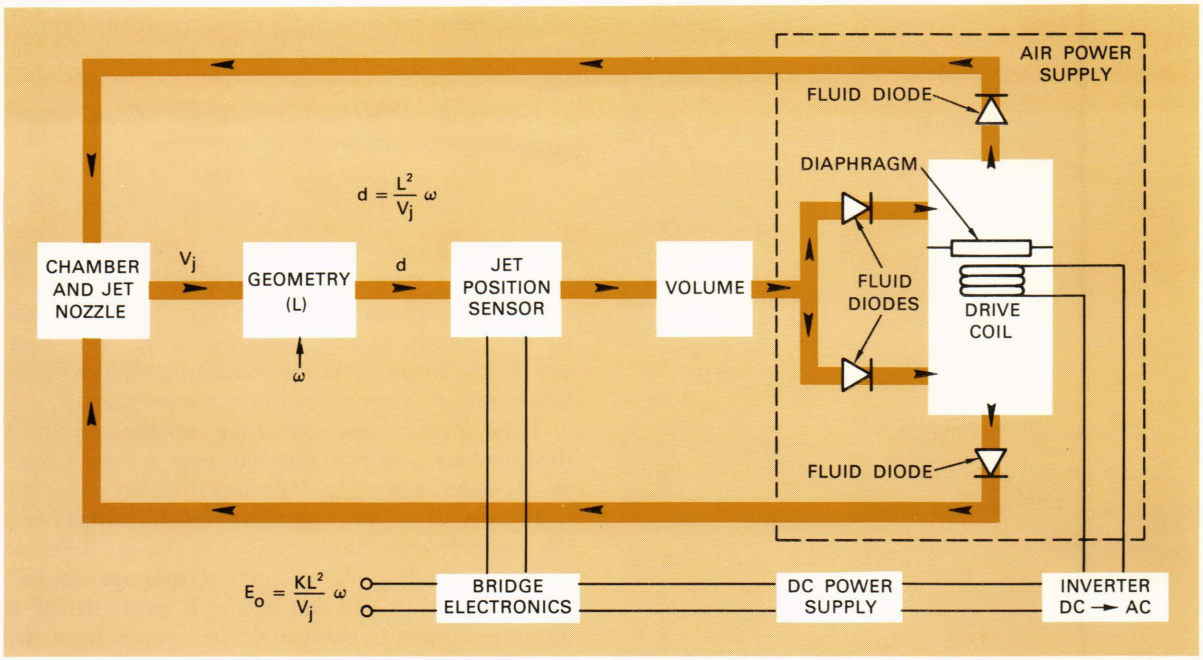

Fig. 5—Functional block diagram of sensor, including air power supply.

pressure that is proportional to input angular rate.

ELECTRONICS—A very simple passive electronic thermistor bridge may be used to get a usable output signal. However the thermistor beads have a thermal time constant in the range of ~ 0.15 to 2 seconds, which limits the dynamic capabilities of the rate sensor. The thermal time constant can be reduced to ~ 0.001 second by connecting the thermistors into an active electronic bridge in which the thermistors are held at a constant temperature. To further improve the dynamic characteristics, hot-wire anemometry techniques can be used; in this method the thermistors are replaced by tiny wire filaments. All of these techniques have been tested with excellent results.

AIR POWER SUPPLY—Rate sensors, like all other inertial sensors, are almost always subject to the system requirements of low cost, long life, and ruggedness.

The first of these, low cost, requires simplicity of design, while the second and third require the minimization of moving parts, etc. The laminar jet angular rate sensor has eliminated the large spinning wheel used in the rate gyroscope. However an air supply must be provided. This could have been a hose from a regulated air pressure source or a simple fan or blower mounted in the sensor itself. ABL eliminated these by developing a long-life, no-rotating-parts air pump as shown in Fig. 4. Early models of the air power supply utilized a Western Electric Type U1 earphone to move air back and forth through special orifice plates to produce a very low pressure pump. More recently developed sensors use a piezoelectric crystal as the driver element.

The pump consists of two parallel orifice plates with a hole in each plate as illustrated in Fig. 4. The holes are opposite each other, and the hole diameter is approximately equal to the distance

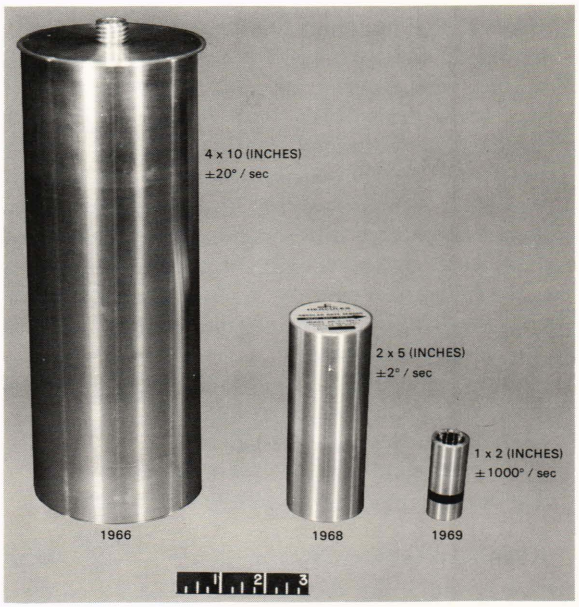

Fig. 6—Evolution of the fluidic angular rate sensor.

between the plates. As the diaphragm is displaced, a jet is formed by the orifice in the upstream plate. The jet diameter contracts in the usual manner as it moves across the gap toward the hole in the downstream plate. As the jet is crossing the gap, fluid between the plates is entrained by the jet and exhausted through the downstream hole. As the motion of the diaphragm reverses, a jet is formed in the opposite direction. Because of the symmetry of the orifices, fluid from between the plates is again exhausted through the downstream orifice. If the space between the plates is connected to a tube, fluid will be drawn through this tube and exhausted through the orifices as the diaphragm is caused to oscillate back and forth. The device, therefore, is a pump and will provide either pressure or suction.

Figure 5 is a functional block diagram of the ABL fluidic angular rate sensor showing how the fluid flows through the pump and the sensor. No attempt is made here to define transfer functions of each block. The jet nozzle and cavities throughout the sensor act as RC type filters to smooth the rectified pump flow to a clean noise-free flow at the jet position sensor location.

The rate sensor has been reduced to a package 1 in. in diameter and 2 in. long for some applications (see Fig. 6). Figure 7 shows actual photographs of one of the ABL experimental fluidic angular rate sensors as delivered to APL as part of a development contract. Figure 8 is an artist's illustration of the fluidic angular rate sensor showing the fluid flow as well as showing the location of each sub-unit of the sensor (e.g., pump, jet position sensor, nozzle, etc.). Note that this fluidic angular rate sensor has a DC output and requires only a DC power supply.

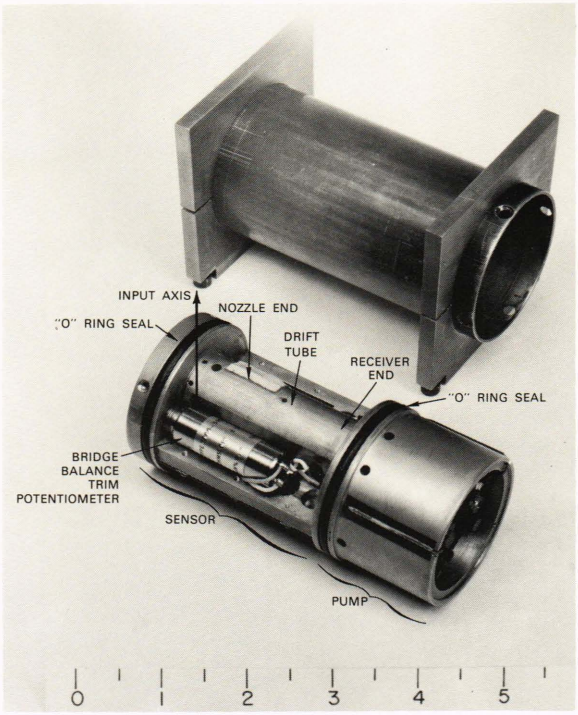

Fig. 7—Sensor with cover removed to show the relative location and size of all major parts.

Performance

Performance testing has been conducted on first, second, and third generation fluidic angular rate sensors at APL and on the fourth generation units at ABL. Table I summarizes the results of these tests to show performance and progress. In general the units have a nonlinearity less than 0.2%, a dynamic range in excess of 2000 to 1, and a frequency response capability up to at least 300 rad/sec.

Generation 1 and 2 sensors were not designed for any specific application but rather as experimental devices. The third generation sensors have been delivered to APL for evaluation as an angular rate sensor for input to a target engageability computer. The fourth generation sensor is a first attempt at missile-type rate sensors. The 1-in.-diameter by 2-in.-long self-contained unit has a linear range to ±1000°/sec with a frequency response in excess of 300 rad/sec. The self-contained power supply uses a small piezoelectric crystal for the pump. Power requirements for the sensors are typically less then 1.5 watts.

The fluidic angular sensor transfer function is basically a transport delay and a first-order lag. The transport delay is caused by the time required

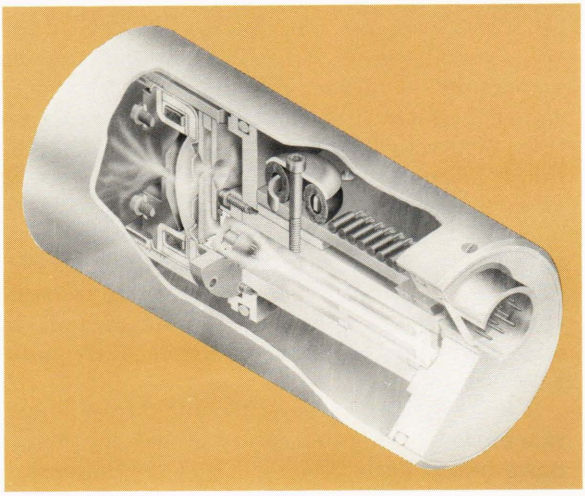

Fig. 8—Artist's concept of the second generation fluidic angular rate sensor.

TABLE I

SUMMARY OF PERFORMANCE PARAMETERS OF THE ABL FLUIDIC ANGULAR RATE SENSOR

Performance Parameter	*1966 First Generation*	*1967 Second Generation*	*1968 Third Generation*	*1969 Fourth Generation*
Range	± 20°/sec	± 20°/sec	± 2°/sec	± 1000°/sec
Nonlinearity	1%	0.2%	0.22%	0.5%
Bias Stability	—	0.001°/sec/day	—	—
Frequency Response	8 rad/sec	22 rad/sec	1 rad/sec	300 rad/sec
Resolution	<0.01°/sec	<0.01°/sec	0.002°/sec	0.3°/sec
Noise (at 0 input)	0.05%	0.05%	0.1%	0.3%
Size	Lunchbox	2-1/4 in. dia. x 4.75 in. long	2 in. dia. x 5 in. long	1 in. dia. x 2 in. long
Acceleration Sensitivity	5%/g	0.48%/g	1.5%/g	0.1%/g
Temp. Sensitivity				
Bias	—	0.07%/°F	0.12%/°F	0.05%/°F
Scale Factor	—	0.4%/°F	0.15%/°F	0.06%/°F
Voltage Sensitivity				
Bias	—	3.75%/V-DC	0.1%/V-DC	—
Scale Factor	—	14.3%/V-DC	0.25%/V-DC	—
Life	—	>16,000 hr (Units have been operating continuously in excess of 2 years)	—	—

(NOTE: All %'s are related to full scale values.)

for a slug of fluid to traverse the distance from the nozzle to the pick-off. The first-order lag is due to the thermal time constant of the thermistor beads. When a constant power bridge is used to improve the frequency response the lag appears at a higher frequency and a higher frequency second-order lag appears in the transfer function.

Table I gives a chronological listing for comparison of the performance parameters of all the fluidic angular rate sensors developed. One immediately sees the vast improvements in most areas and the areas where further improvements are desired. The bias stability (null wander) is caused by change of pick-off characteristics with time. Convective acceleration effects in the area of the jet position sensors are responsible for acceleration sensitivity. Imperfect matching of the two pick-off elements causes temperature sensitivities. Parameter stability (drift) and convective acceleration sensitivity have been reduced to tolerable levels for applications being considered, but remain the major areas of concern for future development.

Two of the early experimental fluidic angular rate sensors having the self-contained, no-rotating-parts pump have been operated continuously at APL for approximately two years (a total of 17,000 hours each) to determine life and stability characteristics. ABL has a similar unit that has operated for the same length of time. This is a total of 51,000 operating hours on the three sensors without any failure. The output wander for zero input rate has been monitored during the life testing. The rate of the "zero" drift has decreased from 0.043°/sec/day to 0.001°/sec/day. This indicates that the sensors get better with age, as was expected. The fluidic angular rate sensor therefore has all the advantages of fluidic elements, i.e., low cost, long life, and ruggedness.

The jet fluidic angular rate sensor is capable of exceptionally high over-ranging without any degradation of performance thereafter. If you highly over-range a gyroscope, you either destroy it completely or permanently change its performance parameters. The usual procedure using rate gyroscopes for such an application is to specify the highest expected rate and then suffer poor performance when operating in the low rate range because of the dynamic range limitation of the sensor.

Before comparing the merits of the jet fluidic angular rate sensor with those of another fluidic angular rate sensor—the vortex type—a brief explanation of the vortex type must be given. The vortex type fluidic angular rate sensor, utilizes a two-dimensional radial sink flow created by fluid flowing from a porous wall into a centrally located sink. This becomes a spiral sink flow when the

system is subjected to a rotation about the sink axis. Case rotation about this axis imparts a tangential component (relative to fixed coordinates) to the radially flowing fluid. Since angular momentum is conserved, a free vortex is generated, increasing the angular velocity of the fluid and resulting in an appreciable value at the sink relative to that at the wall. Tangential pitot tubes located near the center of rotation sense the dynamic pressure caused by the increase in tangential velocity of the fluid over the tangential velocity of the case. Both the sense and the magnitude of the input angular rate are contained in the pressure measurement.

In making a comparison between these two types of fluidic angular rate sensor the following conclusions are apparent. The jet unit has the advantage of simplicity, smaller size, smaller flow, smaller power requirements, and a much higher signal-to-noise ratio. The vortex type rate sensor must have a very high volume rate of flow to reduce the transport delay time. The result of this is turbulence which introduces noise into the receiver area. The jet fluidic angular rate sensor operates at a low Reynolds Number (<500) which is well within the requirement for laminar flow. The vortex type rate sensor must have a large diameter since gain is proportional to diameter and it also requires a precision machining effort. The vortex type rate sensor has gone through approximately nine years of extensive development both by industry and by government as a rate sensor that is useful in fluidic systems. However, its limited dynamic range, high power requirement, and large size have limited its use to the all-fluid systems.

Development of the jet fluidic angular rate sensor continues in both theoretical and experimental areas to establish the performance capabilities and limitations of the basic sensor. It is expected that the sensor will find its way into shipboard systems and other applications where frequency response does not limit its usefulness.

ADDRESSES

Principal recent addresses made by APL staff members to groups and organizations outside the Laboratory.

The following four addresses were given at the 1968 Fall Meeting of the *American Physical Society,* Miami Beach, Florida, November 25-27, 1968:

R. Turner and T. O. Poehler, "Far-Infrared Laser Diagnostics of Transient Plasma;"

W. R. Powell, "Spectroscopic Measurement of Electron Concentration;"

H. M. Stainer, "Some Consequences of Rotation in a Model Theta Pinch;"

C. S. Leffel, Jr., "Ion Analysis of a Theta-Pinch Gun."

R. W. Cole, "Responsibilities, Activities, and Procedures of the Satellite Reliability Group at APL," *Baltimore Chapter, IEEE Reliability Group,* Baltimore, January 27, 1969.

D. D. Zimmerman and R. E. Hicks, "Preparation of Substrates with Bumps for Face-Down Bonding of Hybrid Components," *National Electronics Packaging Conference,* Anaheim, California, February 11-13, 1969.

M. H. Friedman, "Free Swelling of Biological Tissue. The Corneal Stroma," *American Institute of Chemical Engineers, 64th Annual Meeting,* New Orleans, Louisiana, March 17-20, 1969.

W. H. Avery, "Aerial Car Transit System," *New York University Seminar,* March 21, 1969.

V. O'Brien, "Large Circulating Drops in the Gravity Field," *International Union of Applied and Theoretical Mechanics, Symposium on Flow of Fluid-Solid Mixtures, University of Cambridge,* Cambridge, England, March 23-29, 1969.

The following three addresses were given at the *American Physical Society,* Philadelphia, March 24-27, 1969:

F. J. Adrian, E. L. Cochran, and V. A. Bowers, "ESR Spectrum and Structure of HNO_2^- in KCl;"

F. J. Adrian, E. L. Cochran, and V. A. Bowers, "CN Stretching Vibration in HCN;"

J. Bohandy, J. C. Murphy, and A. N. Jette (APL) and D. O'Shea and C. M. Wilson (The Johns Hopkins University), "Raman Scattering in X-irradiated KCl-Ag Crystals."

L. Monchick, "Calculation of Ortho-Para Hydrogen Scattering Cross Sections," *The Johns Hopkins University, Department of Chemistry Colloquium,* Baltimore, March 25, 1969.

R. A. Dickman, "The Use of Functional Job Analysis as an Aid to Personnel," *American Personnel Guidance Association,* Las Vegas, Nevada, April 1, 1969.

A. A. Westenberg, "Atom-Molecule Kinetics Using ESR Detection," *Interagency Chemical Rocket Propulsion Group,* Cleveland, April 10, 1969.

W. E. Radford and R. L. Hickerson, "Measurement of Earth Magnetic Field Oscillations at Synchronous Satellite Altitudes," *1969 International Conference on Magnetics (INTERMAG),* Amsterdam, The Netherlands, April 15-18, 1969.

K. Moorjani, "Elemental Amorphous Semiconductors," *Physics Department, University of Maryland,* College Park, April 17, 1969.

E. Maumenee, L. V. M. Hyvarinen, and T. George (The Johns Hopkins University), and J. T. Massey and B. F. Hochheimer (APL), "Fundus Camera for Retinal Fluorescence Cinematography," *Bascom Palmer Eye Institute, Department of Ophthalmology, University of Miami,* Miami, Florida, April 20-23, 1969.

CHARLES R. BROWN and CHARLES F. MEYER

THE TALOS CONTINUOUS-ROD WARHEAD

INTRODUCTION

The warhead developed by APL for the Unified Talos (SAM-N-6c1) missile was a significant milestone in ordnance technology. Performance objectives were achieved with a configuration in which a double layer of steel rods, welded at the ends to form hinge joints, was accelerated by the detonation of a cast explosive. Structural damage to the target was achieved by the impact of the steel rods projected at high velocity in an expanding circular pattern (Fig. 1). This was shown to be a highly effective counter to any manned aircraft, such as a heavy bomber. An accurate fuze was employed to control burst position so that the rods would strike the target.

The continuous-rod warhead evolved from consideration of the lethality of chunky fragmentation devices and their inability to inflict a decisive kill on a manned aircraft. The optimum fragment velocity for effective target penetration was shown to be considerably higher than that of about 3000 feet per second from an antiaircraft shell. Considerable improvement in lethality was observed when the chunky fragments from a 3-inch/50 shell were replaced by small discrete rods.

A quick, decisive kill was shown to be feasible when a long rod sufficiently damaged the aircraft structure so that failure resulted from normal aerodynamic flight loads. Ordinary fragments, while adequate for damaging vital components, cannot produce such structural failure. The continuous-rod concept was born in 1952 with the suggestion that the rods be connected end to end, thereby providing the capability of inflicting a continuous "line" of structural damage over the target surface.

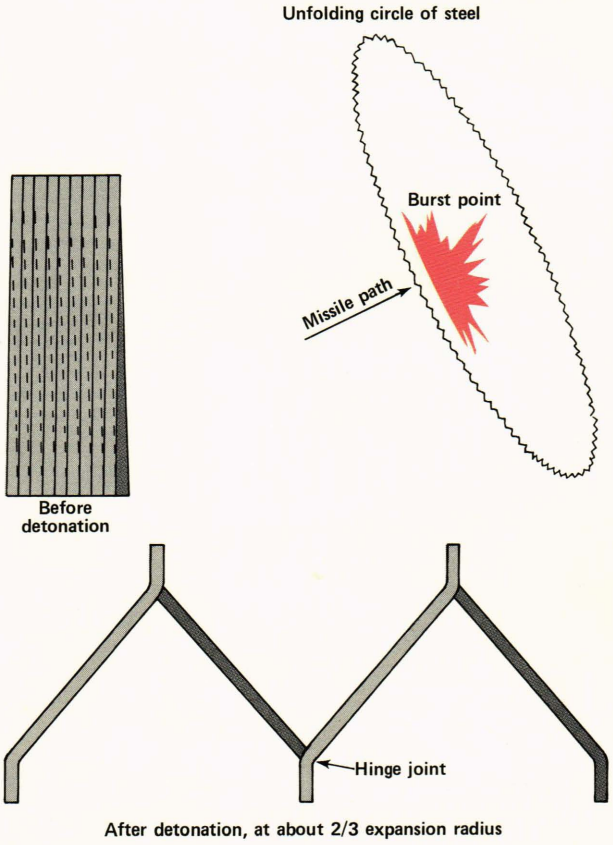

Figure 1 — The continuous-rod warhead was designed to produce an expanding zigzag ring of connected rods. The rod structure expanded like a folding rule.

WARHEAD DESCRIPTION

The Mk 46 continuous-rod warhead, developed for the Unified Talos 6c1, is shown schematically in Fig. 2. Each pair of a double layer of 0.25-inch square rods, 19.25 inches long, was resistance welded at the ends to form a hinge joint. The rods were welded together in two flat sections that were connected by two heli-arc welds after assembly on the cylindrical surface. At the explosive-rod interface, two filter layers — a 0.062-inch layer of steel and a 0.025 inch layer of lead — helped to reduce the explosive shock effect on the steel rods, the steel filter being part of the basic warhead structure. Structural rigidity was achieved by a 0.035-inch steel stress skin over the rods; both rods and stress skin were welded to steel end rings.

Detonation of the explosive composition, nominally 25% RDX and 75% TNT (cyclotol), was centrally

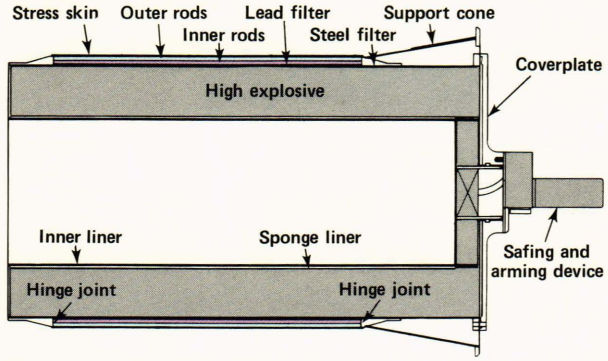

Figure 2 — The Unified Talos 6c1 Mk 46 warhead was a hollow cylindrical structure. Quarter-inch rods arranged in a double layer and surrounding the explosive charge were welded at the ends to form hinge joints. At the explosive/rod interface, two filter layers — a 0.062-inch layer of steel and a 0.025-inch layer of lead — helped reduce the explosive effect on the steel rods.

initiated at the aft end where the detonator and booster were part of the overall safing and arming assembly. A silicone sponge liner was used on the approximately 8.7-inch outer diameter steel inner liner to prevent cracking from shrinkage of the explosive caused by cooling in the casting process.

The overall weight of the warhead was about 465 pounds, and the explosive load was about 225 pounds. Warhead length, not including the end plate and the safing and arming device, was about 29.5 inches and the diameter of the section comprising the rod assembly was about 16.8 inches.

The location of the warhead within the missile structure is shown in Fig. 3. The blowthrough area is the section that has the most effect on warhead performance. Lockfoam was used between the warhead and the inner-body cowl as a cushion to prevent the rods from damaging the magnesium cowl. Coaxial cables, pitot tubes, and their fairings were designed for the most practical, circumferentially uniform distribution of mass to minimize rod breakup.

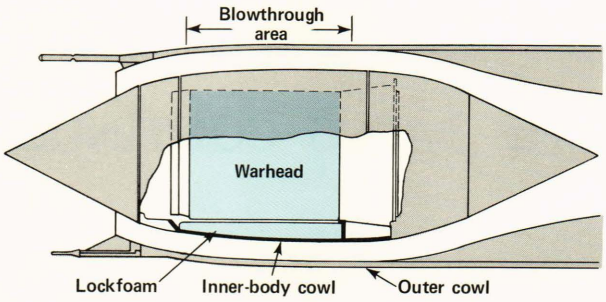

Figure 3 — The missile and warhead structure was designed to place the warhead in the inner body of the multiple-shock diffuser. Lockfoam was used between the warhead and inner-body cowl as a cushion to prevent the rods from damaging the magnesium cowl. Coaxial cables, pitot tubes, and their fairings were distributed to minimize rod breakup.

DEVELOPMENT AND PERFORMANCE OF THE TALOS WARHEAD

Problems solved during the development of the Mk 46 warhead were associated with preventing rod deformation, controlling initial rod motion so that a nearly unbroken rod pattern persisted to the maximum radius, and producing rod velocities high enough to inflict structural damage on the target.

Fastax camera coverage of static testing of the warhead in an arena of steel witness plates (Fig. 4) provided valuable performance data on rod continuity, rod pattern, and velocity. Extensive recovery of sample rod strands yielded vital information on hinge opening and the metallurgical properties of the rods.

The missile structure had a strong influence on warhead performance. About 30% of the kinetic energy of the rods was lost in the process of blowing through the substantial missile structure. The initial velocity was reduced from about 5300 to about 4600 feet per second, a useful speed. However, rod continuity seemed to be somewhat improved because gapping between inner and outer rod layers was reduced.

The maximum radius of continuity was 90 feet. Ideally the rods would produce a uniform "saw-

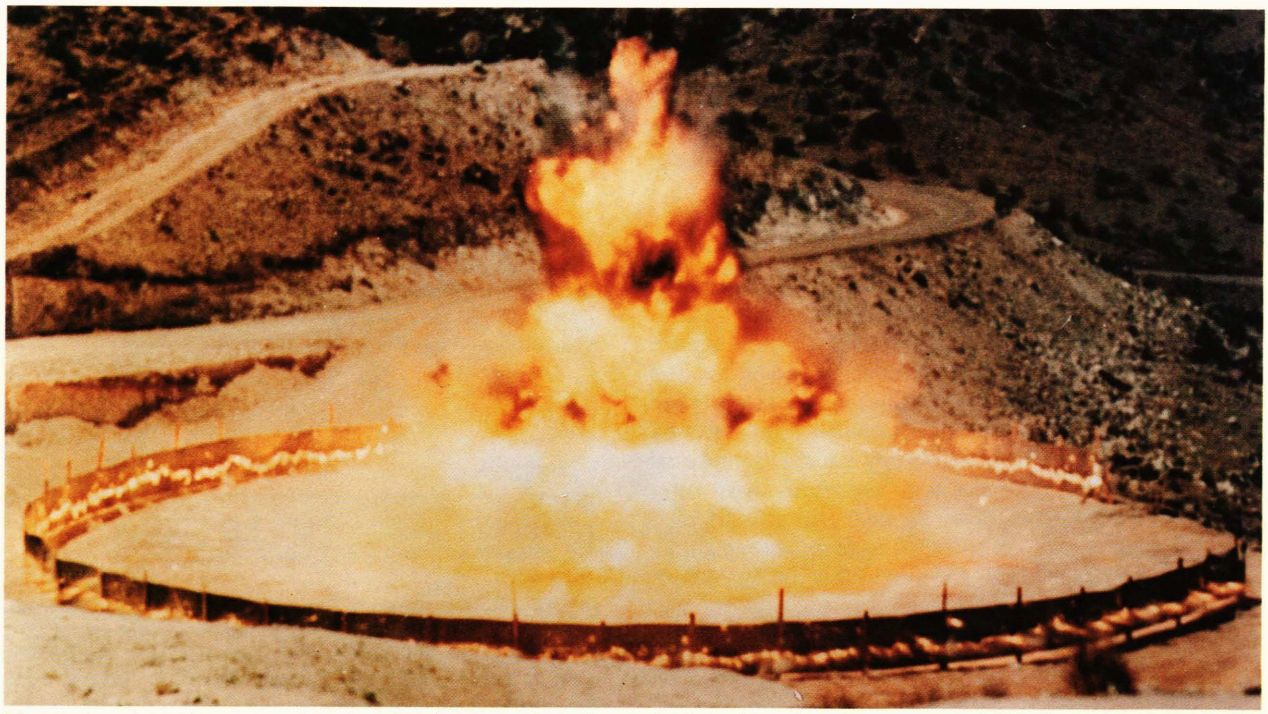

Figure 4 — A continuous-rod warhead test demonstrated an unbroken ring of continuous rods. This photograph shows the continuous rods striking steel target panels located near the maximum possible continuity radius.

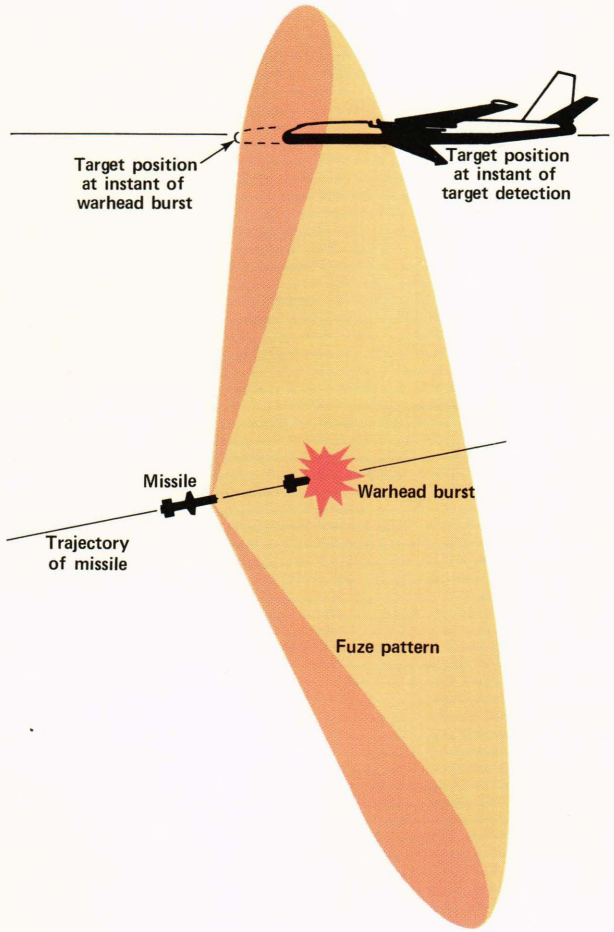

Figure 5 — Warhead burst position was controlled to obtain maximum effectiveness of the continuous-rod warhead. The target was detected by a short-pulse range-gated radar having a fixed-angle antenna pattern. The time delay from detection to burst was controlled by the missile-to-target closing speed.

tooth'' pattern during expansion in such a way that all rods would break simultaneously at the hinges when the maximum radius was reached. In practice, the expansion was not uniform, and some hinges would always break prematurely. Typical continuity performance was 100% out to a radius of 60 feet, with a degradation to 90% at 90 feet.

The hinge weld played an important role in preventing excessive premature rod breakage. It consisted of a strong weld in a primary region and a weaker weld in a secondary region. Progressive failure of the secondary weld helped to control the bending radius during the expansion process, while the primary weld remained intact.

FUZE

The final fuze version (Mk 52), designed by the Naval Ordnance Laboratory, Corona, Calif., was a short-pulse-radar, range-gated device having a fixed-angle radiation pattern (Fig. 5). A sea tracking gate

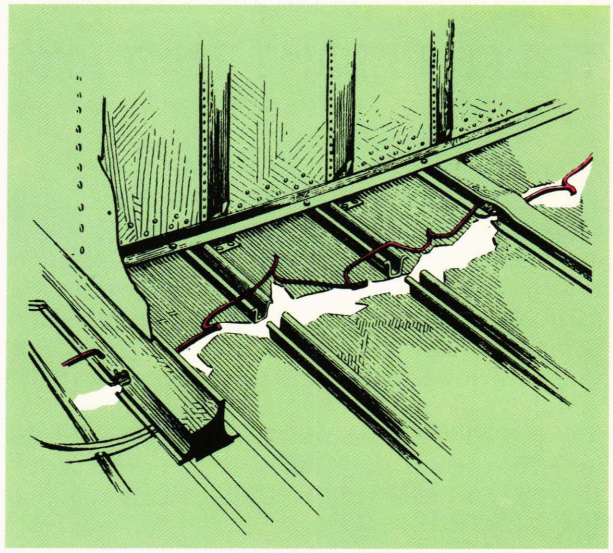

Figure 6 — Cutting action of the rods across the target surface could lead to structural failure and therefore produce a quick kill.

was included to prevent premature firing on the sea when intercepting very-low-altitude targets. The warhead was fired by a signal originating from a valid target detection or by fuze-on-jamming action. The missile-to-target closing rate controlled the time delay of the burst so that optimum effectiveness was achieved.

Analyses of time delay requirements were performed for a variety of targets, intercept-approach aspects, and altitudes. Suitable constants for the time-delay equation were thus derived for optimizing hit probability.

TARGET DAMAGE

The nearly continuous cutting action of the rods across the target surface could lead to structural failure and therefore produce a quick kill. Complete severence of the structure was not necessary. For example, if the skin and stringers of a wing were severed and the heavy spars damaged, the wing could fail under a 1g flight load (Fig. 6).

Structural damage by the impact of rods required a sufficient mass, high impact velocity, and a continuous strand of unbroken rods. For quarter-inch rods, a minimum striking velocity of about 3500 feet per second was necessary to produce structural damage to most aircraft.

Experiments showed that a rod that struck a thin target edge-on tended to break into two pieces during the damaging process. The amount of damage produced greatly depended upon the ability of the rod to resist being pulled apart. On the other hand, a rod striking a target whose thickness was much larger than the rod's thickness was broken into three pieces, the center portion contributing the most to the damage.

APL *and the* VT FUZE

The inexorable movement of the United States toward entry into World War II gave great urgency, in 1940, to the search for new weapons with which to combat a massive enemy air threat. Among many such weapons long envisioned was the proximity fuze—a mechanism for detonating an explosive shell within kill range of an aircraft. While this had long been considered impossible to attain, a project was nevertheless launched in mid-August 1940, to investigate three possible mechanisms for this type of fuze: photoelectric, acoustic, and radio.

Fuze Program Begins

On June 27, 1940, the National Defense Research Committee had been founded, with Dr. Vannevar Bush as its chairman, to serve as a functioning link between the National Academy of Science and the military services. This organization, comprised of eminent scientists and educational leaders, was divided into divisions, of which Division A was to give its attention to problems of armor and ordnance. Division A was further broken down into working teams, or sections, which would investigate certain well-defined problems. One of these had assigned to it the search for a proximity fuze; this was Section T, with Dr. Merle A. Tuve as its chairman (each section was known by its chairman's initial). At the time of his appointment on Aug. 24, 1940, Dr. Tuve was a member of the staff of the Department of Terrestrial Magnetism of the Carnegie Institution in Washington, D. C.

From August 1940, until early in 1942, the radio shell fuze moved at a fast pace through the phases of idea conception, search for components, testing, redesign, firing tests, and organizational growth in both numbers of personnel and the size of facilities required. By Sept. 1941, after frenzied effort, a complete fuze had functioned properly at the end of its trajectory in a test firing. By Jan. 1942, a production contract for a basic model of the fuze, for Navy 5-in. guns, could be written.

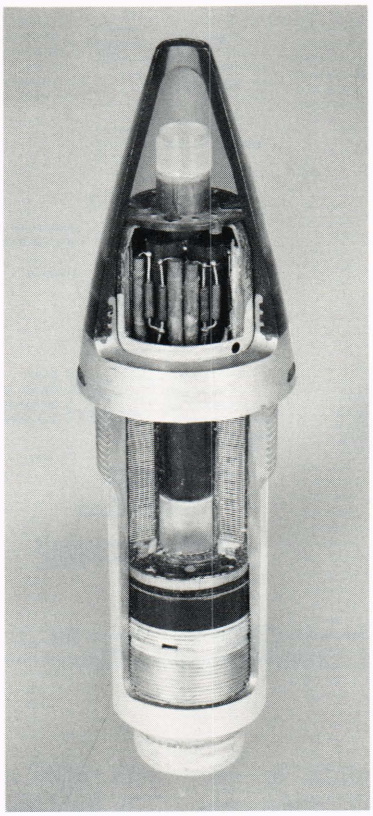

Cutaway view of a typical VT fuze.

The VT (variable time), or proximity, fuze is clearly described by the Bureau of Ordnance: the configuration selected as most promising for anti-aircraft use was one "in which the transmitter and receiver were both located on the projectile. This . . . self-contained unit functions by transmitting a continuous pattern of [radio] waves in space. These signals are reflected back to the oscillator by any target that gives a radio reflection. At first the projectile is so far from the enemy that the signals are not returned with any strength. As the projectile nears the target, however, the reflected waves picked up by the oscillator grow stronger. The outgoing and incoming signals then interact to create a "ripple" signal which is amplified by vacuum tubes. When the projectile comes within a radius of about 70 feet from the target, the ripple pattern becomes strong enough to trigger the thyratron tube that serves as a switch. That action releases the electrical energy in a charged condenser, and the current, in turn, initiates an explosion in the electrical detonator, or squib. That blast activates the standard electrical detonating fuze which sets off the main explosive charge in the projectile. If the triggering pattern of the fuze coincided with the fragmentation pattern of the shell, a "kill" was probable. . . . In completed form, the VT fuze consisted of four principal parts: A radio frequency oscillator and receiver, an amplifier and thyratron tubes, a battery, and an explosive train incorporating vital safety features."[1]

Paralleling the scientific effort in developing the so-called VT fuze, the organization supporting the work was growing apace. Early work, with a handful of scientists, was done at the Carnegie Institution Department of Terrestrial Magnetism. When the proximity fuze had emerged from the "impossible" category and was firmly seated in the "probable," the need for more space became desperate. In consequence, all of Section T's work on projects other than the shell fuze was removed physically and organizationally to the Bureau of Standards.

Founding of APL

This move proved to be only temporary relief, however, with the ultimate result that on Mar. 10, 1942, a contract was signed by the Office of Scientific Research and Development and The Johns Hopkins University which stipulated that the University would furnish laboratory space, equipment, test site, and additional

[1] B. Rowland and W. B. Boyd, "U. S. Navy Bureau of Ordnance in World War II," U. S. Government Printing Office, 1953, 278–279.

personnel for furthering the VT fuze program. Dr. Tuve was to continue as head of the program, and overall administration was transferred to the OSRD. Dr. Tuve conceived the name "Applied Physics Laboratory" for the new organization operating under The Johns Hopkins University.

With this brief background of the emergence of the VT fuze, we may now look in some detail at the vastness of the fuze program and at its impact on the unfolding drama of World War II*.

The Johns Hopkins University entered upon its new responsibilities in a manner that gave promise of continued rapid progress in the development of the VT fuze. The President of the University appointed D. Luke Hopkins, member of the Board of Trustees, as the official representative of the University in all matters pertaining to APL. Mr. Hopkins stated that the University's purpose was "to see to it that the job progressed as smoothly, expeditiously, and efficiently as possible."

The immediate task, of course, was to provide whatever was most needed to enable Section T's expanding program to be carried on effectively by the newly established Applied Physics Laboratory. The most important and most obvious requirement was additional personnel, but before new staff could be taken on, office and shop space adequate to accommodate them had to be acquired. In Silver Spring, Md., a sparsely settled cross-roads community at the time, a garage was found which, it appeared, would serve well for the present at least.

Lease of this property, 8617 to 8621 Georgia Ave., was arranged by the University to include not only the garage floor but also the second and third floors which were then occupied by a Social Security office. Many problems in adapting this building for use by the new Laboratory were overcome in a short time in spite of wartime limitations on materials and a tight labor market. The date of May 1, 1942, may be considered to mark the start of operations by APL at the Silver Spring location.

The pressure for still more space continued, however. The rapidly expanding program seemed always to be exasperatingly ahead of the available physical facilities. In spite of a new building constructed just north of the garage, plus two new floors added to the original building, and a new connecting building, the space available for the Laboratory's work never seemed to be adequate.

Needed facilities other than space to house the Laboratory included a new test field equipped with shelters for the personnel conducting tests, machine tools, instruments of various kinds, and other related equipment for laboratory and field use. A suitable site at Newtown Neck, Md., was leased and equipped for the safe conduct of vertical recovery firings.

In spite of the many details that had to be taken care of in the relocation to Silver Spring, and the establishment of new administrative and communications channels, these tasks were accomplished in good time. The increase in staff from 100 in 1942 to 700 in 1944, under difficult conditions imposed by the need for complete secrecy, probably could never have been done under the restrictions that had existed before the entrance of The Johns Hopkins University in the role of contractor-operator for the OSRD.

Problems of Design

Recalling Dr. Tuve's statement that the success of this type of fuze was dependent on a great number of empirical factors, each dependent upon design of specific components, we can appreciate the need for the continuing program of testing. This included complete fuzes as well as tubes, oscillator circuits, detonators, explosive charges, and other components. Among the latter were the safety switches to prevent the shell from exploding either in the bore of a gun or within 0.3 to 0.5 sec after leaving the muzzle, and self-destruction mechanisms designed to explode the shell after it had passed beyond the target. The self-destruction feature was incorporated to prevent friendly units near the line-of-fire-extended from being endangered and enemy forces from having an opportunity to recover a dud. These components were tested under all conceivable operating conditions for all sizes of guns for which radio fuzes were to be produced, as well as for various changes in design intended to correct previous test failures. The search for glass rugged enough to withstand the shock of gunfire was constant, as it was for filaments, bridge wire, and wax. Even after the fuzes were in production, the test program objectives persisted in the quality control program.

Illustrative of the experience that supported the need for the continual program of testing, even through quantity production, is Dr. Tuve's summarization of the development of rugged tubes:

"Empirical factors enter in other ways than performance. For example, some design factors unpredictably limit production. We started five companies on the design and manufacture of rugged tubes, during 1940 to 1942. All designs were successfully rugged and made into successful fuzes. One failed to make them on anything but a laboratory basis, although large amounts of money were spent on pilot production lines during two years. The second has made rugged tubes continuously since early 1941. Maximum production ever reached was 4000 per day, with limited use of these tubes as substitutes. The third company started 1940 with fairly successful tubes, kept in production to early 1944, but could never exceed 20,000 per day because the design was not adapted to fast production. . . . The fourth company is now our primary supplier (260,000 per day). The fifth company made two million tubes, but characteristics were poor and fuzes variable. The tubes were set aside and production stopped early in 1943. (The sixth company was started and factory built but the factory was turned over to other work at our request.)"[2]

Mass Production Begins

As the first of the production fuzes became available, the need for carrying the test program still farther was recognized. Until that time,

* These historical notes are adapted from a history of the Applied Physics Laboratory being prepared under the direction of Rear Admiral M. R. Kelley, U. S. Navy (Ret.), assisted by staff members of APL.

[2] Letter from M. A. Tuve to Lt. Col. C. F. Fell, Army Member of JPS Subcommittee; subject, "Confirmation of Important Features in Development and Production of VT Fuze," Sept. 28, 1944.

operation of the fuze test samples had been checked only by firings in which the radio waves that triggered the fuze were reflected from the water as the shell returned to the surface on the downward leg of its trajectory. A test that more accurately represented a shell approaching an aircraft was obviously needed. This was done for the first time at Parris Island in April 1942, when a full-scale aircraft target suspended from a balloon triggered the fuze. Later, chicken wire replicas of full-scale aircraft were suspended between two towers, and test fuzes were fired at them for determination of operational performance. Tests of production fuzes were then conducted against drone targets in Chesapeake Bay from the USS *Cleveland*. The three drones allotted to this series of tests were destroyed on the first day of firing by four proximity bursts. Because of this success, these realistic tests were considered a final "dress rehearsal" for the shell radio fuze before its first appearance in a theater of combat. From these results, specifications for a quantity production fuze were crystallized and production began.

High Priority of Safety

For the many models of the shell radio fuze that were manufactured and/or tested, exceptional care was taken to safeguard personnel against bursts in handling or in the bore of the gun, and to insure delay in postfire arming. The standard of safety set up as a requirement was no more than one muzzle burst in a million rounds.

Not only in the design of the safety and arming element was such care taken, but also in the inspection and test program. An example will show the painstaking care used to prevent accidental bursts. The mercury unshorter switch was designed to prevent operation of the fuze during handling and loading and to insure that the shell could not be exploded until it had traveled a certain distance from the muzzle. It was cylindrical in shape, slightly over 0.25 in. in diameter, and about 0.4 in. long. Inside an outer chamber or sump, which was empty prior to high-speed spin of the projectile, was an inner chamber filled with mercury. In this location the mercury maintained an electric short in the cannon-primer circuit so that it could not be fired. The wall of the inner chamber was a diaphragm of relatively porous material through which the mercury could pass under centrifugal force generated by the post-firing spin of the projectile, thereby removing the short in the primer circuit. The purest mercury obtainable commercially was procured for this use, but it was nevertheless subjected to additional distillation before it was considered to have the required purity. Selected samples of the thousands of switches manufactured daily were then spun at a rate to produce the centrifugal force resulting from the projectile spin after firing. The time required for the mercury to pass through the diaphragm was accurately determined and, for acceptance, had to lie within specified limits. Rough handling tests of the switches followed, with each checked by X-ray to insure that it met the prescribed standards. Under a regime of such supervision and testing it is easy to see why safety provisions proved so successful.

Military Demands

In the spring of 1941, priorities had been established to meet requirements of the armed forces in the following order: U. S. Navy, British Navy, U. S. Army, and British Army. Because of the optimism that had grown in the Section T program, the U. S. Joint Chiefs of Staff considered the matter of time and place of introducing the fuze into the various areas of combat operations. The above priorities reflected the viewpoint of the Joint Chiefs in their concern lest the fuze fall into enemy hands shortly after its initial use in combat. This would have made it possible for the Axis powers to develop counter-measures to reduce the effectiveness of the fuze and/or to develop their own versions of the fuze. If either had resulted, the advantage to the Allies of sole possession and use of this new weapon would have been substantially reduced. Aside from the fact that the U. S. Navy had assigned the highest priority to the shell radio fuze and was supporting its development in every possible way, there was, of course, the obvious fact that use of the fuze by naval forces afloat would greatly reduce the likelihood of its being recovered by the enemy.

Colonel H. S. Morton and Drs. L. R. Hafstad and M. A. Tuve (l. to r.) examine early VT fuzes for use in Europe.

With quantity production of a fuze for the Navy's 5-in. guns getting underway in the fall of 1942, a very urgent problem which had already been recognized came to the fore. This was the need for appropriate steps to be taken to indoctrinate the combat forces in its proper handling and use. A necessary follow-on of utmost importance was to build up their confidence in its capabilities so that they would overlook no opportunity to use it in action. Once they had seen results, it was felt by those who were engaged in the development and test program, and by those of the Navy who had followed this program closely, that the users would be enthusiastic.

The proximity fuze did not present the kind of breakthrough that would at once demand a change in either the strategy or tactics of the allied forces. Rather, it gave promise that the strategic plans already in effect, and the tactics being employed, could be confidently adhered to with the expectation of a decisive victory. Without the new fuze, on the other hand, revision of both strategy and tactics at the appropriate levels might be forced upon the Allies because of their losses to attacking aircraft and the German V bombs.

Experienced officers in the Navy Bureau of Ordnance who had close contact with the fuze program were quick to see that indoctrination of the fighting forces in its capabilities and use was of utmost importance if the full benefits of this new weapon were

to be reaped quickly. And Dr. Tuve's instruction on the subject of Section T's moral responsibility would clearly indicate what importance he attached to such indoctrination.

The Fuze Goes into Action

Since the Combined Chiefs of Staff felt strongly that the fuze should not be used where a dud might be recovered on the ground, the South Pacific, where Japanese land-based aircraft were a constant and serious menace, seemed the area of first importance. First deliveries of the new fuzes, then, were to be made to ships in that area having the 5-in. guns for which the earliest production fuzes were designed. During October 1942, 500 fuzes for shipboard use were produced each day and shipped immediately to the Naval Ammunition Depot, Mare Island, where they were inserted in the fuze cavities of 5-in. shells. Of each day's consignment, 10% were withdrawn and flown back to the Naval Proving Ground, Dahlgren, Va., for test. When 5000 proximity-fuzed projectiles had accumulated, Commander W. S. Parsons, Special Assistant to the Director, OSRD, went to Mare Island to supervise loading of the shells for air transportation to Pearl Harbor. He then flew to Hawaii, leaving the ammunition in the care of three scientists from APL specifically commissioned for this duty: Lieutenants N. E. Dilley, R. P. Petersen, and J. A. Van Allen.

First Strike—Pacific Theater

At Pearl Harbor the shells were loaded into the aircraft tender USS *Wright* for transshipment to Noumea, New Caledonia, where Commander Parsons reported to Admiral Halsey. Three ships of the Third Fleet received portions of this first shipment—USS *Enterprise*, USS *Saratoga*, and USS *Helena*—and indoctrination of their personnel commenced immediately. There was a period of relative inactivity in the Third Fleet area at the time, extending into the early months of 1943, an excellent time for indoctrination but giving little opportunity for battle test of the new fuze. On Jan. 5, 1943, however, a Japanese plane was destroyed by a proximity fuze, the first of a long record of encouraging successes that made such an important contribution to total Allied victory.

The Problem of the Fuze in Europe

In addition to the three APL scientists commissioned to assist in introducing the new fuze to Pacific Fleet units, two other APL staff members had been selected for the same duties in the Atlantic and Mediterranean areas: Lieutenants E. R. Chatham and R. Morison. But introduction of the fuze in these areas was intentionally delayed about six months for several important reasons. First, the waters in which the Pacific Fleet units were operating were of appreciably broader expanse and were much less likely to be monitored by high-performance radio countermeasures and direction-finding equipment at strategic points on land. It was thought that the Germans would be much more likely than the Japanese to have such equipment, and at this stage of the war would no doubt have the vital sea areas well monitored. Another factor was that injection of the fuze into combat situations on a broad scale would require time in which to check out battery personnel, tactics, fuze performance under shipboard conditions, and indications of enemy jamming. Early experience gained in the Pacific could be used to modify defects in the fuze, develop the most effective tactics for its use, and check out logistics and handling problems. Successful introduction of the fuze into the Atlantic and Mediterranean areas would be greatly aided by this experience, especially if its safety and performance record proved to be all that was desired.

The VT fuze on Iwo Jima in 1945.

The Navy's indoctrination team arrived in the Mediterranean in the closing days of the North African campaign and had completed introductory instruction for all concerned by the time the Sicilian operations got under way. Confidence in the new fuze was more easily built up because action reports from the Pacific were available to bear out the claims of the instruction teams.

On the Army side, a well-planned program of indoctrination was put into effect. Colonel H. S. Morton, assigned as the Army's liaison officer to Sections T and E, and later to APL, was a key figure in this program. As early as Sept. 1942, the Army had asked for 1,000,000 proximity fuzes. Accompanied by transfer of the necessary funds to support the stated requirement, this indication of faith in the project was of vital importance to its continued progress, especially when the Army's primary effort and financial support had been directed to the photoelectric fuze project of Section E.

Colonel Morton was sent to Europe where, from the beginning, he talked about the proximity fuze to any and all officers who would listen to him. Those in the highest command echelons, as well as officers in the lower echelons who would have the responsibility for using the fuzes in battle, were given thorough briefings on it and on the advantages it offered for use against both ground and air targets. Some of them, of course, already knew about the fuze, and some undoubtedly felt that this was a new "gimmick" that might be worth a try.

Colonel Morton outlined the most effective methods of employment over different kinds of terrain and against low- and high-altitude air attack; also, the dangers involved for U. S. observation aircraft engaged in spotting artillery fire. For the field artillerymen especially, the fuze promized to be an ideal solution to the problem of putting bursts at an optimum altitude above the ground when used against personnel and other battlefield targets.

A pattern of bursts of VT-fuzed anti-personnel shells over a battlefield in France during World War II.

APL Keeps Pace with Changing Demands

As a build-up for indoctrinating the fighting forces in use of the fuze, Dr. Tuve had seen early the desirability of instructing Army and Navy personnel in the design, inspection, handling, and functioning of proximity fuzes. This was in line with his views that the fuze must be closely followed by APL right to the field of battle. The Ordnance Department of the Army, fully appreciating the importance of a program to introduce the fuzes to appropriate Army units, selected 200 officers and men for training at APL and at the Bureau of Standards. These men participated in certain phases of the development work at the laboratories and in field testing, as well as in those methods of handling the fuzes that were pertinent to battlefield operations. The Navy also selected officers and men for advanced training in the shell radio fuze at APL. The trainees of both Services contributed in no small degree to the success of the entire program.

With the start of quantity production in the fall of 1942, many complications arose, resulting in part from the priorities established by the Combined Chiefs of Staff. Many diverse requirements had to be satisfied within a time scale that would permit each of the military forces to bring its full weight to bear in execution of the overall strategic plan. The basic design of the proximity fuze for the Navy's 5-in. guns could not, merely by a process of rescaling the dimensions, be readily adapted for use in the various types of guns in the other three military organizations. There were differences in caliber, muzzle velocity, rate of projectile spin, handling and loading equipment, and of course in the basic missions for which each was designed.

A measure of these complexities is obtained when we note that there were eight models of the shell radio fuze required for the U. S. Navy, four for the British Navy, twelve for the U. S. Army, and six models for the British Army. The modifications that were needed introduced some fears that a modified fuze might prove unsafe in its handling, loading, and firing cycle; hence, the seemingly endless program of testing this one feature continued to demand the greatest care. As if these problems were not complicated enough, many planners and operators in the using services were changing their minds at frequent and unpredictable intervals concerning the number of fuzes of each model they would need.

The Applied Physics Laboratory was not, of course, in the business of producing these different types of fuze. However, APL had the principal responsibility for the design adaptations, a responsibility which certainly could not be dropped at the moment the modified fuzes were put into production. Without full cooperation of the many industrial contractors under Section T, this responsibility could not have been discharged.

The extent of the industrial participation in the program has been succinctly summarized in the official history of the OSRD as follows:
"In the months just preceding V-J Day (there was no slackening in the work of "T" after V-E Day) the Central Laboratory at Silver Spring was the nerve center of a vast, country-wide activity. Five major plants were rolling out some 70,000 VT-Fuzes a day—millions of tiny radio sets designed to "play" for a few moments! Feeding these assembly plants (Crosley, Sylvania, RCA, Eastman Kodak, McQuay-Norris) were a host of more than 2000 interlocking suppliers and subsuppliers. The Sylvania Company, with 23 plants in the eastern part of the United States, supplied over 400,000 tubes per day; the National Carbon Company, with a major plant at Winston-Salem, North Carolina, constructed especially for T, and the Eastman Kodak and Hoover Companies were turning out one tenth of a million batteries a day."[3]

Production Miracle Reviewed

In view of the many complexities of the program, the actual production of proximity fuzes assumed the status of a miracle, as a few figures will indicate. Assembly of production fuzes began in Sept. 1942 and averaged 500 a day during the first month. A little more than a year later (Dec. 1943), 1,164,000 fuzes had been produced for the Navy and 126,000 for the Army. During 1944, a total of 8,301,000 fuzes were produced. By the end of that year, more than 40,000 proximity fuzes per day were coming from the assembly lines. Altogether, 22,073,481 fuzes were produced up to Aug. 14, 1945.

The development and manufacture of proximity fuzes was one of the best-kept secrets of the war. For reasons already given, it is well that this was the case. The success with which the secret was kept seems no less a miracle than the production miracle, in view of the fact that an estimated one million persons participated in the research, development, and production of the fuze in the United States, and in its use in combat. The extraordinary precautions taken to insure this secret are a fascinating story in themselves.

As stated by Admiral Ernest J. King, then Commander in Chief of the U. S. Fleet, "the development of the VT fuze was a major scientific achievement that has contributed greatly toward winning the war for the United Nations."

---

[3] "New Weapons for Air Warfare," ed. by J. C. Boyce; Little, Brown and Co., Boston, 1947, 172. This is one of a series of volumes of the official history of the Office of Scientific Research and Development.

TALOS FLIGHT TEST FACILITIES

From February to December 1945, flight tests to support propulsion and aerodynamic studies for the development of Talos were conducted at Island Beach, N.J. Activities were then transferred to Fort Miles, Del., pending the opening of the Bureau of Ordnance's east coast range at Camp Davis, N.C. Camp Davis was deactivated in 1948 because of lack of funds, and all flight testing in support of Talos was shifted to the Naval Ordnance Test Station (NOTS), China Lake, Calif. Testing of steering test vehicles was undertaken at NOTS as early as August 1945.

Most early flight tests in support of the development of the guidance system were conducted at NOTS. Large (18-inch diameter) ramjet test vehicles were also tested there during the period from 1946 to 1950. When test requirements exceeded the available range at NOTS, the testing was shifted to White Sands Proving Ground, now White Sands Missile Range (WSMR). As time passed and the missile guidance system was in the final stages of development, shipboard prototype equipments were assembled at WSMR into a weapon control complex that was commissioned USS *Desert Ship*. That facility made it possible to test missile system improvements and the compatibility of the missile with the prototype shipboard equipment. *Desert Ship* supported development of the Talos Weapon Control System until about 1965.

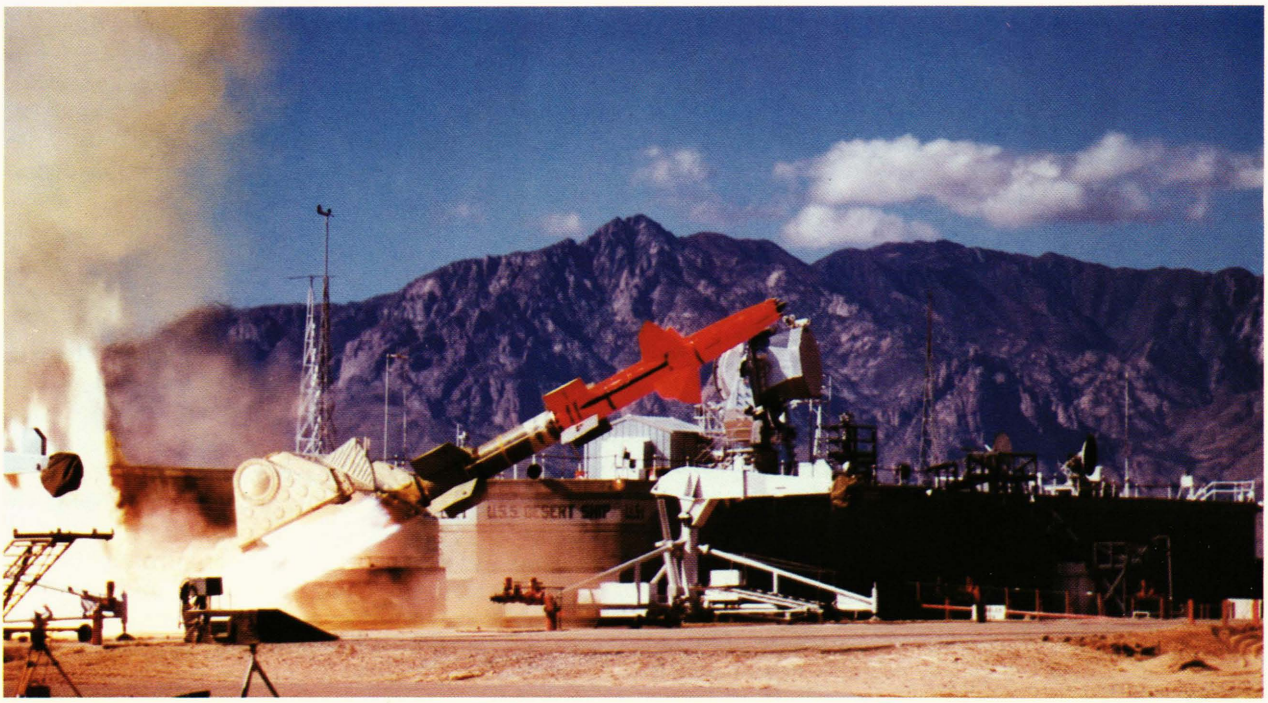

A First Tactical Talos leaves its launcher at USS *Desert Ship*, White Sands Missile Range, N.M. (This is one of hundreds of fine technical photographs taken by the late Clyde T. Holliday during his long and distinguished career at APL.)

THE TALOS LAND SYSTEM

The Talos missile was in a state of advanced development and ready for final production engineering in the early 1950's, although it would be several years more before the first Talos ship was ready for a load of missiles. The Talos missile represented such a considerable advance in the state of the art that it attracted the attention of the Air Force, which was interested at the time in the defense of Strategic Air Command bases. A design proposal of such a land-based system was prepared by the Laboratory and, following approval by the Air Force, a contract was let by the Bureau of Ordnance to RCA, Moorestown (N.J.) Division, to put together a land-based weapon system.

The RCA Talos Land System was the most advanced air defense system developed up to that time and also, because of automatic self-testing and fault identification, one of the most reliable. The basic components of the system were two C-band monopulse radars to track and illuminate targets, four C-band guidance radars to support midcourse guidance, a launching system that used a round-house arrangement for storage of missiles, and digital computers to control and monitor the system operations. It was engineered into an operating entity, ready for test and evaluation, in only 18 months. The figure shows the system installed in its own building at White Sands Missile Range, N.M.

The evaluation of the system demonstrated many firsts, including the completely automatic hands-off operation of an antiair warfare system, from target designation through target intercept. Further, the Land System demonstrated the concept of multiplexing, where several missiles are in flight simultaneously and the illuminator is directed from one target to the next at the right time for each missile's terminal phase. In addition, system capabilities were under study to use the nuclear warhead version of Talos as a last-ditch defense against ICBM's. No tests were ever carried out, but the concept has now resurfaced, some 30 years later, in the attempt to achieve survivability of missile silos.

The Talos Land System evoked a prolonged controversy between the Air Force and the Army, which was supporting the Nike Hercules system. The end of that evaluation, in the fall of 1956, was a jurisdictional decision by the Senate Armed Services Committee. It awarded the responsibility for land-based missiles with a range of up to 100 nautical miles to the Army and responsibility for missiles beyond that range to the Air Force. The Talos Land System, just starting its detailed evaluation and demonstration, was placed under the aegis of the Army, which then took over the evaluation; afterward, the system was disassembled. RCA continued to develop the Talos Land System's fire control radars, which had been under development as part of the Bumblebee Program and which later became the well-known FPS-16 Instrumentation Radars.

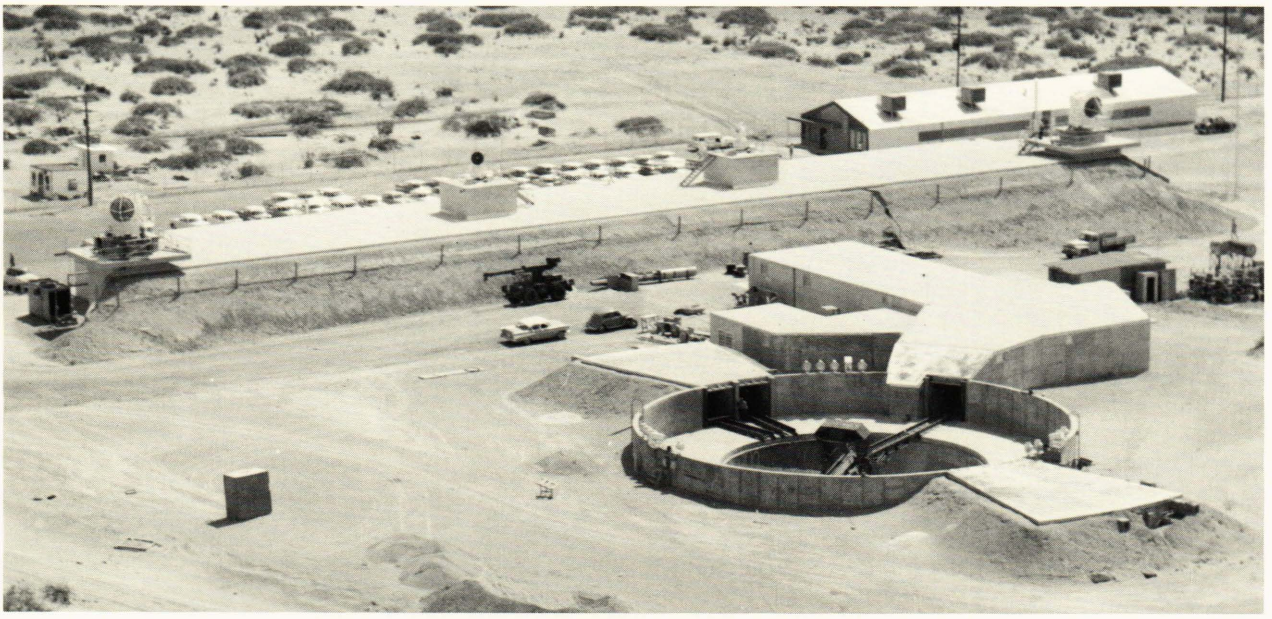

The Talos Land System, installed at White Sands Missile Range, included two C-band monopulse radars, two C-band guidance radars, a launching system, and a partial magazine for six missiles.

ELMER D. ROBINSON

THE TALOS SHIP SYSTEM

The Long Range Talos missile placed requirements on the ship system that were beyond the state of the art during the entire lifetime of the Talos Weapon System. However, valuable lessons were learned that affected the development of later systems. The evolution of the ship system proved that patchwork techniques could not be used to satisfy tactical needs.

The initial concept of the Talos Weapon System was established in 1952 and included antiair, antiship, and shore bombardment capabilities. There were two types of missile, each having intercept ranges up to 50 nautical miles. One missile carried a command-detonated nuclear warhead, and the other, a proximity-fuze-detonated continuous-rod warhead. The nuclear warhead missile rode a programmed guidance radar beam to the vicinity of the target, where it was detonated by a command from the ship. The missile with the continuous-rod warhead employed midcourse beamriding and terminal semiactive homing.

As would be expected, the Talos fire control system was directed from the ship's weapon control center. That center processed search radar data, provided selected coordinate data to the fire control radar, ordered loading of the missile launcher, and controlled missile firing.

To control the missile in flight, a continuous measure of target and missile position was necessary. There were three major subsystems: a target tracking radar to measure target position and to illuminate the target, a guidance radar for beamriding and missile range measurements, and a computer to generate angle-rate signals for positioning the guidance beam and activating the terminal homing system. Three types of trajectory were employed by Talos (Fig. 1).

Talos was constantly improved during the course of the Program. Improvements in missile capabilities became a primary driving force in establishing ship system requirements. Extending the maximum missile range, for example, forced the use of a new generation of search and target acquisition radars. The shift to continuous wave (CW) homing required the installation of CW illuminators. The state of the art was constantly being applied to improve the weapon system. A detailed description of the Talos ship system depended on the ship and the date.

The typical Talos system (Fig. 2) contained:

- Search radars that were used to detect targets and provide position data to the weapon control system;
- A weapon control system that made target assignments to the fire control system, ordered loading of missile launchers, fired missiles, and linked defense responses with Fleet units;
- A fire control computer that interfaced all elements of Talos to control the missile in flight;
- A fire control radar that accurately tracked the designated target and provided illumination for semiactive homing;
- A missile guidance radar that acted as a command link to the missile.

TALOS SHIP INSTALLATIONS

USS *Galveston* (CLG-3) was designated as the first ship to receive Talos missiles and underwent an austere conversion to accommodate the missile. The aft main gun battery and seaplane catapults were removed. A dual-rail missile launcher was installed. The ship's structure was modified to include a missile magazine, a missile handling area, and barbettes for the target tracking and missile guidance radars. Spaces for the radar consoles, the fire control computers, and a weapon control system were included. Missiles were loaded on the launcher by extendable and retractable overhead rails. The fire control system was a functional copy of the ground system used during development testing at White Sands Missile Range. Two fire control channels, consisting of

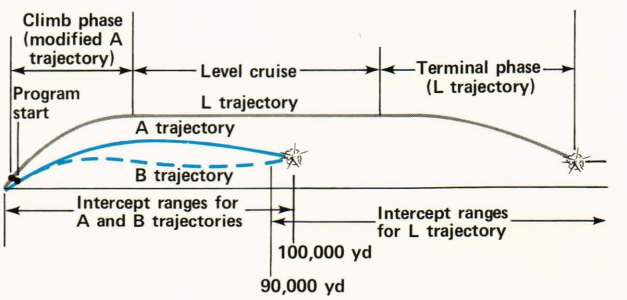

Figure 1 — Talos flight trajectory types depended on the range to the target and the electronic countermeasures environment. The A trajectory was medium range and approximated a circular arc. The B trajectory, also medium range, closed the beams earlier to reduce susceptibility to enemy countermeasures. The long-range L trajectory was used for intercepts at greater than 90,000 yards.

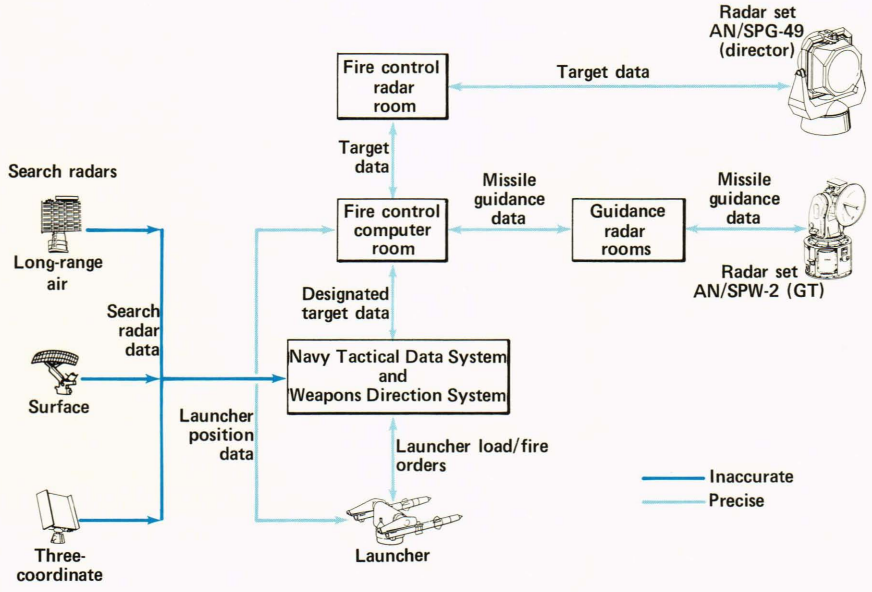

Figure 2 — Typical Talos Weapon System.

tracking radars, computer channels, and guidance radars, were required to support the dual-rail launcher (Fig. 3).

The Combat Information Center in *Galveston* was modified for mounting a television camera above a master plan position indicator and for the installation of two repeater displays. These formed the link between the Combat Information Center and Talos. Information could also be transferred by the use of grease pencils on the televised displays.

The Talos Weapon Control System provided manual tracking of up to six targets and the designation of any two of them to fire control channels. Little thought was given in the early days to a large number of targets, adverse environments (jamming), designation accuracies, and system reaction times.

Shortly after authorization of the *Galveston* conversion, two additional ships were authorized — USS *Little Rock* (CLG-4) and USS *Oklahoma City* (CLG-5). These ship systems were very nearly identical with the system on *Galveston*. The initial installation in these three light cruisers supported the short-range version of the missile (50 nautical miles).

Introduction of the long-range missile (100 nautical miles), and later the CW seeker, imposed changes in the ship system. These changes involved increasing the tracking range of the fire control radar, increasing the instrumented range of the fire control computer channels, and adding a low-noise-level, high-power CW target illuminator. Also required were a computation of the closing velocity between missile and target and the relaying of this information to the missile.

The long-range missiles focused attention on the need for long-range target detection and rapid handling of multiple targets in adverse sea, land, and weather clutter and heavy countermeasure environments. Threat studies showed that the search radars and weapon control system in the light cruisers were inadequate to support Talos in a heavy threat or jamming environment.

Figure 3 — USS *Galveston* (CLG-3) was designated as the first ship to receive Talos missiles. Two of the first tactical Talos missile types, SAM-N-6b and SAM-N-6bW, are shown on the launcher.

The first chance to install an improved ship system occurred with the authorization to convert USS *Long Beach* (CGN-9) to a Talos ship. This first nuclear-powered cruiser had powerful long-range search and acquisition radars that used state-of-the-art, fixed-array, electrically steerable beams and a new Weapon Control System capable of rate-aided manual tracking of up to 24 targets. Digital computer technology

Table 1 — The Talos ships.

Ship	*Commissioned*	*Armament*
USS *Galveston* (CLG-3)	May 1958	46 Talos missiles 6-inch triple-barrel gun 5-inch dual-purpose guns
USS *Little Rock* (CLG-4)	Jun 1960	Same as CLG-3 except for the number of guns
USS *Oklahoma City* (CLG-5)	Sep 1960	Same as CLG-3 except for the number of guns
USS *Long Beach* (CGN-9)	Sep 1961	52 Talos missiles 240 Terrier missiles 5-inch twin-barrel guns
USS *Albany* (CG-10)	Nov 1962	104 Talos missiles 80 Tartar missiles 5-inch twin-barrel guns
USS *Columbus* (CG-12)	Dec 1962	Same as CG-10
USS *Chicago* (CG-11)	May 1964	Same as CG-10

using hard-wired techniques was used for the first time in the Fleet. Solid-state devices were used in the analog fire control computers to improve their reliability. The nuclear-powered cruiser was the first Talos ship to employ the Naval Tactical Data System for ship-to-ship and ship-to-air communications.

The next chance to install an improved ship system came with the authorization for conversion of three heavy cruisers to carry Talos and Tartar. The seven Talos ships, their commissioning dates, and armaments are listed in Table 1.

SEARCH RADARS

Three basic types of search radar were used on the Talos light and heavy cruisers: a short-range surface search radar, a longer-range radar for range and bearing data, and a long-range air search radar for range, bearing, and target height data. Radar video and timing signals were sent to the Combat Information Center in all the ships and to the Weapon Control System in the heavy cruisers.

WEAPON CONTROL SYSTEM

The Talos Weapon Control System served several purposes: classification of targets based on search radar data, assignment of targets to fire-control channels, display of repeat-back data from the fire control radars, determination of open fire and intercept ranges, evaluation of the booster splash point and firing cutout zones, selection of the missile type to be used, assignment and loading of the missile launchers, and firing of the missiles.

The weapon direction equipment in the light cruisers contained two large displays of televised radar scopes and a bank of lights for indicating the status of the weapon system. Data written on the televised radar scopes would appear on the displays. Four smaller repeaters were installed — two in the Weapon Control Center and two in the Combat Information Center. Two target engagement consoles interfaced with the main displays via a symbol generator. Six targets could be processed simultaneously. One target could be designated to each of the two fire control channels and one to the gun system. A missile firing panel enabled missiles to be selected, loaded, and fired. It contained a display of surface radar data and superimposed booster splash point and firing cutout zones. A height storage console interfaced the system with three-dimensional search radars.

At the time that a weapon control system was selected for the nuclear and heavy cruisers, digital systems were being developed and more severe threats were being recognized. A hard-wired digital computer, representing the state of the art at that time, was selected for the Weapon Control System. Two target entry consoles were installed for assigning targets to track consoles and for monitoring the weapon systems (Talos and Terrier in the nuclear cruiser and Talos and Tartar in the three heavy cruisers). Six target tracking consoles were installed, each of which could process four targets. The program for processing data for as many as 24 targets was stored and handled in hard-wired magnetic core memory. Frequent manual entries were required to maintain accurate tracks. Two director assignment consoles interfaced the Weapon Direction System with the fire control systems. Four launcher assignment consoles interfaced the system with the missile launchers — two for Talos and two for Tartar.

The hard-wired digital computer proved to be inflexible and expensive to change. It had a high failure rate and long diagnostic and repair times. The solution of these problems appeared to be the replacement of the entire system with a general purpose digital computer and general purpose consoles. These equipments became available too late in the lifetime of the cruisers to warrant their installation.

FIRE CONTROL RADARS

The Talos missile required an automatic tracking radar that was powerful and accurate, with an acquisition capability to cope with target designation errors from search radar data. In 1949, a survey of available radars resulted in the selection of a gun-laying radar that could be adapted to Talos. It consisted of two integrated radars: a scanning acquisition radar and a monopulse tracking radar (Fig. 4). The antenna director had three degrees of freedom: train, elevation, and traverse. The traverse member permitted the tracking of high-speed crossing targets and gave the radar a track-overhead capability. All of the microwave equipment, antenna control electronics, and high-voltage power supplies were mounted within the director. This location made the radar difficult to service at night or during inclement weather. The directors were mounted on barbettes that extended to the keel of the ship for alignment stability. Two operator consoles were mounted below decks — an acquisition console having a unique five-plane display, which gave a synthetic three-dimensional display of the volume of space containing the target, and a tracking console with a range scope display and a plan position display.

The radar was modified at the same time the long-range missiles were introduced, to increase range and to include a high-power CW target illuminator operating through an indexed target-acquisition antenna system. It became the highest-powered, most accurate radar in the Fleet until the digitally controlled pulse Doppler fire control radar for Tartar was introduced in the late 1960's.

Over the years, numerous modifications were proposed and tested to improve radar performance at low elevation angles, for targets in clutter, for fading targets, and for targets screened by countermeasures. Some of these modifications included pulse compression, fade-coast mode, low-elevation-angle mode, track-on-jamming capability, alarm gate for chaff, and digital range gate processors.

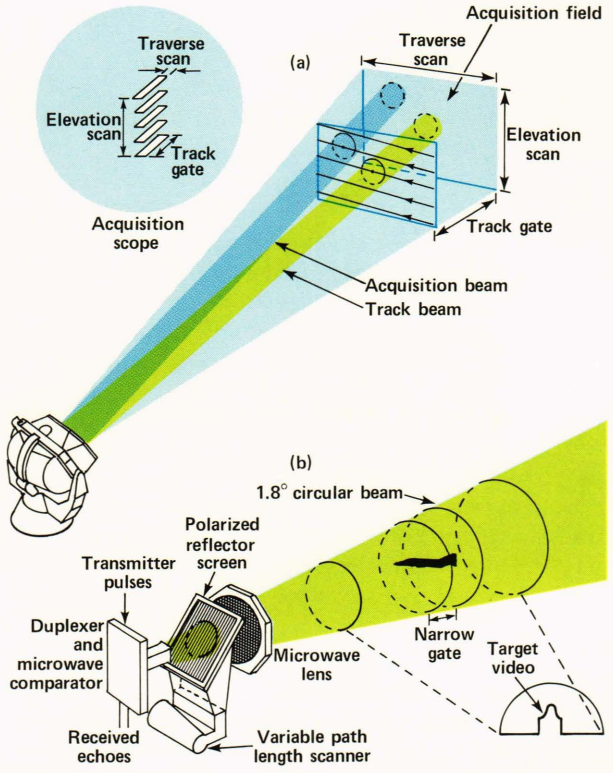

Figure 4 — The Talos fire control radar consisted of two integrated radar systems using a common microwave lens: (a) The acquisition system was scanned by a motor-driven polarized reflector grid and a scanning feed. (b) The tracking radar system, polarized at 90° from the acquisition system, operated through the transparent reflector grid.

FIRE CONTROL COMPUTERS

The fire control computers for Talos were an extension of gun fire control technology of the early 1950's. They were vacuum tube, electromechanical devices performing three-dimensional coordinate conversions in real time and solving both linear and nonlinear equations. These computers implemented the following tasks: target designation; target tracking; launcher assignment and guidance radar control; booster splash point and firing cutout zone calculations; and missile firing and beam programming for antiair, antiship, shore bombardment, and home-on-radiation missions. The computers were originally designed to support the short-range missiles and were later modified to support the long-range missiles.

The analog computers were subject to long settling times and inaccuracies caused by drifting. The drifts were not detectable without comprehensive tests and analysis. As a result, extensive test and adjustment procedures were developed. A high failure rate increased the maintenance burden and system downtime.

The fire control computers for the nuclear and heavy cruisers used solid-state analog technology in the 1958-59 era. However, they suffered from the same problems experienced with the earlier computers — long settling times and inaccuracies.

The problems with the analog computers led to the first studies of digital fire control systems in 1956. The studies, however, were aimed at two additional heavy cruisers and not at existing ships. Cancellation of the cruiser shipbuilding program halted the studies of digital systems until 1961, when APL-built analog-to-digital conversion equipment became available for interfacing with general purpose computers. The operational capability for digital control of guidance radars was demonstrated in 1964. These demonstrations led to evaluation of a digital fire control computer system in USS *Albany* (CG-10) in late 1964 and early 1965. A Univac Model 1218 computer was selected; it became known as the military Mk 152 digital computer.

The development of digital range data processors for the Talos target tracking and guidance radars was paced with the development of the digital fire control

computers. The first conversion to a digital system took place in *Albany* in 1966. Conversion of the nuclear-powered *Long Beach* and of USS *Chicago* (CG-11) soon followed. The three light cruisers and USS *Columbus* (CG-12) were retired before conversion took place.

MISSILE GUIDANCE RADAR

By the end of World War II, several target-tracking fire control radars existed that used conical scanning antenna feeds and time-domain signal processing for tracking targets automatically. Beamriding missiles became an extension of that technology by relocating the radar receiver in the missile and using the output to control the missile.

The missile guidance radar selected for Talos employed a 4°-wide pencil beam that was offset 2° from boresight and nutated about it at a 30-hertz rate. The train and elevation angles in the guidance radar could be controlled manually during collimation testing or remotely by the fire control computer during beam programming. The pulse repetition rate of the radar was frequency modulated sinusoidally at a 30-hertz rate and with a phase related to a stable platform so as to remove the effects on missile attitude of ships' roll and pitch. The frequency modulation provided the missile with a phase reference with which to compare the phase of amplitude modulation resulting from being off boresight. The result of the phase comparison was used to steer the missile in the required direction to follow the boresight line during guidance beam programming.

Instead of a single pulse in conventional radars, the guidance radar used a group of pulses that could be time coded to identify a particular missile with a particular guidance radar and to convey commands to the missile. The coded pulse group also triggered a transponder in the missile to enhance missile tracking by the guidance radar.

The guidance radar for Talos used 1950's technology, and no major modifications were made until digital range data processors were developed in 1966. During its lifetime, several minor changes were made to decrease the receiver noise figure for longer range beacon tracking, improve the settling time of the range tracking output after beacon lock-on, and improve the guidance radar operability and maintainability.

MISSILE LAUNCHING AND HANDLING SYSTEM

Missile magazines and handling areas were installed in the aft end of the light cruisers and the nuclear-powered cruiser. Magazines and handling areas were installed in both ends of the heavy cruisers. A bookkeeping system was incorporated for locating and calling out missiles with continuous-rod or nuclear warheads. Later on, the bookkeeping system was modified to include the location of missiles configured for home-on-radiation missions. In the heavy cruisers, the launchers could be assigned to either the forward or aft fire control channels. Each handling area contained a battery charger and Talos tactical test equipment. The specialized test equipment could exercise the electronics and hydraulics of a missile for periodic tests to determine readiness. On-board repair of missiles could be accomplished by module replacement using on-board spares. At sea, resupply of missiles was accomplished by high-line transfer from ammunition ships. Few changes were made to the missile launching and handling systems during the lifetime of Talos.

EQUIPMENT AND SYSTEM DOCUMENTATION

The introduction of the complex Talos, Terrier, and Tartar Weapon Systems in the Fleet soon demonstrated the inadequacies of available documentation. Failure-reporting procedures were insufficient to highlight problem areas and give direction to the logistic system. Test and evaluation techniques were inadequate to determine the readiness of equipment to meet the needs of an exercise or a real engagement.

A System Operability Test was developed in 1962 to determine system capability to support a mission. This evolved into a Daily System Operability Test that included simulated missile firings and measurement of system parameters for a go/no-go condition. The Daily System Operability Test was also a training aid for maintaining the proficiency of weapon system personnel.

Signal flow diagrams known as pyramids were developed in 1963 to assist personnel in locating faults quickly. This resulted in a new type of documentation known as Improved Maintenance Plans, which evolved into a Planned Maintenance System for surface missile ships. A failure-reporting system was developed that permitted rapid determination of mean-time-between-maintenance events, mean time between failures, mean time to repair, system availability times, and demands on the logistic system.

CONCLUSION

The Talos Program motivated developments in many areas of weapon system technology. The existence of a guided missile having a tactical range in excess of 100 nautical miles most certainly advanced the state of the art in long-range target detection and target data handling. It pointed out the need for:

1. High firing rates for long-range missile systems;
2. Automatic evaluation and reaction to threats;
3. Improved counter countermeasures for radar systems; and
4. Digital computers in all areas for automation, accuracy, flexibility, and maintainability.

The Talos Weapon System provided seven cruisers with a wide-area air defense system unequaled at its time by any other guided missile system in the Navy inventory.

DONALD D. A. GRAY

THE TALOS SHIPBOARD TEST PROGRAM

At-sea tests were necessary to determine weapon system performance and evaluate proposed system improvements. The tests were conducted from combat ships and were squeezed into the ships' schedules of operational commitments.

INTRODUCTION

The basic objective of the shipboard test program was to evaluate the ability of the Talos missile and shipboard weapon system to provide an effective defense against aircraft attack. A major part of the effort dealt with the determination of missile and weapon system deficiencies and the evaluation of proposed improvements.

The test program was not formally chartered or planned, but evolved. The need started with the commissioning and technical evaluation of USS *Galveston* in 1958 and ended, some 27 projects later, on board USS *Chicago* in 1970, with a test involving the use of search radar data to control the midcourse phase of a missile flight.

The program was conducted under the direction of the Talos Project Office of the Bureau of Naval Weapons and with the assistance of the U.S. Naval Ship Weapon System Engineering Station. Other organizations participating were Bendix Aviation Corp., the missile contractor; Sperry Gyroscope Co., the fire control equipment contractor; Northern Ordnance and General Electric Co., the launching system contractors; the Naval Weapons Center, China Lake; the Naval Weapons Laboratory, Dahlgren; and Vitro Laboratories, the system integration contractors. APL's role was to plan the test projects, write the test procedures, and coordinate and supervise the test operations. Providing services and scheduling ships and aircraft were done by the Operational Test and Evaluation Force of the U.S. Navy. Analysis and reporting of test results were largely done at APL. Flight test analysis was conducted in collaboration with the Fleet Missile System Evaluation Group.

PROGRAM HIGHLIGHTS

A chronological summary of the Fleet Test Program is shown in Fig. 1. All of these tests were designed, conducted, and reported by APL, with the assistance of the Talos equipment contractors.

The first Talos cruiser, *Galveston*, was commissioned May 28, 1958, at the Philadelphia Naval Shipyard. The Technical Evaluation of the Talos weapon system started in the fall of 1958 after the ship's fitting out and shakedown period. All aspects of the Talos missile system were checked out and evaluated prior to missile firings in March 1959. This was the first use of the 50-nautical-mile Talos (XSAM-N-6b and -6bW) missiles at sea. The series of tests was followed by a Navy Operational Evaluation conducted by the Operational Test and Development Force of the Navy.

APL conducted Ship Qualification and Acceptance Trials of the 100-nautical-mile Talos system employing RIM-8C pulse homing and RIM-8D nuclear missiles on the newly commissioned USS *Little Rock* and USS *Oklahoma City* in 1960. APL also assisted the Operational Test and Development Force in a Technical Evaluation and Operational Investigation of the same system in *Galveston* in 1960 and 1961.

The first system to support the continuous wave homing, 100-nautical-mile-range missile was evaluated as a part of Ship Qualification and Acceptance Trials of the first nuclear-powered cruiser, USS *Long Beach*, in late 1961 and early 1962 (Fig. 2).

Development Assistance Tests for the introduction and evaluation of missile and shipboard system improvements were started in the early 1960's. That test program provided a realistic environment for the evaluation of missile, fire control, and weapon system improvements. It also provided a vehicle whereby development test work was conducted on board operational ships.

When an improvement or group of improvements was ready for evaluation, a Development Assist Project was proposed to the Navy's Talos System Manager, who would obtain Chief of Naval Operations approval and designate a project assignment. APL would prepare test plans for approval by the Navy, devise test procedures, and, with the assistance of the Operational Test and Evaluation Force, arrange for Talos ship services and any needed tracking aircraft, target aircraft, and surface and shore services. The services of missile and system contractors were provided by the U.S. Naval Missile System Engineering Station at Port Hueneme, Calif. The tests were performed under direction of an APL test conductor, with the very active participation of the Missile Engineering Station.

The primary categories of tests conducted as "Development Assistance Tests" were:

1. Prove-in of new capabilities such as countermeasures resistance, homing against surface

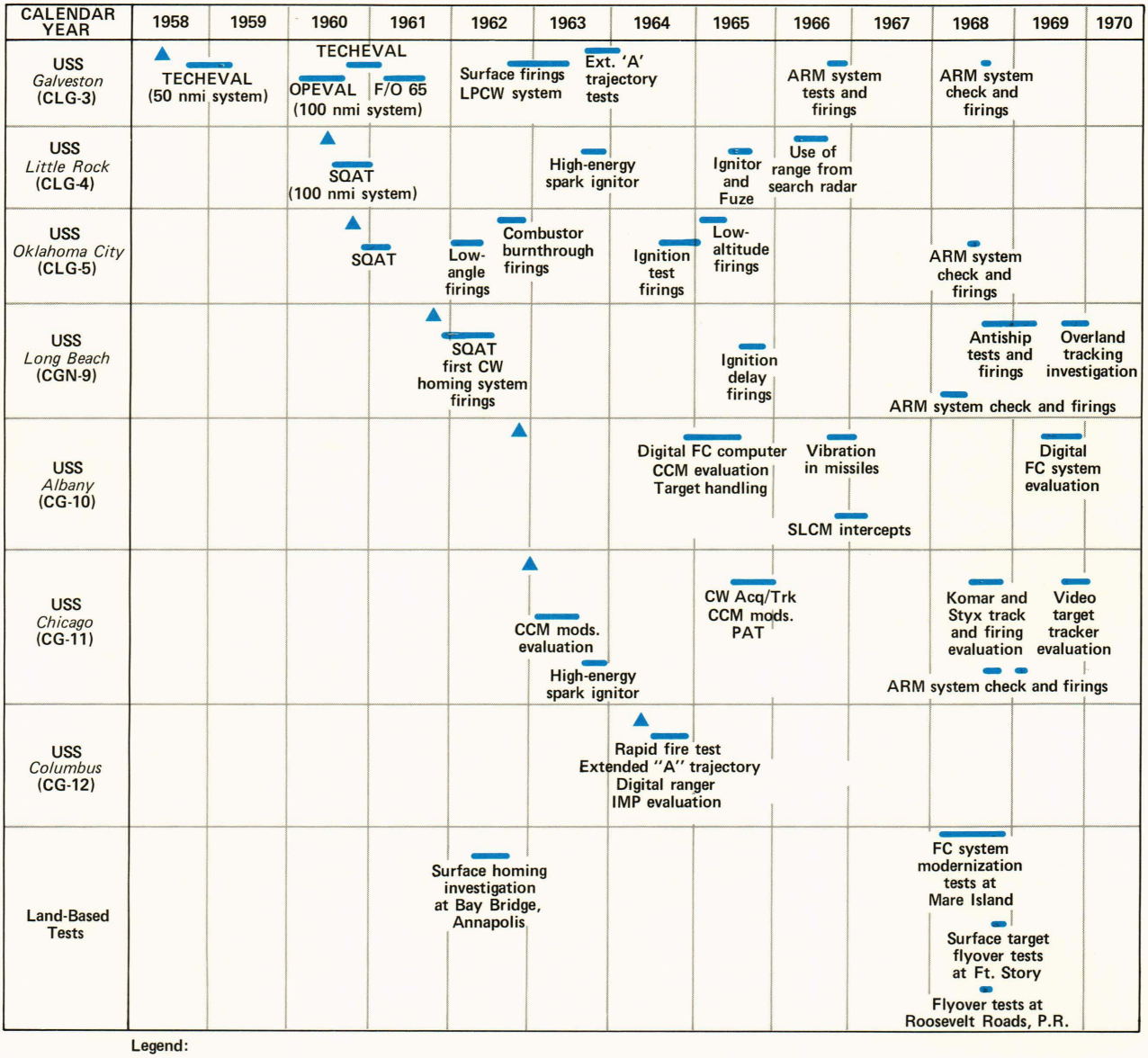

Figure 1 — Development Assistance Tests to evaluate missile and shipboard system improvements were conducted using operational ships. The types of evaluation tests and times involved are shown here.

targets, system coast provisions in case of temporary loss or fading of track, introduction of the digital fire control system, and introduction of antiradiation missile capability;

2. Demonstrations of missile capability against both low-altitude and high-altitude, high-speed targets and the ability of the system to sustain rapid-fire operations;
3. Prove-in of fire control system maintenance aids such as the Daily System Operability Test and the Integrated Maintenance Plan. Some tests and investigations required several project operation periods to be completed successfully, and were actively pursued for a number of years before completely satisfactory results were obtained.

A typical example of a Development Assist Project requiring several years of testing was the assessment of Talos capability against surface targets. The investigation of the technical problems started in 1962 with a series of land-based tests in which a Talos con-

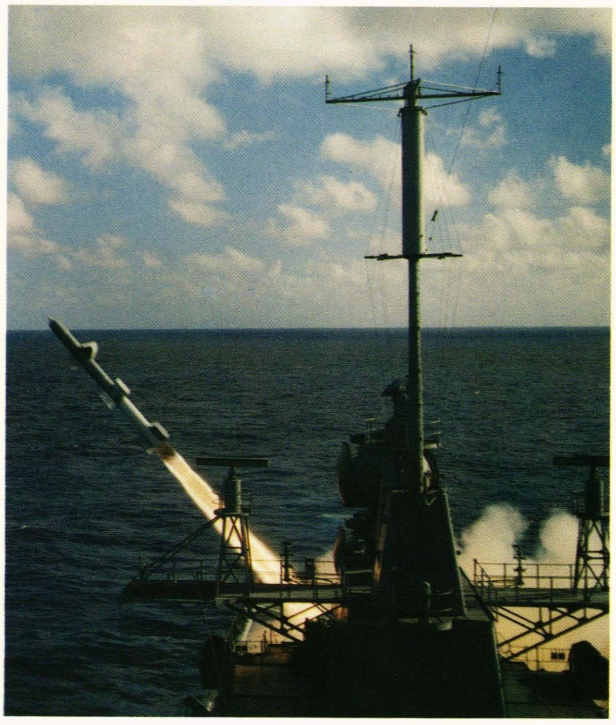

Figure 2 — Talos firing from USS *Long Beach* to evaluate the 100-nautical-mile missile and continuous wave homing system. Missile and weapon system evaluations were part of the *Long Beach* Ship Qualification and Acceptance Trials.

tinuous wave illuminator, a missile front end antenna and receiver assembly, and instrumentation to identify and record signal returns were installed on a pier of the Chesapeake Bay Bridge near Annapolis. The setup was used to gather radar reflection data on maritime traffic passing under the bridge, thus providing an evaluation of the capability of the Talos seeker to track the complex radar returns from ships. Following the Bay Bridge tests, missile firings from *Galveston* against a destroyer hulk were conducted in 1963 with considerable success, in terms of hits on the target and demonstration of extensive damage from missile impact, even though a warhead was not used. A problem revealed by these flight tests was a tendency of the missile seeker to lose track about 1 second before intercept because of the size and complexity of the target. A rapid shifting of the aimpoint along the length of the target caused considerable wing motion and erratic flight. A seeker modification in order to zero the wing control signal when this condition occurred was developed and tested aboard USS *Columbus* in 1964. Tests were also conducted with the Talos seeker mounted in the nose of a P-2V aircraft to evaluate receiver performance more extensively during antiship intercepts. The antiship test program culminated in 1968 with firings from *Long Beach* that demonstrated a Talos capability to intercept surface targets that varied in size from patrol boats to major warships.

The use of tactical ships as at-sea test sites for missile and weapon system development was very ambitious because test work had to be squeezed in between operational commitments. In spite of these heavy operational commitments, the necessary development and evaluation were accomplished and many valuable lessons were learned.

RADM WAYNE E. MEYER and CAPT RICHARD W. ANDERSON (Ret.)

OPERATIONAL LESSONS LEARNED

LESSON ONE

From its beginning, the Talos missile system was conceived as a long-range weapon system. Its propulsion method would have supported still more range than the guidance concepts on which it was based, and its time-to-target was respectably low. The range capability was double or triple that of contemporary naval surface-to-air systems. As the nature of air attack changed from gravity bomb delivery at relatively short range to air-to-surface missiles launched at considerable standoff, Talos promised the ability to reach the enemy's launch aircraft and their jamming support before their antiship missiles were launched. Talos' range capability would force the enemy to stand off to distances that would severely reduce the effectiveness of their antiship weapon delivery. We were proud of the technical achievements of the Talos missile system, but we learned quite vividly that missile systems do not stand alone.

The detection sensors upon which the Talos missile system depended were severely stressed to provide early enough designation to Talos fire control to permit missiles to reach their maximum range capability, especially in a jamming environment. Additionally, the Talos range capability made it a virtually unmanned interceptor, capable of operating in regions where aircraft alone held sway. This posed an additional problem for the search and surveillance components of the air defense system: it was not enough merely to detect approaching enemy aircraft, it was essential to know the movements of friendly aircraft and missiles in relation to each other as well as in relation to enemy aircraft. What we found was that, in general, the defensive system was not up to this requirement, and the problem was "solved" by not using Talos to its full capability, the air defense aircraft being favored due to its established position.

This disuse of long-range missilery, given the existing command and control situation, was probably as large a contributory factor to the demise of the Talos missile system as were the more often stated factors of electronic antiquation and maintenance expense. Had the capability been credible, the age and cost problems would have been solved. This problem of achieving really credible capability still plagues designers of antiair warfare weapon systems. Though weapons have changed, though newer and better sensors have appeared, though superior defensive aircraft have been designed, we still have the problem that good weapons systems are of true military value only if they can be coordinated with the entire ensemble. The secret of this coordination lies in the command and control system, its supporting sensors, its computational power, and its display and communications abilities to gain and make sense of the information about what is going on at great distances from the ships being defended. Talos history provided us with an early identification of a problem that will occupy and plague us for decades to come.

LESSON TWO

Looking back at our experience with the Talos missile system, we are reminded of a basic lesson that runs through all of its history, as well as the history of other missile programs: engineering changes are inevitable, and provisions must be made to accommodate them in an orderly manner. White Sands Missile Range was the only development and test facility nearer the sea than a laboratory bench, but much of the development testing needed to be done at sea. The Talos program never had an at-sea development site, except for the operational ships. That meant that the combatants had to squeeze development test work in with operational commitments. This way of life was acceptable in a programmatic sense only because the number of ships was so small that configuration changes could be kept track of and logistically supported to an acceptable degree. The ships accepted such constraints because it was the only way of getting capability improvements in a timely manner.

Today such methods are unacceptable. Ship classes are too large to be accommodated in such a fashion, and the technical personnel situation will not allow that sort of experimental activity. The lesson learned was that there had to be land-based test sites, combat system development sites, and program maintenance facilities where a much more orderly process of design and development testing could get things well in order before going to sea. The rigors of installation problems needed to be worked out before system components reached the recipient ship and where the details of computer programs could be put in order at relative leisure and without debilitating the ship's operational capability. Thus, we learned that it is not sufficient just to build ships and combat systems; rather, it is essential to consider carefully the need for a complete support system to accommodate orderly evolution of the weapon system.

ANNOTATED BUMBLEBEE INITIAL REPORT

In the first half of 1944, when World War II had not yet run its course, the technical focus of APL shifted from proximity fuzes and gun directors to guided missiles. To recall the events of nearly 40 years ago that set the stage for the development of the Talos antiaircraft guided missile (and of Terrier, Tartar, and Aegis, its offshoots), we reproduce the Bumblebee Initial Report that was issued soon after the assignment of a new task to APL in January 1945. The Annotations accompanying the report are intended to assist the reader in reconstructing the origins of a program that had a profound and lasting effect on the technical direction of APL. *Walter G. Berl*

THE JOHNS HOPKINS UNIVERSITY
APPLIED PHYSICS LABORATORY

SILVER SPRING, MD.

Operating Under a "Section T" Type of Contract
With the Bureau of Ordnance U. S. Navy

BUMBLEBEE
REPORT
No. 1
Copy No. 108

BUMBLEBEE

INITIAL REPORT

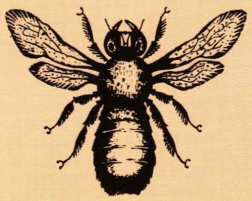

FEBRUARY
1945

Bumblebee_____
Report No._____
Copy No. _____

BUMBLEBEE INITIAL REPORT

As of February 15, 1945

Foreword

This is a statement covering the formulation and general planning of the "Bumblebee" program, as undertaken by the Johns Hopkins University Applied Physics Laboratory under a research contract of the Section T series with the Bureau of Ordnance, Navy Department. It provides an introduction to the activities associated with this problem, indicates the scope and background, and should serve to illuminate the series of progress reports on Bumblebee which will be issued at regular intervals.

The Applied Physics Laboratory, Johns Hopkins University, has acted for the past three years as a consulting technical group for the Research and Development Division of the Bureau of Ordnance, while operating as the Central Laboratory for Section T, Office of Scientific Research and Development. After December 1, 1944, the Laboratory continued its work under a new type of research contract directly with the Bureau of Ordnance, Navy Department. The primary emphasis in its technical program has been directed toward the protection of the Fleet against enemy aircraft. The VT fuze and the Mark 57 fire control system are specific developments to meet this particular military requirement. It has been recognized, however, that the nature of warfare is rapidly changing, and that while refinements can be introduced into fuzes and fire control systems, there is a growing possibility that the effectiveness of our present navy might be very seriously reduced by a large scale introduction of new types of enemy guided missiles during the late phases of this war. The use of the HS 293 and FX 1400 weapons by the enemy foreshadows advanced forms of aircraft attack against naval vessels for which inadequate protection will exist.

In July 1944, the Chief, Bureau of Ordnance requested an initial analysis and evaluation by Section T of the problem of protecting a task force against guided missiles launched from enemy mother-planes beyond the range of present fire control. Accordingly, with Dr. Bush's approval, a small group of Section T technical men explored this problem and submitted a report to Admiral Hussey and Dr. Bush.

It was the opinion of this group that some technical agency should give immediate and concentrated attention to the problem of developing a guided, jet-propelled, antiaircraft missile, preferably with supersonic speed, on a time scale which anticipates at least limited military use in the later stages of the present war.

This conclusion was reached as the result of consideration of a guided missile weighing 2000 pounds and traveling at a rate of 1850 ft. per sec. In this tentative design it was proposed that the missile would be launched to this velocity by means of rockets and driven to its target by a ram-jet motor. A payload of 600 lbs. of explosives was assumed. The auxiliary rocket-launching equipment would weigh an additional 2000 lbs., and would be dropped early in flight. A maximum flight time of 63 seconds would be required at an overtaking range of 38,800 yds. This was computed on the assumption that the misille would be fired at a target flying at an altitude of 10,000 yds. to intercept at a horizontal range of 20,000 yds.

It is of great military importance to the United States to learn whether guided, ram-jet missiles of supersonic speed are feasible as a weapon, since it would indicate what might be expected, for example, from the enemy in the way of surprise attacks on an invasion fleet. If an intensive effort were made by a suitable technical group, even a negative result would be valuable, in that it would provide evidence that no nation could bring such devices into effective use against us in a predictable length of time. 8

In December 1944, the Bureau of Ordnance was directed to proceed with the development of guided, jet-propelled antiaircraft missiles on an urgent basis, and the other Bureaus of the Navy were asked to give all possible support and assistance in carrying forward this program. The Bureau of Ordnance, recognizing the highly technical character of this problem, and cognizant of the fact that various aspects of the guided missile program are matters of prime concern and responsibility to several Government and Service groups, decided to handle this assignment in an unusual manner. The Chief of the Bureau proposed that this program should be made the overall responsibility of a contracting agency outside of the Navy Department, supported by Navy funds and with the responsibility for their activities accepted by the Bureau of Ordnance. This would allow freedom in the technical planning of the work, and would make possible a maximum degree of cooperation and joint participation in the program by other agencies in the general field of guided missiles. The former central laboratory of Section T now operates under a direct Bureau of Ordnance research contract; and the Chief of the Bureau therefore asked the trustees of the Johns Hopkins University to accept an assignment for the Applied Physics Laboratory to undertake a major program on jet-propelled antiaircraft missiles. At the end of December, the Johns Hopkins officials made a tentative decision to accept this assignment (Task F, code word "Bumblebee"), contingent upon being able to obtain additional technical personnel and facilities. 9

The Bureau of Ordnance and the Applied Physics Laboratory technical men recognized that cooperation and, wherever possible, joint acitivity with the agencies already interested in the general problem of guided missiles, is essential if effective results are to be obtained in a minimum time. Although this program was initiated and is supported by the Bureau of Ordnance, the work is of such broad scope and so closely allied to projects already under way in this country and in the United Kingdom that active cooperation with these other agencies is not only desirable, but necessary. This view was presented in letters from the Chief of the Bureau of Ordnance to the Army Air Forces, Army

Ordnance, National Advisory Committee for Aeronautics, the Office of Scientific Research and Development and the Navy Bureau of Aeronautics. All interested groups were asked to participate in the Bureau of Ordnance program with the Applied Physics Laboratory, and each was informed that its participation in the program would be given recognition. 10

The Applied Physics Laboratory will make every effort to work closely with all the technical agencies concerned, and with the various committees investigating the field of guided missiles, such as the Gilliland, Dewey, NACA, and other groups. It is recognized that the Applied Physics Laboratory, being a temporary war agency, is not expected to become a permanent central group 11
for guided missile work as a whole. However, if it can provide an effective technical arm in the immediate future by presenting an opportunity for detailed and continuous technical exchange in an active working laboratory located in close proximity to all of the Washington agencies, it should be of value to each group working in this field.

Representatives of the Laboratory have examined the literature available, and have been in touch with technical men in this country and abroad who are actively engaged in guided missile programs. Through OSRD channels, discussions were held directly with the G.A.P. Committee at two of its sessions in England. Informal liaison with associated technical agencies has been established, and more active collaboration is anticipated as the Applied Physics Laboratory technical program develops.

For several reasons the Applied Physics Laboratory, with the approval of the Bureau, has decided to limit the Bumblebee program to a jet-propelled AA missile of supersonic speed: in the initial phases of the work major emphasis will be given to ram-jets (athodyds), although an alternate based on liquid 12
rocket propulsion will be initiated as soon as personnel needs can be met. 13

During the first year (1945), the technical attack will be on the basic elements necessary to any guided supersonic missile, without major emphasis on a specific missile design. Empirical and laboratory investigations are already in progress, and it has been arranged for the Navy to survey and evaluate the situation at the end of the first year.

The basic problems to be determied are: (a) the thrust of a ram-jet versus the accompanying supersonic drag; (b) supersonice stability and control arrangements versus drag; (c) whether guidance at supersonic speeds presents basic difficulties or practical limitations not yet perceived. It is hoped that at least preliminary answers to these questions may be available by the end of a year of investigation (January 1946).

The Applied Physics Laboratory plans to add roughly three hundred people to the modest group now working on Bumblebee. In addition to maintaining a strong program at the Laboratory, the assistance of university and industrial groups on various technical phases of the problem is being arranged for under associated research contracts of the "Section T series" with the Bureau of Ordnance.

Expansion of the central laboratory space is now in progress; additional building facilities have been obtained at Forest Grove, Maryland, a short distance north of the present location in Silver Spring, which will accommodate the expanding needs of the Bumblebee Project, including a ram-jet laboratory. General administration of the Bumblebee Project will remain at the central laboratory.

The Bumblebee problem has been initially divided into several parts and assigned to groups working under technical supervisors as follows:

1. Burner: Fundamental problems of propulsion, involving stationary ram-jet experiments, thrust measurements, and fuels. Experiments will be performed simulating as nearly as feasible the conditions to be met in flight. This necessitates large blower and compressor facilities and the use of an open-circuit, supersonic wind tunnel, primarily for burner experiments.

2. Aerodynamics: The study of supersonic drag stability and control problems, and designs of wind tunnels and ducts. In the later stages it is expected that this group of necessity will also assume the overall design of the weapon. The facilities of the proposed supersonic wind tunnel will be used in some phases of this work, together with free-flight experiments.

3. Models: Primary emphasis on ram-jet thrust and drag by free-flight experiments at supersonic speeds. Measurements will be made on athodyd models in flight, using radio telemetering methods, together with radar and photographic tracking observations. This group will provide data to supplement the stationary burner experiments. Fuel injection, altitude controls, tracking and telemetering problems are among the secondary concerns of this group.

4. Guiding and Control Systems: Radar guidance, target tracking and gyro-servo systems for control and stabilization.

5. Facilities: Test fields and flight observing facilities, also experimental laboratory and large blower facilities.

6. Launching: This group has been organized to develop and study launching techniques.

In carrying forward a major program of the type indicated, it is planned to allocate specific areas of the problem to industrial and university groups, with several contractors invited to share with the Applied Physics Laboratory a sense of overall responsibility for the success of the program as a whole. The Applied Physics Laboratory expects to invite a major aircraft company to participate in solving the aerodynamic problems and the eventual design of the missile, and to assist with experiments using large blowers and the supersonic wind tunnel. A large industrial concern specializing in prime movers or heavy machinery will be asked to undertake a general program, including the design of a

complete weapon, but with a special emphasis on the ram-jet and propulsion problems. At least one organization specializing in fuels will be asked to accept a contract to develop various types of fuels, and to join in the ram-jet experiments.

A group at Princeton University has begun investigations of telemetering in cooperation with the Models group at the Applied Physics Laboratory.

At the University of Virginia, investigations have been initiated on the burning of fuels in a small-scale burner laboratory. Data from these experiments will be correlated with those obtained by the Burner group at its stationary burner laboratory in Forest Grove, and later with data from the large-scale burner work.

Since no facilities exist for full-scale ram-jet experiments, blower equipment, a power plant, and a facilities building are being provided at Daingerfield, Texas, through the Bureau of Ordnance. These facilities will provide 200,000 cfm at 30 lbs. per sq. in. (gage), and in addition, a high-pressure blower will be fabricated and installed which will convert the 30 psi gage output of one of the 100,000 cfm low-pressure blowers to 120 psi gage. The initial blowers will provide air for low-pressure (high altitude equivalent) ram-jet experiments and for the 24"x36" wind tunnel being designed by the Aerodynamics group. The series combination of the low-pressure and high-pressure blowers will provide air for high-pressure (sea-level equivalent) ram-jet experiments. A test field has been established at Island Beach, New Jersey, and a major test field in the western part of the country is proposed for later experiments.

It is hoped that this report presents a sufficient introductory picture of the interests, aims, and initial progress of the Bumblebee project. A monthly survey of progress will be sent regularly to persons on the present distribution list, and to a limited number of additional persons who may be specifically authorized by the Bureau of Ordnance to receive this information. Requests for Bumblebee reports should be addressed to the Supervisor of Technical Reports, Applied Physics Laboratory, Johns Hopkins University, 8621 Georgia Avenue, Silver Spring, Maryland.

ANNOTATIONS

1. In June 1940, the National Defense Research Council (NDRC) was established by the Council of National Defense, which, in turn, had been created in 1916 "for the coordination of industries and resources for the national security and welfare." In President Roosevelt's letter appointing Vannevar Bush, then the president of the Carnegie Institution of Washington, to be the chairman of this Committee, NDRC was directed to "supplement the activities carried out by the Army and the Navy by extending the research base and enlisting the aid of the scientists who can effectively contribute to the more rapid improvement of important devices, and by study to determine where new efforts on new instrumentalities may be usefully employed." The organization was designed to bring together civilians in universities and research establishments to work on projects that would be of value to the military services.

Its six divisions, subdivided into numerous sections, covered a wide spectrum of science and technology of concern to the Armed Services. In placing contracts, one factor was uppermost in the Committee's thoughts — the need for speed. Contracts were let, permitting key scientists to remain in their laboratories as far as possible. Exceptions, however, were made in such areas as antisubmarine warfare, radar, and rocketry, where large centers were established through contracts with universities. In rocketry, for example, the California Institute of Technology and George Washington University were pressed into service as contract managers.

This unusual, imaginative, and extraordinarily effective mobilization of scientists and engineers was expanded in 1941 into the Office of Scientific Research and Development (OSRD) with the additional functions of liaison with Allied governments and an Office of Field Service with the responsibility of transferring technical developments to the Armed Services and evaluating their effectiveness.

In August 1940, an NDRC contract was signed with Merle A. Tuve of the Department of Terrestrial Magnetism of the Carnegie Institution of Washing-

ton to develop a fuze that would explode an antiaircraft shell by radio signals reflected from a nearby target ("proximity" or "VT" (variable time) fuze). With the assistance of a small number of his colleagues (R. B. Roberts, H. H. Porter, and L. R. Hafstad), Tuve demonstrated in a few months of breadboarding and field testing that such a miniature radio system could be designed and could survive the acceleration of the projectile being shot out of a cannon.

Because of the great military potential of the device and the need to translate the concept speedily into a reliable weapon, Tuve's Section T (the initials of a Section frequently reflected the name of the Chief) was expanded from about 100 persons at the end of 1941 to 365 one year later. A contract was negotiated with The Johns Hopkins University on March 10, 1942, to organize an Applied Physics Laboratory to pursue the fuze work on an enlarged scale. Close relations with industry were established to oversee the design and production of the fuze's components and to improve the reliability of the device. A staff of more than 600 was assembled in the Silver Spring, Md., Laboratory complex in June 1944.

Development and production were telescoped in an intensive coordination effort. Within two years from the enunciation of the initial concept, a workable fuze was in production. Its first successful demonstration took place on January 5, 1943, during an engagement in the South Pacific between USS *Helena* and Japanese war planes.

2. The close ties established with the U.S. Navy Bureau of Ordnance during the development and funding of the VT fuze resulted in a shift in the relationship of Section T and OSRD. The Section T operating philosophy had moved toward the concept of a central laboratory that was responsible for the development of an idea to the demonstration stage, followed by its rapid transformation into production and introduction into service use. This could only be achieved by the early selection of industrial contractors and by close and continued liaison with the ultimate user. Untried in military procurement, except for the Manhattan Project, this broad concept went beyond the immediate charter of OSRD and led, in December 1944, to a formal separation. By then, the staff had grown to nearly 1000. The Bureau of Ordnance negotiated a contract directly with The Johns Hopkins University. However, this "Section T Type" contract retained most of the features evolved during the OSRD period and has been maintained with few changes to the present day.

3. The VT fuze and gun directors were intended primarily for Fleet use during the Pacific operations, where they had a profound impact on the defensive capabilities of ships against conventional air attacks. However, the fuze was equally effective against the V-1 attacks on England that began in July 1944, and as a countermeasure against the German offensive in the Battle of the Bulge in November 1944. While there was reluctance to use the fuze on land for fear the Germans might discover its principle of operation, the war's end was near enough to overcome that objection. In fact, the Germans had made independent efforts to design a proximity fuze of their own, but there was insufficient support and urgency to bring their development to a successful conclusion.

When the APL fuze project was technically completed in 1943, it permitted a switch to new projects. The development of guided antiaircraft missiles and their integration into an effective Fleet system became the major APL effort until the 1960's. New programs were then added on satellite navigation and submarine evaluation and security, as were projects in biomedical engineering and in the fields of energy, environment, and safety.

4. As ideas for a guided missile development program crystallized into action during the early months of 1944, questions were raised as to whether any major new project could be completed in time to play a decisive role in the war. By then, it was evident that the early successes of the Germans in western Europe and in Russia had been checked and had, in fact, been reversed. Britain remained unconquered. The near-disaster for the Germans, in their costly campaign in the Ukraine and entrapment at Stalingrad, had led to continued retreats to the prewar Polish frontier by the beginning of 1944.

Similarly, in the Pacific, the military situation had greatly improved. From Pearl Harbor until the Battle of Midway (June 1942), the war had gone incredibly well for the Japanese — better, in fact, than in their most optimistic forecasts. Within six months, they controlled a vast area stretching from the Aleutian Islands in the north to New Guinea in the south, and from the Indian border in the west to the Gilbert Islands in the east. The defeat at Midway (so aptly named) was the turning point. The Imperial Navy lost four aircraft carriers and never recovered from that blow, even though reconquests of strategic Pacific islands had to be paid for frequently at hideous costs.

The summer of 1944 saw the successful crossing of the Channel in Europe and the approaching invasion of the Philippines in the Pacific. In mid-October, the Battle of Leyte Gulf, one of the fiercest sea battles in history, commenced. The Japanese Second Fleet, containing Japan's main naval strength, was decimated. It marked the end of the Imperial Navy as an effective fighting force, opening the home islands to effective invasion for the first time since Kublai Khan.

5. Postwar surveys of German and Japanese developments in antiship and antiaircraft guided weapons indicated that neither country had pressed vigorously enough for them to be of value in their war efforts. Indeed, the Germans had a long lead from their early commitment to the development of liquid-fueled rockets that culminated with the V-2's

bombing of civilian targets in England and the Netherlands. After successful flight tests in 1941, 5000 V-2's were assembled, half of which reached English targets in the time from September 1944 to the German surrender in April 1945.

However, despite a many-pronged development effort in surface-to-air and air-to-surface missiles, not a single German system was pushed into production on a large enough scale to have a decisive impact. The air-launched HS 293, a 10-foot-long glide bomb propelled by a hydrogen-peroxide-powered rocket and flying at a speed of 500 miles per hour, was put into limited production in 1941 and was instrumental in sinking several British merchant ships in the Bay of Biscay. But later versions with radio-controlled guidance did not become operational. The FX 1400, also radio-controlled and flying faster than 600 miles per hour, arrived too late to be of value. A variety of liquid- or solid-fueled and rocket-propelled missiles reached flight test stage in 1944 but did not become effective antiaircraft weapons. Despite a lead time of four to six years over the Allies, the German program never played an effective role in the prosecution of the war.

The Japanese effort in the high technology of guided missilery was almost nonexistent. During the desperate Leyte Gulf engagement and on virtually one week's notice, the kamikaze attacks were organized in October 1944. Pilots would guide their planes into direct collision with ships in the expectation that the resulting fires and explosions would cause great damage. It is estimated that 5000 sorties were flown in this style. While three capital ships were sunk and 300 other vessels were damaged, the tactic was a failure from a practical point of view.

The Ohka ("Cherry Blossom") bomb, introduced into the Okinawa campaign in the spring of 1945, was even less effective. Slung under a conventional mother plane and accelerated by solid propellant rockets to a speed of 600 miles per hour, it, too, depended on human guidance. Not a single ship was sunk by this device.

6. In view of the limited German effort and the virtual absence of a corresponding Japanese development, it is incorrect to describe the Navy guided missile initiative in the summer of 1944 as a response to kamikaze or Ohka attacks, since neither of those weapons had yet been deployed. Rather, the decision to proceed arose from the fact that technologies had advanced to a point where such a development was, in principle, feasible. M. A. Tuve wrote in a letter to Vannevar Bush on July 19, 1944, about

> *...the new Navy tactical situation which may arise if the enemy adopts guided missiles for attack against task forces from airplanes just beyond the limited range of anti-aircraft for us.... We have thought about this problem for several years, and only in the last eight months have reluctantly concluded that we may have to face it during this war instead of the next one in view of the weapons already in use by the Axis powers and ourselves.... The problem must be faced before very long if we hope for real defense against future air attacks in this shrinking world.*

Information about Axis developments was sketchy and incomplete, at best. Not knowing the magnitude of the German effort, it was unavoidable that actions based on a "worst case" assessment had to be taken. Tuve wrote on November 30, 1944 in a memorandum to Bush and to Rear Admiral G. F. Hussey, Jr., Chief of the Bureau of Ordnance:

> *Various discussions in Section T during the first six months of 1944 indicated the probable necessity for attack on a 'chaser' problem in the immediate future, even if the probability of success were low, since the stakes involved are so large; if high-speed guided missiles are more feasible than has been expected and the enemy discovers this first, the risk for us is very great.*

The request by the Bureau of Ordnance for a formal proposal was, in essence, in response to ideas generated by APL on how to prevent attacks on ships by guided missiles launched from planes beyond the range of conventional antiaircraft guns.

The first APL concept, suggested in early 1944, was a subsonic pilotless "fighter-missile," referred to as Falcon. A more detailed analysis of the problem was undertaken in the summer of 1944. It was concluded that a subsonic chaser would only be marginally effective against a target that could take evasive action. A detailed proposal (largely based on analysis by Jesse Beams, professor of physics at the University of Virginia) specified a supersonic velocity (1850 feet/ second), a promising powerplant (ramjet), a convenient fuel (octane), and a warhead weight of 600 pounds. The small amount of available design data at supersonic velocities indicated that a reasonably compact structure should be adequate to carry this payload to a distance of 20,000 yards. Radar guidance and a homing device were suggested, as were solid-propellant boosters. The code name for the proposed device was Torch.

Early in 1945, the project acquired the code name Bumblebee. Years later, as individual missile types were developed, mostly mythological names starting with the Letter T, were assigned to them (Talos, Triton, Typhon, and Terrier).

7. None of the needed components (powerplant, radar guidance, or booster) existed at the time the overall design was formulated. While there was hope that proof of concept would be available within a year, no tactical missile was foreseen in less than five years. In view of the expectation that the war would end in 1945 or soon thereafter, the likelihood of a useful device before the war's end seemed remote.

In contrast to the VT fuze, which took less than two years from invention to production, the complete guided missile system required a much longer development time. Talos, the culmination of the 1944

Falcon proposal, entered the Fleet in 1958, while the shorter-range rocket-propelled Terrier missile (an offshoot of one of the Talos test vehicles) became operational in 1955. Fully effective antiaircraft systems are only now being introduced into the Fleet.

While the APL proposal was the most ambitious in its specifications (supersonic speed, radar guidance), several other programs were discussed and initiated at the same time. Little Joe, Wac Corporal, and Tiny Tim, all subsonic and rocket propelled, were pursued by different sponsoring agencies, as were radio-controlled air-to-surface bombs (Razon, Tazon, Roc, and Gargoyle). The National Advisory Committee for Aeronautics developed a subsonic, radar-guided air-to-surface missile (Bat).

8. In an October 24, 1944, memorandum to Captain C. L. Tyler, M. A. Tuve wrote:

> *Even a negative result of this kind should be extremely valuable, as the attack aspects of these devices are of at least as great significance as the chaser (defense) aspects. Results of either type are highly necessary for the United States to possess as soon as possible whether ready before the end of the war with Japan or not.*

9. In a memorandum on "Intensive Program on Guided, Jet-Propelled Antiaircraft Missiles," dated January 11, 1945, Rear Admiral G. F. Hussey, Jr., wrote:

> *On the basis of technical considerations and work already in progress, the Commander in Chief, United States Fleet, directed on 4 December 1944 that the Bureau of Ordnance program on the development of guided, jet-propelled antiaircraft missiles is to be carried forward on an urgent basis and further directed that other Bureaus and agencies of the Navy give all possible support and assistance to the Bureau of Ordnance in connection with this program.*

Admiral Ernest J. King, at the same time, instigated a comprehensive survey, by a committee chaired by Prof. E. R. Gilliland of MIT, of jet-propelled missiles and their continuing postwar implications. Its overall purpose was to review the status of such missiles, with particular emphasis on their future possibilities and thus to aid the Navy in shaping requirements for the weapons and for research in the fields related to their use. At Air Force Headquarters, a similar study was undertaken when the high-level Scientific Advisory Group was established under the direction of Theodor von Karman.

10. Representatives of the Air Force and the British Scientific Mission in Washington were assigned to APL as liaison officers.

11. The question of "permanence" was discussed with great intensity for several years following World War II. The relationship and responsibilities of The Johns Hopkins University, APL, its associate contractors, and the sponsoring government agency (Bureau of Ordnance), and the makeup and the technical goals of the Central Laboratory staff were debated at length. For several years, the future of APL as a stable, large research laboratory under Johns Hopkins sponsorship was in doubt.

12. Soon after the formal Task F assignment to APL for the development of an antiaircraft missile, it was realized that the technology could readily be extended to other end-uses as well. Studies were assigned within a year for the design of a long-range ship-to-shore missile (Triton). Task extensions for the development of antiradiation missiles and antiballistic missiles were formulated at a later date.

13. The liquid-fuel rocket alternatives were never seriously considered. However, test vehicles propelled by solid propellants proved sufficiently adaptable to short-range applications that a separate program — Terrier — was organized to exploit the technology. Terrier became a dominant shipboard missile system.

THE TERRIER

a capsule history of missile development

M. R. Kelley

The history of the Applied Physics Laboratory between mid-1948 and mid-1956 was characterized by significant technological achievement, an outstanding part of which was the successful development of the missile named Terrier I. This was the first sea-going antiaircraft guided missile in world history. The Laboratory had, prior to that time, pursued an exploratory research and development program that resulted in, among other things, a supersonic-missile, test-vehicle configuration. The Navy decided to adapt it to tactical use as a rocket-propelled surface-to-air missile for the Fleet. This decision was communicated to the Guided Missiles Committee of the Department of Defense Research and Development Board on June 11, 1948. Dr. R. B. Kershner of APL proposed the name "Terrier" for the new missile, after the canine breeds of relatively small size, aggressive and tenacious by nature, but readily controlled by their masters. This name was approved by the Chief of the Bureau of Ordnance on December 29, 1948.

Development of Terrier presented no major problem in propulsion because enough was known of rocket propellants to afford confidence that it could attain the speed, altitude, and range demanded. However, there were other problems. Even though roll stabilization—a prerequisite of good beam-riding — had been achieved earlier by both subsonic and supersonic test models, and satisfactory beam-riding had already been demonstrated, unexpected difficulties were encountered in the first two STV*–3 flight tests (April and July, 1948). These tests had among their principal objectives the measurement of roll moment and determination of the damping coefficient, information that was urgently needed before a vehicle that incorporated a device for roll stabilization could be tested. Neither test provided the desired data because of malfunctions in the telemetering equipments, cause unknown.

In October 1948, a third test having these same objectives produced good roll data. Confirmatory results were also obtained in another flight test a month later. Shortly thereafter flights of two modified STV–3's, which were intended to be roll-stabilized, proved unsuccessful because of an apparent electrical power failure in one case and, in the other, the occurrence of large acceleration forces at end of boost, which were shown in post-flight analysis to have been present also in two previous STV–3 tests. Such forces had not been encountered in tests of the STV–2's. After careful study of the differences between the two vehicles, the booster-missile attachment was redesigned to minimize the possibility of a collision between it and the missile's tail

These historical notes are adapted from a chapter on the Terrier missile prepared by Rear Admiral M. R. Kelley, U.S. Navy (Ret.) for inclusion in a history of the Applied Physics Laboratory.

* Supersonic test vehicle.

compartment and nozzle extension tube during separation. But the first flight test of this attachment (April 1949) showed that it had not resolved the difficulty; the missile did not roll-stabilize, and a violent disturbance occurred at separation, knocking out half the telemetering channels. Further investigation identified three acceleration forces operating during the boost and separation stage: (1) *acceleration at boost,* which forced the 250-pound sustainer charge rearward against the after face of the case; (2) *deceleration at end of boost,* which thrust the charge hard against the forward face of the case; and (3) *igniter pressure at ignition,* which drove the charge solidly against the after face of the case, producing the damaging shock. Accordingly it was decided to immobilize sustainer charges in all subsequent STV–3's, a "fix" that proved highly effective in later tests.

Meanwhile, during the above tests extending over a period of 18 months, progress was made in two other areas. A so-called "zero-length" launcher was checked out satisfactorily in four of the above-cited tests, and capture of the missile into the guidance beam at end-of-boost was successfully accomplished in the flight of an STV–2.

Prototype Testing Begins

Following the Navy's decision in the spring of 1948 to make a tactical missile of the STV–3, plans were formulated to reach the final design of the new missile through tests of a succession of prototype missiles designated Lots 1, 2, 3, 4, 5, and 7. Lots 6 and 8 were earmarked for development of a higher performance missile at a later date, to benefit from the experience with the earlier lots and from advances in the state of the art. Confident that a tactical version of the STV–3 could be achieved, the Navy early contracted with the Consolidated Vultee Aircraft Corporation for production of a pre-prototype Lot 0 consisting of fifteen missiles. Late in 1949, the Bureau of Ordnance (BuOrd) declared the Terrier to be in the production prototype stage and contracted with the above corporation for the manufacture and delivery of 50 prototype units spread over Lots 1 through 4. Pending delivery of the first Lot 0 missiles, tests of various models of the STV–3 were continued, these tests varying in their objectives as determined by the problems under investigation.

Guidance Problems Investigated

With completion of successful tests of the zero-length launcher and the achievement of roll stabilization in the STV–3, emphasis was more and more centered on solution of the guidance problem. This was at first a matter of beam-riding performance. The very modest effort on an interferometer homing system that had been started in 1948 was viewed only as a possible alternative in case satisfactory beam-riding guidance should prove unattainable. There had been early tests, beginning with two flights of subsonic control test vehicles in 1947 and followed by two successful STV flights in 1948, which inspired confidence that beam-riding guidance could be made effective for tactical employment afloat. In these tests, however, the radar guidance beam had been fixed in space and the test missile was so launched as to be in, or close to, the beam axis at the time of booster separation. This insured that the missile would be in a position to receive guidance signals from the radar. It was obvious that such an accommodation would only accidentally, if ever, occur in a tactical situation at sea.

In another respect, also, these tests were not representative of guidance conditions in actual service afloat. There the radar pulses directed at a high-speed aircraft would be reflected randomly from different surfaces or features of the target and, in combination with random reflections from the sea, would cause the beam to jitter. No beam-riding guidance system could be considered acceptable until a determination had been made that this jitter did not adversely affect the missile's accuracy in guided flight. The opportunity was taken, therefore, in the STV–2 test in April, 1949, marking the first successful use of a capture beam, to test also the missile's ability to ride a jittering beam. Jitter was injected into the beam at the radar source so as to simulate that expected in a tactical situation. Another "first" was achieved when the missile demonstrated in this test that it could ride a jittering beam with acceptable accuracy.

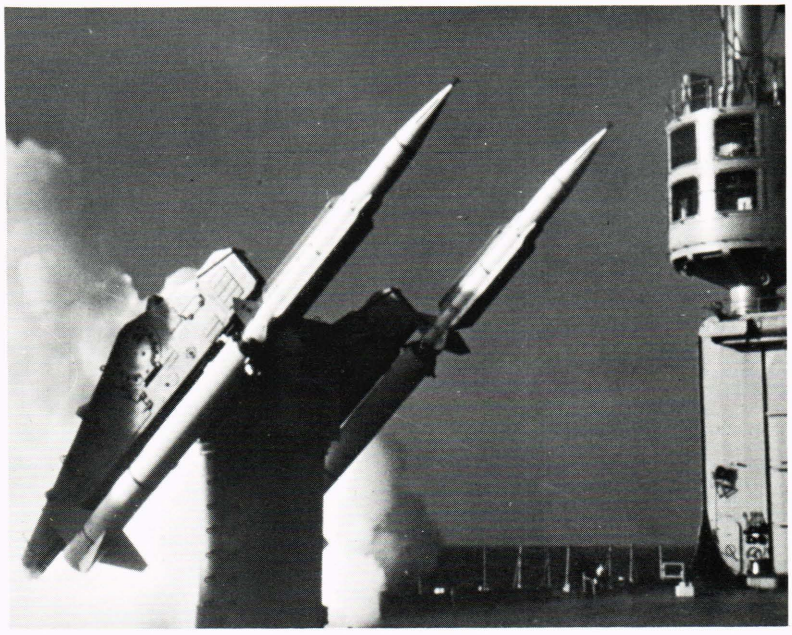

Terrier missiles (BT-3) being fired from the deck of the USS *Norton Sound.*

Meanwhile research and development in beam-riding guidance had been actively carried on with a view to improving the sensitivity of the missile response to control corrections for guidance errors, both near the surface and at altitude. Obviously, the aerodynamic control surfaces would have to be moved through greater angles in the rarified atmosphere at high altitude than in the denser atmosphere near the earth's surface in order to correct promptly any off-beam error. A redesign of the control system for the STV–3 had been completed near the end of 1948, the effectiveness of which was impressively demonstrated in a flight test about a year later when guidance sensitivity was changed in flight for the first time, being increased by a factor of six. The missile responded promptly by closing to within 2 mils of beam center, where it remained more than twice as long as any previous Bumblebee beam rider. This signaled an important advance in beam-riding accuracy. Other less obvious factors also had to be taken into account in devising a system of controlling missile guidance sensitivity, but results achieved in the above test indicated good progress. They were soon well corroborated by another STV–3 test that demonstrated excellent roll stabilization and speed of response.

In December 1949 the first of the initial experimental production missiles (Lot 0) was delivered and, within two months, was flight-tested at the Naval Ordnance Test Station (NOTS). Missile capture was most impressive, and beam-riding proved quite good during much of the flight. Since the Navy had already decided to use the aircraft tender USS *Norton Sound* for preliminary shipboard tests of Terrier, the opportunity was now taken to measure the effect of booster blast on a specially constructed deck section similar to that in the location selected for the ship's launcher. Results showed the deck to be suitable for launching Terrier at quadrant elevations of 35° or less.

Necessary preparations for shipboard testing included the assembly of all the elements of the Terrier system for installation in the ship, plus the elements of an approximately identical system for use at NOTS. The latter system, obviously, did not need to have the capabilities in the weapon-direction, fire-control, and launching subsystems that would be required in the face of the unpredictable motions of the ship at sea.

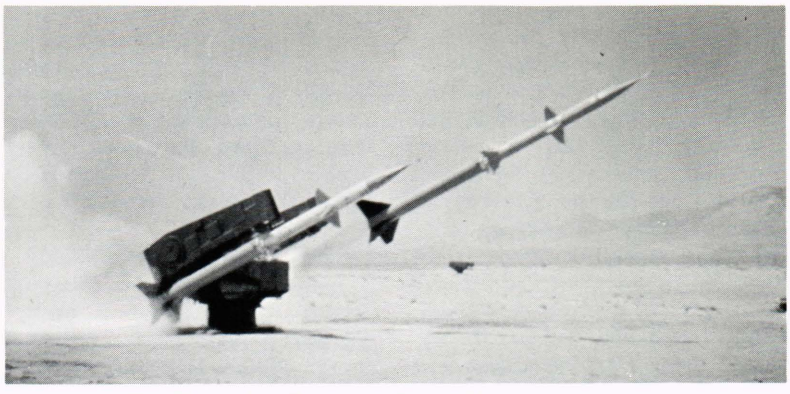

Test firing of the Terrier missile at China Lake, California.

By this time progress made toward a rocket-propelled tactical missile, plus the general advance on all fronts in missile technology, warranted an updated appraisal of the capabilities that seemed possible of attainment in an advanced design. Accordingly, in May 1950 the Navy issued a new operational requirement which set the military characteristics for a higher performance missile that came to be known as Terrier II. The Laboratory, which had contributed to the appraisal of capabilities pertinent to an improved Terrier missile, immediately undertook the necessary studies to formulate specifications for a design aimed at meeting the new requirements.

Action in Korea

But in a matter of weeks there occurred totally unexpected events of great historical importance, which gave new emphasis to the revolution in weapons and created overnight a sense of urgency that had not existed since V–J day. The "cold war" suddenly and unexpectedly came almost to the boiling point. A strong force of North Koreans, behind a phalanx of tanks, invaded South Korea on June 24. The U.N. Security Council in emergency session—in the absence of Russian representatives—adopted a resolution before the day was out condemning this unprovoked aggression, and three days later adopted a second resolution recommending that members of the United Nations furnish such assistance to the Republic of South Korea as might be necessary to restore the status quo in Korea. In compliance President Truman at once directed the U.S. Navy and the U.S. Air Force to give the South Koreans air cover and support; by June 30 U.S. military forces present in the area were quite fully committed.

Fear that the *police action*—so-called by President Truman—might escalate into a major war became a matter of utmost concern to all Americans. Each of the military Services immediately undertook a survey of its overall preparedness to meet such a contingency. This was backed up by individual and collective planning to blunt the edge of any further aggression before it could acquire momentum. As in World War II, the threat from the air, whether in the form of aircraft-launched guided rockets or surface-launched bombardment missiles, was considered most serious of all. This was fully substantiated by the Armed Services' research and development efforts that from 1945 were directed toward an adequate defense against such attack. Although there were several promising development programs, it was recognized that as of the start of hostilities in Korea no surface-to-air or air-to-air missile could be expected to reach the serv-

ice-use stage in less than three years. Within the Department of Defense, after "in-house" surveys of the situation by the military Services, the following views found general acceptance: (1) the antiaircraft missile programs nearest the service-use stage should be pushed at the highest possible level of effort, compatible with the state of the art and good engineering practice, toward acceptance and production for use in combat; and (2) the number of missile programs might well be cut back, permitting continuation of only those that promised to satisfy requirements for which no other adequate program was in hand.

On October 25 Mr. K. T. Keller of the Chrysler Corporation was appointed Director of Guided Missiles by the Secretary of Defense. His mission, essentially, was to direct the military missile program so as to expedite entry into service use of those missile systems most urgently needed. Additional funds, facilities, and technical personnel were expected to be made available from the defense budget and by cutting back other programs less far advanced.

Missile Programs Accelerated

With a staff of civilian-military representatives of the three Services, Keller made a survey of all the guided missile programs and subsequently recommended for special emphasis the Army's Nike, the Navy's Terrier and the Navy's Sparrow, on the basis that each could be put into service at a relatively early date and each would satisfy an immediate need. Within the Research and Development Board of the Department of Defense, the treatment proposed for these three missiles was commonly called "super-acceleration," but in the fellowship of scientists, engineers, executives and administrators engaged in research, test, development, and production of guided missiles it was known as "Kellerization."

An almost immediate result of this treatment prescribed for the Terrier was a decision by BuOrd to have incorporated in the design of the Lot 4 prototype the final tactical features of Lot 7. The latter had been viewed originally as the ultimate production-engineered version of the tactical Terrier. The design of Lot 4, completed in conformity with that decision, was frozen at the end of 1950, anticipating that a satisfactory tactical missile would emerge thereby at least six months earlier than had been previously scheduled.

In addition to acceleration of the missile programs, the Navy decided to install Terrier systems in selected World War II heavy cruisers. Two dual launchers were to be located on the cruiser's after deck, each supplied from its missile magazine below by means of automatic handling and loading equipment. The subsystems needed for controlling two complete missile systems were also to be installed, making it possible for each launcher to fire a two-missile salvo every 30 seconds. The U.S. Marine Corps undertook at once to organize missile battalions for defense of overseas bases. Steps were also initiated by the Army to procure 25 Terriers for training purposes, and preliminary action was taken to have the supporting ground control equipment provided. This resulted early in 1951 in a contract with the Radio Corporation of America to develop an Army Tactical Terrier System. At NOTS a Terrier system similar to that planned for the USS *Norton Sound,* but not suited for use at sea, was installed by mid-1950 and put in operation in the flight-test program. By the end of the year installation of the first Terrier shipboard system, including computer and dual launcher, was completed in the *Norton Sound* at the San Francisco Naval Shipyard. Navy Guided Missile Training Unit No. 21 was transferred from NOTS to the ship for on-board training and checkout of the system in preparation for the first missile firing afloat, which was expected to take place within a few months.

The year 1950 saw a number of other important indications of progress in the Terrier program. Following the successful test of the first Lot 0 in February, several quite satisfactory tests were conducted during the year, marking improvements in the missile-borne guidance receiver, beam-riding in the presence of jitter, and successful launching from a trainable launcher to which aiming intelligence was supplied by the guidance radar and computer in order to facilitate missile capture in a moving guidance beam. Of seven Terrier pre-prototypes flown in this period, the one tested on May 12 marked the first supersonic-missile versus target-drone test in this country, while the firing on October 4 proved noteworthy as the first instance of two missiles being fired in salvo. Other units tested included four early Terriers (Lot 1A), of which the first, fired against a target drone on October 18, demonstrated that the new orientation of the steering wings, 45° from the vertical and horizontal planes, gave satisfactory performance. Although several units tested experienced malfunctions that precluded attainment of all prescribed

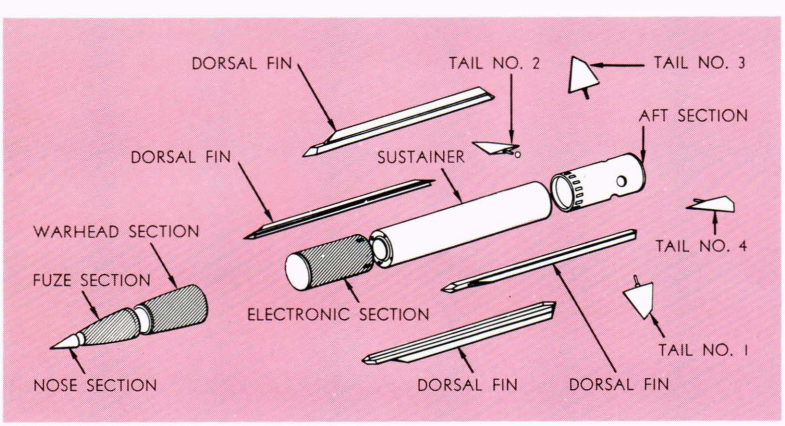

Exploded view of the BT-3 missile.

objectives, review of the test results for 1950 showed that the sum total of objectives had in fact been attained.

Warhead Development

An important part of the super-accelerated Terrier program was the development of a warhead. Studies indicated that controlled fragmentation of material concentrated in the side walls of the warhead, plus an increase in fragment velocity to 10,000 ft/sec or more, would give twice the killing power per pound of the antiaircraft fragmentation shells previously used. Based on results of experimental work with a hydrogen gun conceived and built at the New Mexico School of Mines under Navy contract, APL became the first proponent and sponsor of high-velocity impact studies. In 1949 a new experimental gun built at the Naval Research Laboratory (NRL) to extend the facilities there for investigation of penetration, in cooperation with APL, obtained velocities believed to be the highest ever achieved with ordinary powder propellants. As a result of studies of the relative merits of small, high-velocity fragments, large fragments (rods) of relatively low velocity, and pure blast, the technique of distributing large numbers of small, fairly high-velocity fragments in an annular conical beam was adopted for use with the Terrier missile.

The effectiveness of a warhead is not alone a matter of the weight of explosive and the type and size of fragments. It depends also on detonation at the precise instant that will cause destruction of the aircraft. This is the fuze's function. Although the development of fuzes for the Terrier missile was a responsibility of the National Bureau of Standards at the time, APL had an important part in determining the width and direction of the channels along which target reflections should be received that would cause the fuze to function.

Studies were initiated to find some means of providing guidance intelligence at low altitude that could not be interfered with by random reflections from the surface. This turned out to be a difficult problem. For another problem, however—that resulting from unintentional friendly-radar interference with the guidance intelligence being transmitted to a missile (or missiles) in flight—a solution was found. With the design of an improved guidance receiver that would accept signals only from its own guidance radar, the problem of unintentional interference from friendly sources ceased to exist.

Advent of the Terrier Missile System

By early 1951, the Terrier program had reached a stage that inspired confidence that an effective weapon system was fairly close at hand. Problems still existed but none was considered insoluble. Moreover, it was felt that corrective measures found necessary could be taken without too seriously disturbing existing designs or schedules. This was most important because the situation could brook no delay; Terrier must be gotten into service as quickly as possible. Reports of bitter fighting in Korea against the staggering odds posed by the entry of 12 divisions of Chinese Communist "volunteers" into the war portended further escalation of the fighting, perhaps even to global proportions.

Most of the problems that lay ahead proved to be of the type normally associated with the transition of a development and engineering program to one of quantity production. But growing confidence that the near future would see a successful antiaircraft guided-missile system in operation encouraged the Navy to make two important decisions early in the year. The first was to start construction of a production facility at Pomona, California, to be devoted entirely to the manufacture of guided missiles. Consolidated Vultee Aircraft Corporation, then constructing the Terrier prototype at San Diego, was selected to operate the new facility. Construction proceeded rapidly, and by the end of 1952 all Terrier manufacturing operations were transferred to Pomona, where they have continued to the present.

The second decision was to have the Navy's Operational Development Force (OpDevFor) conduct an evaluation of the Terrier missile system aboard a combatant ship, following preliminary shipboard tests on the *Norton Sound*. The USS *Mississippi* was selected for this purpose, to be modified by having the two after gun turrets removed and two dual launchers installed. In February 1952, the *Mississippi* entered Norfolk Naval Shipyard for installation of the modified Terrier system—a task completed by the end of the year.

Following this shipyard period, APL assisted in checking out the system elements in the performance of their appropriate functions. November 1952 saw the first missile firings from the ship—two Terrier launching test vehicles that performed satisfactorily to demonstrate operability of the handling, launching, and instrumentation systems. Meanwhile, the heavy cruisers USS *Boston* and USS *Canberra* entered naval shipyards to be converted to Terrier missile ships, destined to become the first guided missile cruisers in naval history.

Mention has been made of the Navy's new operational requirement, issued shortly before the start of the Korean War, and of APL's response to it, leading to the formulation of recommendations for a Terrier of considerably improved performance. As a result of detailed investigations, a beam-riding missile was selected for development, which would include an altimeter-control device for effective guidance at low altitude. Homing was considered also, and design dimensions were selected to accommodate a target seeker. Aerodynamic studies had shown by that time that tail control, in which steering and roll stabilization were accomplished by appropriate movement of tail surfaces, had certain distinct advantages over control through movement of wing surfaces. By the end of 1950 early studies and experimental testing had been completed so that APL was able to prepare a set of preliminary military specifications which formed the basis of recommendations that were accepted by BuOrd in January 1951. This inaugurated a new development program leading to an improved version of Terrier, designated Terrier II.

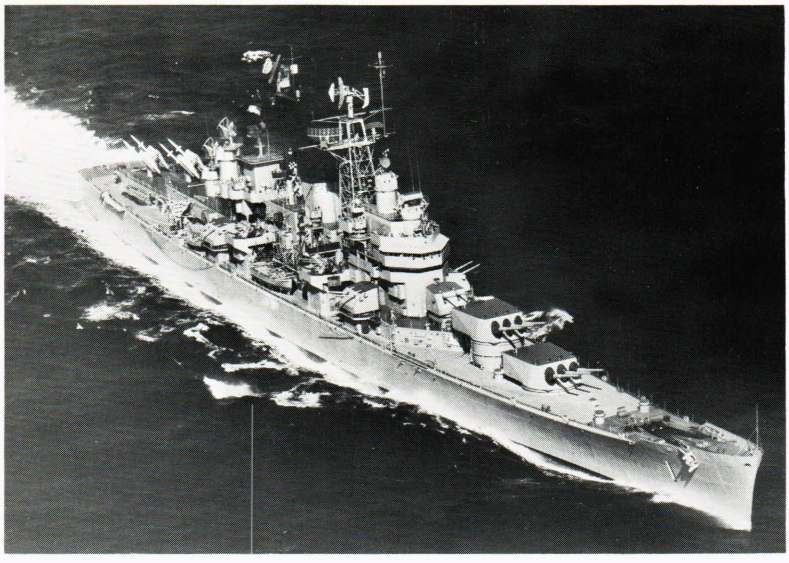

The USS *Boston* (CAG-1) at sea, showing dual launchers and Terrier missiles on the after deck. (Official U. S. Navy photograph)

Terrier II Program

A test program consisting of four test vehicles (STV–4's) was initiated by APL to obtain verification of the tail control studies. One major change had to be made in configuration. Up to that time the outside diameter of Terrier missiles had been 13.5 inches; it appeared now that it would be necessary to increase the diameter to 15 inches to accommodate a sustainer that could provide the impulse necessary to give the improved performance desired.

By mid-1951, the Terrier II program had suffered considerable delay since it was not permitted to interfere in any way with the "super-accelerated" Terrier I. Further delay in the program seemed a certainty in October 1952, so a six-month review was undertaken. Among other conclusions reached in this review was that a wingless and tail-control version of Terrier, which would have many advantages, could be derived from the original winged design.

Meanwhile, the Terrier I program had made good progress as it swung into high gear at the beginning of 1951. Several excellent tests of Lot 1 and Lot 2 missiles were recorded. The distinction of being the first Terrier to be fired from a ship fell to a Lot 2 missile, which achieved all prescribed objectives in a noteworthy test from the *Norton Sound* on September 7, 1951. Another Lot 2 missile, exactly three months later at NOTS, became the first Terrier to engage an aircraft successfully when its fragmentation warhead scored 15 penetrations in a drone target, although the missile was at the limit of lethality at the instant the fuze functioned. The F6F drone was not brought down by these fragments, but examination showed that one of them passed right through the place the pilot would have occupied had the plane been manned—a hit that would undoubtedly have resulted in loss of the plane. On May 16, 1952, this success was followed by flight tests at NOTS of two Lot 3 missiles fired less than two hours apart at separate drones. Each gave an outstanding performance and destroyed its target. The first Lot 4 missile to be flight tested, in April 1952, proved unsuccessful; this, however, was no cause for great concern because in the desire to make the earliest possible test of several new components a number of modifications to the missile had been found necessary.

It was apparent by this time that because of engineering difficulties Convair was far behind schedule in Lot 4 production. Accordingly, six APL staff members were assigned to Convair to assist in the engineering and production program, while special investigation of a number of components and subassemblies was undertaken at the Laboratory. A few weeks later the Terrier Emergency Committee was established by APL to assume responsibility for all efforts toward a solution of these critical problems.

Aware of the production difficulties, BuOrd in the summer of 1952 selected 30 Lot 4 missiles from the production line, to be designated Parameter Test Vehicles (PTV's) and to be used to check Lot 4 operability and performance in flight, with special attention to the roll problem. The Bureau of Ordnance subsequently formed a Terrier Task Group (TTG) of representatives of the Navy, APL, and associate contractors concerned with the critical problems. This committee took over the functions of the Terrier Emergency Committee and was domiciled at Pomona where it worked closely with Convair's production engineers. As a result of the remedial measures taken, Terrier flight tests in January 1953 showed Lot 4 missiles to be good beam riders, with their reliability appraised as "fair." A test series of Terrier Research Test Vehicles (RTV's) in early 1953 supplied much information of value on overall operability and performance characteristics of Lot 4 missiles and further aided in resolution of the production difficulties at Pomona.

Assurance that Lot 4 missiles could carry out the tasks for which they were designed was strengthened as 1953 progressed. An important milestone was reached in May when a missile fired from the *Norton Sound,* carrying a live warhead, rode the beam to interception and destruction of its F6F drone target. Following closely thereafter was another test at NOTS in which a Lot 4 missile made a successful target interception, marked by proper fuze and smoke puff operation, at an altitude appreciably above that of any previous Terrier test. Eleven days later another of this lot, fired from the *Norton Sound* and armed with a live warhead, destroyed its target, also at high altitude. Such early and convincing demonstrations of the effectiveness of the new tacti-

cal Terrier were most encouraging to the Navy, as well as to the Laboratory and its associate contractors.

Of two Lot 4 tests from the *Norton Sound* against targets at low altitude, one was a complete success while the other rode the beam well for 27.5 seconds, then experienced a malfunction of one of the wing controls, the cause of which could not be accurately determined from the test data recorded. All in all, however, on the basis of test performance Lot 4 appeared to be ready for tactical employment at sea. But by this time, the next block of Terriers, designated Lot 5, was in full production. It was not a noticeably different version of Terrier but essentially a continuation of the Lot 4's, incorporating all the design and engineering improvements that experience had dictated in the production and test of its predecessor. The first of this new lot was flown at NOTS in June, a month marked also by the return to Maryland of most of the APL engineers who had been assigned to the Terrier task group at Pomona.

Truce in Korea

The year 1953 witnessed an event of historical importance that gave sanction to a trend that had developed early and almost imperceptibly in the conduct of the accelerated U.S. missile program. The event was the signing of a truce, on July 27, by representatives of the United Nations and the North Koreans, which brought an end to the fighting. The trend was a gradual relaxation of the taut guide lines originally accepted in carrying out the accelerated programs. It was in this atmosphere that the Laboratory began investigations to improve the design of the tactical missile in respect to uniformity and reliability of the production version, without detracting from the main effort.

Recognizing that the early problems had shown a need for engineering improvements to facilitate production, APL initiated a study to demonstrate the feasibility of rearranging missile components so as to simplify assembly, repair, and maintenance. The objective was to group together, into appropriate subassemblies and sections, components that were related either by similarity of technique in manufacture or by test requirements. The new, re-packaged design became known as Terrier IB, to distinguish it from the version then in production, which was based upon the Lot 4 tactical design updated to Lot 5 and labeled Terrier IA.

In April 1953 the Laboratory had prototypes of the re-packaged electronics and hydraulics sections available for examination by the Navy. These were viewed with much favor, and APL was requested to undertake a full-scale engineering program to construct a number of units in order that their performance might be evaluated by extensive ground and flight testing. Two of the newly designed missiles were flown near the end of 1953, after being assembled and checked out with exceptional ease. The first demonstrated excellent beam-riding throughout its long flight, and the second would have done equally well except for a premature smoke puff operation that caused a malfunction in the missile. Additional firing tests were conducted during 1954, with the same or even better success. Laboratory participation in this program terminated in late 1954 when the design was turned over to the Navy, and four missiles were transferred to Convair for evaluation prior to type approval.

Gradual easing of the tensions that had attended the Korean hostilities also permitted a step-up in the Terrier II (Lot 6) program, the six-month review of which had been completed in the spring of 1953. There were four objectives of this program: (1) to increase missile maneuverability for greater effectiveness against targets at high altitudes; (2) to increase missile range; (3) to permit carrying a heavier warhead to achieve greater lethality; and (4) to improve missile performance at low altitudes. On the basis of the program review, a new set of performance requirements was prepared by APL, and BuOrd contracted with Convair to engineer and develop a group of eight test vehicles, designated STV–5s, for flight test under APL's technical direction to determine their ability to meet these requirements.

On July 1, 1954, the OpDevFor evaluation of the Terrier missile system began, following completion of the BuOrd Assist Phase that had been conducted aboard the *Mississippi* to familiarize personnel of the ship with the new weapon system.

Missile Modification Program

As the engineering program undertaken first by APL in 1953, then by Convair, made progress in 1954 toward a better tactical Terrier, the introduction of changes in the roll system, hydraulic power supply components, aerodynamic surfaces, and other improved components required retrofitting of missiles on a systematic basis. Accordingly, a step change in missile production was adopted by which such improvements could be incorporated when they were found to be ready for use in production missiles. At the same time the necessity of differentiating between the types of missiles being produced became apparent. It was decided, therefore, that the required designations would be made up of two letters each, the first indicating the method of guidance and the second, the method of control. For guidance, B would indicate beam-riding and H, homing. For method of control, W would indicate wing control and T, tail control. The number 1, 2, or 3 following these letters would identify the combination of booster and sustainer rockets used by the particular missile. The then-current production missile was assigned the designation BW-O, indicating that it employed the combination of booster and sustainer rockets then in production.

Work on homing guidance was actively continued during this period. As early as 1953, good results had been obtained with the Raytheon target seeker used in Sparrow—one of the super-accelerated missiles of the Korean emergency period—and it was closely watched for possible application to Terrier. Under APL sponsorship Convair established a facility on San Clemente Island, off the California coast, to obtain basic

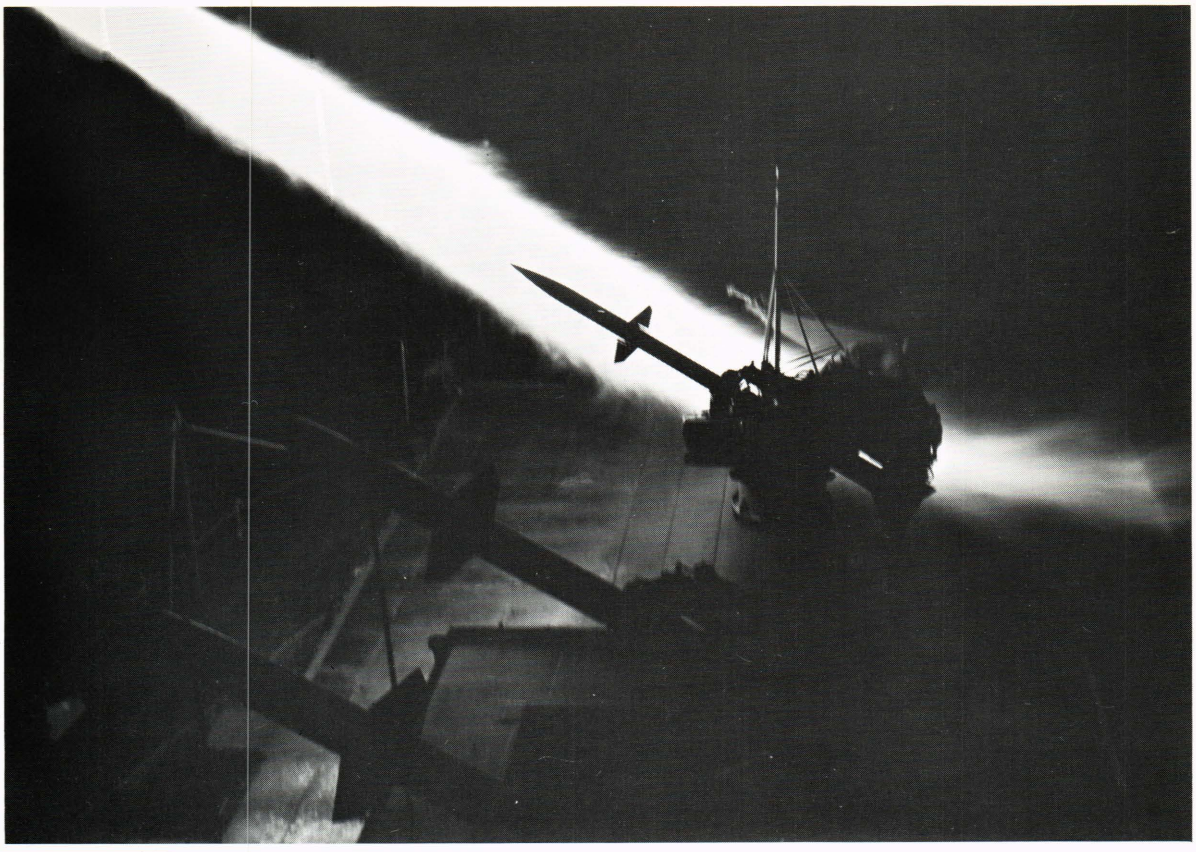

Terrier missiles undergoing test firing at sea from the deck of the USS *Mississippi.*
(Official U. S. Navy photograph)

measurements of sea reflection properties having effect on homing guidance, and to evaluate seekers, such as the one used in Sparrow, for possible service in Terrier. Data recorded there were converted into suitable form to be used in the Raytheon seeker when tested in homing simulators built by Convair.

Late in 1954, the Laboratory began a three-phase program of development of a semiactive homing system for use in Terrier I missiles. Test firings that began in early 1955 and continued for about two years demonstrated the feasibility of homing guidance as well as its effectiveness against low-flying targets.

There were in effect during the latter part of 1953 and all of 1954, two Terrier development programs in addition to the still-basic program of proving-in the tactical Terrier I missile. The first of these development programs was the Terrier improvement program, which had as its objective improvement of the tactical missile through engineering changes designed to simplify missile assembly, checkout, and repair, and to develop effective guidance at low altitude, without seeking to extend the missile's performance beyond that prescribed in pertinent specifications. The second was the improved-performance Terrier (designated Terrier II), which had as its objective the development of a missile with substantially increased performance capabilities in range, altitude, and maneuverability, plus improved effectiveness at low altitude.

Advanced Terrier

From consideration of these two development programs as 1954 advanced, it could be said that they had a common purpose in the sense that both were directed toward achievement of a service missile that would give consistently excellent performance within its designed limits, be easy to produce and maintain, and possess a high degree of adaptability to meet various situations. Certain design and engineering developments in each program were found to be applicable and beneficial to the other. Accordingly, APL and Convair late in the year formulated a long-range program for improvement of the Terrier missile, which was submitted to BuOrd for approval. Its objective was to achieve production by 1960 of an "Advanced Terrier" missile that would be compatible with the stowage and handling facilities being installed for Terrier I in the heavy cruiser missile ships and would be capable of successful interception and destruction of potential air threats in that period.

Development of Advanced Terrier was to be based on the sectionalized configuration of the Terrier IC, then entering the flight-test phase of evaluation, and on the knowledge gained from the Terrier II program of the performance that could be

reasonably expected from the wingless, tail-controlled missile. A stepwise development was planned, therefore, so as to have in the production stage at any given time a missile capable of countering the potential threat for that period.

On the basis of this review, BuOrd early in 1955 redirected the Terrier II program along the lines summarized above, assigning technical direction to APL. Although the program of developing an improved-performance Terrier took on a somewhat different hue as a result of this redirection during early 1955, the test results obtained up to that time in three STV–4 firings contributed substantially to the STV–5 program. Much useful data were obtained. The third STV–4 test confirmed studies that a wingless missile would be both feasible and practical, thereby contributing in large measure to the decision to eliminate wings on all improved-performance Terriers.

Planning started at once on the Advanced Terrier program. A homing-guidance Terrier, to be designated HT–3, was made the ultimate objective of the program, but since development of homing guidance had not progressed as far as that of beam-riding guidance, some doubt existed that missiles employing a homer would be ready for production as early as 1960. It was decided, therefore, to develop the necessary aerodynamics, dynamics, control, and propulsion systems in a beam-rider (BT–3) that could be available by 1960, and then to utilize these developments in a homing missile design when a suitable system of this type was developed. By so doing, maximum use could be made of Terrier BW–1 developments in the areas of guidance, warheads, and fuzes, as well as of the STV–5 series of missiles. The firing of two launching test vehicles and four control test vehicles in this series contributed data that were to prove useful in the advanced program.

First Guided Missile Heavy Cruiser

The ultimate aim of the years of effort in Terrier development was brought a long step closer to realization on November 1, 1955, when the USS *Boston,* having successfully completed the required preliminary acceptance trials, was recommissioned at the U.S. Naval Base, Philadelphia. Its name was unchanged but it bore a new Navy classification, CAG–1, signifying the first of a new class of ship in the U.S. Navy (and in world history)—"guided missile heavy cruiser."

On January 30, 1956, after several weeks devoted to familiarization with the new weapon system, the *Boston* sailed for Guantanamo to undergo shakedown training. There, early in February, the prescribed training began, which, because of the revolutionary weapon system installed in the ship, was extended beyond the usual six weeks. Several important groups of visitors witnessed the missile firings, spanning a period in which 10 Terriers, in the jargon of Navy torpedomen, flew "hot, straight, and normal" to successful achievement of all objectives.

As of July 1, 1956, the development phase of Terrier I was considered to be complete. Terrier had gone to sea.

PUBLICATIONS

The following list is a compilation of recently published books and technical articles written by APL staff members.

J. O. Artman and J. C. Murphy (APL) and S. Foner (M.I.T.), "Magnetic Anisotropy in Antiferromagnetic $\alpha - (Cr_{1-f}Al_f)_2O_3$," *J. Appl. Phys.,* **36**, Mar. 1965, 986–987.

J. G. Parker and R. W. Swope, "Vibrational Relaxation Times of Oxygen in the Temperature Range 100° – 200°C," *J. Acoust. Soc. Am.,* **37**, Apr. 1965, 718–723.

T. O. Poehler and D. Abraham, "Aluminum—Doped CdSe Thin Film Triodes," *Appl. Phys. Ltrs.,* **6**, April 1, 1965, 125–126.

L. Monchick (APL), A.N.G. Pereira (St. Xavier's College, Goa, India), and E. A. Mason (University of Maryland), "Heat Conductivity of Polyatomic and Polar Gases and Gas Mixtures," *J. Chem. Phys.,* **42**, May 1, 1965, 3241–3246.

V. Uzunoglu, "Feedback: Perils and Potentials in Designing Integrated Circuits," *Electronics,* May 31, 1965, 67–71.

S. D. Bruck, "Thermal Degradation of an Aromatic Polypyromellitimide in Air and Vacuum—III—Pyrolytic Conversion into a Semiconductor," *Polymer* (London), **6**, July 1965, 319–332.

R. P. Rich and A. G. Stone, "Method for Hyphenating at the End of a Printed Line," *Communications of the ACM,* **8**, July 1965, 444–445.

D. J. Williams (APL) and G. D. Mead (NASA), "A Nightside Magnetosphere Configuration as Obtained from Trapped Electrons at 1100 Kilometers," *J. Geophy. Res.,* **70**, July 1, 1965, 3017–3030.

W. G. Berl, "A Brief Review on the Combustion of Boron Hydrides," *Progress in Astronautics and Aeronautics,* **13**, Academic Press, New York, 1964, 311–325.

R. R. Newton, "Orbital Elements from the Doppler Tracking of Four Satellites," *J. Spacecraft and Rockets,* **2**, July-Aug. 1965, 634–636.

D. Abraham and T. O. Poehler, "Heat Flow as a Limiting Factor in Thin-Film Devices," *J. Appl. Phys.,* **36**, June 1965, 2013–2020.

The following five papers were published in *Tenth Symposium (International) on Combustion,* The Combustion Institute, Pittsburgh, Pa., 1965:

W. G. Berl (APL), P. Breisacher (Aerospace Corp.), D. Dembrow (NASA), F. Falk, T. O'Donovan, J. Rice, and V. Sigillito (APL),

LESTER L. CRONVICH

MISSILE AERODYNAMICS

This article describes the role of the aerodynamicist as a member of a missile development team, the preliminary design tools available to him, the potential problem areas in designing aerodynamically efficient configurations, and the types and sources of aerodynamic data needed during the engineering development and flight-testing process. The discussions deal primarily with tactical surface-to-air missiles, although the general development philosophy also holds for other types.

SETTING DESIGN REQUIREMENTS

The goal of the development team is to develop a tactical missile system either to counter an expected threat to one's own defended area (a defensive system) or to destroy or do significant damage to the enemy's defended area (an offensive system). For the aerodynamicist, this means designing the external configuration of the airframe so as to provide sufficient capability (speed, range, and maneuverability) to accomplish the mission planned for the system.

The first task of the team is to ascertain the threat and, on the basis of feasible battle scenarios, develop a missile system concept to counter it. That concept will establish broad requirements in most technologies. The aerodynamicist must carry out his preliminary design study while recognizing the limitations on his options that are imposed by necessary choices in the other technologies or subsystems, as indicated in Fig. 1 and discussed in the next section. The mission analysis should lead to design goals for range, speed, and maneuverability of the missile, to fuzing and warhead needs, and to an overall guidance philosophy. At this stage, first-cut individual choices can be made by the several related technologies to achieve the mission. Modifications to those choices will be made as more-detailed interrelated studies of subsystem performance are made. Thus, a baseline configuration can be established from which further development can proceed.

TECHNOLOGY INTERFACES WITH AERODYNAMICS

Launching

Besides restricting the missile's weight, length, and span, the launching system may restrict its permissible motion early in flight. Also, such factors as the motion of the launcher and winds or extraneous flow fields about it will affect the missile's design. The external shape might also be affected by launching shoes or other devices that guide the missile out of the launcher. Such appendages add drag and weight and can affect the missile's stability or controllability. The span limitation for a given launching system may require lifting and control surfaces to be folded, which adds to missile weight and drag and introduces a potential dynamic disturbance during deployment. The aerodynamic design must be done with full knowledge of these considerations so that detrimental effects can be minimized.

Propulsion

A missile's shape may depend strongly on its propulsion system. Designers of airbreathing systems

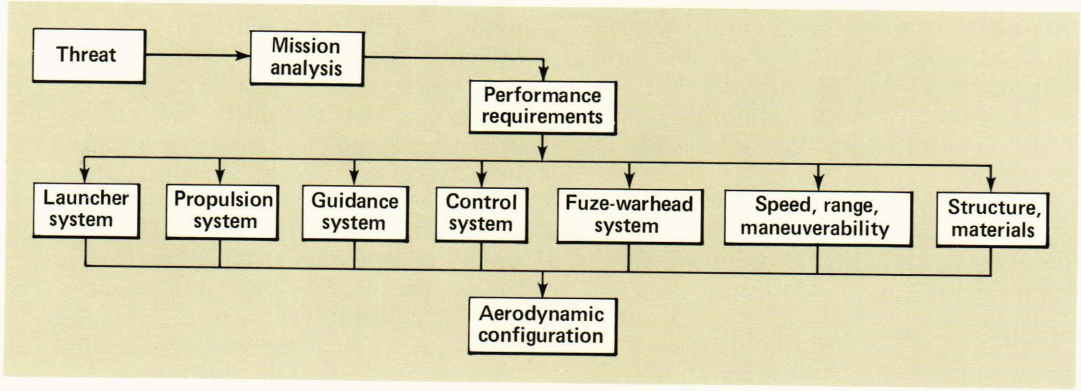

Figure 1 — Factors and systems affecting the design of aerodynamic configurations.

prefer to locate the air inlets in areas free of degrading aerodynamic interference such as shock waves, vortices, or wakes. At the same time, the inlet itself may degrade the aerodynamic performance. Thus, a compromise must be made between propulsion performance and aerodynamic performance, or, if possible, a design should be sought that takes advantage of favorable interactions that improve thrust, lift, stability, and controllability or that reduces drag.

As fuel is consumed, the center of gravity may shift, thereby changing the controllability of the missile. In general, the center-of-gravity shift is more troublesome with solid-fueled propulsion systems than with liquid-fueled propulsion systems, which have more flexibility in the location of fuel tanks. Offsets of the thrust axis from the center of gravity may also occur for certain propulsion systems (e.g., strap-on booster systems) or may result from design tolerances or from center-of-gravity travel that moves the center of gravity off the thrust axis. Such offsets can result in overturning moments that require additional control capability from the airframe.

Guidance

The choice of guidance system will affect the demands on missile maneuverability and response, which, in turn, may affect the choice of lifting and control surfaces. Furthermore, the design of domes to protect guidance sensors usually calls for compromises. For example, a hemispherical dome is usually considered the optimum choice for the sensors, but it has high drag. A dome with a high fineness ratio (i.e., length/diameter ratio) has low drag, as shown in Fig. 2, but tends to degrade the reception of signals by the seeker. A guidance system that uses interferometric homing with spike-like antennas at the nose of the missile (as the Talos missile did) can have significant effects on the stability and control as well as on the drag of the configuration. Air-data probes needed for setting autopilot gains (as in the Terrier I missile) or for regulating fuel flow may have similar effects, depending on their placement.

Warhead and Fuze

The demands of the warhead and fuzing on the aerodynamic performance occur primarily during the brief interval prior to target engagement when the missile should be placed in a position and an attitude that will maximize the kill by the warhead. The other subsystems (guidance, control, propulsion) must work in concert with the airframe to provide this favorable condition.

The aerodynamic design is also influenced by the location of the warhead (usually a very dense package) because it affects the missile's center-of-gravity location and travel.

Autopilot and Control

Three aerodynamic control systems use all-movable control surfaces: canard controls located well forward on the missile, tail controls located well aft, and wing controls located near the midbody. Although several early missiles used wing control (Talos, Terrier I,[1] and Sparrow), the missiles requiring high maneuverability generally resort to tail control. With canard control (Fig. 3a) or tail control (Fig. 3b), maneuverability is achieved by having the entire airframe at an angle of attack to the airstream and is controlled by forces from small surfaces at a large distance from the missile's center of gravity. A wing-controlled missile (Fig. 3c), on the other hand, operates at a much smaller angle of attack and derives a large portion of its lift from the deflected wings. Canard controls can be placed near their source of information – the guidance package (which is usually far forward) – but their effectiveness may be partially compromised by "interference" moments from surfaces situated downstream from them. In some cases the control moment from forward controls (canard or wing) may be greatly diminished or even reversed[2] through interference moments from the aft surfaces. An illustration of interference effects for the wing-controlled missile of Fig. 3c is shown in Fig. 4. The force normal to the missile centerline (proportional to the coefficient C_N) increases nearly linearly with wing incidence when the body is lined up with the flow ($\alpha = 0$), as shown in Fig. 4a. When the tails are not present, the force is given by the colored curve. The downwash on the tails from the deflected wings produces a downward force, causing the resultant force on the configuration to drop to the black line. This downward force results in a nose-up pitching moment (proportional to the coefficient C_m) that overpowers the nose-down pitching moment from the wings (colored line in Fig. 4b) to yield a resultant nose-up pitching moment for the full configuration (black line). The effect of downwash is the difference between the two curves in

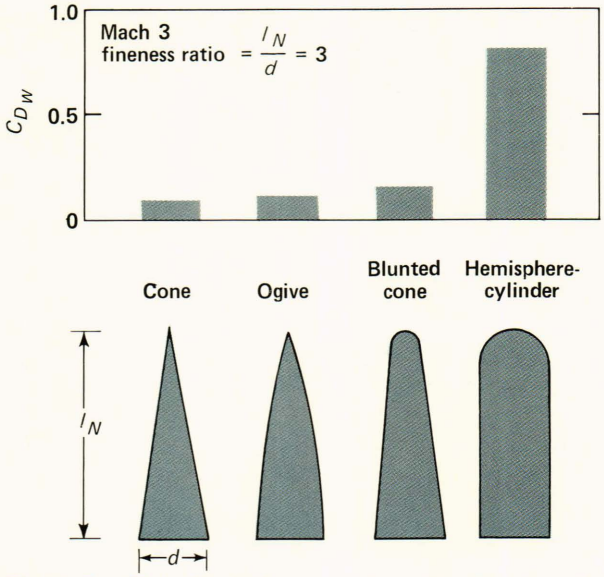

Figure 2 — The effect of sensor dome bluntness on the wave drag coefficient, C_{D_W}.

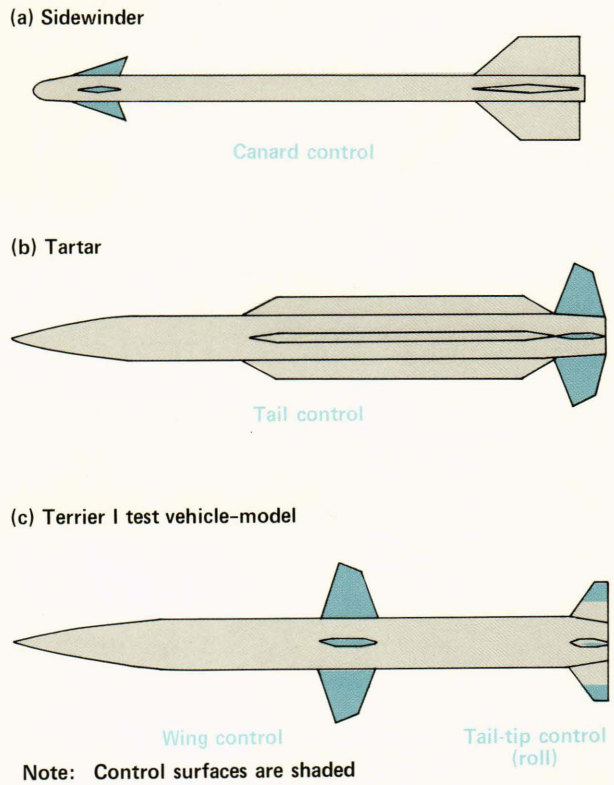

Figure 3 — Types of aerodynamic control.

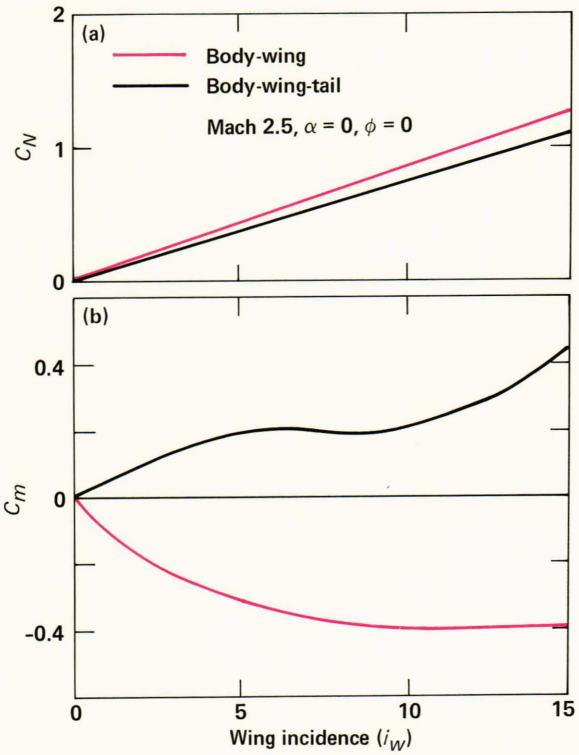

Figure 4 — The effect of downwash from wing on tail as a function of wing incidence, i_W.

each case. Other types of aerodynamic controls are tip controls and trailing edge controls in which only a portion of an aerodynamic surface is rotated to produce control forces.

With thrust vector control, the flow leaving the exit nozzle is deflected to produce a pitching moment. Obviously this system is operable only when the engine is delivering thrust. Such systems are well suited to quick reaction when aerodynamic forces are low, such as for turning a missile shortly after it leaves its launcher or for a rocket missile at an extremely high altitude when aerodynamic forces are small. Control by means of side jets, augmented by natural aerodynamic interference, has been used on some short-range missiles but may not be adequate for high-performance, medium- to long-range tactical missiles.

Thus, the type of control system chosen will determine the locations of lifting and control or stabilizing surfaces and will have a major effect on the missile's stability and control characteristics.

The choice of autopilot to provide proper signals to actuate the controls that guide the missile to the target depends on the airframe and controls selected. For example, with a skid-to-turn autopilot, a missile achieves a maneuver in a given direction by pulling maneuvers in two component directions at right angles to each other. Such an autopilot is appropriate for a cruciform configuration, which has equal lifting capability in two mutually perpendicular directions. On the other hand, with a bank-to-turn autopilot, the missile achieves the desired maneuver by banking (or rolling) to the desired direction and pulling the maneuver in that direction. This is appropriate for a configuration with a preferred lift direction (e.g., a ramjet missile with an air inlet on one side or a missile with a single pair of wings). Some comparisons of homing performance have been made[3] for selected configurations using skid-to-turn or bank-to-turn steering policies.

In summary, the aerodynamic configuration depends strongly on the requirements of the other missile technologies; therefore, achievement of the design goal is usually attained by compromising among them all.

PRELIMINARY AERODYNAMIC DESIGN TOOLS

In preliminary design, the aerodynamicist may use the following tools to develop a baseline configuration and to assess the effects of potential configuration changes:

1. Existing experimental data bases;
2. Theoretical methods;
3. Handbooks of theoretical, semi-empirical, and empirical design charts;
4. Computer programs, including computerized handbooks, computerized theoretical methods, computerized data bases, and computational aerodynamics;
5. Exploratory wind tunnel tests.

Existing Experimental Data Bases

Whenever practical, a designer will base the preliminary design of a missile on an existing data base for similar configurations and use interpolation or extrapolation as necessary. For example, in an evolving program such as Standard Missile, there is a wealth of data for the preliminary design of advanced versions. With such data, the designer can not only get the baseline design started but can also plan the necessary wind tunnel test program.

In general, it is possible to compile data (forces and moments) on the several components of a configuration (body, wings, tails, etc.) with reasonable confidence for moderate angles of attack and Mach numbers. More difficult is the assessment of aerodynamic interactions or interference among those components that add to the total aerodynamic behavior of the missile. Thus, a data base with full-configuration data, complemented with data on its components, is very important because the interference effects can be extracted.

The usual design approach consists of building up the aerodynamic characteristics of a full configuration from a knowledge of the characteristics of its component parts, augmented by estimates of the mutual interference of the parts. The acquisition of information on interference phenomena has usually lagged behind the development of methods for calculating the aerodynamic behavior of individual components. As Mach number and angle of attack increase, the interference effects become much more complex and more difficult to predict. A reliable set of test data on the full configuration is required for the detailed engineering design of the missile. If the design requirements point to a configuration considerably different from those contained in the existing data bases, one may turn to other methods discussed in the following subsections.

Theoretical Methods – Inviscid Flow

Bodies. Most early developments in supersonic missile aerodynamics started with the assumption of inviscid flow that was given a small perturbation by the movement of the missile. If the body were sufficiently long and thin, the "slender body" theory could be used to describe the perturbed flow. A linearized partial differential equation, the potential equation, described the flow field. That simple solution yields estimates of dimensionless coefficients of lift (C_L) and drag due to lift (C_{D_L}) that are independent of Mach number and body shape (within the slenderness restrictions of the theory) and of the static pitching moment (C_m) that depends on missile volume:

$$C_L = 2\alpha, \tag{1}$$

$$C_{D_L} = C_L\ \alpha/2 = \alpha^2, \tag{2}$$

$$C_m = -2\alpha\left(l - \frac{volume}{l\ S_{base}}\right), \tag{3}$$

where α is the angle of attack in radians, l is the body length (reference length), S_{base} is the base area (reference area), and the reference center for C_m is the vertex of the nose. The wave or pressure drag, on the other hand, requires integrations involving second derivatives of the axial distribution of the cross-sectional area.[4]

Eliminating the slenderness restriction but still having the restriction of a small perturbation, the first-order (or linear) theory was applied, which led to theories for axial flow (giving the drag[5]) and inclined flow (giving the lift and the pitching moment at small angles of attack[6]). The equations had to be solved numerically. Similar solutions for ducted bodies of revolution were also obtained, including the effect of the deflected air entering the duct.[7,8] Further improvements, using an iteration process, led to the second-order theory by Van Dyke,[9] which also required a numerical integration. Since the second-order theory could handle axial flow but not cross flow, a hybrid theory combining second-order theory for axial flow and first-order theory for cross flow was adopted. Even with pretabulated functions, the second-order axial calculations were tedious.[10] With modern computers the solutions became more feasible and were included in the original Naval Surface Weapons Center (Dahlgren) computer code.[11] A more exact method for axial flow is the method of characteristics (e.g., Ref. 12), also too tedious for preliminary design calculations. Several of these methods provide pressure distributions in addition to forces and moments.

The foregoing perturbation methods are satisfactory for the lower supersonic regime. Other methods were developed for higher speeds. The most frequently used are the generalized shock-expansion method[13] and an improvement on it, the second-order shock-expansion theory,[14] both of which are based essentially on the fact that at high speed, with a high body fineness ratio, the flow can be considered to be locally two-dimensional, so that basic shock-wave and expansion-wave theories are applicable. For even higher speed, the noses of the bodies are usually blunted to alleviate a local thermal condition; to account for blunt noses, the calculation procedure has been modified to allow the use of the Newtonian impact theory over the forward portion of the body and an appropriate matching at some location where the shock-expansion theory can proceed.[15,16] For very high Mach numbers, the Newtonian impact theory is appropriate.[17]

Although much effort has been expended on the theoretical analysis of base flow (with and without the effects of propulsive jets[18]), one generally has recourse to empirically derived design charts for estimating base drag because the theoretical flow models are quite complex.

For the transonic flow problem, great effort has been expended in analyzing the flow fields for a variety of conditions (e.g., Ref. 19), but the calculations are very tedious because the perturbation equations are nonlinear and require numerical integration. Subsonic flow has been handled by the slender body theory and linear theories (as was supersonic flow). The solution in the slender body theory, $C_{L_\alpha} = 2$, assumes potential flow. The linear theory solutions[20] are satisfactory for incompressible flow (Mach = 0) but generally require a compressibility adjustment at higher subsonic Mach numbers. In the design of high-speed, high-performance missiles, the greatest needs are at high angles of attack, and they cannot be handled by the aforementioned perturbation methods.

Thin Lifting Surfaces. Most early theoretical approaches to the problem of inviscid flow about wings resulted in solutions of the linearized potential flow equation for thin wings at small angles of attack.[21,22] Although the solutions for zero-lift wave drag and slopes of lift and pitching moment coefficients have been published for a variety of wing planforms, their applicability to higher angles of attack is somewhat limited. Higher-order approximations are best obtained by turning to two-dimensional wing theory, which is the basis for the so-called shock expansion theory mentioned for bodies. Using two-dimensional theory along streamwise strips does not account for the tip losses inside the Mach cone associated with the disturbances from the outermost point of the leading edge. However, as the Mach number increases and the Mach cone angle decreases, the affected region becomes smaller, so that the approximation may be satisfactory.

Interference Effects. When a lifting surface is attached to a body, the aerodynamic forces on the combination generally exceed the sum of the forces on the isolated elements because the two flow fields interact.

A research program on supersonic wing-body interaction was conducted in the Bumblebee program at Cornell Aeronautical Laboratory in 1947-1951.[23,24] It provided theoretical methods for calculating the velocity potentials corresponding to the flow perturbation of the body on the wing and the wing on the body. The methods were validated by detailed pressure measurements. Although the results have provided a better understanding of the flow phenomena, the designer can obtain satisfactory engineering approximations with less effort using the method of Morikawa.[25] The solutions are meant to be restricted to small angles of attack and moderate supersonic Mach numbers for wing-body configurations with no afterbody. Nevertheless, the so-called Morikawa factors have been used successfully over a wider range of parameters. An illustration of the several components contributing to the total lift resulting from wing-body interference is given in Fig. 5 for a delta wing mounted on a cylindrical body.

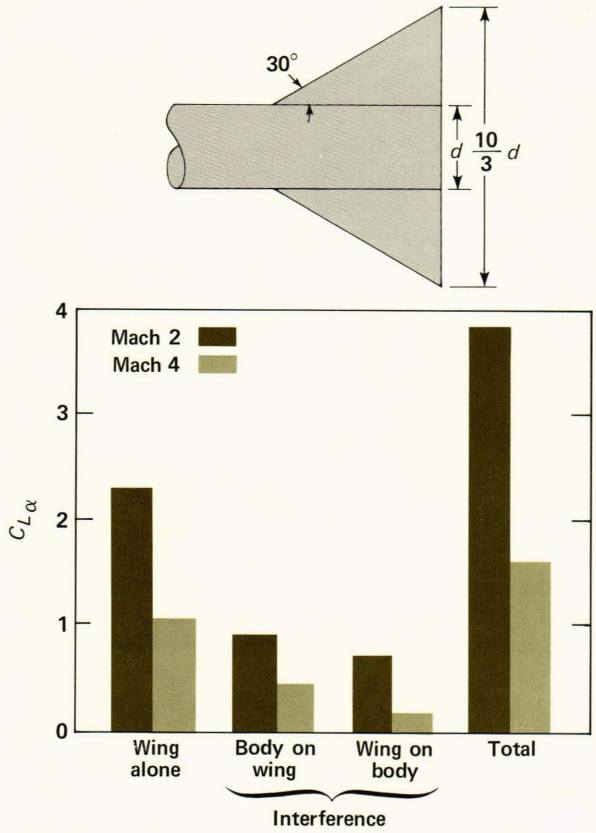

Figure 5 — Wing-body interference – linear theory.

On the other hand, when lifting surfaces are in tandem (such as a canard followed by a wing or a wing followed by a tail), the flow past the forward surface is deflected (downwash) and also loses energy so that less lift is produced on the aft surface. These effects determine the so-called efficiency of the aft surface. Although there are many techniques for calculating the downwash, such calculations[26] may not be warranted if one needs only a rough estimate of tail lifting efficiency for preliminary design.

Combined Angles of Attack and Sideslip. Most theoretical approaches have been developed for cases in which the missile or one of its components is at an angle of attack to the flow with no sideslip. One can also obtain effects of sideslip with zero angle of attack. But the problem of combined angles of attack and sideslip, a truly three-dimensional problem, is not easily handled by these theoretical methods. Some of the most recent attacks on the problem have been made by Nielsen *et al.*[27]

Full Configurations. The characteristics of a full configuration are calculated theoretically by combining the characteristics of the component parts and their mutual interferences. The results are limited by whatever restrictions are inherent in the theories for the components and their interferences. Consequently, nonsymmetrical configurations are usually very difficult to deal with theoretically.

Theoretical Methods – Viscous Effects

The two most important viscous effects are those in the flow direction that produce skin friction drag and those normal to that direction (cross flow) that produce additional lift and pitching moment at higher angles of attack. To calculate skin friction drag during preliminary design, the aerodynamicist generally treats the missile configuration as a set of simple geometric elements (flat plates, cylinders, etc.) on which the turbulent skin friction drag can be calculated by a method such as that of Ref. 28. This skin friction drag is combined with wave and base drags to give total missile drag. The additional lift and pitching moment resulting from viscous cross flow are calculated by a method such as that given in Ref. 29. They are combined with the inviscid lift and pitching moment to give the totals for the missile.

Handbooks

Many of the foregoing theoretical methods and some of the wind tunnel and flight data have been assembled into handbook form as curves and tables so that preliminary design can proceed by a build-up process without individual calculations having to be made. The most well known of these handbooks are:

1. *Handbook of Supersonic Aerodynamics,* NAVORD Report 1488 (published between 1950 and 1966),
2. Royal Aeronautical Society, *Engineering Sciences Data Units (Aeronautical Series, Aerodynamics Sub-Series)* (published between 1943 and the present),
3. *U.S. Air Force Stability and Control DATCOM* (initially issued in 1956 and updated periodically).

The *DATCOM* has been computerized so that much of the data extraction from families of curves has been speeded up, but preparation of the input to the program is time consuming. Consideration is being given[30] to the development of a handbook (based on *DATCOM*) aimed specifically at missile design (rather than at general aircraft design as was the original *DATCOM*).

Computer Programs

The following four programs now being used are representative of those that exist:

Approximate Aeroprediction Code–NSWC/DL.[31,32] Available analytical and empirical procedures are used to calculate static and dynamic coefficents for configurations with axially symmetric bodies and streamwise wing and tail tips. The reported region of validity is $0 < M < 8$, $0 < \alpha < 180°$, although this region does not hold for all components. It is useful for early design studies when drag, normal force, and longitudinal static stability are the primary concerns.

PANAIR–NASA (by Boeing Military Airplane Co.).[33,34] In this program, "panel methods" are used, i.e., a set of linear partial differential equations of potential flow is solved numerically by using "singularity strengths" on the set of panels to describe the configuration geometrically. The configurations can be arbitrary in shape.

Mark IV Supersonic-Hypersonic Arbitrary Body Program–AFFDL (by McDonnell Douglas).[35,36] As an engineering approach to preliminary design, methods are used that can handle configurations not suited to linear theory without going to the method of characteristics or to finite-difference techniques. Many analytical techniques are programmed; the user makes the choice of what is best for his problem. The configuration is represented geometrically by sets of quadrilaterals (panels) on which the forces are calculated. The code is applicable from Mach 2 up to very high Mach numbers. Entering the geometry of the configuration is a tedious task.

Numerical Aeroprediction Code–NSWC/WO.[37,38] The inviscid supersonic flow field about finned configurations is calculated by finite difference techniques using mesh spacing that is adjusted to improve accuracy in regions of expected large flow gradients. It is best suited for selected check calculations because it requires much more computer time than, for example, the Approximate Aeroprediction Code. Also, it provides much more detailed information at each condition. Before using any such code, the user should see how well the calculations have agreed with test data on configurations similar to those being considered for the design.

Exploratory Wind Tunnel Tests

It is always desirable to carry out exploratory wind tunnel tests, guided by the calculations discussed in previous sections. Such tests should be aimed at determining the variations from a basic design by making configurational changes in the components, by spanning the expected Mach number and angle-of-attack ranges, and by validating the calculations made for the baseline configuration. In addition, measurements at nonsymmetric conditions (such as a cruciform configuration maneuvering out of its planes of symmetry) are needed to assess yaw and roll stability not easily calculable by standard methods. Measurements of hinge moments of control surfaces are needed for sizing control servos. It must be remembered, however, that these moments may be changed considerably in the design process by configuration modifications upstream of the surface. The selection of a final hinge line must take into account such modifications.

PROBLEM AREAS IN CONFIGURATION DESIGN

Geometric Limitations

Geometric limitations usually result from the compatibility requirements of the launching and han-

dling systems. Restrictions on length place a limit on available body lift (or normal force). The slope of the normal force coefficient curve, C_{N_α}, generally tends to increase with body fineness ratio (Fig. 6) although this behavior also depends on the Mach number and fineness ratio of the nose section. Since normal force resulting from viscosity is a function of cross-flow drag, the normal force coefficient, C_N, also increases with body fineness ratio because there is an increase of body planform area on which the cross flow can act. The variation of C_N with fineness ratio and angle of attack is shown in Fig. 7 for bodies at Mach 7.69. A further observation is that the Newtonian theory agrees quite well with experimental data at that Mach number except at low angles of attack.

Restrictions on the span of stabilizing and control surfaces result in surfaces of lower aspect ratio, AR, that generally produce a smaller slope of the normal force curve than those of higher aspect ratio having the same planform area, as is shown in Fig. 8 (curve W). Because the viscous normal force at angle of attack depends primarily on the planform area, the total normal force (potential plus viscous) does not show as great a variation with aspect ratio as does the slope of the normal force curve. The carryover normal force from the body to the wing and from the wing to the body also tends to lessen the difference attributed to the difference in aspect ratio. An illustration of the total potential normal force from linear theory is presented in Fig. 8 (curve $W + W_B + B_W$). The contribution from the wing alone (curve W) decreases with the reciprocal of the aspect ratio, whereas the total C_{N_α}, including interference effects, peaks near $AR = 0.5$ for those rectangular wings evaluated at Mach 2.24.

Another limitation is the space available for control servos of tail-controlled configurations. The servos are usually housed in the annular volume around the throat of the propulsion nozzle. Optimum design requires careful attention to the selection of an appropriate hinge line for control surfaces in order to minimize torque requirements over the missile's full operating range. This spatial limitation is generally more severe for a ramjet missile than for a rocket missile because the former requires a larger nozzle throat area to accommodate the greater mass flow from the combustion chamber.

Center-of-Gravity Travel

The static stability of a missile is a measure of its tendency to return to its equilibrium attitude after being disturbed. It depends on the relative location of the center of gravity (the point at which the resultant of the inertial forces acts) and the center of pressure (the point at which the resultant of the aerodyamic

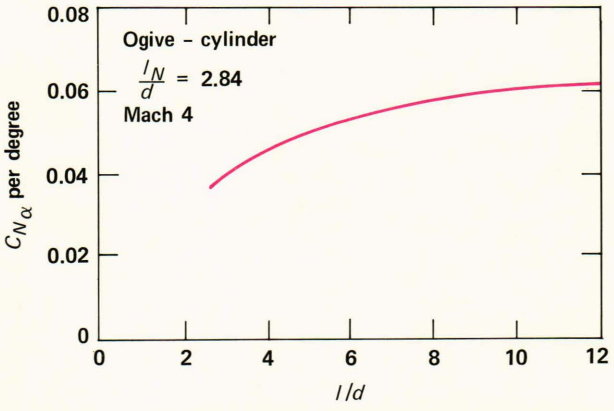

Figure 6 — The effect of fineness ratio on the body normal force coefficient.

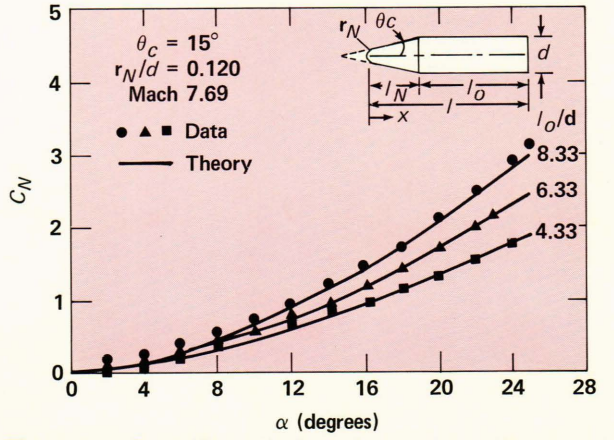

Figure 7 — The effect of aft body length on the normal force coefficient.

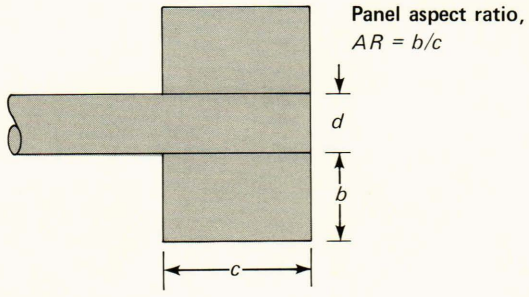

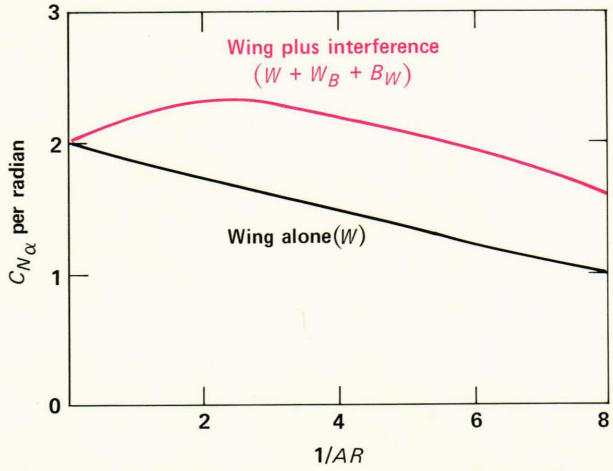

Figure 8 — The effect of wing-body interference on the slope of the normal force coefficient at Mach 2.24.

forces acts). A very stable missile has its center of pressure well aft of its center of gravity and requires a large control authority to maneuver it to another position. For a highly maneuverable missile, it is desirable to minimize the margin of stability.

In the case of missiles propelled by solid rockets, the change in the center of gravity from ignition of the rocket to burnout may be large, so the spread in static stability for a given Mach number may also be large. In order for the missile to accomplish its mission (near or after burnout), it must be maneuverable near the target, at which time the center of gravity is usually in a very forward position. The forward position favors stability and thus requires a large control authority. If the missile is designed for very low stability at that condition, it may result in unacceptable instability early in flight when the center of gravity is in an aftward position. Since the center of pressure of a configuration varies with Mach number, it is clear that the designer should consider simultaneously the time histories of center-of-gravity travel and Mach number in establishing margins of stability.

Spread in Mach Number and Altitude

The center of pressure of a configuration varies with Mach number. Each component contributes to this variation. As Mach number increases, C_N for the body varies only slightly, and the center of pressure (with a few exceptions) moves aft slightly (Fig. 9). C_N for the tails decreases (nearly inversely with Mach number), and the center of pressure varies only slightly. As a result, the center of pressure of such a body-tail configuration moves forward with increasing Mach number because of the lowered tail force coefficient. If intercept occurs at high Mach number, this center of pressure movement with Mach number, which favors instability, is desirable because the demand on control moment is lessened.

Consideration must be given early in the design process to the maneuverability requirements at the highest altitude because maneuverability depends on controllable lift. The latter depends on the configuration lift coefficient attainable with the available control authority and the dynamic pressure, q, at which the missile will operate:

$$\text{Maneuverability (in } g) = \frac{lift\ (lb)}{weight\ (lb)} = C_L q \frac{S}{W}, \text{ and}$$

$$q = \frac{\gamma}{2} pM^2,$$

where C_L is the lift coefficient, S is the reference area upon which C_L is based, W is the missile weight, p is the static pressure at the flight altitude, and γ is the ratio of the specific heats of air.

For example, at the same speed and for the same maneuver, the missile needs a lift coefficient at 80,000 ft altitude that is more than 40 times the sea-level value. Dynamic pressure is also an important parameter in designing the autopilot and in selecting its gain program.

High Angle-of-Attack Phenomena

High angle-of-attack (α) phenomena arise at both ends of the Mach number regime. During launch, un-

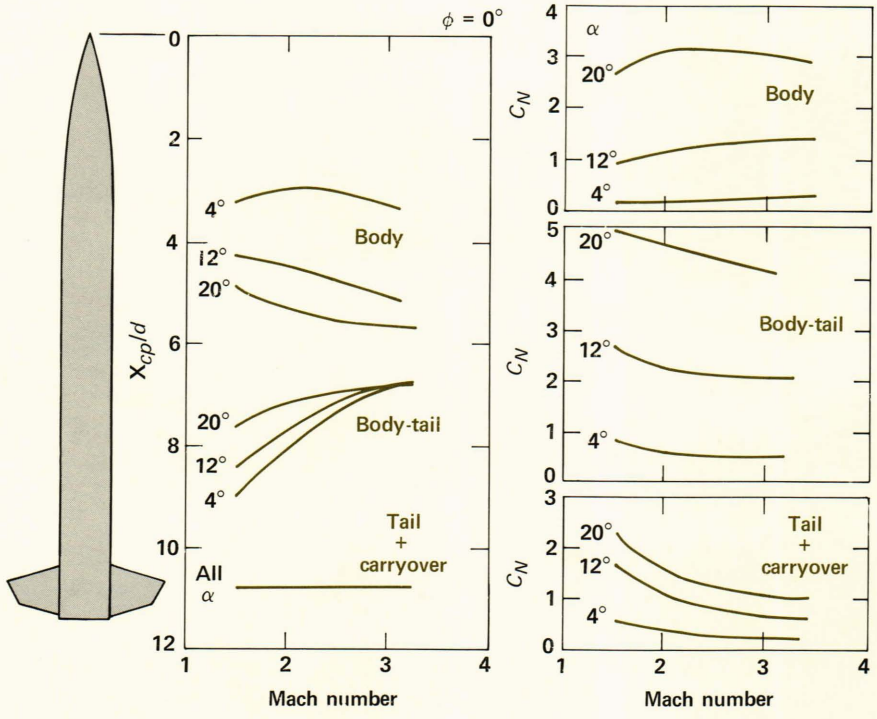

Figure 9 — The normal force coefficient and center of pressure – body, body-tail, tail plus carryover.

der conditions of launcher motion and high winds, the low subsonic motion of the missile may occur with high angle of attack where the stability characteristics are very nonlinear and the control effectiveness is limited because of low dynamic pressure on the surfaces. The dynamic motion required to achieve the proper attitude may dictate a need for a supplementary launch-phase control system or may impose additional requirements on an aerodynamic control system intended for the entire flight phase. During the high subsonic and transonic phases, if the missile is required to operate at high angle of attack in order to maintain its position in a desired trajectory, it may experience a shedding of unsymmetrical vortices from its lee side, resulting in side forces and moments on a symmetrical airframe in a symmetrical attitude.[39] This phenomenon may present another control problem.

Another high angle of attack phenomenon is that of coupling between the yaw and roll modes of motion (pitch-yaw-roll coupling).[40] Coupling occurs when the missile attempts to maneuver in the yaw direction while pulling a large maneuver in the pitch direction. Increased loading on the windward surfaces (behind the strong body shock waves) and decreased loading on the lee side (in vortex flows) combine to produce instabilities in roll and yaw and induced moments resulting from the roll and yaw control deflections that are required to counter those instabilities. The phenomenon is highly dependent on the configuration's shape and attitude in roll. A proper design study of this phenomenon requires a coordinated effort between the autopilot designer and the aerodynamicist in order to achieve maximum controllable maneuverability. The data necessary for such an investigation should be obtained from detailed wind tunnel tests that provide a three-dimensional description of the aerodynamic forces and moments.

Launching Environment

The housing of a folding mechanism may require additional thickness of the inboard cross section, thereby adding to drag. Furthermore, one should investigate the dynamic behavior of the missile during deployment of the surfaces, which usually occurs while the missile is under the influence of somewhat random flow fields near the launcher.

The environment of shipboard launchers includes the ship's angular motions, relative winds, disturbed flow fields about the superstructure, and enveloping gases from the missile's own rocket, each of which taxes the missile's controllability. In the case of launching from aircraft, the aerodynamic interference between the flow fields of the aircraft and those of the missile is a major factor to be considered and has been investigated extensively in recent years.[41]

Staging

For a multistage missile, one must be concerned with the aerodynamic design of the full configuration during each stage, taking into account the Mach number and altitude regimes covered by it. A key problem to be attacked early in the preliminary design is the separation of the stages so as to avoid any possible recontact if the relative drag and thrust forces are not sufficient to ensure clean separation. In addition, the presence of the separating stage (the booster) from the continuing stage (the missile) may result in an interference that adversely affects the missile's stability. It is important that the control system be designed to cope with this change in stability and that it be activated without excessive delay.

DATA NEEDED FOR DETAILED DESIGN, FLIGHT TESTING, TROUBLE SHOOTING

Various methods to provide aerodynamic data for preliminary design were described earlier. Many of the problems discussed in the previous section cannot be addressed using the type of data provided by those methods. Thus, early planning should be made for detailed wind tunnel testing to provide the data needed for such critical analyses.

Three-Dimensional Data for Six-Degree-of-Freedom Simulation

A six-degree-of-freedom simulation should be able to describe the missile motion in three translational and three rotational modes. The appropriate aerodynamic forces (axial, normal, lateral) and moments (pitching, yawing, rolling) must be provided as functions of Mach number, altitude, angle of attack, angle of sideslip, and control deflections in pitch, yaw, and roll. A well planned wind tunnel testing program must be conducted to acquire these data efficiently and economically. First, one must decide how the data will be used and what format might be best for the simulation. Those factors will have significant influence on the test plan. Wherever possible, advantage should be taken of known symmetries or known regions of small variations in the expected data in order to reduce the required testing.

The aerodynamic data will be needed in the engineering design phase in order to design the autopilot and to check it out over a wide range of potential maneuvers. The aerodynamicist should assist in planning the flight tests and in analyzing the flight data to validate the aerodynamic description of the configuration. He also should assist in troubleshooting when flight anomalies appear. The money spent in providing a proper three-dimensional representation of the aerodynamic characteristics is well spent if it makes possible a more productive and less costly flight test program.

Pressure Distributions, Panel Loads, and Moments

Pressure distributions may be needed for structural design and for thermal analysis. In some cases, they may be obtained with sufficient accuracy for preliminary design from theoretical calculations or from

computer codes using finite difference methods to calculate the flow fields. For critical conditions that may involve complex flow fields and shock waves interacting with each other or with the boundary layer, or impinging on surfaces, it is usually necessary to include some wind tunnel tests with a pressure model and with flow visualization techniques to be able to identify critical areas of high temperature or pressure. Because the volume inside the model is limited, the number of points at which pressure may be measured is also limited. Thus, it is important to confine measurements to areas of expected high pressure gradients and to limit them in areas of low pressure gradients. When panel flutter may be a design problem, pressure distributions are needed for the aeroelastic studies.

Accurate measurements of control surface hinge moments are required for sizing the control servos. The design goal is to choose a hinge line that minimizes the hinge moments over the entire flight regime. A surface planform and cross section is desired with minimum center-of-pressure travel over the full range of Mach number, angle of attack, and angle of incidence for the various roll orientations. An important caution is that any changes in the geometry of the surface or of the missile ahead of the surface are likely to affect the hinge moments. For that reason, detailed hinge moment measurements are usually postponed until the preliminary design has reached the point where only minor modifications are expected. Theoretical estimates of hinge moments are rather tedious to make and are not very reliable because the center of pressure of the control forces cannot be calculated with the needed accuracy as a result of the complex flow conditions associated with angle of attack, roll angle, and control deflections, and of the many interferences from the body, the forward surfaces, or protuberances. It is customary to measure panel normal loads, hinge moments, and spanwise bending moments simultaneously. If the model size permits, the measurements are obtained at the same time that the six components of force and moment are measured on the full configuration.

A considerable effort was expended in arriving at a wing planform for the Talos wing-controlled missile in order to minimize the wing hinge moments.[42] That planform proved to have the desired limited center-of-pressure travel and has been used for the control surfaces of Terrier, Tartar, and the Standard Missile family. The hinge line location (in percent of root chord) has been adjusted according to the Mach number regime to keep the center-of-pressure travel to a minimum and thus to minimize the design hinge moment.

Effects of Elasticity on Aerodynamics

Under sufficient loading, a missile may change its shape and thereby cause changes in its aerodynamic characteristics.[42] The body may bend as a freely supported beam, the surfaces may "wind-up" about the hinge line, and the shaft itself may twist. These elastic effects are usually accounted for by making a "quasi-static" correction. A structural analysis, which depends on a sufficiently accurate distribution of air loads and inertial loads, must provide the description of the distorted shape. The distorted shape essentially describes the changes in angle of attack or incidence of the various elements of the configuration. Forces and moments resulting from the changes are added to those of the rigid body to give the quasi-static aerodynamics of the configuration. The process is iterative but converges rapidly for a properly designed airframe. Figure 10 illustrates the effect of elasticity in the Talos missile.

Dynamics of Separation

At separation of the missile from the booster in a two-stage vehicle, at least two goals are sought. The first is a clean, quick separation. That condition can be ensured if the axial forces on the booster greatly exceed the axial forces on the missile at the instant of separation. If the booster cross section is sufficiently larger than that of the missile and if the booster thrust tail-off is steep, a clean, quick separation should be expected since such a relationship between axial forces should exist. One factor that might oppose a clean separation is the existence of an angle of attack on the missile-booster configuration at separation; that factor could result in individual dynamic motion of the missile and the booster where each could be affected by the other. The angle of attack may result from the use of guidance during the boost-phase of flight or, for an unguided boost phase, from manufacturing misalignments (particularly in the booster fins and rocket nozzle) that could cause a stable configuration to seek an equilibrium angle of attack to balance the resultant pitching moments.

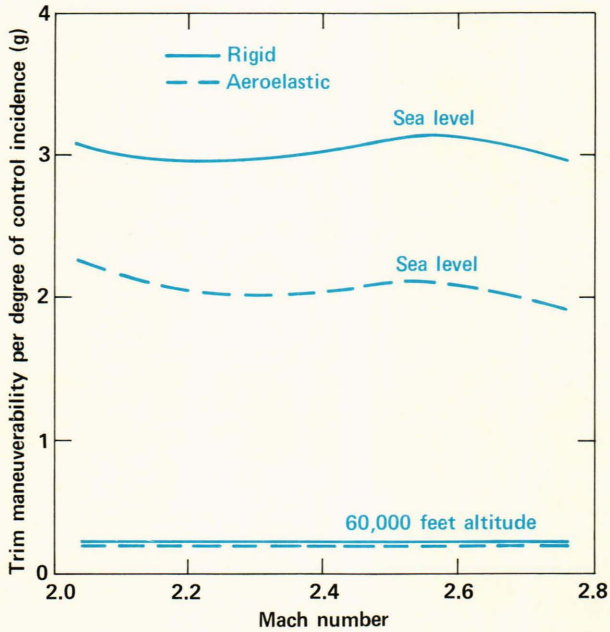

Figure 10 — The effect of aeroelasticity on maneuverability.

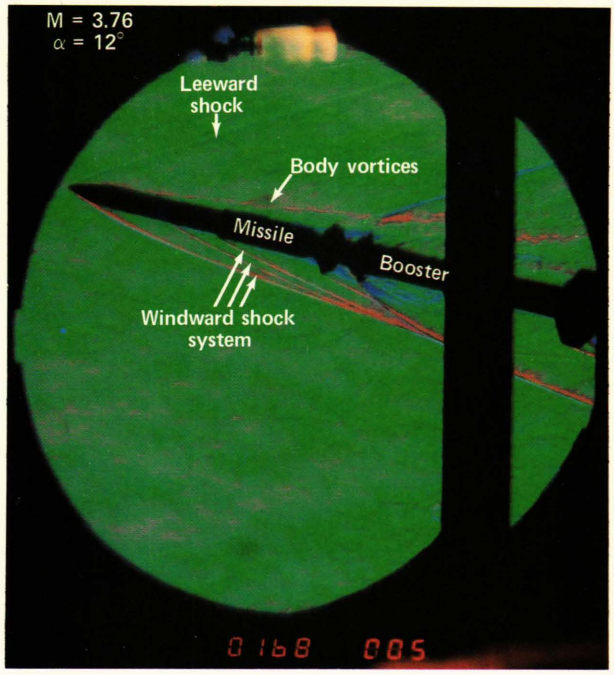

Figure 11 — Missile booster, first stage.

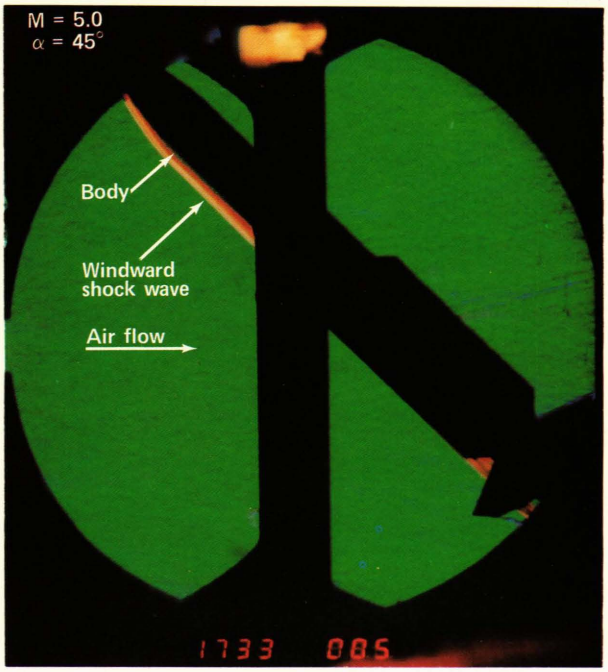

Figure 12 — Missile, second stage.

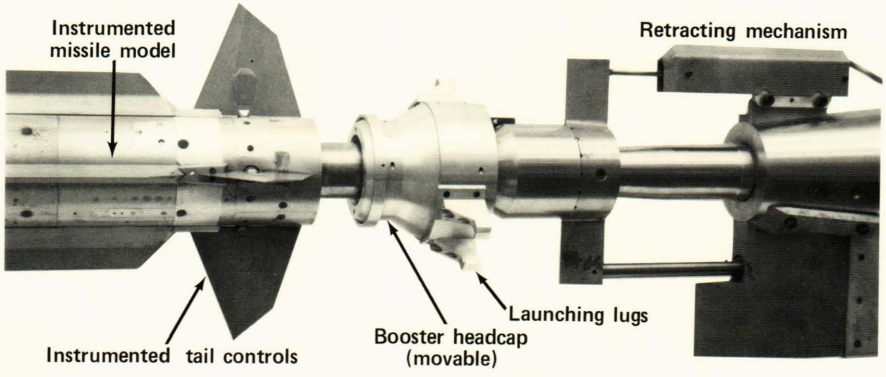

Figure 13 — Missile booster, separation test model.

The second goal is to activate the missile control system as soon as possible after separation. Then, if the missile is unstable in the presence of the separating booster, the transient angle of attack can be minimized, thereby decreasing missile drag and increasing the chance for a clean separation. Since tail stabilization and control may be adversely affected by the flow disturbances caused by the booster head cap, it is desirable to obtain wind tunnel test data simulating missile-booster separation conditions for both the missile alone and the separated booster.

CONCLUDING REMARKS

Missile design involves many interacting technologies, most of which have significant input to the choice of an aerodynamic configuration. The process should lead to a compromise solution that seeks an optimum missile system for the mission. The solution, however, is likely to be less than optimum for each of the technologies contributing to the system.

The many interactions among technologies seeking solutions for the proposed system have a profound effect on the philosophy of the wind tunnel testing needed to arrive at the eventual configuration and to provide an accurate definition of its aerodynamic characteristics for detailed engineering design and flight testing. Preliminary testing over a broad range of parameters should include the so-called "build-up" data, which isolate the contributions of the several configurational elements (body, wings, tails, launcher shoes, etc.) to the overall forces and moments measured on the full missile configuration. As changes are necessitated by findings during the preliminary design process, the aerodynamicist can evaluate quantitatively the effects that will result from those changes, using the body of acquired parametric data. When design has progressed to the point where only minor external changes are expected, extensive testing can proceed for a three-dimensional description of the aerodynamics of each configurational phase of the weapon (first stage (Fig. 11), second stage (Fig. 12), and separation phase (Fig. 13)).

REFERENCES

[1] L. L. Cronvich, "Aerodynamic Development of Fleet Guided Missiles in Navy's Bumblebee Program," AIAA Paper No. 79-0219, 17th Aerospace Sciences Meeting (Jan 1979).

[2] A. R. Eaton, Jr., *Investigation of Roll-Reversal Effects on Generalized Missile Configuration at M 1.73 in the 19 x 27.5-Inch Nozzle for The Johns Hopkins University,* JHU/APL CF-788 (Sep 1947).

[3] R. T. Reichert, *Homing Performance Comparison of Selected Airframe Configurations Using Skid-to-Turn and Bank-to-Turn Steering Policies,* NASA CR-3420 (May 1981).

[4] J. N. Nielsen, *Missile Aerodynamics,* McGraw Hill, Inc. (1960).

[5] T. Von Karman and N. B. Moore, "Resistance of Slender Bodies Moving with Supersonic Velocities with Special Reference to Projectiles," *Trans. ASME* **54** 303-310 (1932).

[6] H. Tsien, "Supersonic Flow Over an Inclined Body of Revolution," *J. Aeronaut. Sci.* **12,** 480-483 (Oct 1938).

[7] C. E. Brown and H. N. Parker, *A Method for the Calculation of External Lift, Moment, and Pressure Drag of Slender Open-Nose Bodies of Revolution at Supersonic Speeds,* NACA Report 808 (1945).

[8] G. N. Ward, "The Approximate External and Internal Flow Past a Quasi-Cylindrical Tube Moving at Supersonic Speeds," *Q. J. Mech. Appl. Math.* **1,** 225-245 (1948).

[9] M. D. Van Dyke, "First- and Second-Order Theory of Supersonic Flow Past Bodies of Revolution," *J. Aeronaut. Sci.* **18,** 161-178, 216 (1951).

[10] M. D. Van Dyke, *Practical Calculation of Second-Order Supersonic Flow Past Non-Lifting Bodies of Revolution,* NACA TN 2744 (1952).

[11] F. G. Moore and R. C. Swanson, Jr., *Aerodynamics of Tactical Weapons to Mach Number 3 and Angle of Attack 15°, Part I, Theory and Application,* NSWC/DL TR-3584 (Feb 1977); *Part II, Computer Program and Usage,* NSWC/DL TR-3600 (Mar 1977).

[12] L. L. Cronvich, "A Numerical-Graphical Method of Characteristics for Axially Symmetric Isentropic Flow," *J. Aeronaut. Sci.* **15,** 155-162 (1948).

[13] A. J. Eggers, Jr., R. C. Savin, and C. A. Syvertson, "The Generalized Shock-Expansion Method and Its Application to Bodies Travelling at High Supersonic Speeds," *J. Aeronaut. Sci.* **22,** 231-238, 248 (1955).

[14] C. A. Syvertson and D. H. Dennis, "A Second-Order Shock-Expansion Method Applicable to Bodies of Revolution Near Zero Lift," NACA Report 1328 (1957).

[15] R. J. Vendemia, *An Engineering Method for Rapid Calculation of Supersonic-Hypersonic Pressure Distributions on Lifting and Non-Lifting Pointed Bodies of Revolution and Several Special Cases of Blunt-Nosed Bodies of Revolution,* JHU/APL TG 752 (Nov 1965).

[16] F. R. DeJarnette and K. M. Jones, *Development of a Computer Program to Calculate Aerodynamic Characteristics of Bodies and Wing-Body Combinations,* NSWC/DL-3829 (Apr 1978).

[17] W. D. Hayes and R. F. Probstein, *Hypersonic Flow Theory,* Academic Press, Ch. III (1959).

[18] G. Batiuk, *A Bibliography of Plume Effects Investigations Conducted by the Army Missile Command,* U.S. Army Missile Command Technical Report RD-76-16 (Dec 1975).

[19] J. W. Wu and K. Aoyoma, "Transonic Flow Field Calculations around Ogive Cylinders by Nonlinear Stretching Method," AIAA Paper No. 70-189 (Jan 1970).

[20] E. V. Laitone, "The Linearized Subsonic and Supersonic Flow about Inclined Slender Bodies of Revolution," *J. Aeronaut. Sci.* **14,** 631-642 (1947).

[21] R. M. Snow, "Aerodynamics of Thin Quadrilateral Wings at Supersonic Speeds," *Q. Appl. Math.* **5,** 417-428 (1948).

[22] A. E. Puckett and H. J. Stewart, "Aerodynamic Performance of Delta Wings at Supersonic Speeds," *J. Aeronaut. Sci.* **14,** 567-578 (1947).

[23] C. Ferrari, "Interference Between Wing and Body at Supersonic Speeds, Part I – Small Perturbation Theory for Interference on the Wing and Also on the Body," *J. Aeronaut. Sci.* **15,** 317-336 (1948)

[24] C. Ferrari, *Aerodynamic Components of Aircraft at High Speeds,* Sect. C, Ch. 2, Princeton University Press (1957).

[25] G. Morikawa, "Supersonic Wing-Body Lift, *J. Aeronaut. Sci.* **18,** 217-228 (1951).

[26] P. A. Lagerstrom and M. E. Graham, "Methods for Calculating the Flow in the Trefftz-Plane Behind Supersonic Wings," *J. Aeronaut. Sci.* **18,** 179-190 (1951).

[27] J. N. Nielsen, M. J. Hemsch, and C. O. Smith, *A Preliminary Method for Calculating the Aerodynamic Characteristics of Cruciform Missiles to High Angles of Attack Including Effects of Roll Angle and Control Deflections,* ONR CR-215-226-4F (Nov 1977).

[28] E. R. Van Driest, "Turbulent Boundary Layer in Compressible Fluids," *J. Aeronaut. Sci.* **18,** 145-160, 216 (1951).

[29] H. J. Allen, and E. W. Perkins, *A Study of Effects of Viscosity on Flow over Slender Inclined Bodies of Revolution,* NACA 1048 (1951).

[30] S. R. Vukelich and J. E. Jenkins, "Evaluation of Component Buildup Methods for Missile Aerodynamic Predictions," *J. Spacecr. Rockets* **19,** 481-488 (1982).

[31] L. Devan, *Aerodynamics of Tactical Weapons to Mach Number 8 and Angle-of-Attack 180°: Part I, Theory and Application,"* NSWC TR 80-346 (Oct 1980).

[32] L. Devan and L. A. Mason, *Aerodynamics of Tactical Weapons to Mach Number 8 and Angle-of-Attack 180°: Part II, Computer Program and Users Guide,* NSWC TR 81-358 (Sep 1981).

[33] A. E. Magnus and M. E. Epton, *PAN AIR – A Computer Program for Predicting Subsonic or Supersonic Linear Potential Flows about Arbitrary Configurations Using a Higher Order Panel Method, Vol. I – Theory Document* (Version 1.0), NASA CR 3251 (Apr 1980).

[34] K. W. Sidwell, P. K. Baruah, and J. E. Bussoletti, *PAN AIR – A Computer Program for Predicting Subsonic or Supersonic Linear Potential Flows about Arbitrary Configurations Using a Higher Order Panel Method, Vol II – User's Manual* (Version 1.0), NASA CR 3252 (May 1981).

[35] A. E. Gentry, D. N. Smyth, and W. R. Oliver, *The Mark IV Supersonic-Hypersonic Arbitrary-Body Program, Vol. 1 – User's Manual,* AFFDL-TR-73-159 (Nov 1973).

[36] A. E. Gentry, D. N. Smyth, and W. R. Oliver, *The Mark IV Supersonic-Hypersonic Arbitrary-Body Program, Vol II – Program Formulation,* AFFDL-TR-73-159 (Nov 1973).

[37] A. B. Wardlaw, Jr., L. B. Hackerman, and F. P. Baltakis, *An Inviscid Computational Method for Supersonic Missile Type Bodies – Program Description and User's Guide,* NSWC/WOL TR 81-459 (Mar 1982).

[38] A. B. Wardlaw, Jr., F. P . Baltakis, J. M. Solomon, and L. B. Hackerman, *An Inviscid Computational Method for Tactical Missile Configurations,* NSWC TR 81-457 (Dec 1981).

[39] L. E. Tisserand, *A Modeling of Aerodynamic Forces and Moments Resulting from Asymmetric Vortex Shedding in the Subsonic and Transonic Speed Regimes,* JHU/APL BFD-1-82-032 (Dec 1982).

[40] L. L. Cronvich and B. E. Amsler, *Pitch-Yaw-Roll Coupling,* AGARD Report 353 (Apr 1961).

[41] A. R. Maddox, J. R. Marshall, G. F. Cooper, and E. F. McCabe, "Store Separation State-of-the-Art Review ," Paper 16, 10th U.S. Navy Symposium on Aeroballistics (Jul 1975).

[42] L. L. Cronvich, "Talos Aerodynamics," *Johns Hopkins APL Tech. Dig.* **3,** 138-141 (1982).

FREDERICK S. BILLIG

TACTICAL MISSILE DESIGN CONCEPTS

The selection of a propulsion system to meet a particular mission requirement is arduous and often controversial. Frequently, when the government solicits proposals for missile concepts from industry, it must choose from a group of fundamentally different propulsion concepts. This article describes a variety of propulsion cycles and presents a methodology for selection based on particular mission requirements and constraints. Engine specific impulse, thrust-to-weight ratio, and propellant mass fraction are shown to be important engine design indices that govern selection. Optimal staging, motor pulsing, and thrust modulation are among the design variables that are examined.

INTRODUCTION

From the Wright Flyer to the Space Shuttle, propulsion has set the pace for the technology of flight. At first it seemed to present an insurmountable barrier, but once overcome by the development of a variety of efficient power plants, new vistas of opportunity have presented themselves.

Tactical missile development was no exception. Initially, the challenge was to produce enough thrust to reach and sustain a velocity with a payload of sufficient size for a viable weapon concept. Later the goal was to produce a thrust greater than the weight of the missile and sufficient to penetrate the so-called "sonic barrier." That challenge was met by the rocket, the subsonic combustion ramjet, the turbojet, and other engine cycles. Currently we seek to fly at hypersonic speeds (greater than five times the speed of sound) to long ranges within the lower atmosphere. Perhaps this will be accomplished when an engine of the supersonic combustion ramjet family (scramjet) is developed. Such a design has already been successful in ground tests.

PROPULSION SYSTEMS

Figure 1 illustrates the three basic types of propulsion system for tactical missiles: the rocket, the ramjet, and the turbojet. In the rocket, the propellant is burned in a combustion chamber to produce products of combustion at high pressure (30 to 200 atmospheres) and high temperature (4500 to 7200°F). The burned gases are accelerated to high velocity as they pass through the exhaust nozzle. Thrust is produced by the high pressure acting on the internal surfaces of the motor.

Instead of explicitly defining this pressure field, Newton's law, $F = ma$,* which establishes the equivalency between force and momentum change, is used to determine the thrust from the momentum of the exhaust gases as they leave the nozzle, i.e.,

$$F = \dot{m}u_{ex} + (p_{ex} - p_0)A_{ex}$$

$$= \dot{m}\,[2(h_t - h_{ex})]^{1/2} + (p_{ex} - p_0)A_{ex} \qquad (1)$$

$$\simeq \sqrt{2}\,\dot{m}\,h_t \simeq \sqrt{2}\,\dot{m}\,c_p T_t\,,$$

*See list of symbols on the next page.

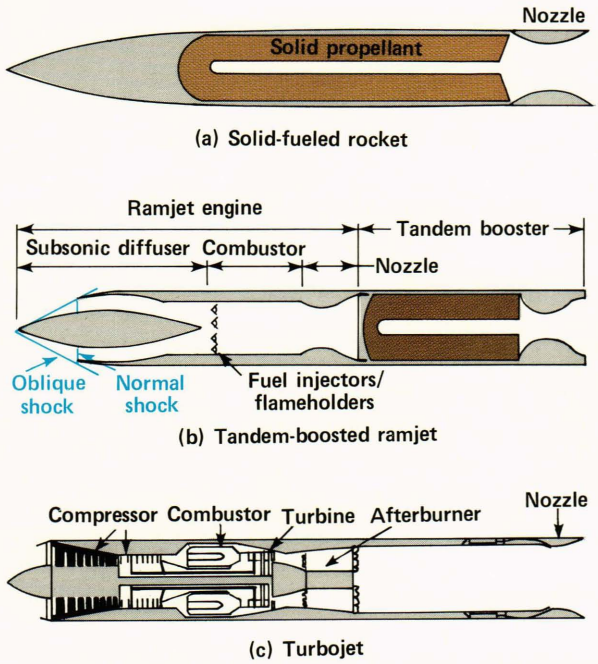

Figure 1 — Propulsion systems for tactical missiles: (a) solid-fueled rocket; (b) tandem-boosted ramjet; (c) turbojet.

SYMBOLS

a	acceleration or constant in burn rate expression, Eq. 4
A_p	surface area of propellant
c_p	specific heat at constant pressure
C_L	lift coefficient
d	diameter
D	drag
ER	equivalence ratio
F	force
g	gravitational constant
h	enthalpy
I_{sp}	specific impulse
L	lift
m	mass
$\dot{m}$	mass flow rate
n	exponent in burn rate expression, Eq. 4
p	pressure
q	dynamic pressure
R	gas constant
t	time
T	temperature
u	velocity
W	weight
x	down-range distance
z	altitude
ϵ	structural coefficient
θ	flight path angle
ν	kinematic viscosity
Π	product function
ρ	density
ψ	elevation angle

Subscripts

b	burnout
c	combustion
ex	nozzle exit
f	final
i	initial or inlet
L	payload
max	maximum value
n	nth stage
p	propellant
R	reference
s	structure
t	total or stagnation
0	free stream or initial

Superscript

*	nozzle throat

where $\dot{m}$ is the propellant flow rate, u is the velocity, p is the pressure, h is the enthalpy, T is the temperature, c_p is the specific heat at constant pressure, subscript t is the stagnation conditions in the rocket motor chamber, subscript ex is the nozzle exit, and subscript 0 is the local ambient. Thus, to produce thrust efficiently, i.e., a large force for a given flow rate or high specific impulse ($I_{sp} = F/\dot{m}$), it is necessary to use propellants that produce gases at high temperatures.

For convenience in handling, rocket-powered tactical missiles generally use solid rather than liquid propellants (Fig. 1a). The propellant is composed of a fuel, an oxidizer (which may be a single chemical compound or a mixture of several ingredients and often contains ignition and burning rate modifiers, catalysts, and inhibitors), and additives to enhance the mechanical and rheological properties (binders, plasticizers, etc.). Typical fuels are organic resins and plastics with or without metal powder additives, typical oxidizers are nitrates or perchlorates, and typical homogeneous monopropellants are the organic nitrates containing fuel and oxidizer in the same substance. Table 1 gives the properties of several typical rocket propellants.

The ramjet (Fig. 1b) differs from the rocket in that air is brought from the atmosphere into the engine to serve as the oxidizer for burning the fuel. The ramjet should be more efficient than the rocket, since it does not have to carry the weight of the oxidizer. On the other hand, this thermodynamic cycle requires compression of the air by slowing it down in the engine inlet prior to heat addition. Such compression is insufficient to produce thrust unless the air speed is greater than about Mach 0.9 (i.e., the speed is 0.9 times the speed of sound). Thus the ramjet must be brought up to this speed or beyond by a booster engine, generally a rocket. The booster can either be a separate stage that is jettisoned after propellant exhaustion, as shown in Fig. 1b, or be integrated with the ramjet, i.e., an integral rocket ramjet. In the latter case, the rocket propellant fills the ramjet combustor during the boost phase, ejectable covers close off the inlet to the combustor, and a rocket throat is used inside the larger ramjet nozzle. After the rocket propellant has been spent and the missile has reached its minimum operating speed, inlet port covers are ejected to permit external air to be captured by the engine inlets and the rocket nozzle insert is ejected.

For speeds between Mach 1 and about Mach 5, the air is compressed by means of a series of shock waves that terminate in a normal shock. The flow into the combustor is subsonic and the engine cycle is called a "conventional" subsonic combustion ramjet. At speeds greater than about Mach 5, a more efficient cycle results if the inlet air is only partially com-

Table 1 — Properties of typical solid rocket propellants.

Propellant	*Metal Content Weight (%)*	*Density (pounds per cubic inch)*	*Flame Temperature (°F)*	I_{sp} *(pounds force-seconds per pound mass)*	*Burning Rate (inches per second)*	*Pressure Exponent n (Eq. 4)*
DB	0	0.058	4100	220 to 230	0.45	0.30
DB/AP/Al	20 to 21	0.065	6500	260 to 265	0.78	0.40
DB/AP-HMX/Al	20	0.065	6700	265 to 270	0.55	0.49
XLDB/AP-HMX/Al	19	0.067	6060	269	0.35	0.50
PVC/AP	0	0.061	4600	230 to 240	0.45	0.38
PVC/AP/Al	21	0.064	5600	260 to 265	0.45	0.35
PS/AP	0	0.062	4700	230 to 240	0.35	0.43
PS/AP/Al	3	0.062	5000	240 to 250	0.31	0.33
PU/AP/Al	16 to 20	0.064	5400 to 6000	260 to 265	0.27	0.15
NEPE	19	0.067	6060	269	0.60	0.50
PBAN/AP/Al	16	0.064	5800	260 to 263	0.55	0.33
CTPB/AP/Al	15 to 17	0.064	5600 to 5800	260 to 265	0.45	0.40
HTPB/AP/Al	4 to 17	0.067	5600 to 5800	260 to 265	0.40	0.40
PBAA/AP/Al	14	0.064	5400 to 6000	260 to 265	0.32	0.35

Al	Aluminum
AP	Ammonium perchlorate
CTPB	Carboxy-terminated polybutadiene
DB	Double base
HMX	Cyclotetramethylene tetranitramine
HTPB	Hydroxy-terminated polybutadiene
NEPE	Nitrate ester plasticizer
PBAA	Polybutadiene-acrylic acid polymer
PBAN	Polybutadiene-acrylic acid-acrylonitrile terpolymer
PS	Polysulfide
PU	Polyurethane
PVC	Polyvinyl chloride
XLDB	Cross-linked double base

pressed and enters the combustor with a speed greater than Mach 1. This cycle is called a supersonic combustion ramjet.

The third basic engine cycle is the turbojet (Fig. 1c). A rotating air compressor is added ahead of the combustor to circumvent the low speed limitation of the ramjet, and a turbine to drive this compressor is added behind the combustor. The turbomachinery more than pays for itself in weight at subsonic and low supersonic speeds because the Carnot efficiency of the engine is much greater than the compressor "expense" as long as sufficient heat can be added in the combustor. However, at speeds above about Mach 3, the adiabatic compression of the air in the inlet raises its temperature to a point where only a relatively small amount of heat can be added in the combustor without damage to the turbine blades from overheating. Moreover, the relatively heavy compressor is no longer needed, and the cycle becomes less efficient than the ramjet.

RAMJET DESIGN TYPES

Many variations and combinations of these basic cycles have been used; typical examples are shown in Fig. 2. Figure 2a is a solid-fueled air-ducted rocket with an integral rocket booster. In the configuration shown, multiple axisymmetric aft-entry air inlets are used. Variations include half-round and two-dimensional inlets, perhaps with inward-turning compression surfaces. Depending on the thrust required and the constraints that may be imposed by the stowage of the missile, one, two, or four air inlets can be used. After the booster propellant has been expended and the small rocket nozzle and air inlet covers have been ejected, the sustain propellant is ignited to produce a hot fuel-rich exhaust that is burned to completion with the captured air in the main combustor. As contrasted to the ramjet where a sheet metal can or metal baffle obstructions are used to stabilize the flame, flame stabilization in this design occurs in recirculation zones that are generated in the region of the air intake ports. Since the solid propellant contains some oxidizer, the specific impulse, $I_{sp} = F/\dot{m}$, is lower than for the pure ramjet. However, the relatively high density of the solid fuel provides a high packaging efficiency that is an important consideration in volume-limited situations.

Figure 2b is an integral rocket liquid-fueled supersonic combustion ramjet. A "chin" inlet is shown that takes advantage of a favorable forebody compression field at angle of attack in the plane of symmetry. On the other hand, bank-to-turn rather than skid-to-turn control is required, which can have detrimental effects on the guidance system accuracy, especially during terminal maneuvers. Rather than a single ejectable nozzle, multiple nozzles are shown, reducing volume at the expense of weight and complexity.

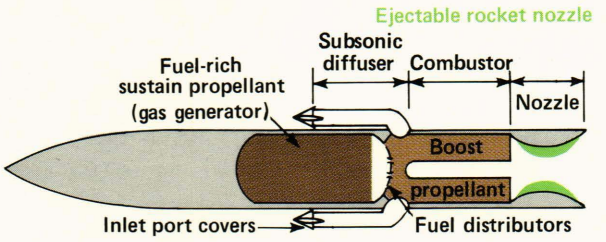

(a) Solid-fueled ducted rocket

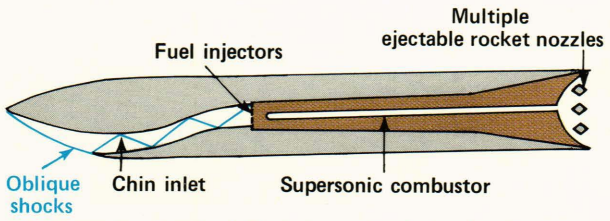

(b) Integral rocket liquid-fueled supersonic combustion ramjet

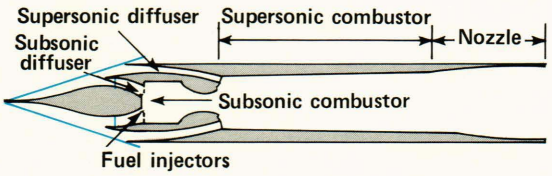

(c) Liquid-fueled dual-combustor ramjet

Figure 2 — Variants of basic propulsion cycles: (a) solid-fueled ducted rocket; (b) integral rocket liquid-fueled supersonic combustion ramjet; (c) liquid-fueled dual-combustor ramjet.

When the rocket propellant is consumed and the nozzles and inlet port covers have been ejected, liquid fuel is injected from the walls into the combustor unencumbered by flame holders that would produce undesired shock losses in the supersonic flow. Since the flow is supersonic, the residence time in the combustor is very short. Therefore, to burn conventional fuels, either the flight Mach number must be high, i.e., above Mach 5, or a highly reactive fuel or fuel blend, such as a hydrocarbon with 20% ethyl decaborane, must be used. Figure 3 is a photograph of a scramjet engine that was developed at APL and tested in the free-jet facilities at the Navy's Ordnance Aerophysics Laboratory in Daingerfield, Tex., at Mach 5 and 6 in the late 1960's and in the APL Propulsion Research Laboratory (PRL) at Mach 7 in 1970-71.

An alternative technique to reactive fuels is to inject simultaneously a highly reactive oxidizer, e.g., chlorine trifluoride (ClF_3), with a conventional fuel at the expense of simplicity, increased safety hazard, and loss in specific impulse.

An engine concept that bridges the gap between the supersonic and hypersonic speed ranges, with logistically acceptable fuels, is the dual-combustor ramjet, shown in Fig. 2c. A portion of the airflow captured by the inlet is diverted to a hot-gas generator, which,

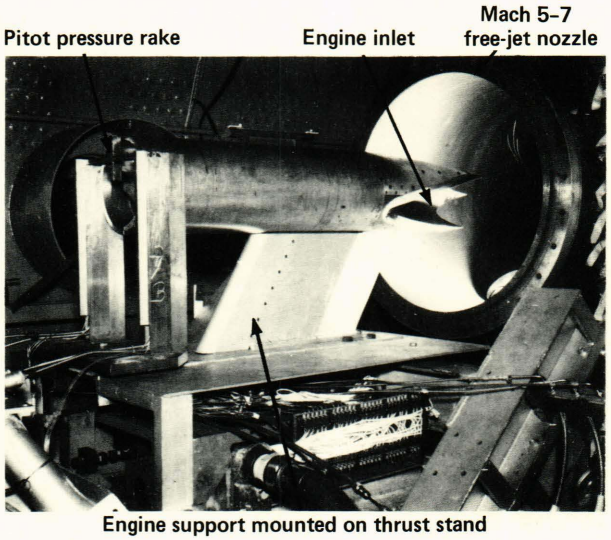

Figure 3 — A Navy/APL heat-sink type scramjet engine model in position for a hypersonic test.

in fact, is a "dump-type" subsonic combustor. To simplify the fuel control and injection system, all of the fuel is injected into the gas generator. Consequently, this combustor must operate considerably in excess of stoichiometry when high thrust is demanded. The hot fuel-rich combustion products pass into the main supersonic afterburner to complete the heat release by reacting with additional air.

Both this engine cycle and the scramjet (Fig. 2b) can, in fact, be dual-mode engines: they can operate in either the subsonic or the supersonic combustion mode. At low flight Mach number and high equivalence ratio, *ER* [*ER* = (fuel/air)/(fuel/air) at stoichiometry], a normal shock is located in the combustor entrance and heat release begins in subsonic flow. Heat addition occurs simultaneously with pressure drop in a diverging duct that accelerates the flow through the sonic point to supersonic conditions at the combustor exit. The price that is paid for the versatility in operation over a wide speed range is the complexity and weight of the split flow inlet compression system and gas generator. Figure 4 includes a schematic illustration and a photograph of the gas generator/supersonic afterburner currently being tested at PRL.

The particular choices of inlet type (e.g., chin, axisymmetric nose, or side mounted), nozzle type (single or multiple), and booster type (tandem or integral) in the configurations shown in Fig. 2 were arbitrary. Indeed, nearly every possible combination of these components has been examined for one or more applications. Moreover, Fig. 1a depicts only the simple, single-stage rocket. As the subsequent discussion will show, in some applications the optimum rocket missile may either have two stages or a propellant designed to burn intermittently in two or more pulses.

SELECTION OF PROPULSION CYCLE

Selection of the optimum propulsion cycle for a given application can be an arduous task. Generally,

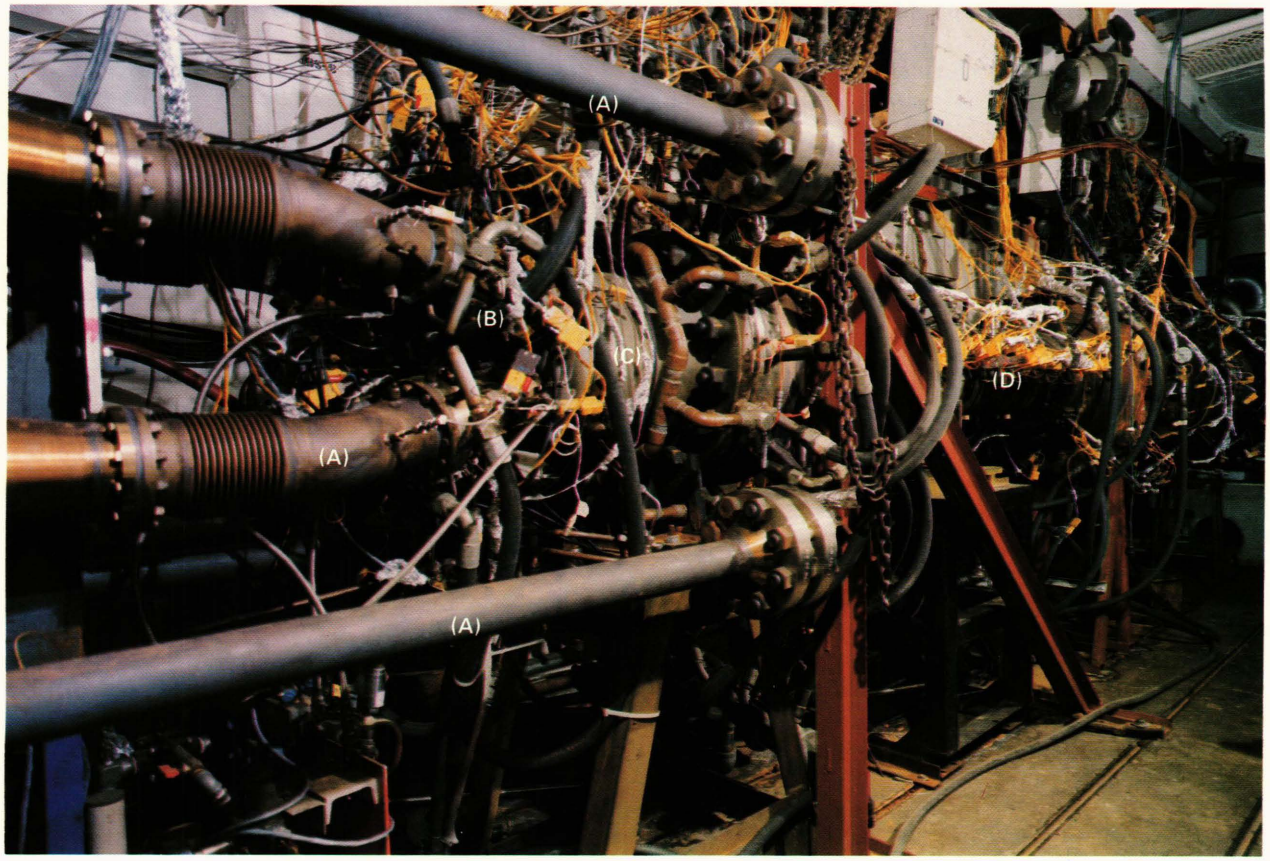

Figure 4 — Dual-combustion ramjet direct-connect test apparatus.

many cycles can be eliminated by a cursory examination, but the final selection often requires a detailed composite design. Even then, the selection may be ambiguous; one cycle may be better for a particular mission, but another may have the versatility to carry out several missions. There may be a trade-off between cost and performance, etc.

Two relatively simple expressions can provide some insight into the factors that ultimately lead to the selection of the candidate engine cycles. The first is the Breguet range equation, which holds for the simple case of cruising at constant velocity u with the lift L equal to the weight W, viz.,

$$R = uI_{sp}\ (L/D)\ \ln\frac{W_i}{W_f}\,, \qquad (2)$$

where D is the drag and W_i and W_f are the weights at the beginning and end, respectively, of the cruise phase.

The second expression is for the velocity change of a vehicle during the climb and acceleration phase, viz.,

$$u_b - u_0 = g\,I_{sp}\ln\frac{W_0}{W_b} - \int_0^b \left(g\sin\theta + \frac{D}{W}\right)dt\,, \qquad (3)$$

where W_0 is the initial weight ($W_S + W_P + W_L$), W_S is the structural weight, W_P is the weight of the propellant, W_L is the payload weight, $W_B = W_S + W_L$ is the burnout weight, g is the acceleration due to gravi-

ty, and θ is the local flight path angle with respect to the horizontal.

In both expressions, performance (either the range or the accelerative ability) is directly related to the specific impulse, I_{sp}. Typical values of I_{sp} for the propulsive cycles depicted in Figs. 1 and 2 are shown in Fig. 5. The values are based on the use of conventional hydrocarbon fuels in the airbreathing engines. The turbojet is the most efficient for speeds up to Mach 2.5, which has led to its near universal use as an aircraft powerplant. If relatively high thrust is required, the turbojet operates with an afterburner and I_{sp} is significantly lower.

Most missile applications require high thrust. As a result, the high cost of the turbomachinery for an expendable engine eliminates the turbojet from consideration unless long range is the dominant requirement and high acceleration and high speed are not mandatory. The current generation of cruise missiles (Harpoon and Tomahawk) are in this category. In the supersonic to moderate hypersonic speed range, the ramjet is attractive despite the booster requirement to bring it up to speed. The choice among subsonic-combustion, supersonic-combustion, or dual-combustor ramjets depends on the velocity requirement for the mission as well as cost and logistic considerations, as noted earlier.

As shown in Fig. 5, the rocket's specific impulse is only 20 to 30% of that of a ramjet. On the other hand, the mass fraction of propellant for a rocket for a tactical missile is typically 50 to 70% of the initial weight as compared to 25 or 35% for the ramjet. Thus the logarithmic terms in Eqs. 2 and 3 are larger by a factor of 2.5 to 2.8 for the rocket. Since the product of the two terms is significantly lower for the rocket, this generally eliminates it from consideration if long range during cruise is required (Eq. 2). However, during rapid acceleration the second term in Eq. 3 can be significant. This term is minimized when dt is small and drag is not too large, which corresponds to a relatively high average thrust to weight ratio, (F/W), of about 10. By tailoring the grain design and using a relatively large exit nozzle throat, it is possible to design a rocket with F/W of about 10, which is essentially independent of altitude. High-speed ramjets can be designed with F/W of about 10 near sea level. But since the thrust is proportional to the ambient pressure, at an altitude of 50,000 feet F/W is approximately 1 and at 100,000 feet about 0.1. Thus, if the missile must climb to high altitude while accelerating rapidly and a long cruise range is not required, the rocket may be the preferred engine.

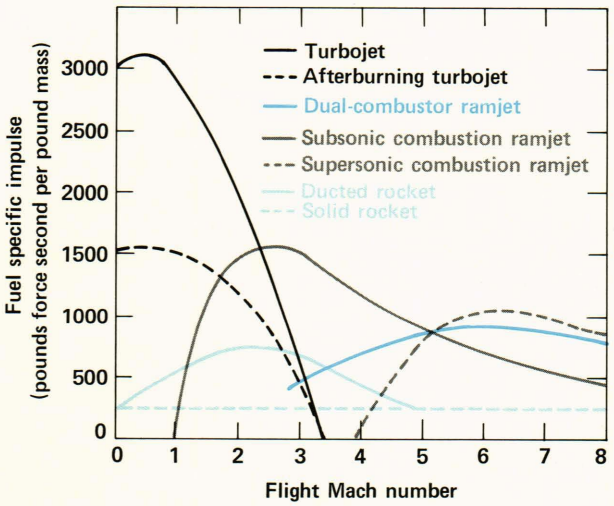

Figure 5 — Fuel specific impulse for various missile propulsion systems.

To develop this argument further and to give some insight into the design of propulsion systems, it is necessary to examine families of climb-out and cruise trajectories. For a given mission objective and constraints inherent to the composite design of the missile, e.g., structural and control limitations, the climb-out trajectory can be optimized by the introduction of lateral aerodynamic force and modulation of the thrust. Lateral force, which affects the missile attitude θ, can only be generated at the expense of induced drag, so the terms within the integrand of Eq. 3 are coupled. Moreover, drag increases with the square of velocity and decreases exponentially with altitude Z. Thus, rapid acceleration reduces dt but not necessarily $\int (D/W)\,dt$. No general solution has been found for Eq. 3, nor is there a rigorous procedure for optimization of the climb-out. However, considerable attention has been directed toward suboptimal schemes[1,2] that use high-speed computations to obtain apparent optimal trajectories for particular missile configurations and missions.

The interdependence of the missile composite design and the optimization of the trajectory will become apparent as particular mission requirements are examined. Typical trajectories for the first generic class of missions to be examined are depicted in Fig. 6. In this case, the missile is to be launched vertically ($\theta \approx 90°$) from a canister, after which it will climb, accelerate, and intercept a target at an altitude Z_A. The criterion for selecting the best propulsion system is maximum velocity at point A, which in general corresponds to minimum flight time.

Consider first the case of a solid propellant rocket. Let us hypothesize that it will be possible to select propellant grains and specify grain shapes and nozzle sizes that will produce constant flow rates of the propellants. Trajectories can now be flown for different flow rates to determine whether flight time is dependent on them. Curve I in Fig. 6 corresponds to a high flow rate, a short duration turn from the vertical, and a zero-lift ascent trajectory, i.e., no normal aerodynamic force is applied. Thus, the vehicle flies ballistically. Maximum velocity is reached when the propellant burns out and the missile coasts with some slowdown from burnout to altitude Z_A.

Curve II is for a lower flow rate. Burnout occurs later at a higher altitude and the trajectory "falls over" farther from the vertical because the velocity during the early phase of the climb-out is lower than

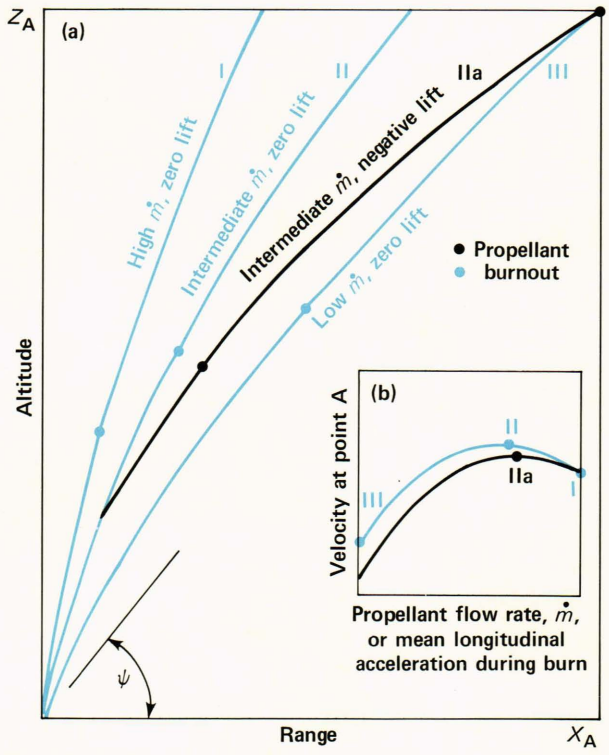

Figure 6 — (a) Ascent trajectories of missiles for target intercept near point A, and (b) determination of optimum propellant flow rate.

for curve I. Curve III is for the lowest flow rate covered in this example. Burnout occurs nearer X_A, Z_A and the trajectory falls over somewhat farther.

By introducing negative aerodynamic lift, it is possible to force trajectories I and II to pass through X_A, Z_A also, as typified by curve IIa for the intermediate value of flow rate. Similarly, trajectories II and III could be forced to pass through the terminal point of trajectory I by introducing positive lift.

Regardless of whether a comparison is made for ballistic ascent trajectories or for lifting trajectories forced to pass through the same point in space, there exists a propellant flow rate that yields a maximum mean velocity, as shown in Fig. 6b. The optimum trajectory corresponds to the case where the integrand in Eq. 3 is minimized. This can best be understood by examining the limiting case of $\dot{m} \rightarrow \infty$, which, from Eq. 3, would produce the maximum velocity immediately after launch. However, the vehicle would experience rapid slowdown due to the high drag at low altitude. With a lower flow rate the missile would climb through the dense lower atmosphere at a lower velocity with lower drag impulse, taking the same time to arrive at an intermediate altitude but with higher velocity.

As an example, consider the case of a rocket weighing 4000 pounds at lift-off, of which two-thirds is propellant that produces an average I_{sp} of 260 pound force seconds per pound mass. The rocket is 18 inches in diameter and 230 inches long, and has a low-drag nose. Taking the unrealistic limiting case of instantaneous burning of the propellant, the burnout velocity would be 9190 feet per second. For a vertical climb, the rocket would reach an altitude of 95,300 feet in 11.99 seconds with a velocity of 7500 feet per second, and an altitude of 204,100 feet at a velocity of 7000 feet per second. For ascent trajectories to targets having elevation angles less than the zenith, the corresponding altitudes at these velocities would be lower because the drag impulse would be higher.

As shown in Fig. 7, there is a range of finite values of propellant flow rates that yields a higher Z_A for a corresponding velocity on a vertical climb. For clarity, the entire $\dot{m} = \infty$ curve is not included. Curves drawn through the loci of points on ascent trajectories corresponding to velocities of 7500 and 7000 feet per second are shown for flow rates from 60 to 200 pounds per second. It is clear that only when targets are near the zenith are high flow rate values desirable. For targets below an elevation angle of about 30°, the optimal flow rate is about 80 pounds per second.

Unless the enemy uses ballistic missiles against ships, the primary role for defense of the Fleet from air attack is from targets at angles below 30°. Consequently, the emphasis will be on propulsion systems designed to cope with this threat. For the case with a constant flow rate of 80 pounds per second, the propellant burn time is 33.3 seconds and the burnout velocities vary from 7260 feet per second for targets at low elevation angles to 7858 feet per second for targets at elevation angles of about 35°. For an evaluation angle of 90°, the burnout velocity drops to 7770 feet per second, which again shows the interaction of the terms within the integrand in Eq. 3. This range of burnout velocities corresponds to a mean longitudinal acceleration during burning, u_b/gt_b, of 6.76 to 7.32 g where t_b is the time at burnout. Although each missile design and mission would have a unique flow rate value, the value that yields a mean acceleration of 5 to 10 g is typical of a wide variety of cases.

Granting that a constant flow rate of 80 pounds per second is a reasonable design point from which departures can be made to examine other effects, the case of nonconstant flow rate can be studied. Two cases are considered: a constant flow rate with an intermediate period without burning and a linear variation of flow rate with time. Figure 8 shows the effect of interrupting the burning of the propellant for periods of 5 to 40 seconds once the vehicle reaches a velocity of 5000 feet per second. For the range of elevation angles of primary interest, pulses up to 30 seconds lead to increases in performance, i.e., the u_A = 7000 feet per second contour is moved farther from the launch point. The shift of the curve for altitudes below 120,000 feet for the 30 seconds pause corresponds to a slowdown of about 400 feet per second for the steadily burning case. Lengthening the pulse beyond 30 seconds causes too great a slowdown to move the contour further and, indeed, if the pulse is long enough the vehicle cannot reach 7000 feet per

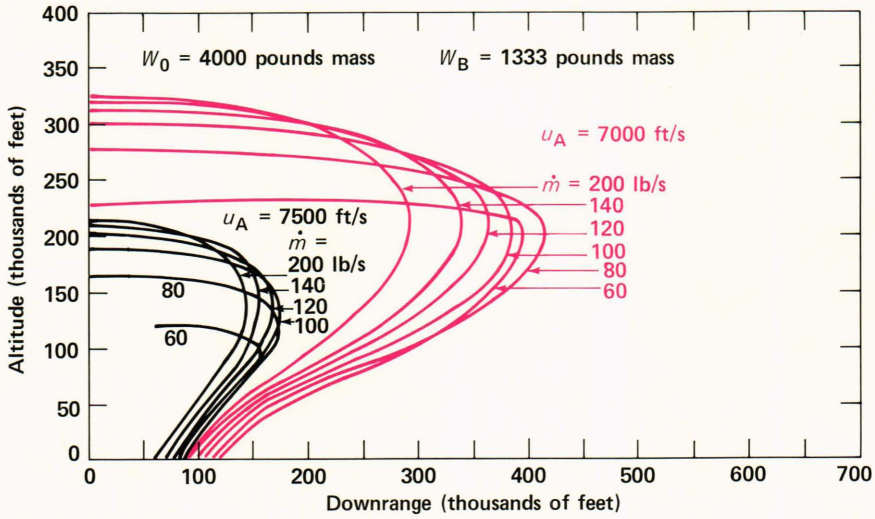

Figure 7 — The effect of propellant flow rate on ascent trajectories.

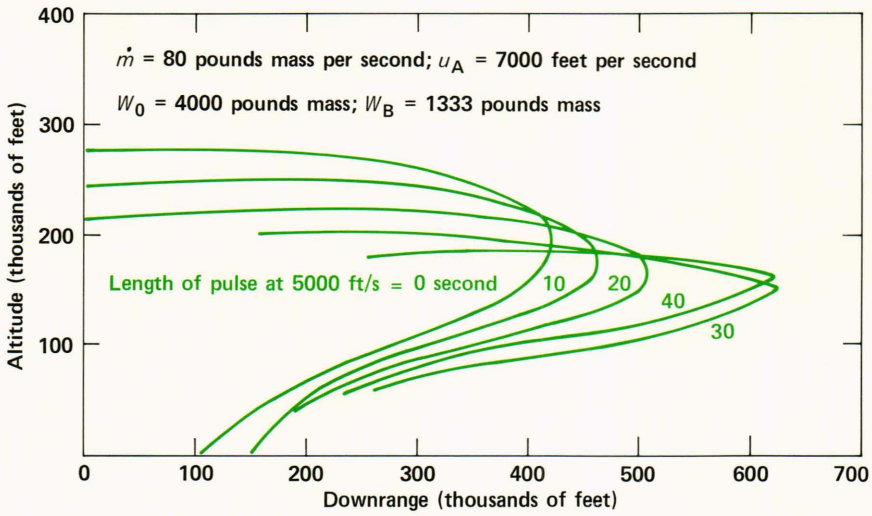

Figure 8 — The performance of pulsed rocket motors.

second. The choice of 5000 feet per second for the point at which the zero flow rate pulse is initiated is about optimum for extending the u_A = 7000 feet per second contour for pulse lengths of 30 seconds. Had the pulse been delayed until u_A = 6000 feet per second, only about half of the gain would have been realized. Whether the added complexity of the motor design to accommodate pulsing is warranted would depend on how crucial the additional performance is in meeting mission requirements. The amount of payload that would have to be replaced by additional propellant to produce an equivalent extension of the 7000 feet per second contour, would be about 85 pounds.

A plot similar to Fig. 8 can be used to compare the performance of linearly varying flow rates with constant flow rates. The 80 pounds per second constant flow rate case is again used as reference. Four cases were examined: linearly increasing flow rates from 60 to 100 pounds per second and from 70 to 90 pounds per second and linearly decreasing flow rates over the same two ranges. As shown in Fig. 9, increasing flow rates degrade performance, whereas decreasing flow rates extend the 7000 feet per second contour.

Unfortunately, from the point of view of grain design, a so-called "regressive" burning rate is difficult to achieve. Figure 10 shows typical cross sections of some radially burning propellant grains. The simplest configurations, shown in Fig. 10a, result in increasing flow rates as the diameter and area of the burning surface(s) increase with time. To obtain a near constant or decreasing flow rate, more complicated internal shapes are required, as shown in Fig. 10b, introducing problems of high stress concentrations in corners and the possibility of producing longitudinal slivers of propellant that could be sheared off and expelled from the rocket chamber without burning.

An "end burning" grain could also produce a constant flow rate, but the required burn rates for the propellant would have to be increased significantly. For a flow rate of 80 pounds per second, the volumetric burning rate for a propellant having a density of 0.067 pound per cubic inch would be 1194 cubic inches per pound. For a grain having a diameter of

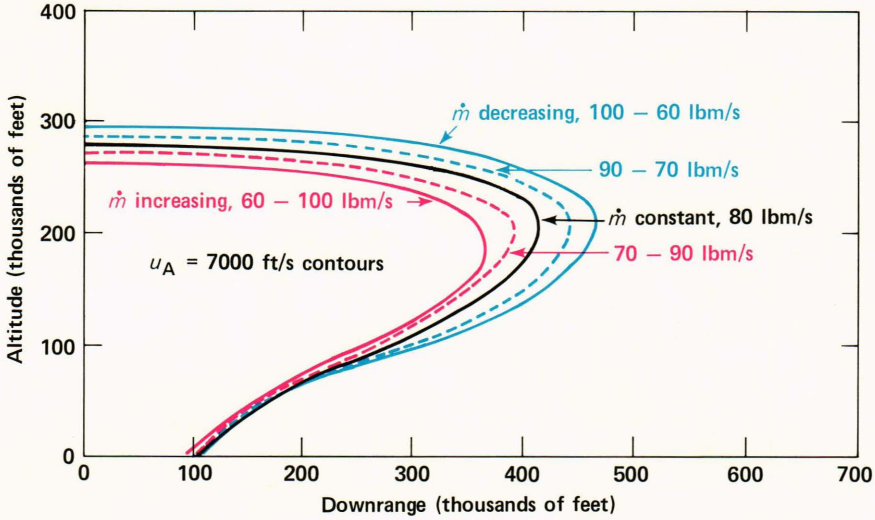

Figure 9 — The effect on rocket motor performance of linearly varying the weight flow of propellant.

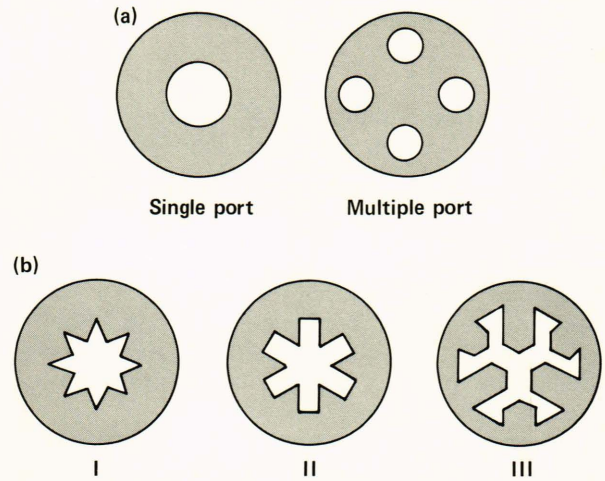

Figure 10 — Cross sections of typical solid propellant grains: (a) progressive burning rate designs; (b) near-neutral (I) and regressive (II and III) burning rate designs.

about 17.5 inches, this would require a linear burning rate of about 5 inches per second, about an order of magnitude larger than can be obtained with the propellants shown in Table 1. The addition of longitudinal metallic wires in the propellant offers the possibility of increasing the burning rate, perhaps to the level required.

The internal star designs have surface areas ranging from 1 to 5 Dl , where D and l are the overall diameter and length of the grains. Assuming that grain length is two-thirds of the 230-inch missile length, the corresponding range in required burning rates would be 0.09 to 0.45 inch per second, which is in the range that can be obtained with the Table 1 propellants.

The burning rate of most propellants is in accordance with Saint Robert's law, viz.,

$$\dot{m} = a A_p \rho_p P_c^{\,n} , \qquad (4)$$

where the lead coefficient a is constant for a given grain temperature. Combining this expression with the equation for flow through a sonic throat, viz.,

$$\dot{m} = p_c A^* u^* / R T^* , \qquad (5)$$

shows that for a fixed nozzle, i.e., A^* constant, and propellant temperature (T^*, u^* constant),

$$A_p \approx (\dot{m})^{1-n} . \qquad (6)$$

The asterisks refer to conditions at the throat of the nozzle. To obtain a regressive burning rate of from 100 to 60 pounds mass per second, the range of percentage reductions in A_p would be from 29 to 54% for the propellants listed in Table 1. The internal star design shown on the right in Fig. 9 would have an A_p that decreases by about 60%. Either this or a somewhat less complex shape could presumably meet the regressive rate selected in the example.

There is a mitigating effect that was not considered in this example, viz., that the structural weight of the linearly varying propellant flow engine would be greater than that of the constant propellant flow engine because the design maximum pressure would be greater. Consequently, most missile designs tend to use burning grain designs that generate gases at approximately a uniform rate.

The trend of these results suggests that for two-stage rocket designs, the flow rate of the first stage should be greater than that of the second stage. To establish this point, it is necessary to examine the differences in performance for two-stage vehicles where flow rate is varied for the two stages. A complete examination of this issue is an arduous task; however, some exemplary results can be discussed that show the general trends that would result from a more thorough investigation. Classical theory (see, e.g.,

Ref. 3) shows that for vehicles having multiple stages, Eq. 3 must be revised to determine the velocity change for an accelerating vehicle. In this case the logarithmic term becomes

$$\ln \left[\prod_{1}^{n} (W_{0i} / W_{bi}) \right] , \qquad (7)$$

where the bracketed term is the product of the n weight ratios of the i individual stages. In general, the burnout velocity of the nth stage u_{bn} is greater than the burnout velocity for a single-stage vehicle having the same ratio of payload to initial weights, W_L / W_0. The higher velocity is a result of discarding the structural weight of the burntout stage at staging, thereby saving the propellant that would have been used to accelerate this mass. For the large velocities required for long-range ballistic missiles and space vehicles, staging is mandatory for high W_L / W_0. Three- and four-stage vehicles are typical for these missions. For tactical missiles the velocity increment is typically one-third to one-half of that required for ballistic missiles, and no more than two stages are required.

Analytical solutions (see, e.g., Ref. 3) to maximize the burnout velocity for particular propulsive and structural characteristics have been found that show, for the idealized case of drag-free/gravity-free climbout of a vehicle having equal I_{sp} and structural coefficients $\epsilon = W_{si} / (W_{si} + W_{pi})$ for all stages, each stage should have the same weight fraction and therefore produce the same velocity increment as every other stage. Here, W_{pi} is the weight of propellant in the ith stage. When drag, gravity, varying I_{spi}, and ϵ_i are considered, the optimum u_{bi} for rocket-powered vehicles occurs when the velocity increment of the stage increases with each succeeding stage. Figure 11 shows that optimum performance for two-stage rockets is obtained when the velocity increment of the first stage is 44 to 46% of the total Δu.

The same trend would also be observed when the second stage is an airbreathing missile. However, this cannot be fully exploited with the fixed geometry engines that are generally used in tactical missiles. Usually it is not possible to design a fixed geometry engine (i.e., the inlet area and the throat of the exhaust nozzle cannot be varied) that will operate over a velocity range below 55 to 60% of the maximum velocity, as shown in Fig. 11b. If variable geometry is practical, the velocity increment of the first stage can be reduced to about 46 to 48% for optimal performance.

A 4000-pound missile with similar characteristics as before, except that it has two stages rather than one, can now be reexamined. If a structural coefficient $\epsilon_i = 0.1$ is taken for the rocket motor case, not including the nozzle and thrust vector control system, 1480 pounds of propellant should be packaged in the first stage to obtain $u_{b_1} \approx 0.45\, u_{b_2}$. At first-stage burnout the total weight would be 2520 pounds, of which 214 pounds would be dropped (164 pounds of rocket motor case and about 50 pounds of nozzle, thrust vector control, and stage clamping devices). The second stage would have an initial weight of 2306 pounds, including 1153 pounds of fuel, 122 pounds of structure, and 20 pounds of nozzle. Thus, both missiles would have effective payload weights of 1006 pounds if it is assumed that the nozzle thrust vector control of the one-stage vehicle is 30 pounds. The effective payload includes the warhead and guidance radome, the forebody, and all other components of the engine other than the rocket motor.

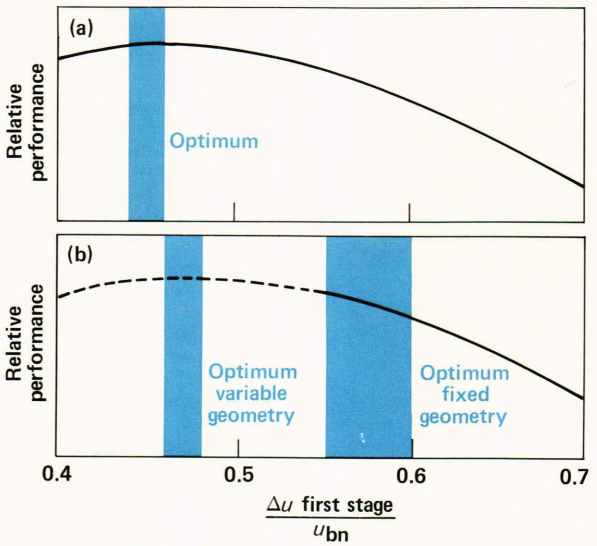

Figure 11 — Optimal staging of tactical missiles: (a) two-stage rocket; (b) rocket booster, airbreathing second stage.

Comparing the performance of one- and two-stage rockets for altitude values of 120,000 feet or lower shows that the u_A = 7000 feet per second curve for the two-stage rocket would extend about 20,000 feet farther when the flow rates are 80 pounds per second for both stages. This increment would about double if the mass flow rates were optimized, i.e., 140 and 60 pounds per second for the respective stages. Again, whether the added cost and complexity would be warranted for a Fleet defense missile targeted at low elevation angle is questionable. On the other hand, for targets at high elevation angles, a two-stage vehicle would be capable of reaching nearly double the range at the same burnout velocity for a given elevation angle.

The domain of velocity values examined so far, i.e., equal or greater than 7000 feet per second, precludes meaningful direct comparisons of rockets and airbreathers since, at present, structural and perhaps propulsive constraints appear to be too formidable to reach these speeds in tactical airbreathing missiles. However, the 4000 to 6000 feet-per-second velocity interval is of considerable interest for Fleet air defense.

Two approaches are possible to compare the performance of rockets and airbreathers in this range. The first is to compare an airbreather capable of

reaching u_A = 6000 feet per second with the rocket over a range of velocity values up to 6000 feet per second. The second is to compare a family of airbreathers, each designed for a particular maximum value. For velocity values less than 6000 feet per second, the latter approach would show better performance for the airbreathers because more of the total weight of the system could be put in the second stage. For example, to meet the u_{b_1} criterion shown in Fig. 11 for a fixed geometry airbreather capable of reaching u_A = 6000 feet per second would require a booster weighing about 1960 pounds, whereas for a u_A = 4000 feet per second missile the booster weight would be about 1259 pounds. Again, these designs are for total weights of 4000 pounds and many assumptions have been made regarding structural weights and other factors.

The procedures used to optimize the airbreather stages and trajectories are complex and the reader is referred to more detailed discussions of the subject (see, e.g., Ref. 4). Suffice it to say that the geometry of the engine, the modulation of thrust during climb-out, and the variation of normal force all enter into the optimization.

The final result of the comparison is shown in Fig. 12 where the single-stage rocket is compared with a family of optimally designed airbreathers for the mission described in Fig. 6, which, from a guidance system point of view, would correspond to commanding the missile by way of a shipboard radar. In Fig. 12, the down-range scale has been compressed. The rocket is the preferred engine for all elevation angles above 10°. The region for the rocket is terminated since, at high altitude, control of the missile would have to be provided by a means other than aerodynamic surfaces. The 160,000-foot limit shown here corresponds to a dynamic pressure q of 45 pounds per square foot for a velocity of 6000 feet per second. Control at lower dynamic pressure would have to be provided by auxiliary thrusters; this not only greatly complicates the missile design, but thrusters generally are not available in tactical missiles. The airbreather is preferred for all velocities that can be reached at $Z_A < Z_{A_{max}}$ prior to fuel exhaustion, since the airbreather still has fuel remaining to maintain a high velocity, whereas the rocket is coasting. The airbreather operating envelope is terminated at fuel exhaustion and at $Z_A = Z_{A_{max}}$, which corresponds to the altitude above which stable combustion cannot be obtained.

Trajectories representative of a second generic class of missions are shown in Fig. 13. Here the objective is to obtain maximum range by accelerating and climbing to an altitude Z_c and cruising in near horizontal flight from c to d. As in the previous example, the rocket has a maximum speed greater than the airbreather. The propellant is consumed relatively early in the climb-out, i.e., 33.3 seconds into a climb-out of about 100 seconds, and the vehicle decelerates following burn-out. To obtain maximum range, the flight path during climb-out and approach to the cruise condition must be optimally shaped. In general, the optimal path corresponds to launch near the vertical (θ = 90°) and continual turn-down (negative lift) up to the apogee. If near vertical launch is not achievable, positive lift (and thrust vector control) are used during the early phase of the climb-out to bring the vehicle close to the $\theta = f(z)$ characteristic of the optimal vertical launch case.

The types of trajectories that must be examined to obtain optimal range of a high thrust-to-weight (F/W) ratio vehicle (e.g., the rocket) are typified by curves IV, IVa, and V in Fig. 13. A high F/W vehicle has the accelerative capability to "overshoot" Z_c and then glide from the apogee back to Z_c by a number of possible paths with the introduction of positive lift. Curve IV corresponds to a case with a lift-to-weight ratio (L/W) > 1 as Z_c is approached. With L/W = 1

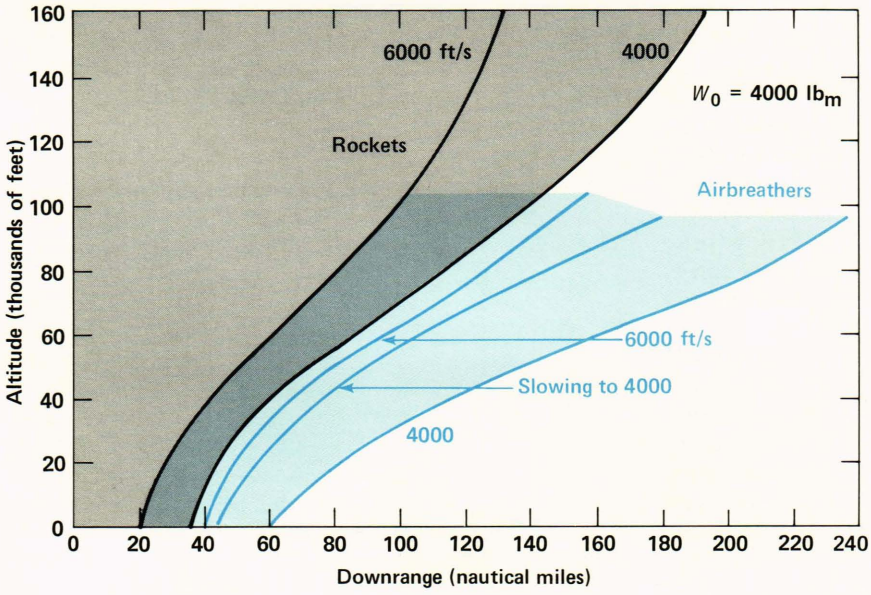

Figure 12 — Comparison of rockets and ramjets for area defense mission.

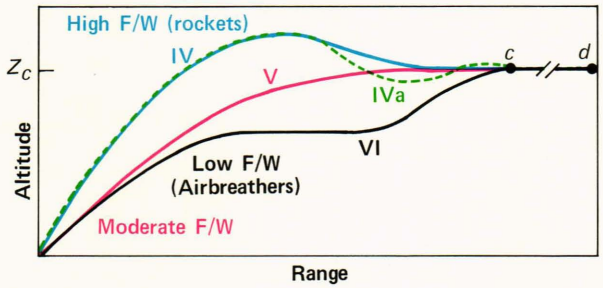

Figure 13 — Effect of thrust-to-weight ratio on ascent trajectories for missiles designed for near-level flight at an altitude Z_c.

at Z_c the vehicle will oscillate about Z_c with a decreasing excursion as time progresses, as typified by curve IVa. With $L/W < 1$, the vehicle can approach Z_c at $\theta = 0$ asympotically from below (not shown). The permissible altitude at apogee is limited to the aforementioned requirement to maintain control but, in general, optimal range is obtained on trajectories having lower apogees. These constraints significantly restrict the region of permissible climb-out trajectories to a narrow corridor in ψ_a, where ψ_a is the elevation angle of the apogee with respect to the launch point. For example, given that the flow rate is 80 pounds per second and that the rocket is constrained to an apogee of 100,000 to 160,000 feet, then the range in elevation angle is from 11 to 15°.

Curve V of Fig. 13 schematically represents the climb-out of a rocket with a moderate thrust-to-weight ratio or of a ramjet having a relatively large ratio of inlet areas to body cross-sectional area. For the same Z_c, however, the optimal climb-out for an airbreather would lie below that of a rocket. That is a consequence of the need to optimize thrust and fuel flow-rate simultaneously with the minimization of the integrand in Eq. 3 in the climb-out of an airbreather. Typically, those trajectories require modulation of the lateral force that produces turn-down following launch, followed by positive lift at low and intermediate altitudes, and negative lift as Z_c is approached.

Curve VI is representative of the climb-out of a low thrust-to-weight ratio engine. The accelerative capability is inadequate to climb to Z_c and accelerate to the desired u_c simultaneously. Instead, the vehicle must climb to a lower altitude, use lift to maintain this altitude, accelerate to u_c, then turn up with $L > W$, and finally approach Z_c with $L < W$. Usually this type of climb-out results in poorer performance than a Case V climb-out, which is one of the factors that influences the choice of the proper thrust-to-weight ratio propulsion system.

Optimal cruise range for the airbreathers or glide range for the rockets usually results when the vehicle flies from c to d at an angle of attack corresponding to $(L/D)_{max}$. The maximum lift-to-drag ratio varies with the aerodynamic configuration, velocity, and altitude, but for tactical missiles in the range of 4000 to 7000 feet per second, $(L/D)_{max} \approx 3$ and the corresponding angle of attack α is between 8 and 12°. During cruise the rocket is lighter than the airbreather, and the optimum altitude at the same velocity is somewhat higher. As the rocket slows down during the glide, the optimum altitude decreases. On the other hand, as the airbreather burns fuel to maintain constant velocity, the optimum altitude increases with the decreasing weight unless that altitude is too high to permit efficient operation of the inlet and combustor.

Figure 14 shows the altitude-range envelope for points d for the same tactical missiles used for the flight envelope of Fig. 12. For the rocket, boundaries are shown for slowdown to u_d = 4000 and 6000 feet per second. For the airbreathers, three boundaries

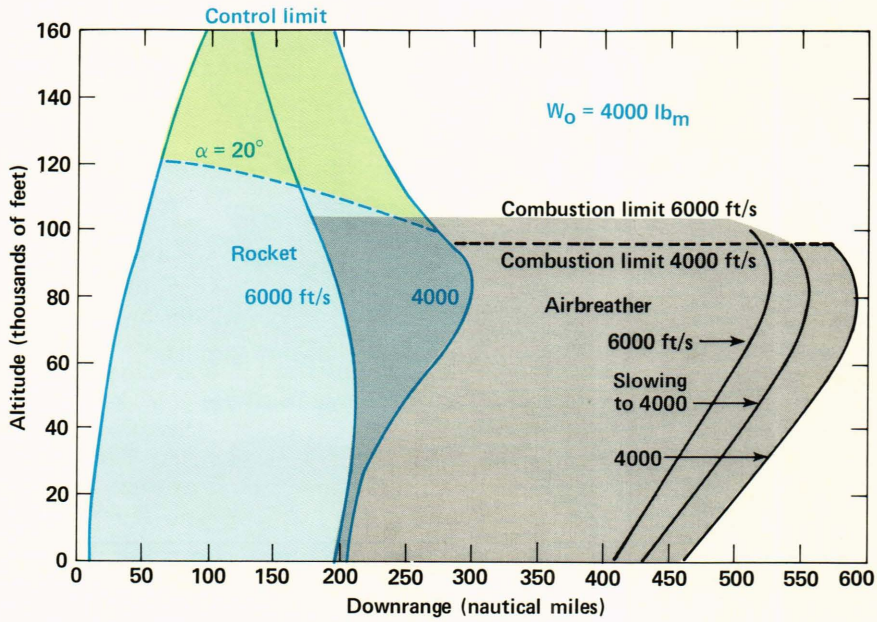

Figure 14 — Comparison of rockets and ramjets for long-range cruise missions.

are shown. The area above the dashed line is shaded in green to show that angles of attack greater than 20° would be required to maintain level flight of a coasting rocket. Indeed, at altitudes above about 130,000 feet, level flight is not possible for this vehicle. The u_d = 6000 feet per second is for a missile designed to cruise at 6000 feet per second. Two 4000 feet-per-second boundaries are shown; the one having the greatest extent is for a missile designed to cruise at 4000 feet per second and the other is for the 6000 feet-per-second design, coasting to 4000 feet per second following fuel exhaustion.

As in Fig. 12, the range that can be reached by the airbreathing missile is considerably greater than that reached by the rocket. On the other hand, for ranges less than that corresponding to equal velocities of the rocket or airbreather (i.e., 6000 or 4000 feet per second) for this example, the rocket could be the preferred propulsion system for a tactical missile, the argument being that the mean velocity would be greater, hence the time-to-target would be less for the rocket. This in turn could perhaps permit more time for assessment prior to firing or time for more salvos in a shoot-look-shoot scenario.

The optimum cruise altitude for the rocket, assuming $C_L = L/q_0 A_R \approx 1$ at $(L/D)_{max}$, where $A_R = \pi D^2/4$, would be about 111,000 feet at u = 6000 feet per second and 93,000 feet at u = 4000 feet per second. Maximum range, however, occurs at lower altitudes because cruise range for the coasting rocket is small compared to the ranges of the optimal paths to points c. For the airbreathers, the corresponding altitudes for flying at $(L/D)_{max}$ would be 2000 to 4000 feet lower at the same velocity, but better performance would be achieved at slightly lower altitudes due to the aforementioned problems of low inlet and combustor efficiency at low pressure levels. Thus the cruise phase of the airbreather occurs at a somewhat lower angle of attack than that which yields $(L/D)_{max}$. For this example, optimum cruise altitude is about 95,000 feet for u = 6000 feet per second and 80,000 feet for u = 4000 feet per second.

The mission postulated in Fig. 13 is typical of a tactical missile that provides for its own guidance during the cruise phase and is, in fact, a long-range weapon. Thus, in the parlance currently in vogue, the performance shown in Fig. 14 is typical of a "wide area defense" missile, whereas that shown in Fig. 12 is typical of an "area defense" missile.

DESIGN PROCEDURES FOR AN AIRBREATHING MISSILE

Even though the details of the procedures used to design and develop an airbreathing missile cannot be covered, the overall approach can be outlined. Figure 15 is a flow chart showing this procedure. Initially, engine performance is determined using assumed efficiencies for the engine components, weights, and aerodynamics based on preliminary composite designs and constraints imposed by the guidance system, ordnance, stowage, etc. Parametric variations

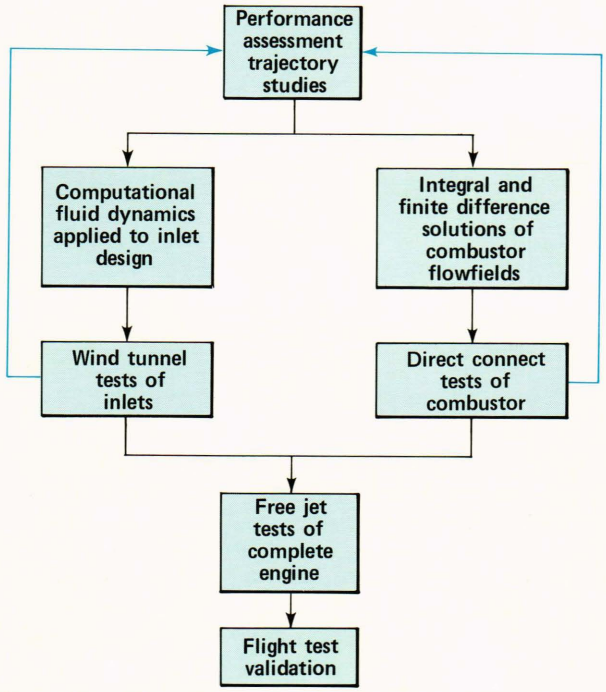

Figure 15 — Flow diagram for the design and development of a ramjet-powered missile.

are made in each of the above categories, and trajectories are flown to determine which candidate engine concepts can perform the proposed mission. Based on these results, computational techniques are used to obtain preliminary designs for candidate inlet configurations. Wind tunnel tests of inlets are made to provide revised performance values. A similar procedure is used in the development of the combustor. One or more iterations is made before a principal candidate engine geometry is chosen for verification in a free jet. The fuel supply and control system design is carried out concurrently with the inlet and combustor development and generally is used in the free-jet engine test. If all goes well, the engine then undergoes a flight test validation. A cursory examination of each of these steps follows.

Figure 16 shows results from one of the steps that take place in sizing the inlet and nozzle throat. Parametric variations of the inlet area A_i and the nozzle throat area A^* at various flight conditions and fuel flow rates are made to determine the thrust level. For a given fuel flow rate there exists a combination of A_i and A^* that yields the maximum thrust. For a subsonic combustion engine, this optimum occurs when the normal shock in the inlet compression process is located at the cowl lip station, as shown in the engine sketches. The solid curve is drawn through the locus of points corresponding to these optimal geometries. The curve terminates at the point where the maximum allowable A^* and the fuel/air equivalence ratio equals 1. This curve gives the performance of a variable geometry engine.

Taking the A_i and A^* that correspond to any point on the curve, e.g., point A, permits comparison of

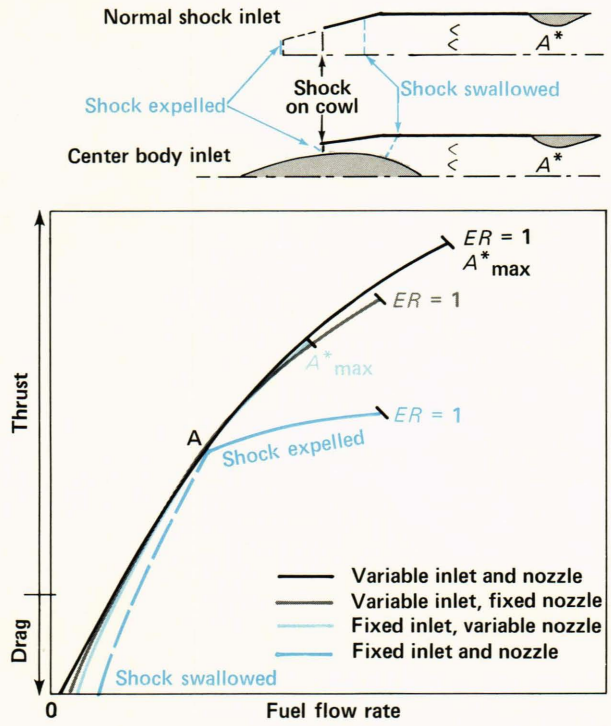

Figure 16 — The procedure used to determine inlet and nozzle throat dimensions.

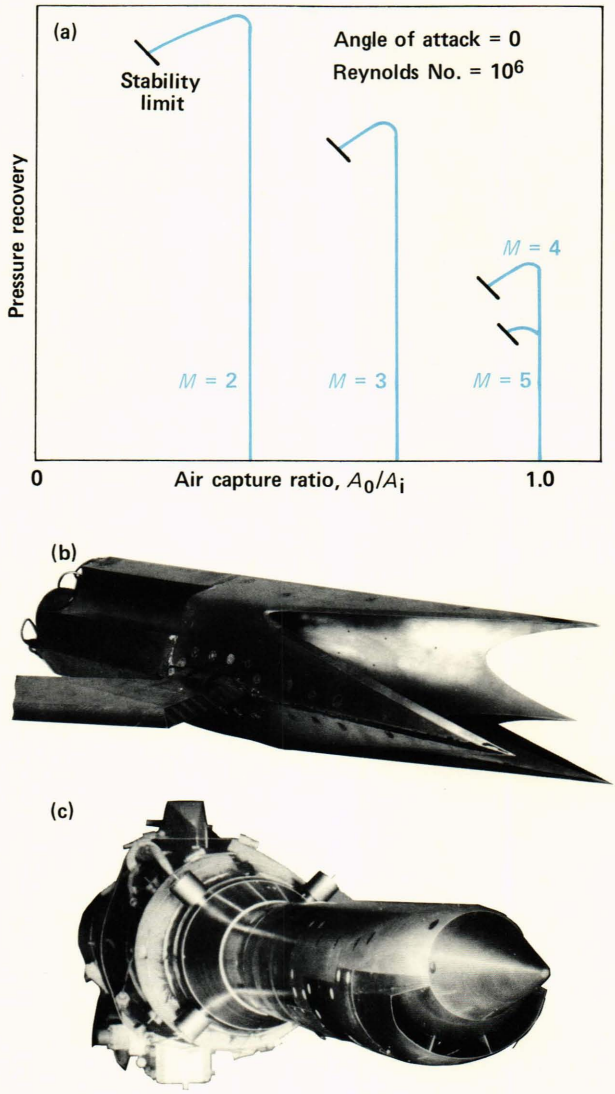

Figure 17 — Inlet testing. (a) Typical air capture-pressure recovery characteristics of an airbreathing missile inlet. (b) Three-module inlet evaluated in seven wind tunnel tests at M_0 = 4.0, 5.3, 6.0, 7.8, 8.1, and 10.0. (c) "Chin" type inlet model for a subsonic combustion ramjet tested at M_0 = 3.0 to 4.5.

partially variable and fixed geometry engines. If only the inlet can be varied, optimum performance is obtained with the shock on the cowl lip, but more fuel is required to produce the same thrust, and an equivalence ratio equal to 1 occurs at a lower thrust level. Likewise, with a fixed inlet and a variable exit, the normal shock is on the cowl lip, more fuel is required than for the variable geometry engine, and the maximum thrust is lower. With a fixed inlet and exit, the normal shock will be located on the cowl lip only at point a. For lower fuel rates, this shock is swallowed, as shown in the sketches, and the performance is correspondingly degraded. For higher fuel flow rates, the normal shock must be expelled, which may or may not be acceptable. In normal shock inlets that are used at relatively low flight speeds (i.e., less than Mach 2.2), no problems are encountered but, as shown in Fig. 16, the gains in thrust accrue only with large increases in fuel flow rates. With centerbody inlets that are used at higher speeds, expelling the shock much beyond the cowl lip generally results in the generation of an unacceptable instability sometimes referred to as "buzz." In a buzz condition, the airflow into the ramjet pulsates with a frequency equal to the fundamental or to a harmonic of the equivalent Helmholtz resonator.

The choice of point A in this discussion was arbitrary, and if more thrust were needed in a fixed geometry engine, a larger inlet would be dictated, albeit with an increased fuel flow and less efficiency at lower thrust levels.

INLET TESTING

Typical inlet testing is illustrated in Fig. 17. The flowfield of an inlet in flight can be simulated in a wind tunnel test as long as the Mach number and Reynolds number [(velocity·diameter)/kinematic viscosity] are duplicated. If the tests are performed at pressures higher than in flight or at temperatures lower than flight or both, the ratio ud/ν can be several times larger, and the diameter can thus be smaller. Typically, wind tunnel tests are carried out at one-fifth to one-third of the flight size. Tests are run over the entire range of Mach numbers and Reynolds numbers at all angles of attack expected in flight. For asymmetric designs, various roll orientations must also be examined.

The principal parameters that are measured in the test are pressure recovery, air capture, and cowl and additive drag. The details of both the internal and external flowfields and the inlet starting characteristics may also be of interest, especially if boundary layer separations or large gradients in the internal flow are present or if problems are expected in starting the engine. In Fig. 17a, pressure recovery as a function of air capture ratio A_0/A_i is shown for Mach 2 through 5 for a centerbody inlet designed for full capture at $M = M_D = 4$, angle of attack = 0 (M_D is the design Mach number). These data are obtained by closing a calibrated throttle attached to the inlet, which simulates the pressure rise that would be caused if combustion were present. As the throttle closes, the normal shock moves toward the cowl lip and the pressure recovery increases. When the normal shock passes upstream of the cowl, air capture decreases; with further closing of the throttle, the inlet reaches the aforementioned stability limit. The ratio of the cross-sectional area of the streamtube captured by the inlet to A_i is 1 for $M \geq M_D$. Pressure recovery corresponding to normal shock at the cowl lip increases with decreasing M.

Figures 17b and 17c are photographs of inlets tested for the Naval Sea Systems Command by APL. The three-module engine shown in Fig. 17b was tested in conjunction with the development of the engine shown in Fig. 3. Tests were made over a range of Mach numbers of 4 to 10 at angles of attack up to 15°. Figure 17c is a chin inlet that has been tested at $M = 2$ to 3.5.

COMBUSTOR DEVELOPMENT

Combustor development involves the direct-connect testing of the combustor chamber to an air ducting system that provides air at conditions simulating those provided by the inlet in flight. Since there is no unique similarity parameter for combustion, the tests must be made in full-scale hardware. In the course of the development of the combustor, numerous fuel injector and flame holder geometries are investigated. Other parameters that may be studied include the nozzle throat area, combustor length, port-to-dump area ratio in sudden expansion burners, and the effects of swirl. The standard measures of performance are combustion efficiency η_c and total (stagnation) pressure loss. The former is the ratio of the heat release actually realized to what is theoretically available in the fuel. The latter is a measure of all of the nonkinetic losses that are present.

Typical direct-connect testing data are shown in Fig. 18. Combustion efficiency varies with equivalence ratio, air total temperature, and pressure or weight flow. Both rich and lean blowout limits can be present, and regions where the combustion is unstable are often encountered. These instabilities can be either longitudinal or transverse. The former, relatively low frequency oscillations, can cause unfavorable interactions with the inlet; the latter, relatively high frequency oscillations, can produce detrimental effects on insulation materials, electronics components, etc.

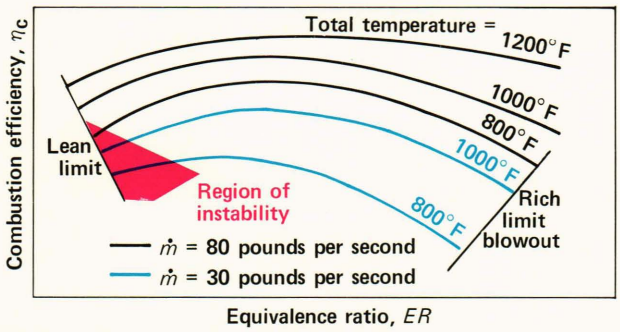

Figure 18 — The effects of temperature, pressure, and equivalence ratio on combustion efficiency in direct-connect testing of the combustion chamber.

Finally, in free-jet testing, the entire engine is placed in a large ground test facility. It is installed on a thrust stand to measure the net force on the engine. The entire test chamber is enclosed so that tests can be made that simulate high-altitude flight. Figure 19a shows an integral rocket ramjet that was tested in the free-jet facility at the Airbreathing Propulsion Test Unit at the Arnold Engineering Development Center, Tenn. Figure 19b shows typical test data. Successful completion of the free-jet engine tests provides the opportunity to proceed into a flight test program with reduced risk.

The development of other types of propulsion systems follows a similar approach to that diagrammed in Fig. 15, but the steps may differ depending on the components that must be tested. For example, rocket motor development obviously does not require inlet testing, but frequently attention must be given to tailoring the propellant composition to meet specific flight requirements. Because the coefficient a and exponent n in Eq. 4 are only weakly dependent on scale, most of the combustion characteristics of propellants can be obtained in a small-scale apparatus. Then, when a candidate fuel has been selected, full-scale motor firings are made to verify the small-scale results and to examine behaviors such as combustion instability that are scale dependent.

Much of the emphasis in the full-scale tests of rocket motors, and indeed in the testing of other propulsion cycles, addresses issues other than propulsion *per se,* e.g., the structural integrity of the propellant, rocket motor case, and nozzle. When the nozzle must provide thrust vector control, the operating characteristics of the actuating system, the structural adequacy of the gimbal or vanes, and the determination of the thrust degradation as a function of the lateral force generated must be examined.

The development of integral rocket ramjets requires not only all of the steps for both the rocket and the ramjet individually, but also a ground test demonstration of the transition from operation as a rocket to that as a ramjet. Even for cycles of this

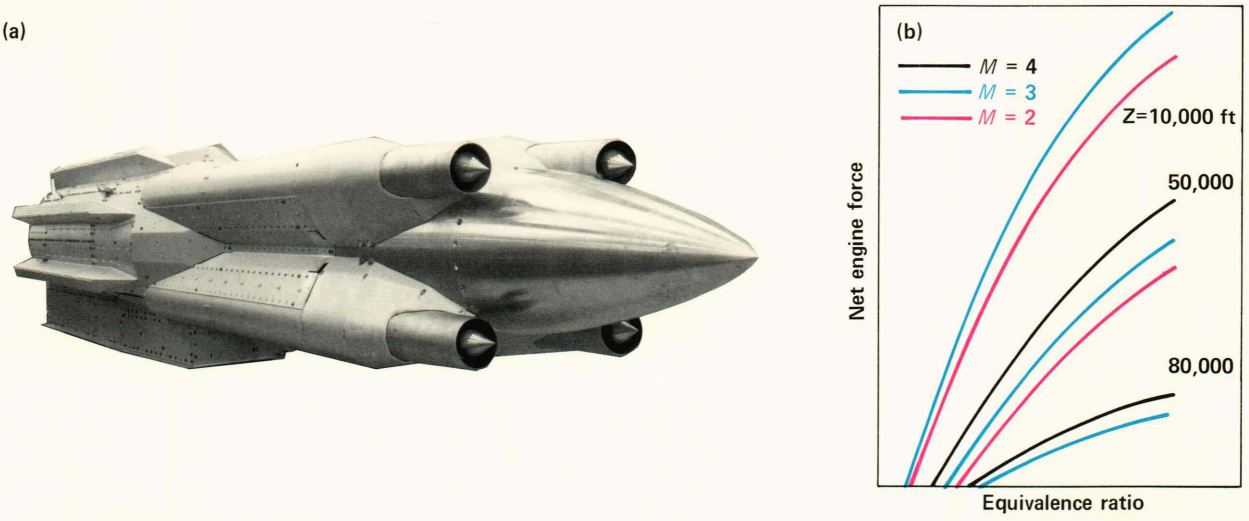

Figure 19 — Free jet engine testing. (a) Photograph of an integral rocket ramjet surface-to-surface engine with test fairings prior to testing in the Arnold Engineering Test Center free jet. (b) Typical measurements of engine force at various fuel flow rates and altitudes.

complexity, experience has shown that when meticulous attention is given to the resolution of all problems encountered in ground tests, near-flawless performance in flight test programs can be expected, as exemplified by the recently completed tests of the Advanced Strategic Air-Launched Missile for the United States Air Force.[5]

REFERENCES

[1] A. E. Bryson, Jr., and Y. C. Ho, *Applied Optimal Control*, Halsted Press, Washington, D.C. (1975).
[2] A. Miele, "Recent Advances in Gradient Algorithms for Optimal Control Problems," *J. Optimization Theory Appl.* **17**, 361-430 (Dec 1975).
[3] P. G. Hill and C. R. Peterson, *Mechanics and Thermodynamics of Propulsion,* Addison-Wesley, Reading, Mass. (1965).
[4] P. J. Waltrup, F. S. Billig, and R. D. Stockbridge, "Engine Sizing and Integration Requirements for Hypersonic Missile Applications," *NATO/AGARD/PEP 58th Symp. Conf. Proc. No. 307* (Oct 1981).
[5] J. Cushman, "Ramjet? Roger, Says DeLauer," *Defense Week,* 6-7 (Sep 27, 1982).

RANDOLPH W. BRUNS and EDWARD C. JARRELL

RAM GUIDED MISSILE WEAPON SYSTEM

The SEASPARROW and the RAM are short range missiles intended for antiair self-defense of surface ships. Versions of SEASPARROW have been deployed for some time.The model RIM-7M SEASPARROW, now being developed, will be supplemented on SEASPARROW ships by the RAM, which will provide more firepower against specific threats. The RAM and its associated ship system may also protect small craft that have no other antiair defense.

INTRODUCTION

A defense in depth is required to defend individual ships and task forces successfully; different defensive weapons are necessary to engage at long, at medium, and at short ranges. The world's navies have developed many weapons to protect their ships against air attack. These weapons include aircraft, missiles, guns, and countermeasure devices to confuse the guidance systems of the attacking threats. While these weapons are reasonably successful in destroying attackers, increased firepower continues to be a very desirable attribute.

The RAM Weapon System currently being developed provides higher firepower than existing weapon systems because it uses different guidance principles. Less equipment is required on the ship to support the missile guidance function. This, in turn, also results in a reduced requirement for operating and maintenance personnel.

The unique design concepts required to achieve this capability were successfully demonstrated by APL, General Dynamics/Pomona Division, and Hughes Aircraft Co. in tests and analyses from 1966 to 1979. In June 1979, the governments of the United States, the Federal Republic of Germany, and Denmark entered into a contract with General Dynamics to proceed with full-scale engineering development of the RAM Missile and one of two systems to control and launch the missile. Since that time, APL has continued to assist the Navy in the technical development of this system. Recently, the Netherlands and Belgium have joined the program, while Canada and Norway currently participate as observer nations.

APL has provided technical support to both the Naval Air Systems Command and the Naval Sea Systems Command during the development and testing of both the SEASPARROW and RAM Missiles, has supported the integration of SEASPARROW Weapons Systems aboard ships, and presently is involved in the integration of the model RIM-7M and associated weapon systems into existing and future ships. APL and General Dynamics/Pomona Division jointly originated and tested the RAM guidance and control concept. The Laboratory provides technical support to the Naval Sea Systems Command in the development and integration of the missile and the shipboard system.

BACKGROUND

Air defense missiles must either hit the target or pass within the lethal range of the warhead (typically 5 to 50 feet). This requires that the missile either home on signals emanating from the target or that the missile be directed to the target by shipboard devices that accurately monitor target and missile locations. Most shipboard air defense missile systems home on signals that are produced by the defending ship and then are reflected from the target. A shipboard radar tracks the target and transmits additional signals directed at the target in a narrow beam. These additional signals are reflected by the target and are then detected and tracked by a receiver in the missile. Information obtained from these reflected signals is used to steer the missile toward the target. This method of controlling missile flight is called *semiactive homing guidance* because the transmitter is located on the ship and the receiver is located in the missile. Another form of missile guidance, *command guidance*, uses radars on board the ship to track both the target and the missile while command signals are transmitted to the missile to steer it. Missiles are also guided toward the target using *beamrider guidance*, in which shipboard radar tracks the target and the missile is launched into the radar's beam. The missile's beamriding guidance receiver detects modulations of the radar signal to maintain the missile at the center of the beam until intercept. Some combination of these methods may also be used.

The shipboard radars used for semiactive, command, and beamrider guidance must maintain track of the target until intercept. Ships will typically have more than one tracking radar aboard; however, the number of targets that can be engaged is limited by the number of these radars. Newer radars are being developed that can provide guidance signals to more than one target at a time, but they will be limited at first to cruisers or larger ships.

An attractive alternative approach is to derive guidance information from emissions from the target. The major air threat to ships today is the cruise missile. At least 27 different cruise missile weapons have been produced by nine different nations.[1] These weapons can be launched from aircraft, submerged submarines, surface ships, and land. A large percentage of these weapons use self-contained active radars for guidance. The RAM Weapon System was conceived in this context. It is designed to acquire and home on the radar guidance signals emanating from antiship missiles. Using target data from shipboard passive sensors instead of from dedicated tracking radars, the launcher is pointed in the direction of the threat and the missile is fired. The firepower resulting from this weapon is much greater than from systems requiring shipboard tracking radars for missile guidance. Advances in guidance technology are under continual consideration for enhancement of the capability of this weapon.

SYSTEM DESCRIPTION

Functional System Operation

The RAM Weapon System uses search radars and passive radar frequency sensors called electronic warfare support measures equipment to detect the presence of radiating threats. Figure 1 illustrates the functional operation of the RAM Weapon System.

Shipboard search radars detect targets and report target direction and range. Electronic warfare support measures equipment detects only targets that are radiating and measures their frequency and target direction. The data from these two sensors are then correlated by computers to establish legitimate targets for RAM engagement. As targets come into RAM engagement range, designation commands are sent to the RAM Weapon System, the launcher is slewed to the target direction, and a missile is fired. The missile radar frequency seeker acquires the target radar signals in flight and initiates homing. The missile also has an infrared passive homing receiver that detects infrared radiation from the heated skin and the engine exhaust of the target. When the missile approaches the target, guidance is transferred from the radar frequency seeker to the infrared seeker for the terminal phase of the flight. As the missile passes close to the target, an active optical target detector detects the presence of the target and triggers the warhead. When the missile scores a direct hit, a contact fuze triggers the warhead.

Hardware Configuration

A major feature of the RAM Weapon System is that it will operate with currently installed shipboard equipment with only minimal software and hardware modifications to the surveillance sensors and the Combat Direction System. The only sizable additions required are a launcher and its peripheral equipment, an operating console, and storage for additional missiles.

Surveillance and Weapon Direction Equipment—Modern warships have search radars and passive equipment that will satisfy RAM targeting requirements. The target data must be processed as rapidly as possible to support the high firepower of the RAM Weapon System. On U.S. warships, this information can be obtained from the AN/SLQ-32(V) Electronic Countermeasures Set and the Mk 23 Target

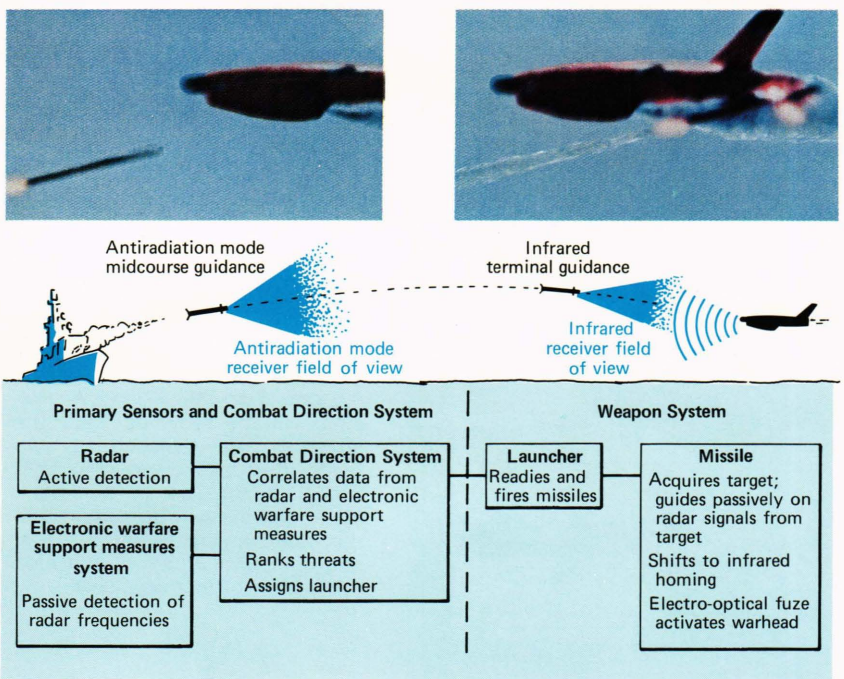

Fig. 1—RAM Weapon System functional operation. In a typical engagement, radar and passive tracks of a target are correlated by the Combat Direction System, which designates the target to the weapon system. A launcher is assigned to the target and subsequently a RAM round is fired. After launch, the RAM Missile detects radar emissions from the target to make midcourse guidance corrections. As the target is approached, guidance is switched to infrared homing for final corrections. Detonation of the warhead within lethal range of the target is initiated by a signal from the optical fuze. The inset shows a test intercept of a drone by the RAM Missile.

Acquisition System search radar. Both of these systems use digital computers to detect and track targets. Computer algorithms are being developed to correlate the data from the Target Acquisition System and the Electronic Countermeasures Set in order to rapidly identify radiating threats and to support the target selection and weapon assignment functions.

Weapon System Configurations—At the present time, the RAM Missile is planned to be deployed in two weapon system configurations. The first uses the present NATO SEASPARROW launcher (Mk 132) in which two of the eight SEASPARROW's are replaced by two guide inserts containing five RAM rounds each (Fig. 2). Modifications to the SEASPARROW software, launcher, and firing officer's console will be made to accommodate the RAM Weapon System. The semiactive guidance NATO SEASPARROW has a longer range than RAM Missiles and can engage both radiating and nonradiating threats, while the RAM Missile measurably increases firepower at shorter range against radiating threats. Computer-assisted weapon employment doctrines are being developed to provide optimum use of these weapons in varying threat situations.

The second RAM configuration, called the Guided Missile Weapon System (EX-31, Mod 0), uses a modified gun mount from the Close-In Weapon System. (The Close-In Weapon System provides close-in defense using 20 mm guns against high speed, low flying missile or aircraft targets.) Twenty-four missile rounds, loaded individually from the rear, are housed in a launching guide assembly that replaces the gun and its associated radars (Fig. 3). The lightweight guide assembly is manufactured from fiberglass composite materials. Many of the components of the EX-31 Weapon System Launcher are being manufactured in Germany. Other major components of the weapon system include the Launcher Servo Control Unit, the Weapon Control Panel, and a small computer assembly for missile control and interfacing with the ship's combat system.

Missile Round—The RAM round consists of the XRIM-116A Missile enclosed in an EX-8 canister that provides environmental protection for the missile and serves as a launching tube. The missile consists of a guidance section, control section, ordnance section (active optical fuze and warhead), and a rocket motor (Fig. 4). The overall length of the missile is approximately 110 inches and the body diameter is 5 inches, although folded wings, tails, and clamps extend beyond this diameter. The nominal weight of the missile is 161 pounds. The missile will roll in flight, permitting use of a single-plane guidance and control system. The missile roll is achieved with a rifling guide designed into the launch tube.

The guidance section consists of an aluminum shroud, a clear infrared dome, four antennas, a modified STINGER infrared seeker, the radar frequency seeker, and guidance mode switching circuits (transition electronics). Facing forward are two wideband interferometer antennas whose output signals provide guidance information; the other two antennas (facing aft) are used in the rear sector gate circuitry to reject radar signals arriving from the rear of the missile. Since the radar frequency seeker provides initial and midcourse guidance and the infrared seeker provides terminal guidance, transition electronics are required to determine when radio- frequency to infrared changeover should occur and to channel the proper signals for steering.

The control section contains the fixed (rectangular) and movable (delta) wing assemblies. The delta wings are mounted on a common shaft and are driven from a single torque motor. The wings are folded into slots in the airframe before launch. All wings unfold from front to back and lock upon deployment. The rectangular forward wings are deployed after rocket motor burnout to compensate for the shift in the missile's center of gravity that occurs as the rocket motor burns out. Also contained within the control assembly are the servo motor, associated electronics, autopilot sensors, and missile batteries. The ordnance sec-

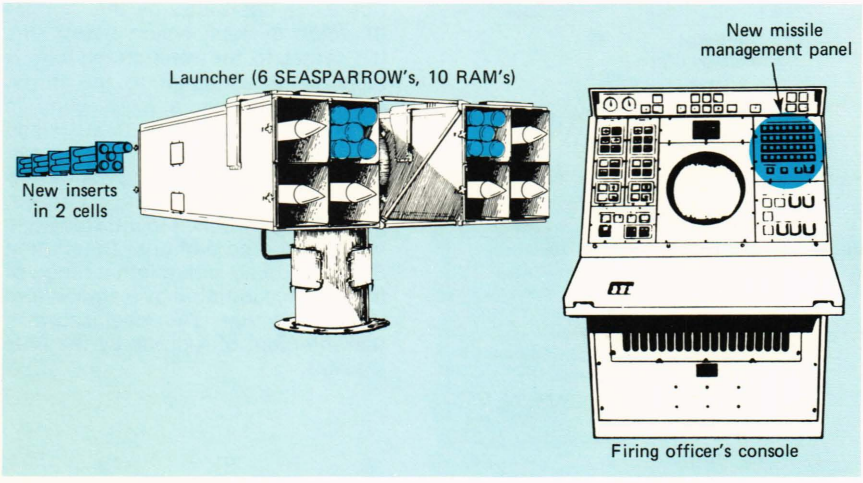

Fig. 2—The RAM modification to the NATO SEASPARROW Missile System. Two SEASPARROW Missiles will be removed from the launcher and replaced by two guide inserts, each able to hold five RAM Missiles in canisters. Modifications will be required in the launcher, in the missile system computer program, and also in the firing officer's console.

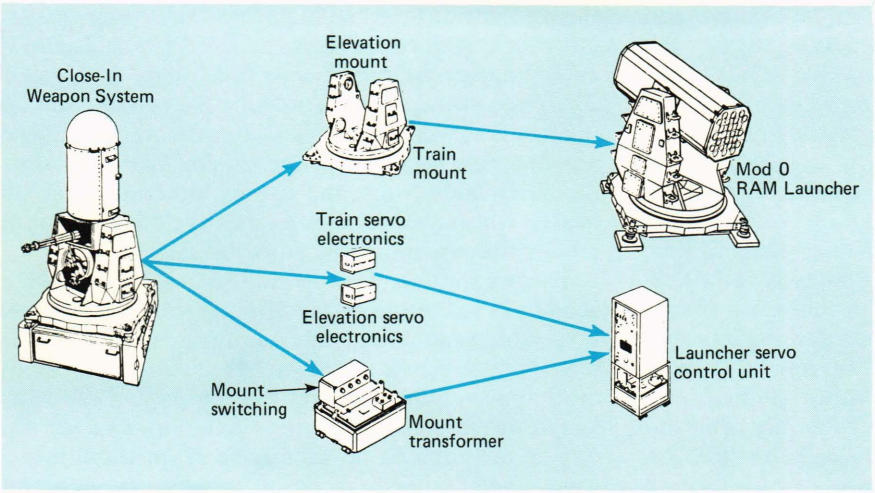

Fig. 3—Conversion of the Close-In Weapon System gun mount to the RAM application. To achieve this conversion, the gun and radar are removed, an additional casting is added in the elevation trunnions to permit clearance for the missile guide assembly, and the launcher base is removed. Electronics for providing control of the launcher are housed in a separate equipment rack. A reinforced fiberglass missile guide assembly is added to the mount, missile-selection electronics are mounted on the bottom portion of the guide assembly, shielding is added to protect the mount from the missile blast effects, and the entire mount is shock-mounted to the deck.

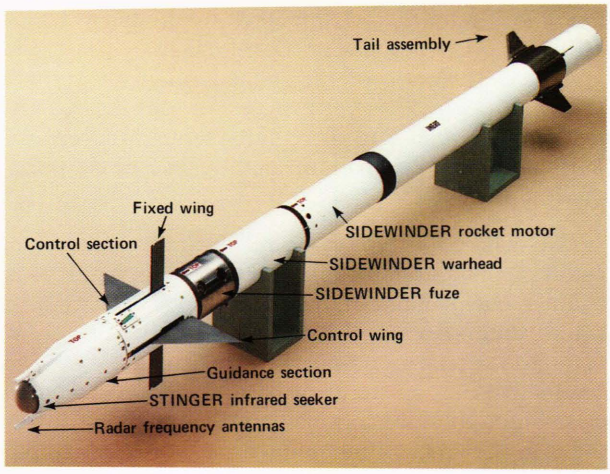

Fig. 4—RAM round. The RAM Missile is enclosed in a canis- ter that also serves as a launching tube. The guidance section consists of a radar frequency seeker and interferometer antennas along with a STINGER infrared frequency seeker. The control section consists of an electromechanical system that directs the movable wings. The ordnance section (optical fuze and warhead) as well as the rocket motor are variants of the SIDEWINDER Missile.

tion contains the SIDEWINDER DSU-15/AB active optical fuze and the SIDEWINDER WDU-17/B warhead.

The rocket motor is a variant of the SIDEWINDER Mk 36 motor. It contains a solid propellant and provides mounting lugs for the folding fixed tail fins. The tail surfaces are folded within the launch tubes and are spring-erected and locked when the missile has cleared the tube after launch. The tails are arranged in a cruciform pattern interdigitated with the wings. To control missile roll rate during the flight, the tail surfaces are slightly canted with respect to the missile axis.

MAJOR TECHNICAL DEVELOPMENTS

The RAM Program is in full-scale engineering development. At this time, much of the early development work has been accomplished. APL contributed heavily to the development of the missile guidance system, the most notable work being that associated with the design of the radar frequency guidance subsystem. Other Laboratory contributions to the missile guidance system were in missile body motion decoupling implementation and in infrared target acquisition. APL also supplied missile guidance hardware for advanced development flight testing.

The development of a high-performance, acceleration-feedback autopilot in a rolling airframe with a single-plane guidance system has been largely the product of General Dynamics. This work is an outgrowth of earlier rolling single-plane control missiles (including the STINGER) now in production and the operational REDEYE. Other major accomplishments have occurred in the areas of aerodynamics, autopilot design, and sensor development. Throughout this development, General Dynamics has conducted the overall missile design, fabrication, and testing activities.

The RAM Weapon System requires a means of rapidly correlating target reports from the search radar and the electronic warfare support measures equipment. The conceptual computer algorithms for this have been developed and tested by APL and Hughes Aircraft Co. The APL work was the outgrowth of other efforts associated with automatic integration of target reports from several search radar sensors.

Although a discussion of all these efforts is not included here, descriptions of the guidance system concept development, the radar frequency seeker design, and the radar and electronic warfare support measures correlation algorithm development are provided below.

Development of the Dual-Mode Guidance Concept

From 1966 to 1973, APL collaborated with General Dynamics/Pomona Division in the investigation of possible applications of these guidance concepts in various missile airframes. During that

period, system analyses as well as laboratory and missile flight tests were conducted to develop the dual-mode guidance system required for RAM.

In 1974, work was initiated to develop a 5-inch-diameter rolling airframe missile to provide Navy ships with an improved self-defense capability against antiship missiles that use active radar guidance. Early in the program validation phase, dual-mode flight tests were successfully completed at White Sands Missile Range against target drones using an early radar frequency receiver design. During the validation phase, the missile configuration used an aerodynamically stable airframe in conjunction with a pitch rate feedback control system. The simulation studies indicated a need for additional maneuverability over that available from the validation missile hardware. An acceleration feedback autopilot was then added to ensure that the tactical missile would have the desired maneuverability.

Radar Guidance Design

As a prelude to final radar system design, a four-month radar study program was performed, which was completed in October 1976. The radar study program addressed the following areas: definition of the operational environment, definition of radar guidance candidate systems, and formulation of a detailed list of radar design questions to be addressed prior to actual hardware design.

In March 1977, a design effort was begun at APL that culminated in the fabrication of a radar guidance system for laboratory testing. System analysis and critical hardware experiments were completed prior to the selection of a candidate system for the detailed hardware design. During the radar guidance development at APL, a parallel design effort was being pursued by General Dynamics. Technical information was exchanged between the two design teams via written reports and design reviews. The resulting candidate system was one of four candidate systems defined in the 1976 study program.

In RAM Missiles, guidance information is derived from a single pair of interferometer antennas mounted on the rolling airframe. The interferometer measures radar frequency phase interference. Rolling both the infrared seeker and the radar frequency seeker along with the control system provides the advantage that only a single plane of guidance and control is required, greatly reducing the quantity of hardware involved in the guidance and control of the missile. The basic guidance information is sinusoidal, with a frequency equal to the missile roll rate. This is, in effect, a scan-on-receive angle tracking system, with the effective scan rate equal to the roll rate.

One of the benefits gained from intentionally rolling the radar interferometer antennas is that the classical angle ambiguity problem is solved. Antenna spacing and radar wavelength cause many electrical degrees of phase to be produced (i.e., more than 180 electrical degrees, which is the maximum field of view) for the geometric angle being measured. Under these conditions the actual direction to the target cannot be ascertained. Rolling the interferometer allows an unambiguous phase detection to be performed. The error voltage that represents the space angle between the target line of sight and the interferometer antenna pair becomes a sinusoidal signal. This alternating signal permits the use of integration (at the missile roll frequency) to obtain the desired pointing error voltage without any ambiguities.

The decoupling of body motion in RAM Missiles is accomplished at microwave frequencies by means of a variable time delay path (digital line stretcher) inserted in one of the microwave frequency lines. Body motion decoupling requires the component of the interferometer signal due to pitch and yaw of the missile airframe to be subtracted from the total interferometer signal in order to generate a signal related only to target motion. The delay inserted in the line stretcher is controlled by a gyro, which measures pitch and yaw of the missile body.

A block diagram of the radar guidance system is shown in Fig. 5. For purposes of discussion, the system is divided into three subsystems: microwave, automatic gain control and gating, and angle information processor.

Microwave Subsystem—The microwave subsystem receives the radar signals, provides discrimination against out-of-band signals by means of high-pass filters, and processes the radar frequency in a pair of orthogonal phase comparators to provide sine and cosine of phase angle information at video frequencies. Since the interferometer provides phase information, the target tracking information is not amplitude dependent. Furthermore, the rolling interferometer provides alternating voltage information (the phase information is basically sinusoidal, with a frequency equal to the missile roll rate). Hence, there is

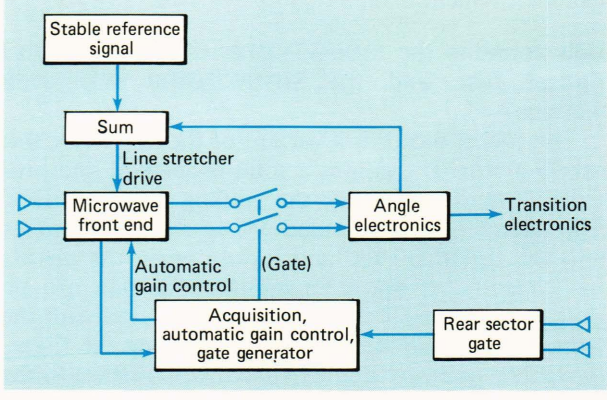

Fig. 5—The RAM radar frequency guidance system processes radar frequency signals from the interferometer antennas to derive seeker pointing and missile steering information. Automatic gain control is used to prevent saturation of the radar receiver. To prevent signals from one's own ship from interfering with guidance, gate electronics generate an inhibit pulse if the signals from the rear antenna exceed those from the forward antenna.

no fundamental requirement for direct-coupled information processing with its attendant bias problems. Since the line stretcher allows the angle information processor to be operated as a closed-loop system, wider tolerances can be allowed in the specifications for the angle-processor operation than would otherwise be possible.

Automatic Gain Control and Gating Subsystem—Because target tracking information is contained in the phase relationships of the incoming signals as opposed to the amplitude, there is no requirement for fast, tight gain control. However, an automatic gain control circuit is required to prevent limiting in the receiver. Two electronically variable attenuators provide automatic gain control at microwave frequencies. Front- and rear-sector signal amplitude information at video frequencies is provided to the automatic gain control circuit. The gating portion of this subsystem makes a pulse-by-pulse decision as to whether the pulse should be gated into the system by generating an inhibit pulse if the radar signal out of the rearward-looking antenna exceeds that out of the forward-looking antenna.

Angle Information Processor Subsystem—This portion of the system takes the in-phase and quadrature video (which represents periodic sampling of the sine and cosine of the sinusoidal radar frequency phase difference) and provides an output that is a sinusoidal voltage proportional to a filtered version of the sinusoidal phase.

The radar guidance system has undergone extensive testing at the subsystem and system levels. A missile digital simulation was designed and implemented at both General Dynamics and APL to support the testing phase. The microwave electronics tests and supporting analysis have indicated that the design is acceptable in terms of overall system performance across the specified radar frequency range (I and J bands). The experimental performance of the automatic gain control and gating subsystems agreed with that expected on the basis of analysis and also verified the analytical models of the various subsystems used in the system analysis.

Development of Radar and Electronic Warfare Support Measures Correlation Algorithm

The need for unambiguous and timely data from radars and passive sensors to support the RAM Weapon System has led to the development of sophisticated signal processing algorithms by APL and Hughes Aircraft. An automatic detection and tracking capability produces much more reliable and timely target data than human operators in complex antiair warfare situations. With these data, the radar and electronic warfare support measures (ESM) correlation algorithms can rapidly sort out radiating versus nonradiating threats. Without these developments, the RAM System's effectiveness would be significantly reduced in multiple target engagements because human operators would become saturated with data and the need for decisions.

The correlation algorithm uses track file data (i.e., digital target information stored in computer memory) from both the radar and electronic warfare support measures systems to find and correlate radar and passive system track pairs that are likely to correspond to the same threat. The algorithm output is a list of correlated radar and passive system track pairs, radar tracks not correlated with a passive system track (radar-only tracks), and passive system tracks not correlated with a radar track (electronic warfare support measures (ESM) equipment-only tracks). Radar-only tracks result when a target is not radiating or when the target's radiation is not detectable. ESM equipment-only tracks typically result when the threat is beyond the maximum radar detection range. The following paragraphs describe the general method used to make the correlation decision.

The radar track file parameters are compared with the ESM equipment track file parameters to find the radar and other track pairs that should be correlated. Some examples of the track file parameters used to make the correlation decisions are shown below.

Radar

Target position	—	Obtained by measuring target bearing and target range. On some radars, target elevation can also be measured.
Target rate	—	Determined by differentiating sequential samples of target position data.
Update time	—	Time of last target report.
Target category	—	Targets are categorized as air or surface, based on target rate and detection range.
Target identification	—	Targets are identified as friend, foe, or unknown, based on (identification, friend or foe) equipment reports.
Track type	—	Indicates whether the target track is firm or tentative, based on the consistency of the target reports.

Electronic Warfare Support Measures System

Track bearing	—	Determined by the direction-finding capability of the receiver.
Update time	—	Time of last target report.
Target category	—	Targets are categorized as air or surface, based on the signal received.

Target identification — Targets are categorized as friend, foe, or unknown, based on the signal received.

Emitter frequency data — Emitter frequency information is obtained and stored.

These parameters are used in a two-step decision process. In the first step, radar and other system track pairs are subjected to a series of gate tests. These tests eliminate grossly mismatched pairs from further correlation processing by comparing parameters, such as bearing separation, to a threshold. Those track pairs that pass all the gate tests are then evaluated in the second step of the decision process.

The second step of the process combines several selected correlation likelihood estimates into a single number that is a measure of the overall likelihood of correlation for each track pair. This value is used to help select the best track pairings in high density situations. A two-hypothesis test of the log likelihood ratio is used to obtain these correlation likelihood estimates. The general form of the correlation likelihood estimate is the logarithm of a probability ratio:

$$LL(D_R,D_E) = \log_a \frac{P[D_R,D_E/H_o]}{P[D_R,D_E/H_i]}$$

where:

$LL(D_R,D_E)$ = log likelihood ratio of the parameters D_R and D_E,

D_R = observed parameter for the radar track,

D_E = observed parameter for the ESM system track,

$P(x/y)$ = conditional probability of observing x given that hypothesis y is true,

H_o = hypothesis that the radar and other system tracks correspond to the same target, and

H_i = hypothesis that the radar and other system tracks correspond to different targets.

The specific form of the correlation estimate will depend on the parameter used in the estimate. Observed parameter values are used either to compute a correlation likelihood or to index a correlation likelihood reference table containing values that were estimated *a priori*.

For example, the radar and the ESM receiver report target identification as either friend, hostile, or unknown. Conditional probabilities for each possible identification combination, i.e., RADAR-FRIEND, ESM-FRIEND/RADAR-HOSTILE, ESM-FRIEND, etc., are estimated *a priori* for the hypothesis that the target reports originate from the same target. Similarly, conditional probabilities are computed for all combinations for the hypothesis that the target reports originate from different targets. The logarithm of the ratio of the conditional probability under the first hypothesis to the conditional probability under the second hypothesis is computed for each identification combination to obtain the correlation likelihood for that combination. All these values are entered in the table and used for the track pair correlation estimate according to the identification categories produced by the radar and the ESM receiver. In a similar manner, other parameters are used to estimate other likelihood values. A number of likelihood functions are summed to obtain the overall likelihood of correlation.

Much effort has been involved in selecting an overall strategy, developing algorithms, determining the statistical models of the parameters and weighting functions, and programming the algorithm in an efficient manner. Limited flight testing involving radiating targets has been successfully conducted and this has led to refinements to the algorithms. Additional testing will be conducted during the remainder of full-scale engineering development.

REFERENCE

[1] R. T. Pretty, ed., *Jane's Weapon Systems, 1979-1980*, Tenth Edition, Franklin Watts, Inc., New York.

ACKNOWLEDGMENTS—Major contributors to the development and design of the radar frequency guidance system at APL are J. F. Gulick, D. R. Marlow, and P. H. Gilbert. Major contributors to the development of the radar and ESM system correlation algorithm at APL are W. G. Bath, W. W. Keys, J. W. Thomas, and R. W. Proue.

MARION E. OLIVER and WILLIAM N. SWEET

STANDARD MISSILE: THE COMMON DENOMINATOR

STANDARD Missile has evolved from the wing-controlled beam rider of 30 years ago into the free world's most advanced operational homing missile. Its design is based upon the proven airframe of its TERRIER and TARTAR surface-to-air missile predecessors. STANDARD Missile has followed the concepts of modular design and commonality throughout its history.

INTRODUCTION

STANDARD Missile is a surface-to-air ship-launched missile for defense against attacking aircraft and antiship missiles (Fig. 1). It is presently deployed, in its various configurations, on over 70 frigates, destroyers, and cruisers of the U.S. Navy. More than 80 new ships, planned and being built, and including the new AEGIS ships, will also use STANDARD Missile. STANDARD Missile is currently operational in 28 ships of eight allied navies; this foreign force is planned to increase to 35 ships by the mid-1980's.

STANDARD Missile is a supersonic, solid-rocket-propelled, tail-controlled missile with all-electric guidance and control equipment. It is modular, permitting maximum commonality among its various configurations. There are extended- and medium-range versions and an inertial midcourse guidance feature that distinguishes the STANDARD Missile-2 from the STANDARD Missile-1. Common guidance receivers, warheads, autopilots, and control sections are found in all versions.

The ability to successfully evolve a missile design to double and redouble its performance through the years and adapt it to a variety of tactical applications is based upon several basic design principles and disciplines. The compact tail control aerodynamic configuration not only provides high performance but can readily accommodate a widely varying flight regime and changes in component sizes and weights. Adherence to the discipline of sectionalized design, with interchangeable components having a high degree of commonality among the several versions of the missiles, provides great flexibility at minimum cost. Finally, strict conformance to the standard physical dimensions of diameter and maximum length is a basic principle.

In reality, STANDARD Missile is a family of missiles rather than a single configuration. The "family history" of this missile is a success story that forms the theme of this article.

Figure 1 — STANDARD Missile-2 launch from USS MAHAN. A STANDARD Missile firing, whether from a land test site or a ship, is an impressive and unforgettable experience. If it were not for the rocket smoke trail, the eye could not follow the path of the missile as it flies under precision control to a target many miles away. The complex, interactive systems required for a STANDARD Missile firing rival the most sophisticated mechanisms developed by man.

HISTORY OF THE STANDARD MISSILE

In 1949, a supersonic test vehicle using a solid fuel rocket was used to test and evaluate the guidance and control system for the TALOS Guided Missile (Fig. 2). A version of that test vehicle performed so well that it was developed into the operational TERRIER Missile.

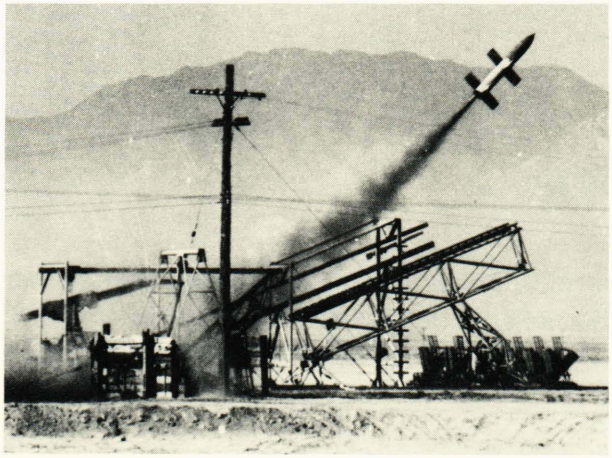

Figure 2 — Early subsonic test vehicle used in the development of TALOS guidance and control systems. This solid fuel rocket, developed in 1949, is shown being launched at Inyokern, Calif.

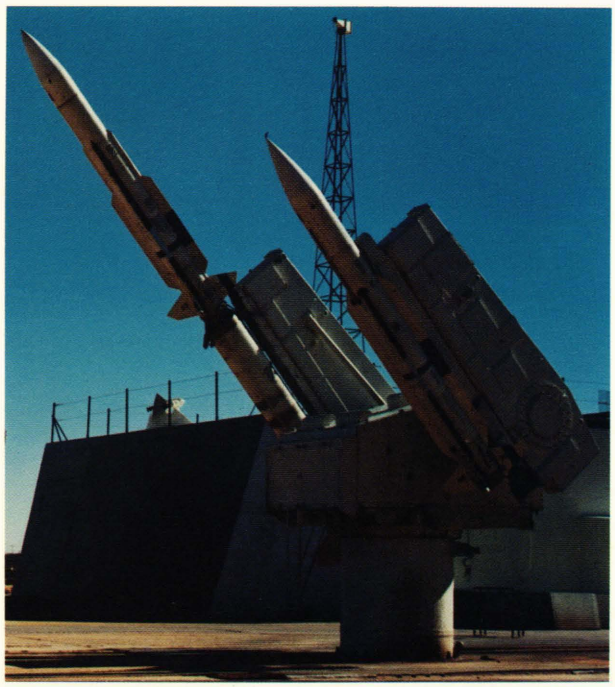

Figure 3 — TERRIER and TARTAR Missiles on launcher at White Sands Missile Range. The extended-range TERRIER Missile has a separate booster.

The first significant improvement to the TERRIER Missile was the change in the control system from wing control to tail control. This was prompted by the need for better maneuverability to counter evasive maneuvers on the part of the attacker. The second major improvement was the change from a beamrider guidance system to semiactive homing. The third major change, concurrent with the second, was the development of an integral dual-thrust rocket motor (a single rocket that provides a high thrust for boost followed by a much lower thrust for the sustain phase). This version became the TARTAR Missile (Fig. 3).

In the early 1960's, the technological advances of solid-state electronics had matured sufficiently to justify the redesign of both the TERRIER and the TARTAR Missiles to improve their reliability and manufacture. The TERRIER Missile became STANDARD Missile, Extended Range [SM-1(ER)]and the TARTAR Missile became STANDARD Missile, Medium Range [SM-1(MR)]. With the use of modular construction, performance improvements by block changes (a collection of related design changes introduced during production) were possible and have led to a progressive family of STANDARD Missiles. SM-1(ER) is a two-stage configuration having a single thrust booster that separates from the missile a few seconds after launch. The rocket sustainer then ignites and provides thrust until burnout. The missile coasts for the remainder of flight. SM-1(MR) employs a dual-thrust, solid rocket developed earlier for the TARTAR Missile. This type of rocket permits both the boost and sustain phases to be implemented in a single rocket.

In the 1960's, the air threats to Naval forces began undergoing a transition from aircraft to antiship missiles. Such missile attacks may be coordinated with the use of various countermeasures and special tactics, making antiair defense more complex and stressful. At this point, the Advanced Surface Missile System Study Group, involving the Navy, industry, and APL, concluded that the nature of the projected threat dictated the need for a new weapon system combining high performance, quick reaction time, an inherent countermeasures capability, and high reliability. In 1969, the contract was awarded for the AEGIS Weapon System, which would utilize improved versions of STANDARD Missile.

As initially conceived, the ASMS (AEGIS) was to include a new missile with improved performance, including midcourse command and semiactive terminal guidance. During the deliberations of Technical Planning Group II, it was perceived that, with certain modifications, STANDARD Missile might be upgraded to provide the new capability, and the study report so indicated. In late 1969, just prior to award of the contract, the new missile was deleted from the budget and a modified version of STANDARD Missile was substituted. This version incorporated a new inertial guidance system and missile/radar data link and was designated STANDARD Missile 2, Medium Range [SM-2(MR)].

These modifications substantially improve the performance of the missile in range, altitude and terminal homing accuracy and also provide a capability for simultaneous control of multiple missiles in flight.

In the early 1970's, subsequent to award of the AEGIS contract, the Navy, with APL as technical lead, sponsored a new study group to determine how these new capabilities might be used to enhance the performance of the TERRIER/TARTAR combat systems. This group soon evolved a concept incorporating those advantages that could be used with both sys-

tems. The TARTAR concept used the medium-range missile designed for AEGIS, with minimal changes. The TERRIER system, incorporating the previously developed booster, was officially designated STANDARD Missile 2, Extended Range [SM-2(ER)].

In 1975, projections showed that the threat would become increasingly severe in terms of speed, maneuverability, and countermeasures. A study performed by APL concluded that once again the threat could be countered through evolutionary improvements to STANDARD Missile in propulsion, signal processing, and warhead technology.

The Surface Warfare Directorate of the Office of the Chief of Naval Operations chartered a study group in 1980 to assess current and projected threats and make recommendations for further upgrades in surface-to-air missile capability.

THE APL ROLE

In January 1945, the Laboratory was directed by the Navy Bureau of Ordnance in the following manner:

> "A comprehensive research and development program shall be undertaken, embracing all technical activities necessary to the development of one or more types of rocket-launched, jet-propelled, guided, and anti-aircraft missiles. . . .This program shall include pertinent basic research, investigations, and experiments, and the design, fabrication and testing of such missiles, their component parts, and supplementary equipment. . . ."

During the years following this initial assignment, APL has supported the Navy in antiaircraft missile development in keeping with these general guidelines established in the 1940's.

APL has made vital contributions to the development of U.S. Navy antiair warfare missiles since the mid-1940's. These contributions include threat assessments, performance requirements definitions, concept definitions and engineering, design monitoring, and performance tests and evaluations.

APL's participation in the development of STANDARD Missile has been as Technical Direction Agent and Technical Support Agent. In these assignments, APL has conducted assessments of design, development, and improvement programs. The Laboratory has coordinated and conducted test activities during the initial design stages, through production, and when in use by the Fleet.

THE COMMON DENOMINATOR

The operational use of any guided missile requires direct support from a combat system whether it be launched from land, sea, or air. In the surface Navy, many missile system design requirements are unique, not only because of the sea environment, but, more significantly, because the supporting systems are combatant ships with varied missions and tactical requirements. This means that missile weapon system designs are under severe constraints in terms of physical size, weight, and shipboard location. Additionally, the missile system must be totally consolidated within the ship command structure, which deals with all weapons aboard the ship. Because of this close weapon-to-ship integration requirement, it is technically and economically practical to upgrade the missile system's performance provided forethought in planning and special design concepts are incorporated.

Development of STANDARD Missile has followed these concepts throughout its history. There have been incremental missile upgrades based on long-term requirements, in which improvements are made by building solidly on existing resources and knowledge. Each module is designed with a tolerance to change so that missile upgrades have a minimum impact on other ship elements and support activities. In a word, STANDARD Missile is based on commonality: commonality of critical components within the missile from one generation to the next; commonality among versions fired from TERRIER, TARTAR, and AEGIS ships; commonality of interfaces with supporting launchers and radars; and commonality in engineering expertise, technical data base, and logistic support.

Because STANDARD Missile subsystems (radome, guidance electronics, warhead, autopilot, etc.) are common to versions for TERRIER, TARTAR, and AEGIS ships, there is essentially only one production line. In some instances, major components are identical; in others, only subcomponents differ. Because of this commonality, production acceptance testing is simplified. The handling and transporting equipment within factories, and the shipping and transporting containers as well, can also be common in order to simplify the whole logistics chain from the production line to a shipboard supply of combat ready missiles (Fig. 4). Two design features of STANDARD Missile predominate in permitting an efficient logistics chain: a diameter of 13.5 inches, which has remained constant for over 30 years, and a uniform approach to sectionalization whereby major pieces of the missile are physically separable into major subsections that are functionally unique (Fig. 5).

A missile's capabilities must keep pace with the threat. Often this mandate requires significant modification at the component level, e.g., guidance electronic upgrades demanded by the changing electronic countermeasures environment. To minimize the development time and cost of production change, STANDARD Missile is typically upgraded by a block change program. In this process, specific design changes are made only for those subsections affected by the operational need. Unaffected performance specifications, production drawings, and subcontract elements can therefore be retained. Economic savings are therefore obtained at all levels of development.

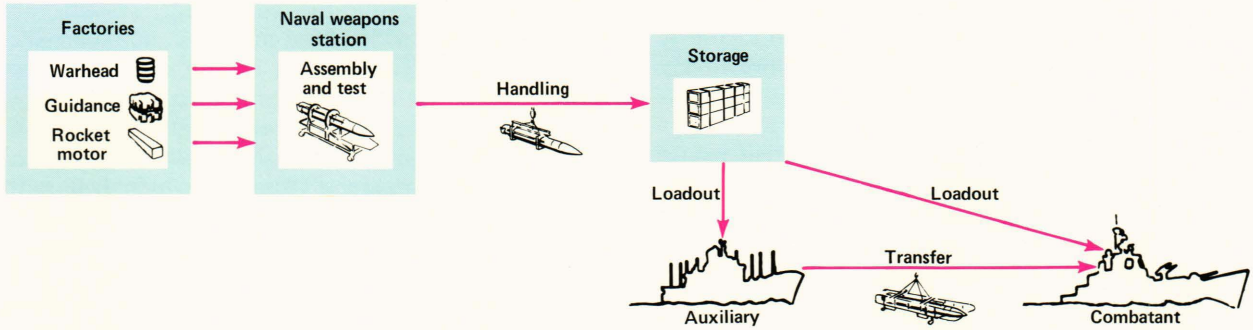

Figure 4 — STANDARD Missile logistics chain. The common characteristics of STANDARD Missile versions allow an efficient logistic chain from factory to ship.

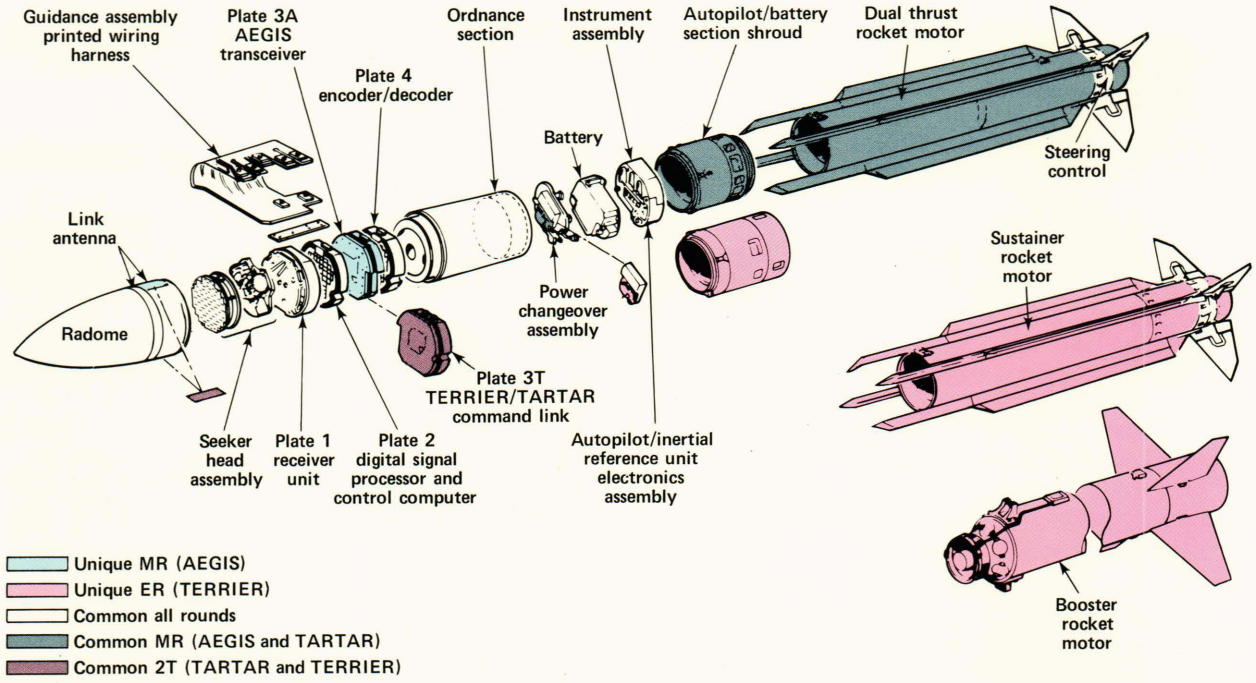

Figure 5 — STANDARD Missile's modular construction permits maximum commonality between missile configurations and allows improvements to be made efficiently.

Today, all STANDARD Missiles are fired from rail launchers that move in azimuth and elevation to provide the desired launch direction (Fig. 6). Because of the demanding mechanical operation of these launchers, missile designers must observe a number of constraints such as launch attachment devices. Additionally, a number of launcher-to-missile connectors are required to prepare the missile properly for launch and conduct the actual firing. With launchers within a major ship class having common loading, holding, and firing mechanisms, the corresponding connecting points on the missile can be standardized. Because this logistics principle is observed in STANDARD Missile and its corresponding ship weapon systems, it is possible, for example, to fire SM-1(MR) from a variety of ship classes. Obvious benefits are reduced ship installation costs as well as increased flexibility in resupplying ammunition.

The team associated with Naval antiair missile development for over 30 years includes a large industrial base headed by General Dynamics/Pomona, the prime contractor; Navy laboratories and support agencies; and APL. In spite of the normal attrition and migration of technical and management personnel from the program, there has remained a surprisingly large cadre of technical experts within these organizations. These people represent a very strong base of corporate knowledge and are, indeed, a real part of the common denominator.

LOOKING AHEAD

As hostile forces utilize new technology to improve their ability to attack our surface Navy, we must continue to upgrade our weapon systems to keep pace. As a particular threat vehicle appears with increased

Courtesy General Dynamics/Pomona

Figure 6 — STANDARD Missile is fired from dual rail launchers. The Mk 10 launcher fires the extended-range version from TERRIER ships while the Mk 26 launcher fires the medium-range version from TARTAR and AEGIS ships. Missiles are loaded horizontally onto the Mk 10 launcher and vertically onto the Mk 26 launcher.

speed and operating altitude, for example, a countering increase in missile rocket impulse is generally required. Fortunately for the missile designer, a new vertical launcher is currently being developed that will permit major increases in rocket impulse. The Vertical Launching System is planned for installation in new ship construction. Unlike current launching systems, the Vertical Launching System is fixed and will be installed below decks. Storing and firing of missiles will be in a vertical position (Fig. 7). Because of this arrangement, the overall length and diameter of STANDARD Missile can be increased if necessary. The aerodynamic shape and the size of the dorsals and steering tails also can be modified. This new flexibility in design will provide a new dimension in the growth potential for surface-to-air missiles for decades to come.

For immediate application, the next major upgrade in STANDARD Missile will make use of the additional length in the Vertical Launching System to provide a substantial increase in total rocket impulse. This upgrade will be only one of many improvements

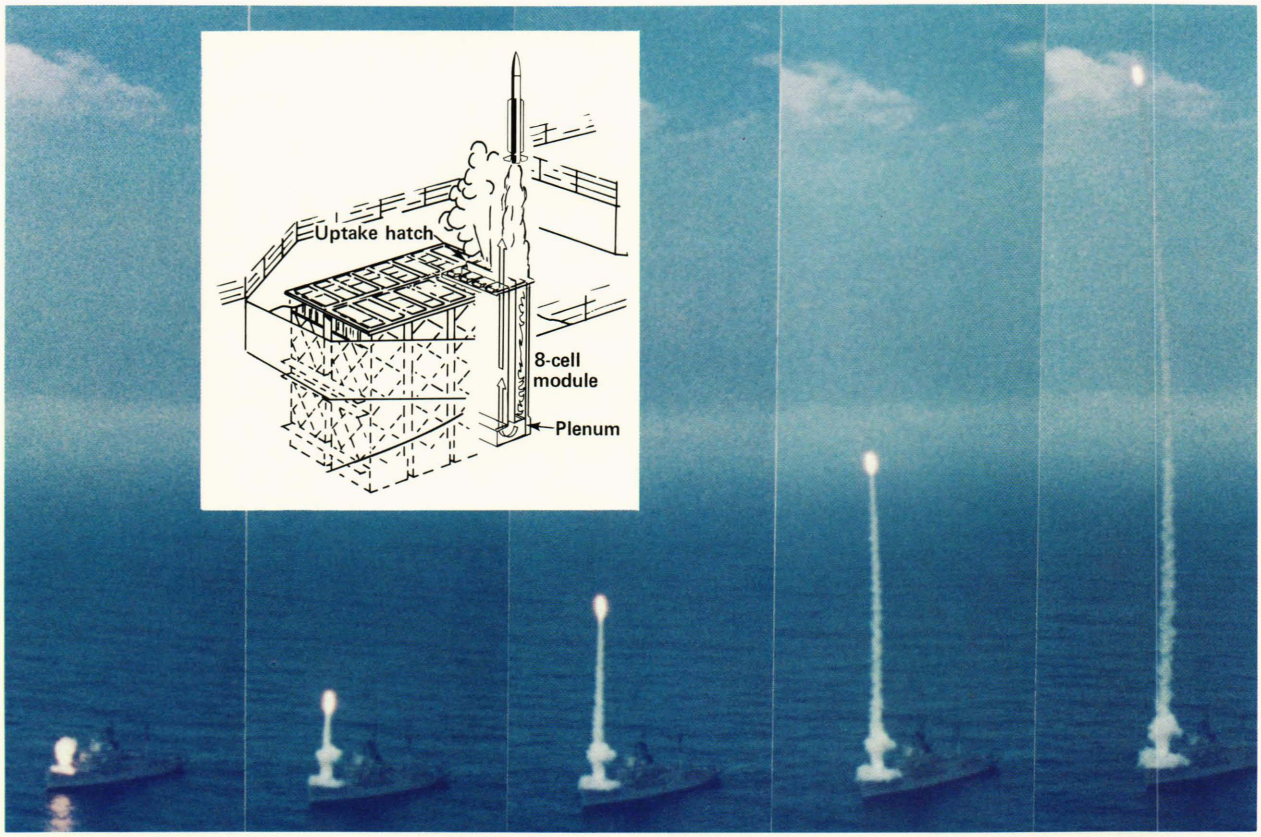

Figure 7 — STANDARD Missile test firing from the Vertical Launching System in USS NORTON SOUND. The flush deck vertical launch concept will eliminate the above-deck rail launcher and permit modifications in missile length and diameter.

planned for meeting the challenges of the next decade. Other improvements will include an enhanced guidance and control capability.

SUMMARY

STANDARD Missile has evolved from the wing-controlled beamrider of 30 years ago to the free world's most advanced operational tail-controlled homing missile. Its design is based upon the proven airframe of its TERRIER and TARTAR surface-to-air-missile predecessors. Today's STANDARD Missile uses solid-state devices throughout, reducing warm-up time and eliminating the need for shipboard checkout. Continued advancements in performance, introduced in a series of evolutionary block changes, will keep the STANDARD Missile family ready to meet threats to the United States Fleet.

ROBERT W. WITTE and ROBERT L. MC DONALD

STANDARD MISSILE: GUIDANCE SYSTEM DEVELOPMENT

To achieve a missile capability that is commensurate with the long-range, high data-rate, target-detection characteristics of the AN/SPY-1A radar, an evolutionary upgrade of the existing STANDARD Missile-1 was authorized. Designated STANDARD Missile-2, it adds a command midcourse flight phase, thereby providing the AEGIS Combat System with increased intercept range and higher firepower. STANDARD Missile-2 with inertial midcourse guidance also provides upgraded TERRIER and TARTAR Combat Systems with a corresponding increase in capability. Terminal guidance accuracy has also been improved by incorporating a new homing receiver common to all STANDARD Missile-2 variants.

INTRODUCTION

The development of STANDARD Missile-2 (SM-2) began in the early 1970's, with General Dynamics/Pomona as the Design Agent and APL as Technical Advisor. At the time, STANDARD Missile-1 (SM-1) was in production as the primary weapon for Fleet air defense by TERRIER and TARTAR ships. The principal modification to SM-1 envisioned at the outset was to add a midcourse guidance system consisting of communication links, a digital guidance computer, and an inertial reference unit. These additions were incorporated as shown in Fig. 1. For terminal guidance, the original plan had been to use the existing SM-1 scanning receiver. However, shortly after becoming the Naval Sea Systems Command AEGIS Project Manager in 1972, Rear Admiral W. E. Meyer made the decision to include a new monopulse terminal homing receiver. Thus, the final SM-2 configuration consisted of a largely new guidance section, a repackaged autopilot to accommodate the inertial reference unit, and the existing SM-1 ordnance, propulsion, and steering control systems.

To accelerate the development of the new homing receiver, General Dynamics/Pomona and APL engineers embarked on an intensive cooperative effort. The design evolved over a two-year period, during which frequent meetings were held to review every aspect of the signal processing and logic. During that time, the communication links had progressed to the point where hardware interface tests were being conducted to demonstrate ship system compatibility. Prior to the beginning of flight testing at White Sands Missile Range in 1975, a guidance section design model was supplied to APL for an assessment of its performance. Hundreds of hours of tests were conducted in the Guidance System Evaluation Laboratory. As that evaluation proceeded, SM-2 began to acquire a reputation as a highly accurate missile. The results obtained in the APL tests were confirmed in subsequent flight tests of SM-2 and an upgraded SM-1 that also uses the new homing receiver. To date, both missiles have achieved a sizable percentage of direct hits in intercepting target drones.

The development and deployment of SM-2 cannot realistically be a stopping point in providing the future Navy with an effective antiair warfare capability. Because the threat has continued to increase, the initial SM-2, now designated Block I, is being improved. Currently, Block II is in engineering development, with APL technical support being provided in many areas, including guidance.

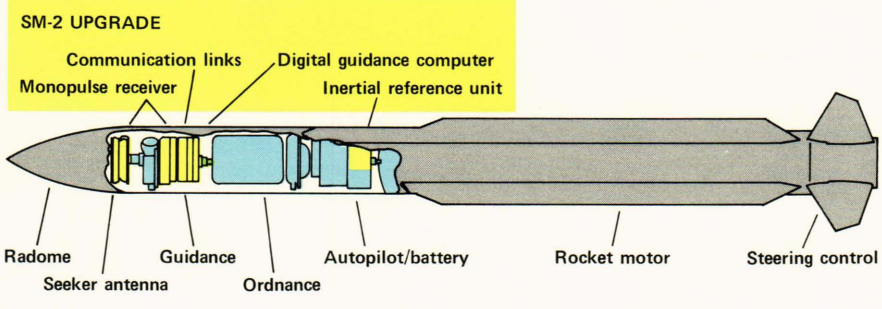

Figure 1 — STANDARD Missile-1 (SM-1) showing STANDARD Missile-2 (SM-2) additions. Evolutionary improvements to STANDARD Missile have been facilitated by the use of modular packaging. The SM-2 upgrade consisted of a new guidance section and additions to the autopilot/battery section, while other sections remained essentially unchanged.

MISSILE GUIDANCE TECHNIQUES

Semiactive Guidance

A feature common to both SM-1 and SM-2 is an ability to "home," i.e., to guide either some or all of the flight by means of target-reflected energy. The source of this energy is a high power, continuous wave, shipboard radar illuminator. A portion of the illuminator signal is received directly by the missile for use as a Doppler frequency reference. To accomplish this, the illuminator antenna combines a narrow beam directed toward the target with a broad reference beam that encompasses the missile throughout flight (Fig. 2). This type of guidance is called "semiactive" because the transmitter and receiver, although linked, are not colocated.

A semiactive missile must also be able to home passively on electronic countermeasures signals radiated by the target. Such signals may be used to screen the target-reflected signal or otherwise deceive the semiactive receiver. Home-on-jam processing is automatically selected when the target skin return cannot be identified and when incoherent energy is present whose frequency and angle of arrival are approximately correct.

Home-All-the-Way Guidance

A home-all-the-way guidance policy is one in which the missile derives its own steering commands throughout flight based on the processing of signals received from the target. Such a policy requires that the target be acquired either prior to or shortly after launch. Figure 3 illustrates the various phases in the firing of an SM-1, which uses home-all-the-way guidance. On the launcher, the missile is provided with a post-launch prediction of where it should look for the target in angle and Doppler frequency. Following an unguided boost phase, the missile seeker acquires either target-reflected energy from shipboard illumination or jamming energy emanating from the target. The seeker consists of a gimballed antenna and a radar receiver that measures the angle of arrival of the received signal (Fig. 2). The seeker tracks the target and provides information to the missile guidance computer concerning the line-of-sight angle and the closing velocity as determined from the Doppler frequency. Using a proportional navigation steering law, discussed below, the guidance computer generates steering commands that ideally keep the missile on a collision course with the target.

Semiactive, home-all-the-way guidance is used in many missile systems throughout the world. Its primary advantage is that it provides moderately good area defense coverage, i.e., intercept range, by virtue of high power ship-based or ground-based illumination combined with up-and-over flight trajectories. (Such trajectories are achieved by launching the missile at a relatively steep angle and allowing it to climb above the target early in flight so as to better maintain available kinematic energy.) One of the major limitations of home-all-the-way guidance is its relatively low firepower, since one of only a few illuminators must be committed to a single target for the entire missile flight. A second limitation is illustrated in Fig. 4, which shows the many signals that may be present at the missile's receiving antenna. Clearly, a missile receiver that must pick out the target signal immediately after launch has a much more difficult task than it would if acquisition could be delayed until later in flight.

Midcourse Plus Terminal Guidance

Midcourse guidance implies an intermediate flight phase in which an external source supplies sufficient information to allow the missile to guide or steer toward the target without having to home. Two types

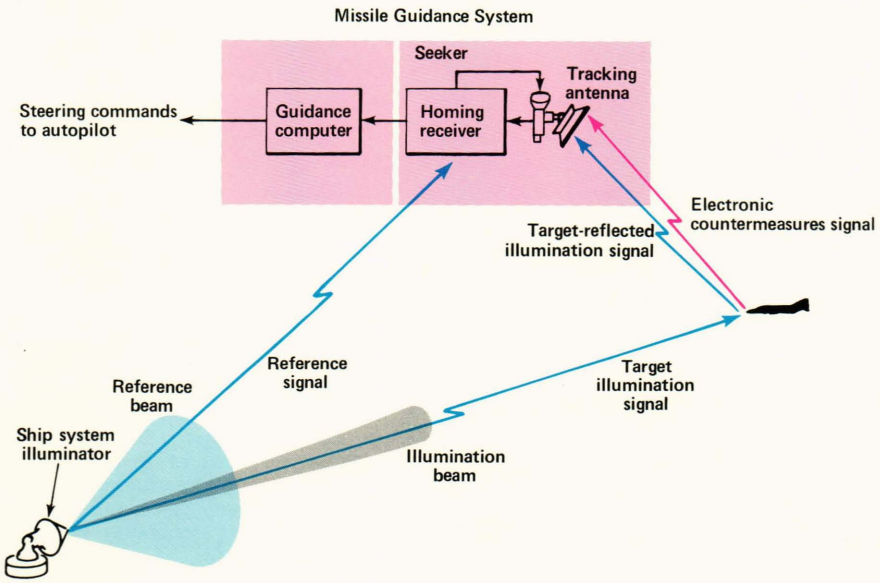

Figure 2 — Semiactive guidance concept. Both SM-1 and SM-2 employ continuous wave, semiactive guidance. The target is illuminated by highly pure, sinusoidal RF energy that allows objects to be distinguished on the basis of their velocity by the Doppler shift of the reflected energy. Homing is semiactive in the sense that the transmitter, in this case a high power shipborne radar, and the missile receiver are linked but not colocated. A passive homing capability is also provided to cope with possible jamming by the target. The combination of the onboard homing receiver and the steerable front antenna is known as a "seeker." In addition to target tracking, the seeker supplies information to the guidance computer for computing missile steering commands.

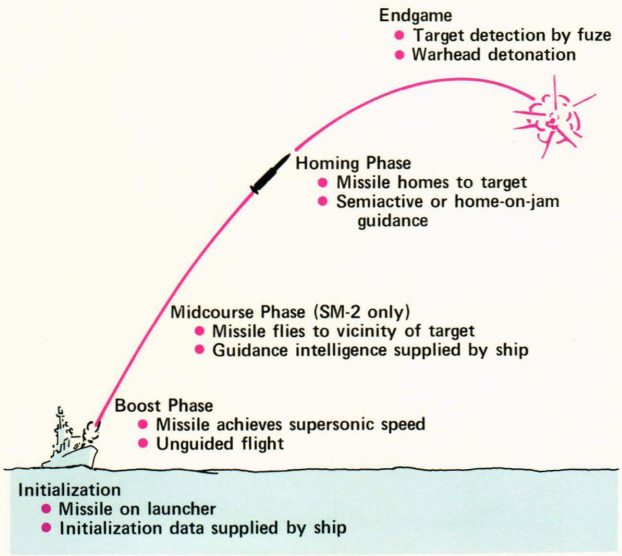

Figure 3 — STANDARD Missile operational sequence. On the launcher, the SM-1 is supplied with target acquisition data and begins homing shortly after the unguided boost phase of flight. The SM-2, however, undergoes a midcourse phase under ship control; at a predetermined point much later in flight, target acquisition occurs and homing begins. In the endgame phase, the target is detected by a missile-borne proximity fuze and the warhead is detonated close to the target.

of midcourse guidance are commonly used — command and inertial. In a command system, missile steering signals are directly supplied in an agreed-upon coordinate frame. In an inertial system, the missile guides toward a point or a succession of points in inertial space based on externally supplied information.

The use of midcourse guidance followed by a relatively short period of terminal homing offers a significant improvement in firepower and missile intercept coverage if the ship system can provide the necessary support. Firepower is clearly increased over home-all-the-way guidance because semiactive homing is restricted to the terminal portion of flight. Thus, the shipboard illuminators can be used more efficiently to engage a larger number of targets. If the missile has the kinematic capability and if the midcourse trajectory control is sufficiently accurate, then a small target can be engaged at a longer range than would be possible if seeker acquisition were required early in flight, as in the home-all-the-way case.

The shorter missile-to-target propagation distance at the start of the terminal homing phase also tends to enhance the target return relative to some of the sources of interference shown in Fig. 4. In particular, the missile has a much better chance of "seeing" the target in the presence of standoff jamming following a period of midcourse guidance than it would immediately after launch.

STANDARD MISSILE-2 MIDCOURSE GUIDANCE

Midcourse guidance has been implemented in SM-2 by adding to SM-1 an inertial reference unit together with missile-ship communication links. The inertial reference unit consists of an instrument package coupled with a special-purpose computer. The instruments include three accelerometers, two rate-integrating gyros for measuring angular motion perpendicular to the missile body, and a space-stable, single-axis platform for monitoring missile roll. The computer solves the equations of motion to keep track of missile position, velocity, and attitude in the inertial coordinate frame established prior to launch.

AEGIS Command Midcourse Guidance

In the AEGIS Combat System, SM-2 is command-guided during midcourse flight under direct control of the ship (Fig. 5a). The AN/SPY-1A radar performs missile and target tracking and also serves as the shipboard data link transceiver. Steering commands are computed by the ship weapon-control computer and transmitted on the uplink to the missile, which acknowledges receipt via the downlink. The midcourse guidance law is a form of proportional navigation with appropriate trajectory-shaping modifications. The inertial reference unit is used primarily as an atti-

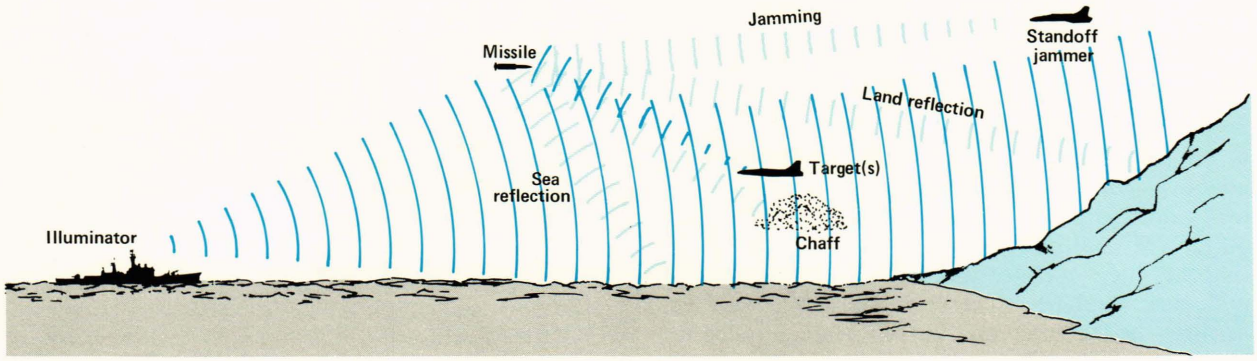

Figure 4 — Typical signals received by the missile in flight. Good steering information can usually be derived from either target-reflected energy or jamming energy from the target. Interfering signals, which can exceed the target skin return by many orders of magnitude, must be rejected. Interference derives from natural and man-made environments, both friendly and unfriendly.

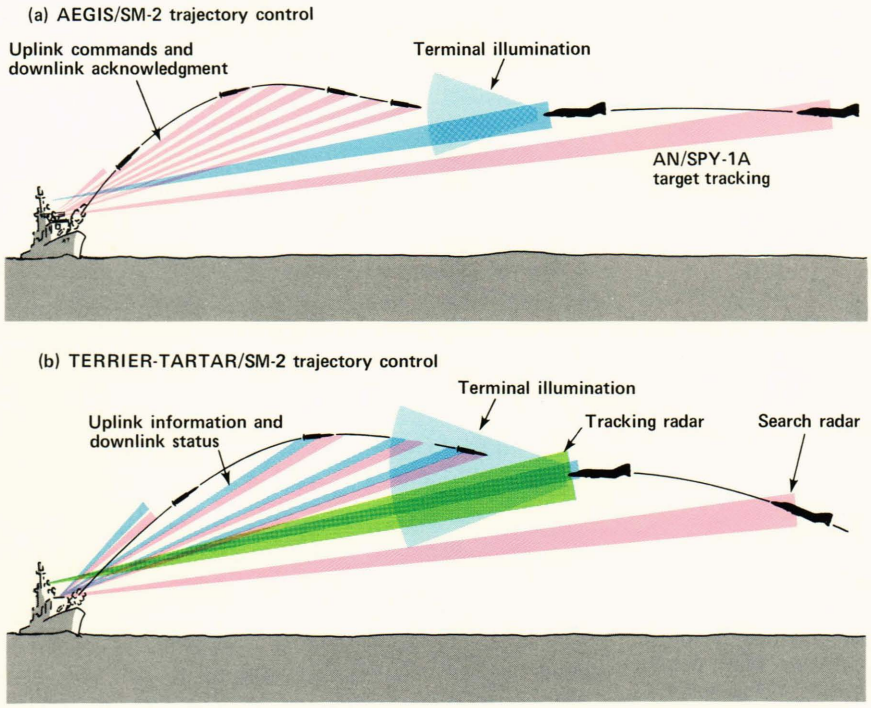

Figure 5 — SM-2 midcourse plus semiactive terminal guidance. In the AEGIS application (a), SM-2 is guided by the ship through the midcourse phase of flight. Uplink acceleration commands, which are acknowledged via the downlink, are converted into steering signals by the missile inertial reference unit. Terminal homing is commanded by uplink and can be delayed longer than in TERRIER or TARTAR because of greater midcourse accuracy.

In TERRIER and TARTAR Combat Systems (b), the SM-2 uses its inertial reference unit to guide itself to a point in space. New points are sent to the missile by the ship via uplink if course changes are required. Missile flight progress is monitored by means of downlink information. The missile switches to terminal homing at a predetermined time prior to intercept, subject to uplink revision.

tude reference system, transforming the uplink guidance commands in inertial coordinates to steering commands in missile body coordinates. At a predetermined time prior to intercept, the weapon system assigns an illuminator to the engagement to support the terminal phase. Shortly thereafter, the missile is told to search for the target based on updated seeker pointing and Doppler frequency information. The change from midcourse to terminal guidance, known as "handover," occurs following target acquisition by the missile seeker. The improvement in intercept capability relative to SM-1 is substantial in both downrange and crossrange because of the use of midcourse guidance.

TERRIER and TARTAR

Inertial Midcourse Guidance

In the TERRIER and TARTAR application, SM-2 uses inertial midcourse guidance for self-navigation, command guidance being impractical because these combat systems do not track the missile. Instead, using target data derived from a three-dimensional search radar, these ship systems direct the missile to a point in space, or to a succession of points in case the target changes course and/or speed (Fig. 5b). New guidance points, along with target position and velocity data, are communicated via the uplink as required. Missile information is downlinked, permitting the ship system to monitor flight progress. The midcourse guidance law is known as explicit guidance because the steering equations are explicit functions of the current and desired boundary conditions (position and velocity). The missile's knowledge of its own position and velocity is, of course, provided by the inertial reference unit.

As in AEGIS, at a predetermined time in the flight, the weapon system assigns an illuminator to support the terminal homing phase. Doppler frequency and angle information required for target acquisition by the missile seeker are computed from inertial reference unit and uplink data. Terminal handover, which follows acquisition, cannot be delayed as long as in AEGIS because of greater uncertainties in missile position and heading. Intercept coverage of TERRIER and TARTAR ships with SM-2 is also substantially increased relative to SM-1 against both incoming and crossing targets.

APL Contributions

Initially, APL contributed significantly to the development of SM-2 midcourse guidance in the TERRIER and TARTAR application by formulating the initial requirements and defining many of the basic concepts. This was a challenging undertaking, for not only was it to be the first tactical missile to use inertial midcourse guidance, but it had to be compatible with two existing shipboard systems. For a time, this work proceeded in parallel with the development of the new AEGIS Combat System. When the advantages of a common missile became apparent, APL helped define the resulting configuration through participation on a number of steering groups chartered by the Naval Sea Systems Command.

Subsequently, APL played a major role in connection with the development of both the AEGIS and TERRIER data links. From 1973 to 1976, extensive AEGIS link-compatibility tests were periodically conducted with APL participation. Concurrently, the Naval Sea Systems Command requested that APL design and evaluate an alternative AEGIS uplink re-

ceiver/decoder using improved signal processing concepts. The resulting design, successfully tested in 1977, was shown to be highly tolerant of expected variations in the uplink signal waveform. Subsequently, many of the features of the design were incorporated in the production version of the receiver/decoder. In addition, APL guided the development of the TERRIER and TARTAR uplink and downlink systems, performing much of the preliminary design work for the downlink system. Test and evaluation equipment for these systems was also designed and built at the Laboratory, culminating in final system integration testing at APL in 1976 prior to flight testing at sea.

STANDARD MISSILE-2 TERMINAL GUIDANCE

"Terminal guidance" refers to the self-navigation phase following midcourse guidance during which SM-2 homes on the target until intercept occurs and the missile warhead is detonated. A terminal guidance mode is necessary because midcourse guidance is not sufficiently accurate, even at short range, to consistently achieve miss distances less than the lethal radius of the warhead. The same terminal guidance equations are used in all SM-2 missile variants.

Many factors affect the success or failure of the missile during the terminal guidance phase. At the desired time of handover, seeker acquisition is the primary consideration. As intercept is approached, the kinematic capability of the missile (i.e., speed and maneuverability) relative to that of the target is critical. As might be expected, crossing and/or maneuvering targets tend to be more stressing than directly incoming, nonmaneuvering threats. Other factors having a major effect on guidance accuracy are an angle scintillation phenomenon known as target glint and, occasionally, severe fades in the target-reflected signal at a critical time prior to intercept. The extent to which the missile is not steering toward the actual intercept point at handover, i.e., the missile heading error, can also affect the final miss distance.

Figure 6 is a block diagram of the SM-2 terminal guidance loop. The characteristics of the signal received from the target (most importantly, angle of arrival) vary with target and missile motion. The seeker antenna receiving the signal is inertially stabilized to remove missile pitch and yaw motion. The missile receiver has two primary outputs, a line-of-sight angle measurement and a closing velocity (Doppler) measurement. The guidance computer uses these measurements to generate steering commands in accordance with a proportional navigation guidance law. In the same manner as during the midcourse guidance phase, the autopilot converts the guidance computer's electronic commands to missile tail deflections so as to alter the missile's trajectory. The result is lateral missile motion. With longitudinal motion provided by propulsion, the missile heads toward an intercept with the target.

The final phase of flight, known as the endgame, is characterized by a high-speed encounter with the target. Accurate timing of the warhead detonation is essential in this phase. When the missile and the target are close, a small radar aboard the missile, known as a target detection device or proximity fuze, senses the target's presence. A calculation is then performed to determine the optimum time to trigger warhead detonation. If the missile collides with the target before that time, a contact fuze detonates the warhead upon impact.

MONOPULSE RECEIVER DEVELOPMENT

As previously indicated, the purpose of the missile homing receiver is to provide an accurate measurement of the angle of arrival of the target signal with respect to the boresight axis of the seeker antenna. Three basic methods are commonly used in missile receivers to measure angle error: scan, interferometer, and monopulse[1] processing. As explained below, scanning receivers induce an amplitude variation on the received signal in order to derive a measurement of angle error. On the other hand, an interferometer measures the phase difference in the return signal as received at different antenna ports to obtain an estimate of the off-boresight angle. Monopulse receivers can be designed to make use of either amplitude or phase differences depending on the type of antenna

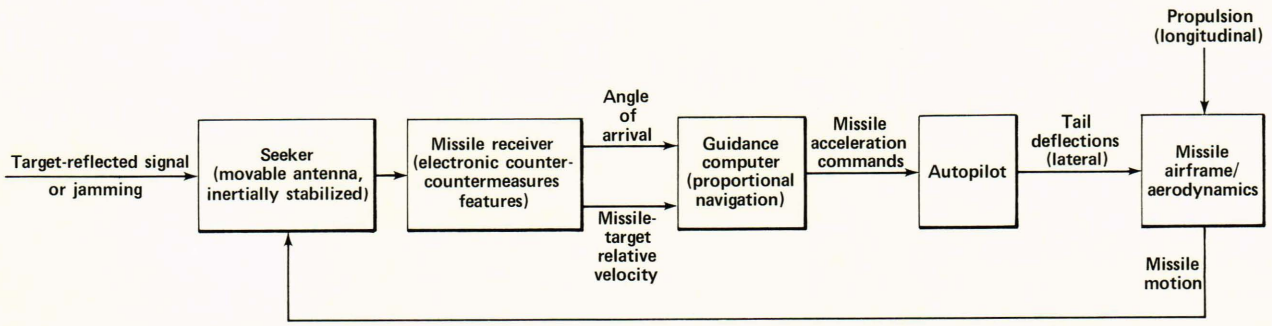

Figure 6 — Terminal guidance functional block diagram. STANDARD Missile terminal guidance is accomplished by processing an RF signal received from the target. The receiver determines the angle and relative velocity of the target while the guidance computer translates this information into steering commands. The autopilot adjusts the aerodynamic control surfaces to alter the missile's trajectory as required. Kinematic energy is provided by a solid rocket propulsion system.

PROPORTIONAL NAVIGATION

The problem of guiding a missile to an eventual near miss or collision with a target using only the observed motion of the missile-target line of sight has a number of potential solutions. Probably the most obvious is a simple pursuit course, in which the missile always flies directly toward the current target location. The disadvantage of this approach is the stringency of the missile maneuvers that are generally required as intercept is approached. A more favorable trajectory is a constant bearing course in which the missile leads the target, similar to the manner in which a projectile is traditionally fired at a moving object. If the missile flies a course that keeps the relative missile-target velocity aligned with the line of sight, a collision will always occur. If missile speed and target speed and course are constant, the missile trajectory is a straight line to the intercept point, as is shown in the illustration.

Proportional navigation is a steering law that is intended to yield a constant bearing course even if the target maneuvers. This is achieved by making the rate of change of the missile heading directly proportional to the rate of rotation of the line of sight. Ideally, this implies that the missile respond instantaneously to changes in the line-of-sight direction. In reality, there is some delay in returning to a constant bearing trajectory following a target maneuver because of finite missile responsiveness and filtering that is introduced to reduce the effects of noise.

In mathematical terms, the proportional navigation steering law is given by

$$\dot{\gamma}_M = N\dot{\sigma}, \qquad (1)$$

where $\dot{\gamma}_M$ is the rate of change of missile heading, $\dot{\sigma}$ is the rate of rotation of the line of sight, and N is a parameter known as the navigation ratio.

The navigation ratio governs the responsiveness of the missile in correcting for line-of-sight rotation. Theory indicates that its value should be proportional to the missile-target closing rate, i.e., the higher the closing rate, the more responsive the missile must be. With a continuous-wave-illumination homing system, a good estimate of the closing rate can frequently be derived from the Doppler frequency of the target return.

The angular rate of line-of-sight rotation, $\dot{\sigma}$, is measured by the missile seeker. The seeker antenna assembly, which is stabilized with respect to missile body motion, tracks the target. The tracking error, ϵ_m, derived from the signal processor, together with the antenna rotation rate, $\dot{\sigma}_p$, measured by antenna-mounted gyros, provides the information to compute the line-of-sight rate; i.e.,

$$\dot{\sigma} = \dot{\sigma}_p + \dot{\epsilon}_m . \qquad (2)$$

Computation of steering commands is performed by the missile guidance computer according to the above relationships. In addition to noise filters, compensations are usually introduced to account for such factors as variations in missile velocity and radome effects. Steering command limits are also imposed so that the missile maintains aerodynamic stability and does not exceed its structural capability.

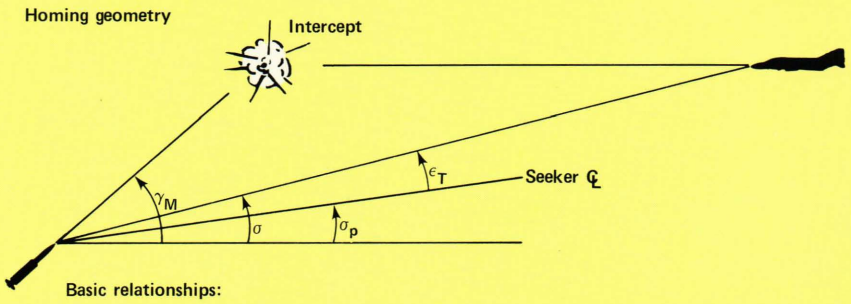

Basic relationships:

1. Steering equation for proportional navigation is $\dot{\gamma}_M = N\,\dot{\sigma}$.
2. From geometry, $\dot{\sigma} = \dot{\epsilon}_T + \dot{\sigma}_p$.
3. To obtain a measure of $\dot{\sigma}$, the signal processor provides ϵ_m ($\approx \epsilon_T$) and seeker-mounted rate gyros provide $\dot{\sigma}_p$.

employed. Phase-comparison monopulse receivers have become by far the most popular choice in modern missile receiver applications based on performance and hardware implementation considerations.

Until recently, scanning techniques were most common as a result of their relative simplicity. A scanning receiver measures angle by either mechanically or electronically nutating the antenna to form a conical pattern about the seeker axis (Fig. 7). The magnitude of the resulting amplitude modulation on the received signal can be shown to be proportional to the target off-boresight angle, while the phase is directly related to the polar orientation of the target. This information can be extracted by the receiver by processing the first harmonic of the scan sideband frequency. (In the frequency domain, the amplitude modulation of the received signal caused by the nutating antenna pattern is evidenced by sidebands displaced from the primary return signal at multiples or harmonics of the scan frequency.)

One of the major disadvantages of scan systems has been their inherent susceptibility to amplitude

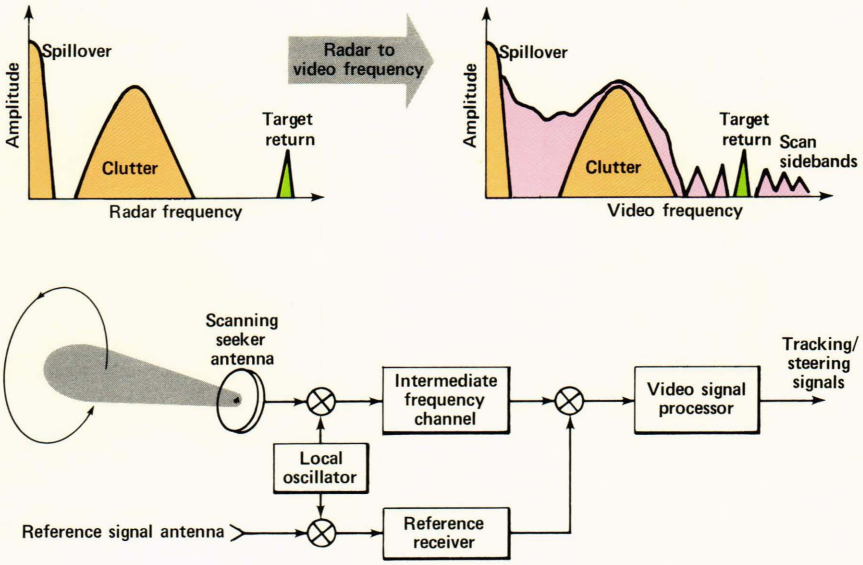

Figure 7 — Scanning receiver operation. Nutation of the scanning seeker antenna introduces an intentional amplitude modulation on the received signal. The modulation causes sidebands about each return, whether from the target or from clutter. Seeker angle error information is derived from the magnitude of the first scan sideband associated with the target signal. Scan sidebands associated with clutter can interfere with target detection and tracking.

modulation. While more modern scanning receivers have been developed using electronic techniques that are relatively immune, scan systems are basically at a disadvantage because they make a time-sequential determination of angle rather than a simultaneous measurement. A second disadvantage of scan processing is that the generation of scan sidebands can cause interference in the receiver. This is illustrated in Fig. 7, in which the scan sidebands of clutter overlap those of the desired target even though the fundamental signals are separated in Doppler frequency. Both monopulse and interferometer receivers avoid these disadvantages.

STANDARD Missile-2 Receiver Objectives

A primary objective in designing the SM-2 receiver was to take advantage of available technology to obtain the high degree of angle measurement accuracy afforded by one of the simultaneous signal processing techniques. Of course, it was recognized that this alone would not guarantee the desired level of performance in all of the signal environments considered possible for SM-2 operation. Consequently, a number of additional key features were defined at the outset to guide the design of the receiver and associated logic. As testing proceeded in conjunction with development, problems were found that invariably were traced back to a violation of the original basic principles. The performance of the final configuration, as demonstrated by extensive ground-based and flight tests, has since confirmed the soundness of the design approach. A brief discussion follows of the basic operation of the receiver, divided into angle error processing and Doppler processing functions.

Angle Error Measurement

SM-2 employs phase-comparison monopulse angle processing, enabling target direction to be determined on an instantaneous basis in two angular coordinates by comparing the signals received in appropriate lobes of the subdivided front seeker antenna. The directivity pattern for the SM-2 antenna consists of four parallel lobes, as shown in Fig. 8. By summing and differencing combinations of these four lobes, the Σ, $\Delta_{azimuth}$, and $\Delta_{elevation}$ signals are formed. Although these three signals contain all the necessary information for computing angle errors, they are not in a useful form and must be amplified, filtered, normalized, and translated to a lower frequency ("video") before final processing can be performed. In many respects, these operations are similar to those performed in ordinary radio sets.

Following the microwave arithmetic, the information needed for computing the angle error is contained in the amplitude and sign of each of the Δ channel signals relative to the Σ signal. Although separate channels might conceivably have been maintained for each of these signals until the final angle error computation was performed, the approach taken was to combine the Σ signal with each of the Δ signals in phase quadrature. Since the Δ signals are typically small compared to the Σ signal, the phase quadrature combination is approximately equal in amplitude to the Σ signal and has a phase shift relative to the Σ signal that is proportional to the angle error. The new signals are multiplexed through a common limiting amplifier that normalizes the amplitudes but preserves the phase relationships. Following normalization, the signals are demultiplexed, filtered, and phase compared to reproduce the desired angle errors for use in pointing the seeker and providing missile guidance information. This implementation requires less hardware than the separate channel approach, and also facilitates the preservation of relative gain and phase between the Σ and Δ signals.

Doppler Processing

When several competing signals are received, the one with the largest amplitude will inherently be pre-

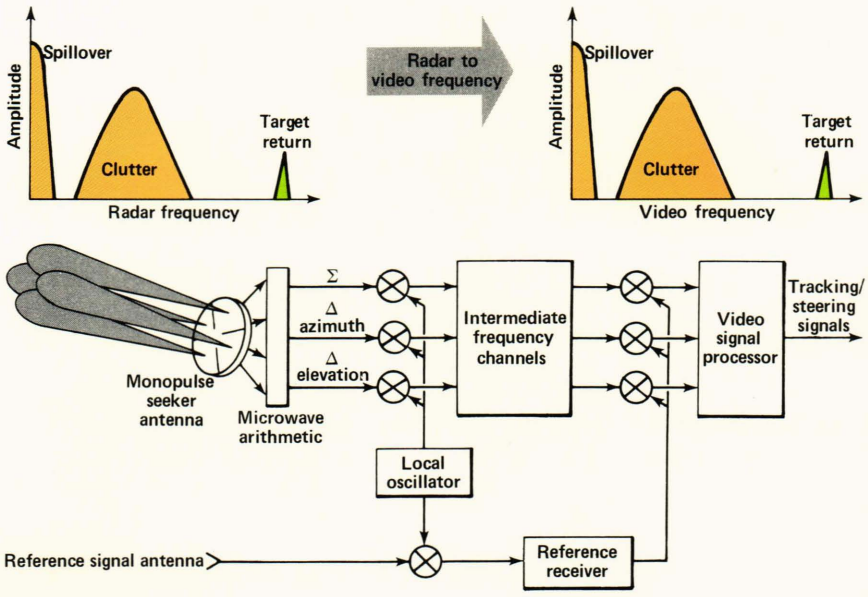

Figure 8 — Monopulse receiver operation. Angle error information is contained in the relative magnitudes of the Σ and Δ signals formed by summing and differencing the signals received by the four symmetrically offset lobes of the monopulse antenna. This simultaneous measurement approach circumvents the amplitude modulation in time-sequential measurement (scanning) receivers, resulting in a significant reduction in Doppler-band interference.

ferred. Therefore, in most signal environments, the desired target signal must be isolated from unwanted signals that may be many orders of magnitude larger. In a continuous-wave semiactive system, this is usually accomplished by taking advantage of the fact that the various signals received will possess different Doppler frequencies because of velocity differences (Fig. 8). Spillover, the signal resulting from energy that enters both the front and reference receivers via the direct path from the illuminator to the missile, will have a zero Doppler frequency. Chaff and clutter have near zero velocity relative to the illuminator, so their Doppler frequency is primarily dependent upon the missile velocity. Relative to stationary objects, the Doppler frequency of an incoming target will be higher, that of a crossing target will be approximately the same, and that of an outgoing target will be lower. Although it is not shown, inherent receiver noise is present throughout the Doppler spectrum. In addition, jamming may occur selectively or at all frequencies.

To acquire a desired target signal, a technique similar to that used in tuning an FM radio receiver is used. This consists of searching the spectrum in the neighborhood of the desired signal until it is located. At that time, automatic frequency control is used to maintain frequency tracking. In the missile receiver, the search is programmed and the switch to frequency tracking is automatic, based on the results of a signal bandwidth, or coherency, test. A comparison of the spectra in Figs. 7 and 8 indicates that tracking the target signal with a monopulse receiver in a dynamic situation should be easier because it is not contaminated with scan sidebands.

APL Contributions

APL contributed to the design and development of the SM-2 monopulse receiver by defining the primary requirements, formulating techniques in close cooperation with General Dynamics/Pomona personnel for achieving the specified performance, performing trade-off studies where alternative approaches were apparent, and conducting a comprehensive test program on the final configuration. Some early APL contributions to the design were made with the aid of a simulator that greatly facilitated the optimizing of circuit parameters over a variety of threat environments. Subsequently, the first closed-loop homing tests with actual guidance hardware were made at APL. Throughout the development program, strict adherence was paid to the fundamental principles defined at the outset despite occasional pressures to do otherwise. The resulting performance, as demonstrated by nearly 100 flight tests, has confirmed both the soundness of the approach and the initial predictions of the APL and General Dynamics/Pomona designers.

TEST AND EVALUATION

The SM-2 guidance system was subjected to an extensive series of ground-based and flight tests throughout its development, with significant APL participation. In retrospect, the Naval Sea Systems Command's "build-a-little, test-a-little" philosophy was crucial to the success of the development process. As soon as guidance hardware was made available to APL, emphasis shifted from the simulator to testing in the APL Guidance System Evaluation Laboratory. Subsequently, flight tests were conducted, including instrumented test-range firings and tactical system evaluations at sea.

Guidance System Evaluation Laboratory

The Guidance System Evaluation Laboratory (GSEL) has been used continuously for testing guidance hardware since it was established in 1965. Upgraded substantially in 1980 to better support SM-2 development, the facility consists of an anechoic test

chamber that houses the guidance section to be tested, generating equipment to reproduce electromagnetic signal environments representative of actual flights, and a hybrid computer system to control test conditions and simulate the dynamic interactions of the missile and the target. Tests can be performed to simulate a wide variety of threat situations, including those involving countermeasures.[2]

SM-2 testing in GSEL began in 1975 with an evaluation of a prototype SM-2 guidance section. Follow-on evaluations were performed using both preproduction and production units. The primary objectives of those tests were to conduct an in-depth evaluation of the guidance system design and to determine guidance accuracy in intercepting both known and projected threats. In the early stages of development, the first objective tended to dominate as design shortcomings were invariably uncovered. Working closely with the missile Design Agent, solutions to each problem involving either hardware or computer program modifications, or both, were developed and verified. After the design was reasonably firm, a comprehensive series of tests was conducted to assess guidance accuracy in terms of miss distance. That evaluation included tests involving a broad spectrum of threats. The overall conclusion of the test program was that the design objectives of SM-2 had been achieved.

Another important facet of the GSEL test effort was in support of flight test activities. The conditions to be employed in planned flight tests were simulated to provide performance predictions and to ensure that the tests provided a significant demonstration of capability with a reasonable margin for success. Occasionally, unexpected phenomena were encountered in a firing with a suspected link to the signal environment. Missile hardware would then be tested in GSEL over a range of environmental conditions bracketing those of the flight. Such examinations often led to a better understanding of missile operation.

Flight Testing

The initial flight tests of SM-2 were conducted at the White Sands Missile Range in New Mexico. While White Sands is part of the National Range System operated by the U. S. Army, the Navy as a tenant has access to the range communication, tracking, and support facilities necessary for missile testing. In addition, a weapon control system and launcher have been installed at the Navy installation (USS DESERT SHIP) so that the system-to-missile interface is functionally equivalent to an actual shipboard system.

SM-2 test firings were conducted with a Navy crew supported by civilian contractors (Fig. 9). APL maintains a close working relationship through a field office and a resident engineer. In addition, APL heads the Computer Programming Committee that develops Weapon Control System computer programs to support individual flight test scenarios. APL is also represented on the Test Coordination Panel and participates in post-flight analyses.

After completion of the engineering development flight test phase at White Sands, combat system tests were conducted in an operational shipboard environment. From a missile standpoint, at-sea testing enables modes of operation to be evaluated that are beyond the capabilities of White Sands, partly because of range safety considerations. AEGIS at-sea testing was conducted in USS NORTON SOUND (AVM-1) in 1976, 1977, and 1978; TERRIER testing was conducted in USS WAINWRIGHT (CG-28) in 1976 and in USS MAHAN (DDG-42) in 1978 and 1979. Preceding shipboard testing, the TERRIER/SM-2 Combat System was assembled and tested at the APL Land Based Test Site. After successful completion of this evaluation, the equipment was transferred to the firing ship. During the initial phases of this test program, APL advisors assisted in the training of Navy personnel.

Based on the successful SM-2 flight test program in USS MAHAN, the TERRIER Combat System with the SM-2 missile was approved for service use on October 2, 1979, by the Chief of Naval Operations. AEGIS with SM-2 will become operational when the first AEGIS ship, TICONDEROGA (CG-47), is deployed.

STANDARD MISSILE-2 UPGRADE PROGRAM

With the initial version of the SM-2 in production, attention has focused on extending its guidance system's ability to counter the growing threat of high-speed, high-altitude, antiship missiles launched from aircraft. Taking advantage of recent advances in digital processing techniques, the SM-2 guidance section has been provided with a fast Fourier transform digital signal processor. This processor is functionally equivalent to a set of contiguous analog Doppler filters, each having a small bandwidth. The objective is to enhance acquisition and tracking of returns from

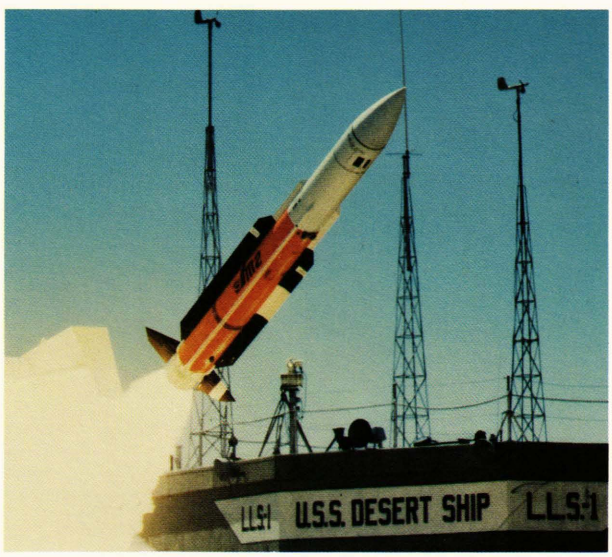

Figure 9 — Launch of an AEGIS SM-2 flight test round at the USS DESERT SHIP at White Sands Missile Range.

targets in the presence of obscuring jamming noise. APL's most significant contribution to the digital signal processor design was the development of a digital automatic gain control that provides the processor with the ability to handle signals of widely varying amplitudes.

In addition to signal processing improvements, missile propulsion has been increased to provide the kinematic capability for successful high altitude intercepts. This, in turn, led to the need for radome accommodations to compensate for the effects of increased aerodynamic heating. APL again played a key role, in conjunction with General Dynamics/Pomona, in defining the required changes. The resulting improved version of SM-2, designated Block II, is currently in engineering development.

ADVANCED GUIDANCE POSSIBILITIES

The feasibility of multiple guidance modes is currently being examined in an exploratory development context with potential applicability to a future STANDARD Missile. Homing modes being considered, in addition to semiactive, include active (in which each missile carries its own transmitter), infrared, and wideband home-on-jam. Some of the more attractive multimode combinations include semiactive terminal supplemented by either active or infrared, active terminal supplemented by infrared, and these plus wideband home-on-jam.

Currently, several programs have been initiated to demonstrate the technology required for alternate or supplemental guidance modes. Examples include development of high power, active transmitters; multiband antenna systems; and infrared domes for high speed flight. Physical integration of multiple sensors into a guidance package and definition of multimode guidance system control logic are also being addressed.

NOTES

[1]The word "monopulse" originally referred to a radar system that required a single pulse to measure the target off-boresight angle. When applied to a continuous-wave receiver, it implies that angle error is measured by simultaneously comparing the return signal as it is received in various sections of a subdivided antenna.

[2]For further information on the Guidance System Evaluation Laboratory, see W. M. Gray and R. W. Witte, "Guidance System Evaluation Laboratory," *Johns Hopkins APL Tech. Dig.* **1**, 144-147 (1980).

The control and tracking of modern high-speed aircraft, guided missiles, and the giant vehicles of the space age require visual display systems of far greater flexibility than are now available. The development of an experimental integrated data display system having two- and three-dimensional capabilities and a controllable memory using coherent fiber optics is a major advance in this field. Used in conjunction with advanced data-gathering systems, such equipment will reduce the chance of errors in operator judgment and will accelerate decision-making.

Experimental

Radar technology has advanced to the stage of development where we may realistically postulate a single radar that can simultaneously and automatically search for, acquire and track with precision a large number of aircraft, providing accurate data as to their dimensional position and velocity. High-speed digital computers that can assimilate large volumes of coordinate information from such radars and from other data-gathering devices will permit the construction of integrated automatic data-gathering, processing, and decision-making control systems. However, it will prove impossible to predetermine all possible operational situations in air traffic environments of increasingly high density and speed and to supply the "canned" answers that will be required by such systems. Consequently, there exists a requirement to develop new visual display devices that can work with advanced data-gathering equipment. Such devices must display quantities of coordinate data in a form suitable for rapid, intelligent monitoring and evaluation by a trained operator in order to allow him to override the automatic control system in times of malfunction or when it is confused by a particular operational situation.

An experimental three-dimensional (3-D) display that exhibits trajectories of both aircraft and satellites has been built at APL (Fig. 1). This is the first step toward demonstrating the technical feasibility of a display system that can display coordinate data in three, as well as in two, dimensions.* A device like this, with trained operators, can perform the key functions of a general-purpose display system for both advanced-weapon and commercial-air-traffic control systems.

The system is also suitable for use with sonar and could be used in a Naval Combat Information Center to display simultaneously both sub-surface and surface tactical situations for evaluation.

* Success of the display system described herein is due in large measure to J. B. Garrison who conceived many of the basic requirements and techniques used.

A. C. Schultheis

3-D Radar Display

Also, as the requirements for space control systems become better defined, we believe that the display system will find uses in such areas as surveillance, navigation, and orbital rendezvous.

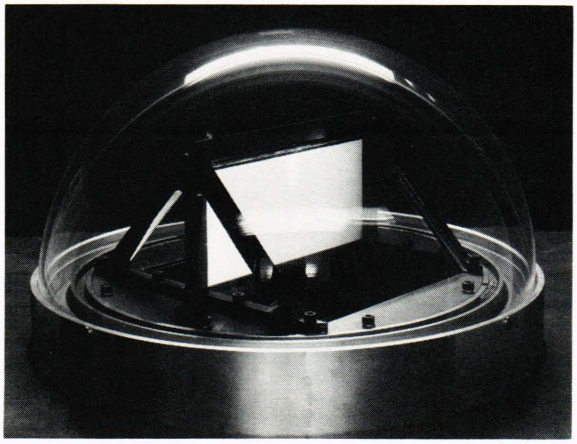

Fig. 1—Experimental three-dimensional display mounted under a plastic dome. Trajectories are displayed on the rotating, vertical, translucent screen.

Display System Characteristics

Because we see the world in three dimensions, it is natural that a 3-D display will provide an operator with information that he can assimilate and evaluate intelligently in the shortest possible time. Furthermore, in a heavily-populated, high-speed air situation, it will be highly advantageous for an operator to watch only one display for all his information rather than to be forced to make a composite mental picture from several 2-D displays, each giving only two categories of information, e.g., range-azimuth, range-elevation, etc. The higher the degree of saturation and the higher the air traffic speeds, the more critical will be his need of such equipment. To be effective, the display must present a large volume of information, have good resolution, and be able to present a controllable time history of a particular situation.

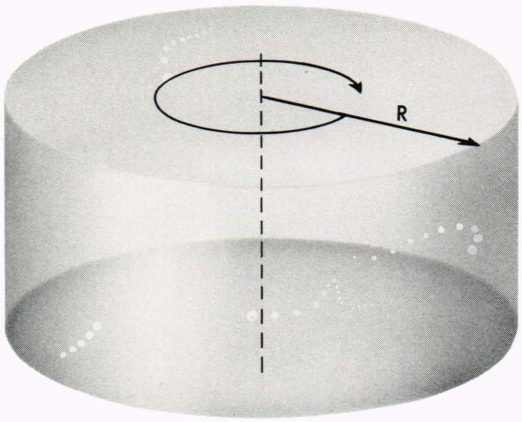

Fig. 2—Cylindrical volume with several trajectories suspended within it to illustrate the 3-D display concept.

To illustrate the concept of a 3-D display, a series of points forming individual trajectories suspended within a volume (arbitrarily chosen to be cylindrical) are shown in Fig. 2. The heaviest point in each trajectory represents the current position of the object under observation, while the others form a selected portion of its past-time position history—a variable for time periods from seconds to hours. With this ability to control the time-history display of an operational situation, an operator can avoid excess data display and more easily detect and evaluate operational trends.

The time lag for display of data after being received must be minimal. Also, the data insertion system must have access to all volume resolution elements within a minimum reaction time since there is no possible control over where objects will appear. A data access time of 1.0 sec was selected as being reasonable and practical, thus permitting all displayed data to be updated every second.

Displayed data must also be easily broken down into categories of information; color coding was therefore selected as being of greatest use to an operator. A capability of inserting symbols and cursors was also provided. With such tools as these an operator can intervene effectively in a fast-changing, high-density, operational environment.

Display Technique and Principles of Operation

Among several ways of generating a 3-D effect of the character shown in Fig. 2, a rotating vertical display screen (Fig. 3) of a semitransparent light-diffusing substance (e.g., frosted glass) was selected. As the screen rotates, it scans the entire volume of a sphere of radius R. For example, at each revolution of the screen, we turn on a small spot of light at the same angular position ϕ of the screen; the spot is then imaged on the screen at location x_o, y_o. The time duration of the spot is very short so that it appears to hang in mid-air at that location. Rotating the display at 20 revolutions per second removes any noticeable flicker as the spot is turned on and off once each revolution; the observer is not aware of the screen itself since its rotational speed makes it invisible.

There are several important advantages inherent in this type of 3-D display. It is truly three dimensional to the *naked* eye and requires no aids to vision. Because of the semitransparent material of the screen, it can be observed from any position. The light spot (data point) is diffused by the screen surface so that it is scattered almost equally in all directions, with the exception, perhaps, of a small angle defined by the plane of the screen and its thickness.

This type of display has a four-color potential. At any angular position of the display screen, four independent quadrants—two at an azimuth angle of ϕ and two at an angle of $(\phi + 180°)$ on opposite sides of the screen—are available to image light spots of different colors that may be viewed simultaneously. (Note in Fig. 3 that only a semicircular screen is needed to generate a spherical volume about the axis of rotation; the light spots need be imaged on only one side of the screen.)

One thousand such vertical planes distributed equally in angle (which is consistent with the

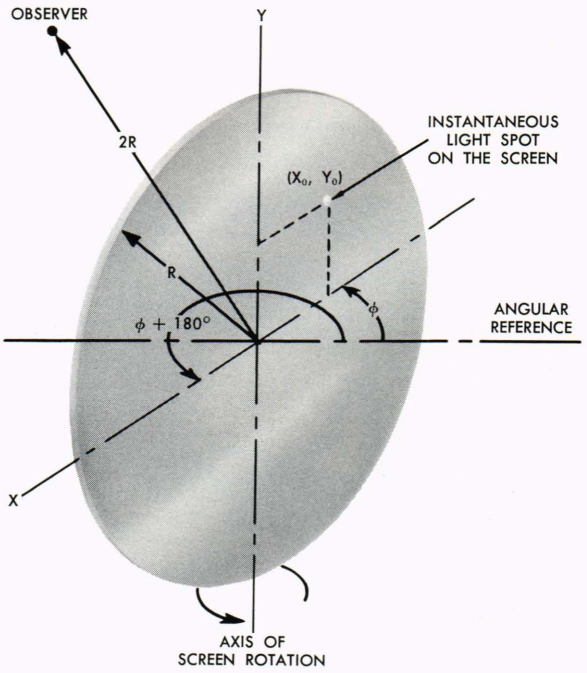

Fig. 3—Rotatable, vertical display screen that scans the complete volume of a sphere of radius R.

resolution stated) define a system angular resolution (azimuth) of 0.36°. Since each circular plane contains 10^6 resolution elements, the entire display volume will therefore contain 10^9 volumetric resolution elements regardless of the radius of the display volume.

Data Processing and Insertion

During each of the 20 revolutions of the screen per second, there are 1000 azimuth locations at which we wish to see all objects (light spots). Thus, the screen spends a total time of 0.05 sec/1000 (50 μsec) at each discrete angular position during a single revolution. In this instant there are 10^6 resolution elements that conceivably could require illumination. This means that a single light spot could spend approximately only 10^{-11} sec at each one of the million resolution cells in order to illuminate them all sequentially in 50 μsec at that location. A realistic example might be to assume 100 objects, at a particular azimuth angle, each being updated with latest position information every second. If we wish to display about 10 minutes of time history on each object, then the light spot must illuminate 60,000 different positions each revolution of the display (100 objects $\times$ 60 points per object per min $\times$ 10) in 50 μsec. This means, assuming they were equally distributed in time, that a single light spot could, on the average, dwell at each position for only about 10^{-9} sec.

The factors important to design of the data-processing and insertion portions of the system were determined from these considerations. The total number of data points that must be displayed in the short times involved (10^4 or 10^5 points in 10^{-5} sec) makes single-channel, sequential, lightspot scanning systems using cathode ray tubes and digital memories appear impractical. Hence, analog techniques allowing use of many parallel channels, each with a controllable memory, appeared to provide a potential solution. It was decided to investigate the use of 2-D, opaque, data memory surfaces that simultaneously could store data and be used to provide a controllable parallel channel light readout to the display.

Display Implementation

The technique chosen to image light points on the display screen (a rectangular screen rather than the circular screen in Fig. 3 that generates a cylindrical display volume) is shown in Fig. 4. The horizontal plane generated by the rotating X-axis represents the surface of the earth. If we take the bottom center of the display (O) as the coordinate origin, then the position of any object is determined by its height y_o above the earth and its

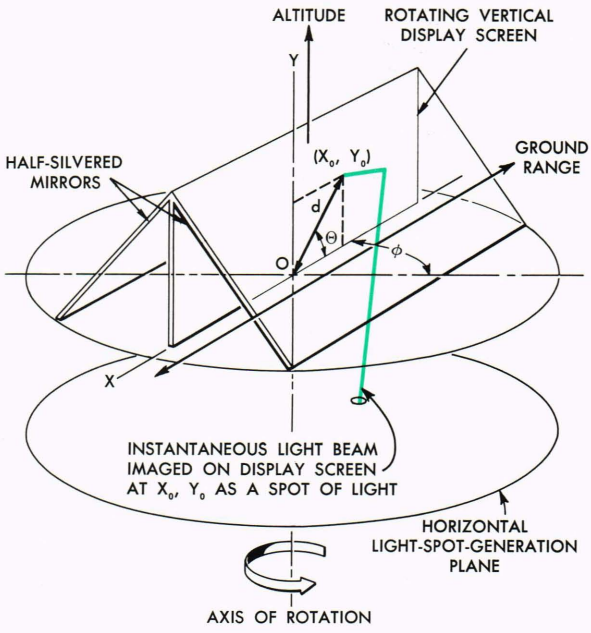

Fig. 4—Diagrammatic representation of the rotating experimental display shown in Fig. 1 and the display principle presented in Fig. 3.

ground range x_o at any azimuth of ϕ or $(\phi + 180°)$ on the screen. Assuming a minimum resolution cell of radius $R/1000$, where R is the radius of the cylindrical volume, we can place 500 such cells side by side along the X and Y axes of the screen. This establishes resolution of the display in both ground range and altitude of 1 part in 500 for the display system.*

Rapid on-off gating of the light spots in synchronization with the display rotation at the desired azimuths is accomplished in a horizontal light-spot-generation plane located directly under the display volume as shown in Fig. 4. At any instant, the picture on the horizontal plane is imaged on both sides of the vertical display screen by means of a simple projection-lens system and semitransparent half-silvered mirrors. These mirrors deflect the light rays projected from the horizontal plane so that they are imaged as spots on the vertical display screen without distortion; because they are semitransparent, they allow the observer to see the spots of light through them.

2-D Display System

The characteristics and operating principles of the analog memory data storage, insertion, and processing system can be described by referring to Fig. 5. Figure 5A shows a simple 2-D display system having two closely-spaced data surfaces of

* Target altitude and ground range can be easily derived from object radial range d and elevation angle θ.

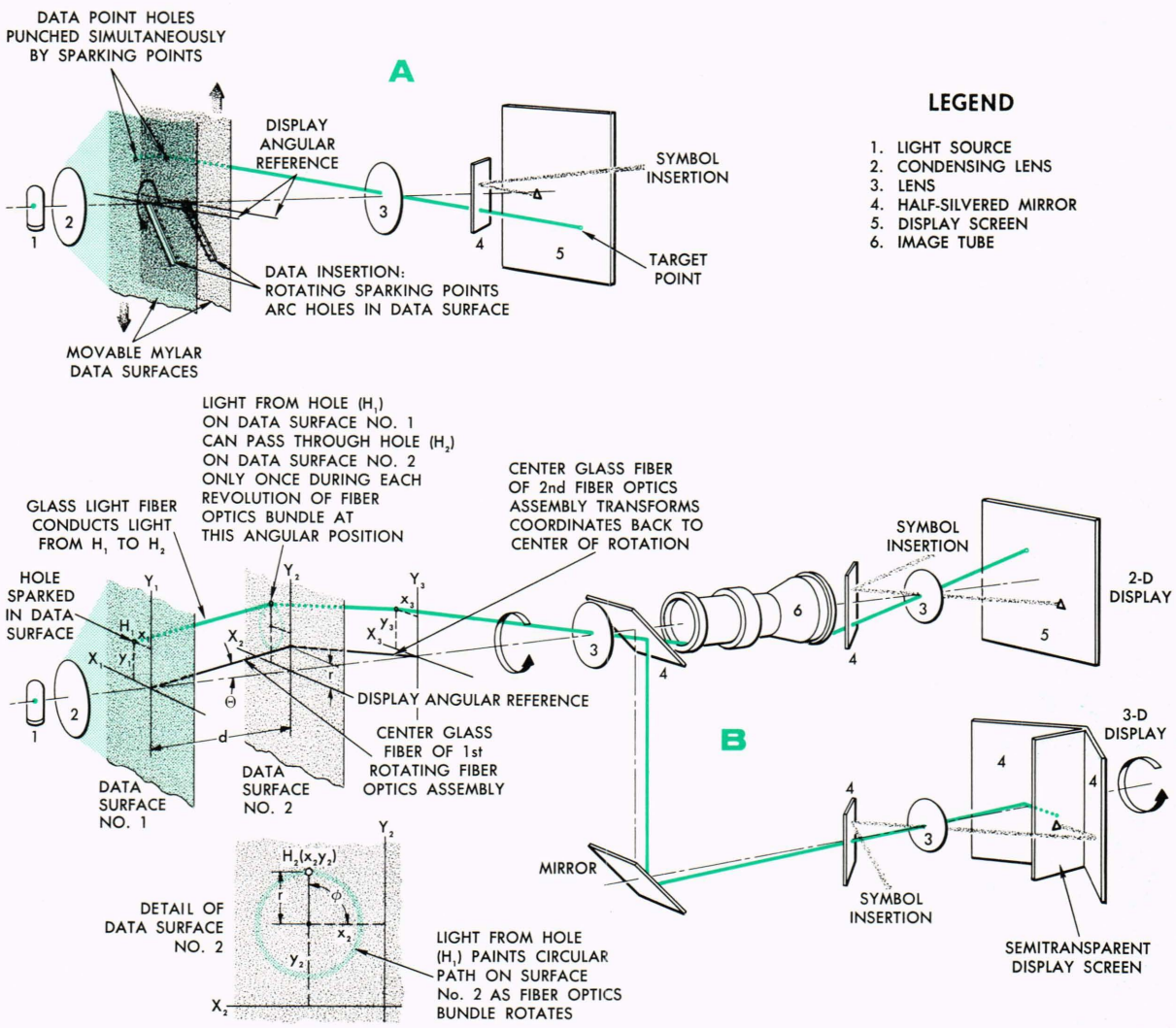

Fig. 5—(A) Simplified 2-D system showing principles of data insertion, storage, and display. (B) Principles of combined 2-D and 3-D displays. Note that fiber optics bundles are represented by a single glass fiber.

aluminum-coated Mylar tape. With aluminum coating on one side, this normally-transparent flexible plastic film forms an opaque memory surface. After making a data point hole in each surface (by removing spots of the aluminum coating) so that these holes are directly aligned, light can pass through both holes and be imaged on the screen via the lens and half-silvered mirror to represent a target coordinate point.

DATA INSERTION—To make the data point holes, we use an electric discharge from a rotating set of sparking points onto the aluminum surface of the Mylar. By controlling the total energy in the sparking pulse (width, voltage, etc.), the hole size can be controlled quite easily. Typical pulse widths of approximately 0.2 μsec and 5000 volts in amplitude are being used. The spark generator is a simple modulator that can be triggered readily from an external source. To reduce the number of sparking points required to scan the complete data surface, radial motion is applied to the sparking arm as it rotates. If the desired accuracy of data insertion is one-half a minimum resolution element, then in 20 revolutions, or one second (the required system access time), each point is made to move a distance of 10 resolution diameters.

If the data point holes are to align properly in angle, the timing accuracy must be related to the maximum usable radius of the data surface and to the minimum resolution element of radius $R/1000$. Since the circumference of the usable display area is $2\pi R$, there are about 3000 resolution elements scanned every 0.05 sec by the outermost sparking point. Thus, to locate the holes in

angle to half a resolution cell requires system timing accuracy of approximately 8 μsec.

DISPLAY PERSISTENCE—The purpose of the two Mylar data surfaces is to permit control of the variable memory (display persistence) by moving the display surfaces at a controlled rate in opposite directions, as shown in Fig. 5A. This serves two purposes. It erases old points from the display by destroying hole alignment between the two surfaces (thus, new data points on a trajectory are perfectly aligned and old points gradually disappear), and it introduces new data surface to the system, thus preventing the system from becoming saturated.

The rate at which the surfaces must move relative to each other is determined by the required memory time and the size of a minimum resolution cell (or hole diameter). If the minimum resolution cell is 0.005 in. in diameter on the display data surface and the memory time required is 5.0 min, the rate of tape usage would be 0.001 in./min. If the full display capacity must be available at all times, the Mylar film speed must be $2R$/memory time, or 1000 times as fast as that required to erase points. If complete independence is required between desired memory time and display capacity, it would be possible to have a double channel memory system in which either or both systems could display points on the screen.

3-D Display Systems

The implementation shown in Fig. 5A is not suitable for the 3-D display, however, since there are no provisions for independently controlling light spot readout from the memory as a function of azimuth angle and in proper time synchronism with the 20-cps rotational speed of the 3-D display screen.

Figure 5B shows the basic operating principle of the combined 2- and 3-D display system. In order to gate the light spot on and off, a rotatable light spot nutator made of coherent fiber optics is inserted between the two data surfaces. Coherent fiber optics are a solid mass of many parallel glass fibers, each approximately 0.001 in. in diameter. When bundled together, these fibers act as independent light guides.

If, for example, we image small spots of light on one face of a coherent bundle (ends of the individual fibers), the light will be conducted almost perfectly and with negligible loss and will appear as light spots imaged precisely in the same location on the opposite face. If, as shown in Fig. 5B we place a fiber optics bundle between the two data surfaces so that the center glass fiber (and consequently all other fibers in the bundle) is not parallel but is at an angle to the axis of rotation, the following results are obtained.

1. If the bundle is rotated about the rotation axis defined by a dotted line connecting the intersections of X_1 and Y_1 on data surface No. 1, and X_2 and Y_2 on data surface No. 2, any hole such as H_1, continuously illuminated by light on data surface No. 1, will paint a light spot (via the fiber optics) on data surface No. 2 having a locus forming a circle of radius r (Fig. 5B).

2. The position x_2, y_2 of the light spot on surface No. 2 at any angle of rotation defined by ϕ can be determined from the simple transformation equations, $x_2 = x_1 + r\cos\phi$, and $y_2 = y_1 + r\sin\phi$, where $r = d\tan\theta$, and ϕ is defined by the angular position of the center glass fiber with respect to the display angular azimuth reference. These equations show that the center of the light circle painted on data surface No. 2 is located at the same position x_1, y_1 of hole H_1 on data surface No. 1.

3. If we place a second hole H_2, as shown in Fig. 5B, at some position (x_2, y_2), defined by the above equations and thereby located at some position on the circular path, the light spot will trace as the fiber optics bundle rotates; we can very effectively control the parallel light readout of the memory as a function of time or angle. The continuous light beam from H_1 can pass through H_2 only once during each revolution of the fiber optics bundle.

By rotating this bundle in synchronism with the 3-D display, the light spot can be imaged only via lens, mirrors, etc., on the display screen at one angular azimuth position, for each altitude and range (determined by x_1, y_1) once each revolution. The second fiber optics bundle shown in Fig. 5B is required to transform the coordinates (x_2, y_2) back to the original coordinate positions (x_1, y_1) with respect to the center of rotation, before projection to the display screen. Since we defined 1000 discrete azimuth locations for display resolution, the circumference of the scanning light circle must contain at least 1000 minimum-resolution cell diameters or be equal to $2R$.

Figure 5B also shows the manner of adding a 2-D display. The process is self explanatory.

Complete Display System Implementation

Figure 6 is the planned complete 3-D display system, with a third data surface added to eliminate false trajectories which may be generated in a two-surface system as different trajectories cross one another. With a third surface, the possibility of a false trajectory is minimized since only scattered false points can occur. We expect that by

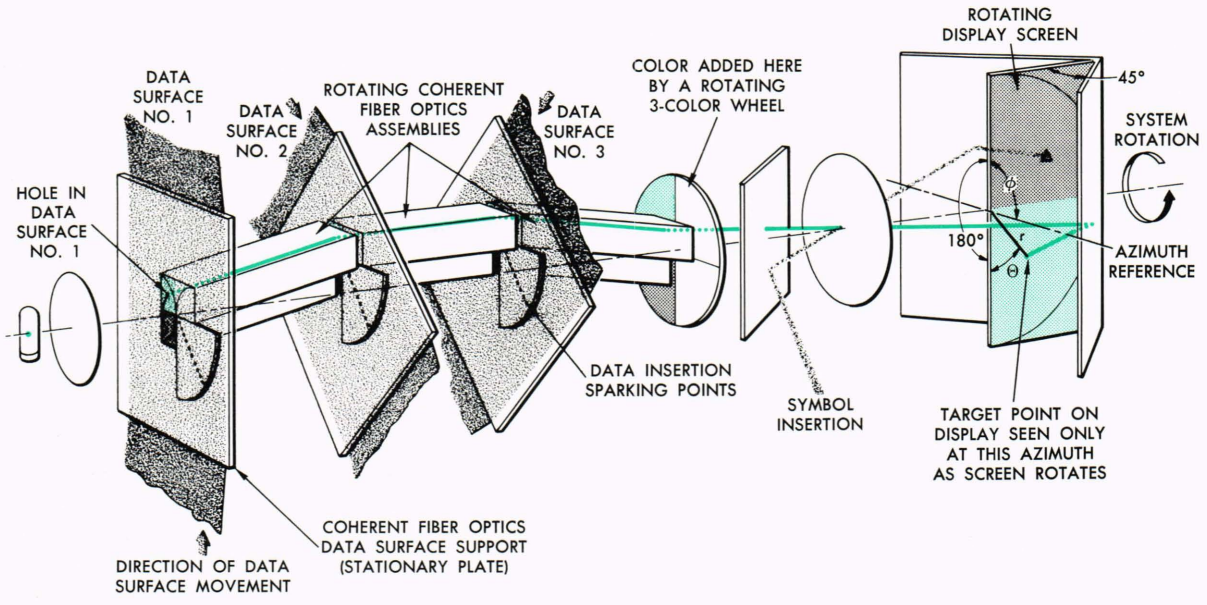

Fig. 6—Proposed complete 3-D display system showing use of a third data surface to eliminate false trajectories, and also showing three skewed fiber optics assemblies.

using 10% of the data surface area, or about 100,000 target points, the number of false points will be about 0.1% of the total number of points displayed. Since we are only interested in displaying trajectories, this level of false target information can be tolerated.

The operating principle of the rotating fiber optics assemblies is the same as in Fig. 5B. Color is inserted by a transparent three-color wheel (red, green, and white) that rotates synchronously with the fiber optics and display. Light spots appearing on the last data surface must pass through the color wheel before being imaged on the screen. This can be better understood by remembering that an image on the display screen at any azimuth position is really a vertical image of the last horizontal data surface at that instant of time via the projection lens and half-silvered mirrors inclined at a 45° angle.

This technique of color insertion utilizes the four-color capability in the display and permits division of the rotating fiber optics assemblies into four imaginary longitudinal sections. Each section is always reserved for a single color. Note that one fiber optics section is eliminated to allow insertion of sparking points. This prevents the sparking points from passing in front of the data surface at a time when they would interfere with the passage of light and prevent projection of data points. A typical, skewed, experimental, coherent fiber optics assembly is shown in Fig. 6. The assembly is 1.0 in. square and has fibers about 1.5 in. long and 10 microns in diameter.

Alternative Data-Insertion Techniques

Investigations have been made of the use of a moderate-power ruby laser to supply energy via the fiber optics to burn a data point hole through the three data surfaces simultaneously. This technique of data insertion, in lieu of the rotating sparking points described previously, was successful, but the duty factor of the laser is still too low to make such a system practical. Investigations of this possibility are continuing. Another interesting possibility is the use of photochromic materials that change from an opaque to a clear state when exposed to light of certain wavelengths.

Experimental Display

Figure 7 illustrates the experimental system that has been successfully used to display synthetic aircraft and satellite trajectories. The display screen itself is 7.0 in. wide and 3.5 in. high. A 3.5 magnification is supplied by a projecting-lens system having a focal length of about 6.0 in. and light-gathering aperture of about 2.8 in.

Two memory surfaces are used to generate the simulated aircraft and satellite trajectories. The circular memory surface in the object plane of the projection lens is attached to the lens and rotates with the display. Fixed data point holes representing discrete range and elevation coordinates have been made in this surface. Beneath the rotating data surface, and separated from it by about 0.01 in., a second fixed data surface has been placed

which has data point holes that match the rotating set at certain angular (azimuth) positions of the display. Light continually floods the underside of this second fixed memory surface so that when two holes align themselves as the display rotates the light is imaged as a spot on the display screen at that angular position. By moving the rectangular fixed data surface, trajectories in the display volume can be made to appear and disappear to simulate a dynamic situation.

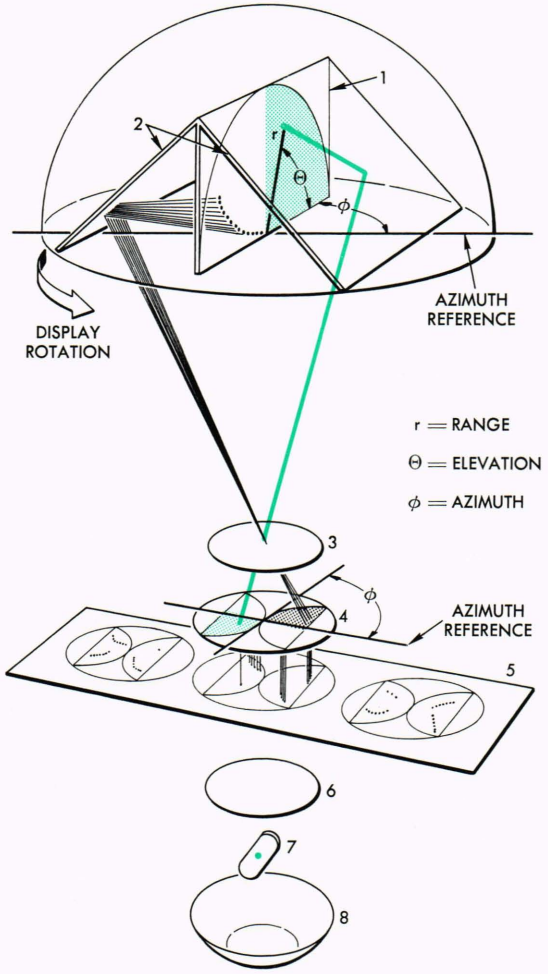

LEGEND

1. VERTICAL FROSTED GLASS PROJECTION SCREEN
2. HALF-SILVERED MIRROR
3. PROJECTION LENS
4. ROTATING DISPLAY SURFACE WITH COLOR QUADRANTS AND DRILLED COORDINATE HOLES
5. ADJUSTABLE DATA SURFACE FOR DISPLAY OF FIXED SYNTHETIC TRAJECTORIES
6. CONDENSING LENS
7. LIGHT SOURCE
8. REFLECTOR

Fig. 7—Experimental 3-D system that has successfully demonstrated aircraft and satellite trajectories.

Holes from 10 to about 4 mils in diameter have been successfully used in the memory surface and displayed in three dimensions. A 4-mil hole results in an altitude and range resolution of 1 part in 250. If the maximum range of the display is set at 100 nautical miles and altitude at 50,000 ft, this gives a range resolution cell of 2400 ft and an altitude resolution cell of 200 ft.

Through magnification, a 4-mil hole on the data surface yields a 14-mil light spot on the display screen. The minimum discernible spot size, as derived earlier, would be $R/1000$ where R is 3.5 in.; this would give a 7-mil-diameter spot.

There has been no difficulty in observing trajectories on the screen using the 14-mil resolution cell which subtends about 2 angular mils at the eye when viewing the display at 7.0 in. from the center. Light from a 750-watt projection bulb has been found adequate in a room that is only moderately darkened. Data points separated by about a resolution cell in a trajectory are discernible.

A number of screen materials other than frosted glass have been tried, and the most satisfactory material found so far is ordinary drawing vellum. Synthetic memory surfaces of thin metal with holes drilled in them, and surfaces of aluminum-coated glass sparked manually, have been successfully used to place points in the display. Color identity codes of red, green, blue and white have been used.

As predicted, the display described is easily visible from all sides, and the angle at which vision is restricted by the plane of the screen is of no consequence. Display trajectories are easily distinguishable from false noise points. There is a small amount of blocking of light from the posts supporting the half-silvered mirrors, and there are some slight refraction effects when part of a trajectory is viewed through the half-silvered mirror and the other part through air. These effects have been completely eliminated, however, in a newer display similar to that shown in Fig. 1 but which uses a single full-silvered mirror on one side of the screen only.

Actual results obtained from the experimental equipment have verified that the display technique and the basic principles of data insertion are feasible and meet predicted display performance objectives. The experimental system is severely limited in flexibility because of the synthetic method of inserting data points and the fact that only two surfaces are available. However, a more flexible, dynamic data insertion and processing system is planned which will allow more detailed testing and evaluation of the overall design objectives.

TRIAD INCREMENTAL PHASE SHIFTER

T. L. McGovern and L. J. Rueger

The TRIAD experimental satellite carried a new digitally controlled electronic instrument that has the capability of keeping time in the satellite for weeks to a precision previously available for less than a day. This instrument is an electronic frequency synthesizer whose frequency transfer function (input to output frequency) can be remotely programmed to compensate for frequency and time errors caused by an aging and drifting reference oscillator. The design allows for frequency adjustment in incremental steps of 7×10^{-13} *over a continuous range of* ± 20 *Hz. This report describes the design interfaces with the spacecraft, ground test results, and the tactics for operation in orbit.*

Introduction

In previous satellites in the Transit program, time and frequency were both derived from stable crystal oscillators, but only time was normalized to a predetermined value; the transmitter carrier frequency was allowed to drift with the frequency drift of the reference oscillator. Time normalization was accomplished by subtracting or deleting pulses in the timing chain in a pattern that very nearly repeats every two minutes. The deleted pulses were at 104 kHz, corresponding to 9.6 microsecond time jumps, each deletion being denoted in the transmitted message format. As a result, the Transit system, for all practical purposes, has a design limitation of ± 5 μs in time keeping. Although, in principle, knowledge of these time deletions is provided, because of the logistics in providing complete data and the instrumental difficulties of recovery, the use of this timing has never been promoted as a means of time transfer.

In order to eliminate or reduce this limitation, the time deletion system provided on TRIAD has a 200 nanosecond unit size, intended primarily for initialization of the satellite time system, with the frequency normalized by an incremental phase shifter (IPS) performing the function of an electronic frequency synthesizer. The time deletion circuit is not activated and the pattern is not identified in the message format when the IPS is used. The normalized frequency precedes the RF multiplier chain for the transmitter carriers and precedes the divider chain for the timing system.

To provide 2-minute time marks in previous Transit satellites, the reference oscillator frequency was selected to be $5\,[1 - (80 \pm 2) \times 10^{-6}]$ MHz and the timing chain had the divisions shown

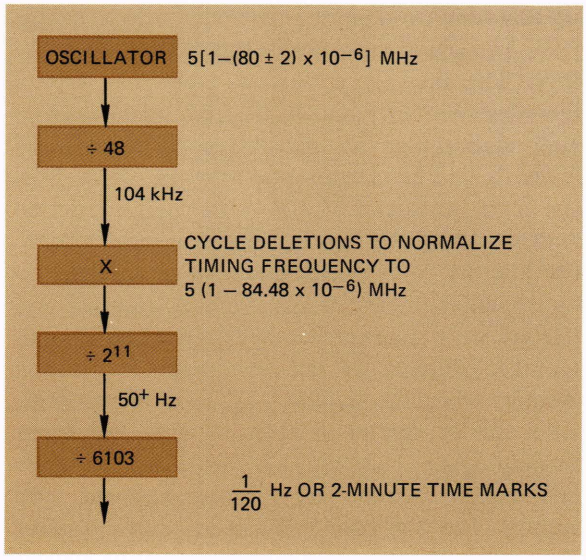

Fig. 1—Previous Transit timing chains.

in Fig. 1. The TRIAD system provided redundant methods of operation pending the successful demonstration of IPS in orbit, and a provision was also made for operating the satellite at a new frequency outside the operationally assigned channel during the testing of the DISCOS system.

Internal to the IPS package are RF switches that allow the Oscillator #1 signal to either bypass or not bypass the IPS circuits. Likewise the Oscillator #2 signal can either bypass or not bypass the IPS circuit. With this combination of circuits and oscillators, the system can operate on either the new frequency channel or operational channel without IPS by using the bypass. On the other hand, IPS can be initially tested in orbit in the new frequency channel and later operated on the operational frequency channels by selections of the proper reference oscillator. The timing chain for TRIAD is shown in Fig. 2. Note that the primary differences are in the position in the chain of the deletion operation and the addition of the IPS.

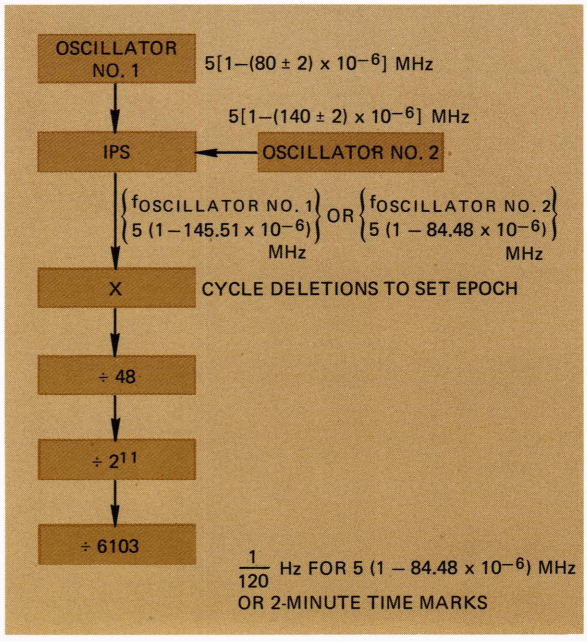

Fig. 2—TRIAD timing chain.

Principle of Operation

The principle of operation employed in the IPS is to provide 200 equally spaced phases over the span of 2π radians of a 5 MHz signal and then to electronically switch sequentially through these phases as shown in Fig. 3. If the electronic switch scans all 200 phases in one second, the smoothed frequency seen on the switch arm is one hertz higher or lower in frequency depending on whether the switch sequencing is toward advanced phases or toward retarded phases respectively. If the electronic switch advances one phase step in a time determined by dividing the 5 MHz input frequency by N, it is clearly observed that the frequency synthesizer has a unique transfer function. Unfortunately, the resolution in frequency adjustment for N adjusted by $\pm$ 1 unit was unacceptably coarse, so a system of alternating between N and $(N + 1)$ was devised; temporary operation at $(N + 1)$ is referred to as γ deletions in the text that follows. The alternating between N and $(N + 1)$ is maintained at the highest rate possible so that although the frequency is alternating between two values, all users on the ground have finite bandwidths and will integrate the received signal to the mean frequency. For one unit in N, the frequency adjustment is 3 or 4×10^{-7} in frequency; there are 2^{20} steps (1,048,576) between N and $(N + 1)$. Therefore it takes $(N \times 2^{20})/f_0$ seconds to realize the maximum frequency resolution (approximately fifteen seconds).

Detailed Design

A simplified block diagram of IPS is shown in Fig. 4. Referring to this diagram, the input RF signal from the reference oscillator enters the delay line and is picked off at one and only one

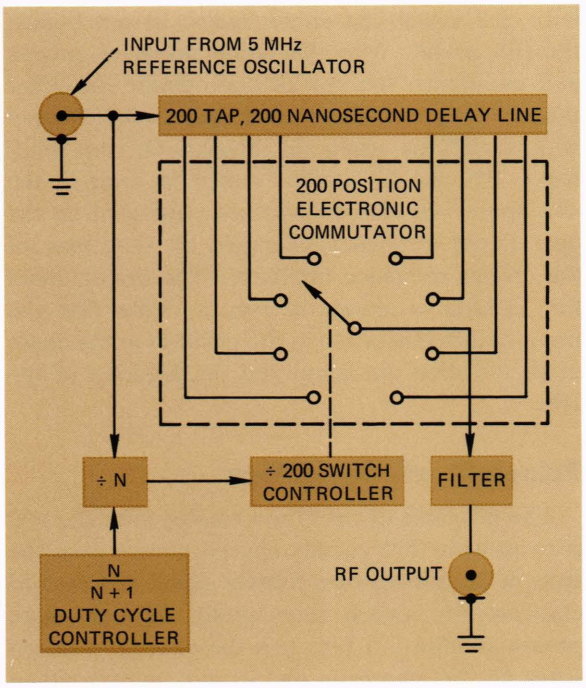

Fig. 3—Principle of operation of IPS.

tap at a time by digitally controlled diode bridge gates. The signal flows out of the diode gates to the filter. The filter is a narrow band-pass crystal filter designed to pass the desired signal derived from smoothing the phase-stepped signal and reject the initial carrier put into the delay line. The input RF signal also goes through a deletion control circuit and into a 7-bit, N-divider circuit. The number N by which this divider operates on the RF signal is selected and remotely inserted into a reference n counter. Comparison circuits monitor the contents of the N divider and the n counter; when the numbers agree in all bit positions, the N divider is reset to zero and starts dividing again. The reset also advances the diode gate switch position by incrementing the 200 counter. The 200 counter is an up/down counter to provide respectively either a higher or a lower frequency in the RF output; the up or down condition is set by an external signal from the spacecraft computer. In addition to the above functions, the reset signal increments a 20 bit γ divider. Each time the γ divider is incremented, comparisons are

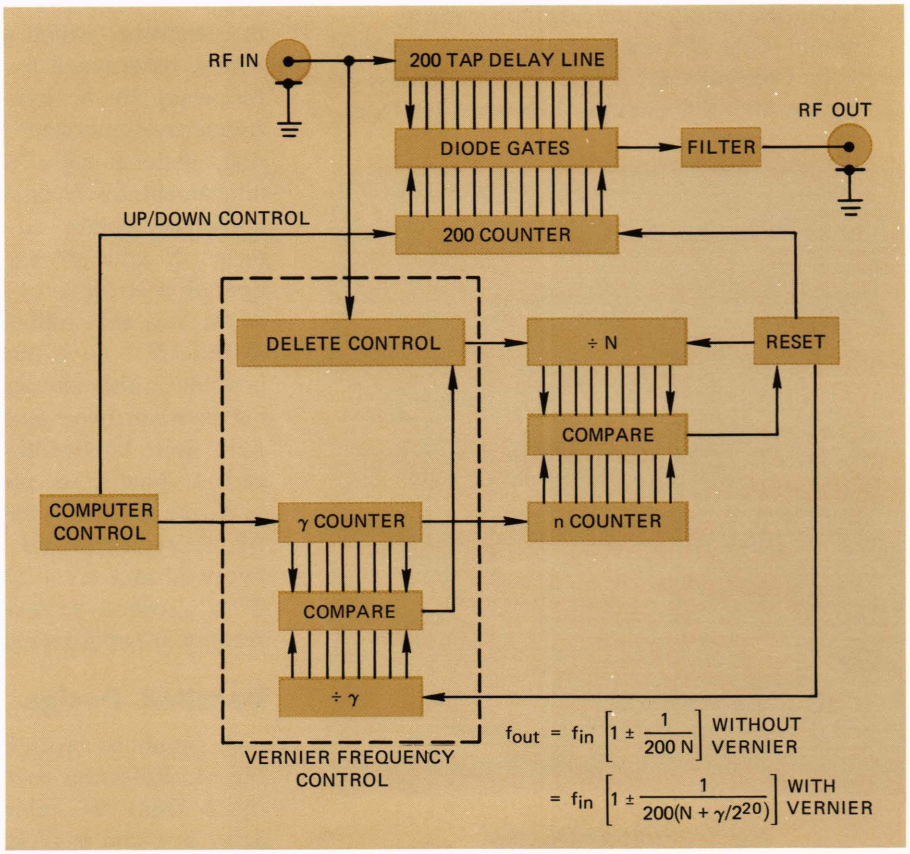

Fig. 4—Simplified block diagram of IPS.

made with the contents of a γ counter for any bits that have a transition to equality. Note that these comparisons are made by comparing the least significant bits of one with the most significant bits of the other; the number of matches is identical regardless of the order in which the comparisons are made, but the distribution in time is astoundingly different. For the method chosen, the comparisons (or deletions that cause the divide by N circuit to look like a divide by $(N + 1)$ circuit) are distributed as uniformly as a binary counting device can achieve over the period required for the divide-by-γ to process 2^{20} divide-by-N resets.

The contents of the γ counter and n counter are set by pulses provided remotely by the spacecraft computer. Pulses are clocked into the γ counter with controls set to count up or count down. When 2^{20} counts are reached in either direction, the overflow increments the n counter one unit in the corresponding direction. The computer control of these numbers enables the IPS to correct not only for frequency bias but also for linear or quadratic functions of frequency drift in the reference oscillator. If very precise timekeeping is desired, the computer can alternate or duty cycle the IPS between two sets of values for greater time resolution than provided by the smallest resolvable frequency increment.

The frequency of the output signal generated by the IPS is a specific function of the input frequency. Without the vernier control, the relation is given by

$$f_{out} = f_{in}\left[1 \pm \frac{1}{200\,N}\right]. \qquad (1)$$

When the vernier frequency control is used, the relation is given by

$$f_{out} = f_{in}\left[1 \pm \frac{1}{200\left(N + \frac{\gamma}{2^{20}}\right)}\right], \qquad (2)$$

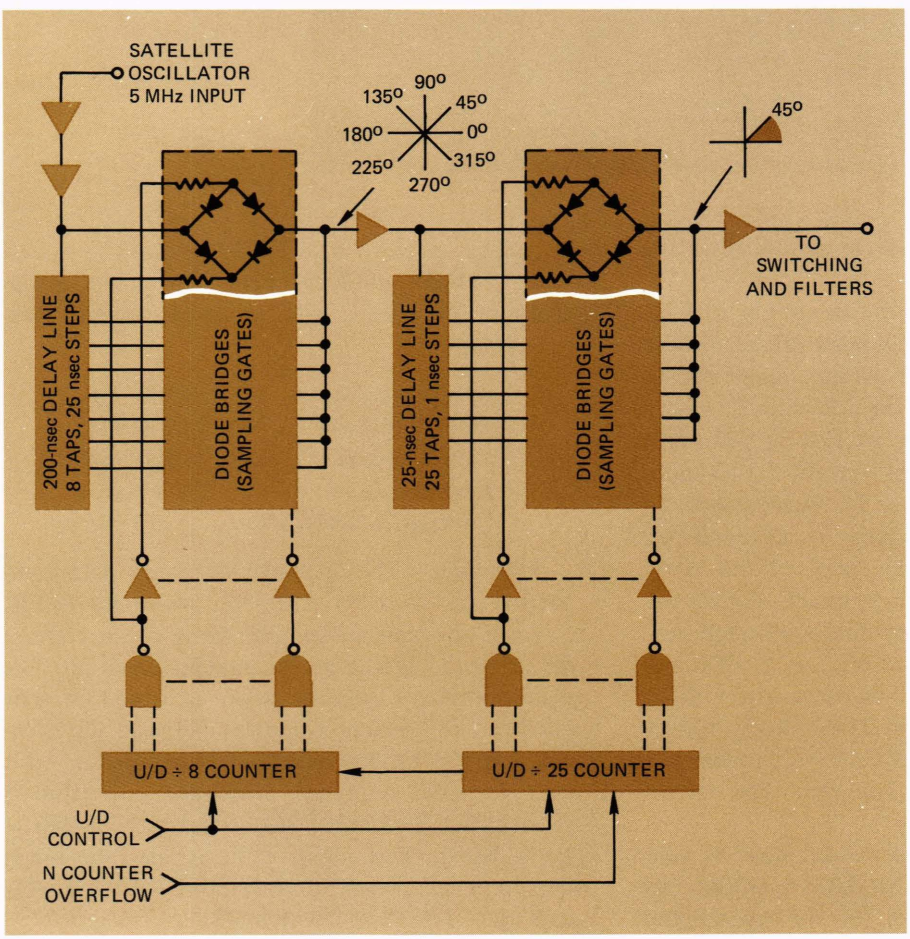

Fig. 5—Diode gates.

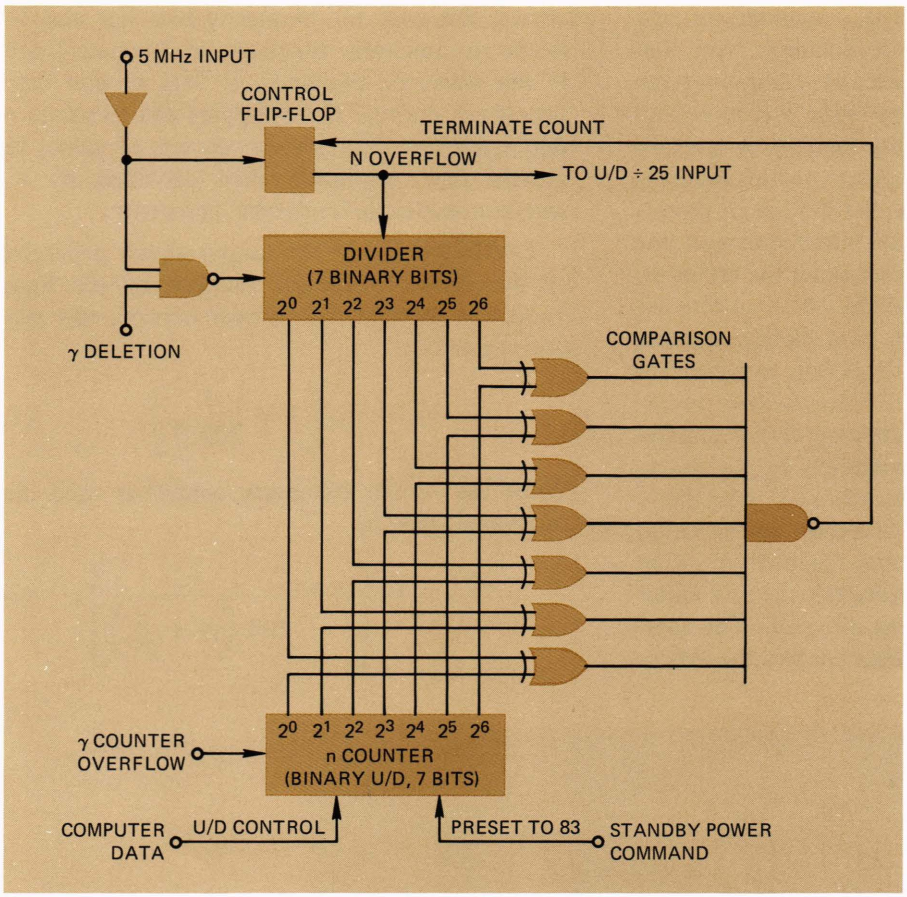

Fig. 6—*N* and *n* counters and controls.

where N and γ are the numbers contained in the N and γ counters.

Diode Gates—For economy in circuits and increased reliability, the 200 phases of the 5-MHz signal are generated by providing eight phases spaced 45° apart as inputs to a 25-tap, 25-nanosecond delay line as shown in Fig. 5. The eight phases are provided by eight taps on a 200-nanosecond delay line in steps of 25 nanoseconds. In this way the work of 200 gates is accomplished by $8 + 25 = 33$ gates. The detail of the diode gating is also shown in Fig. 5; digital signals impressed across the bridge of diodes through current limiting resistors turn on the diodes and provide a low impedance path between the delay line tap and the next circuit. These diode bridges pass an analog 5-MHz signal and switch from one tap to the next in much less than one microsecond.

Filter—The narrow-band crystal filter is centered in its pass band at the desired output frequency. There is one filter for the operational frequency centered at 5 MHz − 84.48 ppm and one at 5 MHz − 145.51 ppm. The general properties of the filters relative to their center frequency are:

3 dB bandwidth	±100 Hz
>10 dB rejection	±200 Hz
>15 dB rejection	±300 Hz
Insertion Loss	3.7 dB
Impedance IN/OUT	50 ohms

***N* Divider**—The divide-by-N circuit and comparison circuits to the n counter are shown in Fig. 6. As a convenience in initializing the n counter for using the IPS, a preset number is set into the n counter every time the power is turned on. The number is 83 which is midway between the nominal numbers used—76 and 90. The number 76 is used to raise reference Oscillator #2 from 5 $[1 - (140 \pm 2) \times 10^{-6}]$ MHz to 5 $(1 - 84.48 \times 10^{-6})$ MHz. The number 90 is used to lower Oscillator #1 from 5 $[1 - (80 \pm 2) \times 10^{-6}]$ MHz to 5 $(1 - 145.51 \times 10^{-6})$ MHz.

Pseudo-Symmetric Time Distribution of Deletions (γ Functions)—The computer-controlled up/down binary γ counter holds a maximum of $(2^{20} - 1)\gamma$ deletions. The fixed interval of 2^{20} N counter overflows takes approximately 15 seconds and is considered the minimum integration time over which the finest resolution of the system may be seen. Within this interval the vernier IPS distributes, in evenly spaced time positions, the total quantity of γ held in the γ counter.

Figure 7 shows the γ counter, comparison counter, and the associated comparison gates in a simplified logic diagram.

The comparison counter is the same length as the γ counter and is clocked continuously by the overflow of the N counter. Since the γ functions are keyed to the N counter, this arrangement gives synchronism to the distribution scheme. Comparisons between the γ and comparison counters are made at the bit level by a cross comparison, i.e., highest order of one to the lowest order of the other, and continue in this manner throughout the length. Each bit comparison independently inserts γ deletions in its time position in an uninterrupted repetitive cycle. The γ counter remains at the same count unless a change in frequency or epoch is desired, in which case the comparison timing eliminates the possibility of erroneous comparisons.

The following example illustrates the γ distribution scheme employed. Assume, as shown in Fig. 8, that a γ count of 63 is held statically in the γ counter. This number, as shown in powers of 2, contains 2^0, 2^1, 2^2, 2^3, 2^4, and 2^5, which would place the first six bits of the γ counter in the "one" state.

Assuming the γ register contained 63 and the comparison counter started at 0, the first comparison would be made at 2^{15} counts. This is compared with the 2^5 bit in the γ counter. The comparisons and subsequent γ deletions occur continuously every 2^{15} counts. The next comparison will be at the 2^{16} count, and since it occurred at the 2^{15} count overflow it would be positioned between 2^{15} counts at alternate counts. The 2^{17}, 2^{18}, 2^{19}, and 2^{20} bits are compared with and distribute the respective 2^3, 2^2, 2^1, and $2^0\gamma$ values in an identical format.

Since all binary levels of γ counts are generated independently, they are combined or "OR'ed" to give a total of all levels evenly positioned as shown in Fig. 8. In the above example the combined levels give equally spaced γ deletions for each 2^{14} count minus the first count after t_0. It follows that $(2^6 - 1) = 63$ and $2^6 \times 2^{14} = 2^{20}$.

To summarize, the 63 γ deletions would delete one 5-MHz pulse from the input to the N counter, changing its count modulus from N to $(N + 1)$

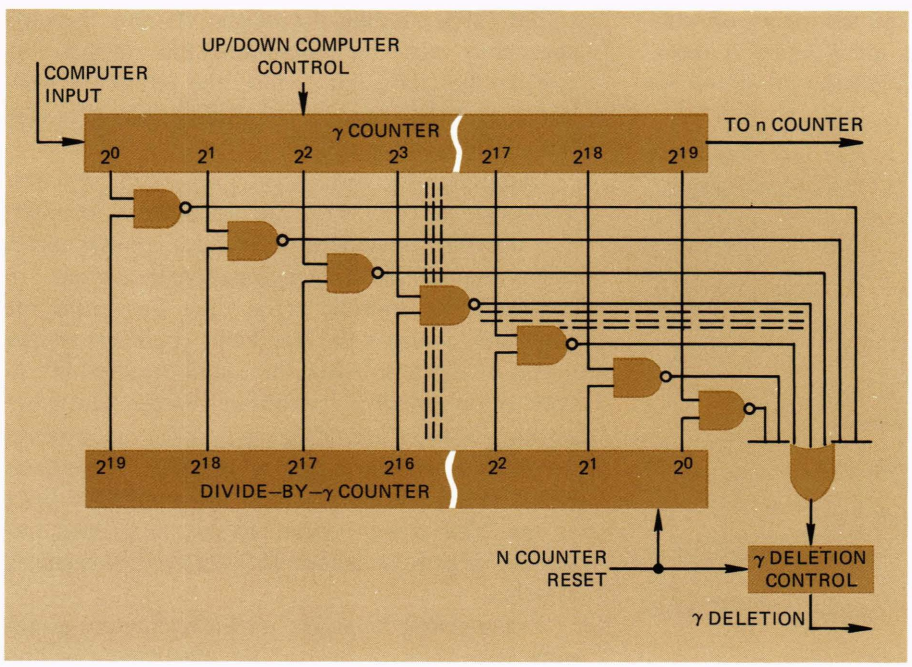

Fig. 7—Gamma counter, divide-by-γ circuit, and deletion control.

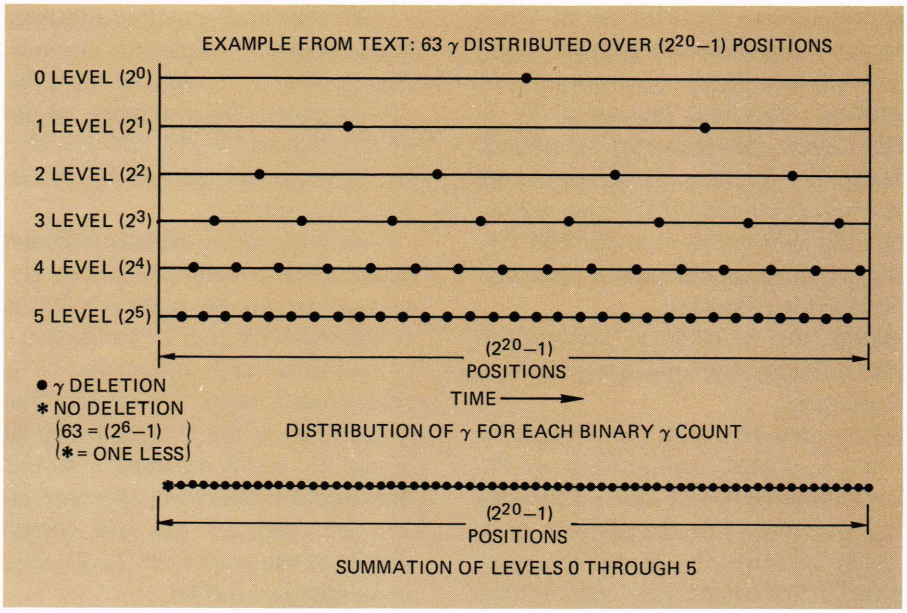

Fig. 8—Binary pseudo-symmetric distribution of γ deletions.

63 times over the 15-second interval. Thus, the N count is effectively changed to N plus the fraction $63/2^{20}$ for the integration time. The process for each succeeding interval is identical if the γ count remains unchanged.

Another way of looking at the effects of the N-counter and γ-counter effects is to observe the 5 MHz input signal phase as a function of time. In Fig. 9, the effects of resets of the N divider show up as transitions in phase as the risers on stair steps. The length of time a given phase is transmitted to the output filter is the time required for a divide-by-N circuit to go through its count and be reset. When the γ-deletion pulse appears, the constant phase period is extended by the period of the input 5 MHz signal which is shown in Fig. 9 as a γ deletion time. After the 200th step, the phase drops to zero and the steps sequence through again.

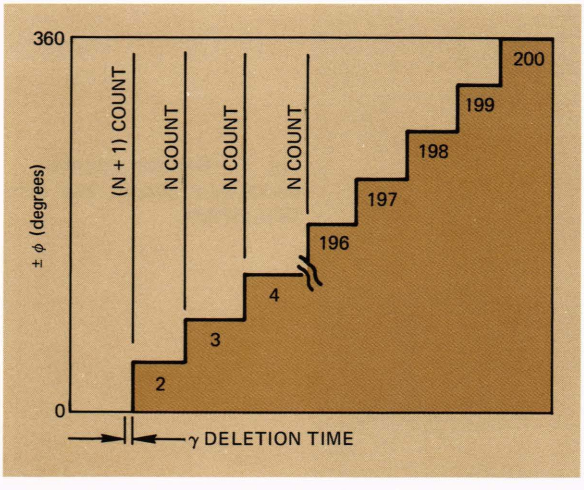

Fig. 9—Deletion of input pulse.

IPS Interfaces

The IPS module interfaces in the TRIAD spacecraft with the computer, the telemetering system, the command system, the reference oscillators, and the frequency multiplier/phase modulator (FM/φM) module.

Computer-IPS Interface—The computer communicates directly with the up/down γ counter. The overflow or underflow of the γ counter increments up or down respectively the binary n counter. The transfer serial data line from the computer controls the up/down condition of the γ and n counters. After the initial "power off" to "power on standby" condition change, the states of the γ counter are arbitrary and the n counter is preset to a predetermined value (83). The adjustments to the γ and n counters are completed prior to the "full power mode" to ensure proper frequency alignment before IPS drives the on-board systems.

Telemetering Interface—Two telemetering telltales have been assigned to the electronics portion

of the IPS: one defines the first bit of the data and remains in the "one" state for this time; the second contains the 32 data bits.

The data from the γ and n counters are parallel shifted, four bits at a time, into a four-bit parallel input (serial output) shift register. The TM frame signal from the telemetering electronics controls the sequence of the parallel shift by incrementing a five-bit binary counter in the IPS. The frame signal also controls the serial shift of the four-bit register, the output of which goes to the TM electronics.

The following lists the assigned TM channels, telltales, and commands for the IPS package:

TM Channel

IPS Temperature (8 bits)

Telltales

1. Oscillator #1 (−145.51 ppm IPS Filter)
   Oscillator #2 (−84.48 ppm IPS Filter)
2. IPS Full Power ON
   IPS Full Power OFF and IPS Bypass
3. IPS TM Marker Bit
4. IPS TM Data (32 bits)
5. IPS Standby Power ON
   IPS Standby Power OFF

Command Interface

1. Oscillator Select #1 (−145.51 ppm IPS Filter)
   Oscillator Select #2 (−84.48 ppm IPS Filter)
2. IPS Full Power ON
   IPS Full Power OFF
3. IPS Standby Power ON
   IPS Standby Power OFF

Satellite Oscillator and FM/ϕM to IPS Interface—Figure 10 shows the signal flow from the IPS to the FM/ϕM and from the satellite oscillator to the IPS.

The selection of the −140 ppm or the −80 ppm oscillator is made by the command system through ground control. Since the IPS must accommodate both oscillators, provisions are made for both inputs in the IPS electronics. A buffer circuit with an input resistive summation network accommodates either input while the other oscillator provides a moderately high impedance in the "power off" mode. The buffer is a one-stage transformer coupled output amplifier with an output impedance of 50 ohms and will drive the IPS electronics when the IPS is "on" and drive the cable, through the "bypass" relay, when the IPS is "off". The FM/ϕM electronics package contains a similar summation network, but three individual amplifier stages drive the FM/ϕM electronics, the PRN, and the memory/computer electronics.

IPS Adjustment Procedures

There are two operational modes for the IPS; they are:

1. The adjustment to compensate for satellite oscillator long term frequency drift.
2. The adjustment of epoch timing marks (2-minute marks) to a degree of accuracy greater than the present 200-nanosecond lumped time adjustments.

Frequency Adjustment—The resolution for one γ deletion in the IPS system is in parts in 10^{13}. Satellite oscillator long term drift has been typically parts in 10^{11} per day. In correcting for this first order drift curve the IPS system, through computer control, would be updated at the rate of

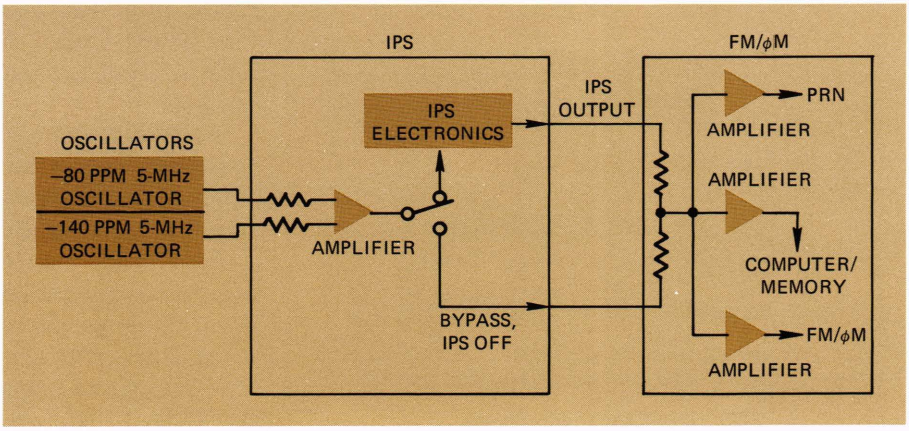

Fig. 10—IPS-oscillator and IPS-FM/ϕM interface.

100 γ functions per day. Considering the 720 2-minute marks occurring each day, this would represent a rate approximately equal to a γ function for each fourteen minutes.

IPS may be commanded to perform a smoothing γ rate function (the rate of which will be second or third order) to provide a first order corrected frequency curve as illustrated in Fig. 11.

Epoch Adjustment—The TRIAD timing system has a cycle deletion process for adjusting time under computer control to the nearest 200 nanoseconds. The IPS system can be used to refine this adjustment to a resolution of better than one

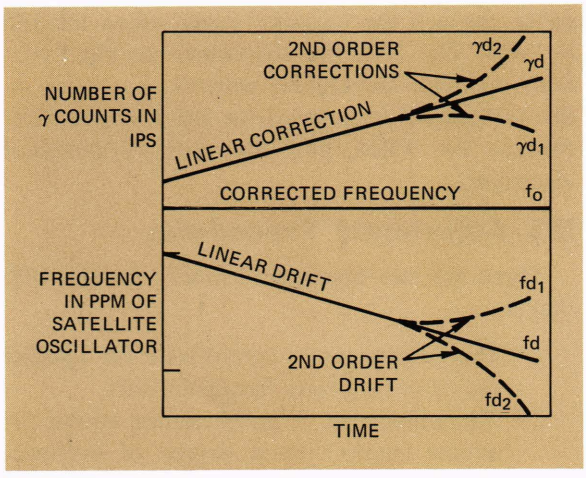

Fig. 11—First and second order distribution of γ for the correction of first and second order frequency drifts.

nanosecond. The procedure is illustrated in Fig. 12. The IPS is commanded through the computer to go to an offset frequency, there to dwell until the epoch error is reduced to zero and then commanded back to provide a frequency that accumulates no time error.

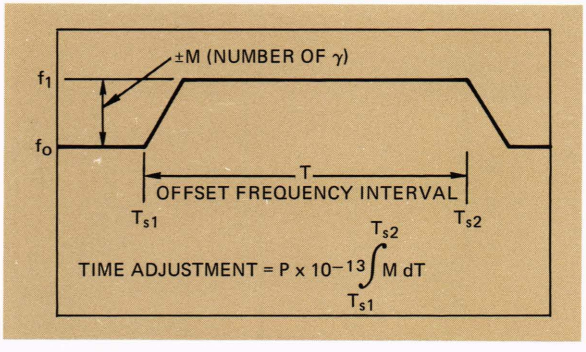

Fig. 12—Epoch adjustment.

Ground Tests with IPS

Tests were performed on combinations of cesium frequency standards, laboratory crystal oscillators, the TRIAD flight reference oscillators, and the IPS. The instrument noise in the IPS was determined by the setup shown in Fig. 13. IPS plus a divider provided one clock. Another divider provided the other clock. Both clocks were driven by the same stable cesium frequency standard. The difference in time between these two clocks showed an instrumentation noise of about 300 picoseconds.

Long Term Aging—The aging rate of the TRIAD oscillator to be used with IPS to generate standard satellite time was determined over a 30 day test with the oscillator in a laboratory vacuum chamber. At best, 7 or 8 $\times$ 10^{-11} per day was attained, or about five microseconds per day for timekeeping.

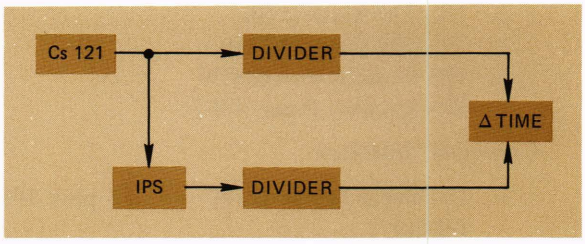

Fig. 13—Cesium (SN 121) versus IPS (offsetting cesium (SN 121)) instrumentation noise.

Long Term Aging Corrections—When two cesium frequency standards were used to drive two clocks, with the frequency of one standard adjusted by IPS to the frequency of the other standard, as shown in Fig. 14, the difference in accumulated time was under the best case observed to be less than ten nanoseconds error in four hours. Under the worst case observed the time accumulated ten nanoseconds difference in one hour.

When a laboratory oscillator replaced the IPS controlled cesium standard of Fig. 13, the best result obtained was a time error of 100 nanoseconds accumulated over three days.

Tests made on the TRIAD flight oscillator over a 30 day period showed that the best that could be done was about 200 nanoseconds over seven hours. The problem in keeping any better time was due to frequency jumps that occurred in the TRIAD oscillator. These jumps were as large

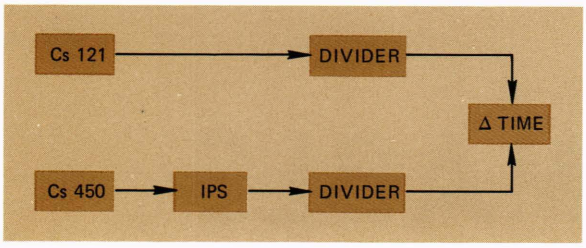

Fig. 14—Cesium (SN 121) versus cesium (SN 450) IPS controlled best case.

as 5×10^{-11} and occurred as infrequently as one in two days or as frequently as four in one day.

Short Term Frequency Stability—The short term frequency stability of a clock driven by an oscillator with and without IPS was measured against a quality rubidium frequency standard. The IPS was observed to modify the inherent short term stability of the oscillator for periods less than five seconds averaging time as shown in Fig. 15.

In-Orbit Tests with IPS

During the post-launch operations, the IPS device was exercised and performed the precise frequency translations commanded by the computer. The epoch setting process was fully confirmed and refined time adjustments were being made when the spacecraft malfunction occurred that suspended use of the computer and the operation of the IPS in TRIAD. The IPS operation in orbit disclosed some operational problems that will be corrected in future models. For instance, switching between oscillators introduced a step in time of nearly three milliseconds because mechanical relays were used.

The IPS epoch adjustment experiments in the TRIAD post-launch operations were of two kinds. First, engineering checks were made to confirm the proper communication between the power, command, telemetry, and computer with the IPS. Second, known values were placed in the IPS to offset the frequency by a magnitude where confirmation could be made via downlink epoch pulses on the received satellite frequency.

The initial settings for frequency offset were large in magnitude since gross time adjustments were attempted for the four-day period. During this time all computer programs and all modes of operation were confirmed.

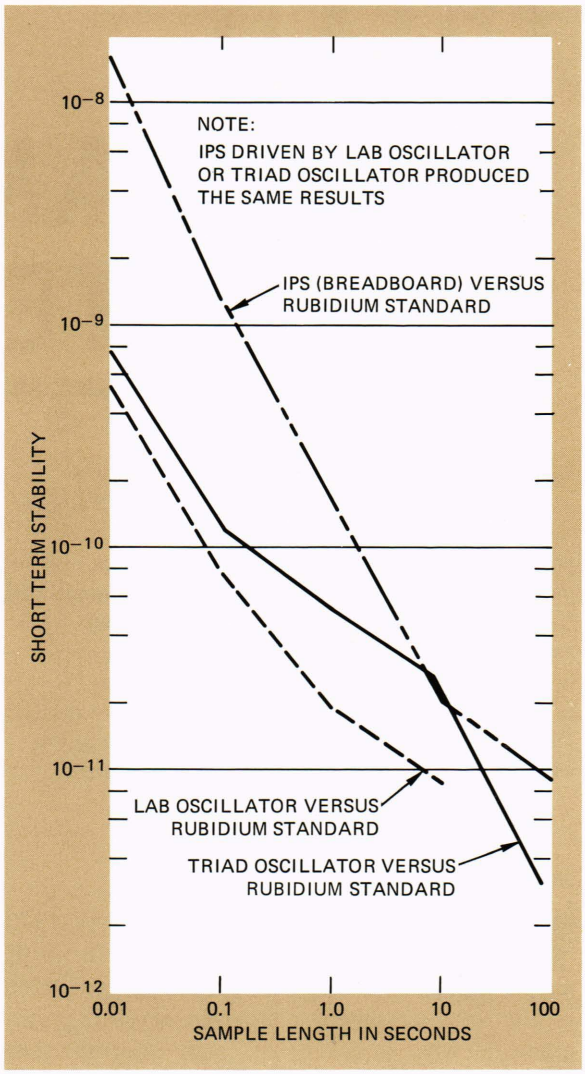

Fig. 15—Short-Term stability.

The second series of tests was intended to refine the epoch steering to the nanosecond region. These tests were never completed because of the computer malfunction.

Conclusion

The Incremental Phase Shifter can adjust the frequency of a spacecraft oscillator, limited only by the ability to predict the rate of drift. IPS can adjust the time of a spacecraft clock, limited only by the ability to measure the time in the spacecraft from signals received on the ground.

A TIME-DIVISION MULTIPLEXING SYSTEM for ASYNCHRONOUS HIGH-RATE TELEMETRY

R. L. Appel and C. T. Pardoe

A time-division multiplexing system has been developed that is significantly different from commercially available equipments. Multiplexing is achieved by interleaving blocks of data from each source preceded by a short coded bit pattern specifying the source of that particular block of data. Data blocks are transmitted as they become available from each particular source. Hence, synchronism of the input and output rates is not required. The prototype system can accommodate input rates as high as 461 kbps on a single input channel and output rates as high as 953 kbps. The system makes possible use of an excess of 90% of channel capacity for information transmittal.

Introduction

ONE OF THE PROBLEM AREAS encountered in adapting the Manned Space Flight Network to support the telemetry requirements for the Earth Resources Technology Satellite (ERTS) Program is that from one to three bit streams at rates from 1 to 32 kilobits per second (kbps) must be relayed from the Corpus Christi tracking station to the Goddard Space Flight Center for processing in approximately real time. It is possible that a general-purpose digital computer such as the Univac 642-B, currently used at remote sites, could perform this task, but little processing time would remain for doing any other computations in the computer.

Multiplexers, per se, are neither new nor hard to obtain. However, after a cursory investigation of available equipments, it appeared that none precisely met the requirements of the ERTS problem. Several manufacturers were agreeable to making modifications to their standard line equipment, but these efforts would have required considerable expenditures of both time and money.

The development of the Time-Division Multiplexer was sponsored by the National Aeronautics and Space Administration. The funding for the work was provided by NASA through APL's contract with the Navy.

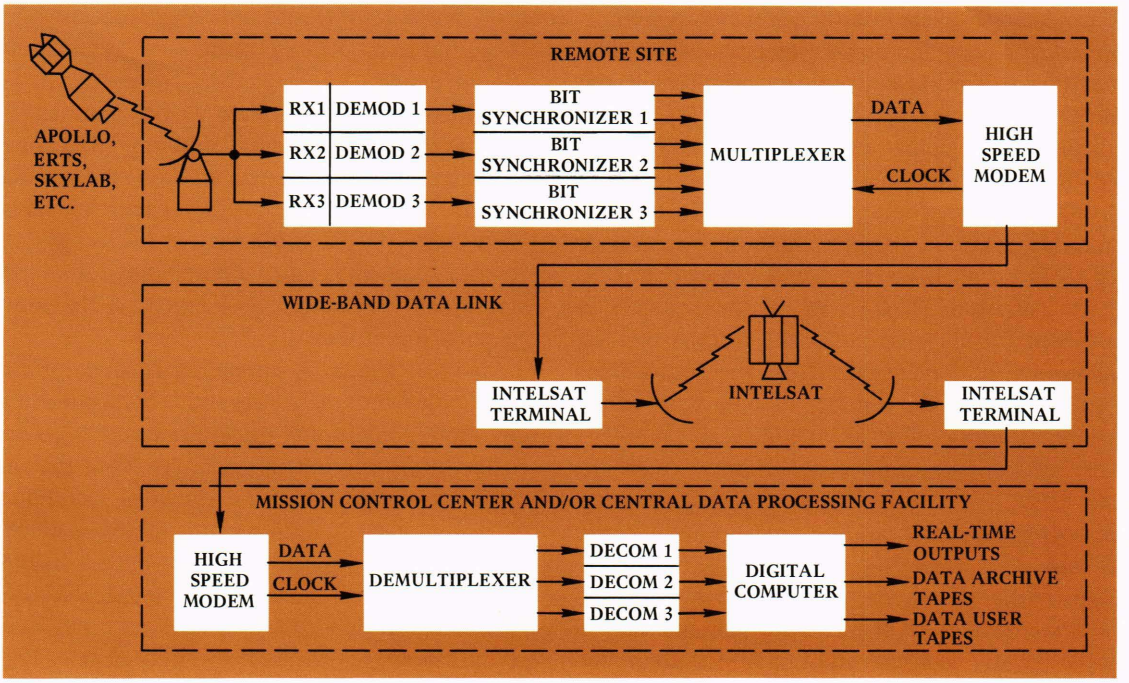

Fig. 1—Proposed application of APL time-division multiplexing system.

At the request of the Manned Flight Planning and Analysis Division of the Goddard Space Flight Center, it was agreed that the Applied Physics Laboratory would design and construct a prototype multiplexing system to satisfy the requirements for ERTS telemetry. This task was undertaken to demonstrate that a small, relatively inexpensive device could be used for the proposed application.

Further impetus was given to the project by the requirements for a similar multiplexing system in a wideband data link/central data processing facility concept (see Fig. 1) presently under consideration. In this application, it is necessary to accommodate a greater number of input channels and a higher output rate than for the ERTS program. The concepts used for the ERTS multiplexing system should, however, be easily expandable to satisfy these requirements.

System Design Considerations

Bit-Stuffing Techniques—All of the commercially available equipments studied in the early stages of this project were of the so-called "bit-stuffing" type. These systems were intended to be used for multiplexing a large number (typically 20) of relatively low rate (typically 150 bps) sources. Furthermore, the sources frequently had to be synchronous. To accommodate input rates greater than the specified input limitation, a sufficient number of inputs were connected together until the required rate total was achieved.

Multiplexing by bit-stuffing, in its simplest form, is no more or less, than commutation. The input signals are sampled at the output rate in an established sequence. If all sources are exactly synchronous with each other and with the multiplexer output rate, the system is highly efficient in regard to the amount of hardware required. However, when this synchronism is not a characteristic of the input signals (which is typical for space communications), considerable effort must be taken to avoid the ambiguity that occurs when an input signal changes state while it is being handled. This problem is compounded if the input rates are subject to reasonably large variations around their nominal value (this variation is typically as much as $\pm$ 10% of the nominal rate for space telemetry) and especially if more than two signals must be multiplexed, one of which is greater than one-half the output rate.

Block Multiplexing Techniques—The underlying concept of the APL multiplexer system is that data will enter the device and be stored as a block. At some later time this block will have an identifying label appended and the data will be

transmitted at a faster rate than it was received.

Simplest Form. Numerous techniques for implementing this basic concept are possible. If the nominal input rates are integer multiples of the lowest rate, one might consider a scheme using twice the integer number of storage registers for each input. These storage registers would then be emptied in a cyclic manner, half of the storage registers from each source being emptied during each output cycle. The length of the registers is determined by allowing sufficient storage for the maximum variation expected on the input rate. Information as to the number of bits of information in each block must be included as a label.

This system is attractive if the input rates are equal, since, then, only two storage registers for each source are required. Also, decommutation is relatively easy since the sources are interlaced synchronously. However, if the input rates differ by a large factor, or if they are not an integer multiple of the slowest rate, such a system becomes very cumbersome.

Storage Register Pairs. Another approach might be to use pairs of storage registers for each input source. By counting modulo the storage register length, one could recognize that a register for a given source had filled. This storage register would then be emptied as output while the incoming information was being stored in the other storage register of the pair.

If no input storage register was filled, then output information would be provided by an auxiliary source. This source might contain a synchronization word (or words), message routing information, or low priority data (e.g., station status, dump telemetry, etc.).

The output bit stream would then consist of blocks of data (with an identifying label appended to each block) from the various sources, but the blocks would not necessarily occur in any specified order. Decommutation for such a system becomes somewhat more difficult since the label bits must now be examined to ascertain the source of a particular block.

Such a system is appealing because of its simplicity and modularity. It could be expanded easily by adding additional pairs of storage registers and a minimum of control circuitry. Also, the rate restrictions imposed in the previous technique and in elementary bit-stuffing are removed since data blocks do not appear as output until a fixed number of bits has been accumulated. However, it does have a major inadequacy; no input rate may be greater than one-half the output rate. If this is exceeded, data will be lost by attempting to fill and empty a storage register at the same time.

Storage Register Pairs Plus Output Registers. The input rate restriction can be removed if additional storage registers are used and if a high rate internal clock is provided to transfer the data from a filled input register to an output register (see Fig. 2). If these additional registers are filled and emptied in a cyclic manner, the output data will be in proper time sequence. Providing that a filled input register from the highest input rate source is given transfer priority over all other sources, and

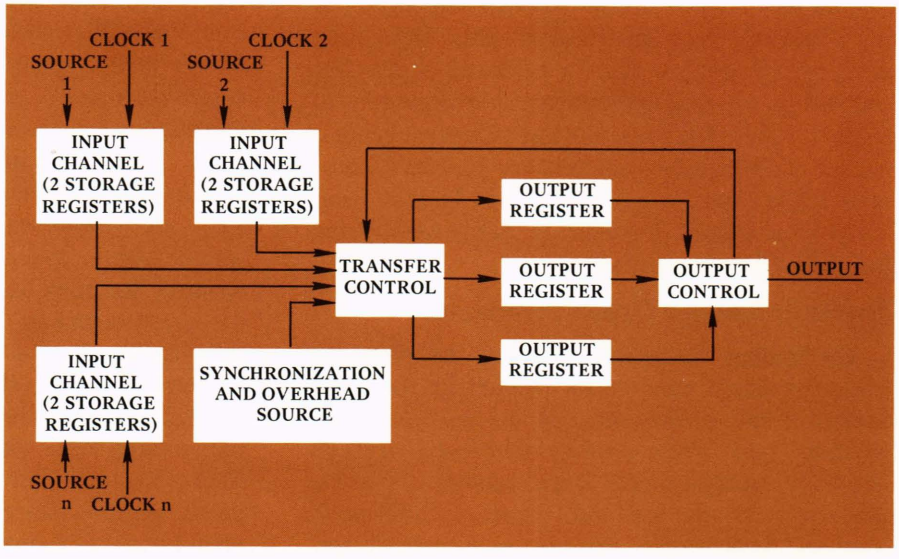

Fig. 2—Improved storage register pairs system.

not allowing for the periodic insertion of synchronization information, three additional registers are sufficient for this purpose. If synchronization information must be periodically included (e.g., if every 20th block must contain the synchronization word), then the number of output registers required is four regardless of the number of input sources.

By using the high-rate internal transfer clock, the restriction of the previous system (that no input rate exceed one-half the output rate) is now improved to the point that no input rate exceed approximately one-half the transfer rate. Since this rate can easily be on the order of 1 to 10 MHz, this restriction poses no real limitation for telemetry data.

Formatting and Channel Efficiency—Up to this point, efficiency has been discussed only from the aspect of the amount and complexity of hardware required to perform a given multiplexing and demultiplexing task. Another, and perhaps more important, aspect of efficiency is concerned with the amount of multiplexed information that can be transmitted over a channel with a known capacity. For this report, multiplexer efficiency will be defined to mean the ratio of the number of information bits to the minimum number of bits required by the demultiplexer to properly process these information bits times 100%. Symbolically, multiplexer efficiency E_m is defined as:

$$E_m = \frac{d}{d + \ell} \times 100\%,$$

where

d = number of information bits and
ℓ = minimum overhead for "d" bits.

It should be noted that this definition removes the effects of periodic synchronization words, automatic routing codes, fixed frame length requirements, and input total rate to output channel rate ratios on the efficiency of the multiplexer unless this information is required by the demultiplexer. It further assumes a perfect (i.e., error-free) transmission channel.

Bit-Stuffing. Representative formats for bit-stuffing multiplexer systems are shown in Fig. 3 (a), (b), and (c) for various input conditions. It can be seen that in the fully synchronous case, in which all input rates and the output rate are derived from a single clock, the efficiency can be as high as 100%. However, as this synchronism is removed, and the input rates allowed to vary independently, the amount of information that must be supplied by the multiplexer to enable the demultiplexer to function properly can be significantly large. This inefficiency can be overcome, but probably at the expense of considerable time delay through the system and/or very complex control circuitry.

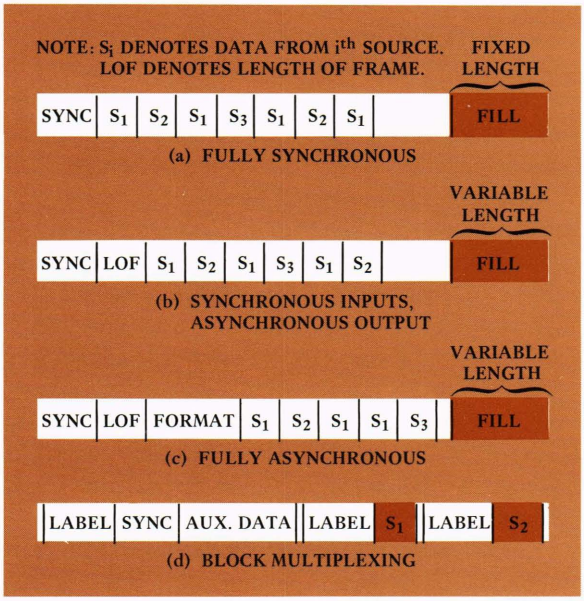

Fig. 3—Typical multiplexing formats.

Block Multiplexing. The general format for a block multiplexer is quite different from that for bit-stuffing, as is shown in Fig. 3(d). Each fixed length block of data from a particular individual source has appended to it a number of bits (referred to as a "label") with a specific pattern that the demultiplexer uses to route the data bits to the appropriate output. If no restrictions on time delay are imposed, the efficiency of a block multiplexer system can be made to approach 100%, limited only by the cost of additional storage registers. The designer must, therefore, choose a storage register size that is compatible with these factors of channel efficiency, time delay, and cost.

The number of bits used as a label has some effect on the efficiency, but since it will generally be much less than the number of bits in the data block, this effect can be kept rather small. However, since a misinterpretation of the relatively few bits in the label will result in the improper routing of the entire block of data bits that follow, the

number of bits in the label should generally be considerably greater than the minimum. This is done so that error detection and correction coding can be included in the labels. The number of bits to be added is determined by the bit-error-rate and over-all error characteristics of the transmission channel that is to be used.

Demultiplexing Techniques—The function of the demultiplexer is to separate the multiplexed composite bit stream into the original data sources. Hence, the design of the demultiplexer is essentially dictated by the format, or manner, in which the data are multiplexed. The first problem, of course, is for the demultiplexer to establish synchronization on the composite bit stream. This is generally accomplished by sending a synchronization word, or specific bit sequence, that has good correlation properties to minimize the probability of obtaining false synchronization. This synchronization word may be sent periodically (which is necessary for bit-stuffing multiplexing systems) or at random intervals (which may be used in block multiplexing systems). The important point is that it be transmitted often enough to minimize the time to reacquire synchronization once it has been lost.

Once synchronization has been established on the incoming bit stream, the data may then be separated, or unpacked, in the manner prescribed by the multiplexer design. For example, a bit-stuffing demultiplexer for nonvarying, synchronous sources and output clock is essentially identical to a decommutator. The demultiplexer simply counts bit-by-bit after synchronization is acquired, and each count routes the given bit to the proper output channel. The main advantage of this technique is that it is relatively simple to implement.

If the sources are rate-variable and nonsynchronous, the design of the bit-stuffing demultiplexer may or may not be more complex. For this case, the bit-stuffing multiplexer complexity increases significantly. However, once the data have been multiplexed and a concomitant data clock generated, the demultiplexer really cannot tell if the sources were synchronous or nonsynchronous. The dynamic range of the fill bits generally will be increased for this case, and, hence, the demultiplexer decoding circuitry may correspondingly increase.

Description of the Multiplexer/ Demultiplexer System

Multiplexer Design—The system selected to demonstrate the feasibility of achieving block multiplexing with a small special-purpose equipment is that shown in Fig. 2. It was constructed with three input channels to meet the requirements for ERTS telemetry. In operation, this system stores incoming data in one of the two registers available to each source. The transfer control section recognizes when a register is filled and shifts the data, with label appended, into the next available output register. During this time, input data are being stored in the other register of the input channel. The output control section needs to merely cycle through the output registers, sequentially shifting data out of each.

Input Channel. The logical flow of information for an input channel is shown in Fig. 4. The data bits are entered into either shift register SR_{IA} or SR_{IB} at the data source clock rate. Selection of the A or B register is accomplished by input and output selector circuits, as well as clock selectors for each register. All selectors for a single input channel are under the control of a single bistable element that changes state after each "d" transition (in one direction) of the data clock.

An additional "ℓ" bits are added to the data block via binary-coded-octal thumbwheel switches on the front panel. These switches generate the correct inputs to a parallel input shift register, SR_L. This information is used as a label for the "d" data bits so that correct demultiplexing may be accomplished. The label information is entered immediately after completely filling an input buffer and is not released until just prior to transferring the "$\ell + d$" bits from an input channel register to an output register.

The remaining input channel logic is used to establish a "fill command", F_i. The presence of this signal in the "true" state indicates that an input register for this channel has been filled, that a periodic synchronization data block is not required (n), and that this input channel has been selected for transfer of data to an ouput buffer.

In order to avoid the simultaneous occurrence of the F signal for more than one channel that would result in an ambiguous decision, the channels are sequentially strobed by an MC_i signal. Each application of this signal, which is derived from the master clock, occupies a distinct and unique time position. (Specifically the MC_{i+1} signal has a duration of one-half the master clock

period and occurs one-half a master clock period after the termination of MC_i.) The MC_i signal also provides the necessary priority for any input with a rate greater than one-half the output rate providing that source is connected as source #1.

Transfer Control. The major purpose of the transfer control section is to recognize that an input channel has a full register and, under the proper conditions, to transfer the contents of that register to the next available output register. In order to ease rate restrictions, this must be done at a high clock rate, which is generated internally.

Also, only the data from one input channel can be transferred at a time and data from a high rate source must be given priority over sources of a lower rate. Both of these functions have been accomplished by generating "strobing" pulses from the internal clock signal ("*MC*" in Fig. 5). When the transfer control section completes the transfer of "$\ell + d$" bits (detected by the transfer bit counter), the input to a modulo 5 counter is enabled and the five strobing pulses are generated (MC_0, MC_1, . . . MC_4). The first pulse, MC_0, resets to zero all the bistable elements generating the F_i signals, particularly the one F_i signal that has been in a true state during the transfer of data just completed. The next pulse, MC_1, strobes the conditions for setting the *F*-generating bistable element in channel 1. If all conditions are met (a full input register and no periodic synchronization block required), the *F* signal will be set, data will be transferred from input channel 1, and no further MC_i pulses will be generated.

If a register has not been filled in channel 1, no *F* signal is generated in that channel, and the MC_2 pulse strobes the conditions in channel 2. MC_3 does the same in channel 3. When no input channel has data to be transferred and the next output register to be emptied has not yet been filled, the MC_4 pulse causes synchronization and overhead source data to be entered into the output register.

The "2-bit comparator" in Fig. 5 is used to prevent the transfer of information from an input register to an output register when the output register still contains data from a previous transfer. This is accomplished by detecting the equality of the states of the transfer cycle counter and the read cycle counter. When these counter states are identical, the modulo 5 counter that generates the strobing pulses is held in a reset condition. Once the output register is emptied, this reset signal is removed, and the generation of strobing pulses can be resumed.

The proper routing of information from an input channel to a selected output register is accomplished by the "4:1 selector" followed by a "1:3 selector" to route data and a second "1:3 selector" to apply a clock signal to the proper output register. The 4:1 selector is an AND-OR gate in which each of the S_i* signals is gated with its corresponding F_i signal so that a "data bus" line is formed as the input to the 1:3 selector.

In the event that a periodic synchronization word is required, it can be provided by counting the blocks of data that are transferred and generating a signal "*n*" for the appropriate block. This signal then inhibits the generation of *F* signals for the data channels and causes MC_4 to

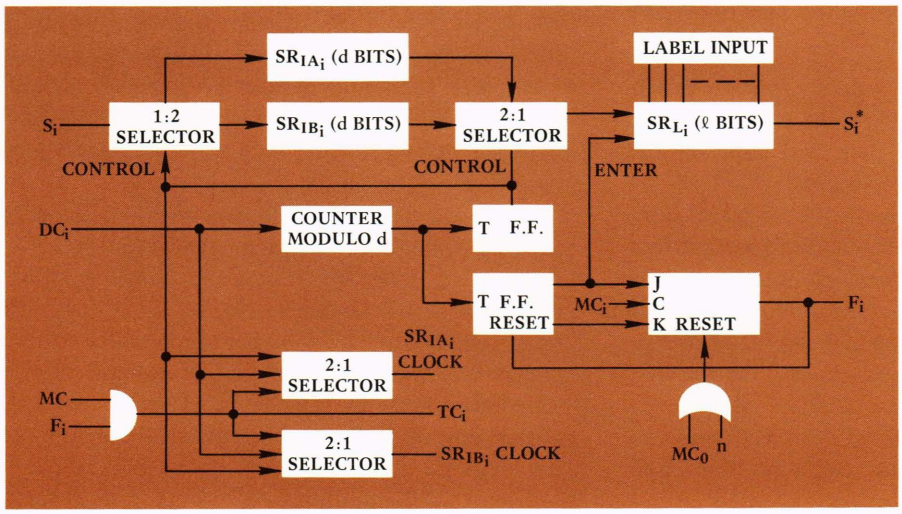

Fig. 4—Multiplexer input channel section.

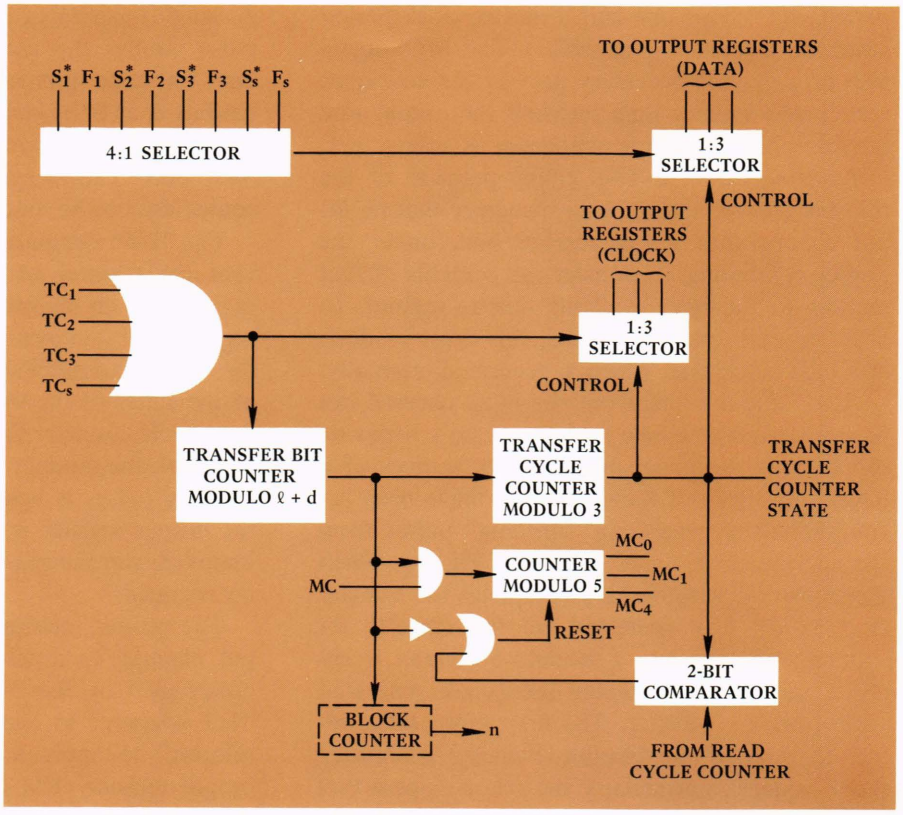

Fig. 5—Transfer control section.

initiate the transfer of information from the synchronization and overhead source channel.

Data Formatting—The selection of the multiplexer output data format is important in that it dictates the design of the demultiplexer and determines to a large extent the efficiency of utilization of the output channel capacity. Many factors influenced the choice of the format for the APL multiplexing system, some of which are discussed in the following.

Synchronization and Overhead Source. When the condition arises that no input channel has a storage register filled with data and data are required by the output, the necessary "filler" information is provided by the synchronization and overhead source. Since in block multiplexing this condition persists for a complete block of bits rather than occurring as pseudo-random bits as it does in bit-stuffing, some use can be made of this otherwise wasted transmission channel capacity. If nothing else, at least synchronization information can be transmitted so that the demultiplexer can verify its synchronism at frequent, although aperiodic, intervals.

The condition requiring the insertion of information from the synchronization and overhead source is detected by a comparison circuit, which compares the states of the read cycle counter in the output control section and the transfer cycle counter in the transfer control section. Whenever the transfer counter state is only one greater than the read state, a command is given to transfer information from the synchronization and overhead source to the output register. A second condition for inserting synchronization data is the requirement that such information be supplied periodically. As discussed previously, this is accomplished with the "n" signal inhibiting all F_i's except F_S and causing F_S to be set.

Block Length. The selection of a block length for any transmission system generally involves a number of tradeoffs. From an intuitive standpoint, the block should not be so short that overhead information is being sent frequently and the channel capacity is inefficiently utilized, nor so long that the delay time from reception to multiplexer output will become significant for low rate data.

For the APL multiplexing system, a third factor

entered into the block length selection. In this system, it is essential that the block labels be received by the demultiplexer correctly to protect against erroneously routing the data from one source to the output channel of another source. To accomplish this, a study was made of error-correcting codes that would be short enough so as not to significantly decrease the efficiency of the system, yet powerful enough to correct a significant number of errors.

Four labels or code words were required for the APL system (three source and one synchronization label), and an 8-bit near-equidistant code for four messages was selected. Equidistant codes are those for which the distance between pairs of code words are all equal to the maximum possible mean distance. By selecting the code word length to be 8-bits, a minimum distance of five was obtained between the four labels. This minimum distance allows the correction of up to two errors. Thus, three errors would have to be made in the eight bits of a label before invalid decoding of a label would occur.

The probabilities of *not properly* identifying a label (i.e., the label cannot be decoded as one of the four known labels) and *incorrectly* identifying a label (i.e., the label is decoded as the label from a different source) have been calculated. The probability that a label is not properly identified is approximately $56p^3$, where p is the bit error probability. The probability that the label is incorrectly identified is approximately $20p^3$ in the worst case, tending toward $10p^3$ in more favorable cases. With a bit error probability of 10^{-6}, these probabilities are of the order of 10^{-16} to 10^{-17}. Even with a bit error probability as high as 10^{-3}, the probability of not correctly recognizing the label is 5.6×10^{-8}, and the probability of incorrect identification is 1 or 2 times 10^{-8}.

Since the label length is considered overhead information and thus affects the efficiency of utilization of the output channel capacity, the block length of the APL multiplexing system was chosen to be 104 bits. This length was selected so that the overhead would contribute less than 10% of the total block length. This block length appears reasonable in that a channel capacity utilization in excess of 90% may be obtained and the time delay from multiplexer input to output is kept rather small (e.g., for a 1 kbps data source and a 50 kbps output rate, the maximum time delay is approximately 100 ms).

Block Formats. The final decision regarding the multiplexing system data format was to transmit a synchronization block 104 bits long so all blocks would be of equal length. This not only simplifies the demultiplexer hardware, but provides some additional flexibility. The format of a synchronization block is shown in Fig. 6(a). The block consists of a special 8-bit synchronization label, the 24-bit synchronization pattern, three 8-bit words to indicate the source, destination, and format of the data, and 48 bits that may contain additional housekeeping information or data from an auxiliary source.

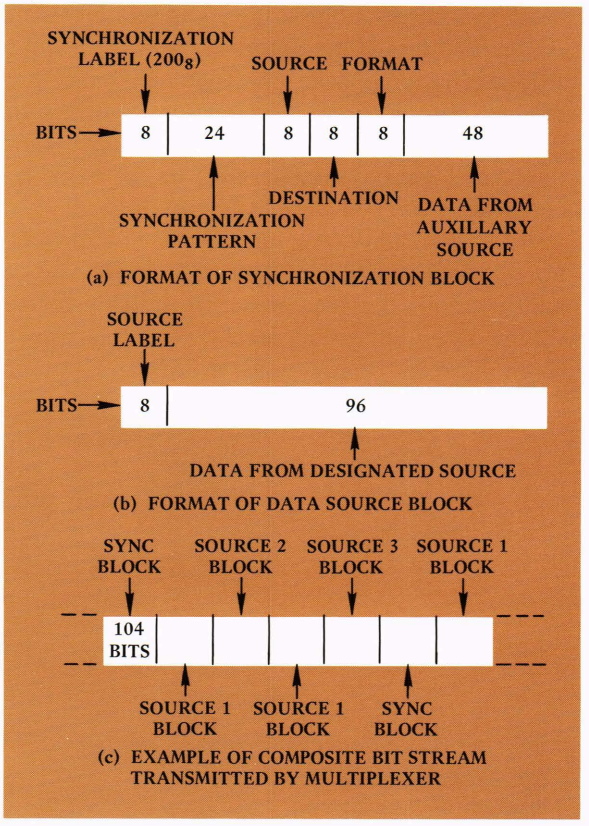

Fig. 6—APL multiplexing system format.

Figure 6(b) shows the format of a data source block, and Fig. 6(c) shows an example of the composite bit stream transmitted by the multiplexer. Note that the multiplexer output is simply a series of equal length blocks, each block being decodable by a distinct label that indicates either a synchronization block or one of the three data source blocks. The number of synchronization blocks transmitted per second is determined by the

multiplexer output line rate and the arithmetic sum of the input sources it is multiplexing. For example, if three 10-kbps sources are multiplexed and transmitted via a 40-kbps data line, approximately 20%, or one out of every five blocks, will be synchronization blocks. This includes the 8% overhead to transmit each data source. If no data are present to be multiplexed, the multiplexer simply sends a series of synchronization blocks, an operation analogous to the generation of an idler pattern by a modem when no data are present for transmission.

Demultiplexer Design—As previously discussed, the functions of the demultiplexer are to establish block synchronization on the composite bit stream transmitted by the multiplexer (Fig. 6(c)) and to separate the composite bit stream into the three original data sources. This section describes the basic operation of the demultiplexer on a functional or logic basis rather than on an individual component level.

Basic Operation. An operational flow diagram for the demultiplexer is shown in Fig. 7. The demultiplexer is designed to search initially for the special synchronization label, which consists of seven "zeroes" followed by a "one". The composite input bit stream is examined bit-by-bit until a run of seven consecutive "zeroes" is found. The next "one" received activates a bit-by-bit serial comparison of the following 24 bits in the input data stream with the selected master synchronization pattern.

If no errors are found in the received pattern, the demultiplexer is considered to have established synchronization. Upon reception of any bit that does not agree with the known pattern, the demultiplexer is considered to have lost synchronization, and a bit-by-bit search for the synchronization label is resumed. Assuming that a perfect 24-bit pattern has been verified, the next three 8-bit words may be stored for future use if required (see Fig. 6(a)). The remaining 48-bits are presently fill bits, and the demultiplexer simply counts until the end of the block occurs (i.e., 96 bits after the initial synchronization label was found).

Having completed examination of the synchronization block, the next 8 bits in the data stream are examined to determine if the next block is another synchronization block or a data source block. If one of the three possible source labels is found, the next 96 bits are data from that particular source, as shown in the data source block for-

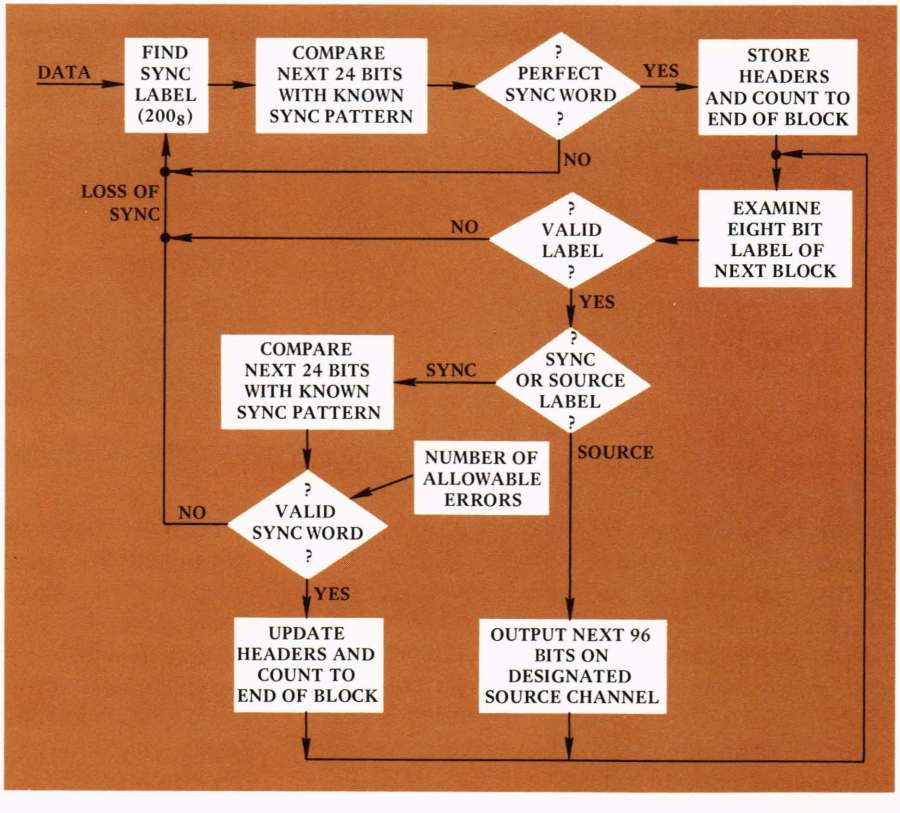

Fig. 7—Operational flow diagram of time-division demultiplexer.

mat of Fig. 6(b). The data bits are then routed to the proper output channel as dictated by the source label.

If the next 8 bits were determined to be the synchronization label, the next 24 bits would again be compared to the known synchronization pattern. In this case, however, some number of disagreements may be tolerated; this allowable number of errors is switch-selectable from zero to seven. Hence, a less stringent bit error rate criterion is allowed once a perfect synchronization pattern has been found.

If the following 8 bits after the synchronization block contain too many errors and cannot be decoded as either the synchronization label or one of the three source labels, synchronization is assumed to be lost, and the bit-by-bit search for the synchronization label and an error-free 24-bit synchronization pattern is resumed.

System Characteristics—The multiplexer and demultiplexer (shown in Fig. 8) are each constructed as self-contained units on a standard 19-inch panel 7 inches high. Each has its own power supply integrally mounted with the unit. The electronics for both units consist exclusively of transistor-transistor logic (TTL) circuits manufactured by both Texas Instruments and Fairchild Semiconductor. The multiplexer consists of 11 printed circuit boards containing up to 16 dual-in-line integrated circuit packages per board. Approximately 150 discrete packages are used. The demultiplexer uses four such printed circuit boards and contains approximately 60 discrete packages.

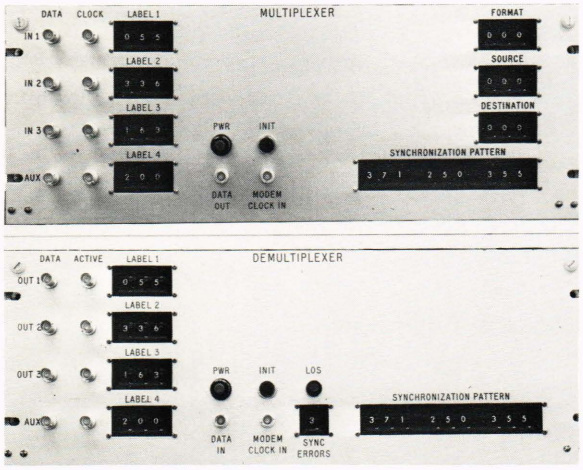

Fig. 8—Multiplexer and demultiplexer units.

Binary-coded-octal thumbwheel switches are used on the front panel of both units. These switches are used to set the three 8-bit source identification labels, the special 8-bit synchronization label, and the 24-bit synchronization word on the multiplexer and demultiplexer. Additionally, the multiplexer has three 8-bit switches to set the format, source, and destination of the data, and the demultiplexer includes a single switch to set the allowable number of errors in a synchronization word.

The system is capable of multiplexing up to three serial pulse-code modulation (PCM) bit streams and may be used for any non-return-to-zero (NRZ) coded data. The maximum output rate limitation for the multiplexer is 953 kbps with a maximum single-channel input bit rate of 461 kbps. These limitations are imposed by the internal multiplexer clock rate of 1 Mbps and the input register configuration.

System Expansion Potential

The time-division multiplexing system described in this report meets all of the requirements for the ERTS telemetry application. Moreover, the system may be utilized in a wide range of similar applications in which several high-rate bit streams must be multiplexed into a single output channel (e.g., the Central Data Processing Facility application). Numerous possibilities exist for expanding the capabilities of the APL multiplexing system to satisfy additional requirements.

If an increased number of input channels is required (i.e., in excess of three channels), the most direct approach is simply to duplicate the current equipment (both multiplexer and demultiplexer units) and connect two of each in a cascade arrangement. In this way, the number of inputs that can be accommodated is increased from three, for a single multiplexer unit, to five, for two cascaded units. A suitable clock rate would have to be provided to serve as the output clock from one multiplexer and the input clock for the second. Such an arrangement, for example, would probably be satisfactory for relaying data from a remote site to a Central Data Processing Facility for most Skylab telemetry conditions.

Input capacity expansion by cascading multiplexers does have the disadvantage of decreasing channel usage efficiency. This results from having

to provide synchronization and block labeling information in the output of the first multiplexer and then similar type information again in the second multiplexer. Also, some small increase in the delay encountered by those sources that must go through both multiplexers will occur.

Both of these difficulties can be circumvented by increasing the number of basic input channels available. Physically accomplishing this with the current equipments is a nontrivial task, but it can be accomplished with relative ease in a redesigned system. The most significant change is that the modulus of the modulo 5 counter in the transfer control section (Fig. 5) must be made equal to the number of input sources desired plus two. This, then, allows for the generation of a sufficient number of strobing pulses to accommodate the additional inputs. Additionally, an input channel (Fig. 4) must be provided for each source, and such secondary units as the 4:1 selector and the transfer clock combining gate in Fig. 5 must be expanded.

Data Rates—In the event that the absolute single channel input rate limitation on the multiplexer of 461 kbps proves inadequate for future missions, this limit may be increased within the current system by replacing the 1-MHz master clock with a 2-MHz clock. This would effectively double both the single channel input rate limit and the output channel rate limit so that inputs of up to 922 kbps and an output as high as 1.9 Mbps could be accommodated. It is not expected that such a change would involve anything further in the multiplexer.

To exceed the above limits would entail a redesign of the entire system using some form of higher-speed logic. Integrated circuits of the "ECL" (emitter-coupled logic) type are now readily available that can be operated at clock rates in excess of 100 MHz. The use of such circuits would result in a multiplexing system design that could easily handle input rates up to 10 Mbps with an output rate at approximately 20 Mbps. It is well known, however, that the physical construction of systems operating at these rates is a nontrivial task.

Data Rate Regeneration—The final area for expanding the capabilities of the APL multiplexing system is in the demultiplexer output portion of the system. At present, the data from the various sources are transmitted in bursts of data at the input, or modem, clock rate. This type of operation will suffice for most digital processing applications as now envisioned. However, there may be cases where it is desirable to have continuous serial bit streams as the outputs from the demultiplexer (e.g., for analog chart recording, oscilloscope presentations, etc.).

A prototype single channel data rate smoothing system has been designed and constructed to demonstrate the feasibility of obtaining continuous or smoothed serial bit streams from the burst-type demultiplexer outputs. The system basically consists of a long shift register that provides temporary storage for the data which enter the register in bursts at the modem clock rate. Data are continuously emptied from the register at or near the expected nominal rate of the source (i.e., the original downlink frequency prior to multiplexing). A voltage-controlled oscillator (VCO) is used as the source for the output clock frequency.

Control of the rate smoothing operation is accomplished by maintaining the number of data bits in the storage register at approximately one-half the register length. If data are entering the register rapidly so that the register is over half full, the VCO or output clock rate is increased. If data are entering the register at a lower rate, so that the register is less than half full, the output rate is correspondingly decreased. Thus, the output rate is continuously adjusted so that the register is always approximately half full, and a continuous serial bit stream is provided. Rate smoothing by this approach does not restore the original instantaneous rate variation of the source. The method, however, does provide a long-term approximation of the original rate and yields gap-free outputs for analog display purposes.

Since the APL multiplexing system uses 96-bit data block lengths, the prototype rate smoothing system was designed to provide a storage capacity of 10 data blocks, or 960 total bits. The system may be used for smoothing original source rates up to 1 Mbps with a maximum modem clock rate of 2 Mbps.

Acknowledgment

The authors would like to acknowledge the significant contributions, especially in the area of coding, made by A. G. Carlton, whose technical guidance and direction aided the project immeasurably.